

EMF-2103(NP)  
Revision 2

# Realistic Large Break LOCA Methodology for Pressurized Water Reactors

November 2010


AREVA NP Inc.

ISSUED IN ON-LINE-  
DOCUMENT SYSTEM  
DATE: 11/12/10

EMF-2103(NP)  
Revision 2

**Realistic Large Break LOCA Methodology for  
Pressurized Water Reactors**


Prepared:

  
B. M. Dunn  
Realistic LBLOCA

11/12/2010  
Date

Contributors (in alphabetical order): Charlie Bott, Andrei Burghilea, Ken Carlson, Hueiming Chow, Mireille Cortes, Eric Coryell, Philippe Dias, Scott Franz, Michael Garrett, Scott Ghan, Monte Giles, Gene Jensen, Rachel Love, Thomas Luedeke, Robert Martin, Harold Massie, Brian Mays, Jeff McElroy, Mark Miller, Larry Nielsen, Nithian Nithianandan, Wanda Roman, Parvez Salim, Paul Sohn, Hong Tang, Don Todd, Maggie Wang, Albert Yang

Reviewed:

  
J. R. Biller  
Realistic LBLOCA

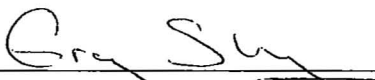
11/12/2010  
Date

Approved:

  
R. L. Baxter, Supervisor  
Realistic LBLOCA

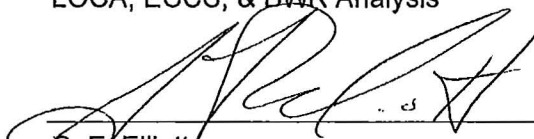
11/12/2010  
Date

Approved:

  
G. S. Uyeda, Manager  
LOCA, ECCS, & BWR Analysis

11/12/2010  
Date

Approved:

  
G. F. Elliott  
Regulatory Affairs

11/12/2010  
Date

AREVA NP Inc.

**U.S. Nuclear Regulatory Commission  
Report Disclaimer**

**Important Notice Regarding the Contents and Use of This Document**

***Please Read Carefully***

This technical report was derived through research and development programs sponsored by AREVA NP Inc. It is being submitted by AREVA NP to the U.S. Nuclear Regulatory Commission as part of a technical contribution to facilitate safety analyses by licensees of the U.S. Nuclear Regulatory Commission which utilize AREVA NP fabricated reload fuel or technical services provided by AREVA NP for light water power reactors and it is true and correct to the best of AREVA NP's knowledge, information, and belief. The information contained herein may be used by the U.S. Nuclear Regulatory Commission in its review of this report and, under the terms of the respective agreements, by licensees or applicants before the U.S. Nuclear Regulatory Commission which are customers of AREVA NP in their demonstration of compliance with the U.S. Nuclear Regulatory Commission's regulations.

AREVA NP's warranties and representations concerning the subject matter of this document are those set forth in the agreement between AREVA NP and the Customer pursuant to which this document is issued. Accordingly, except as otherwise expressly provided in such agreement, neither AREVA NP nor any person acting on its behalf:

- a. makes any warranty, or representation, express or implied, with respect to the accuracy, completeness, or usefulness of the information contained in this document, or that the use of any information, apparatus, method, or process disclosed in this document will not infringe privately owned rights;
- or
- b. assumes any liabilities with respect to the use of, or for damages resulting from the use of, any information, apparatus, method, or process disclosed in this document.

AREVA NP Inc.

EMF-2103(NP)  
Revision 2

**Realistic Large Break LOCA Methodology for  
Pressurized Water Reactors**

**Copyright © 2010**

**AREVA NP Inc.**

**All Right Reserved**



## Nature of Changes

Item	Page	Description and Justification
1.	All	Changes incorporated into Revision 2 are too extensive to itemize. Therefore, this version is considered to be an entire rewrite.

## Contents

1.0	Introduction .....	1-1
2.0	Methodology Roadmap .....	2-1
2.1	Requirements and Code Capabilities .....	2-1
2.2	Assessment and Ranging of Parameters .....	2-3
2.3	Sensitivity and Uncertainty Analysis .....	2-4
3.0	Requirements and Code Capabilities .....	3-1
3.1	Scenario Specification (CSAU Step 1) .....	3-1
3.2	Nuclear Power Plant Selection (CSAU Step 2) .....	3-4
3.3	Phenomena Identification and Ranking, PIRT (CSAU Step 3) .....	3-6
3.4	Frozen Code Version Selection (CSAU Step 4) .....	3-8
3.4.1	COPERNIC2 and RODEX3A Fuel Rod Performance Codes .....	3-8
3.4.2	S-RELAP5 .....	3-10
3.5	Provision of Complete Code Documentation (CSAU Step 5) .....	3-11
3.6	Determination of Code Applicability (CSAU Step 6) .....	3-12
3.6.1	Field Equations .....	3-12
3.6.2	Closure Equations .....	3-13
3.6.3	Code Numerics .....	3-13
3.6.4	Structure and Nodalization .....	3-14
4.0	Assessment and Ranging of Parameters .....	4-1
4.1	Establishment of Assessment Matrix (CSAU Step 7) .....	4-1
4.1.1	PIRT Considerations .....	4-2
4.1.2	Nodalization Considerations .....	4-2
4.1.3	Scaling Considerations .....	4-3
4.1.4	Compensating Errors .....	4-3
4.1.5	Summary .....	4-3
4.2	Define Nodalization for NPP Calculations (CSAU Step 8) .....	4-9
4.2.1	Nodalization Methodology .....	4-10
4.2.2	Numerical Considerations .....	4-11
4.2.3	Loop Model .....	4-12
4.2.3.1	Hot Leg .....	4-13
4.2.3.2	Steam Generator .....	4-14
4.2.3.3	Pump Suction .....	4-14
4.2.3.4	Reactor Coolant Pump .....	4-15
4.2.3.5	Cold Leg and Break .....	4-15
4.2.3.6	ECCS .....	4-16
4.2.3.7	Pressurizer .....	4-16
4.2.4	Reactor Vessel Model .....	4-17
4.2.4.1	Downcomer .....	4-17
4.2.4.2	Lower Vessel .....	4-18
4.2.4.3	Core, Core Bypass, and Fuel .....	4-19
4.2.4.4	Upper Plenum/Upper Head .....	4-21
4.2.5	Containment Model .....	4-22

4.2.6	Plant Model Summary .....	4-23
4.3	Determine Code and Experimental Accuracy (CSAU Step 9).....	4-33
4.3.1	Separate Effects Tests .....	4-33
4.3.1.1	THTF Heat Transfer.....	4-34
4.3.1.2	THTF Level Swell.....	4-38
4.3.1.3	GE Level Swell .....	4-42
4.3.1.4	FRIGG-2 .....	4-46
4.3.1.5	Bennett Tube .....	4-59
4.3.1.6	FLECHT and FLECHT-SEASET.....	4-62
4.3.1.7	PDTF SMART Tests .....	4-80
4.3.1.8	Marviken Tests .....	4-88
4.3.1.9	Westinghouse/EPRI 1/3 Scale Tests .....	4-101
4.3.1.10	AREVA CCFL Tests.....	4-106
4.3.1.11	UPTF Tests.....	4-110
4.3.1.11.1	UPTF Tests 6 and 7.....	4-110
4.3.1.11.2	UPTF Test 8.....	4-114
4.3.1.11.3	UPTF Tests 10 and 29.....	4-116
4.3.1.11.4	UPTF Tests 10 and 12.....	4-119
4.3.1.11.5	UPTF Test 11.....	4-120
4.3.1.12	CCTF Tests .....	4-147
4.3.1.13	SCTF Tests.....	4-176
4.3.1.14	ACHILLES Tests.....	4-214
4.3.1.15	Multi-Dimensional Flow Testing .....	4-226
4.3.1.16	Moby Dick Test 3141 .....	4-233
4.3.1.17	Assessment of Total Heat Transfer in FLECHT-SEASET Test 31504.....	4-237
4.3.2	Integral Effects Tests.....	4-243
4.3.2.1	LOFT Assessments .....	4-243
4.3.2.1.1	LOFT Facility.....	4-244
4.3.2.1.2	LOFT Test Descriptions .....	4-246
4.3.2.1.3	LOFT Assessment Summary .....	4-247
4.3.2.1.4	LOFT Test L2-3 Assessment .....	4-249
4.3.2.1.5	LOFT Test L2-5 Assessment .....	4-249
4.3.2.1.6	LOFT Test LP-02-6 Assessment .....	4-249
4.3.2.1.7	LOFT Test LP-LB-1 Assessment .....	4-250
4.3.2.2	Semiscale Tests .....	4-260
4.3.2.2.1	Semiscale Facilities .....	4-260
4.3.2.2.2	Semiscale Test Descriptions.....	4-262
4.3.2.2.3	Test S-06-3 Assessment.....	4-264
4.3.2.2.4	Test S-07-1 Assessment.....	4-264
4.3.3	Methodology Treatment of PIRT Phenomena.....	4-268
4.3.3.1	Important PIRT Phenomena Not Treated Statistically .....	4-268
4.3.3.1.1	Core Multi-Dimensional Flow and Void Distributions .....	4-268
4.3.3.1.2	Liquid Entrainment in the Core .....	4-270
4.3.3.1.3	Core Flow Reversal/Stagnation .....	4-271
4.3.3.1.4	Upper Plenum Liquid Entrainment/Deentrainment .....	4-271

	4.3.3.1.5	Countercurrent Flow Limit .....	4-273
	4.3.3.1.6	Hot Leg Entrainment/Deentrainment .....	4-273
	4.3.3.1.7	Two-Phase Pump Degradation .....	4-273
	4.3.3.1.8	Pump Differential Pressure Loss .....	4-274
	4.3.3.1.9	Noncondensable Transport .....	4-274
	4.3.3.1.10	Downcomer Entrainment .....	4-274
	4.3.3.1.11	Downcomer Liquid Level Oscillations .....	4-275
	4.3.3.1.12	Lower Plenum Sweepout .....	4-275
	4.3.3.1.13	Steam Binding .....	4-276
	4.3.3.1.14	Cold Leg Condensation .....	4-276
	4.3.3.1.15	Fuel Rod, Stored Energy, Gap Conductivity .....	4-277
	4.3.3.1.16	Fuel Rod, Stored Energy, Axial and Radial Peaking .....	4-278
	4.3.3.1.17	Fuel Rod, Decay Heat, Ballooning, Rupture and Post-Rupture Fuel Relocation .....	4-278
	4.3.3.1.18	Downcomer, Flow Pattern, CCFL, Slug Flow, and Non-Equilibrium .....	4-282
	4.3.3.1.19	Downcomer, Multi-D Phenomena .....	4-283
	4.3.3.1.20	Downcomer, Downcomer Boiling, Noding .....	4-284
	4.3.3.1.21	Loop, Flow Oscillation .....	4-284
4.3.3.2		Important PIRT Phenomena Treated Statistically .....	4-291
	4.3.3.2.1	Stored Energy .....	4-291
	4.3.3.2.2	Oxidation .....	4-293
	4.3.3.2.3	Decay Heat .....	4-294
	4.3.3.2.4	Departure from Nucleate Boiling .....	4-296
	4.3.3.2.5	Core Post-CHF Heat Transfer .....	4-296
	4.3.3.2.6	$T_{min}$ .....	4-298
	4.3.3.2.7	Break Flow .....	4-299
	4.3.3.2.8	Accumulator Discharge .....	4-299
	4.3.3.2.9	Reactor Vessel Hot Walls .....	4-299
	4.3.3.2.10	Containment Pressure .....	4-300
	4.3.3.2.11	Upper Head Temperature, Initial Coolant Temperature .....	4-300
4.3.4		Application of Code Biases .....	4-306
4.4		Determine Effect of Scale (CSAU Step 10) .....	4-308
4.4.1		Test Scaling .....	4-308
	4.4.1.1	Blowdown .....	4-309
	4.4.1.2	Refill .....	4-309
	4.4.1.3	Reflood .....	4-310
4.4.2		Code Scaling .....	4-310
	4.4.2.1	Post-CHF and Reflood Heat Transfer .....	4-311
	4.4.2.2	Scaling from Tests .....	4-315
	4.4.2.2.1	Film Boiling Heat Transfer .....	4-315

	4.4.2.2.2	Core Entrainment .....	4-315
	4.4.2.2.3	Critical Flow at Break .....	4-316
	4.4.2.2.4	Carry-over to Steam Generator .....	4-316
	4.4.2.2.5	Pump Scaling .....	4-317
	4.4.2.2.6	Cold Leg Condensation .....	4-318
	4.4.2.2.7	ECC Water Bypass of Downcomer during Refill and Lower Plenum Sweep-Out .....	4-318
	4.4.2.2.8	Loop Oscillations .....	4-320
5.0		Sensitivity and Uncertainty Analysis .....	5-1
5.1		Determination of the Effect of Reactor Input Parameters and State (CSAU Step 11) .....	5-1
	5.1.1	Fixed Design Factors .....	5-2
	5.1.2	Operational Process .....	5-2
	5.1.2.1	Determining Important Process Parameters .....	5-2
	5.1.2.2	Quantifying Uncertainty for Process Parameters .....	5-3
	5.1.2.3	Treatment of Time in Cycle .....	5-4
	5.1.2.4	Treatment of Axial and Radial Power Shapes .....	5-5
	5.1.2.5	Treatment of GDC-35 Criteria .....	5-6
5.2		Performance of NPP Sensitivity Calculations and Determination of Combined Bias and Uncertainty (CSAU Steps 12 and 13) .....	5-6
	5.2.1	Statistical Approach .....	5-6
	5.2.2	Application of Methodology .....	5-13
5.3		Determination of Combined Bias and Uncertainty and Determination of Total Uncertainty (CSAU Steps 13 and 14) .....	5-14
6.0		References .....	6-1
Appendix A		Time Step Sensitivity .....	A-1
Appendix B		Sample PWR Licensing Analyses .....	B-1
B.1		Introduction .....	B-1
	B.1.1	Analysis .....	B-2
	B.1.2	Description of Analytical Models .....	B-2
	B.1.3	GDC-35 Limiting Condition Determination .....	B-3
	B.1.4	Overall Statistical Compliance to Criteria .....	B-5
	B.1.5	Application of Heat Transfer Correlations .....	B-5
B.2		Westinghouse 3-Loop PWR .....	B-19
	B.2.1	Summary .....	B-19
	B.2.2	Plant Description and Summary of Analysis Parameters .....	B-19
	B.2.3	Realistic Large Break LOCA Results .....	B-20
	B.2.4	Conclusions .....	B-21
B.3		Westinghouse 4-Loop PWR .....	B-52
	B.3.1	Summary .....	B-52
	B.3.2	Plant Description and Summary of Analysis Parameters .....	B-52
	B.3.3	Realistic Large Break LOCA Results .....	B-53
	B.3.4	Conclusions .....	B-54
B.4		CE 2x4 PWR .....	B-85

B.4.1	Summary .....	B-85
B.4.2	Plant Description and Summary of Analysis Parameters .....	B-85
B.4.3	Realistic Large Break LOCA Results .....	B-86
B.4.4	Conclusions .....	B-88
B.5	References .....	B-141
Appendix C	Incorporation of M5 <sup>®</sup> Cladding Properties .....	C-1
C.1	References .....	C-1

## Tables

Table 3.1: Phenomena Identification and Ranking Table for PWR LBLOCA.....	3-15
Table 3.2: Models Added to S-RELAP5 from COPENIC2 and RODEX3A .....	3-17
Table 3.3: Field Equations/Models in S-RELAP5 .....	3-18
Table 3.4: Phenomena/Processes in S-RELAP5.....	3-19
Table 4.1: Validation Needs for Important PIRT Entries .....	4-4
Table 4.2: Assessment Matrix Tests and Phenomena Addressed .....	4-7
Table 4.3: Large Break LOCA Nodalization .....	4-24
Table 4.4: Parameters, FRIGG-2 Void Distribution Experiments.....	4-47
Table 4.5: PDTF SMART Tests Chosen for S-RELAP5 Verification and Validation .....	4-82
Table 4.6: Comparison of Effluent Temperature for the Plant-Consistent Model, Westinghouse/EPRI 1/3 Scale Tests .....	4-104
Table 4.7: UPTF Test 6 and Test 7 Conditions.....	4-122
Table 4.8: Test Phase Parameters for Test 10 Run 081 .....	4-123
Table 4.9: Test Phase Parameters for Test 29 Run 212/211 .....	4-123
Table 4.10: CCTF Test Conditions .....	4-151
Table 4.11: Summary Comparison of Measured and Calculated PCT, CCTF Tests 54, 62, 67, and 68 .....	4-151
Table 4.12: Test Data for SCTF-II Tests Modeled .....	4-181
Table 4.13: Phase I Assessment Results, SCTF Tests .....	4-183
Table 4.14: Phase II Assessment Results, SCTF Tests .....	4-183
Table 4.15: Moby Dick Facility Dimensions .....	4-235
Table 4.16: LOFT Nuclear Large Break Test Parameters .....	4-251
Table 4.17: Event Sequence for LOFT Test L2-3 .....	4-252
Table 4.18: Event Sequence for LOFT Test L2-5 .....	4-253
Table 4.19: Event Sequence for LOFT Test LP-02-6 .....	4-254
Table 4.20: Event Sequence for LOFT Test LP-LB-1 .....	4-255
Table 4.21: Methodology Treatment of Important PIRT Phenomena .....	4-286
Table 4.22: Summary of Evaluated Uncertainties of Important PIRT Parameters.....	4-289
Table 4.23: Film Boiling Multiplier .....	4-302
Table 4.24: Dispersed Flow Film Boiling Multiplier .....	4-302
Table 4.25: Biases Used in Assessments.....	4-307
Table 4.26: Test Ranges for Film Boiling Heat Transfer Test Comparison.....	4-322

Table 5.1: NPP Parameters for Consideration in the Performance of a RLBLOCA Analysis .....	5-15
Table 5.2: Relationship of PIRT to Operational Parameters .....	5-16
Table B.1: Sampled LBLOCA Parameters.....	B-13
Table B.2: Identification of Heat Transfer Parameters during a Limiting LBLOCA Simulation .....	B-14
Table B.3: Simulation and Application Space for CHF during Blowdown .....	B-15
Table B.4: Simulation and Application Space for Film Boiling Heat Transfer Including Thermal Radiation .....	B-16
Table B.5: Simulation and Application Space for Transition Boiling Heat Transfer .....	B-17
Table B.6: Simulation and Application Space for Nucleate Boiling Heat Transfer (late reflood) .....	B-17
Table B.7: Summary of Full Range of Applicability .....	B-18
Table B.8: 3-Loop Westinghouse Summary of Major Parameters for Minimum Margin Case .....	B-22
Table B.9: 3-Loop Westinghouse Plant Operating Range Supported by the RLBLOCA Analysis .....	B-23
Table B.10: 3-Loop Westinghouse Containment Initial and Boundary Conditions .....	B-26
Table B.11: 3-Loop Westinghouse Passive Heat Sinks in Containment .....	B-27
Table B.12: 3-Loop Westinghouse Statistical Distribution Used for Process Parameters.....	B-28
Table B.13: 3-Loop Westinghouse Compliance with 10 CFR 50.46 .....	B-29
Table B.14: 3-Loop Westinghouse Calculated Event Times for Limiting Margin Case .....	B-30
Table B.15: Westinghouse 3-Loop Heat Transfer Parameters for Limiting Margin Case .....	B-31
Table B.16: Summary of Limiting Values for Top Minimum Margin Cases within the Set Used to Establish the Probability Evaluation .....	B-32
Table B.17: Summary of 4-Loop Westinghouse Plant Major Parameters for Limiting Transient.....	B-55
Table B.18: 4-Loop Westinghouse Plant Operating Range Supported by the LOCA Analysis .....	B-56
Table B.19: 4-Loop Westinghouse Containment Initial and Boundary Conditions .....	B-59
Table B.20: 4-Loop Westinghouse Passive Heat Sinks in Containment .....	B-60
Table B.21: 4-Loop Westinghouse Statistical Distribution Used for Process Parameters.....	B-61
Table B.22: 4-Loop Westinghouse Compliance with 10 CFR 50.46 .....	B-62



Table B.23: 4-Loop Westinghouse Calculated Event Times for Limiting Margin Case .....	B-63
Table B.24: Westinghouse 4-Loop Heat Transfer Parameters for Limiting Margin Case .....	B-64
Table B.25: Summary of Limiting Values for Top Minimum Margin Cases within the Set Used to Establish the Probability Evaluation .....	B-65
Table B.26: CE 2x4 Summary of Major Parameters for Limiting Transient .....	B-89
Table B.27: CE 2x4 Plant Operating Range Supported by the LOCA Analysis .....	B-90
Table B.28: CE 2x4 Containment Initial and Boundary Conditions .....	B-93
Table B.29: CE 2x4 Passive Heat Sinks in Containment .....	B-94
Table B.30: CE 2x4 Statistical Distribution Used for Process Parameters .....	B-95
Table B.31: CE 2x4 COPENIC2 Compliance with 10 CFR 50.46 .....	B-96
Table B.32: CE 2x4 RODEX3A Compliance with 10 CFR 50.46 .....	B-97
Table B.33: CE 2x4 Calculated Event Times for Limiting Margin Case .....	B-98
Table B.34: CE 2x4 Heat Transfer Parameters for Limiting Margin Case (COPENIC2) .....	B-99
Table B.35: CE 2x4 Heat Transfer Parameters for Limiting Margin Case (RODEX3A) .....	B-100
Table B.36: Summary of Limiting Values for Top Minimum Margin Cases within the Set Used to Establish the Probability Evaluation (COPENIC2 with M5® Cladding) .....	B-101
Table B.37: Summary of Limiting Values for Top Minimum Margin Cases within the Set Used to Establish the Probability Evaluation (RODEX3A with Zirc-4 Cladding) .....	B-102

## Figures

Figure 2.1: Code Scaling, Applicability, and Uncertainty Methodology Flow Chart .....	2-6
Figure 4.1: Sample Loop Nodalization for NPP .....	4-25
Figure 4.2: Sample Steam Generator Secondary Nodalization for NPP .....	4-26
Figure 4.3: Double-Ended Guillotine and Split Break Nodalization.....	4-27
Figure 4.4: Sample Reactor Vessel Nodalization for NPP .....	4-28
Figure 4.5: Westinghouse/AREVA 3- and 4-Loop and CE 2x4 Plant Vessel Downcomer Configurations .....	4-29
Figure 4.6: NPP Core Nodalization.....	4-30
Figure 4.7: Sample NPP Upper Plenum Nodalization – Axial Plane .....	4-31
Figure 4.8: Sample NPP Upper Plenum Nodalization – Cross-Sectional Plane .....	4-32
Figure 4.9: Comparison of Calculated HTC to Measured HTC, ORNL THTF.....	4-36
Figure 4.10: Distribution for HTC Scaling, ORNL THTF .....	4-37
Figure 4.11: Comparisons of Void Profiles, ORNL THTF Test 3.09.10j.....	4-39
Figure 4.12: Comparison of Void Profiles, ORNL THTF Test 3.09.10m .....	4-40
Figure 4.13: Comparison of Void Profiles, ORNL THTF Test 3.09.10dd .....	4-41
Figure 4.14: Void Profiles at 40 seconds for the 1 foot GE Level Swell Test 1004-3 .....	4-44
Figure 4.15: Void Profiles at 100 seconds for the 1 foot GE Level Swell Test 1004-3 .....	4-45
Figure 4.16: Comparison of Calculated and Measured Void Fraction, FRIGG-2 Test 313007 .....	4-48
Figure 4.17: Comparison of Calculated and Measured Void Fraction, FRIGG-2 Test 313014 .....	4-49
Figure 4.18: Comparison of Calculated and Measured Void Fraction, FRIGG-2 Test 313016 .....	4-50
Figure 4.19: Comparison of Calculated and Measured Void Fraction, FRIGG-2 Test 313020 .....	4-51
Figure 4.20: Comparison of Calculated and Measured Void Fraction, FRIGG-2 Test 313060 .....	4-52
Figure 4.21: Comparison of Calculated and Measured Void Fraction, FRIGG-2 Test 313010 .....	4-53
Figure 4.22: Comparison of Calculated and Measured Void Fraction, FRIGG-2 Test 313013 .....	4-54
Figure 4.23: Comparison of Calculated and Measured Void Fraction, FRIGG-2 Test 313017 .....	4-55

Figure 4.24: Comparison of Calculated and Measured Void Fraction, FRIGG-2 Test 313019 .....	4-56
Figure 4.25: Comparison of Calculated and Measured Void Fraction, FRIGG-2 Test 313030 .....	4-57
Figure 4.26: Comparison of Calculated and Measured Void Fraction at the Same Location for all 27 FRIGG-2 Tests .....	4-58
Figure 4.27: Wall Temperature Profiles, Bennett Heated Tube Test 5358 .....	4-60
Figure 4.28: Wall Temperature Profiles, Bennett Heated Tube Test 5379 .....	4-61
Figure 4.29: Maximum Clad Temperature at All Measured Elevations, FLECHT- SEASET Test 31805 .....	4-66
Figure 4.30: Maximum Clad Temperature at All Measured Elevations, FLECHT- SEASET Test 31504 .....	4-67
Figure 4.31: Maximum Clad Temperature at All Measured Elevations, FLECHT- SEASET Test 31203 .....	4-68
Figure 4.32: Maximum Clad Temperature at All Measured Elevations, FLECHT- SEASET Test 31302 .....	4-69
Figure 4.33: Maximum Clad Temperature at All Measured Elevations, FLECHT- SEASET Test 31701 .....	4-70
Figure 4.34: Maximum Clad Temperature at All Measured Elevations, FLECHT- SEASET Test 34209 .....	4-71
Figure 4.35: Maximum Clad Temperature at All Measured Elevations, FLECHT- SEASET Test 32013 .....	4-72
Figure 4.36: Maximum Clad Temperature at All Measured Elevations, FLECHT Skewed Test 13609 .....	4-73
Figure 4.37: Maximum Clad Temperature at All Measured Elevations, FLECHT Skewed Test 13914 .....	4-74
Figure 4.38: Calculated and Measured Rod Surface Temperature at 78 inches, FLECHT-SEASET Test 31504 .....	4-75
Figure 4.39: Steam Temperatures Calculated at 75.6 inches and Measured at 72 inches, FLECHT-SEASET Test 31504 .....	4-76
Figure 4.40: Accumulated Water Mass in the Test Section, FLECHT-SEASET Test 31504 .....	4-77
Figure 4.41: Rod Quench Time, FLECHT-SEASET Test 31504 .....	4-78
Figure 4.42: Maximum Cladding Temperatures versus Axial Elevation from FLECHT-SEASET Test 31504 Time Step and Node Size Sensitivities .....	4-79
Figure 4.43: Comparison of Predicted PCT and Measured Data, PDTF SMART .....	4-83
Figure 4.44: MCT versus Elevation Comparison to Data for 4-in/s-Flooding-Rate Test, PDTF SMART .....	4-84

Figure 4.45: MCT versus Elevation Comparison to Data for 2-in/s-Flooding-Rate Test, PDTF SMART .....	4-85
Figure 4.46: MCT versus Elevation Comparison to Data for 1-in/s-Flooding-Rate Test, PDTF SMART .....	4-86
Figure 4.47: MCT versus Elevation Comparison to Data for Variable-Flooding-Rate Test, PDTF SMART .....	4-87
Figure 4.48: Comparison of Break Mass Flow Rates, Marviken Test 2 .....	4-90
Figure 4.49: Comparison of Break Mass Flow Rates, Marviken Test 6 .....	4-91
Figure 4.50: Comparison of Break Mass Flow Rates, Marviken Test 8 .....	4-92
Figure 4.51: Comparison of Break Mass Flow Rates, Marviken Test 16 .....	4-93
Figure 4.52: Comparison of Break Mass Flow Rates, Marviken Test 17 .....	4-94
Figure 4.53: Comparison of Break Mass Flow Rates, Marviken Test 20 .....	4-95
Figure 4.54: Comparison of Break Mass Flow Rates, Marviken Test 22 .....	4-96
Figure 4.55: Comparison of Break Mass Flow Rates, Marviken Test 24 .....	4-97
Figure 4.56: Comparison of Break Mass Flow Rates, Marviken Test 25 .....	4-98
Figure 4.57: Comparison of Calculated and Measured Mass Fluxes (All Nine Marviken Tests).....	4-99
Figure 4.58: Break Flow Uncertainty, Marviken Tests .....	4-100
Figure 4.59: Comparison of Calculated and Measured Effluent Temperature for the Plant-Specific Model, Westinghouse/EPRI 1/3 Scale Tests.....	4-105
Figure 4.60: Comparison between Mini-Loop CCFL Data of a Westinghouse 17x17 UTP and Bankoff.....	4-107
Figure 4.61: Comparison between Mini-Loop CCFL Data of a Westinghouse 15x15 UTP and Bankoff.....	4-108
Figure 4.62: Comparison between Mini-Loop CCFL Data of a Combustion Engineering 14x14 UTP and Bankoff.....	4-109
Figure 4.63: Lower Plenum Liquid Level Comparison UPTF Test 6 Run 131 .....	4-124
Figure 4.64: Lower Plenum Liquid Level Comparison UPTF Test 6 Run 132 .....	4-125
Figure 4.65: Lower Plenum Liquid Level Comparison UPTF Test 6 Run 133 .....	4-126
Figure 4.66: Lower Plenum Liquid Level Comparison UPTF Test 6 Run 135 .....	4-127
Figure 4.67: Lower Plenum Liquid Level Comparison UPTF Test 6 Run 136 .....	4-128
Figure 4.68: Lower Plenum Liquid Level Comparison UPTF Test 7 Run 203 .....	4-129
Figure 4.69: Broken Cold Leg Liquid Temperature UPTF Test 6 Run 135.....	4-130
Figure 4.70: Lower Head Liquid Temperature UPTF Test 6 Run 135 .....	4-131
Figure 4.71: Total Cold Leg Break Flow UPTF Test 6 Run 135 .....	4-132
Figure 4.72: Cold Leg Temperature Comparison UPTF Test 8 Run 111.....	4-133

Figure 4.73: Flow Regime Comparison UPTF Test 8 Run 111 .....	4-134
Figure 4.74: Cold Leg Temperature Comparison UPTF Test 8 Run 112.....	4-135
Figure 4.75: Flow Regime Comparison UPTF Test 8 Run 112 .....	4-136
Figure 4.76: Countercurrent Flow of Steam and Water UPTF Test 10 Run 081 .....	4-137
Figure 4.77: Countercurrent Flow of Steam and Water UPTF Test 29 Run 212/211 .....	4-138
Figure 4.78: Carryover to Steam Generators UPTF Test 10 Run 081 .....	4-139
Figure 4.79: Cumulative Water Carryover to Steam Generators UPTF Test 29 Run 211/212.....	4-140
Figure 4.80: Countercurrent Flow of Steam and Water UPTF Test 10 Run 080 .....	4-141
Figure 4.81: Upper Plenum Pressure Comparison UPTF Test 10 Run 080 .....	4-142
Figure 4.82: Calculated Downflow Comparison UPTF Test 10 Run 080 .....	4-143
Figure 4.83: Countercurrent Flow of Steam and Water UPTF Test 12 Run 014 .....	4-144
Figure 4.84: Upper Plenum Pressure Comparison UPTF Test 12 Run 014 .....	4-145
Figure 4.85: Calculated Downflow Comparison UPTF Test 12 Run 014 .....	4-146
Figure 4.86: Calculated and Measured Vessel Bottom Pressures CCTF Test Run 54.....	4-152
Figure 4.87: Calculated and Measured Upper Plenum Pressures CCTF Test Run 62.....	4-153
Figure 4.88: Calculated and Measured Upper Plenum Pressures CCTF Test Run 67.....	4-154
Figure 4.89: Calculated and Measured Upper Plenum Pressures CCTF Test Run 68.....	4-155
Figure 4.90: Calculated and Measured Downcomer Differential Pressure CCTF Test Run 54.....	4-156
Figure 4.91: Calculated and Measured Downcomer Differential Pressure CCTF Test Run 62.....	4-157
Figure 4.92: Calculated and Measured Downcomer Differential Pressure CCTF Test Run 67.....	4-158
Figure 4.93: Calculated and Measured Downcomer Differential Pressure CCTF Test Run 68.....	4-159
Figure 4.94: Comparison of Core Differential Pressures CCTF Test Run 54 .....	4-160
Figure 4.95: Comparison of Core Differential Pressures CCTF Test Run 62 .....	4-161
Figure 4.96: Comparison of Core Differential Pressures CCTF Test Run 67 .....	4-162
Figure 4.97: Comparison of Core Differential Pressures CCTF Test Run 68 .....	4-163
Figure 4.98: Comparison of Liquid Level in Containment Tank II CCTF Test Run 54.....	4-164

Figure 4.99: Comparison of Liquid Level in Containment Tank II CCTF Test Run 62 .....	4-165
Figure 4.100: Comparison of Liquid Level in Containment Tank II CCTF Test Run 67.....	4-166
Figure 4.101: Comparison of Liquid Level in Containment Tank II CCTF Test Run 68.....	4-167
Figure 4.102: Comparison of Rod Surface Temperatures for High Power Bundles at 2.035 meters Elevation CCTF Test Run 54 .....	4-168
Figure 4.103: Comparison of Rod Surface Temperatures for High Power Bundles at 2.035 meters Elevation CCTF Test Run 62 .....	4-169
Figure 4.104: Comparison of Rod Surface Temperatures for High Power Bundles at 2.035 meters Elevation CCTF Test Run 67 .....	4-170
Figure 4.105: Comparison of Rod Surface Temperatures for High Power Bundles at 2.035 meters Elevation CCTF Test Run 68 .....	4-171
Figure 4.106: Comparison of Peak Surface Temperatures versus Elevation for High Power Bundles CCTF Test Run 54 .....	4-172
Figure 4.107: Comparison of Peak Surface Temperatures versus Elevation for High Power Bundles CCTF Test Run 62 .....	4-173
Figure 4.108: Comparison of Peak Surface Temperatures versus Elevation for High Power Bundles CCTF Test Run 67 .....	4-174
Figure 4.109: Comparison of Peak Surface Temperatures versus Elevation for High Power Bundles CCTF Test Run 68 .....	4-175
Figure 4.110: Fuel Assembly Pressure Comparison SCTF-II S2-11 .....	4-184
Figure 4.111: Fuel Assembly Pressure Comparison SCTF-II S2-AC1 .....	4-185
Figure 4.112: Fuel Assembly Pressure Comparison SCTF-II S2-10 .....	4-186
Figure 4.113: Fuel Assembly Pressure Comparison SCTF-II S2-SH1 .....	4-187
Figure 4.114: Fuel Assembly Pressure Comparison SCTF-II S2-17 .....	4-188
Figure 4.115: Fuel Assembly Pressure Comparison SCTF-II S2-18 .....	4-189
Figure 4.116: Core Differential Pressure Comparison SCTF-II S2-11 .....	4-190
Figure 4.117: Core Differential Pressure Comparison SCTF-II S2-AC1 .....	4-191
Figure 4.118: Core Differential Pressure Comparison SCTF-II S2-10 .....	4-192
Figure 4.119: Core Differential Pressure Comparison SCTF-II S2-SH1 .....	4-193
Figure 4.120: Core Differential Pressure Comparison SCTF-II S2-17 .....	4-194
Figure 4.121: Core Differential Pressure Comparison SCTF-II S2-18 .....	4-195
Figure 4.122: Differential Pressure: Upper Plenum – Downcomer SCTF-II S2-11 .....	4-196
Figure 4.123: Differential Pressure: Upper Plenum – Downcomer SCTF-II S2-AC1 .....	4-197

Figure 4.124: Differential Pressure: Upper Plenum – Downcomer SCTF-II S2-10 .....	4-198
Figure 4.125: Differential Pressure: Upper Plenum – Downcomer SCTF-II S2- SH1 .....	4-199
Figure 4.126: Differential Pressure: Upper Plenum – Downcomer SCTF-II S2-17 .....	4-200
Figure 4.127: Differential Pressure: Upper Plenum – Downcomer SCTF-II S2-18 .....	4-201
Figure 4.128: Liquid Level in S/W Separator SCTF-II S2-11 .....	4-202
Figure 4.129: Liquid Level in S/W Separator SCTF-II S2-AC1 .....	4-203
Figure 4.130: Liquid Level in S/W Separator SCTF-II S2-10 .....	4-204
Figure 4.131: Liquid Level in S/W Separator SCTF-II S2-SH1 .....	4-205
Figure 4.132: Liquid Level in S/W Separator SCTF-II S2-17 .....	4-206
Figure 4.133: Liquid Level in S/W Separator SCTF-II S2-18 .....	4-207
Figure 4.134: Temperature Comparison at 1.905 meters SCTF-II S2-11 .....	4-208
Figure 4.135: Temperature Comparison at 1.905 meters SCTF-II S2-AC1 .....	4-209
Figure 4.136: Temperature Comparison at 1.905 meters SCTF-II S2-10 .....	4-210
Figure 4.137: Temperature Comparison at 1.905 meters SCTF-II S2-SH1 .....	4-211
Figure 4.138: Temperature Comparison at 1.905 meters SCTF-II S2-17 .....	4-212
Figure 4.139: Temperature Comparison at 1.905 meters SCTF-II S2-18 .....	4-213
Figure 4.140: Thermocouple Variation Range at the PCT Elevation ACHILLES ISP 25 .....	4-218
Figure 4.141: Nitrogen Insurge Impact at 1.08 meters ACHILLES ISP 25 .....	4-219
Figure 4.142: Nitrogen Insurge Impact at 1.81 meters ACHILLES ISP 25 .....	4-220
Figure 4.143: Nitrogen Insurge Impact at 2.13 meters ACHILLES ISP 25 .....	4-221
Figure 4.144: Nitrogen Insurge Impact at 2.33 meters ACHILLES ISP 25 .....	4-222
Figure 4.145: Nitrogen Insurge Impact at 2.65 meters ACHILLES ISP 25 .....	4-223
Figure 4.146: Nitrogen Insurge Impact at 3.18 meters ACHILLES ISP 25 .....	4-224
Figure 4.147: Downcomer Pressure Comparison ACHILLES ISP 25 .....	4-225
Figure 4.148: Axial Velocities at 32.5 inches, Asymmetric Flow - Test 1 .....	4-228
Figure 4.149: Axial Flow Fractions for Asymmetric Flow - Test 1 .....	4-229
Figure 4.150: Axial Velocities at 32.5 inches, for Asymmetric Flow - Test 2 .....	4-230
Figure 4.151: Axial Flow Fractions for Asymmetric Flow – Test 2 .....	4-231
Figure 4.152: Axial Velocities at 32.5 inches, for Asymmetric Flow - Test 3 .....	4-232
Figure 4.153: Comparison of Moby Dick Data and S-RELAP5 Calculated Pressures .....	4-236
Figure 4.154: Ratio of Convective to Total Heat Transfer, Calculated and Measured .....	4-240

Figure 4.155: Total Heat Transfer Coefficient, Calculated and Measured .....	4-241
Figure 4.156: Convective Heat Transfer Coefficient .....	4-242
Figure 4.157: Comparison of PCTs versus Core Elevations LOFT Test L2-3 with S-RELAP5.....	4-256
Figure 4.158: Comparison of PCTs versus Core Elevation, LOFT Test L2-5 .....	4-257
Figure 4.159: Comparison of PCTs versus Core Elevations, LOFT Test LP-02-6.....	4-258
Figure 4.160: Comparison of PCTs versus Core Elevation, LOFT Test LP-LB-1 .....	4-259
Figure 4.161: Assessment of Semiscale LBLOCA Test S-06-3, PCTs.....	4-266
Figure 4.162: Assessment of Semiscale LBLOCA Test S-07-1, PCTs versus Elevation .....	4-267
Figure 4.163: CONMAS Multiplier as a Function of Cold Leg Void Fraction .....	4-290
Figure 4.164: COPENIC2 Cumulative Centerline Fuel Temperature Error Distribution .....	4-303
Figure 4.165: RODEX3A Bias as a Function of Fuel Pin Burnup .....	4-304
Figure 4.166: Temperature Distribution in the Vessel Wall – S-RELAP5 versus Exact Solution .....	4-305
Figure 4.167: Data Based Nusselt Number versus Reynolds Number for FLECHT-SEASET Steam Cooling Tests Compared with Dittus-Boelter Correlation.....	4-314
Figure A.1: Time Step Sensitivity of Westinghouse 3-Loop Analysis .....	A-3
Figure A.2: Variability of Westinghouse 3-Loop Analysis .....	A-4
Figure A.3: Time Step Sensitivity of Westinghouse 4-Loop Analysis .....	A-5
Figure A.4: Variability of Westinghouse 4-Loop Analysis .....	A-6
Figure A.5: Time Step Sensitivity of CE Analysis .....	A-7
Figure A.6: Variability of CE Analysis .....	A-8
Figure B.1: 3-Loop Westinghouse Scatter Plot of Operational Parameters.....	B-33
Figure B.2: 3-Loop Westinghouse PCT versus PCT Time Scatter Plot from the Case Set .....	B-35
Figure B.3: 3-Loop Westinghouse PCT versus Break Size Scatter Plot from the Case Set .....	B-36
Figure B.4: 3-Loop Westinghouse Maximum Oxidation versus PCT Scatter Plot from the Case Set .....	B-37
Figure B.5: 3-Loop Westinghouse Total Oxidation versus PCT Scatter Plot from the Case Set .....	B-38
Figure B.6: 3-Loop Westinghouse Peak Cladding Temperature (Independent of Elevation) for the Limiting Margin Case .....	B-39
Figure B.7: 3-Loop Westinghouse Break Flow for the Limiting Margin Case .....	B-40



Figure B.8: 3-Loop Westinghouse Core Inlet Mass Flux for the Limiting Margin Case .....	B-41
Figure B.9: 3-Loop Westinghouse Core Outlet Mass Flux for the Limiting Margin Case .....	B-42
Figure B.10: 3-Loop Westinghouse Void Fraction at RCS Pumps for the Limiting Margin Case .....	B-43
Figure B.11: 3-Loop Westinghouse ECCS Flows (Includes Accumulator, Charging, SI and RHR) for the Limiting Margin Case .....	B-44
Figure B.12: 3-Loop Westinghouse Upper Plenum Pressure for the Limiting Margin Case .....	B-45
Figure B.13: 3-Loop Westinghouse Collapsed Liquid Level in the Downcomer for the Limiting Margin Case .....	B-46
Figure B.14: 3-Loop Westinghouse Collapsed Liquid Level in the Lower Plenum for the Limiting Margin Case .....	B-47
Figure B.15: 3-Loop Westinghouse Collapsed Liquid Level in the Core for the Limiting Margin Case .....	B-48
Figure B.16: 3-Loop Westinghouse Containment and Loop Pressures for the Limiting Margin Case .....	B-49
Figure B.17: 3-Loop Westinghouse Pressure Difference between Upper Plenum and Downcomer .....	B-50
Figure B.18: 3-Loop Westinghouse Validation of BOCR Time using MPR CCFL Correlation.....	B-51
Figure B.19: 4-Loop Westinghouse Scatter Plot of Operational Parameters.....	B-66
Figure B.20: 4-Loop Westinghouse PCT versus PCT Time Scatter Plot from the Case Set .....	B-68
Figure B.21: 4-Loop Westinghouse PCT versus Break Size Scatter Plot from the Case Set .....	B-69
Figure B.22: 4-Loop Westinghouse Maximum Oxidation versus PCT Scatter Plot from the Case Set .....	B-70
Figure B.23: 4-Loop Westinghouse Total Oxidation versus PCT Scatter Plot from the Case Set .....	B-71
Figure B.24: 4-Loop Westinghouse Peak Cladding Temperature (Independent of Elevation) for the Limiting Margin Case .....	B-72
Figure B.25: 4-Loop Westinghouse Break Flow for the Limiting Margin Case .....	B-73
Figure B.26: 4-Loop Westinghouse Core Inlet Mass Flux for the Limiting Margin Case .....	B-74
Figure B.27: 4-Loop Westinghouse Core Outlet Mass Flux for the Limiting Margin Case .....	B-75
Figure B.28: 4-Loop Westinghouse Void Fraction at RCS Pumps for the Limiting Margin Case .....	B-76

Figure B.29: 4-Loop Westinghouse ECCS Flows (Includes Accumulator, Charging, SI and RHR) for the Limiting Margin Case .....	B-77
Figure B.30: 4-Loop Westinghouse Upper Plenum Pressure for the Limiting Margin Case .....	B-78
Figure B.31: 4-Loop Westinghouse Collapsed Liquid Level in the Downcomer for the Limiting Margin Case .....	B-79
Figure B.32: 4-Loop Westinghouse Collapsed Liquid Level in the Lower Plenum for the Limiting Margin Case .....	B-80
Figure B.33: 4-Loop Westinghouse Collapsed Liquid Level in the Core for the Limiting Margin Case .....	B-81
Figure B.34: 4-Loop Westinghouse Containment and Loop Pressures for the Limiting Margin Case .....	B-82
Figure B.35: 4-Loop Westinghouse Pressure Difference between Upper Plenum and Downcomer .....	B-83
Figure B.36: 4-Loop Westinghouse Validation of BOCR Time using MPR CCFL Correlation.....	B-84
Figure B.37: CE 2x4 Scatter Plot of Operational Parameters (COPERNIC2).....	B-103
Figure B.38: CE 2x4 PCT versus PCT Time Scatter Plot from the Case Set (COPERNIC2).....	B-105
Figure B.39: CE 2x4 PCT versus Break Size Scatter Plot from the Case Set (COPERNIC2).....	B-106
Figure B.40: CE 2x4 Maximum Oxidation versus PCT Scatter Plot from the Case Set (COPERNIC2) .....	B-107
Figure B.41: CE 2x4 Total Oxidation versus PCT Scatter Plot from the Case Set (COPERNIC2).....	B-108
Figure B.42: CE 2x4 Peak Cladding Temperature (Independent of Elevation) for the Limiting Margin Case (COPERNIC2) .....	B-109
Figure B.43: CE 2x4 Break Flow for the Limiting Margin Case (COPERNIC2) .....	B-110
Figure B.44: CE 2x4 Core Inlet Mass Flux for the Limiting Margin Case (COPERNIC2).....	B-111
Figure B.45: CE 2x4 Core Outlet Mass Flux for the Limiting Margin Case (COPERNIC2).....	B-112
Figure B.46: CE 2x4 Void Fraction at RCS Pumps for the Limiting Margin Case (COPERNIC2).....	B-113
Figure B.47: CE 2x4 ECCS Flows (Includes SIT, Charging, SI and RHR) for the Limiting Margin Case (COPERNIC2) .....	B-114
Figure B.48: CE 2x4 Upper Plenum Pressure for the Limiting Margin Case (COPERNIC2).....	B-115
Figure B.49: CE 2x4 Collapsed Liquid Level in the Downcomer for the Limiting Margin Case (COPERNIC2) .....	B-116

Figure B.50: CE 2x4 Collapsed Liquid Level in the Lower Plenum for the Limiting Margin Case (COPERNIC2) .....	B-117
Figure B.51: CE 2x4 Collapsed Liquid Level in the Core for the Limiting Margin Case (COPERNIC2) .....	B-118
Figure B.52: CE 2x4 Containment and Loop Pressures for the Limiting Margin Case (COPERNIC2) .....	B-119
Figure B.53: CE 2x4 Pressure Difference between Upper Plenum and Downcomer (COPERNIC2).....	B-120
Figure B.54: CE 2x4 Validation of BOCR Time using MPR CCFL Correlation (COPERNIC2).....	B-121
Figure B.55: CE 2x4 Scatter Plot of Operational Parameters (RODEX3A) .....	B-122
Figure B.56: CE 2x4 PCT versus PCT Time Scatter Plot from the Case Set (RODEX3A).....	B-124
Figure B.57: CE 2x4 PCT versus Break Size Scatter Plot from the Case Set (RODEX3A).....	B-125
Figure B.58: CE 2x4 Maximum Oxidation versus PCT Scatter Plot from the Case Set (RODEX3A) .....	B-126
Figure B.59: CE 2x4 Total Oxidation versus PCT Scatter Plot from the Case Set (RODEX3A).....	B-127
Figure B.60: CE 2x4 Peak Cladding Temperature (Independent of Elevation) for the Limiting Margin Case (RODEX3A).....	B-128
Figure B.61: CE 2x4 Break Flow for the Limiting Margin Case (RODEX3A).....	B-129
Figure B.62: CE 2x4 Core Inlet Mass Flux for the Limiting Margin Case (RODEX3A).....	B-130
Figure B.63: CE 2x4 Core Outlet Mass Flux for the Limiting Margin Case (RODEX3A).....	B-131
Figure B.64: CE 2x4 Void Fraction at RCS Pumps for the Limiting Margin Case (RODEX3A).....	B-132
Figure B.65: CE 2x4 ECCS Flows (Includes SIT, Charging, SI and RHR) for the Limiting Margin Case (RODEX3A).....	B-133
Figure B.66: CE 2x4 Upper Plenum Pressure for the Limiting Margin Case (RODEX3A).....	B-134
Figure B.67: CE 2x4 Collapsed Liquid Level in the Downcomer for the Limiting Margin Case (RODEX3A) .....	B-135
Figure B.68: CE 2x4 Collapsed Liquid Level in the Lower Plenum for the Limiting Margin Case (RODEX3A) .....	B-136
Figure B.69: CE 2x4 Collapsed Liquid Level in the Core for the Limiting Margin Case (RODEX3A) .....	B-137
Figure B.70: CE 2x4 Containment and Loop Pressures for the Limiting Margin Case (RODEX3A) .....	B-138

Figure B.71: CE 2x4 Pressure Difference between Upper Plenum and Downcomer (RODEX3A) .....	B-139
Figure B.72: CE 2x4 Validation of BOCR Time using MPR CCFL Correlation (RODEX3A).....	B-140

## Nomenclature

Acronym	Definition
ACC	accumulator
ANP	advanced nuclear products
ANS	American Nuclear Society
ASME	American Society of Mechanical Engineers
BIASI	Biasi CHF multiplier
BLCL	broken loop cold leg
BLHL	broken loop hot leg
BST	blowdown suppression tank
BWR	boiling water reactor
CCFL	countercurrent flow limitation
CCTF	Cylindrical Core Test Facility
CE	Combustion Engineering
CFR	Code of Federal Regulations
CHF	critical heat flux
CONMAS	interfacial condensation heat transfer coefficient multiplier
CONMSG	interfacial condensation heat transfer coefficient multiplier, vapor
CSAU	Code Scaling, Applicability, and Uncertainty
DEG	double-ended guillotine
DFFBHTC	dispersed flow film boiling heat transfer coefficient
DIW	deionized water tank
DMS	document management system
DNB	departure from nucleate boiling
ECC	emergency core cooling
ECCS	emergency core cooling system
EDR	Experimental Data Report
EHL	end of heated length
EPRI	Electric Power Research Institute
FCTF	Fuel Cooling Test Facility
$F_{ij}$	Interphase friction multiplier
FILMBL	film boiling
FIMIST	post-CHF mist flow regime
FLECHT	Full Length Emergency Cooling Heat Transfer
HEM	homogeneous equilibrium model
HHSI	high head safety injection
HPC	high probability of compliance
HPI	high pressure injection
HPSI	high pressure safety injection
HTP	high thermal performance

IET	Integral Effects Test
ILCL	intact loop cold leg
ILHL	intact loop hot leg
INEEL	Idaho National Environmental Engineering Laboratory (formerly INEL)
INEL	Idaho National Engineering Laboratory
JAERI	Japan Atomic Energy Research Institute
KWU	Kraftwerk Union (SPC), now AREVA GmbH
LANL	Los Alamos National Laboratory
LBLOCA	large break loss-of-coolant accident
LHGR	linear heat generation rate
LHSI	low head safety injection
LOCA	loss-of-coolant accident
LOCE	loss-of-coolant experiment
LOFT	Loss of Fluid Test
LOOP	Loss of Offsite Power
LPCI	low pressure coolant injection
LPSI	low pressure safety injection
MCT	maximum clad temperature
MLHGR	maximum linear heat generation rate
MSIV	main steam isolation valve
NAI	Numerical Applications, Inc.
NPP	nuclear power plant
NRC	United States Nuclear Regulatory Commission
ORNL	Oak Ridge National Laboratory
PCT	peak cladding temperature
PDF	probability density function
PDTF	Product Development Test Facility
PFM	pipe flow meter
PIRT	Phenomena Identification and Ranking Table
PLC	programmable logic controllers
PWR	pressurized water reactor
QLR	Quick Look Report
RABS	reflood assisted bypass system
RABV	reflood assisted bypass valve
RCP	reactor coolant pump
RCS	reactor coolant system
RLBLOCA	realistic large break loss-of-coolant accident
RWST	refueling water storage tank

SBLOCA	small break loss-of-coolant accident
SCTF	Slab Core Test Facility
SDR	Software Development Record
SEASET	System Effects and Separate Effects Tests
SET	Separate Effects Test
SIT	Safety Injection Tank
SMART	SMall Array Reflood Test
SPC	Siemens Power Corporation
SRP	Standard Review Plan
THTF	Thermal-Hydraulic Test Facility
TMDPJUN	time-dependent junction
TMDPVOL	time-dependent volume
TMINK	maximum temperature for transition boiling
UCSP	upper core support plate
UPTF	Upper Plenum Test Facility
UTP	upper tie plate

## 1.0 Introduction

This report describes the AREVA NP Inc. (AREVA) methodology developed for the realistic evaluation of a large break loss-of-coolant accident (LBLOCA) for pressurized water reactors (PWRs) with recirculation (U-tube) steam generators. Specifically Westinghouse 3- and 4-loop designs, Combustion Engineering (CE) 2x4 designs and AREVA 3- and 4-loop designs all with fuel assembly lengths of 14 feet or less, and emergency core cooling system (ECCS) injection to the cold legs, are covered. The methodology was originally developed by AREVA in the early 2000s and approved by the U.S. Nuclear Regulatory Commission (NRC) as EMF-2103(P)(A) Revision 0 in April 2003. In 2006, AREVA submitted EMF-2103(P) Revision 1 as a limited scope change to the methodology. During the review it was recognized that the limited scope of Revision 1 was insufficient for future licensing. Revision 1 was, therefore, withdrawn from review and replaced by a development program culminating in the Revision 2 methodology documented herein. The documentation provided for and labeled as Revision 2 is complete in its intended scope. Between the withdrawal of Revision 1 and the submittal and approval of this revision, plant licensing was accomplished with an interim approach, termed the “Transition Program,” based on Revision 0 but incorporating methodology changes to address NRC concerns. This methodology is documented on a plant specific basis when applied for licensing.

Although the Revision 2 documentation is complete and self-contained, the methodology does build on and incorporates much of the Revision 0 approach and generally incorporates the “Transition Program” modifications by directly including them in the methodology. The most significant modifications to the Revision 0 methodology are:

1. The Forslund-Rohsenow correlation is no longer used in determining the fuel cladding temperature. For the dispersed flow film boiling regime in the core, Wong-Hochreiter with enhancements replaces the use of Sleicher-Rouse. This alteration is presented in Sections 4.3.1.1 and 4.3.1.6 and is assessed in Sections 4.3.1.17 and 4.3.3.2.5.
2. A rod-to-rod radiation model has been incorporated into the methodology and the reflood heat transfer benchmarking has been redone. This alteration is presented in Sections 4.3.1.17, 4.3.3.2.5, and 4.4.2.1.



3. A cold leg condensation model, specific to the pumped injection period of the accident, has been incorporated. In Revision 0, the cold leg condensation was underpredicted during the post-accumulator phase resulting in subcooled water entering the downcomer, and the potential suppression of downcomer boiling. This alteration is presented in Sections 4.3.1.9, 4.3.1.11, and 4.3.3.1.14.
4. The statistical evaluation has been upgraded, with the application of the Tukey methodology, to resolve concerns over a multi-variant versus uni-variant evaluation. This alteration is presented in Section 5.2.
5. The COPERNIC2 fuel performance code has been added as a source of fuel initial conditions. COPERNIC2 is NRC approved and addresses the issue of burnup-dependent fuel pellet thermal conductivity. For RODEX3 applications, an additional conservatism is incorporated in the code bias to account for thermal conductivity degradation. These alterations are presented in Section 4.3.3.2.1.
6. The methodology has been upgraded such that a direct calculation of second cycle fuel performance is accomplished. This expands the range of evaluations and assures that fuel experiencing its second burn will be evaluated and, if limiting, recognized as limiting. This alteration is presented in Section 5.1.2.3.
7. The break modeling was altered from Revision 0 to concur with the approach outlined in Regulatory Guide 1.157. This alteration is presented in Section 4.3.3.2.7.
8. The interfacial drag package has been modified with improved logic for transition between flow regimes to cover a wider range of experimental data. This change does not address a specific concern or issue, but serves to update the state-of-the-art of S-RELAP5. The details of this alteration are presented in Reference 11.
9. The interphase heat transfer for mist flow was modified to raise steam temperatures. The details of this change are presented in Reference 11.

The methodology complies with the revised LOCA ECCS rule as issued by the NRC in 1988 (Reference 1). This rule allows the use of realistic LOCA evaluation models in place of the prescribed conservative evaluation models specified by 10 CFR 50 Appendix K, provided that it can be established with a high probability that the criteria of 10 CFR 50.46 are met.

The basis for the revised rule is a large body of research performed after the 1973 LOCA ECCS rule was implemented, which shows the prescribed Appendix K analysis methods are unnecessarily conservative. A compendium of ECCS research (Reference 2) was issued by the NRC in 1988 and references the relevant thermal-hydraulic research upon which the realistic LOCA rule was based.

The realistic evaluation model rule does not prescribe the analytical methods or uncertainty techniques to be used. However, a Regulatory Guide (Reference 3) was issued to provide guidance for realistic LOCA analyses. The NRC also independently developed and demonstrated the code scaling, applicability and uncertainty (CSAU) methodology (Reference 4) for quantifying uncertainties in realistic codes. The 95<sup>th</sup> percentile of the probability distribution is accepted (Reference 3) as providing the level of conservatism required by the rule.

This report provides a description of the AREVA PWR realistic LBLOCA (RLBLOCA) methodology and demonstrates its application to representative nuclear power plants. The methodology documentation is provided in a format consistent with that outlined in the "CSAU Evaluation Methodology," which specifies that a roadmap be provided for the methodology followed by a detailed discussion. Each of the steps outlined in CSAU is addressed in both the roadmap section (Section 2.0) and the detailed description sections (Sections 3.0, 4.0, and 5.0).

As outlined in CSAU, the development of this methodology relies on documentation of the associated computer codes. The models and correlations document (Reference 11) demonstrates the applicability of the codes to the chosen event scenario and Nuclear Power Plant (NPP) types through the use of a phenomena identification and ranking table (PIRT) process. The PIRT identifies the models and correlations in the codes for which biases and uncertainties are required or conservatisms demonstrated.

The results of the computer code assessments reported in the verification and validation report (Reference 5) provide the information required to define how the important PIRT phenomena are treated in the uncertainty analysis. The treatments range from simply acknowledging and accepting conservatism in code results to defining biases and uncertainties, including their distributions that are required to treat the PIRT phenomena statistically.

## 2.0 Methodology Roadmap

This section provides an overview of the methodology and its development. Revision 2 is a comprehensive improvement to the original RLBLOCA methodology documented in EMF-2103(P)(A) Revision 0 (Reference 6). A large body of the work that supported Revision 0 still remains applicable to Revision 2. Thus, although the documentation provided herein is complete and self sufficient, much of the content is the same as was provided in Revision 0. This section outlines the CSAU methodology followed by AREVA and points to where detailed discussions of the individual steps are presented. The CSAU approach to realistic LOCA analysis is diagramed in Figure 2.1. The CSAU procedure has three major elements:

- Requirements and Code Capabilities (Section 3.0)
- Assessment and Ranging of Parameters (Section 4.0)
- Sensitivity and Uncertainty Analysis (Section 5.0)

AREVA's RLBLOCA evaluation methodology is defined and documented consistent with the CSAU procedure as shown in the following three sections. AREVA's CSAU-compliant procedure for PWRs is applicable to various plant designs as detailed in Section 1.0.

### 2.1 *Requirements and Code Capabilities*

The requirements and code capabilities discussion identifies and compares scenario-modeling requirements with code capabilities to determine the applicability of the code to the particular scenario and to identify potential limitations. This is accomplished through the performance of the following six CSAU steps:

- Scenario Specification (Section 3.1)
- Nuclear Power Plant Selection (Section 3.2)
- Phenomena Identification and Ranking (Section 3.3)
- Frozen Code Version Selection (Section 3.4)
- Provision of Complete Code Documentation (Section 3.5)
- Determination of Code Applicability (Section 3.6)

The scenario being addressed in this report is the LBLOCA. The licensing criteria for this event are:

- *The calculated maximum fuel element cladding temperature shall not exceed 2200 °F.*
- *The calculated total oxidation of the cladding shall nowhere exceed 0.17 times the total cladding thickness before oxidation. As used in this subparagraph total oxidation means the total thickness of cladding metal that would be locally converted to oxide if all the oxygen absorbed by and reacted with the cladding locally were converted to stoichiometric zirconium dioxide. If cladding rupture is calculated to occur, the inside surfaces of the cladding shall be included in the oxidation, beginning at the calculated time of rupture. Cladding thickness before oxidation means the radial distance from inside to outside the cladding, after any calculated rupture or swelling has occurred but before significant oxidation. Where the calculated conditions of transient pressure and temperature lead to a prediction of cladding swelling, with or without cladding rupture, the unoxidized cladding thickness shall be defined as the cladding cross-sectional area, taken at a horizontal plane at the elevation of the rupture, if it occurs, or at the elevation of the highest cladding temperature if no rupture is calculated to occur, divided by the average circumference at that elevation. For ruptured cladding the circumference does not include the rupture opening.*
- *The calculated total amount of hydrogen generated from the chemical reaction of the cladding with water or steam shall not exceed 0.01 times the hypothetical amount that would be generated if all of the metal in the cladding cylinders surrounding the fuel, excluding the cladding surrounding the plenum volume, were to react.*
- *Calculated changes in core geometry shall be such that the core remains amenable to cooling.*
- *After any calculated successful initial operation of the ECCS, the calculated core temperature shall be maintained at an acceptably low value and decay heat shall be removed for the extended period of time required by the long-lived radioactivity remaining in the core.*

The first three of these criteria are addressed by the RLBLOCA methodology. The remaining two require evaluations beyond the capability of the methodology and are treated separately during plant evaluations.

The selected NPP types to which the methodology is to be applicable includes those PWRs with recirculating (U-tube) type steam generators and initial ECCS injection into the cold legs. Provided herein (Appendix B) are sample problems for a Westinghouse 4-loop PWR design, a Westinghouse 3-loop PWR design, and a Combustion Engineering 2x4 loop design.

A PIRT was prepared for the scenario and NPP types covered by this evaluation model. The PIRT was developed by AREVA from a combination of published PIRTs (Reference 2), reviews by external experts, and a peer review conducted by AREVA personnel and external experts. The PIRT that resulted from this process is provided in Table 3.1.

The codes selected for the performance of the RLBLOCA analysis include the RODEX3A and COPERNIC2 fuel rod codes (References 7, 8, 9 and 10) and the S-RELAP5 system code (References 5, 11, 12, and 13). Documents were developed for each of the codes to address the models and correlations used, the theory applied, and the validation against data. Guidelines were constructed to assist users in the development of S-RELAP5 plant models and the execution of RLBLOCA application analyses. Verification was also performed to confirm the models reported in the documentation are the models actually contained in the codes (Reference 5). In addition, the ICECON containment code (References 14 and 15) was incorporated into the S-RELAP5 code to closely couple the containment and the primary system.

The final step in the requirements and code capabilities element is to demonstrate that the code is applicable to the chosen scenario and NPP types. This objective is accomplished by comparing the important scenario phenomena from the PIRT and the selected NPP modeling requirements with the capabilities of the chosen codes. The results of this comparison demonstrate that the chosen codes are applicable to the scenario and NPP types, as shown in Section 3.6.

## **2.2    *Assessment and Ranging of Parameters***

The assessment and ranging of parameters element is used to quantify the uncertainties and biases that are to be addressed in the analysis of the chosen scenario with the chosen codes. This element includes four steps:

- Establishment of Assessment Matrix (Section 4.1)
- NPP Nodalization Definition (Section 4.2)
- Definition of Code and Experimental Accuracy (Section 4.3)
- Determination of Effect of Scale (Section 4.4)

The assessment matrix identifies those experimental benchmarks necessary to quantify the biases and uncertainties that must be encompassed within the calculation approach of the methodology. The matrix was largely established in Revision 0, and includes separate effects tests (SETs) and integral effects tests (IETs) chosen to demonstrate individual model validity, combined methodology validity and scalability. For Revision 2, the original assessment matrix

was preserved with some additions. Section 4.1 and Table 4.1 provide a detailed discussion of the matrix and its basis. The NPP nodalization is a refinement of that implemented in Revision 0. Section 4.2 describes the NPP noding arrangement and its justification, including those changes incorporated into Revision 2. The execution of the assessment matrix is presented in Section 4.3. Each of the assessment tests is modeled with S-RELAP5 and the appropriate auxiliary code (COPERNIC2 or RODEX3A), incorporating the methodology guidelines to the extent possible given the limitations imposed by experimental benchmarks. The results of these benchmarks are presented and interpreted in Section 4.3, along with a presentation of the uncertainties and biases developed and how they are incorporated into the methodology for each key PIRT phenomena. Scalability considerations are presented in Section 4.4.

### 2.3 ***Sensitivity and Uncertainty Analysis***

The sensitivity and uncertainty analysis element combines the code and model uncertainties and the plant specific contributors needed to obtain a total uncertainty and to provide a basis for making an acceptability statement with respect to the established safety criteria. The following steps are included in this CSAU element:

- Determination of the Effect of Reactor Input Parameters and State (Section 5.1)
- Performance of NPP Sensitivity Calculations and Determination of Combined Bias and Uncertainty (Section 5.2)
- Determination of Combined Bias and Uncertainty and Determination of Total Uncertainty (Section 5.3)

The NPP input parameters and possible operating states were reviewed to determine the applicable input parameters and state. This review identified a list of inputs that might impact the RLBLOCA event. Actual NPP operating conditions and typical technical specifications were assessed to identify allowed operating conditions. A discussion of these types of parameters, including the identification of those necessary for the application of the methodology (power peaking for example), is provided in Section 5.1.

The methodology for determination of the combined biases and uncertainties, and the development of a final statement of probability of compliance with the criteria of 10 CFR 50.46,

is addressed in Section 5.2. Section 5.3 discusses the determination of a measure of total uncertainty. To perform these last two CSAU steps, a non-parametric statistical approach has been used. Non-parametric statistics allows for the treatment of a large number of parameter and plant initial condition uncertainties through direct calculations with the model and associated computer codes. A large number of case inputs are generated by randomly selecting values for all parameters being treated statistically. For this methodology, the number of cases is determined in accordance with the requirements put forth in Section 5.2. The method determines that the three applicable criteria of 10 CFR 50.46 (2200 °F PCT, 17 percent local oxidation, and 1 percent core average oxidation) are met with at least a 95 percent probability with 95 percent confidence. The method does not specifically determine the limiting values for each of these three parameters. Rather, a minimum margin to any of the criteria, determined with 95 percent coverage and a 95 percent confidence is determined. This minimum margin is reported as demonstrating compliance to the 10 CFR 50.46 criteria. To provide further guidance as to plant performance against the criteria, the values of the three parameters for the most limiting cases used to establish the probability and confidence will also be reported. Appendix B provides examples of the application of the methodology and the reporting of compliance for three sample plant applications.

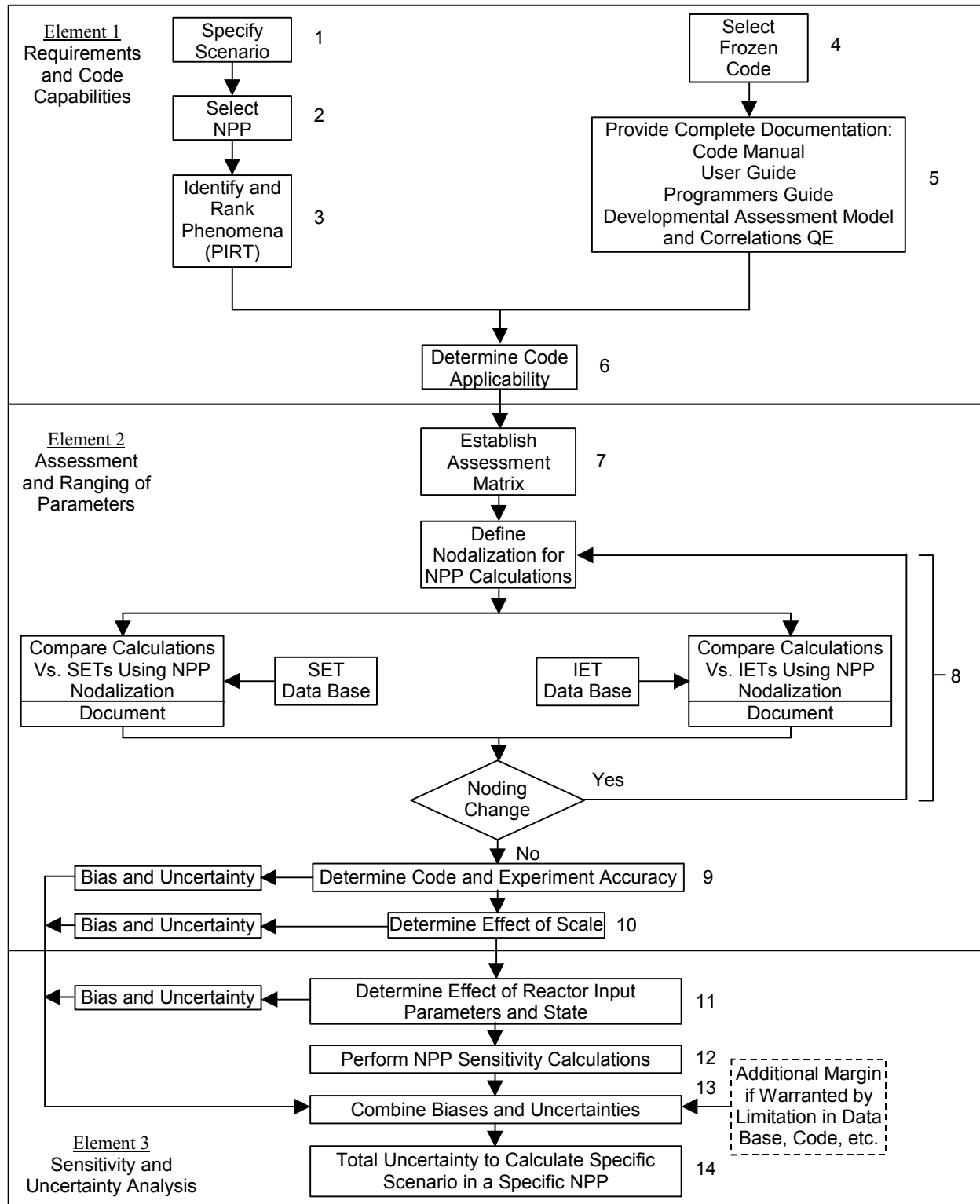


**Figure 2.1: Code Scaling, Applicability, and Uncertainty Methodology Flow Chart**



### 3.0 Requirements and Code Capabilities

The objective of the first element of the CSAU methodology is to establish the analysis requirements and to demonstrate the chosen codes can address these requirements. The important phenomena are determined from the event scenario and NPP types and documented in the PIRT. The ability of the codes to address the important phenomena must then be demonstrated. Documents must be developed that contain sufficient detail to permit the code models to be correlated with the important PIRT phenomena.

#### 3.1 Scenario Specification (CSAU Step 1)

According to the CSAU process, the first step in the construction of a realistic evaluation model is the identification and description of the event to be evaluated. This is termed the event scenario. For the modeling described herein, the event is that of a LOCA. A reasonable and useful definition is provided by the standard review plan for RLBLOCA (Reference 16).

*Loss-of-coolant accidents (LOCA) are postulated accidents that would result from the loss of reactor coolant, at a rate in excess of the capability of the normal reactor coolant makeup system, from piping breaks in the reactor coolant pressure boundary. The piping breaks are postulated to occur at various locations and include a spectrum of break sizes, up to a maximum pipe break equivalent in size to the double-ended rupture of the largest pipe in the reactor coolant pressure boundary.*

A large break LOCA initiates with an instantaneous rupture of a reactor coolant system (RCS) pipe, resulting in the rapid loss-of-coolant from the RCS. It is the coolant loss and its replacement with emergency coolant that is the subject assessment of LBLOCA evaluation models. Two top level considerations apply to the model presented here:

1. The rupture or break occurs in the RCS piping. Although it is possible to envision ruptures in components, those events are considered beyond the design basis and not subjects for this evaluation model.
2. This evaluation model applies only to the larger possible breaks, break areas greater than 0.1 times the cross-sectional area of the largest flow area pipe within the RCS. Smaller breaks are evaluated with a separate evaluation model.

The rate of coolant loss is governed, in part, by the break area, which ranges from 0.1 times the largest pipe area to twice the area of the pipe within which the rupture occurred. For plants covered by this evaluation model, the break can occur in three locations:

1. The hot leg pipe between the reactor vessel and the steam generator (hot leg break),
2. The cold leg between the steam generator and the reactor coolant pump (pump suction break), and
3. The cold leg between the reactor coolant pump and the reactor vessel (pump discharge break).

A LBLOCA evaluation must consider breaks at all of these locations. However, as will be shown in the following text, the pump discharge break comprises the greatest challenge to the emergency equipment and results in the most severe consequences for the reactor core. Although a great deal of the modeling herein is applicable to any of the break locations; it is specific only for pump discharge breaks.

To support the pump discharge as the worst break location, it is useful to describe a simplified LBLOCA scenario:

The break occurs and substantial RCS coolant is expelled to the containment. The emergency systems are activated and inject replacement coolant into the cold legs between the reactor coolant pump and the reactor vessel. This coolant transfers to the reactor vessel and the core to provide core cooling.

When the break is in the pump discharge piping up to one-third, depending on the plant being evaluated, of the emergency coolant can flow directly out the break and not provide core cooling. Because of the design of the RCS loop, this loss can not occur for a hot leg break; essentially all of the emergency coolant must pass through the reactor vessel, providing core cooling in the process. Thus, a hot leg break, with its high flooding rate, refills the core with water sooner than either pump discharge or pump suction breaks and is much less severe.

The relation of a pump suction break to a pump discharge break is similar to that with a hot leg break in that there is no immediate loss of emergency coolant to the break. Although it is possible to lose emergency coolant to the break by entrainment, the efficiency of that process is less than that for a pump discharge break. The resistance to the break from the reactor vessel is higher for a pump suction break and the resistance from the core outlet through the hot

leg pipe connecting to the break is lower, making emergency coolant delivery to the core easier for pump suction breaks. Therefore, because a pump discharge break more easily discharges all coolant, particularly liquid coolant, to the containment and is most likely to discharge the emergency coolant to the break, it can be identified as the worst break location. Accordingly, the hot leg and pump suction locations can be eliminated from specific consideration within this methodology.

The following details the progression of the scenario. A LBLOCA event is typically described in three phases: (1) blowdown, (2) refill, and (3) reflood. For realistic evaluations, the blowdown phase is defined as the time period from initiation of the break until flow from the accumulators or safety injection tanks (SITs) begins to discharge. This definition is different than the traditional definition of blowdown, which extends the blowdown period until the RCS pressure approaches containment pressure. The blowdown phase typically lasts between 12 to 25 seconds, depending on the break size. The refill phase lasts from the end of blowdown until a fluid mixture, supported by ECCS water, penetrates the bottom of the active core region. The reflood phase lasts from the end of refill until the core is quenched.

Following the initiation of the break, the blowdown phase is characterized by a sudden depressurization from operating pressure down to the saturation pressure of the hot leg fluid. For larger cold leg breaks, an immediate flow reversal and stagnation occurs in the core due to flow out the break, which causes the fuel rods to pass through critical heat flux (CHF), usually within 1 second following the break. Following this initial rapid depressurization, the RCS depressurizes at a more gradual rate. Reactor trip and emergency injection signals occur when either the low-pressure setpoint or the containment high-pressure setpoint are reached. However, for LBLOCA, reactor trip and scram are essentially inconsequential, as reactor shutdown is accomplished by moderator feedback. During blowdown, core cooling is supported by the natural evolution of the RCS flow pattern as driven by the break flow.

When the system pressure falls below the accumulator (or SIT) pressure, flow from the accumulator is injected into the cold legs ending the blowdown period and initiating the refill period. Once the system pressure falls below the respective shutoff heads of the high head safety injection (HHSI) pumps and the low head safety injection (LHSI) pumps, and the system startup time delays are met, Safety Injection System flows begin injecting into the RCS. While some of the ECCS flow bypasses the core and goes directly out of the break, the downcomer

and lower plenum gradually refill until the mixture in the lower head and lower plenum regions reaches the bottom of the active core and the reflood period begins. Core cooling is supported by the natural evolution of the RCS flow pattern as driven by the break flow and condensation on the emergency coolant being injected. Towards the end of the refill period, heat transfer from the fuel rods is relative low, steam cooling and rod-to-rod radiation being the primary mechanisms.

Once the lower plenum is refilled to the bottom of the fuel rod heated length, refill ends and the reflood phase begins. Substantial ECCS fluid was retained in the downcomer during refill. This provides the driving head to move coolant into the core. As the mixture level moves up the core, steam is generated and liquid is entrained, providing cooling in the upper core regions. As the two-phase mixture expands into the upper plenum, some liquid may deentrain and flow downward back into the cooler core regions. The remaining entrained liquid passes into the steam generators where it vaporizes, adding to the steam that must be discharged through the break and out of the system. The difficulty of venting steam is, in general, referred to as steam binding. It acts to impede core reflood rates. With the initiation of reflood, a quench front starts to progress up the core. With the advancement of the quench front, the cooling in the upper regions of the core increases, eventually arresting the rise in fuel rod surface temperatures. Later the core is quenched and a pool cooling process is established that can maintain the cladding temperature near saturation, so long as the ECCS provides makeup for the boiling.

The RLBLOCA methodology must analyze the probable and possible consequences of the scenario (a LBLOCA at the pump discharge) and determine the plant will meet the 10 CFR 50.46 criteria, as discussed in Section 2.1, with high probability.

### **3.2     *Nuclear Power Plant Selection (CSAU Step 2)***

The selected NPP types to which the methodology is to be applied include those PWRs with U-tube type steam generators and initial ECCS injection into the cold legs. The specific plant types are enumerated in Section 1.0. These NPP types have similar hot and cold legs, pressurizers, steam generators, and vessels. The largest difference among the NPP types is the number of hot and cold legs, and steam generators. However, experience in the performance of LBLOCA analyses for these NPPs has shown that all three types behave similarly.

All of these NPP types have inverted U-tube steam generators; a pressurizer connected to a hot leg; and initially injects ECCS coolant into the cold legs. The steam generators can all be modeled with downcomer, boiler, plenum, dryer/separator, and steam dome regions. The pressurizers are essentially the same and can be modeled with axial nodes, associated heat structures, heaters, sprays, and a surge line connected to a hot leg. The plant nodalization for a loop is described in Section 4.2 and is illustrated in Figure 4.1.

The configuration of the vessels for all three-plant types is also essentially the same and can be modeled in the code with the same major divisions and nodalization schemes. The coolant enters the vessel through the inlet nozzles and flows into the downcomer. In the downcomer, a small fraction of the flow diverts into the upper head, but the majority of the flow goes down the downcomer (for upflow plants) into the lower head/plenum region.<sup>1</sup> From here the majority of the flow goes up through the active core with some flow bypassing the core through the baffle and guide tubes. From the core, the flow enters the upper plenum and exits the vessel through the hot leg nozzles.

The principal difference in the vessels is in the connection between the downcomer and the lower plenum/lower head. In some CE designs, there may be a flow skirt that is intended to force part of the flow to pass through the lower head before going into the lower plenum region. The NPP model of the lower plenum has been nodalized to address this vessel configuration difference. The plant nodalization for the vessel is described in Section 4.2 and illustrated in Figure 4.4.

As indicated above, a principle difference between these NPP types is in the number of hot and cold legs, and steam generators. The Westinghouse and AREVA 3-loop designs have three hot legs, cold legs and steam generators. The Westinghouse and AREVA 4-loop designs have four hot legs, cold legs, and steam generators. CE 2x4 designs have two hot legs, four cold legs and two steam generators.

---

<sup>1</sup> For down flow baffle plants, the flow into the downcomer splits, with some flow going into the bypass region and the remainder of the flow continuing down the downcomer. In this plant configuration, the downcomer and bypass flow both enter the core.

A typical vessel loop configuration is shown in Figure 4.5. This figure shows the location of the cold legs (arrows pointing into vessel) and hot legs (arrows pointing out of vessel) for the three NPP types. Since the hot legs pass through the vessel downcomer region into the upper plenum, they essentially provide a flow path blockage at the elevation of the hot and cold legs in all three NPP types. As illustrated in this figure, the flow paths for the 4-loop and the 2x4 plants are similar in relation to their hot and cold legs.

Provided in Appendix B are sample problems for a Westinghouse 4-loop PWR design, a Westinghouse 3-Loop PWR design, and a CE 2x4 PWR design. Table B.9, Table B.18, and Table B.27 provide values for some of the important NPP parameters. As illustrated, a major difference in the important NPP parameters is the accumulator pressure for the Westinghouse and AREVA designs, and the SITs in the CE designs. The impact of this difference is shown in the sequence of events given in Table B.14, Table B.23, and Table B.33, where the SIT flow initiation is delayed in the CE design until the pressure in the cold legs drops below the SIT pressure. Taking into account this delay in the SIT delivery, the sequence of events is similar for all three of the NPP types.

### 3.3 ***Phenomena Identification and Ranking, PIRT (CSAU Step 3)***

A key step in the CSAU process is to identify and rank the important phenomena that should be addressed in analyzing the selected scenario. This step is performed by experts who are knowledgeable regarding LBLOCA phenomena that occur during each transient phase. The resultant PIRT provides the basis for: (1) determining code applicability (does the code properly model the important phenomena); (2) establishing the assessment matrix (identifying test data that contain the appropriate phenomena during each accident phase); and (3) identifying phenomenological parameters to be ranged and quantified for evaluating uncertainties.

The AREVA PIRT for the chosen scenario has evolved through multiple stages of review (including experts within AREVA and from outside the company) and adjustment. Its foundation includes an independently developed PIRT (Reference 2), review and development by an expert panel (including experts both within AREVA and from outside the company), and adjustments or updates to incorporate improved understanding of the phenomena. Table 3.1 provides the current version upon which Revision 2 of this methodology is based. Each phenomena is given a ranking, where importance is proportional to the numerical value (e.g.,

9 = extreme importance and 1 = least importance). The ranking indicates the important phenomena that should be simulated by a RLBLOCA evaluation model.

The following definitions apply to the PIRT in Table 3.1:

1. Blowdown: The blowdown phase of the LOCA is defined as the time period from initiation of the break until flow from the accumulators or safety injection tanks begins.
2. Refill: The refill phase of the LOCA begins when the accumulators or SITs begin injecting and continues until the mixture level in the vessel refills the lower plenum and begins to flow into the heated core region.
3. Reflood: The reflood phase of the transient begins when the lower plenum fills and emergency core cooling (ECC) begins flowing into the bottom of the active core and continues until the temperature transient throughout the core has been terminated. At that time, the LOCA stored energy and decay heat are being removed and the LOCA has been reduced to an issue of maintaining long-term cooling.

The following items were revised or added to the EMF-2103(P)(A) Revision 0 final PIRT:

- Fuel rod, stored energy - Increased from Level 2 to a Level 5 importance during refill. Higher energy within the pellet will affect cladding temperatures during this period, which may, for some plants with capable ECCS systems, become the peak cladding temperature (PCT).
- Upper head, initial temperature - Increased to a Level 5 during refill. It is possible for water within the upper head of a Westinghouse designed  $T_{cold}$  plant to suspend and dump during refill potentially reducing the cladding temperatures.
- Hot leg, entrainment/deentrainment - Increased from Level 5 to a Level 6 during reflood to better reflect its potential impact on steam binding.
- Pressurizer, early blowdown quench – Reduced from Level 5 to Level 3 to reflect the importance attributed to this issue in the final Revision 0 methodology.
- Cold leg, condensation during pumped injection - Separated from the accumulator injection to reflect the effect that heating the ECCS injection water closer to saturation

would have on downcomer boiling during reflood after accumulator injection ended. This item was rated as importance level 7 during reflood as compared to the combined accumulator pumped injection reflood rating of Level 5 in Revision 0.

- Downcomer, multi-D phenomena - Increased from Level 2 to Level 5 during reflood to better capture the importance of downcomer nodalization on code stability.
- Downcomer, saturated nucleate boiling - Increased from Level 2 to Level 7 during reflood to capture the importance of downcomer boiling on the prediction of the scenario for high power plants with low pressure containments.
- Break, containment pressure – Decreased from Level 7 to Level 6 to better reflect the sensitivity of the scenario to changes in break backpressure during refill and reflood.

### 3.4 ***Frozen Code Version Selection (CSAU Step 4)***

The codes selected for use in the RLBLOCA methodology include the RODEX3A (References 7, 8, and 9) and COPENIC2 (Reference 10) fuel performance codes, and S-RELAP5 (References 5, 11, 12, and 13) for system analysis. RODEX3A will be used to set the initial fuel temperatures for the evaluation of Zircaloy-clad fuel and COPENIC2 will be used for M5<sup>®</sup>. The S-RELAP5 code is a RELAP5-based thermal-hydraulic system code used for performing LOCA and non-LOCA analyses. The versions of these codes used in the development of this methodology are UOCT09 for S-RELAP5, UDEC02 for COPENIC2 and UFEB07 for RODEX3A.

#### 3.4.1 COPENIC2 and RODEX3A Fuel Rod Performance Codes

A key to a RLBLOCA analysis is the model used for calculating fuel rod performance. In particular, the initial operating temperature of the fuel pellets (stored energy), the internal fuel rod gas pressure, and the transient gap conductance are significant parameters, which affect the calculated PCT. AREVA will use COPENIC2 to calculate the required fuel characteristics as a function of fuel rod exposure and power history except for Zircaloy-clad fuel for which RODEX3A will be used. This particular arrangement is necessary since the use of COPENIC2 is restricted to M5<sup>®</sup> cladding. This restriction is not due to limitations in the physical models in the code, but is rather based on SER restrictions associated with the current



NRC approval of COPENIC2. The physical models in COPENIC2 could be extended for use with Zircaloy cladding, and some of the validation of the code (the Loss of Fluid Test (LOFT) assessments in Section 4.3.2.1) was based on test results using Zircaloy cladding.

The COPENIC2 and RODEX3A fuel rod performance codes were originally developed and NRC-approved for use by AREVA with respect to fuel rod mechanical design. Portions of these codes were incorporated in S-RELAP5 to permit coupled calculations of fuel rod thermal properties (thermal conductivity, heat capacity, and gap conductance), during both the steady-state and the transient phases of an S-RELAP5 LBLOCA analysis. The COPENIC2 and RODEX3A (Reference 11, Sections 7.5 and 7.3, respectively) routines incorporated into S-RELAP5 were for the calculation of fuel pellet temperature, thermal expansion, cladding elastic strain, gap width and gap gas pressure, which in turn determine the fuel rod thermal properties and gap conductance. Table 3.2 provides a description of the models and routines incorporated into S-RELAP5.

Long-term burnup dependent “permanent” fuel rod effects such as pellet densification and swelling, cladding creep, and fission gas release will not change appreciably during the course of a LBLOCA transient. Calculations of these effects are performed to initialize the fuel rod parameters, but are not altered during the transient and, thus, not included in the fuel rod model routines in S-RELAP5. The fuel pellet and cladding strains associated with these “permanent” effects are calculated in separate executions of the standalone COPENIC2 or RODEX3A codes (which burn the fuel rods through the exposure histories required for the individual rods being analyzed). The results of these exposure analyses are then transferred to S-RELAP5 and used to initialize the values of the burnup dependent “permanent” effects in the COPENIC2 or RODEX3A routines.

The fuel rod analysis for an S-RELAP5-based LBLOCA calculation then proceeds in three steps:

1. The standalone fuel rod code (COPENIC2 or RODEX3A) is used to determine fuel rod properties at the end of a specified exposure history.
2. An S-RELAP5 steady-state analysis is performed using the fuel rod models in S-RELAP5, with the permanent burnup dependent fuel properties being defined by data transferred from Step 1. During this steady-state analysis, power related properties such as fuel

temperatures and thermal properties are allowed to migrate to values consistent with the final steady-state power of the system. The initial transient stored energy is determined and adjusted for uncertainty and bias during this phase.

3. An S-RELAP5 transient analysis is performed using initial fuel rod thermal conditions from Step 2, and using the fuel rod models in S-RELAP5 to determine fuel rod thermal properties and gap conductance during the transient.

### 3.4.2 S-RELAP5

S-RELAP5 is an AREVA-modified version of RELAP5/MOD2 (Reference 17), which incorporates the computer portability aspects of RELAP5/MOD3 (Reference 18) and modifications to the constitutive package to provide congruency with literature correlations and to improve the simulation of key LBLOCA experiments. The field equations are basically in the same form as RELAP5/MOD2 with the addition of full two-dimensional momentum equations. This two-dimensional capability is only applied to the downcomer, core and upper plenum regions in the RLBLOCA methodology, but can be applied anywhere in the reactor system through input. The S-RELAP5 code structure was modified to be essentially the same as RELAP5/MOD3. The coding for reactor kinetics, control systems, and trip systems was also replaced by that from RELAP5/MOD3.

The following list summarizes the major modifications and improvements incorporated into S-RELAP5 relative to RELAP5/MOD2:

- Multi-dimensional Capability: A full two-dimensional treatment was added to the hydrodynamic field equations.
- Energy Equations: The energy equations were modified to better conserve energies transported into and out of a control volume.
- Numerical Solution of Hydrodynamic Field Equations: The reduction of the hydrodynamic finite-difference equations to a pressure equation is obtained analytically in S-RELAP5.
- State of Steam-Noncondensable Mixture: The state relations were modified to correctly simulate accumulator depressurization and to prevent code failures during the period of accumulator ECC water injection.

- Hydrodynamic Constitutive Models: Significant modifications and enhancements were made to the interphase friction and interphase mass transfer models.
- Choked Flow: The computation of the equation of state at the choked plane was modified.
- Countercurrent Flow Limiting: A Bankoff form correlation was implemented, which can be reduced to either a Wallis type or Kutateladze type countercurrent flow limitation (CCFL) correlation.
- Component Models: A revised two-phase pump degradation model based on Electric Power Research Institute (EPRI) data was implemented.
- Fuel Model: Initial fuel conditions are supplied by either COPENIC2 or RODEX3A. To be consistent, the fuel deformation and conductivity models from both of these codes have been included in S-RELAP5.
- Containment Back Pressure: ICECON coding and subroutines were placed in S-RELAP5 to a cocurrent containment pressure calculations.

To provide a realistic time variant containment boundary condition for break flow calculations, the coding for ICECON was essentially inserted as a subroutine into S-RELAP5. Break flows and enthalpies are transferred to the containment routines, which continuously feed back calculated pressure and temperature to S-RELAP5 time dependent volumes, against which the break flows are calculated. ICECON (References 14 and 15) is based on CONTEMPT LT-022 (Reference 19). ICECON was originally approved for calculating a conservative containment back pressure under Appendix K rules, but it can also be used with realistic input, and only minor modifications, to give an approximate realistic back pressure calculation. AREVA performed sensitivity calculations to evaluate the effects of containment back pressure. The results showed that, although the RLBLOCA model does not demonstrate a high sensitivity of calculated PCT to containment back pressure, there is a slight impact on cladding temperatures. Therefore, the containment back pressure calculation is designed to provide a reasonable, yet slightly conservative, approximation to the containment pressure.

### 3.5 ***Provision of Complete Code Documentation (CSAU Step 5)***

The documentation for the codes used in the development of this methodology is provided in References 7, 8, and 9 for the RODEX3A code, Reference 10 for COPENIC2, References 5,

11, 12, and 13 for the S-RELAP5 code, and References 14 and 15 for the ICECON code. The documentation describes the models and correlations used in the codes; defines the code inputs and provides a description of the code structure. These documents were verified against the actual coding to ensure the documentation and coding are consistent (Reference 5).

The code validation is provided in Reference 5, which compares the code predictions to measured data in a number of SET and IET facilities. In addition, AREVA has guidelines covering the development of S-RELAP5 input for the NPP model and procedures for performing an actual analysis.

### 3.6 ***Determination of Code Applicability (CSAU Step 6)***

The objective of the determination and code applicability step of CSAU is to demonstrate that the selected codes are capable of modeling the chosen event for all NPP types. This is accomplished by comparing the event and important phenomena identified in the PIRT with the models and correlations documents for the selected codes. Four attributes are needed to make this comparison:

- **Field equations** that provide code capability to address global processes.
- **Closure (constitutive) equations**, which support the conservation equations by providing code capability to model and scale specific phenomena or processes.
- **Code numerics** that demonstrate code capability to perform calculations efficiently and reliably.
- **Structure and nodalization**, which address code capability to model the NPP geometry and components, and to provide efficient and accurate NPP predictions.

These four attributes are discussed in the following sections.

#### 3.6.1 Field Equations

The field equations (conservation of mass, momentum, and energy) must possess the capability of simulating each of the distinct phases (blowdown, refill, and reflood) of a LBLOCA. During the refill and reflood phases, countercurrent flow occurs at various locations in the RCS, and subcooled liquid coexists with superheated steam in parts of the reactor core. Therefore, for realistic analyses, the field equations must be non-homogeneous (unequal velocity for each

phase) and non-equilibrium (unequal temperature for each phase). The presence of nitrogen in the accumulator requires an additional field equation to model and track the movement of this noncondensable gas.

The required field equations are given in Table 3.3. The relationships to specific PIRT-important phenomena along with references to specific models are provided in Table 3.4. As indicated in Table 3.3 and Table 3.4, the S-RELAP5 code has the required field equations and models to address the important LBLOCA phenomena.

### 3.6.2 Closure Equations

Closure equations (constitutive models and correlations) are required to support the basic field equations. The closure equations are essential for modeling the processes and phenomena given in the PIRT (see Table 3.1). The S-RELAP5 constitutive models and correlations are presented in Reference 11. The verification and validation of the code models and correlations are given in Reference 5. The two documents together demonstrate that the S-RELAP5 code adequately simulates LBLOCA events with a high level of confidence.

The capability of the S-RELAP5 code closure equations to meet the requirements of the PIRT (see Table 3.1) is summarized in Table 3.3. The closure equations address wall friction, interphase friction, mass transfer (interphase heat transfer), wall-to-fluid heat transfer, form-losses, and similar functions. The various models require flow regime maps, boiling curves, state relationships, and fluid and material properties for completeness. As indicated in Table 3.3, the S-RELAP5 code has the required closure equations to address the important LBLOCA phenomena.

### 3.6.3 Code Numerics

The numerical solutions contained in S-RELAP5 were extensively tested and checked (Reference 11, Section 2.6). For the RLBLOCA methodology, the adequacy of S-RELAP5 numerics is demonstrated in the performance of the assessments reported in Reference 5 and summarized in Section 4.3 herein. In addition, the adequacy of the numerics was also demonstrated by the time step sensitivity analysis reported in Appendix A.

#### 3.6.4 Structure and Nodalization

To properly model a NPP, a code must be able to adequately model the important components and control systems of the NPP with respect to the chosen accident scenario. The S-RELAP5 code has the ability, as indicated in Table 3.4,(Reference 11), to model all the major components and associated control systems of the reference plants (listed in Section 1.0). The modeling of each of the NPP components is discussed in detail in AREVA guidelines and summarized in Section 4.2. Section 4.2 also describes the studies that were performed to determine the final plant nodalization.



This image shows a full page of blank graph paper. The grid consists of small squares formed by thin black lines. There are 20 columns and 20 rows of squares. A thicker vertical line runs down the center, creating two equal halves of 10 columns each. A thicker horizontal line runs across the middle, creating two equal halves of 10 rows each. These thicker lines intersect at the center of the page. The entire grid is enclosed within a double-line border.



**Table 3.2: Models Added to S-RELAP5 from COPENIC2 and  
RODEX3A**


--	--

**Table 3.3: Field Equations/Models in S-RELAP5**

<b>Scenario and PIRT Requirements</b>	<b>S-RELAP5 Model Existence</b>	<b>Field Equations/Model</b>
Non-equilibrium Two-phase Flow	Yes	Six equation unequal velocity, unequal temperature
Non-condensable Gas Flow	Yes	Gas mass balance in vapor flow field
Multi-D Flow Capability	Yes	2-D components available as required
Separation Due to Gravity	Yes	Gravity pressure differential in flow field equations
Interphase Exchange Terms	Yes	Mass and energy transfer between phases, vaporization and condensation

**Table 3.4: Phenomena/Processes in S-RELAP5**

--	--





**Table 3.4: Phenomena/Processes in S-RELAP5 (*continued*)**

--	--

## 4.0 **Assessment and Ranging of Parameters**

The assessment and ranging of parameters element establishes the assessment matrix to be used in defining the NPP nodalization, quantifying the code accuracy, and demonstrating any code or model scale effects.

### 4.1 ***Establishment of Assessment Matrix (CSAU Step 7)***

The following four considerations are taken into account in establishing the assessment matrix. The first consideration is the important phenomena identified in the PIRT process described in Section 3.3 (CSAU Step 3) and presented in Table 3.1. The assessment matrix, Table 4.2, includes experiments that address the important phenomena, defined as those phenomena ranked 5 or higher in Table 3.1. The selected experiments must have sufficient data to determine code accuracy, including bias and uncertainty, for the important phenomena.

The second consideration is that of NPP nodalization. Here experiments are selected that are representative of the types of NPPs being addressed and cover the identified phases of the selected scenario. Thus, for this application, experiments are selected that are representative of Westinghouse/AREVA 3- and 4-loop designs and CE 2x4 designs. The experiments also should cover one or more of the LBLOCA phases identified in Section 3.1 (CSAU Step 1)—blowdown, refill, and reflood.

The third consideration is to demonstrate that the code and NPP nodalization have the ability to scale from experiments of different sizes to a full size NPP for which analyses will be performed. Generally this is done by selecting a number of assessments in facilities of different scale and demonstrating that the code and NPP nodalization are capable of consistently predicting the experimental data from all the experiments.

The fourth and final consideration is with respect to compensating code errors. The development process embodies substantial methodology verification and validation. The use of a PIRT process and the benchmarking of the methodology during validation against experiments chosen to measure the methodology performance regarding the PIRT phenomena provide substantial assurance that compensating errors do not significantly impact the methodology predictions. These tests include both SETs and IETs dealing with the most

important LOCA phenomena. With a comprehensive set of such benchmarks setting the validity and final assessment of the methodology, it can be concluded that if the methodology contains compensating errors, these errors do not impugn the ability of the methodology to reliably predict the course and outcome of LBLOCA transients.

#### 4.1.1 PIRT Considerations

The PIRT presented in Section 3.0 (see Table 3.1) provides a qualitative expression of what is perceived to be the degree of importance of key phenomena present in a LBLOCA. All these phenomena are accounted for either statistically or with a bias (perhaps a null bias), and a justification for the selected treatment is provided. Within Revision 0 of this methodology, sensitivity studies were used, in part, to determine which phenomena or processes required assessment by the validation matrix. However, once a decision to validate the treatment of a phenomena or process is made, the process by which the decision was made is no longer of consequence unless the decision is changed. In that case, a revised decision process and result must be described and justified. The Revision 2 validation matrix includes all of the phenomena or processes selected for validation in Revision 0 and will not repeat the discussion of sensitivity studies for those parameters, phenomena, or processes. An accounting, including PIRT revisions made in Revision 2, of the validation matrix is made in Table 4.1. Where an item ranked 5 or higher is not included in the validation matrix, an explanation, sensitivity study or other, is provided in Table 4.1 and Section 4.3.3.1 to justify the exclusion.

Table 4.1 lists the moderate and high ranked PIRT phenomena or processes (ranked five or higher) and the analytical parameters that primarily affect them. These are then cross referenced to the decision on including them in the validation matrix or the reason for exclusion. If a sensitivity study is part of the justification, the conclusion from the study is also provided. The final entry includes the reference section within which additional discussion is provided.

#### 4.1.2 Nodalization Considerations

In the selection of the specific tests to be analyzed in each test facility, plant nodalization was an important consideration and, given the extensive experimental facility database developed, provided considerable support for that selected for plant modeling. One additional test facility was identified strictly to address nodalization effects. That test facility was the Slab Core Test



Facility (SCTF), where specific assessments were performed to address radial nodalization with variations in radial power distributions.

#### 4.1.3 Scaling Considerations

Within the test facility database developed to support the PIRT considerations are facilities that span a scaling range of 1:1500 to 1:1. In addition, some specific tests were performed as a counterpart to tests performed in other facilities. Where data are available, these tests were added to the assessment matrix.

#### 4.1.4 Compensating Errors

The issue of compensating errors arises primarily from the use of correlations and closure relations in the code. The interaction of the various correlations and closure relations can be such that an error in one of these models is compensated for by an error in another model. These compensating errors can result in the code being able to predict specific tests but incapable of predicting other tests. For the LBLOCA, only those compensating errors, which could function in one manner in the assessments and in an entirely different manner in the LBLOCA, are a concern. Thus, the assessment matrix must include tests that can be scaled up and that cover the range of the LBLOCA PIRT phenomena. The compensating error issue is addressed in the test matrix through the FLECHT-SEASET, SCTF, CCTF, and THTF for the core phenomena and Upper Plenum Test Facility (UPTF) for most of the other major RCS components. The LOFT and Semiscale benchmarks provide further assurance by benchmarking the methodology as an integral.


#### 4.1.5 Summary

Given these four considerations, the assessment matrix described in Table 4.2 was developed. Table 4.2 lists the test facilities, the actual tests analyzed from each test facility, and the associated phenomena being examined.

**Table 4.1: Validation Needs for Important PIRT Entries**

**Table 4.1: Validation Needs for Important PIRT Entries (*continued*)**

**Table 4.1: Validation Needs for Important PIRT Entries (*continued*)**





#### 4.2 **Define Nodalization for NPP Calculations (CSAU Step 8)**

Reference 4 ("Quantifying Reactor Safety Margins") makes the following statements regarding nodalization:

*The plant model must be nodalized finely enough to represent both the important phenomena and design characteristics of the NPP but coarsely enough to remain economical.*

*Thus, the preferred path is to establish a standard NPP nodalization for the subsequent analysis. This minimizes or removes nodalization, and the freedom to manipulate noding, as a contributor to uncertainty.*

*Therefore, a nodalization selection procedure defines the minimum noding needed to capture the important phenomena. This procedure starts with analyst experience in previous code assessment and application studies and any documented nodalization studies. Next, nodalization studies are performed during the simulation of separate- and integral-effects code data comparisons. Finally, an iterative process using the NPP model is employed to determine sufficiency of the NPP model nodalization.*

Given these general recommendations, the goal of a nodalization methodology is to optimize somewhat independent priorities. These include preserving dominant phenomena, minimizing code uncertainty, conforming to design characteristics, and minimizing computational expense. The AREVA RLBLOCA guidelines are quantitatively explicit wherever possible to remove nodalization as a contributor to uncertainty. Because not all plants of the same type are identical, the guidelines provide guidance for deriving the appropriate nodalization. This strategy serves both to remove nodalization as a contributor to uncertainty and to define a method for automating the generation of input for a RLBLOCA analysis.

As described by Step 8 of the CSAU process, this task is iterative and was so during development of Revision 0 (Reference 6) of the methodology. Revision 2 of the methodology initiates the basic nodalization with the Revision 0 model and improves it, in selected areas, based on studies, described later in this section. Because the nodalization requirements are strictly applied, uncertainty associated with nodalization becomes part of the studies to determine the statistics of key uncertainty parameters.

The derived input prescription defines the standardized nodalization scheme, specifies a logical numbering system, and recommends key parameter inputs for the S-RELAP5 input model. Noding details were determined from experience with simulation of integral- and separate-effects tests (Reference 5) that result in a technically and economically sound

nodalization scheme for simulating LBLOCA in a PWR. Assessment calculations of the FLECHT-SEASET reflood experiments provide data for the axial nodalization of the core region. Studies of the Cylindrical Core Test Facility (CCTF) and SCTF were used to identify two-dimensional modeling techniques for the downcomer and core. Analyses of the LOFT and Semiscale experiments gave information describing the primary coolant loops, reactor coolant pumps, reactor vessel, and steam generators. Assessments of UPTF tests also were used to identify two-dimensional modeling techniques and provide useful plant information, including experimental data on full-scale downcomer fluid behavior during all phases of a LBLOCA.

Column 1 of Table 4.3 defines a particular NPP component or coolant system region and the S-RELAP5 components generally used for its simulation. Column 2 lists the important phenomena associated with the component as evaluated through the PIRT process (Section 3.3). Column 3 defines the number of cells required, based on user experience and assessment calculations, to provide adequate detail.

#### 4.2.1 Nodalization Methodology

The necessary conditions for a satisfactory nodalization methodology are to discriminate key structural characteristics, to obtain reasonable steady-state agreement with plant data, to preserve first order accuracy of dominant phenomena, and to minimize PCT sensitivity to nodalization. The ability of the code and associated nodalization to describe key structural components is addressed in Section 3.6.4, where it is demonstrated that the code is capable of modeling key components. Obtaining reasonable steady-state results is implicitly aided by strict conformance to structural design characteristics (e.g., elevations and volumes).

The most challenging of the necessary conditions is the task to preserve dominant phenomena. The ability of a computer code to capture LBLOCA phenomena cannot separate the contributions of the applicable phenomenological models and nodalization. While it was stated that strict adherence to nodalization transfers the burden of code uncertainty to the uncertainty analysis of key LBLOCA parameters, every effort was made to provide a nodalization scheme that minimizes nodalization uncertainty.

Experience indicates that S-RELAP5 plant models of Westinghouse/AREVA 3- and 4-loop PWRs and CE 2x4 loop PWRs require between 200 and 500 volume component nodes, junction flow paths, and heat structures. The AREVA 3- and 4- loop plants closely pattern the



Westinghouse 3- and 4- loop plants and do not require separate nodalization schemes. The following figures show the modeling techniques.

Figure 4.1: Sample Loop Nodalization for NPP

Figure 4.2: Sample Steam Generator Secondary Nodalization for NPP

Figure 4.3: Double-Ended Guillotine and Split Break Nodalization

Figure 4.4: Sample Reactor Vessel Nodalization for NPP

Figure 4.5: Westinghouse/AREVA 3- and 4-Loop and CE 2x4 Plant Vessel Downcomer Configurations

Figure 4.6: NPP Core Nodalization

Figure 4.7: Sample NPP Upper Plenum Nodalization – Axial Plane

Figure 4.8: Sample NPP Upper Plenum Nodalization – Cross-Sectional Plane

The following sections discuss the nodalization of each major plant component in the context of the PIRT (Section 3.3), and describe the evolution of the nodalization schemes.

#### 4.2.2 Numerical Considerations

The nodalization of a particular model translates into a computational array used to solve the mass, momentum, and energy equations; thus, numerical constraints also must be considered in the sizing and configuration of component volumes. The primary numerical issues are accuracy, numerical stability, and code variability. While optimizing all three of these is necessary to have useable results, some code variability can be tolerated provided it is reasonably defined. However, numerical stability must be assured before performing production calculations to assess accuracy through code/data comparisons.

In general, the RELAP5 series of codes have a solid foundation regarding numerical stability. This is discussed in Reference 11. However, both nodalization and time step decisions can influence numerical stability. It is generally understood that numerical solutions are well behaved if the number of mesh points is sufficiently small. Such small nodes necessitate equally small time steps to satisfy the Courant stability requirement, leading to long uneconomical code execution times. Conversely, it was shown that modeling interfacial drag contributes to the stability of coarser mesh models for two-phase flow codes, such as RELAP5

(Reference 20). While modeling interfacial drag works to destabilize the solution for small mesh sizes, it supports the courser mesh models required for economical code execution times. As a result, considering hydraulic phenomena exclusively, spatial mesh configuration is not a high concern for numerical stability.

For code accuracy, mesh sizing becomes more important for heated surfaces. Steep temperature gradients influence the adjacent fluid conditions. For this reason, small mesh sizes are used on heated surfaces to capture expected phenomena.

The final figure-of-merit for quantifying code variability comes from the calculation of the hot rod PCT. For a set of equivalent input models, differing only in time step (constrained to be less than the Courant limit), comparisons of PCT traces can be used to evaluate expected code variability. By using this approach, nodalization decisions can be made in an effort to minimize the impact of code variability.

In summary, the iteration process for defining a nodalization methodology included decisions to change a component nodalization based on the analysis of either assessments (integral- and separate-effects) or plant sensitivity studies. These calculative results were generally used to confirm the adequacy of a chosen nodalization scheme.

#### 4.2.3 Loop Model

The loop includes those components outside the reactor vessel, including the pressurizer and ECCS. All loops are modeled individually (i.e., the unbroken loops are not lumped into a single combined loop). Each loop models the hot leg piping, steam generator primary and secondary fluid volume and heat transfer, pump suction piping, and pump discharge cold leg piping. Each loop also contains modeling of the accumulator, and high- and low-pressure injection ECCSs. The nodalization scheme is presented in Figure 4.1 for a sample loop with the pressurizer.

The following are key features and assumptions for the reactor coolant loops.



- The nodalization detail for the coolant loops, pressurizer, and primary and secondary sides of the steam generators was selected to give consistent results.

Assessment of loop nodalization comes from various facility test programs, including SCTF, CCTF, LOFT, Semiscale, and UPTF. In addition, the Westinghouse/EPRI 1/3 Scale Steam/Water tests, a separate-effects test examining ECC mixing in the cold leg, is also a useful assessment. Acceptance of nodalization schemes was based on the general agreement in code/data comparisons for pressures, differential pressures, mass flow rates, and heat structure temperatures.

#### 4.2.3.1 Hot Leg

The hot leg connects the reactor vessel to the steam generator inlet plenum. [

] The entrainment of droplets from the reactor vessel will enhance the effect of steam binding, which inhibits reflood. Code-to-data comparisons of tests performed at the CCTF and the UPTF (Sections 4.3.1.12 and 4.3.1.11.3, respectively) show that S-RELAP5 predicts entrainment between the reactor vessel and the steam generator inlet plenum accurately to a slight overprediction. This is acceptable because the result will be a reasonable to slightly conservative simulation of steam binding and its impact on cladding temperature.

#### 4.2.3.2 Steam Generator

The steam generator nodalization scheme is essentially identical to the traditional approach used by other large thermal-hydraulic codes such as TRAC and RELAP5 (References 4 and 21, respectively). [

]

The dominant phenomena of importance are the steady-state heat balance and steam binding during reflood. Heat balance is ensured by the use of control systems controlling feed water and steam flow depending on steam generator inventory. Benchmark simulations of the CCTF tests (Section 4.3.1.12) showed S-RELAP5 conservatively estimates the steam binding effect in the steam generator tubes. Therefore, the nodalization scheme is acceptable.

#### 4.2.3.3 Pump Suction

[

]

#### 4.2.3.4 Reactor Coolant Pump

The pump is a component model, meaning that the pump physics is independent of nodalization; hence, the primary objective of the nodalization scheme is to ensure consistency with the structural characteristics. [

]

#### 4.2.3.5 Cold Leg and Break

The cold leg extends from the RCS pump discharge to, and including, the reactor vessel inlet nozzle. [

] The break model is either a double-ended guillotine with discharge from both cold leg volumes or a split with discharge from both cold leg volumes. The difference between the guillotine and the split is that the flow path between the two cold leg volumes at the break plane is preserved for a split break and closed for a guillotine break. The noding configuration for the two break types is shown in Figure 4.3. [

]

Condensation driven by the cold ECCS water coming in contact with steam is also a primary phenomenological concern for cold leg modeling. This parameter was identified as a key uncertainty parameter for RLBLOCA and any nodalization dependence is absorbed within the assessment that quantifies this uncertainty.

#### 4.2.3.6 ECCS

The ECCS includes models for the accumulator and the piping connecting it to the RCS with sufficient detail to allow the code to accurately predict coolant flow splits for low-pressure injection flows. Figure 4.1 includes a typical nodalization for the ECCS of a three-loop plant. The accumulators are the dominant component in the ECCS. [

]

The dominant phenomena of importance are the accumulator liquid discharge, the pumped injection rate, and the noncondensable gas transport following accumulator liquid discharge. Activity in the accumulator lines can be characterized as a period of single-phase incompressible flow (accumulator water discharge) followed by a two-phase mixture; nitrogen from the accumulator and water from the low pressure injection system. Noncondensable gas transport to the cold leg can continue for several seconds after the end of liquid discharge and may, for some events, be limited by critical flow. The nitrogen in the accumulator will transport from the accumulator to the RCS by gas expansion and pressure forces. Dissolved nitrogen will come out of solution as the system pressure decreases.

#### 4.2.3.7 Pressurizer

The pressurizer vessel is modeled with [

] The dominant phenomena of interest are early lower core quench and critical flow in the surge line. Neither phenomenon shows much sensitivity to nodalization

because the surge line remains choked during the period in which these concerns are important (blowdown).

#### 4.2.4 Reactor Vessel Model

The key components of the reactor vessel are the downcomer, lower head and plenum, core, and upper head and plenum. The nodalization is presented in Figure 4.4. The key features and assumptions for the reactor vessel are:



##### 4.2.4.1 Downcomer

The reactor downcomer is modeled using [

]

For asymmetric cold and hot leg connections to the reactor vessel, the only practical nodalization option is [

]

The dominant downcomer LBLOCA phenomena (condensation, hot wall effects, multi-dimensional flow, CCFL, and entrainment) affect the refill period. These phenomena primarily influence the duration of ECCS bypass. The hot wall effect is conservatively treated by forcing nucleate boiling for any portion of the downcomer in contact with water.

The UPTF Test 6 (Section 4.3.1.11.1) experiments investigated the countercurrent flow of steam, reactor coolant and ECC water in the downcomer during the refill phase for a 4-loop PWR LOCA and were used to validate the downcomer nodalization.

A downcomer noding sensitivity study was also done on a 4-loop plant model. The base modeling comprises [

]. The

conclusion from the study was that the lower plenum refill is relatively insensitive to downcomer nodalization for uniform ECC water injection into all intact loops.

[

] This improvement to the axial and azimuthal noding density gives a well converged model of the downcomer, which captures relevant geometric features.

#### 4.2.4.2 Lower Vessel

The lower vessel includes all volumes [

]



- [

]

The dominant nodalization-influenced LBLOCA phenomena of importance are liquid sweep-out and steam water mixture content as the plant approaches the bottom of core recovery. The nodalization of the lower vessel region is shown in Figure 4.4. As demonstrated in the UPTF Test 6 assessment (Section 4.3.1.11.1), the calculation of the sweep-out phenomenon is conservatively overpredicted.

#### 4.2.4.3 Core, Core Bypass, and Fuel

The core region extends from the bottom of the active core to the top of the upper core support plate. [

]

The most important contributor to nodalization sensitivity is expected to be core nodalization because it directly affects the liquid distribution in the core. The key phenomena of importance influenced by nodalization are the heat transfer modes, entrainment/deentrainment, multi-dimensional flow, stored energy, oxidation, core power distribution, and decay heat. Since the heat transfer modes, entrainment/deentrainment, hot region power, decay heat and stored

[

AREVA NP Inc.

#### 4.2.4.4 Upper Plenum/Upper Head

The upper plenum region extends from the top of the upper core support plate to the core support ledge in the vessel wall (the bottom of the upper head wall). [

]

The dominant phenomena of importance are entrainment/deentrainment, fallback (CCFL), and upper head temperature. The entrainment phenomenon is considered in the same manner as it was for the hot legs. The upper head temperature is treated statistically. [

] This configuration captures the preference for fallback to colder assemblies as demonstrated in the plant sample problems (Appendix B), showing a general conservatism in the treatment of liquid fallback.

In many plants, flow asymmetry into the upper plenum can exist. Flow can either travel directly into the upper plenum or be forced through a support column or mixer vane nozzle and then deposited in the middle of the upper plenum. [

] The configuration is necessary to allow for the possibility that the hot assembly is beneath a standpipe or mixer vane nozzle. For

plants without mixer vane nozzles, only a single TOODEE component (again with a 3x3 geometry) is employed.

#### 4.2.5 Containment Model

Nodalization of the containment for the RLBLOCA is defined in a separate input file from the normal S-RELAP5 input. The containment model input is equivalent to the input used for the ICECON code (Reference 14), which is the AREVA proprietary version of the CONTEMPT code (Reference 19). ICECON was incorporated as a routine in S-RELAP5. The S-RELAP5 input file contains a link between the S-RELAP5 input and the ICECON input. [

] S-RELAP5 drives the containment calculations with mass flow and enthalpy, and the ICECON subroutines return containment pressure and temperature to update the S-RELAP5 time-dependent volumes.

Because the ICECON model provides only containment pressure and temperature for S-RELAP5, a simple model is adequate. For a dry containment, the ICECON model is a single volume representing the containment space within the inner steel liner. This simple model is also used for annular or sub-atmospheric containments. For an ice condenser containment, the model has four volumes: (1) the lower compartment containing the reactor primary coolant system; the upper compartment containing the refueling channel, (2) refueling equipment and polar cranes; (3) the ice chest containing borated ice for condensing steam discharged to the containment; and (4) the dead-end volume containing the auxiliary pipe tunnel, the fan accumulator compartments and the instrument room.

The dominant parameter of interest related to the containment model is containment pressure. The goal of the modeling is to provide a reasonable prediction that remains responsive to the industry held perception that lower containment pressures increase steam binding and restrict the reflooding process by imposing higher steam specific volumes. Three modeling concepts assure this:

1. The heat structure modeling is in line with the recommendations of NUREG-0800 Branch Technical Position 6.2 (Reference 16). This assures that the interior heat absorbing structures are modeled with recognition of the probable best-estimate characterization.

2. The containment condensing heat transfer is a practical bound of benchmark data for ten experiments. Although the benchmarks were conducted using GOTHIC (Reference 68, Figure 5-42, page 5-48), the result was the establishment of a benchmark data set for the condensing heat transfer coefficient to the Uchida correlation. [

]


3. The containment volume is treated statistically by ranging from its best-estimate value to the maximum possible free volume within the containment exterior walls. The free volume is a major determinant in establishing the containment pressure. This volume can not be larger than the volume within the outer containment walls. Because the volume within the outer walls is easy to compute, the use of this volume as an upper bound to the free volume assures that a reasonable-to-conservative volume is applied.

The combination of these three factors provides assurance that the containment pressure applied in the RLBLOCA calculation is conservative but not so much so as to seriously bias the results.

#### 4.2.6 Plant Model Summary

The nodalization described in this section was developed by applying the approach described in Reference 4. This nodalization development methodology was an iterative approach. The base nodalization originated through experience gained by RELAP5 users at the Idaho National Engineering Laboratory and by ANF-RELAP and S-RELAP5 users at AREVA. The nodalization was refined from both plant and code assessment tests, which used the same nodalization and modeling choices as in the full NPP model for those portions of the assessment model that would affect the phenomena being examined.

The uncertainty associated with the nodalization is considered minimal and is subsumed in the uncertainties determined for key LBLOCA parameters because, to the extent possible, the NPP nodalization was used in determining those uncertainties.



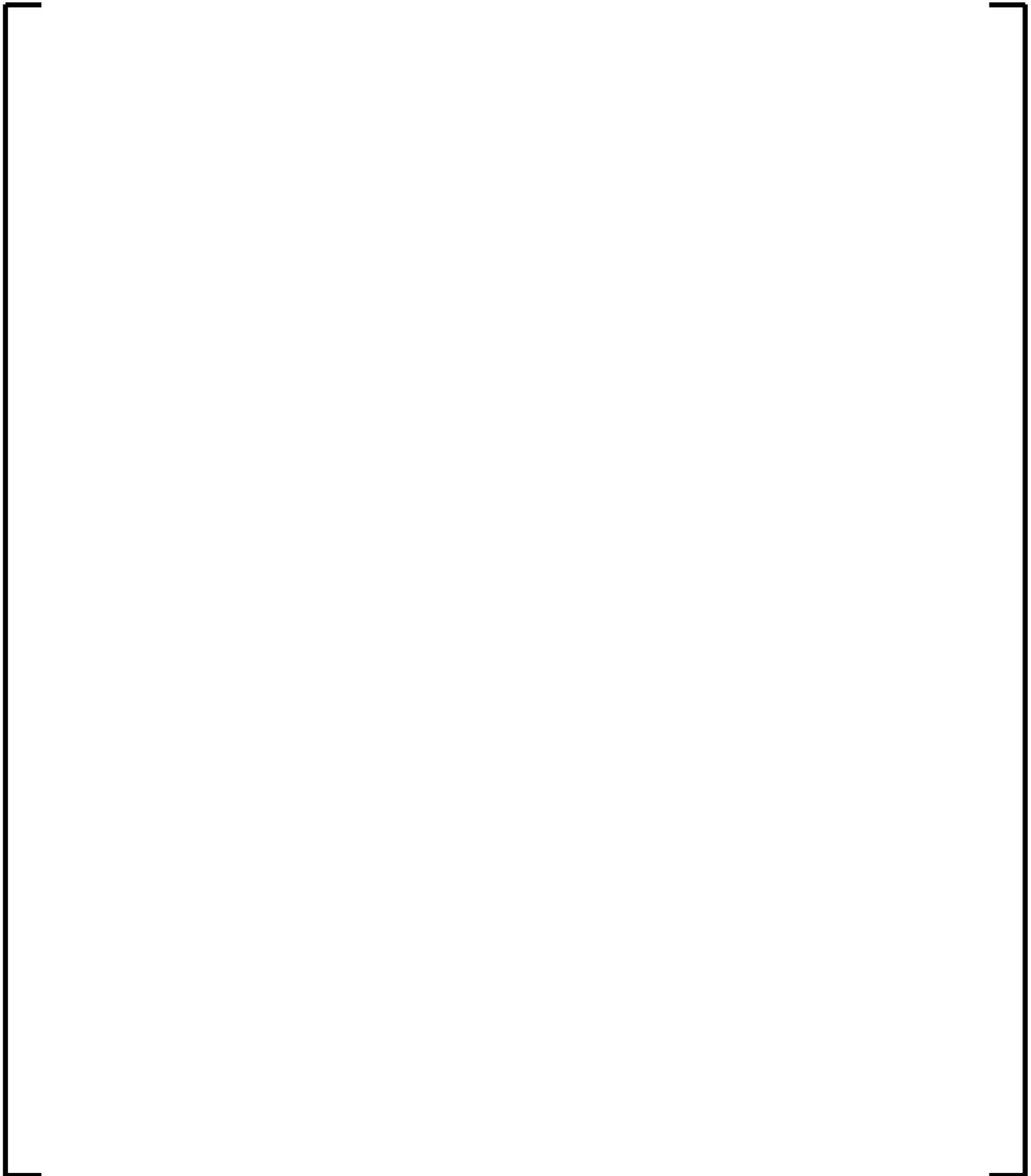


**Figure 4.1: Sample Loop Nodalization for NPP**

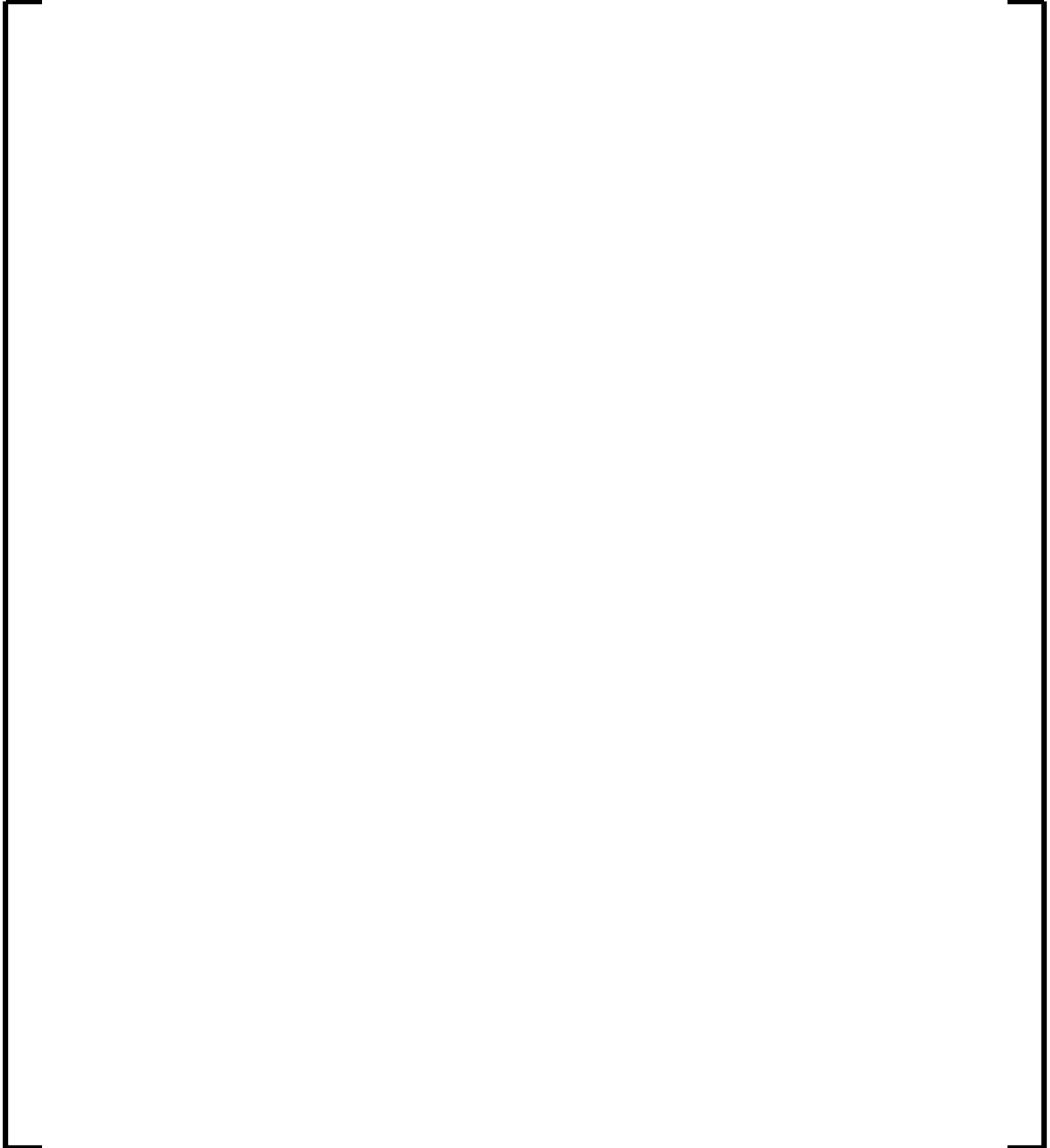


**Figure 4.2: Sample Steam Generator Secondary Nodalization for  
NPP**



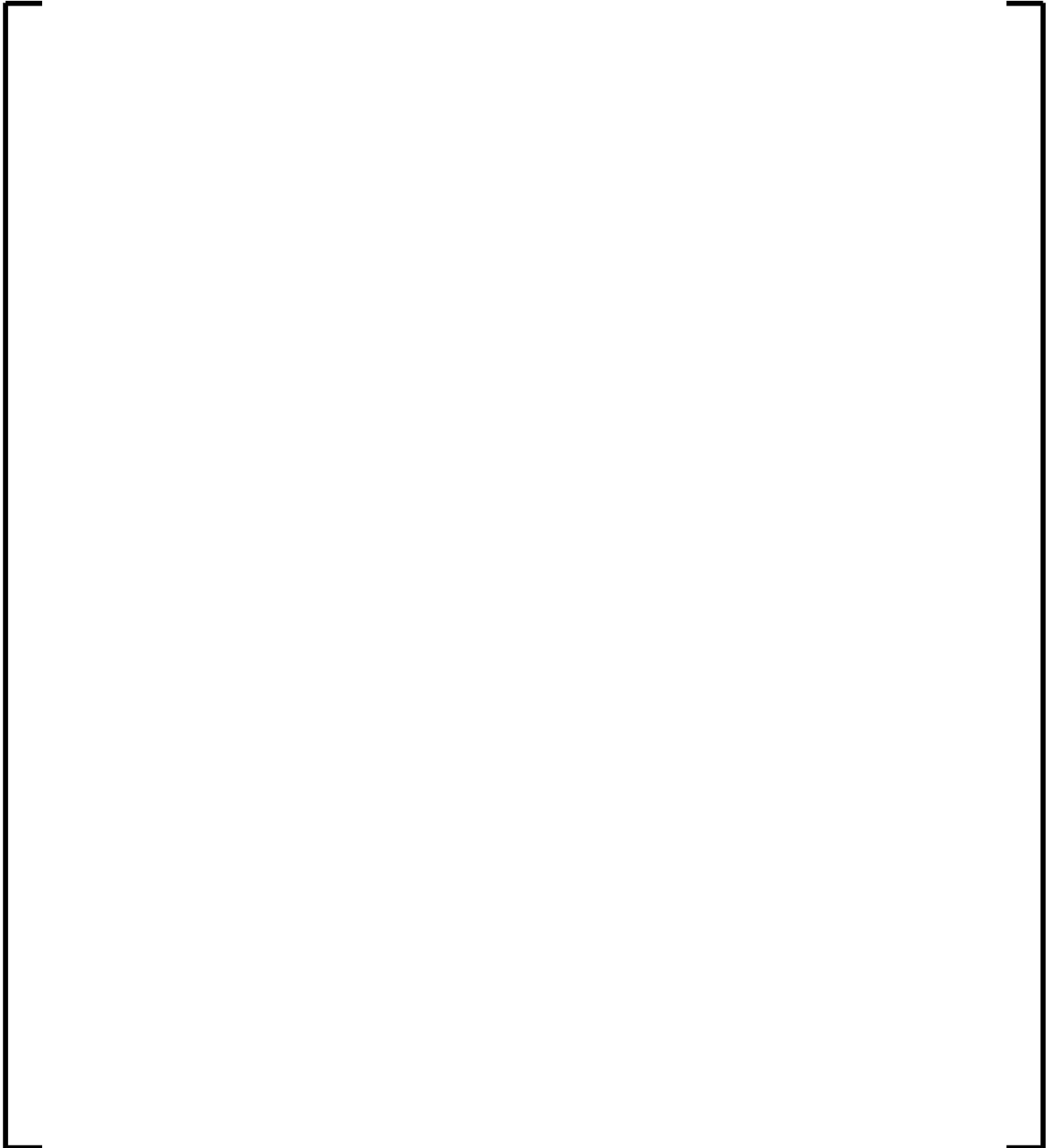


**Figure 4.3: Double-Ended Guillotine and Split Break Nodalization**

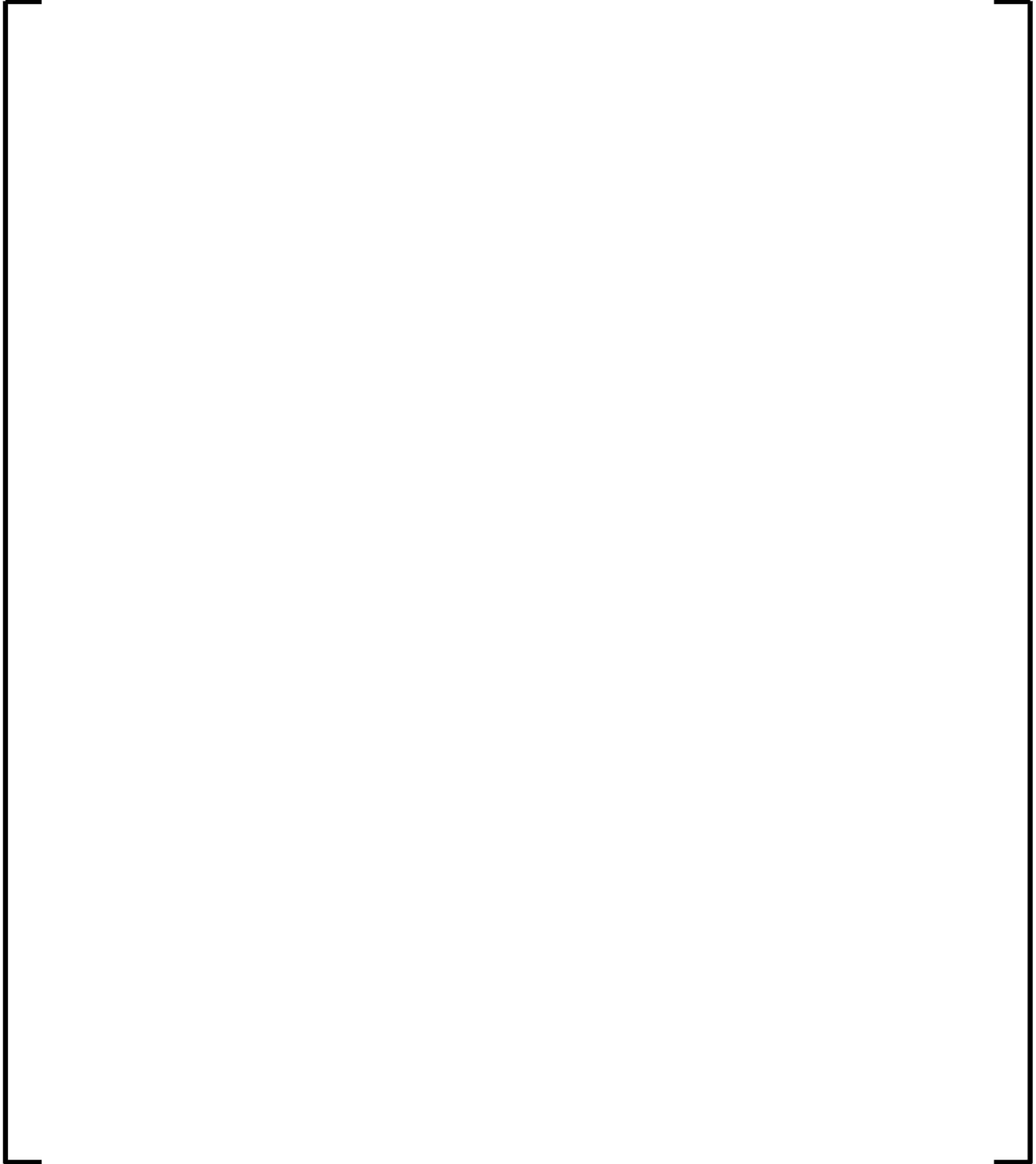


**Figure 4.4: Sample Reactor Vessel Nodalization for NPP**

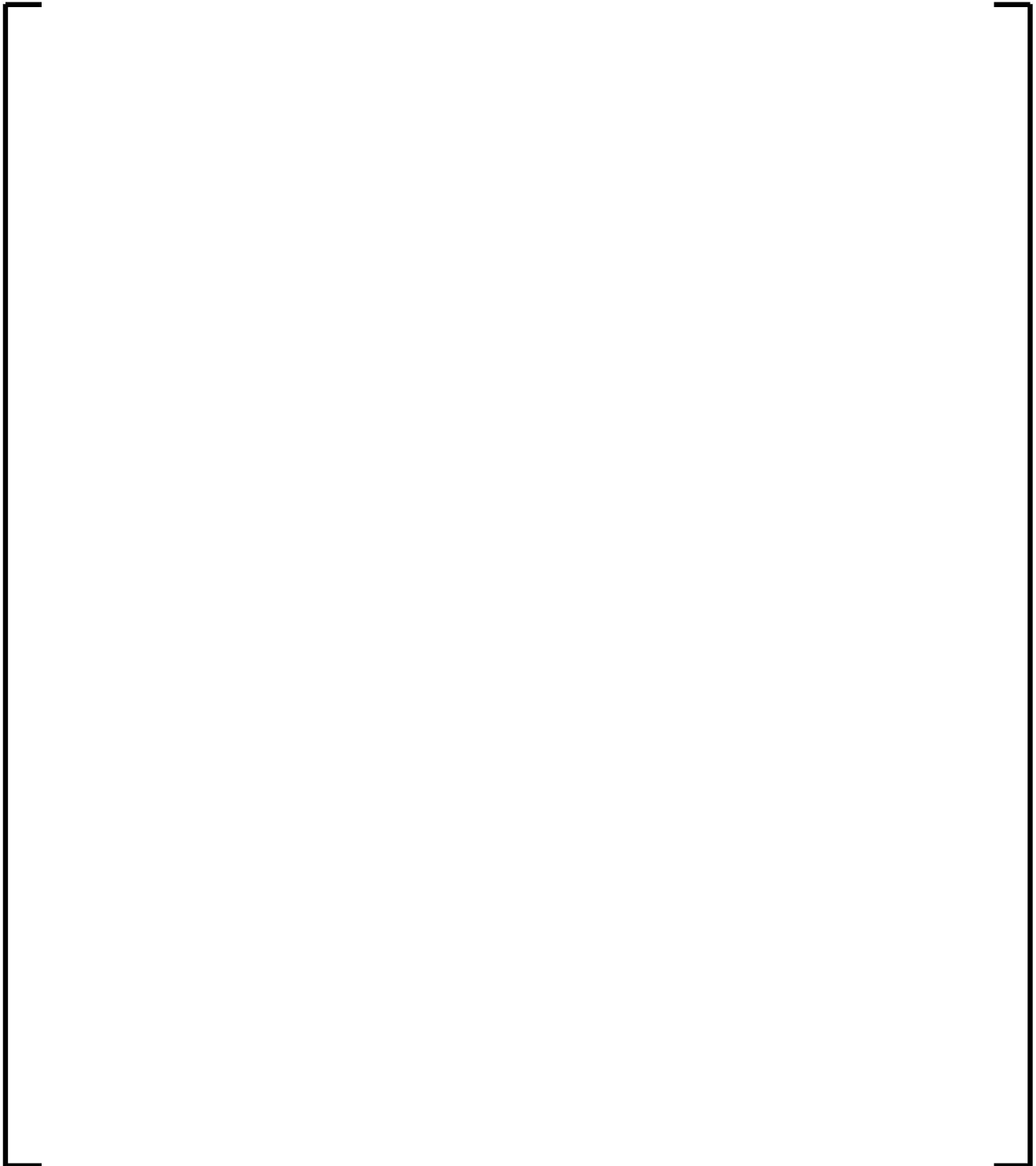


**Figure 4.5: Westinghouse/AREVA 3- and 4-Loop and CE 2x4 Plant  
Vessel Downcomer Configurations**

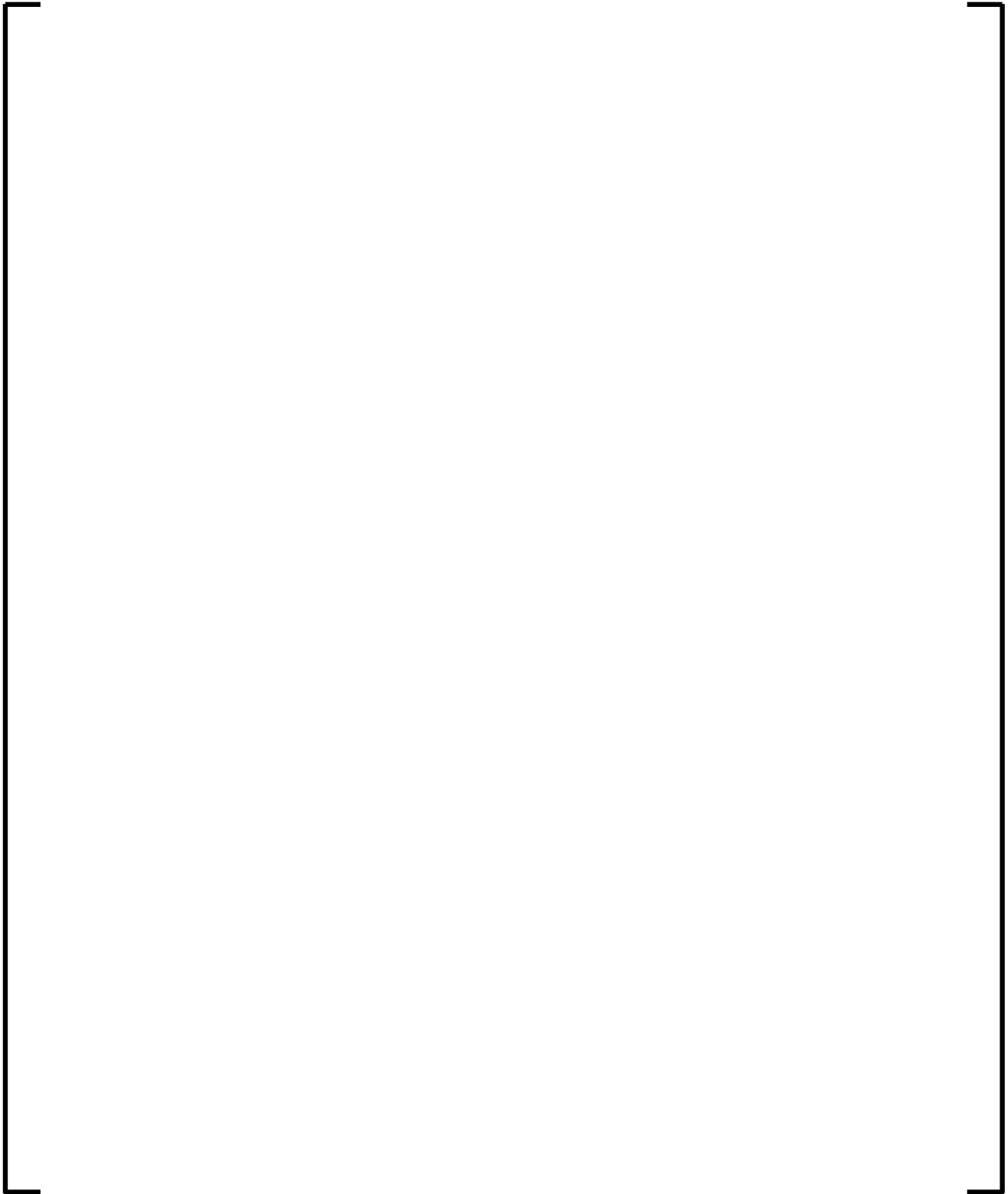


**Figure 4.6: NPP Core Nodalization**

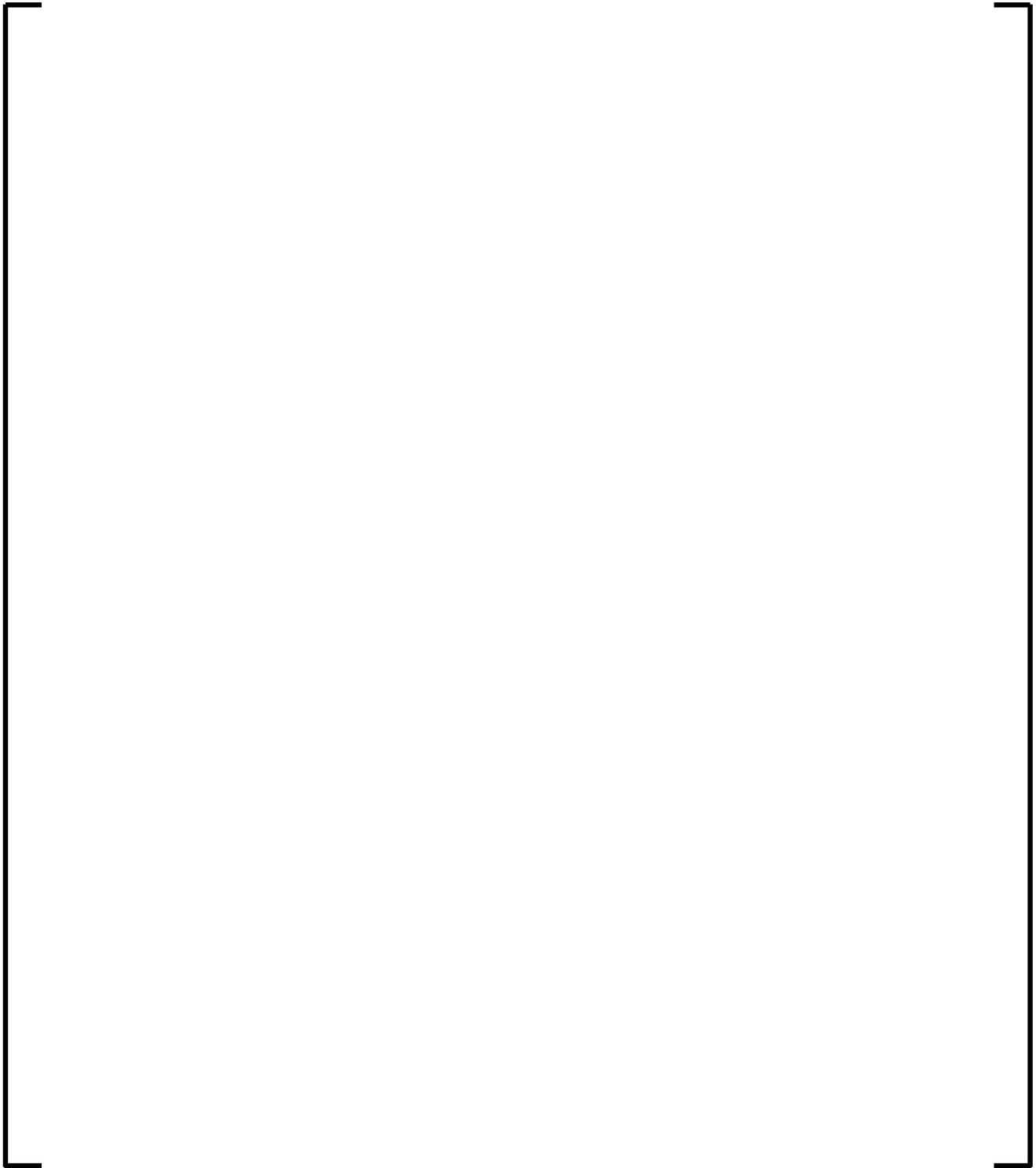


**Figure 4.7: Sample NPP Upper Plenum Nodalization – Axial Plane**

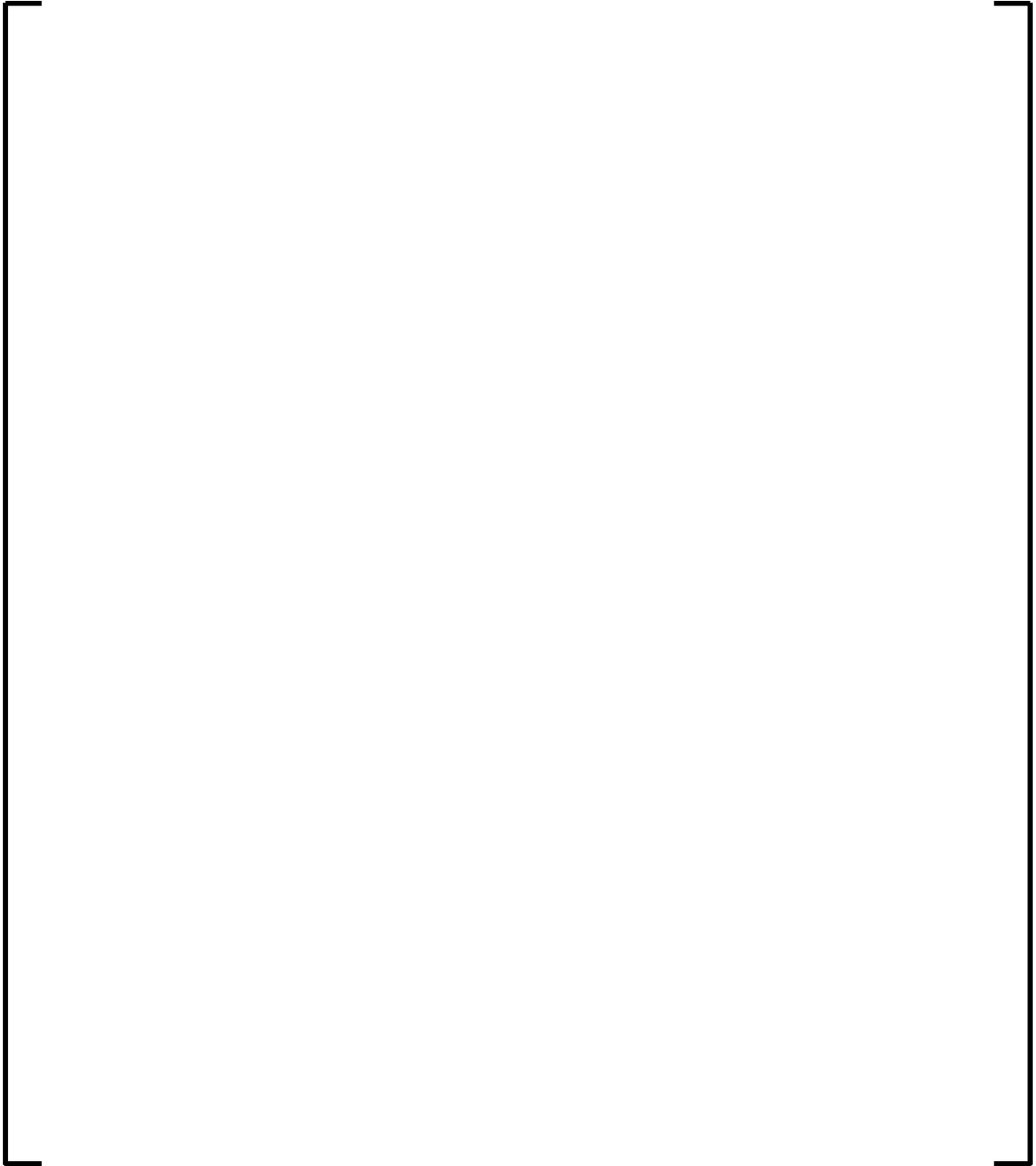


**Figure 4.8: Sample NPP Upper Plenum Nodalization –  
Cross-Sectional Plane**

#### 4.3 ***Determine Code and Experimental Accuracy (CSAU Step 9)***

This section provides the evaluation of the code assessments reported in Reference 5 with respect to the RLBLOCA methodology. The code assessments from Reference 5 applicable to the RLBLOCA methodology are those discussed in Section 4.1 and listed in the assessment matrix, Table 4.2. These assessments were chosen to address the important PIRT phenomena identified in Table 3.1. The cross correlation between assessments and PIRT phenomena is provided in Table 4.2. In addition, some assessments were chosen to address issues of code scalability; these assessments and the discussion with respect to scalability are provided in Section 4.4.

One purpose of the assessments is to determine the capability of S-RELAP5 to predict the important phenomena in large-scale PWR systems. Section 4.2 discussed the appropriate nodalization to represent PWR system components. For the assessment results to apply to large-scale PWRs, the nodalization used in the assessments must be consistent with the large-scale plant nodalization in the regions where the phenomena are being assessed. As far as possible, AREVA used the plant nodalization described in Section 4.2, Table 4.3, and internal S-RELAP5 input guidelines to derive assessment nodalizations which are consistent with the PWR application nodalization. However, unique features of small-scale facilities can require deviations from the guidelines. The detailed nodalizations for the experimental facility assessments are given for each assessment in Reference 5. For the most part, the assessment nodalizations are consistent with the plant application, and where deviations were made, the reasons for the deviations and the effects on results are discussed.

##### 4.3.1 Separate Effects Tests

SETs from numerous different facilities were used to assess the capabilities of the S-RELAP5 methodology to predict LOCA and transient phenomena. The detailed results comparing calculations against measured test data are given in the S-RELAP5 code verification and validation report, Reference 5. The SET assessments in Reference 5 also provide the information necessary to assess code capability for the RLBLOCA methodology. Detailed results from Reference 5 will be summarized herein with respect to the LBLOCA phenomena addressed. Table 4.2 shows the SET facilities, the tests selected, and the PIRT phenomena to be addressed.

#### 4.3.1.1 THTF Heat Transfer

The Oak Ridge National Laboratory (ORNL) thermal-hydraulic test facility (THTF) was used to perform numerous heat transfer tests using full-length electrically heated fuel rod simulators. The facility, tests, and assessments are detailed in Section 3.1 of Reference 5. The assessment tests consisted of numerous steady-state film boiling tests, transient boiloff tests, and reflood tests. [

]

The THTF is a high-pressure, thermal-hydraulic loop designed as a tool for heat transfer studies. The test section consists of a simulated fuel bundle placed inside a cylindrical pipe with inlet and outlet plena. There is no flow in the annular region between the test bundle and the test section barrel. The test bundle is, in terms of geometry, quite similar to an 8x8 segment of a Westinghouse 17x17 fuel design and is instrumented with a large number of thermocouples. The simulated fuel rods consist of a central heating element, thermocouples, and simulated cladding. The heating element is a nickel alloy, the electrical insulation is boron nitride, and the outer sheath is stainless steel.

The S-RELAP5 model for the THTF test bundle was a single rod with a flow channel and heat structures appropriate for single channel with volumes attached to the inlet and outlet to apply the flow, inlet temperature, and pressure boundary conditions. The model used 6 inch nodes since bulging and rupture are not an issue for these tests (they use heater rods to simulate the core). [

] Each of the test cases were evaluated using the appropriate boundary conditions associated with the test cases. The pressures ranged from 300 to 2100 psia.



[

]

Overall the results of the S-RELAP5 transient test predictions [ ] are acceptable. In the bulk of the cases, the uncertainties for the HTC bias were sufficient to make the data and the predictions agree. For reflood cases that had data outside the predicted range, the predictions by S-RELAP5 were conservative. [

]

The CHF bias developed in this analysis is applied to all RLBLOCA NPP calculations. The development of the bias and the uncertainty for post-CHF heat transfer is presented in Section 4.3.3.2.

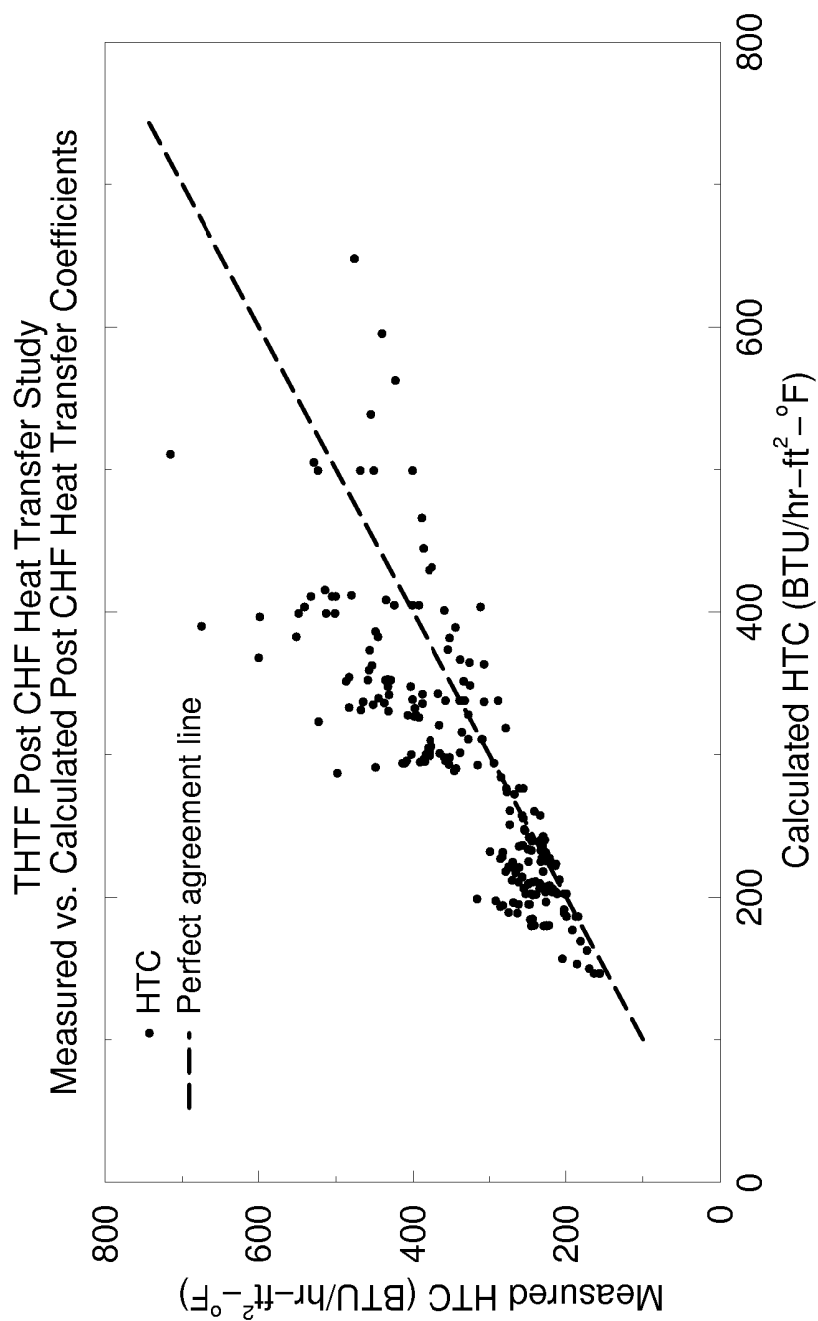


**Figure 4.9: Comparison of Calculated HTC to Measured HTC, ORNL THTF**

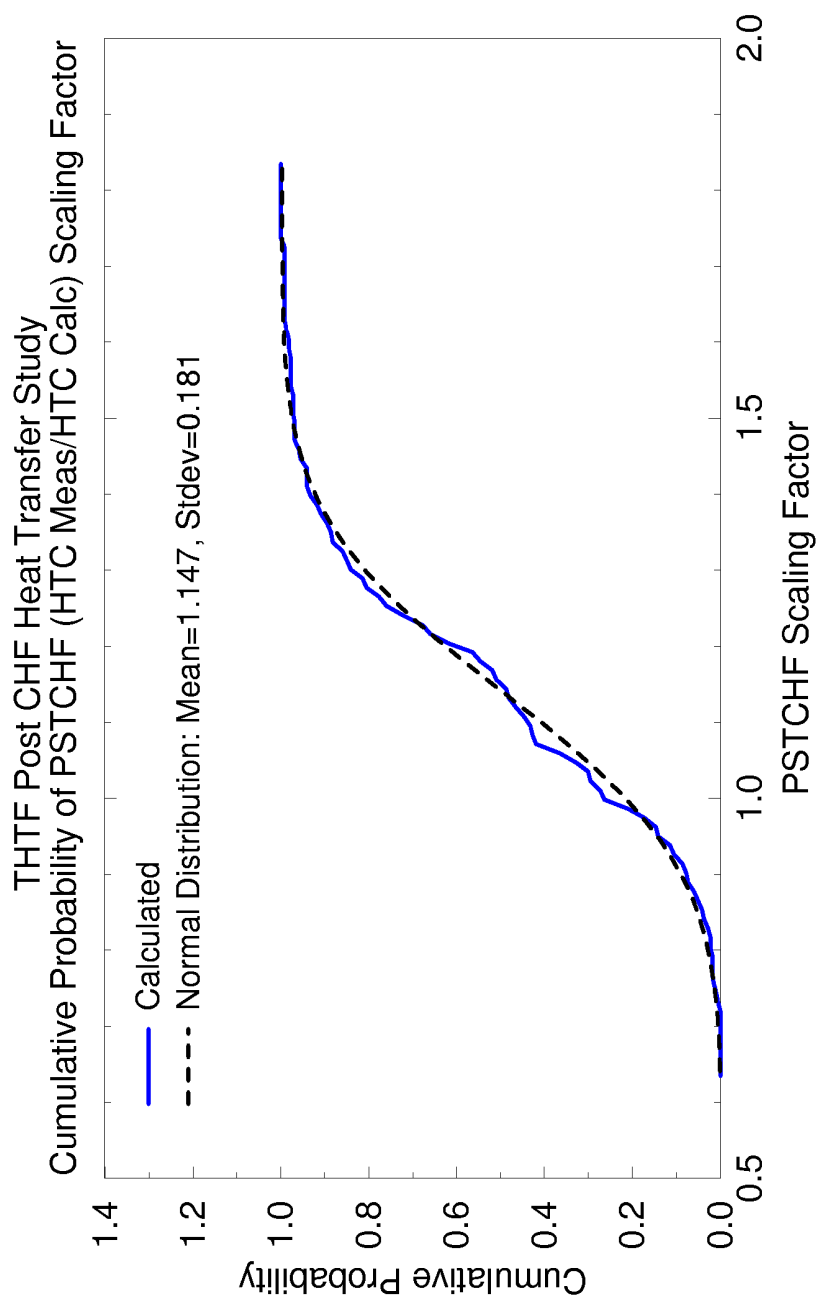


**Figure 4.10: Distribution for HTC Scaling, ORNL THTF**

#### 4.3.1.2 THTF Level Swell

Calculations for the ORNL THTF Level Swell Tests (3.09.10j, 3.09.10m, and 3.09.10dd) were carried out with S-RELAP5. Section 3.1 of Reference 5 presents the details of these assessments. This experiment is useful for assessing code performance in calculating subcooled boiling, interphase friction for slug flow, and interphase mass transfer in slug flow. The tests were performed at relatively high pressures; 609 psia for 3.09.10j, 1009 psia for 3.09.10m, and 1173 psia for 3.09.10dd. While these conditions typically occur during the boiloff period in small break LOCA, these tests provide additional assessment data for the slug flow regime in tube bundles and helps complete the range of applicability of S-RELAP5 to all pressures and temperatures. Furthermore, the transition logic between flow regimes, which is fundamentally the same under all conditions, is indirectly validated by the observed void fractions spanning the range from all liquid to all vapor. [

]

Comparisons between calculated and measured void fractions for the tests are shown in Figure 4.11 through Figure 4.13. The void fractions calculated by S-RELAP5 are generally within the data uncertainty with the exceptions occurring just before the abrupt change to 100 percent void. S-RELAP5 also tends to predict this level change slightly lower in elevation and slightly more rapidly than observed from the data.

In these experiments, the dry-out location is determined by the mixture level elevation. Tests 3.09.10j and 3.09.10m both show good agreement with the measured level, Figure 4.11 and Figure 4.12 respectively, while Test 3.09.10dd, Figure 4.13, shows slightly lower than measured level. Also, the figures show that the onset of voiding is well predicted, especially at the lower pressures. Both of these results indicate there is little variation with pressure variation. Overall, the results show that S-RELAP5 is in good agreement with the data and, therefore, acceptable.

In summary, the simulation of THTF Level Swell tests using S-RELAP5 demonstrates that the code will calculate proper void distributions in the slug flow regime occurring in tube bundles.

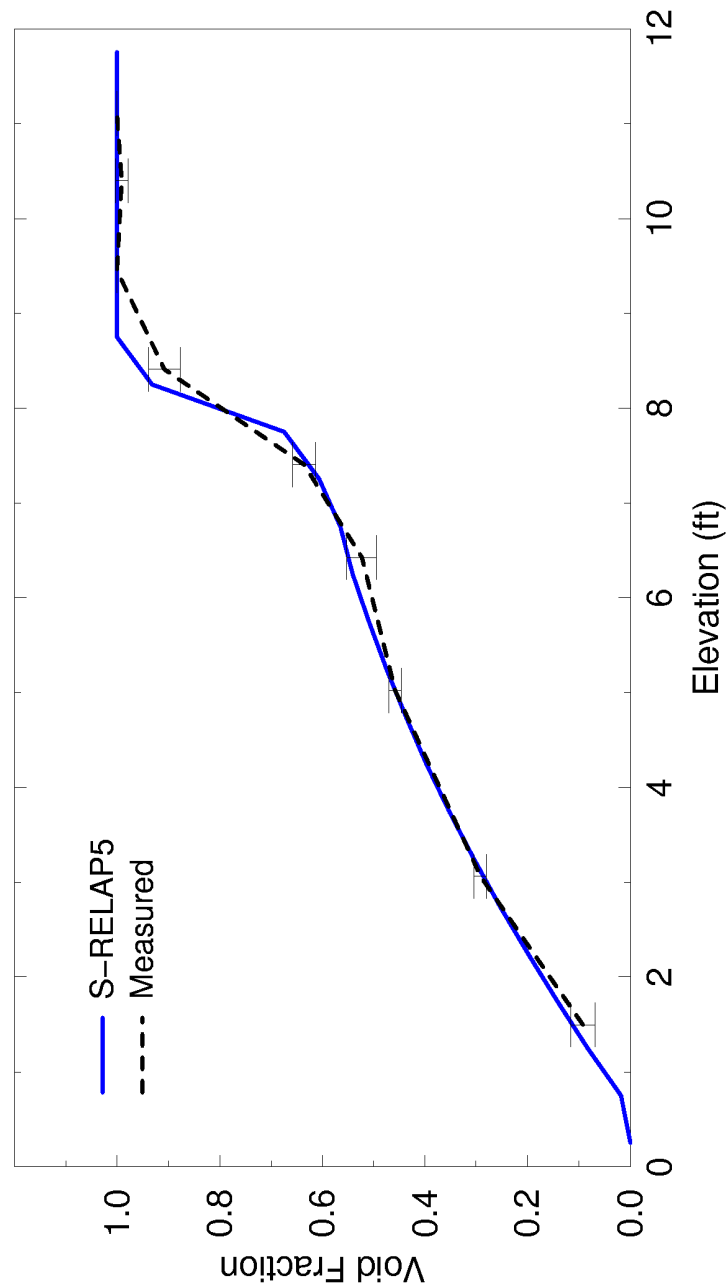


Figure 4.11: Comparisons of Void Profiles, ORNL THTF Test 3.09.10j

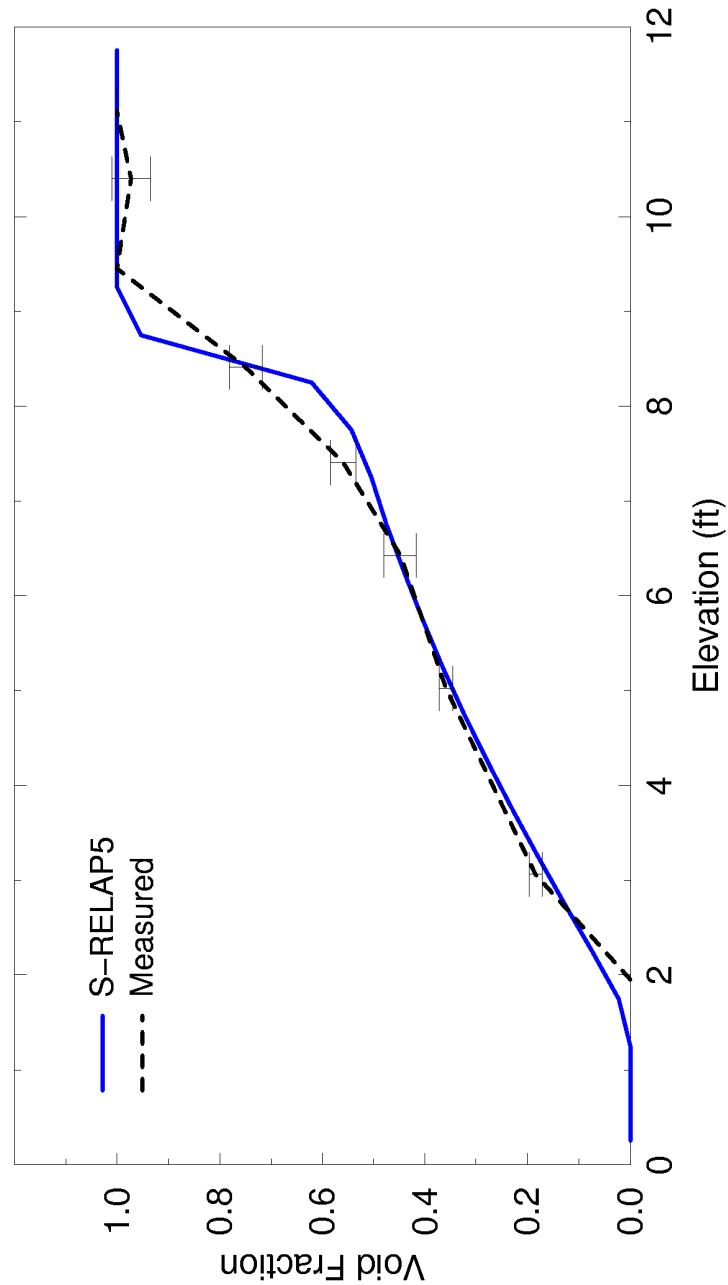
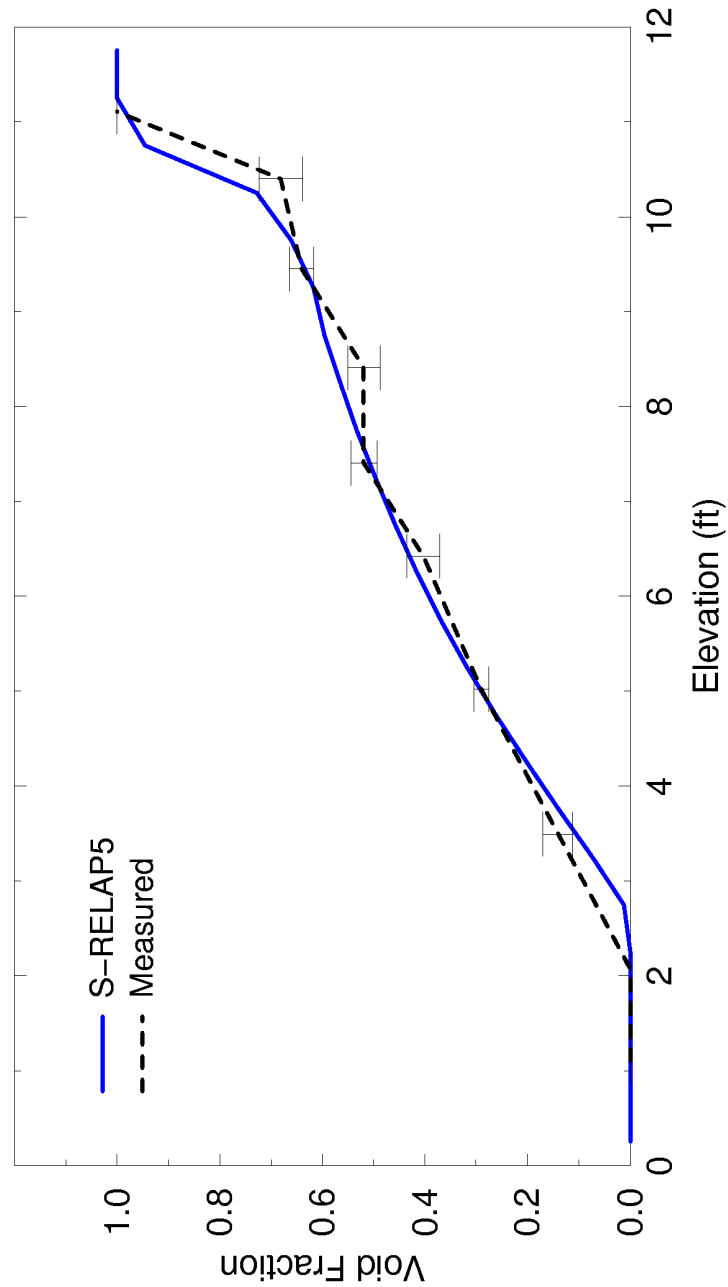


Figure 4.12: Comparison of Void Profiles, ORNL THTF Test 3.09.10m



**Figure 4.13: Comparison of Void Profiles, ORNL THTF  
Test 3.09.10dd**

#### 4.3.1.3 GE Level Swell

The GE Level Swell Test 1004-3 was simulated using S-RELAP5 to validate the interphase heat transfer and the interphase friction models for the bubbly and slug flow regimes. The test is essentially a small break blowdown of a vertical vessel 14 foot high by 1 foot in diameter. The vessel was initially pressurized to 1011 psi and filled with saturated water up to the 10.4 foot elevation. The void fraction distribution was measured axially in the test. This assessment provides a test of the two-fluid interphase models in predicting the flow regimes and void fraction distributions that occur under depressurization conditions.

Since the GE test facility is atypical of a PWR, a simple nodalization approach is used to model the facility. The test vessel is modeled using a 27 node PIPE component with an average node height of approximately 0.5 feet. A two-phase discharge (flow) coefficient of 0.7 is required to simulate the pressure response. Section 3.6 of Reference 5 provides details of the GE Level Swell test, the S-RELAP5 input model, and a discussion of results.

The purpose of this assessment was to validate some of the interphase heat transfer and interphase friction models in the bubbly and slug flow regimes. Comparisons of measured versus calculated void fraction distributions are made at two transient times, 40 and 100 seconds. Figure 4.14 and Figure 4.15 show the S-RELAP5 calculated void fraction results along with data at 40 and 100 seconds, respectively. It can be seen from these figures that, at both times, the S-RELAP5 calculated void distributions provide excellent agreement and are within the range of experimental uncertainty. The calculated flow regimes are bubbly flow below the void fraction of 0.25; slug flow from the void fraction of 0.25 up to the two-phase mixture level position (which occurs at around the void fraction of 0.3 to 0.6); and annular-mist flow (close to single-phase steam) above the mixture level. The results indicate, for this slow transient condition, the two-fluid interphase friction and heat transfer models implemented in S-RELAP5 are applicable.

The jump of void fraction from ~0.4 to ~0.99 within neighboring volumes distinctly defines the location of a two-phase mixture level. The interphase friction models for slug flow, vertical stratification, and annular-mist flow work in harmony to produce a smooth, but sharp transition from a low void fraction region to a high void fraction (close to 1.0) region.



In a non-equilibrium code such as S-RELAP5, the phase exchange (vapor generation) process during blowdown is calculated using flow regime dependent interphase heat transfer models. The calculated liquid and vapor (steam) temperatures are close to the saturation temperature. This shows that the interphase heat transfer submodels described in Section 3.4 of Reference 11, particularly those for the metastable state conditions, are appropriate and adequate for treating the depressurization phenomena.

In summary, the simulation of GE Level Swell Test 1004-3 using S-RELAP5 demonstrates the code will calculate proper void and fluid temperature distribution in bubbly and slug flow regimes in large diameter vertical pipes. The assessment validates the interphase heat transfer and the interphase friction models for the bubbly and slug flow regimes in S-RELAP5.

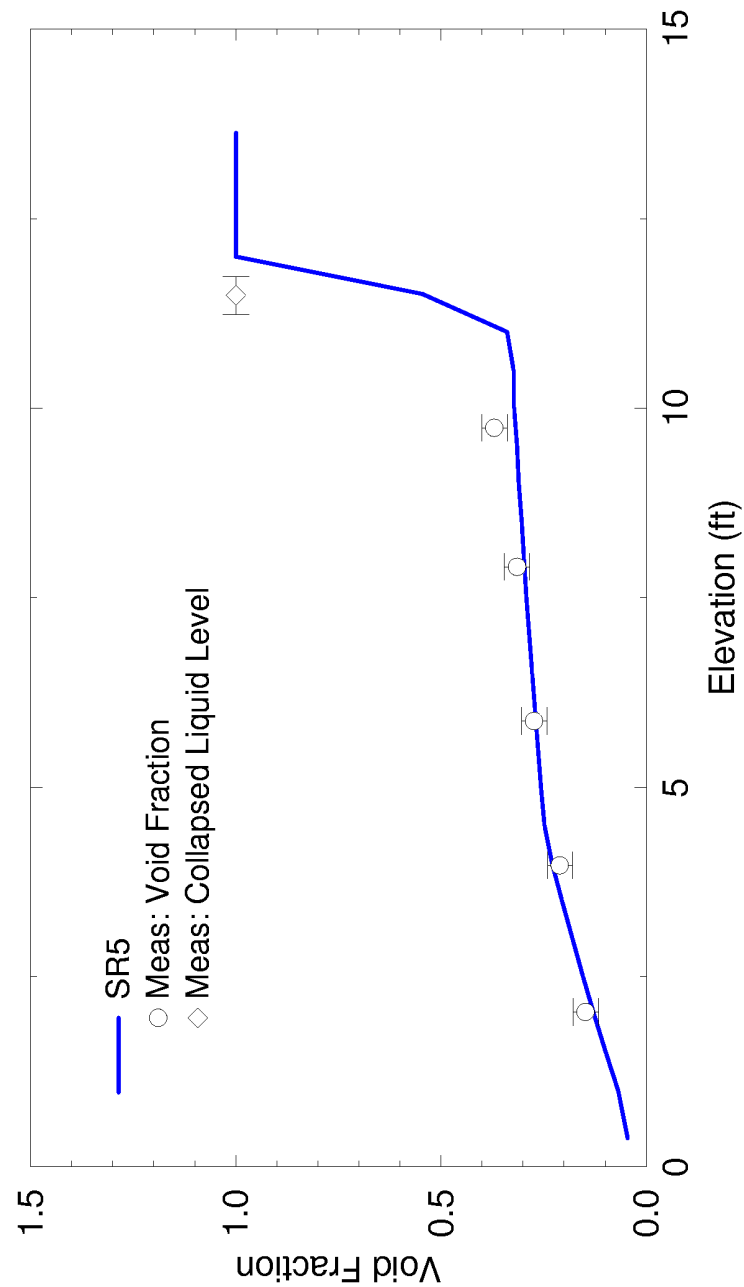


**Figure 4.14: Void Profiles at 40 seconds for the 1 foot GE Level  
Swell Test 1004-3**

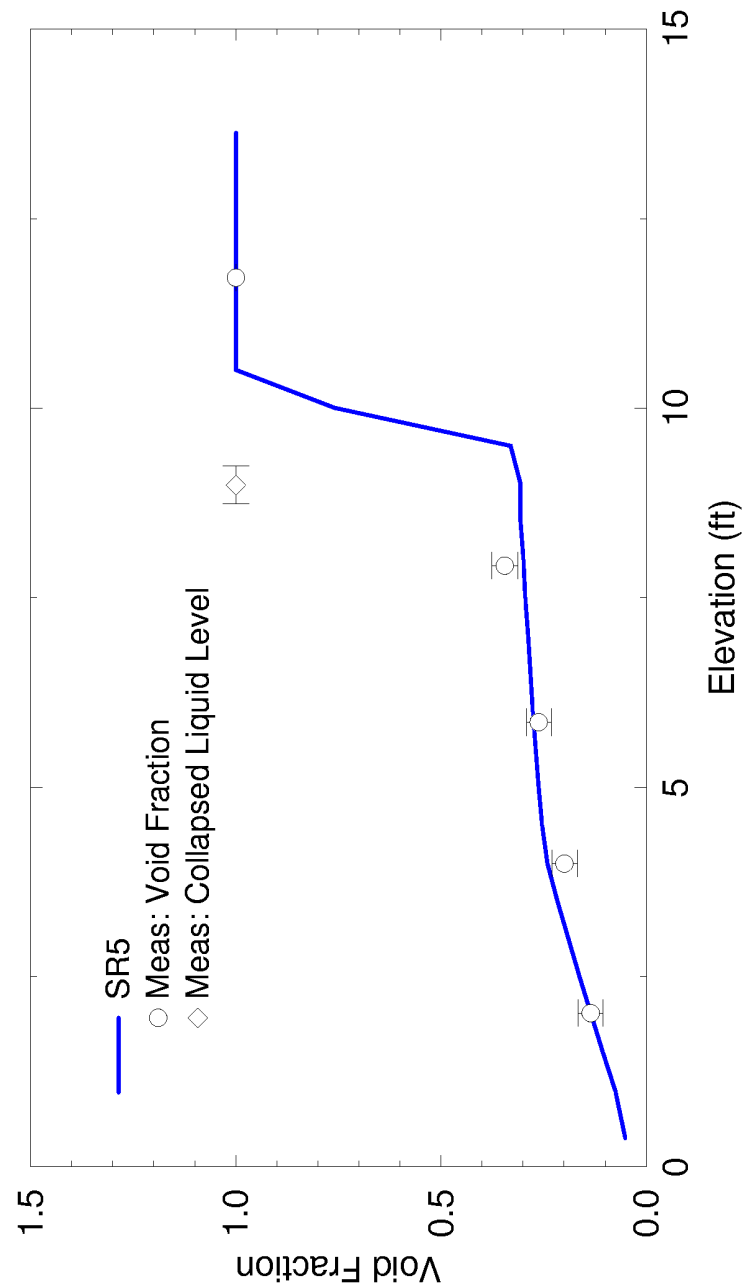


**Figure 4.15: Void Profiles at 100 seconds for the 1 foot GE Level  
Swell Test 1004-3**



**Table 4.4: Parameters, FRIGG-2 Void Distribution Experiments**

<b>Test Number</b>	<b>Pressure (bar)</b>	<b>Inlet Subcooling (C)</b>	<b>Heat Flux (W/cm<sup>2</sup>)</b>	<b>Mass Flux (kg/m<sup>2</sup>s)</b>
313001	49.6	5.0	22.0	1492
313003	49.6	2.6	22.0	1096
313004	49.8	3.7	22.0	1103
313005	49.8	3.7	22.0	1110
313006	50.0	3.7	22.0	729
313007	50.0	11.7	22.0	1110
313008	50.0	4.3	43.9	1471
313009	50.0	4.4	43.6	1107
313010	50.0	4.6	43.6	687
313012	49.7	4.2	20.9	1457
313013	49.7	4.6	42.9	1120
313014	49.7	11.0	42.9	1163
313015	49.7	11.0	42.7	1163
313016	49.6	19.3	42.6	1208
313017	49.6	2.4	64.4	1464
313018	49.7	3.7	64.3	1124
313019	49.5	8.6	64.3	1177
313020	49.7	22.4	64.6	1159
313024	49.7	4.2	21.6	858
313027	50.0	4.9	41.3	886
313030	50.0	5.1	66.7	823
313034	50.0	4.6	22.0	1012
313037	50.0	4.4	43.9	1026
313040	50.0	4.4	22.0	792
313043	50.0	3.5	43.9	823
313056	49.9	9.5	43.9	918
313060	49.4	10.5	21.5	792

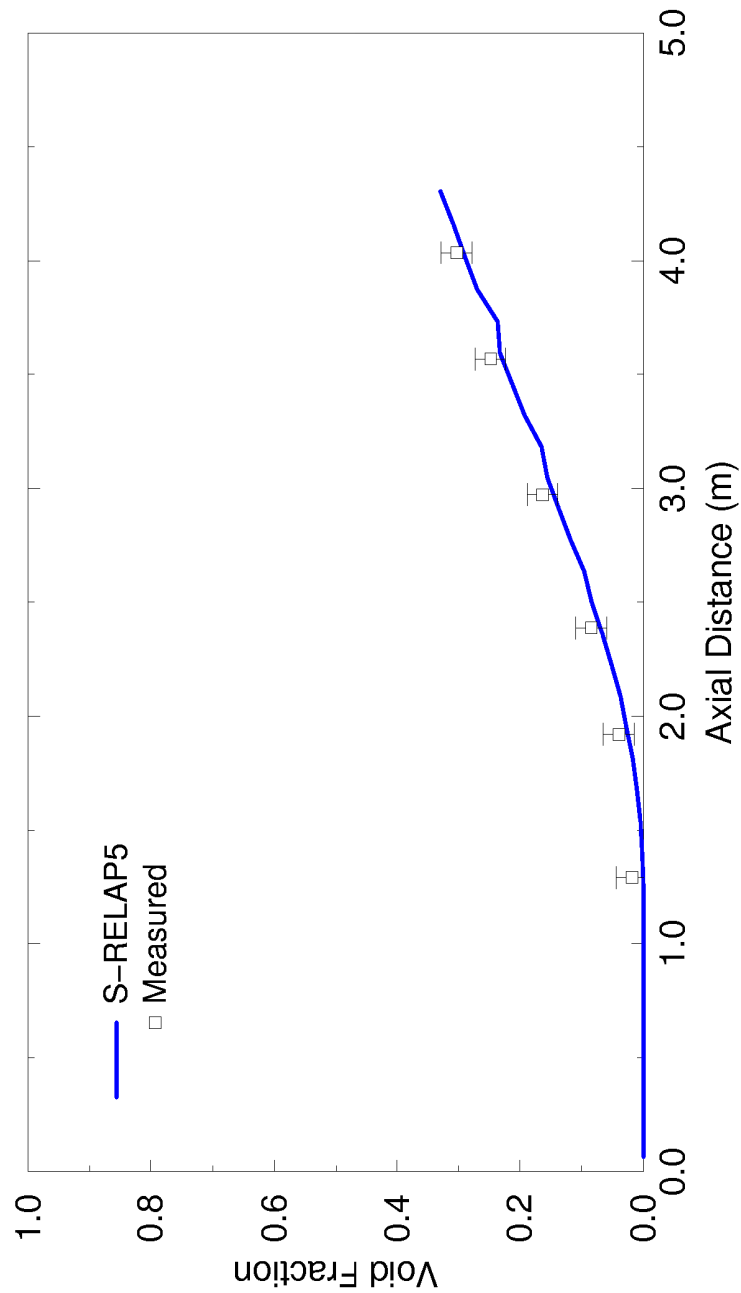


**Figure 4.16: Comparison of Calculated and Measured Void Fraction,  
FRIGG-2 Test 313007**

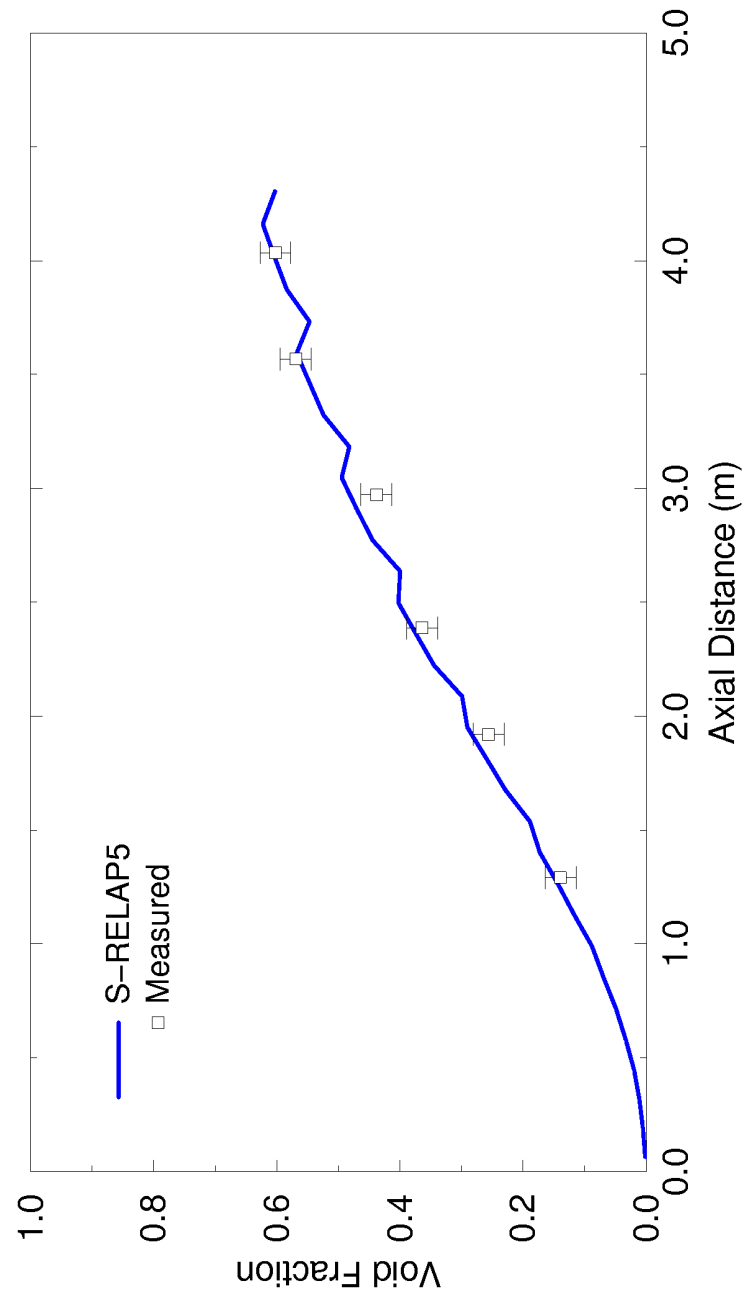


**Figure 4.17: Comparison of Calculated and Measured Void Fraction,  
FRIGG-2 Test 313014**

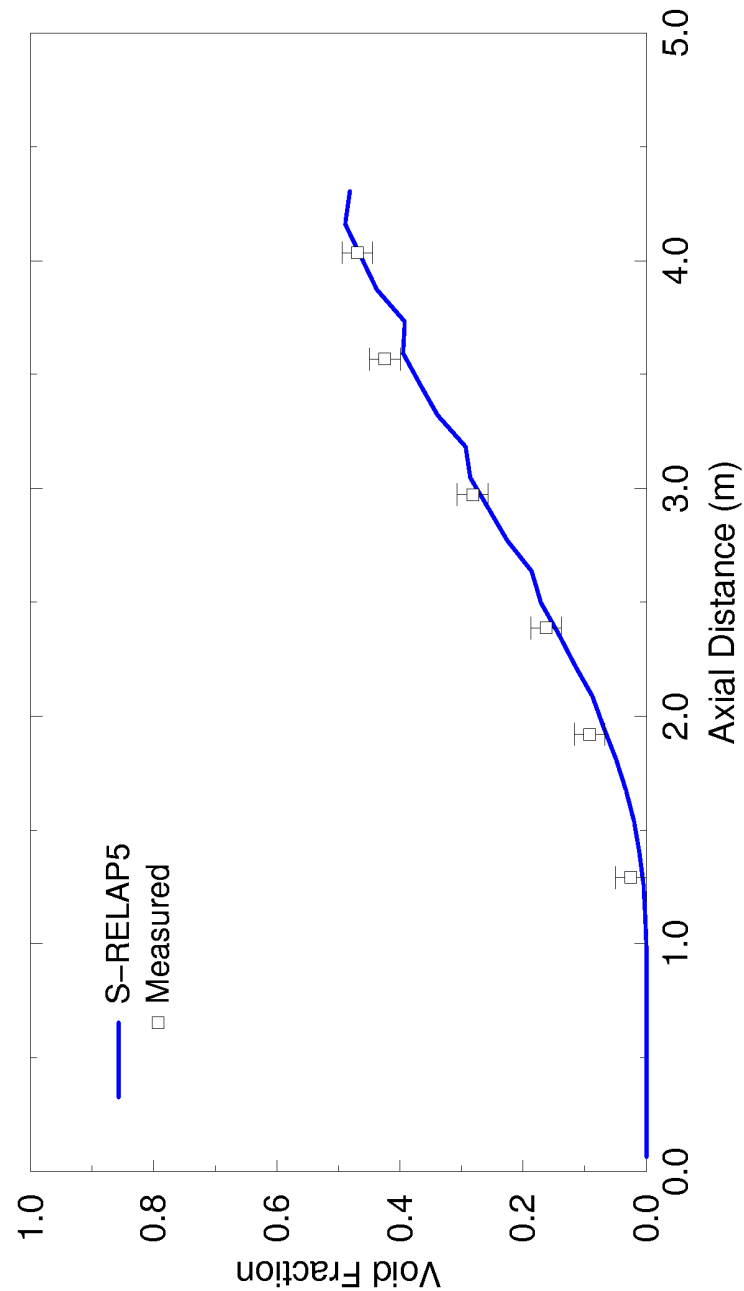


**Figure 4.18: Comparison of Calculated and Measured Void Fraction,  
FRIGG-2 Test 313016**



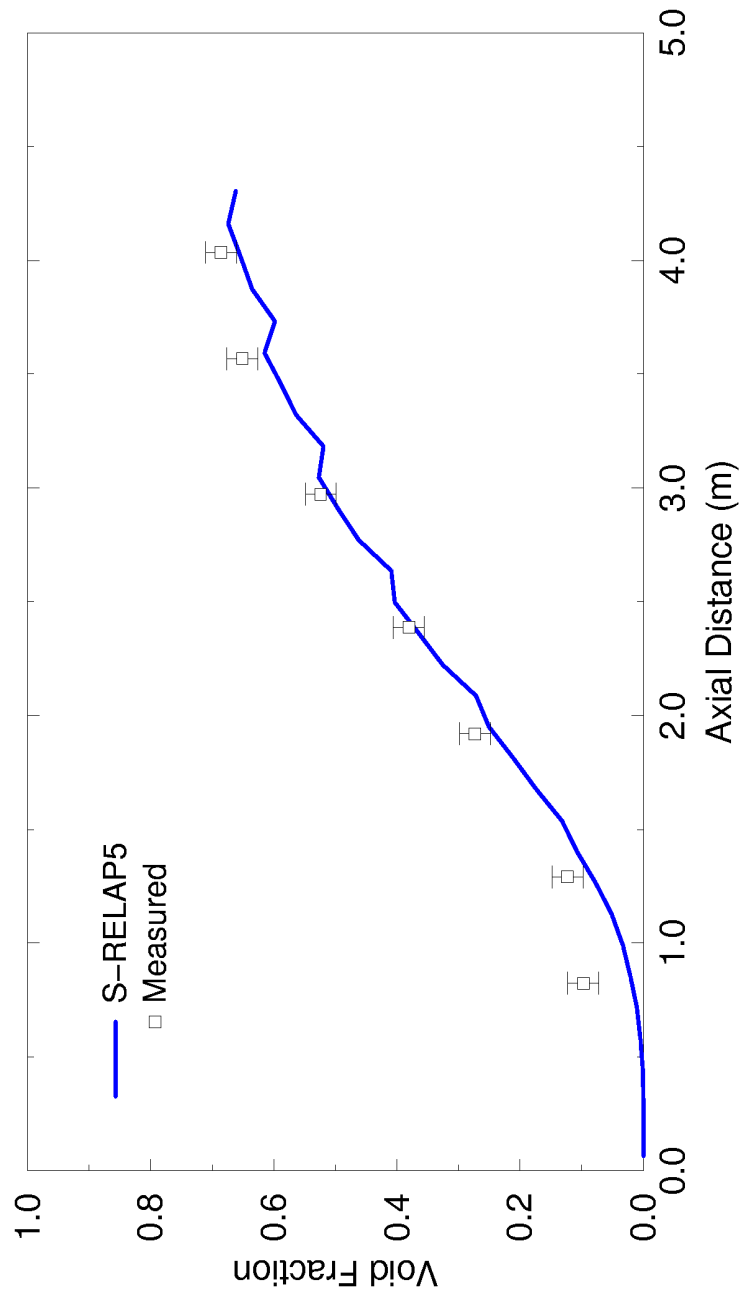


**Figure 4.19: Comparison of Calculated and Measured Void Fraction,  
FRIGG-2 Test 313020**

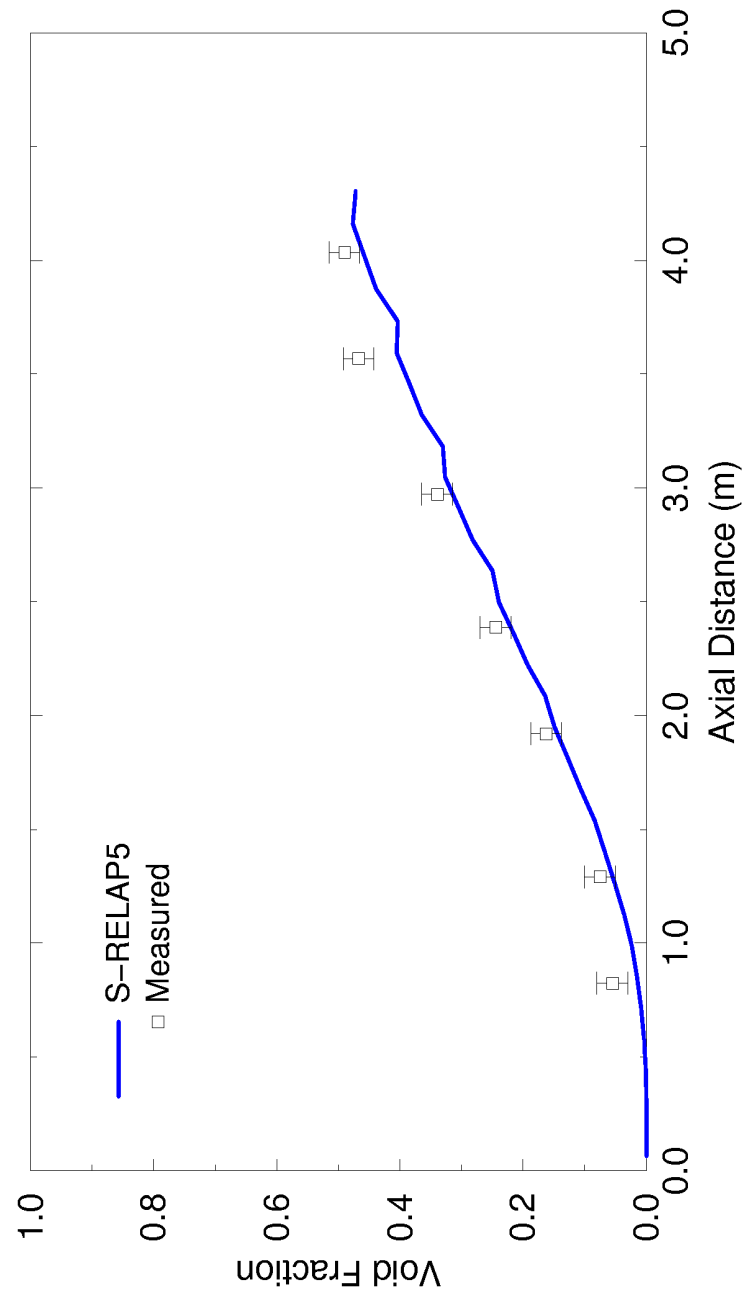


**Figure 4.20: Comparison of Calculated and Measured Void Fraction,  
FRIGG-2 Test 313060**

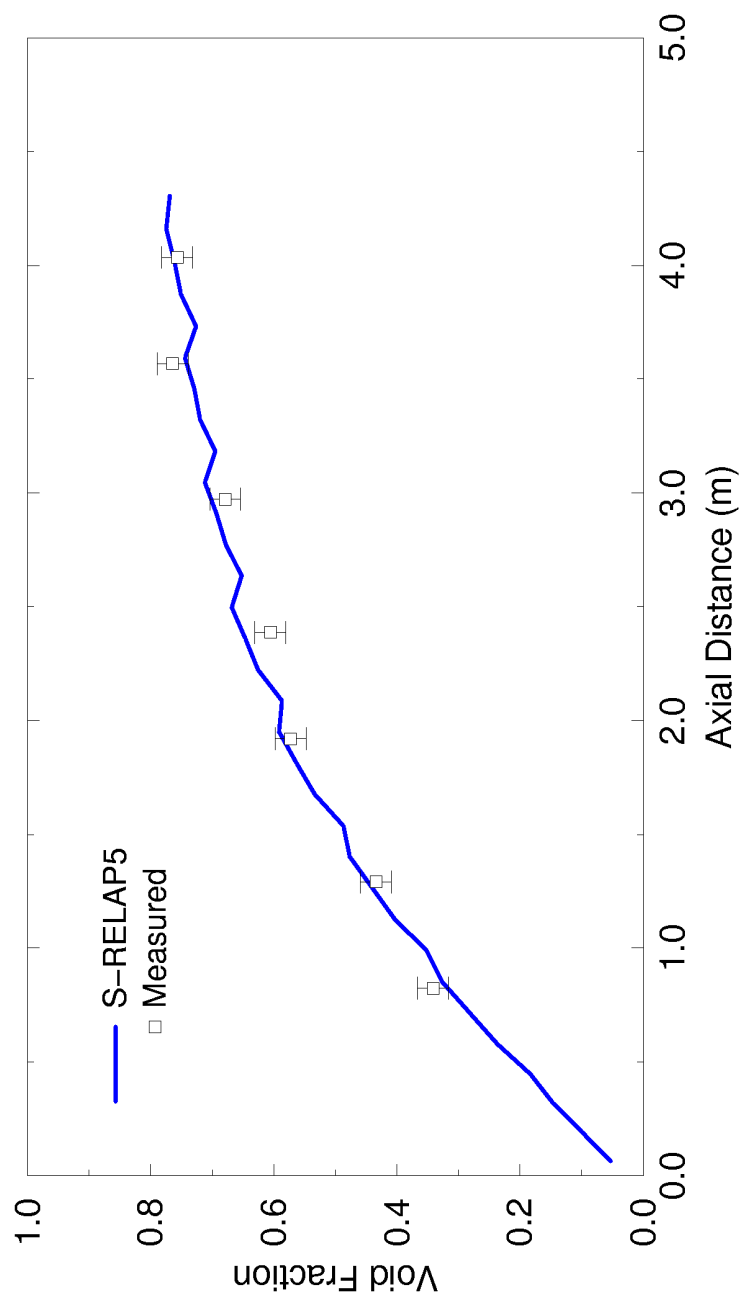


**Figure 4.21: Comparison of Calculated and Measured Void Fraction,  
FRIGG-2 Test 313010**

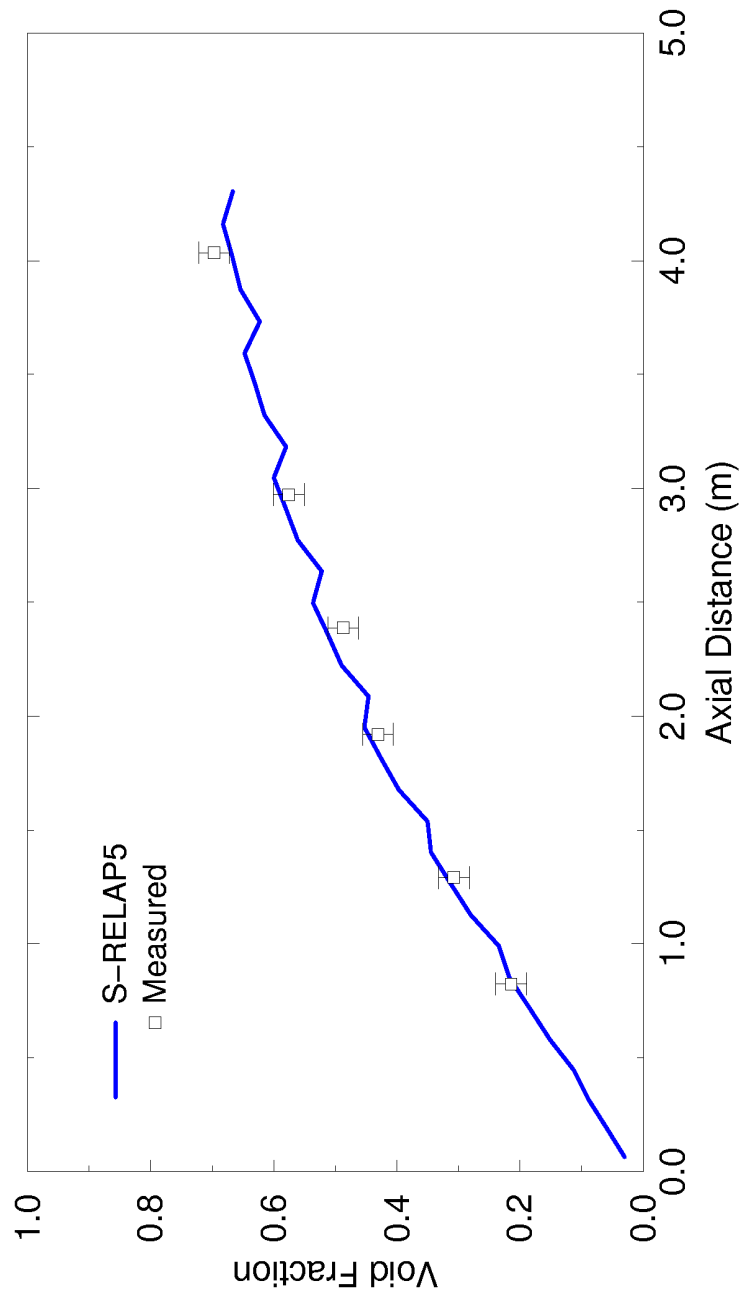


**Figure 4.22: Comparison of Calculated and Measured Void Fraction,  
FRIGG-2 Test 313013**

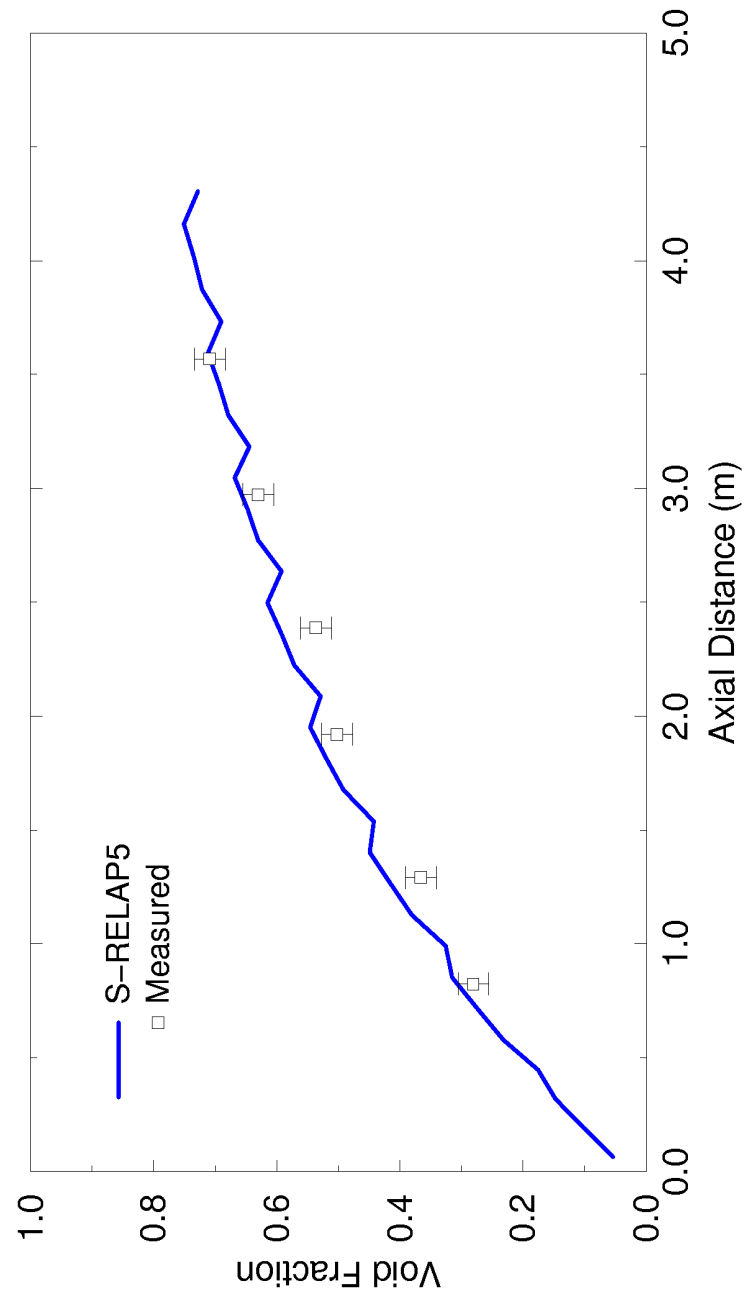


**Figure 4.23: Comparison of Calculated and Measured Void Fraction,  
FRIGG-2 Test 313017**

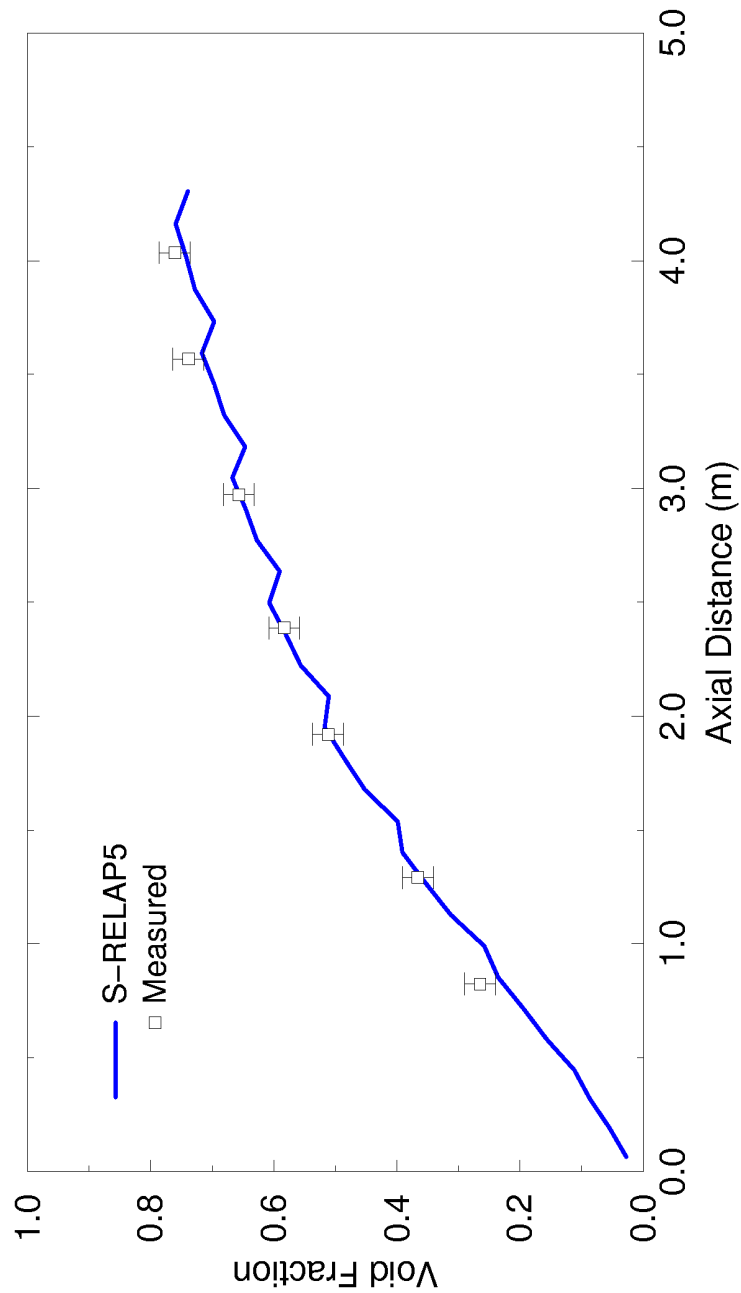


**Figure 4.24: Comparison of Calculated and Measured Void Fraction,  
FRIGG-2 Test 313019**

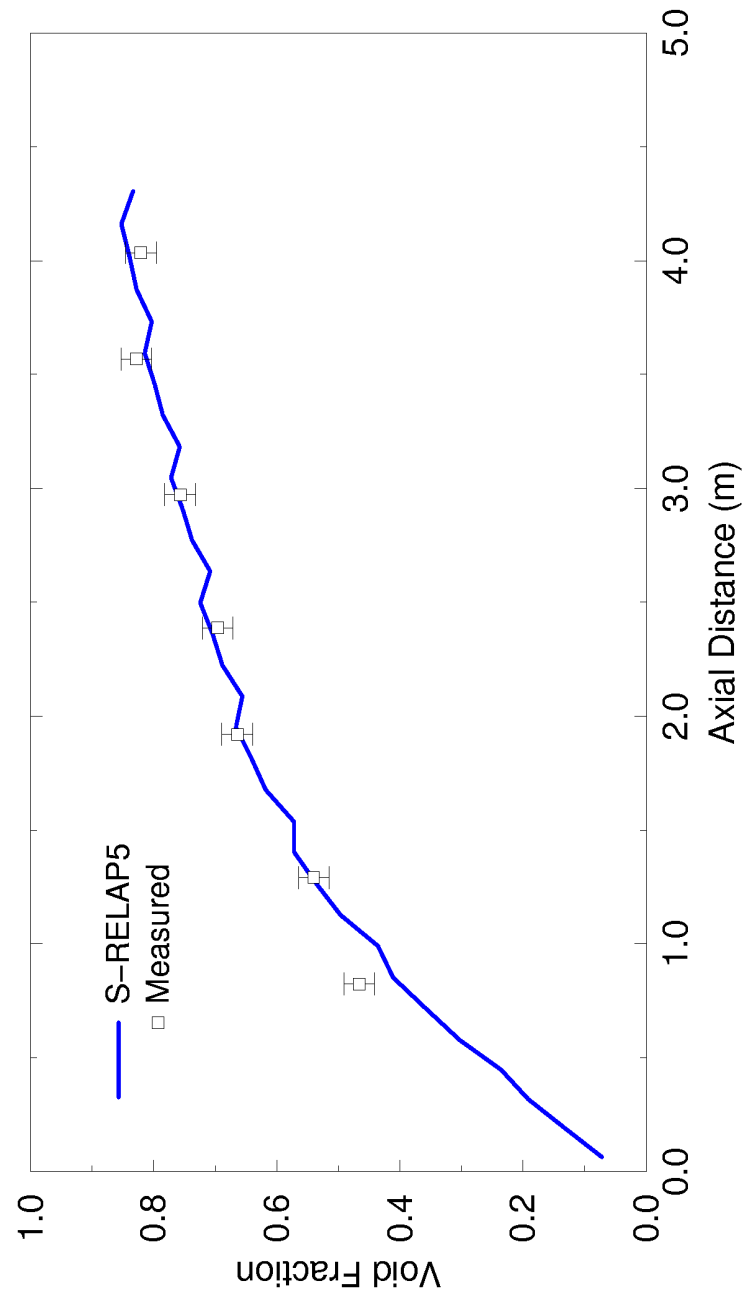


**Figure 4.25: Comparison of Calculated and Measured Void Fraction,  
FRIGG-2 Test 313030**

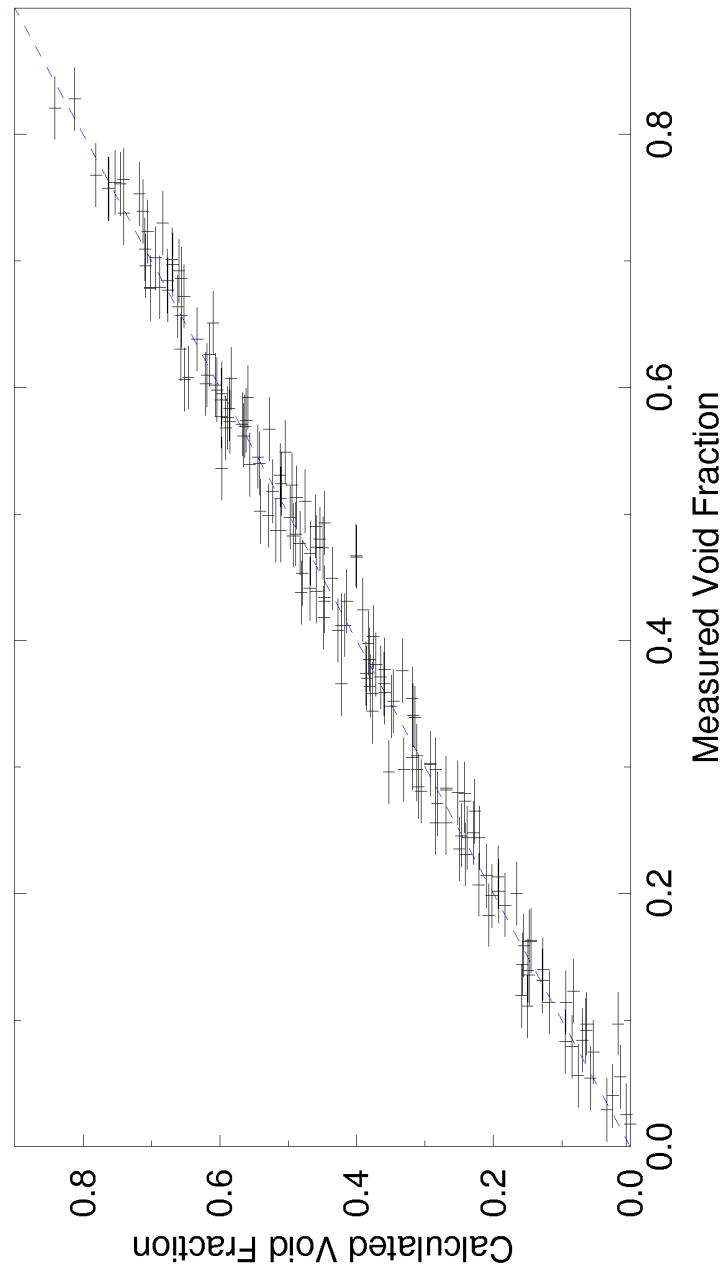


**Figure 4.26: Comparison of Calculated and Measured Void Fraction  
at the Same Location for all 27 FRIGG-2 Tests**



#### 4.3.1.5 Bennett Tube

Bennett Heated Tube Tests 5358 and 5379 were simulated using S-RELAP5 to evaluate the applicability of the Biasi and post-CHF heat transfer correlations in the code. The Bennett heated tube tests were conducted by the UKAEA Research Group to measure the dry-out [ ] location and the surface temperature profiles in the region beyond the dry-out point. Test 5358 is a low flow test with mass flux of  $379.7 \text{ kg/m}^2\text{-s}$  and Test 5379 is a high flow test with a mass flux of  $3797.4 \text{ kg/m}^2\text{-s}$ .

The test tube was a simple heated tube with a 0.497 inch inner diameter, a 0.625 inch outer diameter, a total length of 228 inches, and a heated length of 219 inches for the two selected tests. A simple input modeling approach was used to develop the S-RELAP5 input model. The heated test section was modeled using a 26 node PIPE component. Larger node heights were used in the lower and upper portion of the test section. However, a node height of 6.0 inches was used in the middle region of the test section that is of interest to assess the heat transfer correlations. This node height is within the recommended maximum node height of 7.2 inches (Section 4.2.4.3). The flow and pressure boundary conditions were input as boundary conditions to the input model. The details of the two tests, the S-RELAP5 input model, and the assessment results are discussed in Section 3.2 of Reference 5.

As shown in Figure 4.27 and Figure 4.28, the calculated CHF positions agree well with the data for both tests. Figure 4.27 shows that for the low mass flux case, the wall temperatures in the film boiling region are well predicted. Figure 4.28 shows that for the high mass flux case, the calculated wall temperatures stay rather flat in the post-CHF region and are higher than the data in the top-end region. In the simulation, the bias on the Biasi CHF correlation is not used. Since the bias is less than 1.0, the predicted CHF position would have moved slightly below the current position, resulting in the prediction of a slightly higher cladding temperature in the film boiling region.

In summary, the simulation of the Bennett heated tube tests using S-RELAP5 demonstrate that the code will calculate CHF and post-CHF heat transfer reasonably well during a LBLOCA in a PWR.

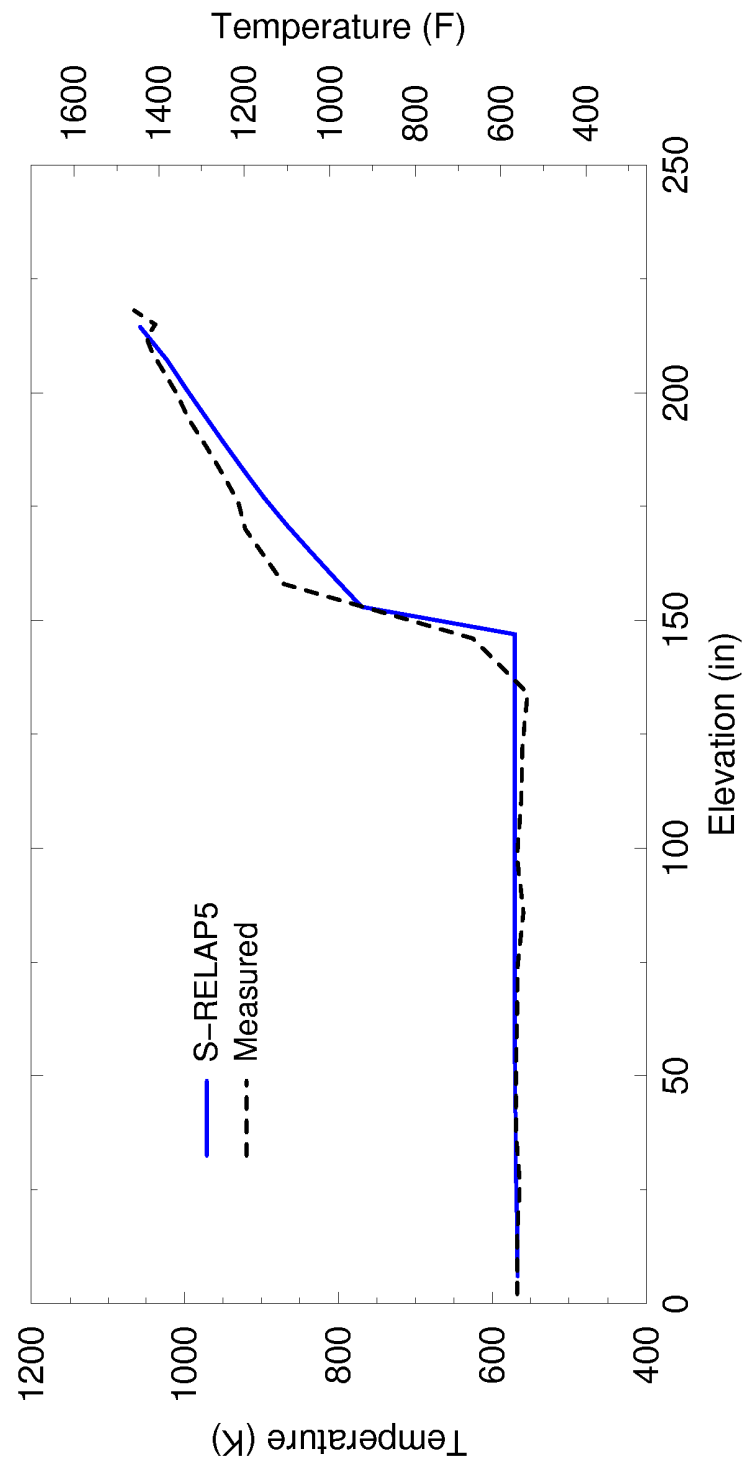


**Figure 4.27: Wall Temperature Profiles, Bennett Heated Tube Test 5358**

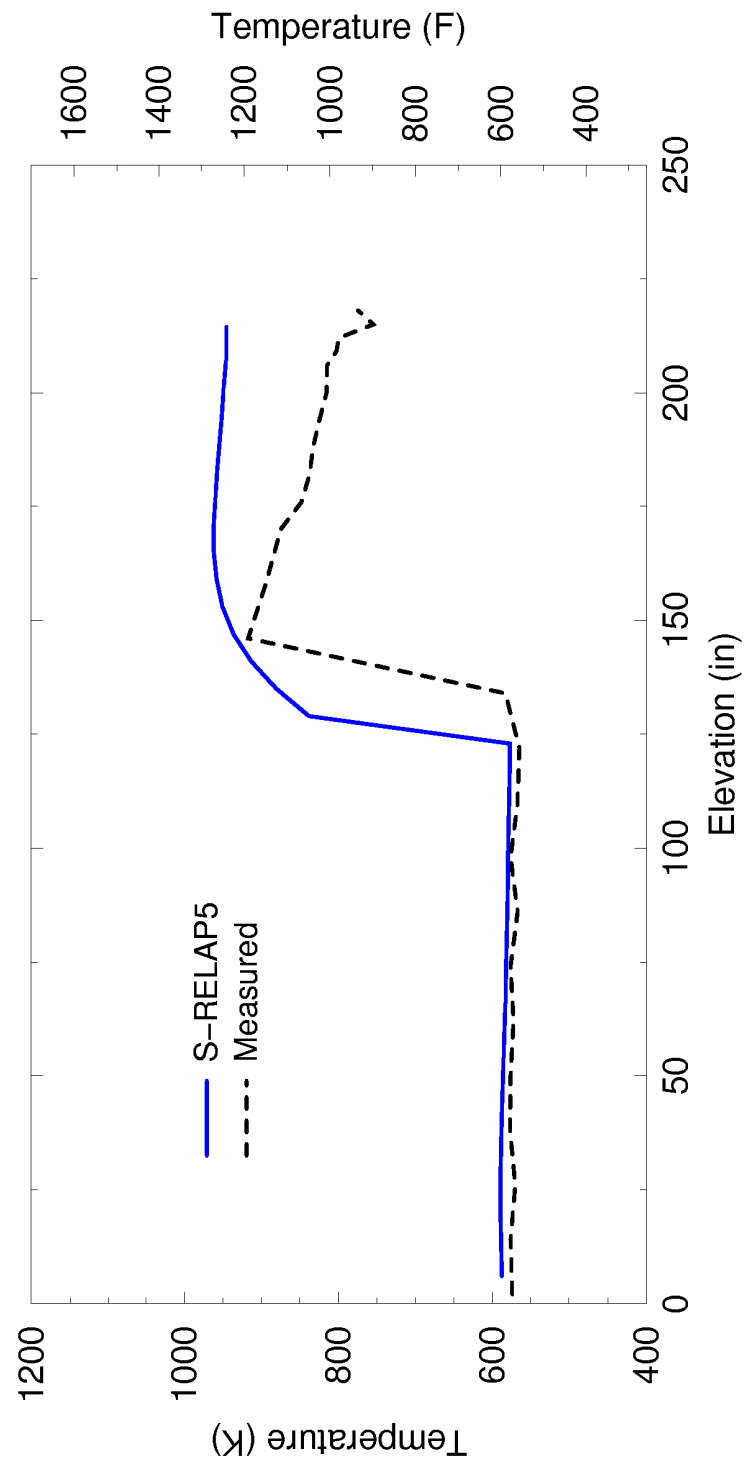


**Figure 4.28: Wall Temperature Profiles, Bennett Heated Tube  
Test 5379**

#### 4.3.1.6 FLECHT and FLECHT-SEASET

Full Length Emergency Cooling Heat Transfer - System Effects and Separate Effects (FLECHT-SEASET) Tests and Full Length Emergency Cooling Heat Transfer (FLECHT) Low-Flooding-Rate Skewed Tests (Skewed) are widely used to assess system codes. The detailed S-RELAP5 assessments for these facilities are given in Section 3.3 of Reference 5.

The purpose of these assessments was to evaluate the S-RELAP5 code reflood heat transfer and hydrodynamics, using different axial power profiles and reflood rates.

[

]

The FLECHT-SEASET facility used the Westinghouse 17x17 geometry for the reference fuel design while the FLECHT facility used the Westinghouse 15x15 geometry for the reference fuel design. The forced reflood SETs are with injection or flooding rates that are very demanding for simulations with the realistic system codes. AREVA selected the FLECHT-SEASET

Tests 31504, 31701, 31302, 31203, 31805, 32013, and 34209, and FLECHT Skewed Tests 13609 and 13914 to validate the reflood modeling capability of S-RELAP5 for the RLBLOCA methodology. For LBLOCA reflood, the selection covers the whole range of pressure, subcooling, and flooding rate, and includes cosine and skewed axial power profiles.

[

]

In the remainder of this section, key code-to-data comparisons are presented with minimal discussion. Consequently, Section 3.3 of Reference 5 should be consulted for the complete analysis.

Figure 4.29 through Figure 4.37 show the calculated maximum surface temperatures and the measured temperature data at various elevations in the simulated fuel assemblies for the FLECHT-SEASET and FLECHT Skewed tests. The S-RELAP5 calculated PCT is generally within the measured data and slightly exceeds the data above the 100 inch elevation. These results are sufficiently close to the expected outcome where the best-estimate calculations are in good agreement with the data and conservatism is brought in through the uncertainty multipliers. The results from the FLECHT Skewed comparisons, Figure 4.36 and Figure 4.37, show the calculated maximum temperatures slightly exceeding the data at the lower elevations, and then greatly exceeding the measurements near the top of the test section. With respect to plant calculations, it is expected that clad temperatures for top-peaked cases will be overpredicted while bottom- and mid-plane-peaked cases will be well predicted.

The calculated and measured temperatures at the 78 inch elevation, approximately the PCT location, are shown for Test 31504 in Figure 4.38. For this case, the calculated rod surface temperature during the temperature rise and peak portion of the test compares well with the measured data and after the peak temperature tends to underpredict the temperature. Although the measured temperature is underpredicted slightly, the calculated quench is delayed by approximately 50 seconds.

Steam temperature is one of the important parameters in determining the heat transfer rate during the reflood phase. Figure 4.39 shows the calculated and measured steam temperatures for FLECHT-SEASET Test 31504. Test 31504 shows excellent agreement up to 200 seconds and then overpredicts the measurements until the calculated quench time is approached.

In both the wall and steam temperature comparisons, the calculated results were in good agreement with the data until approximately 200 seconds, and then the data comparisons show differences between measured and calculated temperatures from 200 seconds to 300 seconds. In this time frame, the void fraction is decreasing from 0.98 at 200 seconds to 0.75 at 300 seconds, and decreases further at later times. In terms of heat transfer, this time frame marks the transition from highly dispersed flow film boiling to dispersed flow film boiling, and then to film boiling when the void fraction drops below 0.90. This is also the region where the turbulence enhancement factor to the vapor convection heat transfer starts influencing the overall heat transfer, and, to a lesser extent, the transition to film boiling heat transfer. The truncation of the turbulence enhancement and the transition to film boiling heat transfer were determined empirically by examining the results from the heat transfer bias and uncertainty determination discussed in Section 5.1 of Reference 5. The heat transfer biases, having values close to 1.0, indicate that the best overall fit was obtained. Since the PCT is not affected, these results are considered acceptable.

The calculated water mass accumulation is generally less than measured. Most of the mass accumulation occurs early in the transient, as the lower half of the test section is filled. Once the water accumulation reaches the high power mid-plane region of the test bundle, the water accumulation becomes a balance between injected water entering, and entrained and evaporated water leaving. Figure 4.40 compares the calculated versus measured liquid mass inventory from Test 31504.

The measured quench times correspond to the time at which the cooldown rate shows a distinct increase (Section E-12 in Reference 23) at an elevation. The time at which this occurs is calculated from the mean of all the thermocouples at that elevation. The calculated quench time is the time at which the wall temperature drops below the value of TMINK (700 K in this analysis) and the void fraction is less than 0.95. The results from Test 31504, Figure 4.41, shows the comparison between measured and calculated quench times. The comparison shows relatively good agreement between the calculated and measured quench times.

Time step and nodalization sensitivity studies were also performed using FLECHT-SEASET Test 31504 to demonstrate solution convergence of the S-RELAP5 treatment of the reflood transient. FLECHT-SEASET Test 31504 was chosen because it is a demanding low flooding rate, 0.97 in/s (2.46 cm/s), test. [

]

The maximum cladding temperatures as a function of elevation are shown in Figure 4.42 along with the measured data. The calculated results are from the 20 node time step study (using time step sizes of 0.01, 0.005, 0.0025, and 0.00125 seconds) and the 40 node time step study (using time step sizes of 0.0025 seconds and 0.00125 seconds). Section 3.3 in Reference 5 contains additional figures comparing the temperature histories at the 78 inch elevation that show minimal differences with respect to time step size. [

]

Summarizing, selected FLECHT-SEASET and FLECHT Skewed tests were used to assess the S-RELAP5 reflood heat transfer. The input models used similar nodalizations and options to those used in the plant model. The calculated PCT was either bounding or within the data scatter from these tests. The notable bounding cases were the FLECHT Skewed tests, which indicate that the plant model will also calculate bounding (hence conservative) PCT from plant applications whenever the axial peaking occurs at elevations above mid-plane. The wall and steam temperature comparisons show the new heat transfer model gives the appropriate amount of energy transfer to the fluid during the heat-up and peak temperature periods of the reflood phase. They also show that the period after PCT is mispredicted and the quench times are delayed. This indicates that the plant calculations will show later than expected quench times.

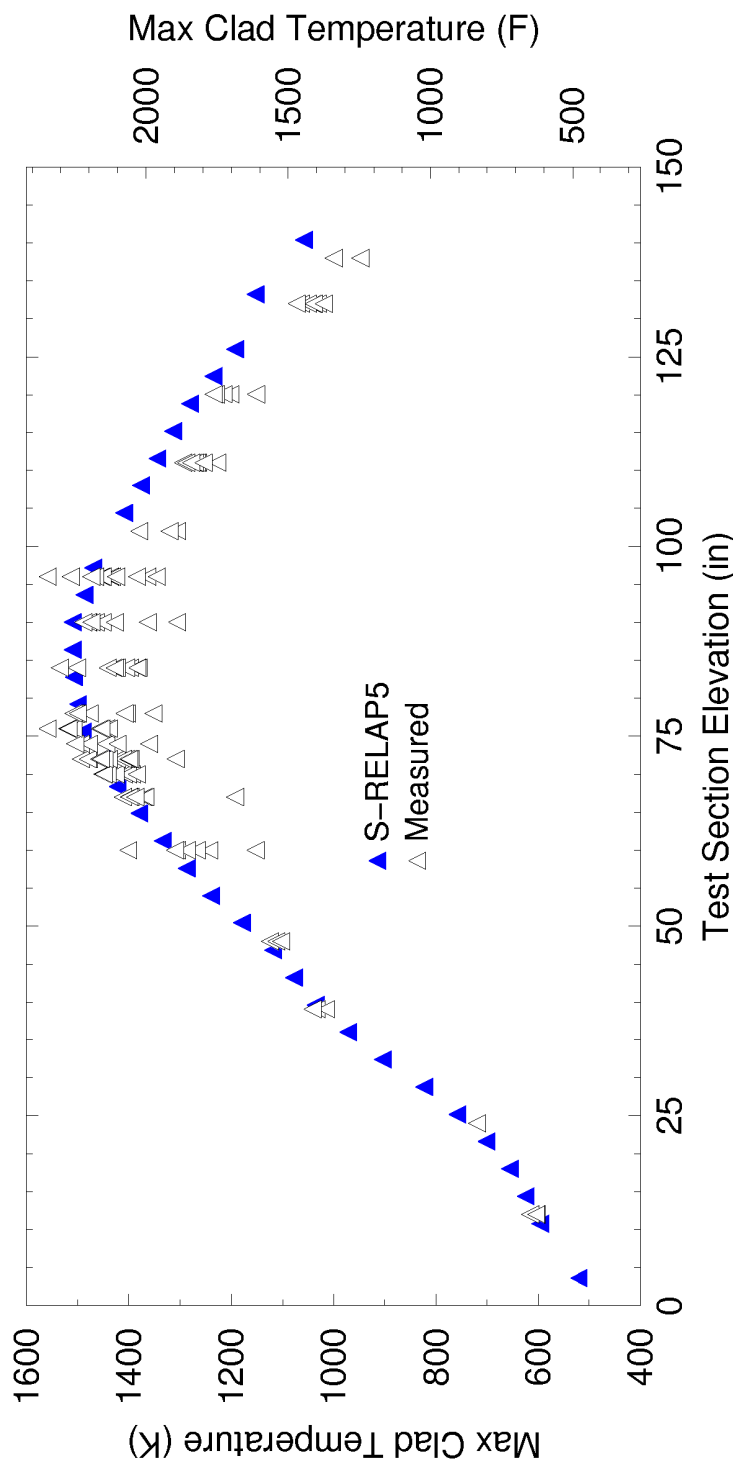


**Figure 4.29: Maximum Clad Temperature at All Measured Elevations, FLECHT-SEASET Test 31805**



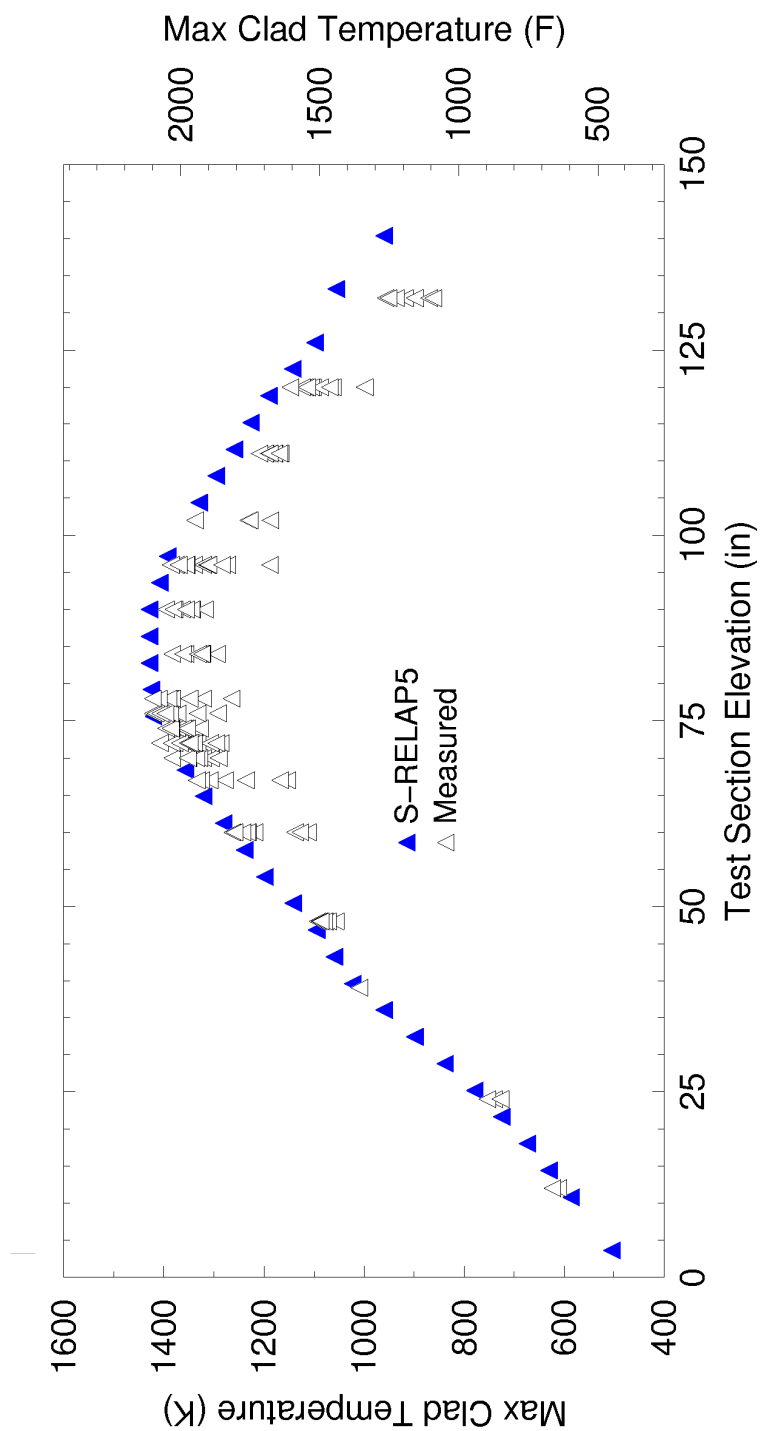


**Figure 4.30: Maximum Clad Temperature at All Measured Elevations, FLECHT-SEASET Test 31504**

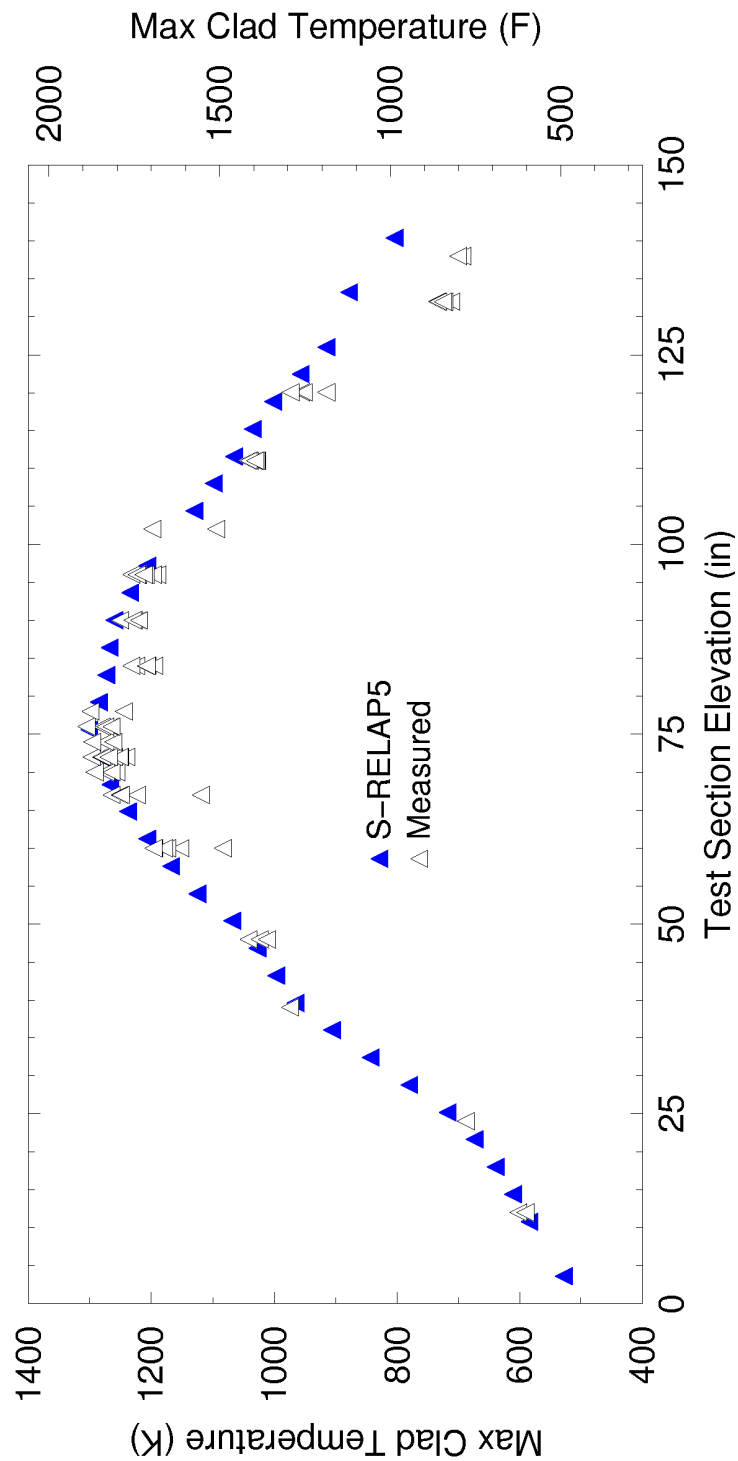


**Figure 4.31: Maximum Clad Temperature at All Measured Elevations, FLECHT-SEASET Test 31203**

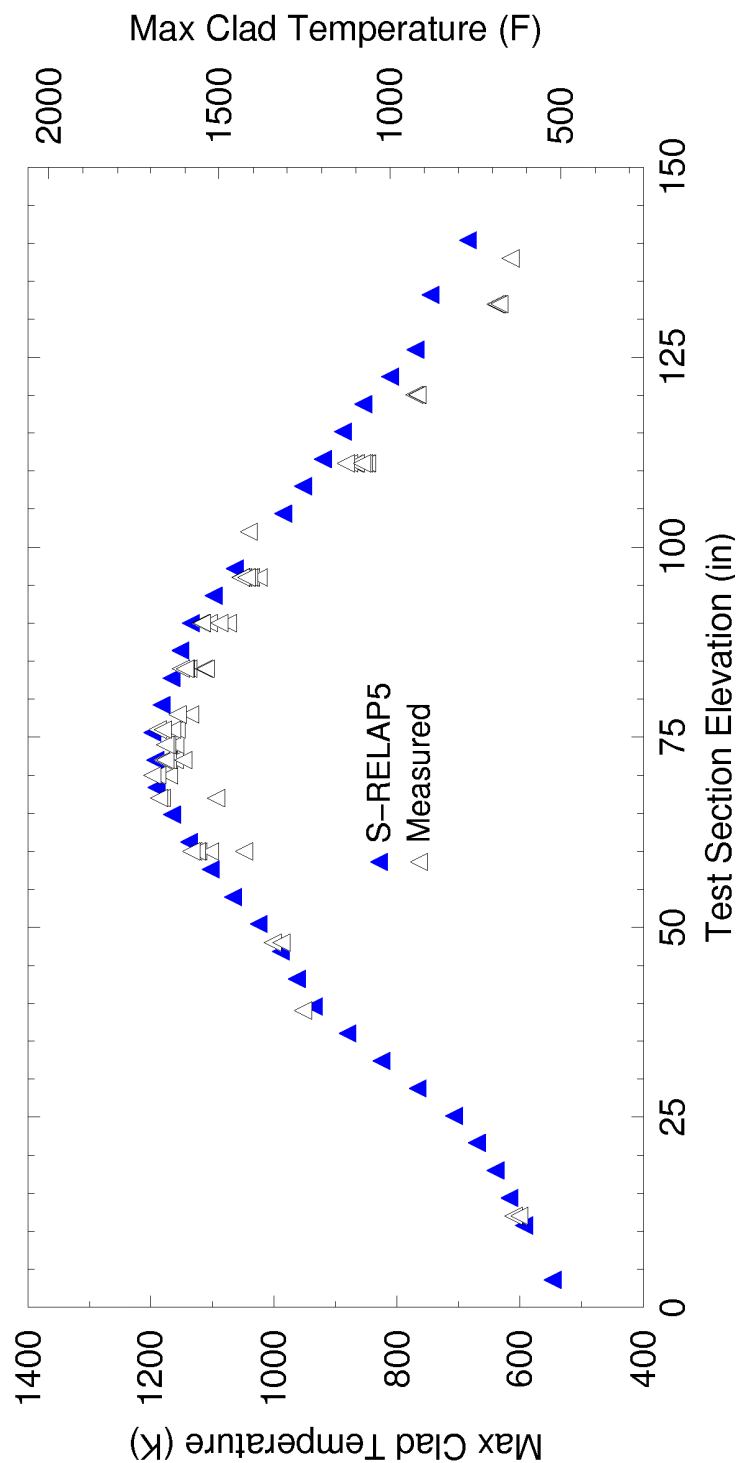


**Figure 4.32: Maximum Clad Temperature at All Measured Elevations, FLECHT-SEASET Test 31302**

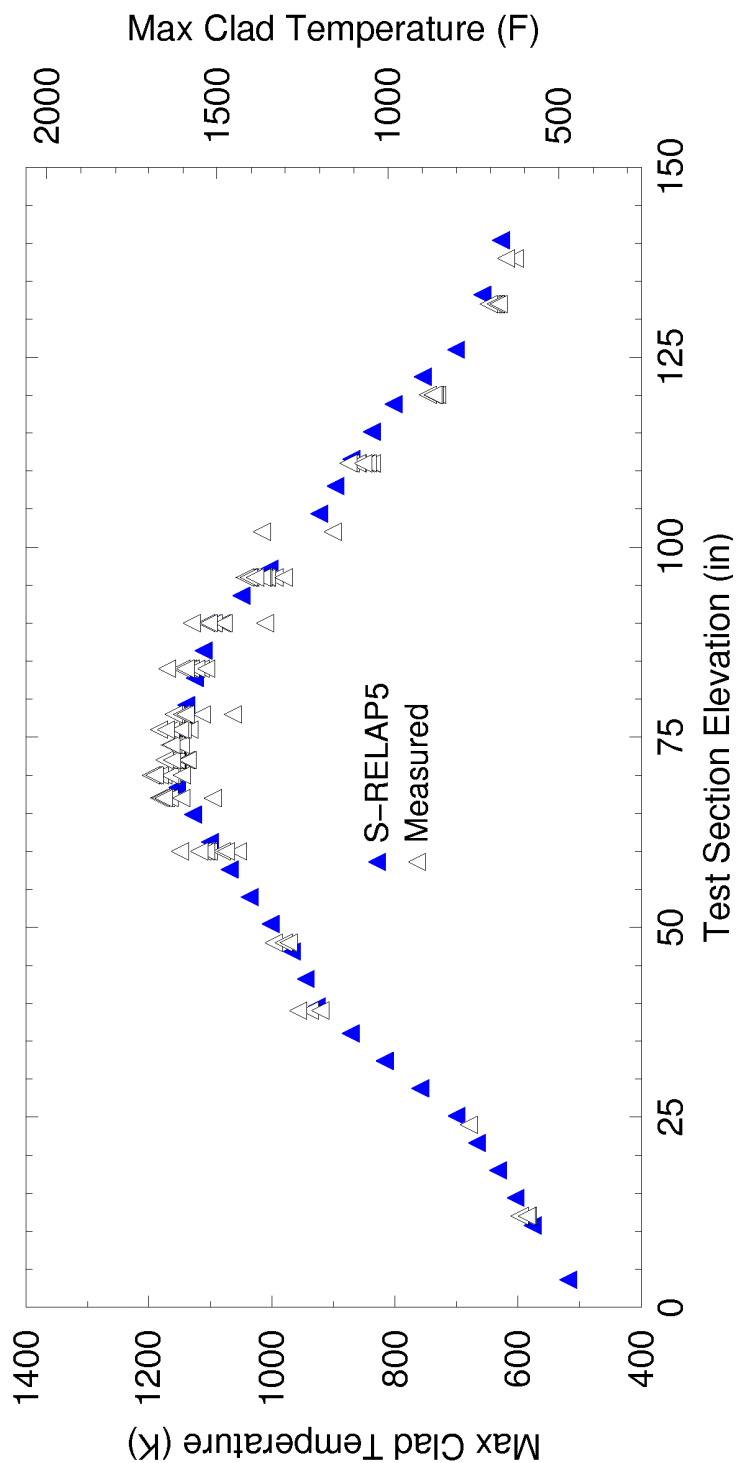


**Figure 4.33: Maximum Clad Temperature at All Measured Elevations, FLECHT-SEASET Test 31701**

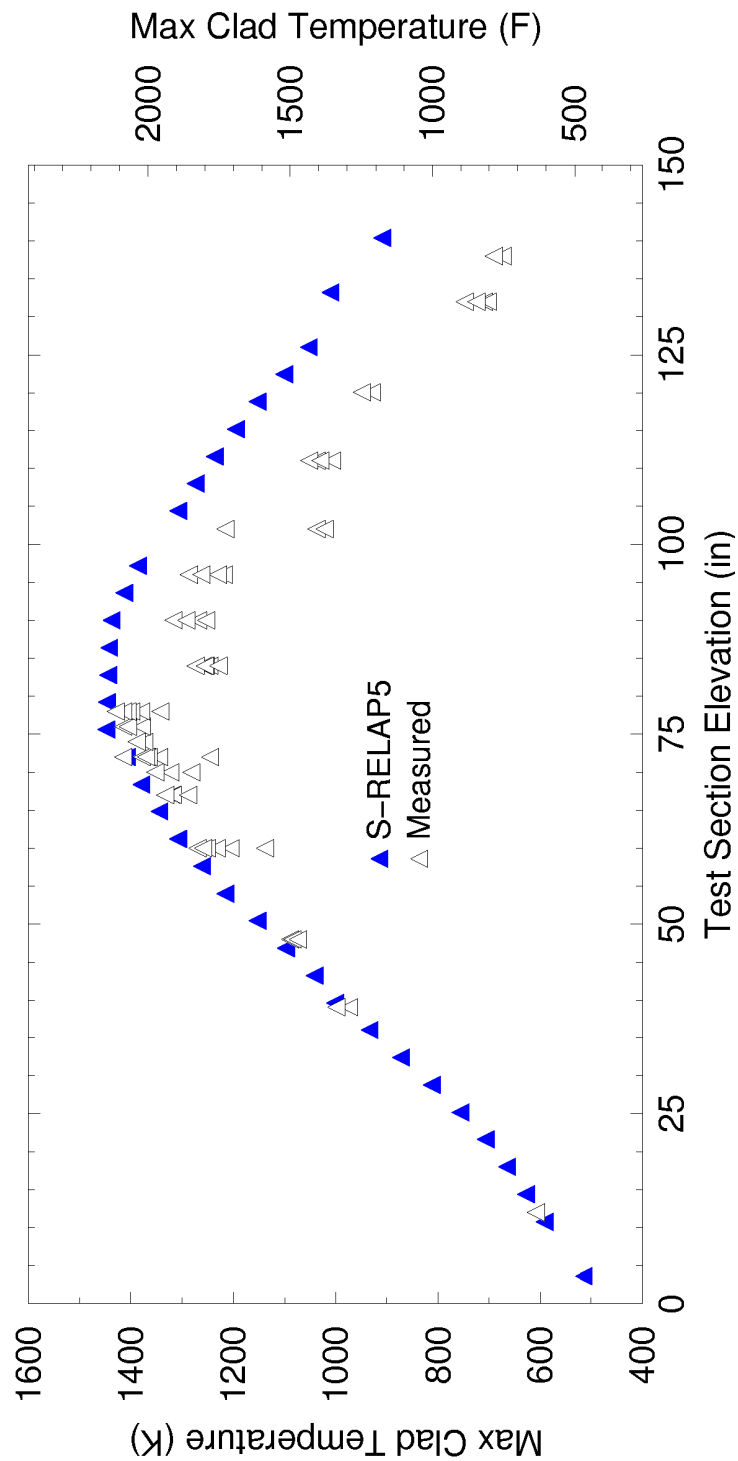


**Figure 4.34: Maximum Clad Temperature at All Measured Elevations, FLECHT-SEASET Test 34209**

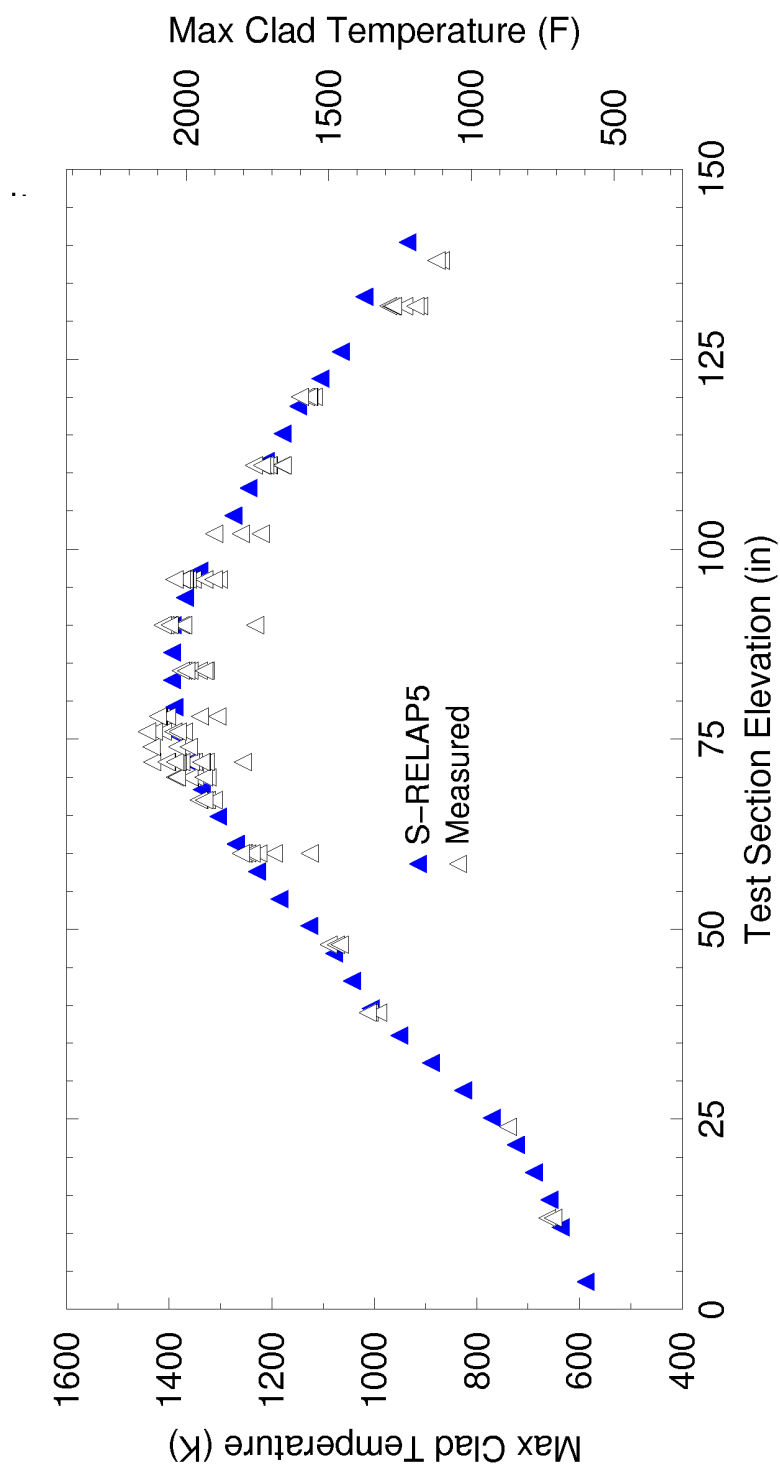


**Figure 4.35: Maximum Clad Temperature at All Measured Elevations, FLECHT-SEASET Test 32013**

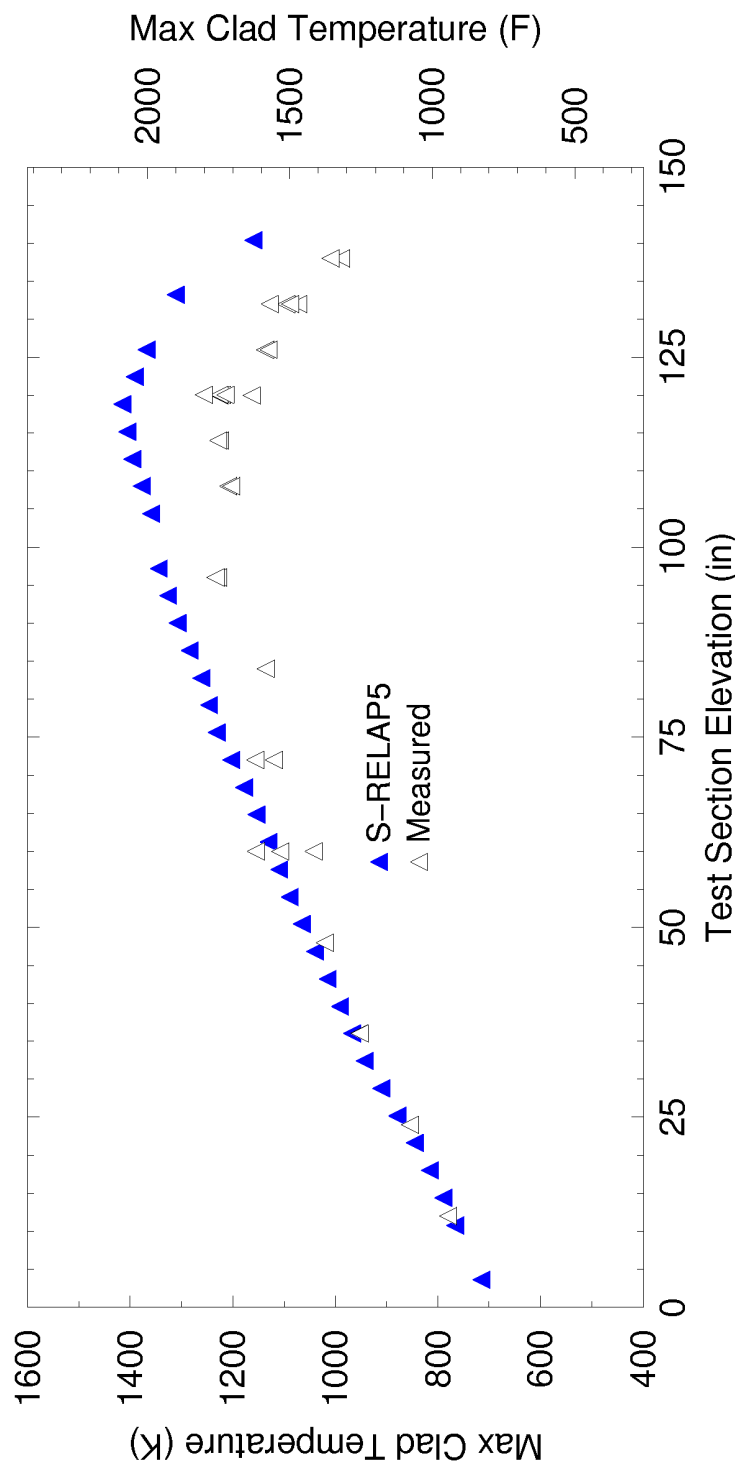


**Figure 4.36: Maximum Clad Temperature at All Measured Elevations, FLECHT Skewed Test 13609**

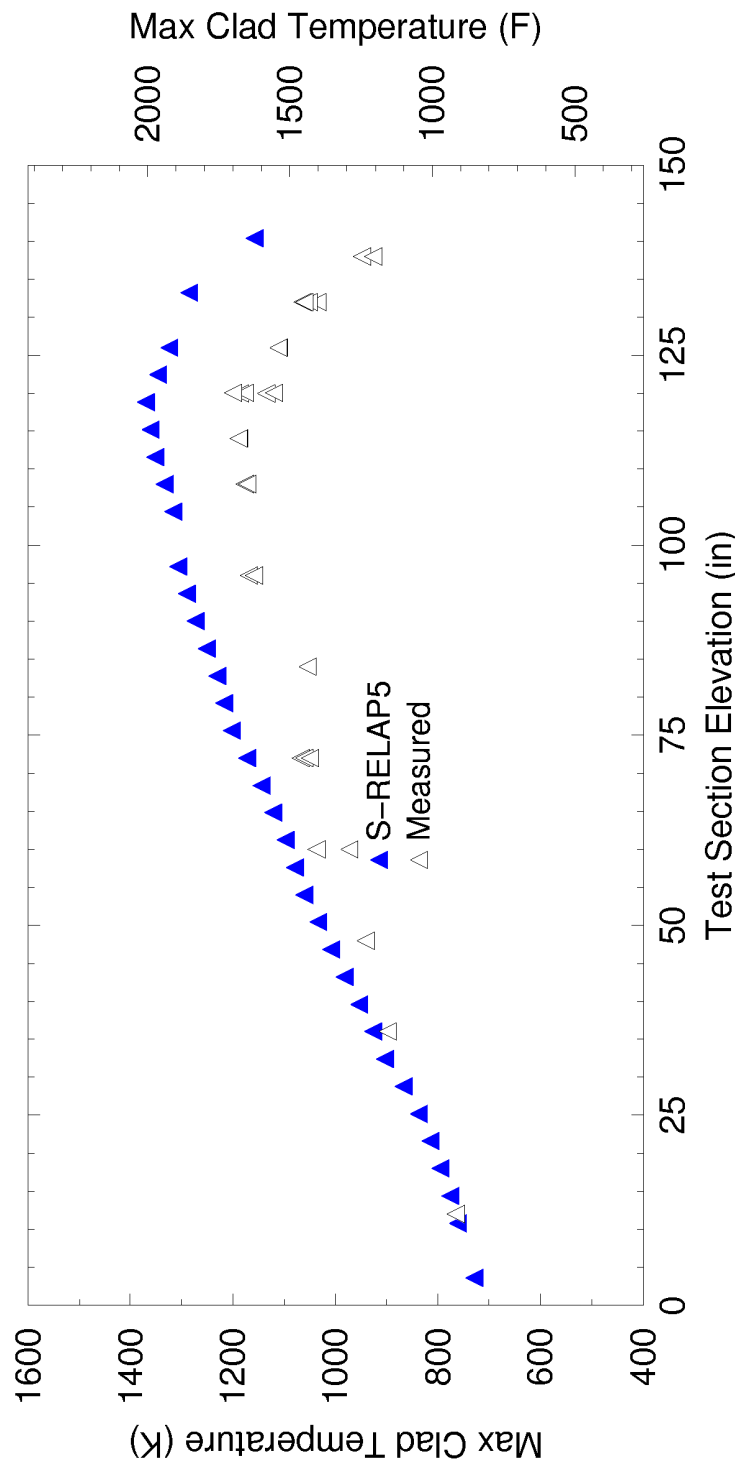


**Figure 4.37: Maximum Clad Temperature at All Measured Elevations, FLECHT Skewed Test 13914**



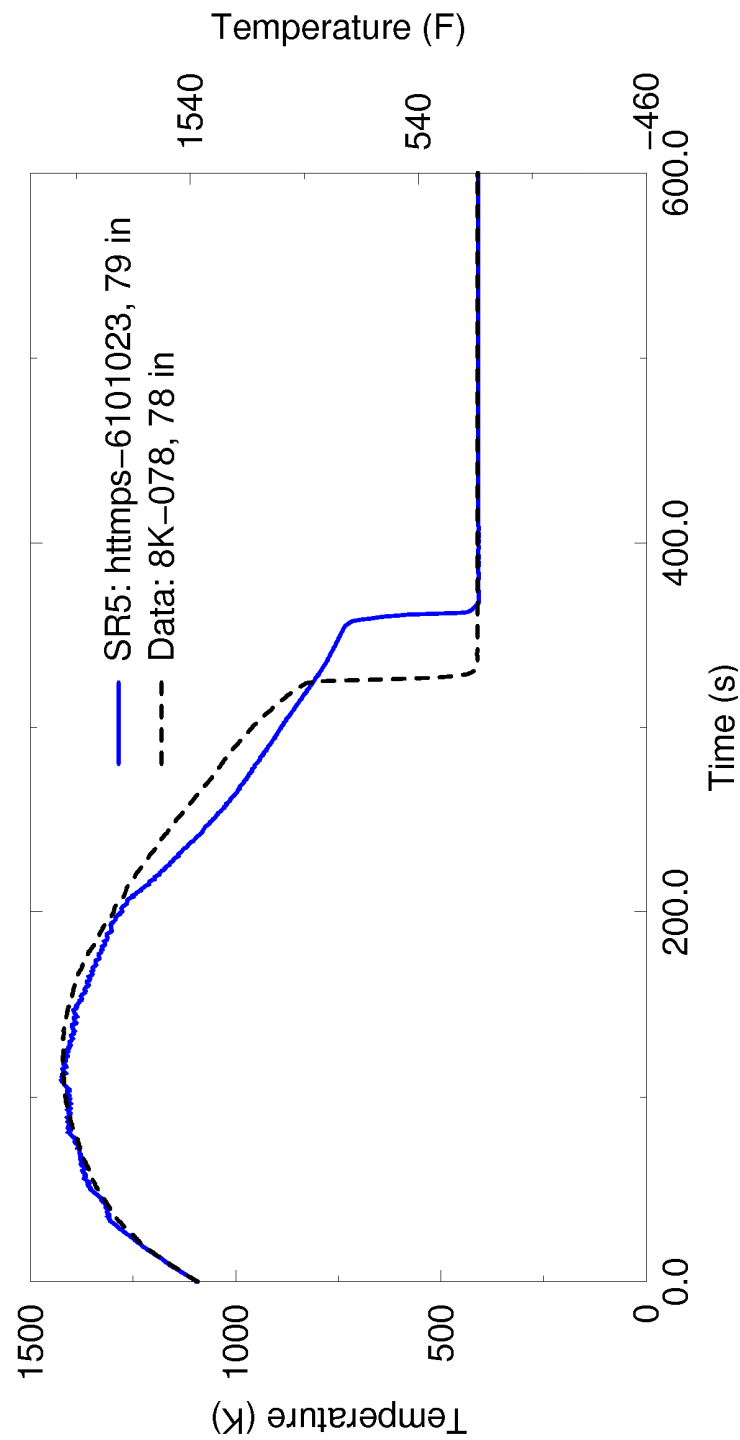


**Figure 4.38: Calculated and Measured Rod Surface Temperature at 78 inches, FLECHT-SEASET Test 31504**

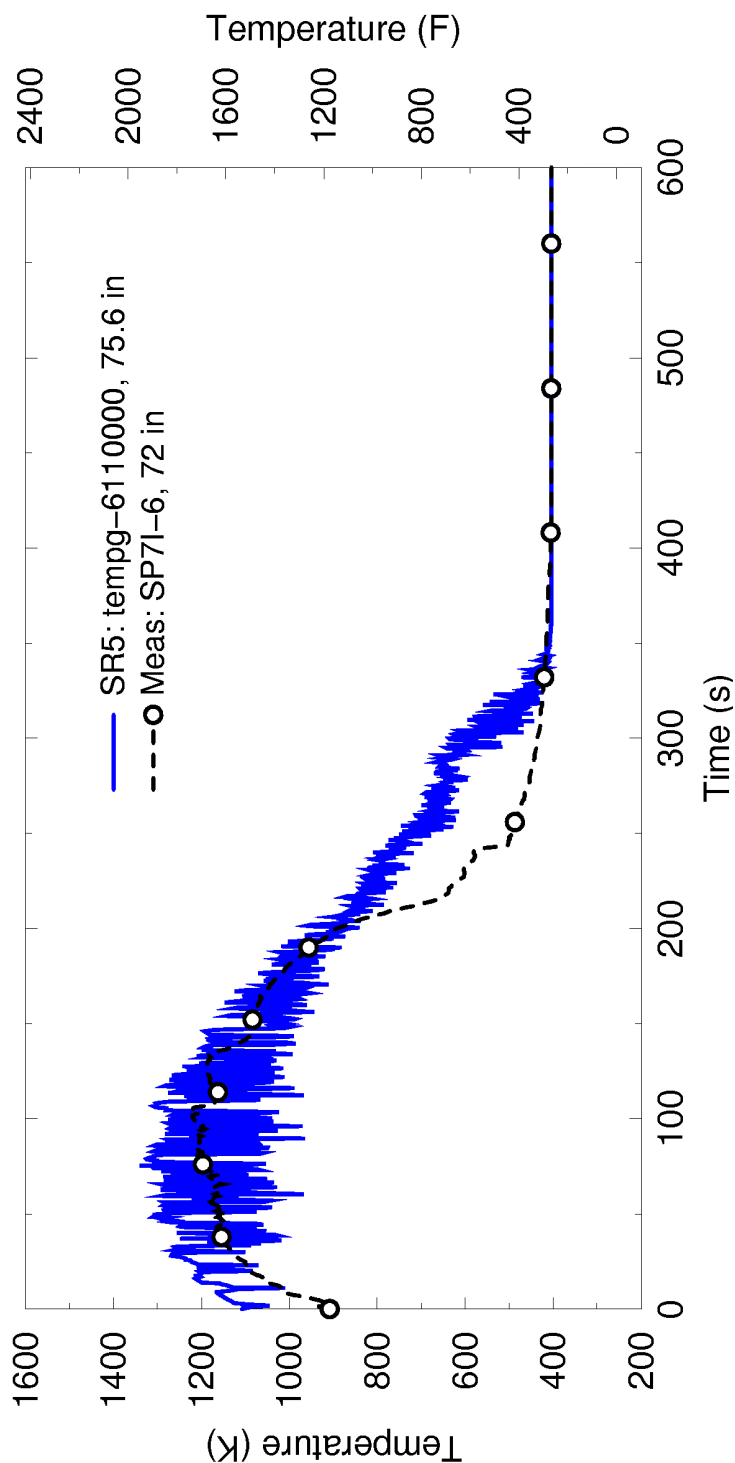


**Figure 4.39: Steam Temperatures Calculated at 75.6 inches and Measured at 72 inches, FLECHT-SEASET Test 31504**

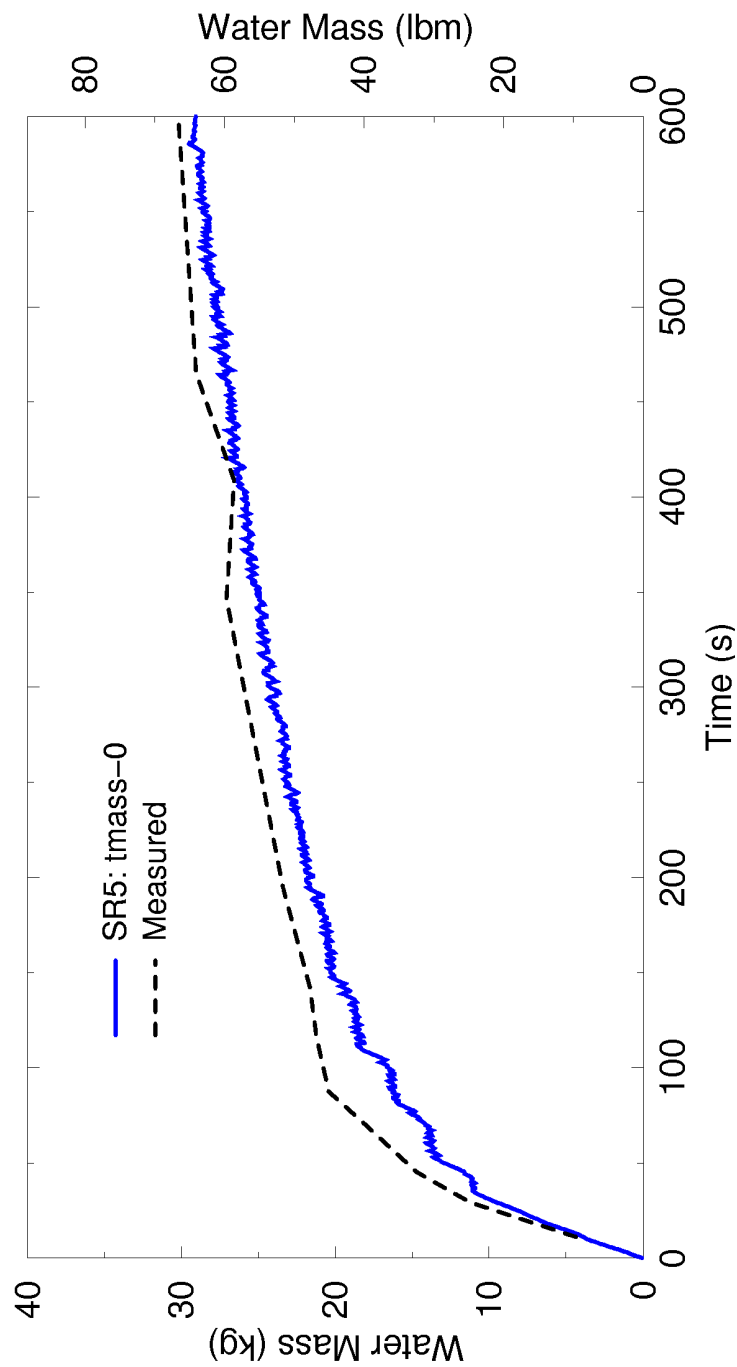


**Figure 4.40: Accumulated Water Mass in the Test Section,  
FLECHT-SEASET Test 31504**

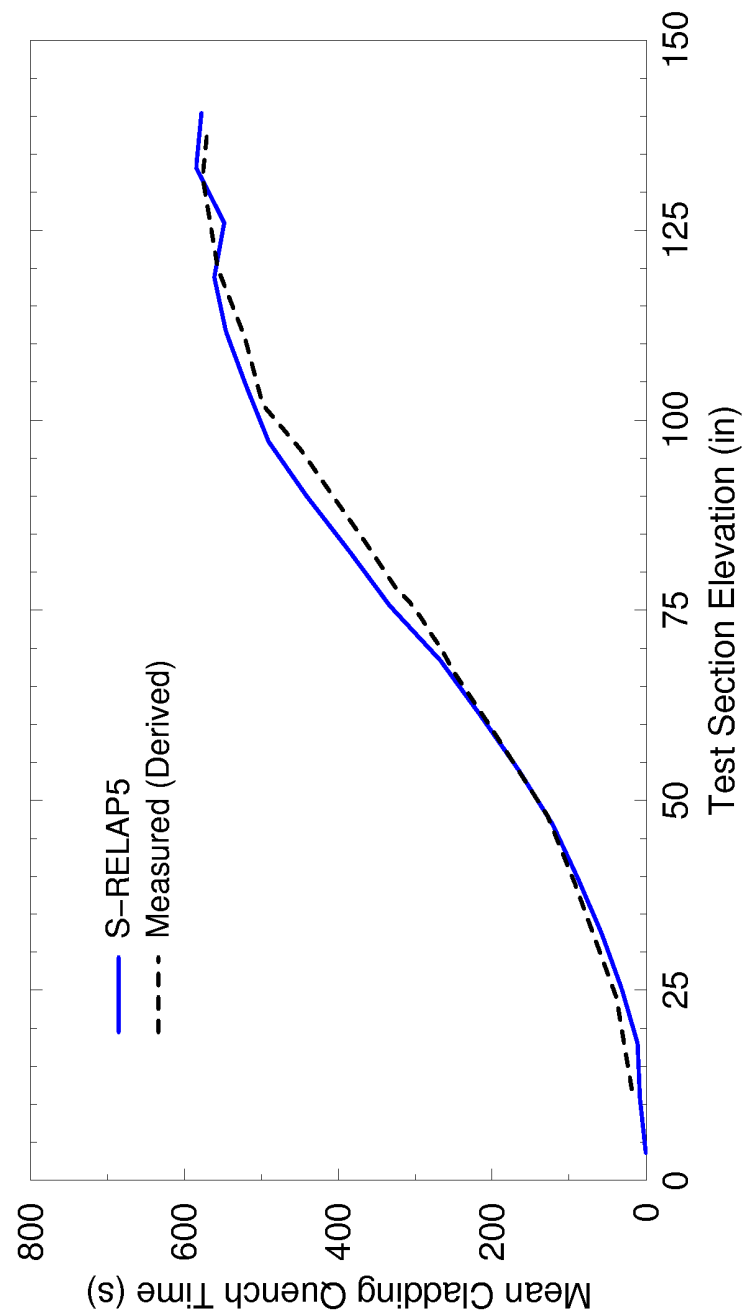
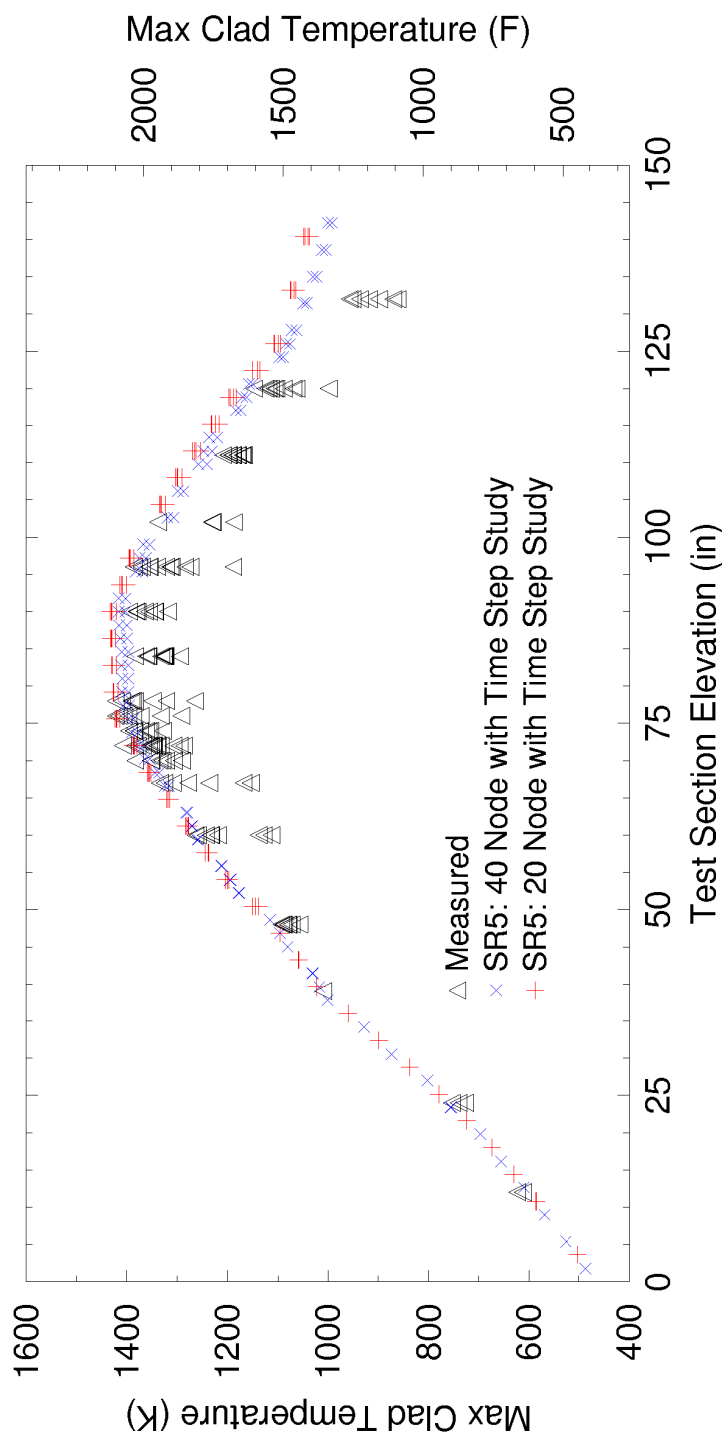


Figure 4.41: Rod Quench Time, FLECHT-SEASET Test 31504



**Figure 4.42: Maximum Cladding Temperatures versus Axial Elevation  
from FLECHT-SEASET Test 31504 Time Step and Node Size  
Sensitivities**

#### 4.3.1.7 PDTF SMART Tests

The Product Development Test Facility (PDTF) Small Array Reflood Test (SMART) tests were performed by AREVA to show that the HTP spacer was thermodynamically equivalent to a mixing-vane-type spacer with respect to reflood and PCT. The purpose of the facility was primarily to demonstrate equivalence between differing fuel designs and not to demonstrate the performance of either. That being said, a reasonable benchmark of the reflood test results does offer insight as to the range of capability of the S-RELAP5 code in simulating reflood behavior.

The PDTF SMART tests were similar to the FLECHT-SEASET tests, but performed in an AREVA facility. The test assemblies were 6x6, full-height, simulated PWR assemblies. The rod diameter and pitch were characteristic of AREVA's 15x15 PWR fuel design. The test assembly had a uniform radial power distribution and a chopped cosine axial power distribution. The tests simulated five different flooding conditions. Of the five flooding rate conditions, four were constant-flooding-rate tests and one was a variable-flooding-rate test. The constant-flooding-rate tests had flooding rates of 0.6, 1.0, 2.0, and 4.0 in/s. The variable-flooding-rate tests started at 8.0 in/s and ramped rapidly to a constant 1.0 in/s flooding rate. The 0.6 in/s tests were terminated prematurely; therefore, they were eliminated for the verification and validation of S-RELAP5. The tests selected for the simulation are listed in Table 4.5. Further details of the tests and the test facility are provided in Reference 5 (Section 3.4).

Two S-RELAP5 models were developed; one with HTP spacer grids and one with mixing-vane type spacers. Since the test bundle is small, there will be rod-to-shroud radiation heat transfer. Therefore, for each model, each benchmark was run with and without the core shroud explicitly modeled. The heated portion of the assembly for these models was divided into 20 hydrodynamic and heat structure sections of approximately equal length, with one additional section for the unheated portion of the bundle at the top of the assembly. The input model is described in detail in Section 3.4 of Reference 5.

Figure 4.43 shows the PCT for each of the benchmarks. Figure 4.44 through Figure 4.47 show the maximum cladding temperature as a function of elevation and independent of time for all four benchmarks and the two test sets. With a few exceptions, the data lie within or below the range of the S-RELAP5 predictions.

In summary, from the simulation of the PDTF SMART reflood tests, it can be concluded that the S-RELAP5 code can adequately predict the core thermal-hydraulic behavior during the reflood phase of a LBLOCA.

**Table 4.5: PDTF SMART Tests Chosen for S-RELAP5 Verification and Validation**

<b>Test Designator</b>	<b>Test Description</b>
<b>KH01A</b>	HTP spacer test with constant flooding rate of 4.0 inches per second
<b>KH01B</b>	HTP spacer test with constant flooding rate of 4.0 inches per second (repeat experiment of KH01A)
<b>KH02A</b>	HTP spacer test with constant flooding rate of 2.0 inches per second
<b>KH02B</b>	HTP spacer test with constant flooding rate of 2.0 inches per second (repeat experiment of KH02A)
<b>KH03A</b>	HTP spacer test with constant flooding rate of 1.0 inch per second
<b>KH03B</b>	HTP spacer test with constant flooding rate of 1.0 inch per second (repeat experiment of KH03A)
<b>KH05A</b>	HTP spacer test with variable flooding rate from 8.0 to 1.0 inches per second
<b>KV01A</b>	FOCUS spacer test with constant flooding rate of 4.0 inches per second
<b>KV02A</b>	FOCUS spacer test with constant flooding rate of 2.0 inches per second
<b>KV02B</b>	FOCUS spacer test with constant flooding rate of 2.0 inches per second (repeat experiment of KV02A)
<b>KV03A</b>	FOCUS spacer test with constant flooding rate of 1.0 inch per second
<b>KV03B</b>	Reported FOCUS spacer test with constant flooding rate of 1.0 inch per second (repeat experiment of KV03A)
<b>KV05A</b>	FOCUS spacer test with variable flooding rate from 8.0 to 1.0 inches per second
<b>KV05B</b>	FOCUS spacer test with variable flooding rate from 8.0 to 1.0 inches per second (repeat experiment of KV05A)



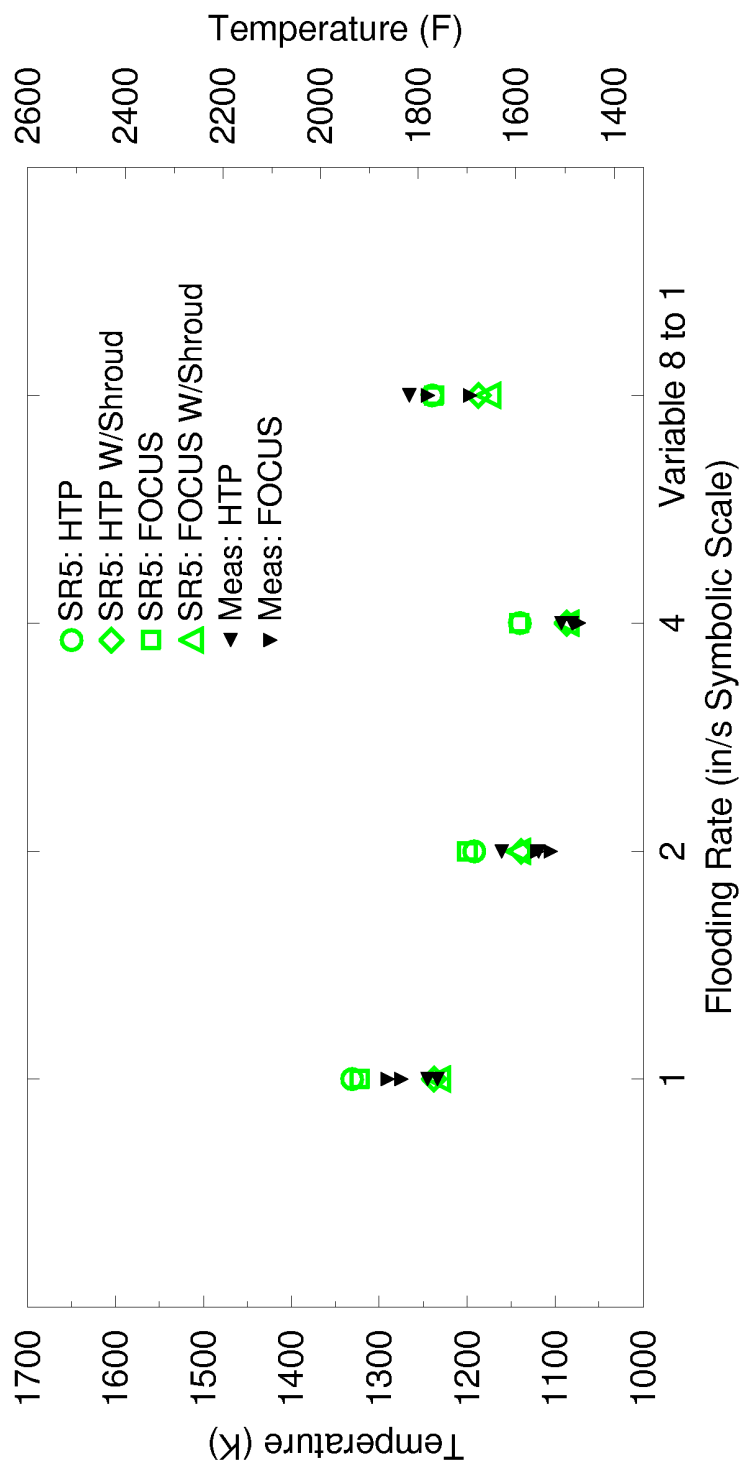


**Figure 4.43: Comparison of Predicted PCT and Measured Data, PDF SMART**

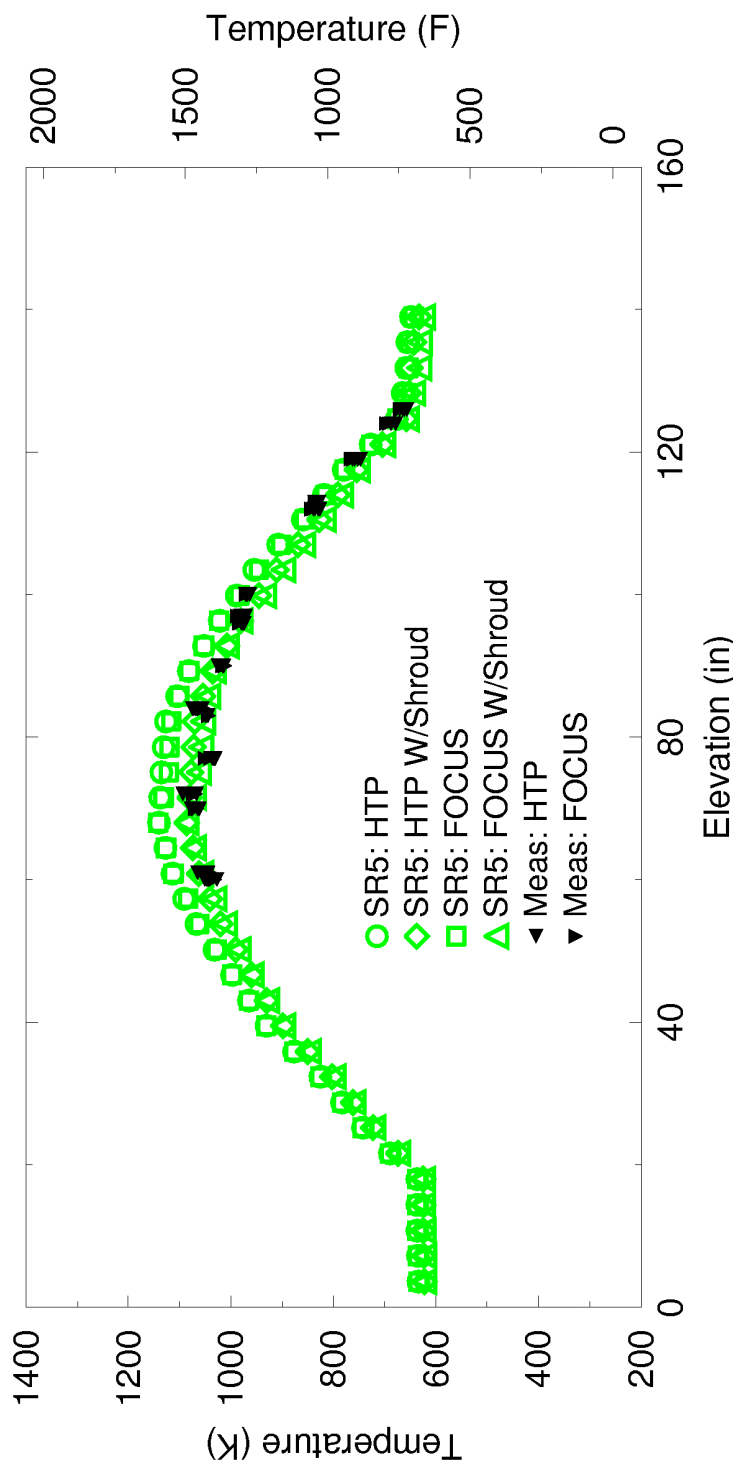


**Figure 4.44: MCT versus Elevation Comparison to Data for 4-in/s-Flooding-Rate Test, PDTF SMART**

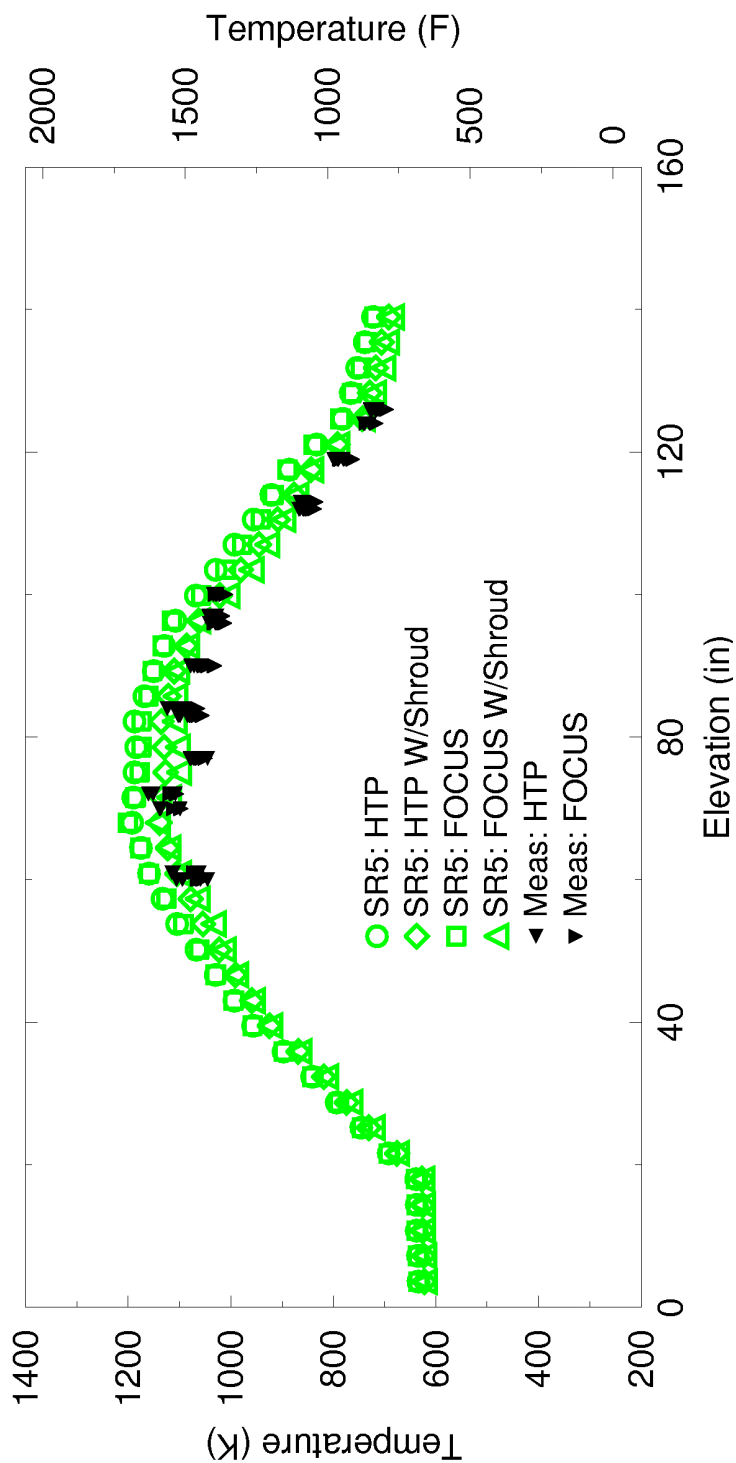


**Figure 4.45: MCT versus Elevation Comparison to Data for 2-in/s-Flooding-Rate Test, PDTF SMART**

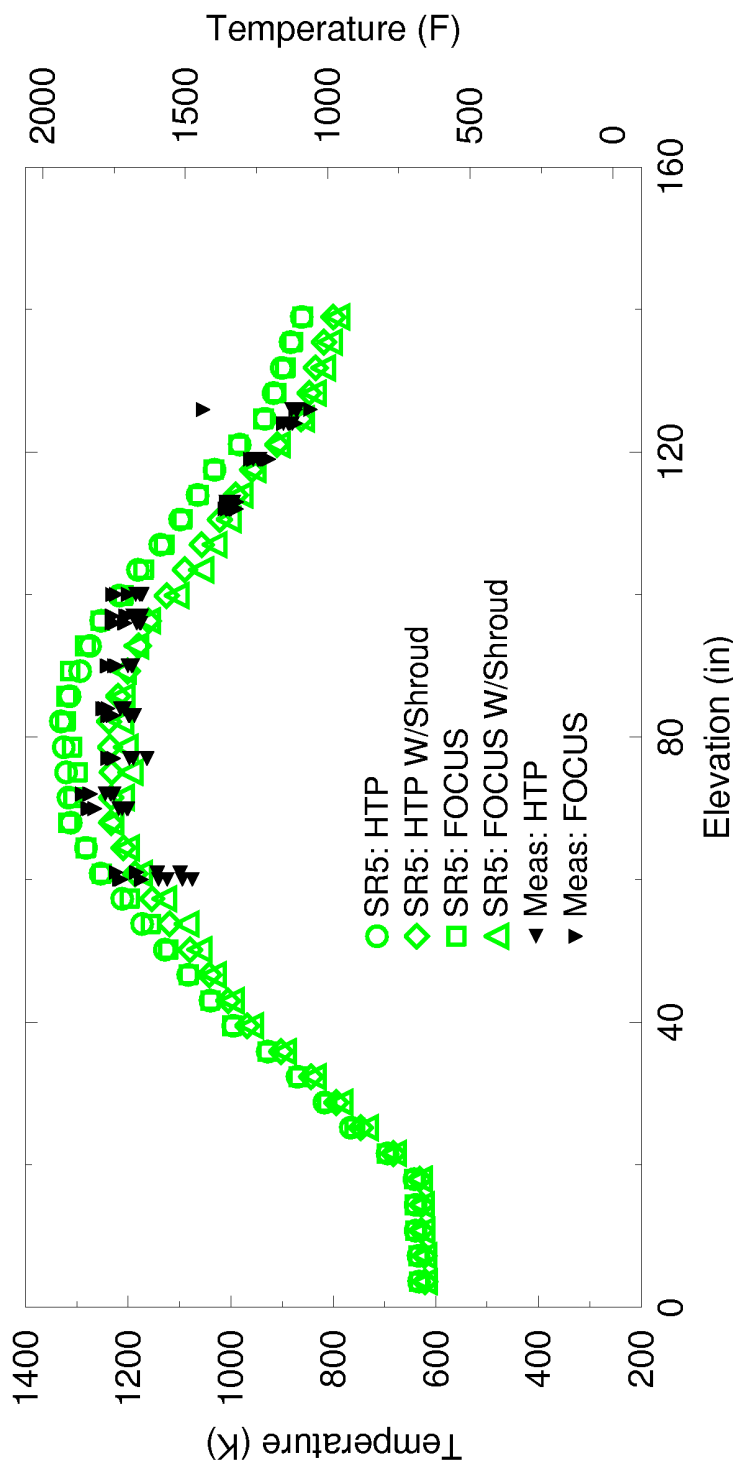


**Figure 4.46: MCT versus Elevation Comparison to Data for 1-in/s-Flooding-Rate Test, PDTF SMART**

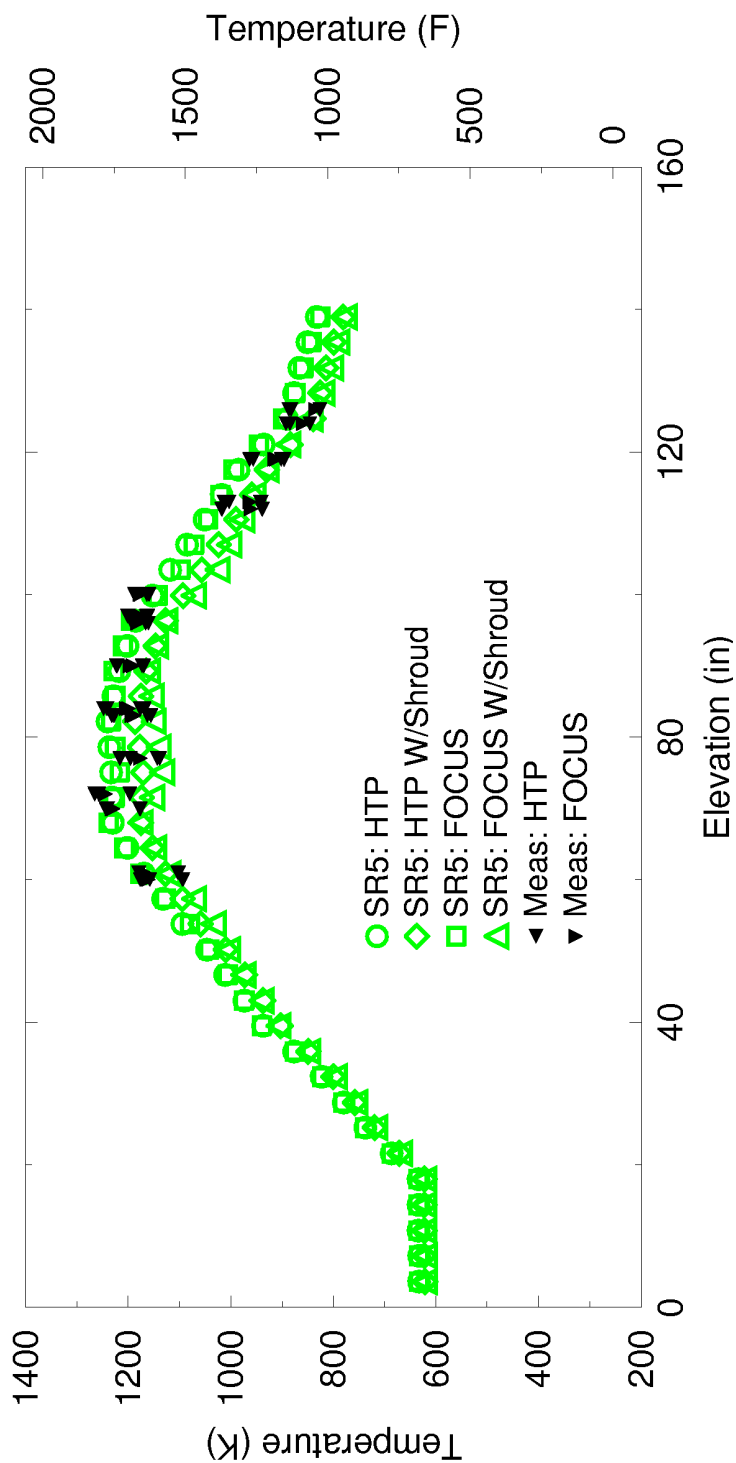


**Figure 4.47: MCT versus Elevation Comparison to Data for Variable-Flooding-Rate Test, PDTF SMART**

#### 4.3.1.8 Marviken Tests

Nine Marviken full-scale critical flow tests were simulated using S-RELAP5 to provide uncertainty information for the critical flow model. The Marviken full-scale critical flow test data were used in the CSAU methodology (Reference 4) to determine the critical flow multipliers and uncertainties for the break flow model. The Marviken test data are also widely used in assessing critical flow models for various system codes. The tests selected for the assessments are Tests 2, 6, 8, 16, 17, 20, 22, 24, and 25.

The Marviken test facility and test data are well documented. The facility has four main parts: (1) a full-scale boiling water reactor (BWR) vessel; (2) a discharge pipe attached to the bottom of the vessel; (3) a test nozzle connected to the downstream end of the discharge pipe, and (4) a rupture disk assembly attached to the downstream end of the nozzle. Nozzles of various length-to-diameter (L/D) ratios were used in the tests.

Since the primary purpose of the test simulation is to benchmark the HEM critical flow model in S-RELAP5, the break junction and the upstream node L/D are important in calculating the critical flow. The test vessel was modeled using 42 nodes with fine nodalization at the bottom of the tank, in order to properly represent the fluid conditions at the inlet to the discharge piping. The discharge piping, together with the nozzle, was modeled using seven nodes. The node that connects to the break junction consisted of the nozzle and a 0.4 meter discharge pipe resulting in an L/D variation for this node from about 1.1 to 5.0. The L/D variation for the break node in the plant cases typically are within this range. The HEM critical flow model option and the abrupt area change option “2” were selected at the break junction. Details of the test facility, the S-RELAP5 input model, and the results are discussed in detail in Section 3.5 of Reference 5. A summary of the results is discussed below.

The S-RELAP5 calculated critical flow mass fluxes and the measured values are sampled at one second intervals. A total of 535 pairs of calculated and measured values from the nine tests were collected. Figure 4.48 to Figure 4.56 show the code-to-data comparisons of mass flow rates at the break. The calculations agree well with the data. The worst situation is in the subcooled-to-two-phase transition region where the differences are larger.

Figure 4.57 shows the comparison of the calculated mass flux versus the data for all nine cases. The figure clearly shows that the comparison points are uniformly scattered around the

45 degree line. The ratios of (calculated mass flux minus data)-to-data are used to compute the statistics.

The ratios given in Figure 4.58 were evaluated first by separating the subcooled choking and two-phase choking and then as an overall data set. [

] Reference 2

(Section 6.1.2) states the maximum extended mass flux error in two fluid code simulations of Marviken is on the order of  $\pm 20$  percent; the Marviken data report (Reference 24) gives a mass flux error of  $\pm 15$  percent. Thus, the calculation benchmark uncertainty is approximately equal to the reported test value, indicating excellent agreement.

In summary, the HEM critical flow model in S-RELAP5 was shown to adequately calculate the critical break flow.

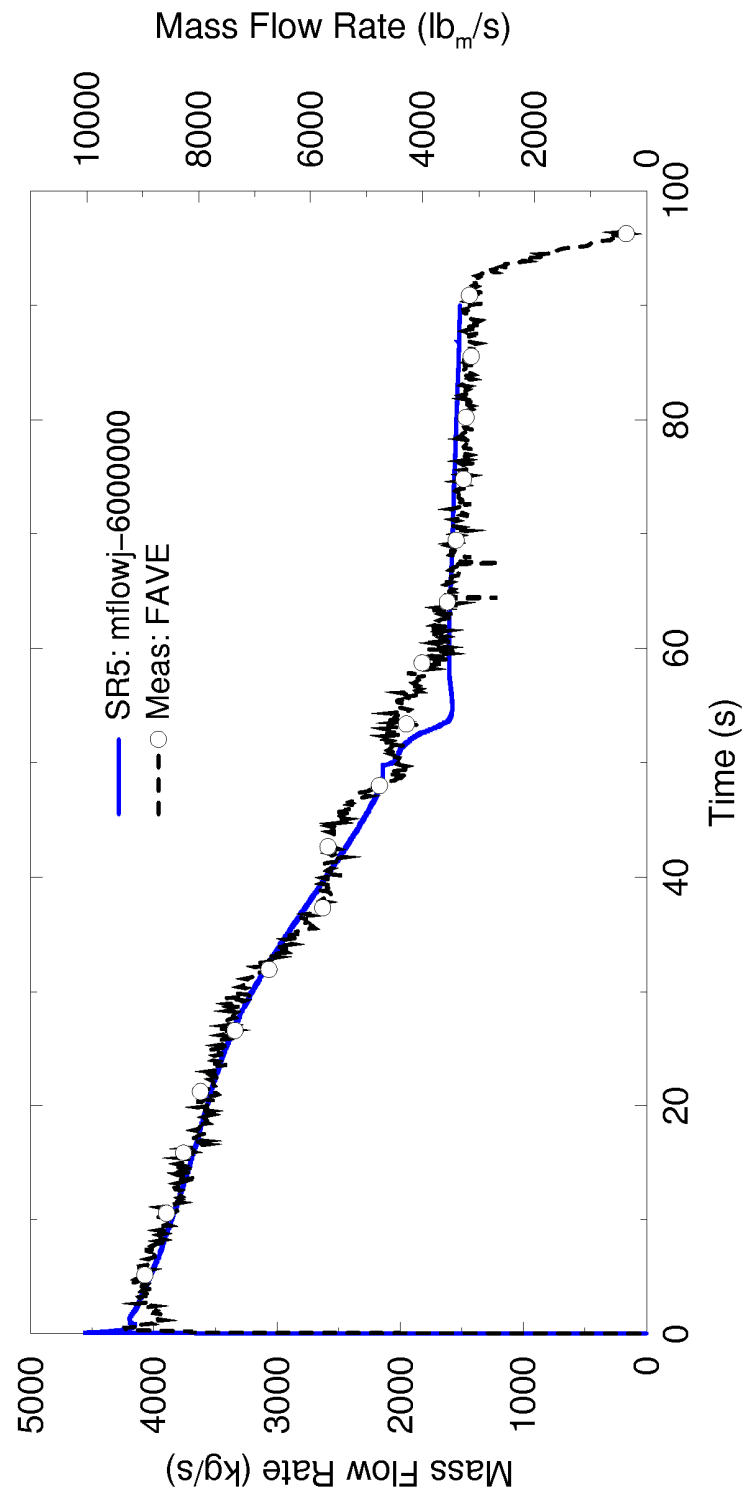


Figure 4.48: Comparison of Break Mass Flow Rates, Marviken Test 2



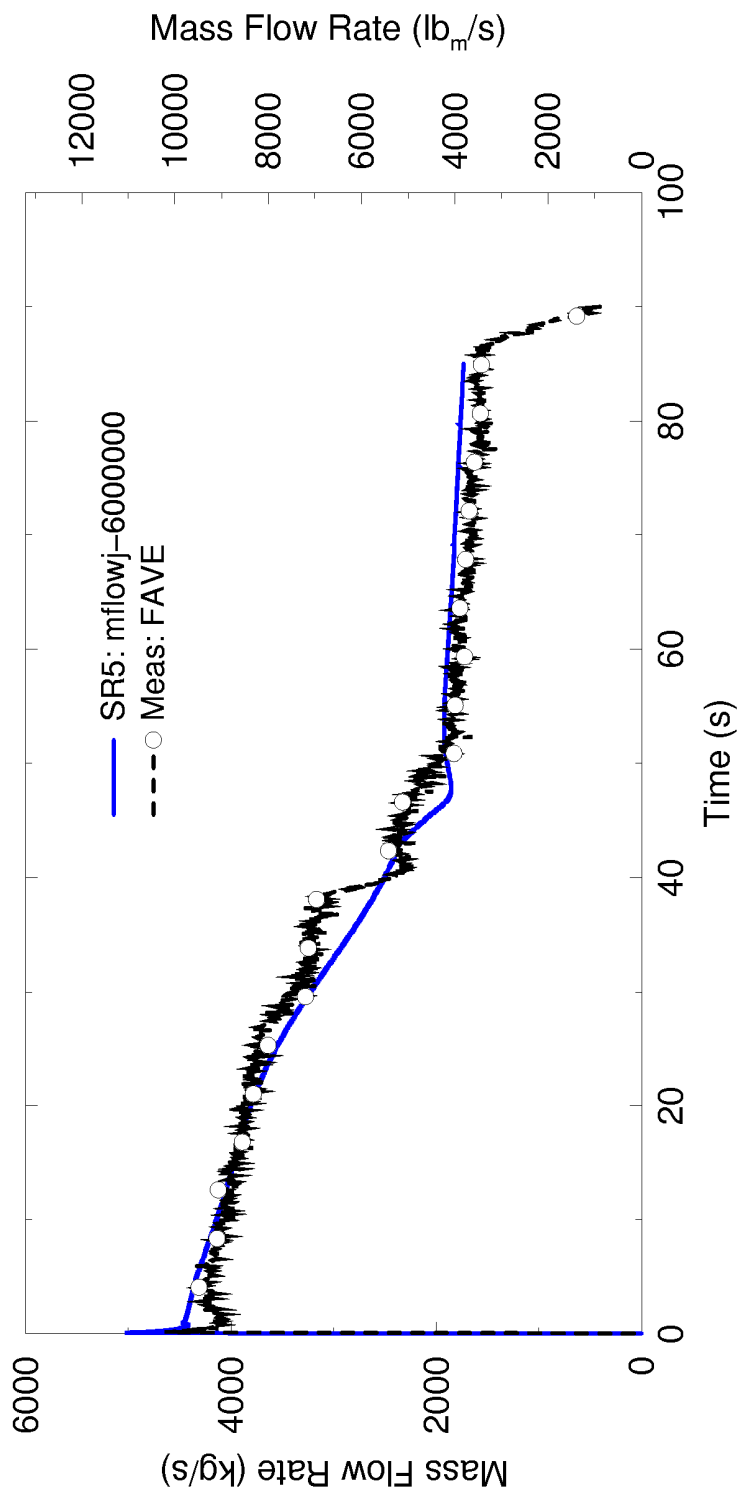


Figure 4.49: Comparison of Break Mass Flow Rates, Marviken Test 6

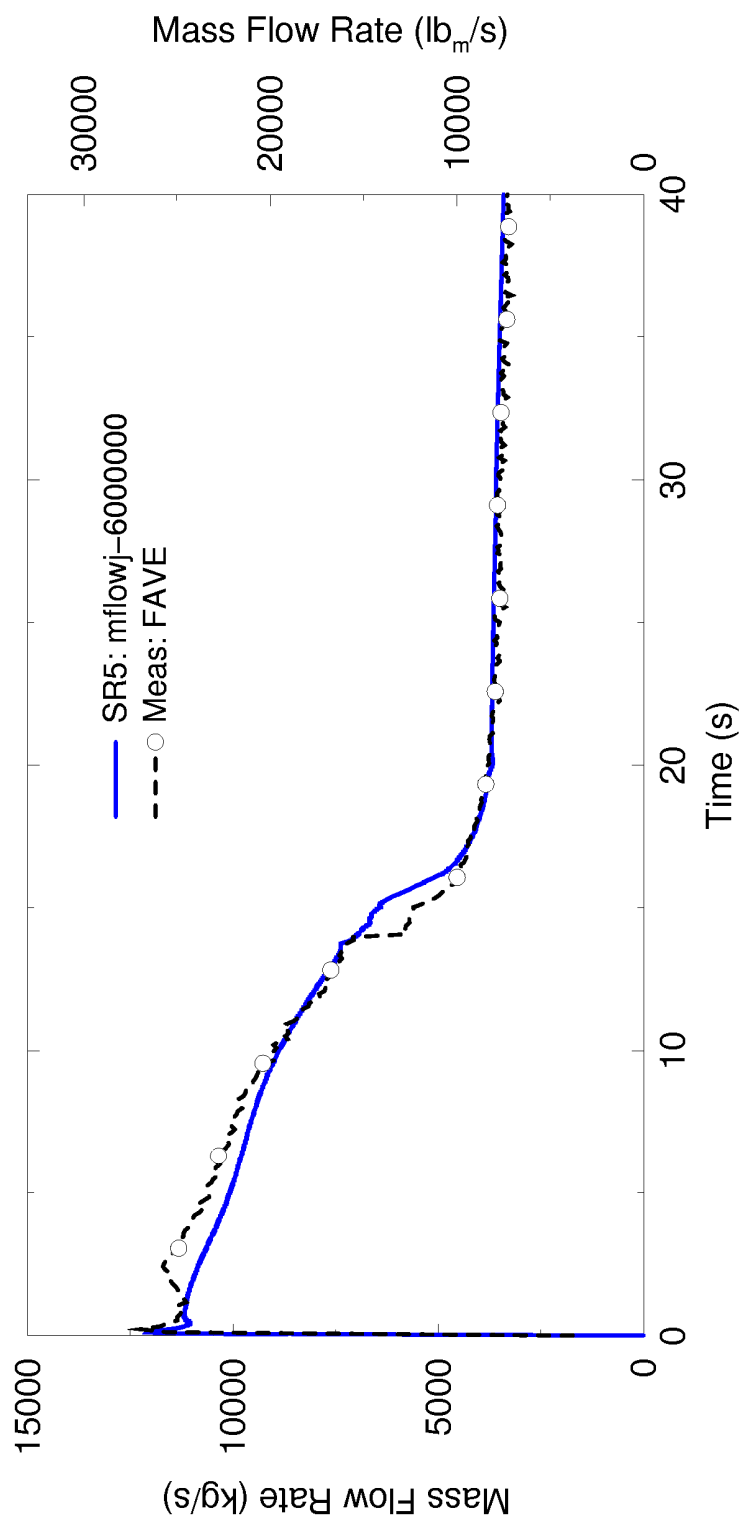


Figure 4.50: Comparison of Break Mass Flow Rates, Marviken Test 8

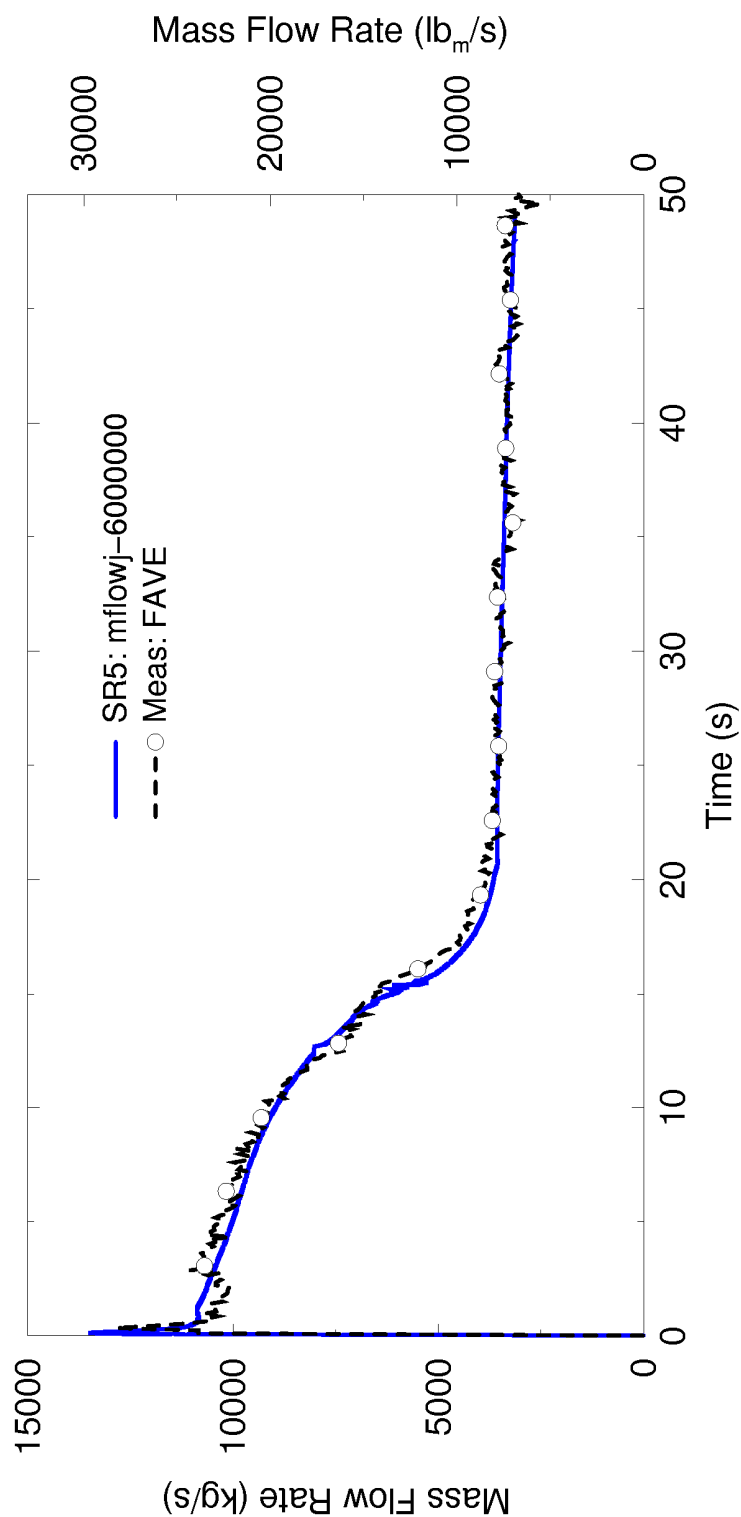


Figure 4.51: Comparison of Break Mass Flow Rates, Marviken Test 16

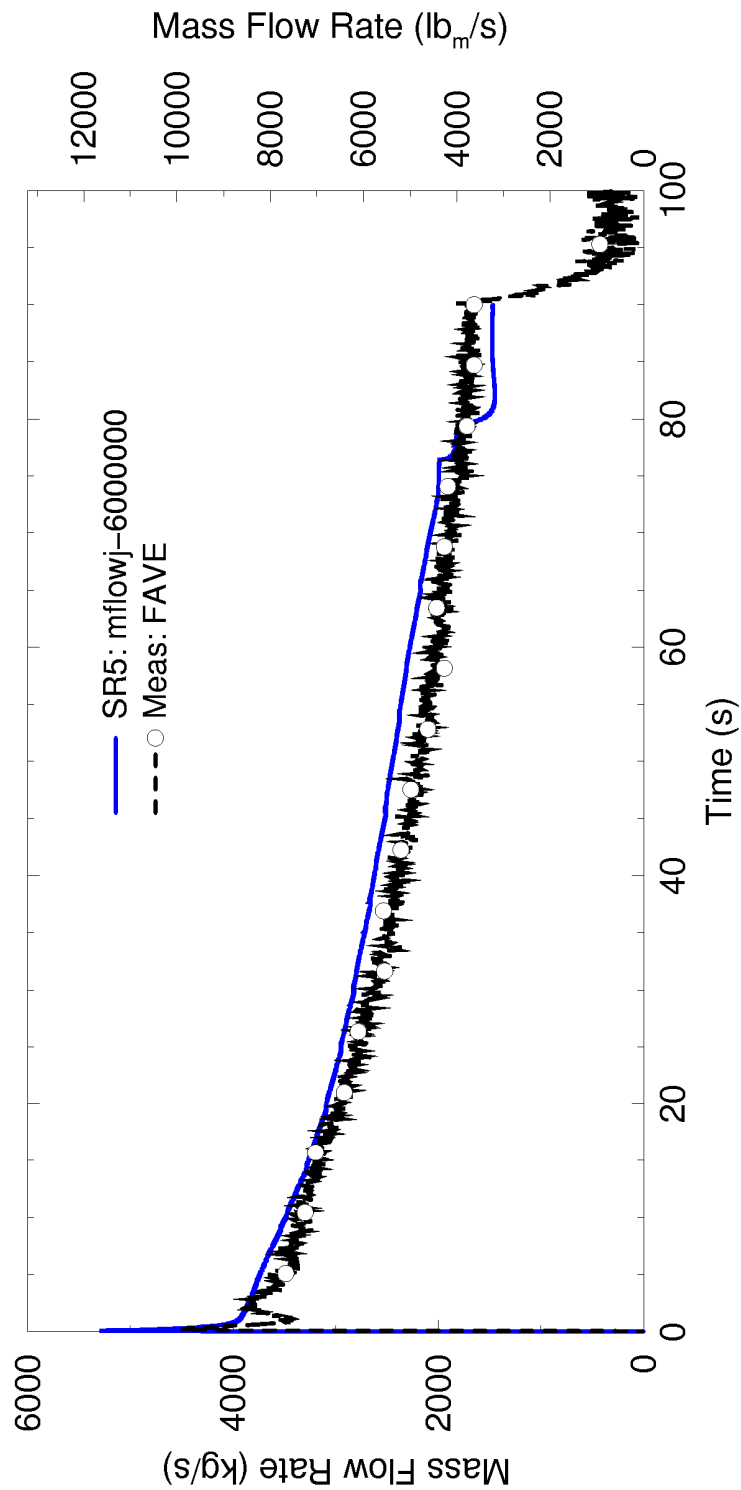


Figure 4.52: Comparison of Break Mass Flow Rates, Marviken Test 17

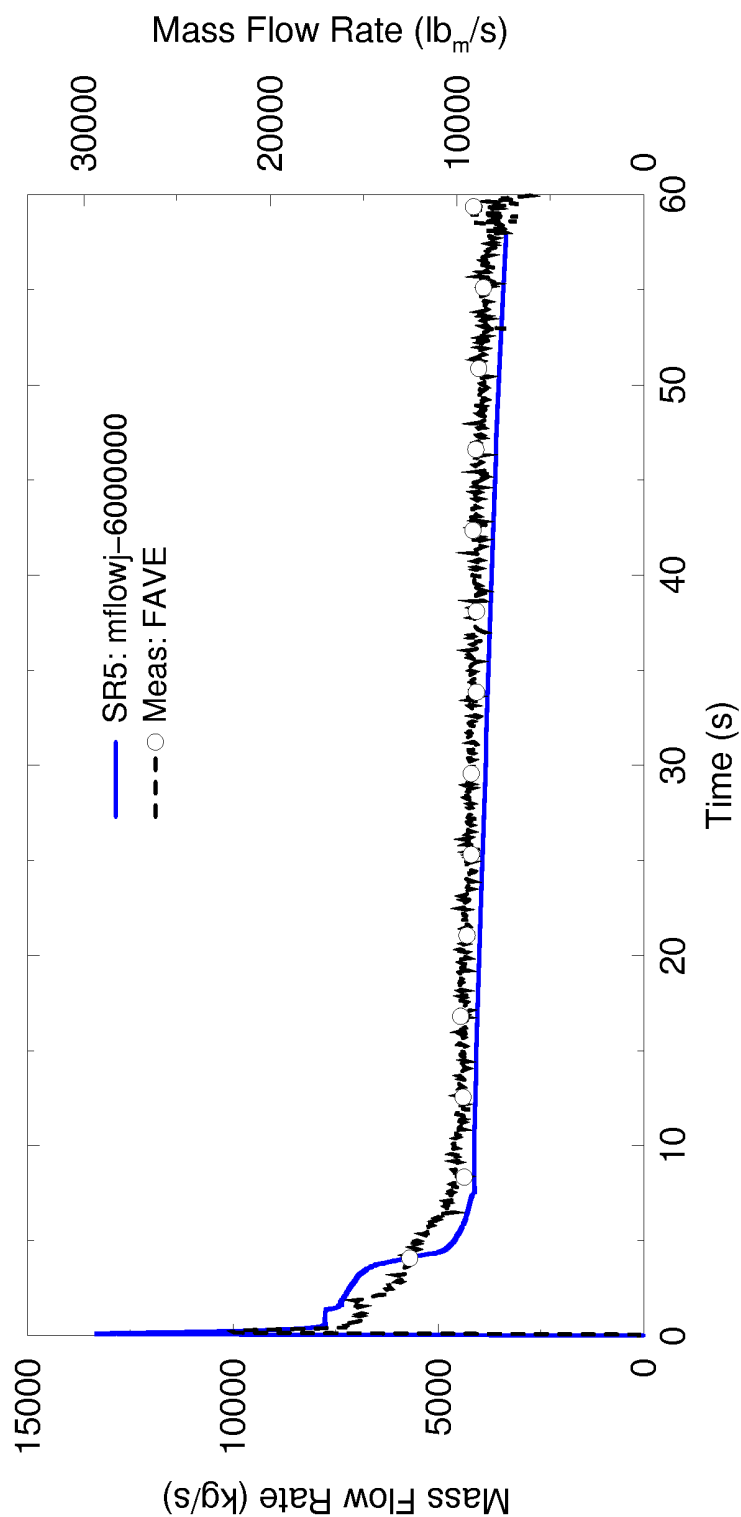


Figure 4.53: Comparison of Break Mass Flow Rates, Marviken Test 20

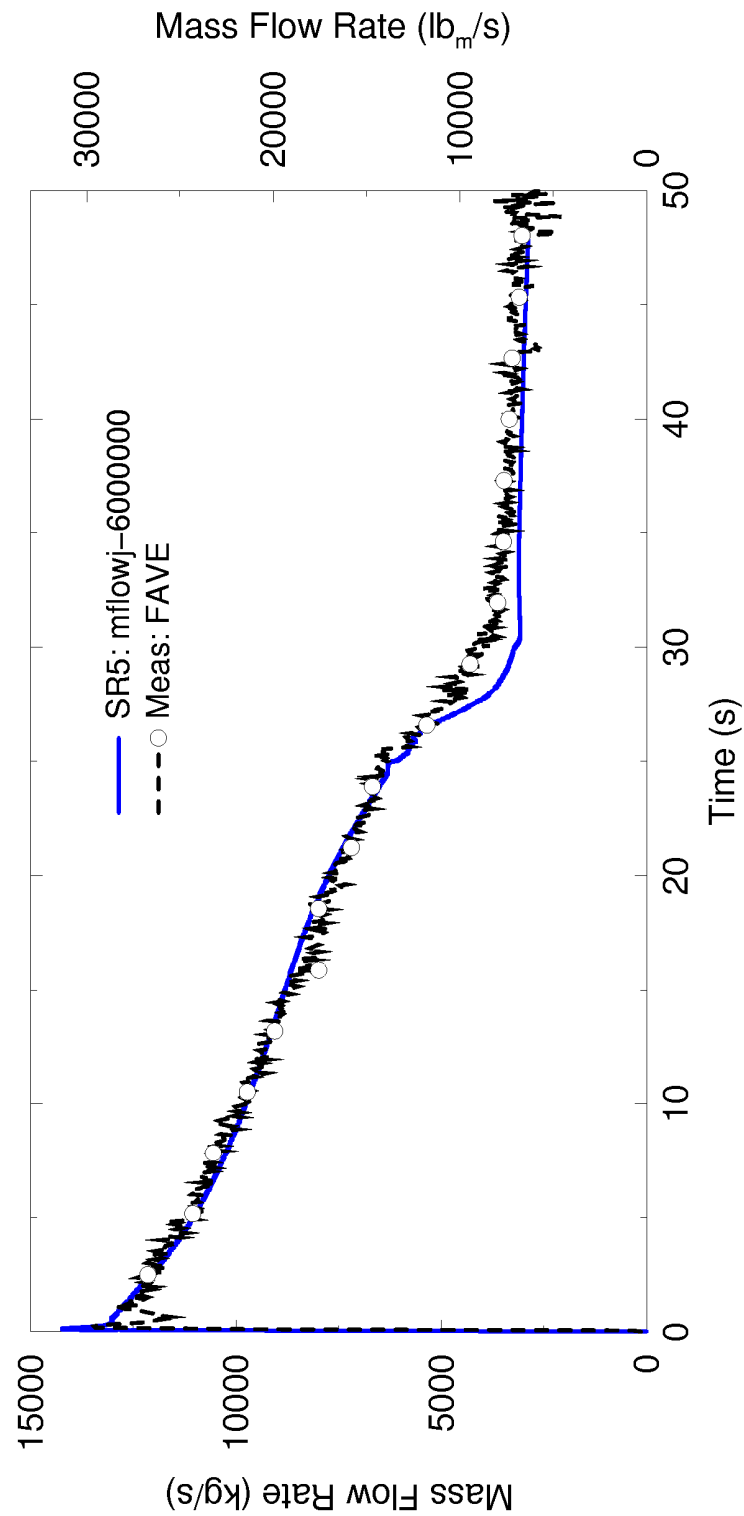


Figure 4.54: Comparison of Break Mass Flow Rates, Marviken Test 22

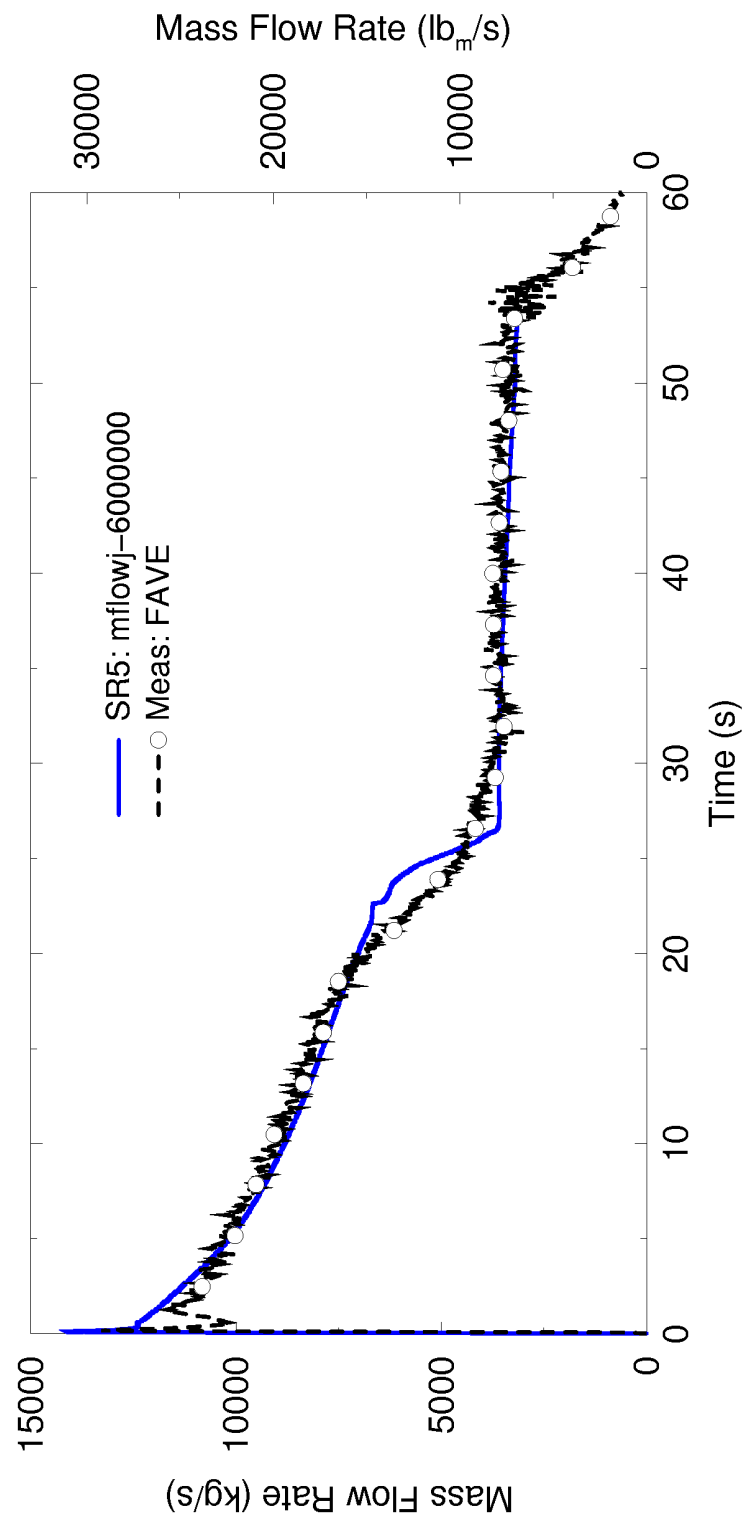


Figure 4.55: Comparison of Break Mass Flow Rates, Marviken Test 24

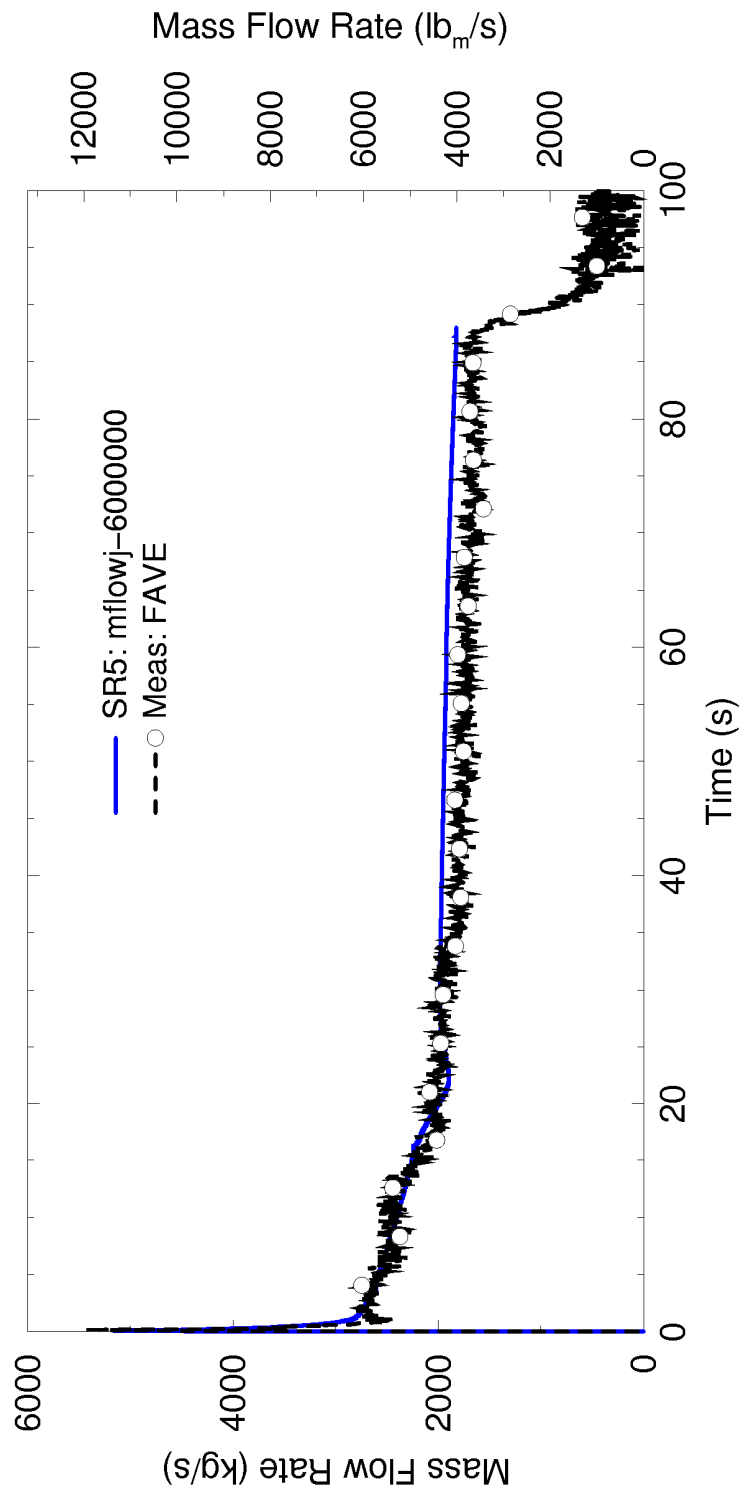
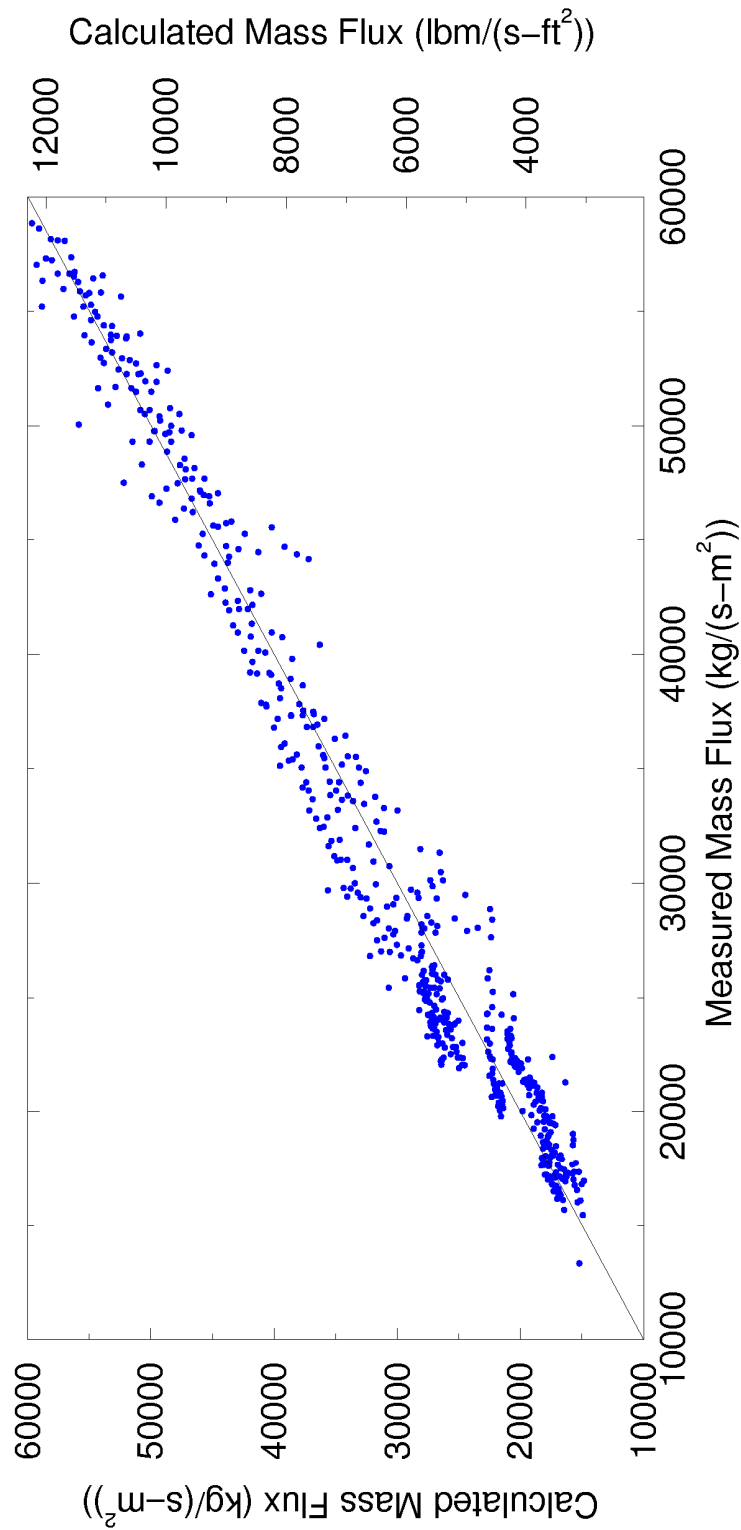
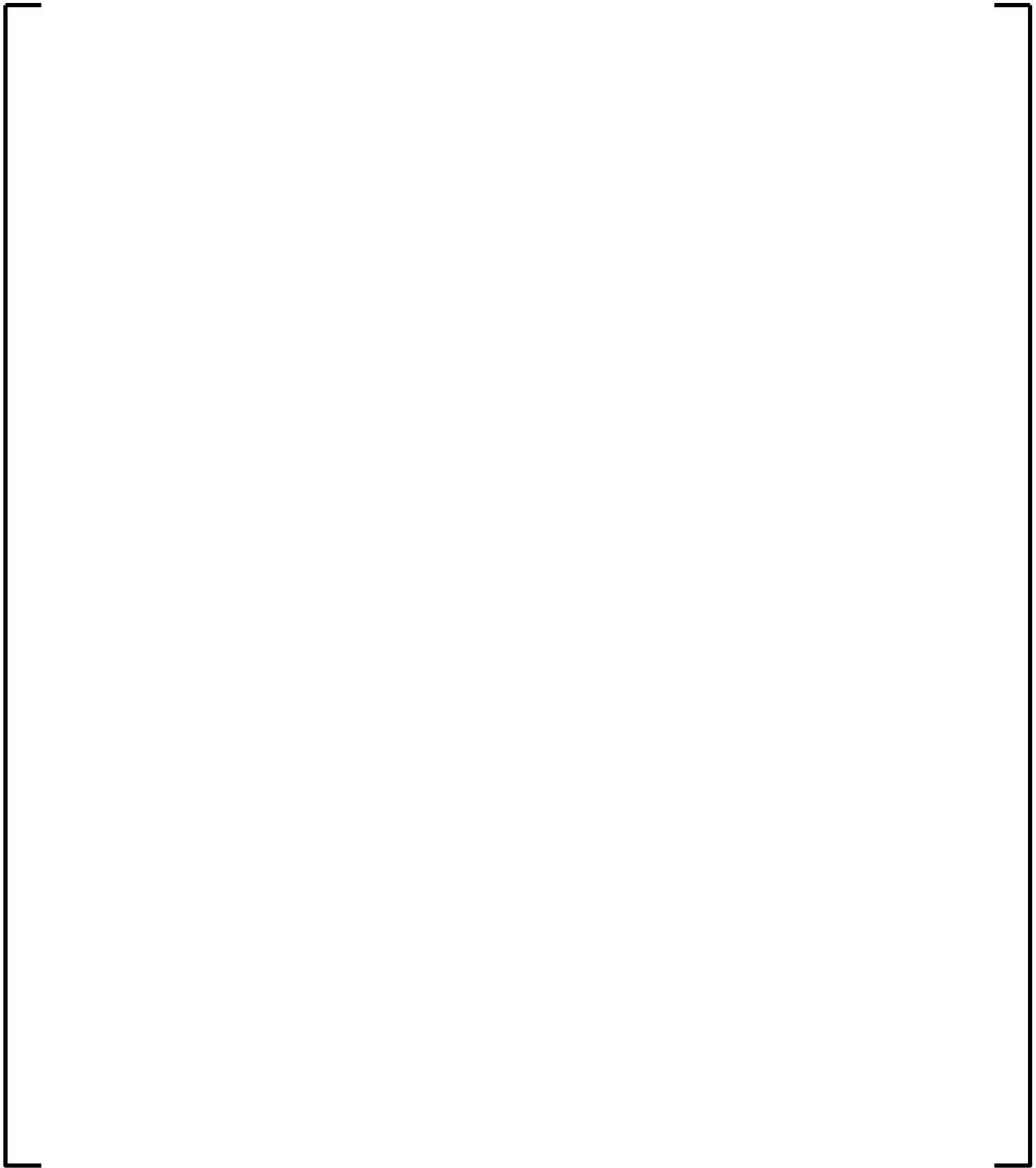


Figure 4.56: Comparison of Break Mass Flow Rates, Marviken Test 25





**Figure 4.57: Comparison of Calculated and Measured Mass Fluxes  
(All Nine Marviken Tests)**



**Figure 4.58: Break Flow Uncertainty, Marviken Tests**

#### 4.3.1.9 Westinghouse/EPRI 1/3 Scale Tests

Twenty-three Westinghouse/EPRI 1/3-scale tests were simulated using S-RELAP5 to assess the ability of the code to calculate the cold leg condensation during the accumulator and pumped-safety injection periods of a LBLOCA.

The principal feature of the test facility was a simulated cold leg break in a 10.42-inch, inside diameter straight pipe. Two ECC injection points were provided so that the pipe lengths downstream of the injection point were either scaled to a typical PWR or were full length. Superheated steam from the boiler flowed through the inlet surge tank and an inlet flow chamber before entering the test section. The inlet flow chamber was designed to yield a uniform velocity profile entering the test section. Cold water from the storage tank entered the test section through either the scaled length ECC injection point or the full length injection point. The effluent fluid exited the test section into the outlet surge tank. The surge tanks upstream and downstream of the test section help maintain constant pressure boundary conditions for circumstances where large pressure oscillations occurred inside the test section. A tank of air connected to the downstream surge tank is used to control the test specific constant pressure boundary conditions. The test section was fitted at the top and bottom with thermocouples, which provided temperature data for both the vapor and liquid phase in the case of stratified flow inside the test section. Pressure drops along the test section also were measured.

One of the important phenomena identified in PWR LBLOCA is the mixing of the ECCS water with the steam in the cold leg during the LBLOCA refill and reflood phases. The controlling parameter is the interphase condensation heat transfer coefficient. As part of Revision 2 of the RLBLOCA methodology, an interphase condensation model was developed using UPTF Tests 8 and 25, and several Westinghouse/EPRI 1/3-scale tests. These tests generally cover both the accumulator and pumped injection period of a LBLOCA. The cold leg condensation model is summarized in Section 4.3.3.1.14 and discussed in detail in Section 5.2 of Reference 5.

Section 3.8 of Reference 5 documents the assessment results and a sensitivity study of the multiplier on the interfacial heat transfer coefficient. The results are used to support the overall application of the RLBLOCA methodology.

The S-RELAP5 input model consists of the test section and the upstream and downstream surge tanks. The nodalization of the test section is consistent with the RLBLOCA methodology guidelines. The cold leg piping from the ECC injection point to the downcomer is divided into three nodes. The nodalization of the cold leg piping upstream from the ECC injection point is not important since it only provides the steam flow boundary to the model. The condensation model is used in the ECC injection and cold leg nodes downstream of the injection node. Time dependent volumes and junctions are used to provide the flow and pressure boundary conditions. Air is modeled in the test vessel boundary node in order to allow air flow back into the test sections (which was observed in some of the high ECC injection tests).

For the S-RELAP5 assessments, the difference between the liquid effluent temperature and the injection temperature was the primary data because it relates directly to the interfacial condensation heat transfer rate over the entire test section. The capability of S-RELAP5 in predicting the interfacial condensation heat transfer in the mixing of ECCS water and steam can be assessed by calculating and comparing this temperature difference to measured data.

Twenty three runs were assessed; thirteen correspond to the reflood phase after accumulator injection and the other ten to the reflood accumulator injection phase. The primary result sought in this study is the effluent liquid temperature (i.e., the liquid phase temperature at the exit of the test section). For all the cases run, the thermal-hydraulic variables were sufficiently steady at 100 seconds except for several reflood-accumulator tests. Hence the effluent temperatures at 100 seconds were used to compare with the measured data.

Table 4.6 compares the calculated and measured effluent temperature for all the cases. The information from Table 4.6 is plotted in Figure 4.59. The total amount of interfacial heat transfer is approximately proportional to the difference between the liquid effluent temperature and the inlet temperature (i.e., ECC liquid temperature). Denote this difference by  $\Delta T$ . The ratio of the calculated  $\Delta T$  and the measured  $\Delta T$  approximates the ratio between the code-predicted condensation heat transfer and the actual value. Hence, R is defined as

$$R = \frac{(T_{\text{effluent}} - T_{\text{in}})_{\text{measured}}}{(T_{\text{effluent}} - T_{\text{in}})_{\text{calculated}}}.$$

Deviation from unity of R represents a code bias in predicting the interfacial condensation heat transfer during the ECC/steam mixing process. [

] The results show that S-RELAP5 calculated acceptable cold leg condensation rates for the tests that cover both the scaled accumulator and the pumped injection ECC flow rates.

In summary, the EPRI 1/3-scaled test benchmarks show that by using the cold leg condensation model described in Section 4.3.3.1.14, S-RELAP5 will calculate acceptable cold leg condensation rates during the accumulator and pumped injection phases of a LBLOCA in a PWR.

**Table 4.6: Comparison of Effluent Temperature for the  
Plant-Consistent Model, Westinghouse/EPRI 1/3 Scale Tests**

<b>Test Number</b>	<b>Liquid, Data (°F)</b>	<b>Liquid, Calculated (°F)</b>	<b>Vapor, Data (°F)</b>	<b>Vapor, Calculated (°F)</b>
5-18	189.0	185.9	183.0	185.9
5-23	249.0	245.1	243.0	245.1
5-24	222.0	219.3	216.0	219.3
5-25	281.0	281.2	282.0	281.9
5-27	229.0	229.1	224.0	229.1
5-30	236.0	237.0	238.0	237.7
5-33	261.0	259.9	254.0	259.9
5-34	228.0	228.1	224.0	228.1
5-48	261.0	261.6	262.0	261.6
5-52	209.0	210.5	230.0	210.6
5-53	184.0	184.0	176.0	184.0
5-57-1	280.0	281.4	282.0	283.1
5-60	231.0	232.6	233.0	233.4
6-41	195.0	198.6	197.0	195.9
6-65	180.5	178.4	182.0	178.4
6-67	157.5	153.1	158.0	153.1
6-69	174.0	174.4	175.0	174.4
6-73	168.0	172.6	169.0	193.9
6-83	174.0	175.3	176.0	175.9
6-88-1	172.0	171.0	174.0	171.0
6-93	134.0	129.4	134.9	132.3
6-95	196.0	197.7	198.0	213.4
6-99	151.0	155.7	153.0	177.2

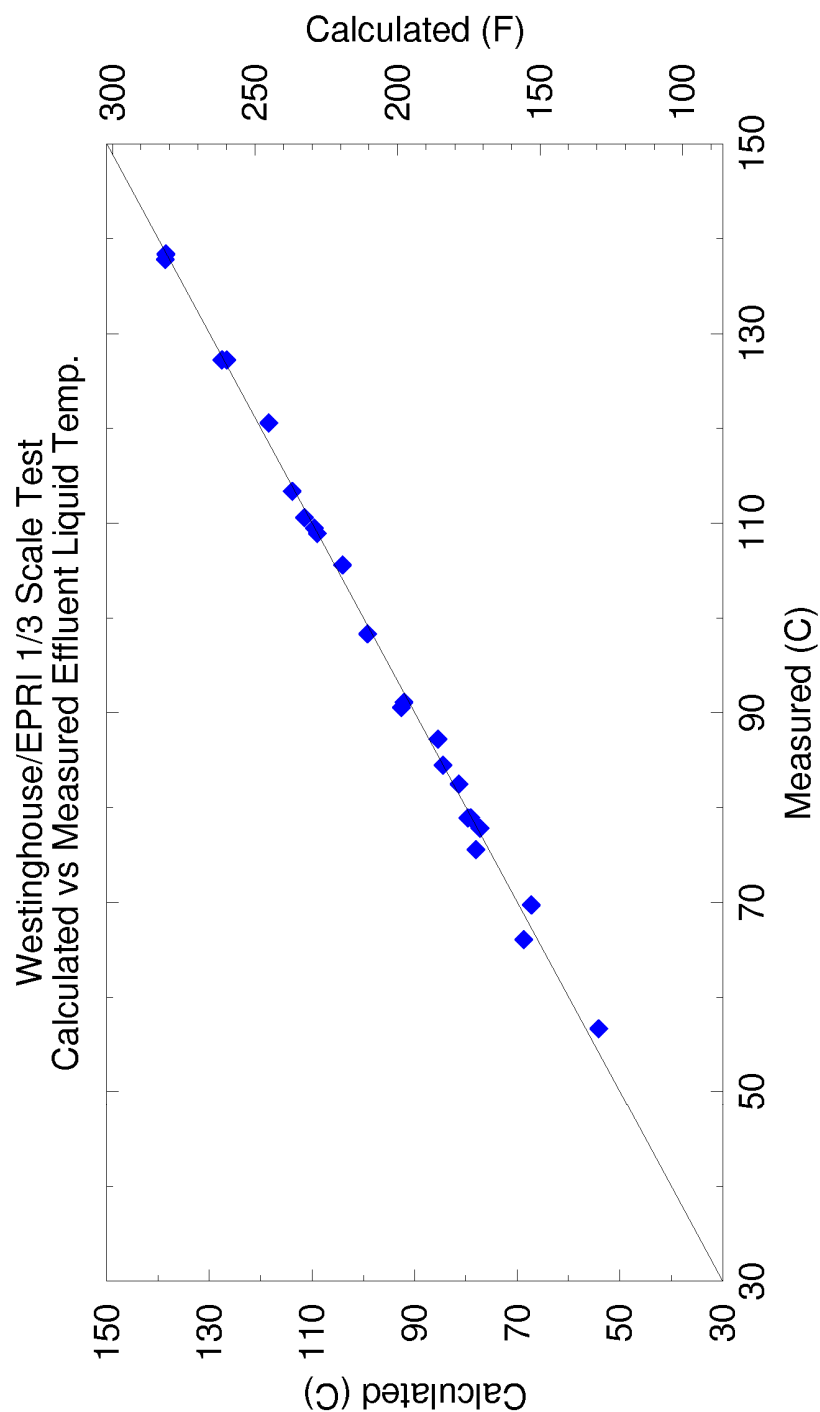


**Figure 4.59: Comparison of Calculated and Measured Effluent Temperature for the Plant-Specific Model, Westinghouse/EPRI 1/3 Scale Tests**

#### 4.3.1.10 AREVA CCFL Tests

As described in Section 3.9 of Reference 25, a small-scale test facility was used to flow test the upper tie plates (UTPs) of interest and determine whether or not the S-RELAP5 calculation of CCFL was sufficient (i.e., accurate or conservative). UTPs from AREVA designs for Westinghouse 15x15 and 17x17 fuel assemblies and a CE 14x14 fuel assembly were obtained and flow tested in the mini-loop of the PDTF. The testing consisted of measuring the liquid penetration in an upflow air channel containing the UTP. CCFL parameters were estimated from the measured data and compared to the corresponding flooding curve predicted for the geometry by the Bankoff correlation (Reference 11) used in the S-RELAP5 CCFL model.

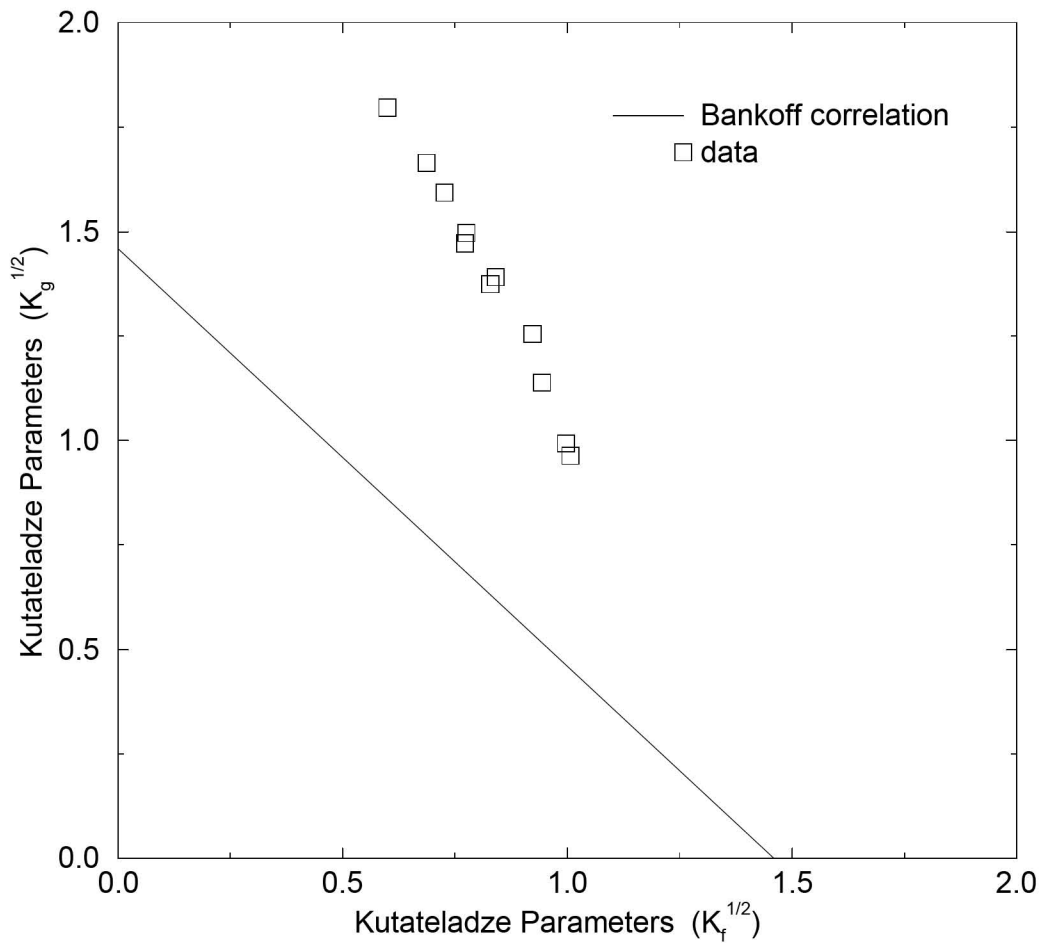
For the geometries used in the experiments, the following hydraulic diameters and resulting intercept (c') were used to calculate the Bankoff flooding curves used for comparison purposes:



Figure 4.60, Figure 4.61, and Figure 4.62 compare mini-loop data with Bankoff. In all cases, the measured data are conservative (acceptable agreement) with respect to the flooding curves using the RLBLOCA parameters [ ].

In summary, the Bankoff CCFL model applied to the AREVA Mini-Loop CCFL data demonstrates this model computes conservative CCFL with respect to the measured CCFL from representative UTPs.





**Figure 4.60: Comparison between Mini-Loop CCFL Data of a Westinghouse 17x17 UTP and Bankoff**

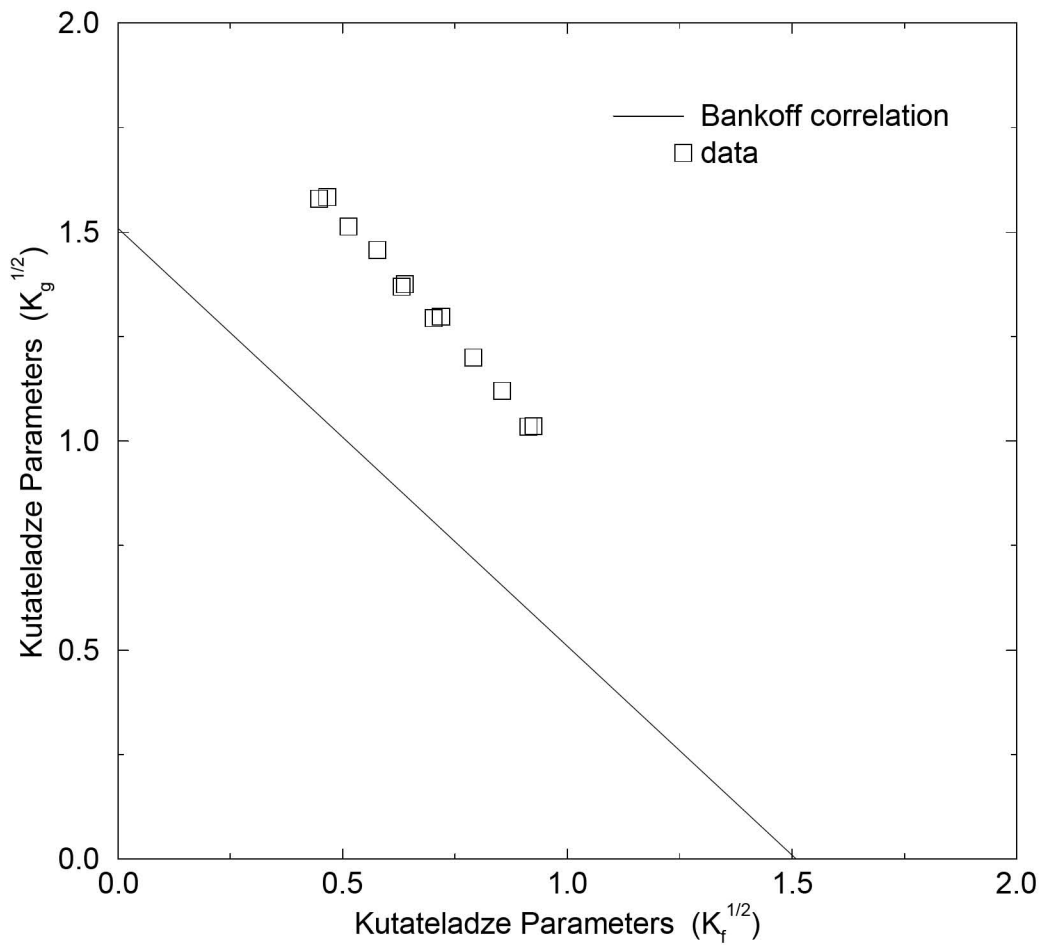


**Figure 4.61: Comparison between Mini-Loop CCFL Data of a Westinghouse 15x15 UTP and Bankoff**

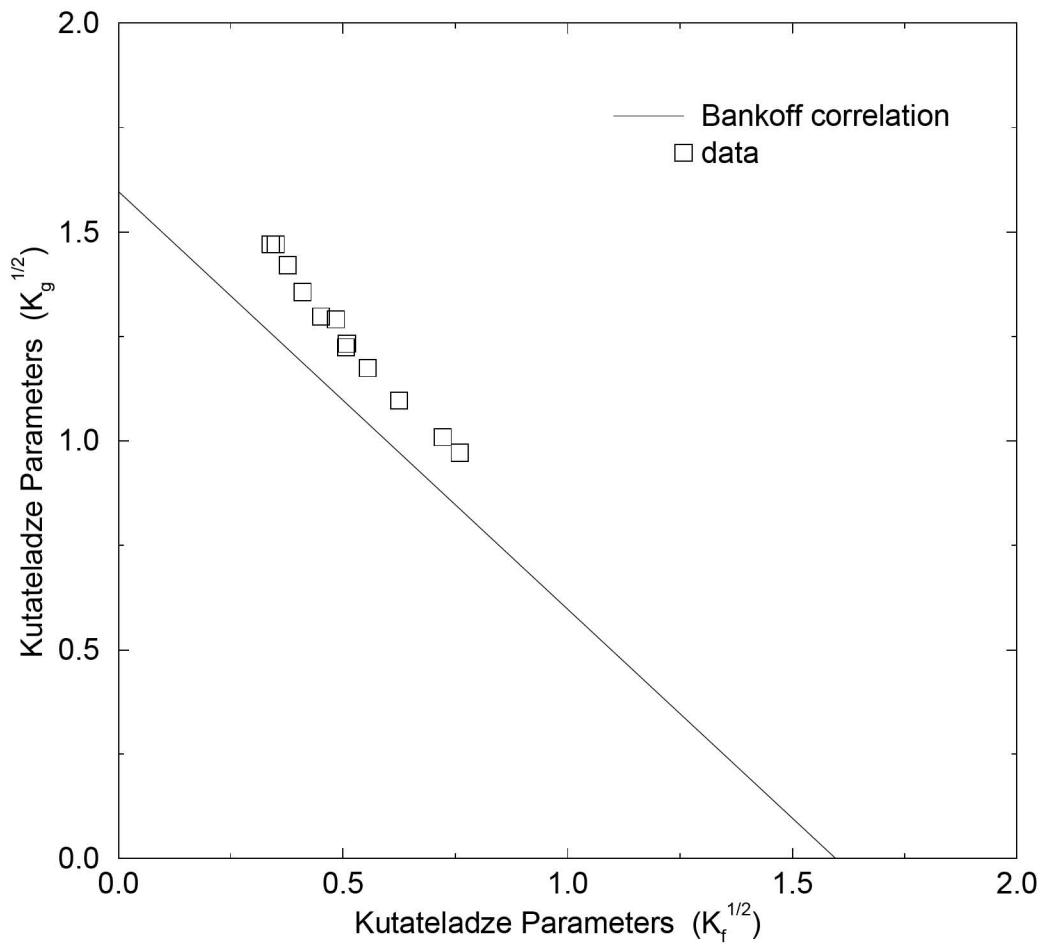


**Figure 4.62: Comparison between Mini-Loop CCFL Data of a Combustion Engineering 14x14 UTP and Bankoff**

#### 4.3.1.11 UPTF Tests

UPTF was operated by Kraftwerk Union AG (KWU) where several separate and integral effects tests were conducted under the 2D/3D Program. UPTF was designed to simulate a German four-loop, 3900 MWt PWR primary system. It was intended to provide a full-scale simulation of thermal-hydraulic behavior in the primary system during the end-of-blowdown, refill, and reflood phases of a PWR LBLOCA. (Note that the refill period, as defined for the RLBLOCA PIRT, includes the end-of-blowdown and refill as defined in UPTF experimental reports).

The reactor vessel, the core barrel, and the greater part of the vessel internals were a full-sized representation of a PWR, as were the four hot and cold legs that simulated three intact loops and one broken loop. The reactor core, steam generators, and coolant pumps were replaced by simulators. Steam produced in a real core during refill/reflood, and the water entrained by this steam, were simulated by steam and water injection sources in the core simulator. Steam production on the primary side of an actual intact-loop steam generator was simulated by injecting steam into the steam generator simulator. The system was capable of simulating both cold and hot leg breaks, including ECC water injection into both intact and broken cold legs and hot legs and into the downcomer. Additional details of the test facility are given in Section 3.7 of Reference 5.

The specific tests assessed with S-RELAP5 include selected runs from the following test series, Tests 6, 7, 8, 10, 12, and 29. The CCFL correlation developed under the 2D/3D program by MPR Associates uses UPTF Test 11 directly in the input model and, therefore, this test was not explicitly simulated.

##### 4.3.1.11.1 UPTF Tests 6 and 7

UPTF Test 6 (Runs 131, 132, 133, 135, and 136) and UPTF Test 7 (Phase IV Run 203) were simulated using S-RELAP5 to demonstrate the ability of S-RELAP5 to self-limit countercurrent flow in the downcomer and to predict acceptable lower plenum refill behavior, including ECC bypass during the refill phase of a LOCA in a PWR. These tests were conducted under the 2D/3D program and were designed specifically to investigate the ECC penetration and countercurrent flow phenomena in the downcomer of a PWR during the refill portion of a LOCA. During the blowdown phase of a LBLOCA, the reactor vessel rapidly depressurizes, causing most of the liquid in the primary system to either flash to steam or flow out through the break.

When the primary system pressure falls below the accumulator pressure, ECC from the accumulators flows into the cold legs. The ECC interacts with the loop steam in the cold legs and with the steam flowing upwards in the downcomer. This steam-water interaction creates a complicated multidimensional flow pattern in the downcomer. The resulting countercurrent flow in the downcomer is important since it affects how quickly the lower plenum refills and when core reflooding starts.

For Tests 6 and 7, the UPTF system was configured to simulate the refill phase of a cold leg break PWR LBLOCA. These tests were steady-state runs. The pump simulators were closed and only the cold leg valve was opened. In Test 6, five benchmark runs (Runs 131, 132, 133, 135, and 136) were performed, each with a different steam injection rate in the core and the steam generator simulators, to establish points on the flooding curve for UPTF. ECC was injected at approximately 485 kg/s to each of the intact cold legs. Test 7 consisted of four runs (Runs 200, 201, 202, and 203), each performed with several combinations of steam flow and ECC injection. In all runs, steam was injected only through the core simulator and various combinations of loops were used for ECC injection. Since the loops were blocked and the hot leg break valve was closed, the injected steam was forced to flow up through the downcomer, interacting with the ECC water before finally flowing out through the broken cold leg. Only Run 203 was simulated using S-RELAP5 in order to complete the low steam flow flooding curve. Table 4.7 shows the Test 6 and Test 7 conditions.

Since the primary purpose of Tests 6 and 7 was to evaluate the CCF behavior in the downcomer, a simplified S-RELAP5 input model was used for test simulations. The intact cold legs, the downcomer, and the lower plenum were modeled using the RLBLOCA guidelines. The remaining portion of the vessel and hot legs were modeled using a simplified approach. The complete loops were not modeled. The cold leg section, from pump discharge to downcomer, is modeled as four nodes. The downcomer is modeled using a 9x8 two-dimensional ( $z, \theta$ ) component. A loss coefficient of [ ] is applied at the  $\theta$ -junctions to account for the blockage effect due to the hot leg penetrations in the downcomer. The cold leg condensation model, summarized in Section 4.3.3.1.14 and described in more detail in Section 5.2 of Reference 5, was applied in the intact cold legs. In the Test 6 input model, mixture level tracking is turned on in all the lower head/lower plenum nodes. Since lower head draining is activated in Test 7, the mixture level tracking in both nodes of the lower head is turned off to avoid interaction with lower head draining. UPTF Tests 6 and 7, the S-RELAP5 input model, and the results of the

simulation are discussed in more detail in Section 3.7.2 of Reference 5. A summary of the results is provided below.

- Little water was delivered to the downcomer and lower plenum during the period that the intact cold legs were filling with ECC water. Only after the cold legs were filled to a quasi-steady level did a significant amount of ECC begin to penetrate the downcomer and lower plenum.
- When ECC penetration to the lower plenum did occur, the penetration rate tended to vary inversely with the rate of steam flow in the downcomer.
- In both tests, during the period of ECC penetration, ECC water from the two cold legs opposite the broken cold leg tended to penetrate directly downward to the lower plenum. ECC water from the cold leg adjacent to the broken cold leg tended to be bypassed to the broken cold leg. Even though the source of the bypassed water is difficult to identify from the S-RELAP5 results, an acceptable amount of water is bypassed in the calculation for all the runs.
- Highly unstable flow conditions were observed in the downcomer during the tests, as well as in the S-RELAP5 results, during the entire transient period.

Specific LBLOCA refill phenomena addressed by the Tests 6 and 7 benchmarks include:

- Lower plenum refill and ECC bypass

Figure 4.63 through Figure 4.68 show the lower plenum liquid level measured and calculated by S-RELAP5 for each test run. The code is shown to consistently underpredict the lower plenum fill rate. Figure 4.71 shows, as an example, the predicted and estimated (by MPR Associates, Reference 26) integrated vessel side break flow for Run 135. The results for other cases are given in Section 3.7.2 of Reference 5. These results show S-RELAP5 overpredicted the ECC bypass in all the Test 6 runs and slightly underpredicted the bypass in the Test 7 Run 203. It is to be noted that in Run 203 water was drained from the lower head in order to avoid the water entering the core simulator injectors. The Run 203 prediction may be influenced by the interaction of the lower head draining with the lower head sweep-out. The lower head draining is atypical to LBLOCA. These results show S-RELAP5 will calculate acceptable to conservative ECC bypass during the refill phase resulting in an acceptable beginning of core recovery time.

- Downcomer multi-dimensional effects

Highly separated downcomer flows were observed in the tests. This phenomenon is difficult to simulate using system codes like S-RELAP5, which was found to distribute water more uniformly in the azimuthal direction in the downcomer. The primary reason for this behavior is that S-RELAP5 results are based on the use of an average void fraction in a fluid node and numerical diffusion. This homogenization of fluid in the downcomer in the S-RELAP5 calculation can affect the flow distribution between the downcomer and lower plenum during the refill phase of a LBLOCA. However, this homogenization is also one of the major reasons for the acceptable-to-conservative ECC bypass prediction.

- Downcomer countercurrent flow

The various runs were performed with a wide range of downcomer steam flow rates and with two-phase flow conditions, including countercurrent flow. In all cases, the code with the interphase drag models predicted either conservative or acceptable downcomer penetration of ECC water. These results justify that there is no need to use an explicit CCFL correlation to calculate acceptable ECC bypass using S-RELAP5 during the refill phase of a LBLOCA.

- Downcomer condensation

The measured and predicted liquid temperatures in the broken cold leg and lower head for Run 135 are shown as an example in Figure 4.69 and Figure 4.70, respectively. From Figure 4.66 it can be seen that the test started at about 30 seconds, and the period of interest is from approximately 60 to 120 seconds. Therefore, the initial mismatch between the input and the data will have no effect with respect to the period of interest. These results show S-RELAP5, with the cold leg condensation model summarized in Section 4.3.3.1.14 and described in detail in Section 5.2 of Reference 5, calculates acceptable condensation rates due to the steam-ECC water interaction in the cold legs and downcomer. This means that there is no need to apply biases to the interphase condensation models to calculate the condensation in the downcomer due to the steam-ECC water interaction.

- Lower plenum sweepout

The code was shown to overestimate the lower plenum sweepout rate, which is partially responsible for the acceptable ECC bypass. This is primarily due to the 1-D modeling of the

lower plenum/lower head where, as expected, the flow behavior during the refill phase is highly multi-dimensional.

In summary, from the simulation results of UPTF Tests 6 and 7, it can be concluded that S-RELAP5 will conservatively calculate lower plenum sweep-out, lower plenum refill, and ECC bypass rates. This results in a conservative beginning of core recovery time during a LBLOCA in a PWR. S-RELAP5 also calculates acceptable downcomer condensation rates due to steam-ECC water interaction.

#### 4.3.1.11.2 UPTF Test 8

UPTF Test 8 was used to verify the S-RELAP5 cold leg condensation model. UPTF Test 8 was performed under the 2D/3D program to investigate the thermal-hydraulic behavior of ECC water injection in the cold legs during the end-of-blowdown, refill, and reflood phases of a postulated LOCA. Of particular interest in the test are the pressure and fluid oscillations occurring in the cold legs and the ECC entrainment through the reactor vessel side break. Oscillations can be induced by the condensation of steam from the injection of subcooled ECC water, the formation of a liquid plug in the cold leg (slug flow regime), and the transition to the stratified flow regime.

UPTF Test 8 was performed by: (1) isolating the intact loop (Loop 1) closest to the broken loop (Loop 4) at the pump simulator; (2) opening one of the two intact loops (Loop 3) opposite to the broken loop, stabilizing the pressure drop between the upper plenum and the downcomer; (3) opening the break valves in the broken loop; (4) injecting steam into the test vessel; and (5) varying ECC water injection into the other intact loop (Loop 2) cold leg. UPTF Test 8 consisted of two runs (Run 111 and Run 112) that differed by the value of the flow resistance applied in the pump simulator of intact Loop 2. The different resistance results in a different steam rate into intact Loop 2.

Since the primary purpose of the S-RELAP5 simulation is to verify the adequacy of the cold leg condensation model, only the Loop 2 steam generator outlet plenum to downcomer are modeled. The cold leg piping from the pump discharge to the downcomer is modeled as four nodes as described in the RLBLOCA analysis guidelines. The modeling of the remaining cold leg segment is not important since it just provides the steam inlet flow boundary. The cold leg condensation model is applied to the ECC injection node and all downstream nodes. This includes the selection of the non-stratified option in the ECC injection node. The cold leg



condensation model is summarized in Section 4.3.3.1.14 and is described in detail in Section 5.2 of Reference 5.

The measured flow and pressure are input as the boundary conditions to the model. UPTF Test 8, the S-RELAP5 input model, and the benchmark results are discussed in detail in Section 3.7.3 of Reference 5.

The primary results from the comparisons of S-RELAP5 to the UPTF data for Test 8 Run 111 and Run 112 (Figure 4.72 through Figure 4.75) are:

- The primary objective of the test simulation was to validate the adequacy of the prediction of the water temperature entering the downcomer, due to its effect on downcomer boiling during the post-accumulator injection period of a postulated LBLOCA. From Figure 4.72 and Figure 4.74 it can be seen that S-RELAP5 correctly predicted the cold leg liquid temperature for both runs.
- Figure 4.73 and Figure 4.75 show the measured steam temperature upstream of the ECC injection node (A900), the measured liquid temperature near the top of the cold leg (A391—just downstream of the ECC injection location), and the S-RELAP5 calculated flow regime in the injection node for Runs 111 and 112, respectively. The fluid temperature near the top of the pipe is an indication of the flow transition from plug flow (subcooled temperature, Flow Regime 5) to stratified flow (fluid temperature is close to the steam temperature). Since the non-stratified option is selected in the ECC injection node, the predicted flow regime is annular-mist (Flow Regime 6) instead of stratified (Flow Regime 10), and there are some flow regime oscillations in the S-RELAP5 calculation for Run 112. [

] The S-RELAP5 calculated flow regimes are in general agreement with the MPR evaluation as well as from the indication of the thermocouple data shown in Figure 4.73 and Figure 4.75.

In summary, it can be concluded that the S-RELAP5 cold leg condensation model correctly calculates the temperature of the water entering the downcomer during the reflood phase of a postulated LBLOCA.

#### 4.3.1.11.3 UPTF Tests 10 and 29

UPTF Test 10, Run 081 (Test 10B), and Test 29, Runs 211 and 212 (Test 29B), were analyzed to provide specific S-RELAP5 input modeling guidelines for the hot leg and steam generator inlet plenum regions to ensure adequate prediction of the liquid entrainment to the steam generator tube region, and to limit countercurrent flow at the UTP during the reflood phase of a postulated LBLOCA. These tests were separate effect tests specifically designed under the 2D/3D program to investigate water mass distribution in the upper plenum, hot leg, and steam generator inlet plenum, and tube regions during reflood. Limiting water down flow into the core is important because it provides a source of additional core cooling and reduces the likelihood of water carryout to the steam generators. Water carryover to the steam generators is directly related to the prediction of steam binding, which results from liquid vaporization in the steam generator tubes.

For UPTF Tests 10 and 29, the UPTF system was configured to simulate the reflood phase of a cold leg break PWR LBLOCA. For these tests, the lower plenum and lower downcomer were filled with water to block steam flow directly from the core to the downcomer and cold legs. A mixture of steam and water was injected into the core simulator to simulate reflood steam generation and water entrainment. The injected steam and entrained water then flowed to the hot legs via the upper core support plate and upper plenum. From the hot legs, the steam/water mixture flowed into the steam generator simulator inlet plenum and to the cyclone separators where water was separated from the mixture. The separated water was stored and measured in holding tanks, while the steam (and any unseparated water) flowed onward through the pump simulators, intact cold legs, upper downcomer and broken cold leg, and flowed out the break into the containment simulator. Each test consisted of a sequence of phases using different steam and water injection rates. Test 10 Run 081 was a 300 second transient consisting of four different flow phases. The conditions for the four phases of this test are given in Table 4.8.

Test 29 Runs 211 and 212 were 900 second transients consisting of six different flow phases. Each phase consisted of a period of constant steam and water flow rates, followed by a period of no flow. The first two phases of Run 211 and last three phases of Run 212 were flawed. Consequently, the S-RELAP5 predictions will be compared to Run 212 data from Phases 1 and 2 (0 through 300 seconds), and Run 211 data from Phases 3 through 6 (300 through

900 seconds). The test parameters for the six phases in combined Run 212/211 are shown in Table 4.9.

The specific LBLOCA reflood phenomena addressed by UPTF Tests 10 and 29 benchmarks are:

- Steam generator steam binding
- Upper plenum two-phase flow
- Core-to-upper plenum countercurrent flow
- Upper plenum, hot leg, and steam generator inlet plenum entrainment and deentrainment

Since UPTF Tests 10 and 29 are separate effect tests to investigate water mass distribution in the upper plenum, hot leg, and steam generator inlet plenum and tube regions during reflood, a simplified modeling approach was used. The models for the core simulator, upper plenum, hot leg and steam generator inlet plenum were developed using the RLBLOCA modeling guidelines. Loops are not modeled, instead pressure boundaries are provided at the cold leg, as well as the cyclone separator region. A lumped modeling approach is used for the intact hot legs. The input model is summarized below:



These specific modeling options promote entrainment of liquid to the steam generator tube region and limit liquid down flow from the upper plenum to the core region. UPTF Tests 10 and 29, the S-RELAP5 input model, and the simulation results are discussed in detail in Section 3.7.5 of Reference 5.

The following general observations can be made regarding the S-RELAP5 simulations of UPTF Tests 10 and 29.

- Overall the predictions of total water carryover to the steam generator simulators indicate that the code overpredicts (adequate agreement with data) the liquid carryover to the steam generators. This is conservative because it will result in an overprediction of steam binding, which in turn will reduce the reflood flooding rate.
- Overall the predictions of total fallback to the lower plenum region also were shown to be conservative in that the fallback to the core was underpredicted (adequate agreement with data). This is consistent with the overprediction of liquid carryover to the steam generators because more liquid will be present in the upper plenum to be carried over to the steam generators.

Figure 4.76 and Figure 4.77 present plots of Kutateladze parameters at the core exit calculated from the S-RELAP5 results for UPTF Tests 10 and 29, respectively. Values, that were calculated using the UPTF correlation (which was developed using the UPTF CCFL tests), are also shown in these figures. The figures clearly show S-RELAP5 calculates conservative liquid down flow relative to the UPTF correlation.

Figure 4.78 and Figure 4.79 show the liquid carryover to the steam generators for UPTF Tests 10 and 29, respectively. Again, both plots clearly show S-RELAP5 generally overpredicts the carryover of liquid to the steam generators.

In summary, it can be concluded that S-RELAP5 will calculate acceptable liquid entrainment to the steam generator tube region and countercurrent flow at the upper core tie plate for a PWR during the reflood phase of a LBLOCA.

#### 4.3.1.11.4 UPTF Tests 10 and 12

UPTF Test 10 (Run 080) and Test 12 (Run 014) were simulated using S-RELAP5 to demonstrate the ability of the code to properly limit countercurrent flow at the UTP (which connects the core region to the upper plenum region of a PWR) during the LBLOCA reflood phase. Limiting water down flow into the core is important because it provides a source of additional core cooling. It also increases the likelihood of water carryout to the steam generators with the associated steam binding effect. These tests, conducted under the 2D/3D program, were specifically designed to simulate the upper core, the upper plenum, and hot leg fluid flow behavior during the reflood phase of a LBLOCA transient. These tests differed from Test 10 (Run 081) and Test 29 in that flow was allowed between the downcomer and core region and Test 12 included nitrogen injection.

UPTF Test 10, Run 080 was performed to examine countercurrent flow through the UTP. The lower plenum was filled with water to a level of 1.2 meters (3.94 feet), steam was injected into the core, and subcooled water was injected into the intact hot legs. The boundary conditions set up countercurrent flow of steam and water through the UTP.

UPTF Test 12, Run 014 was performed to examine countercurrent flow through the UTP. The water level in the lower vessel at the start of the test was low enough (0.56 meters, 1.84 feet) to allow steam to flow from the core to the downcomer and broken cold leg. Steam was injected into the core, and subcooled water was injected into the intact hot legs. These boundary conditions setup countercurrent flow of steam and water through the UTP.

Since the primary purpose of these benchmarks is to demonstrate the ability of S-RELAP5 to properly limit countercurrent flow at the upper tie plate, a simplified modeling approach was used to model the test facility. [

] The  
tests, input model and benchmark results are discussed in detail in Section 3.7.4 of  
Reference 5.

The key parameters to be compared between the S-RELAP5 simulations and the test results are the down flow of water to the lower vessel region, the Kutateladze countercurrent flow parameters calculated at the junctions between the core and upper plenum, and the upper plenum pressure. Reduced down flow of water to the lower vessel generally is considered to be

conservative because it leads to reduced core cooling. Figure 4.80 through Figure 4.82 show results for UPTF Test 10, Run 080. Figure 4.83 through Figure 4.85 give similar results for UPTF Test 12, Run 014.

Figure 4.80 and Figure 4.83 show plots of Kutateladze parameters calculated from the S-RELAP5 results for Test 10, Run 080 and Test 12, Run 014, respectively. The Kutateladze parameters are calculated using the MPR correlation, which was developed using these tests and are also shown in the figures. From these figures it can be concluded that S-RELAP5 calculated conservative liquid down flow through the UTP. The comparison between the measured and predicted mass flow rate at the UTP (shown in Figure 4.82 and Figure 4.85, respectively) for these two tests also support the conservative liquid down flow conclusion.

Figure 4.81 and Figure 4.84 show the calculated and measured upper plenum pressures for Runs 080 and 014, respectively. These results show S-RELAP5 correctly calculates the pressure for both test cases.

The presence of nitrogen in the system does not appear to have a significant impact on CCFL. One of the differences between Test 12, Run 14, compared to Test 10, Run 080, is that nitrogen was injected into the system in Test 12. Comparisons of the Kutateladze parameters indicate that the presence of the nitrogen in the system does not affect either the S-RELAP5 calculation or the UPTF experimental results for CCFL.

In summary, the results for simulation of UPTF Test 10, Run 080, and Test 12, Run 014, show S-RELAP5 adequately calculates the liquid down flow during the reflood phase of a LBLOCA in a PWR.

#### 4.3.1.11.5 UPTF Test 11

UPTF Test 11 is a series of quasi-steady-state SETs conducted under the 2D/3D program to investigate countercurrent flow of steam and saturated water in the hot leg of a PWR under LBLOCA conditions. The test consisted of a series of flow conditions to map out countercurrent flow curves at two different pressure conditions, 0.3 MPa (low pressure case) and 1.5 MPa (high pressure case). Also under the 2D/3D program, MPR Associates (Reference 27) developed a Wallis form CCFL correlation by using a least square fit to the data. [

]

[ ] Since the CCFL correlation was developed from UPTF Test 11 data, the assessment of the phenomena is best performed with independent data. Therefore, the UPTF Test 11 assessment was not performed as part of the Revision 2 methodology. However, since other UPTF CCFL assessments demonstrated that the code calculated CCFL replicates the input parameters used in the analysis, further assessment is unnecessary.

The UPTF test facility is full-scale. Therefore, the CCFL model developed from UPTF Test 11 will be applied at the junction between the hot leg and the steam generator inlet plenum for analyses of PWR plants and all the appropriate small/full-scale tests (refer to Table 4.2).

**Table 4.7: UPTF Test 6 and Test 7 Conditions**

	Test 6 Runs					Test 7
	135	131	132	133	136	203/IV
Downcomer Pressure (kPa)	1130	978	727	543	360	337
Water Level (m)	0	0	0	0	0	2.0
Vessel Inventory (kg)	0	0	0	0	0	17070
Steam Injection (kg/s)						
Total ( core + steam generators)	436	396	295	202	102	51
Steam Generator (per loop)	30	30	30	30	0	0
ECC Injection (kg/s per loop)	480	483	491	493	490	490
ECC Temperature (C)	129	120	115	119	114	133
ECC Subcooling (C)	56	59	52	36	26	2
Nitrogen Injection (kg/s)	1.03	1.01	1.03	1.02	1.03	0



**Table 4.8: Test Phase Parameters for Test 10 Run 081**

Phase	Start Time (s)	End Time (s)	Steam Injection Rate (kg/s) (lb <sub>m</sub> /s)	Water Injection Rate (kg/s) (lb <sub>m</sub> /s)
1	35	75	125 276	60 132
2	75	135	125 276	16 35
3	135	196	110 243	16 35
4	195	255	87 192	16 35

**Table 4.9: Test Phase Parameters for Test 29 Run 212/211**

Phase	Start Time (s)	End Time (s)	Steam Injection Rate (kg/s) (lb <sub>m</sub> /s)	Water Injection Rate (kg/s) (lb <sub>m</sub> /s)
1	35	175	102 225	140 309
2	175	320	87 192	153 337
3	320	465	100 221	90 198
4	465	615	85 187	101 223
5	615	770	101 223	47 104
6	770	900	85 187	63 139

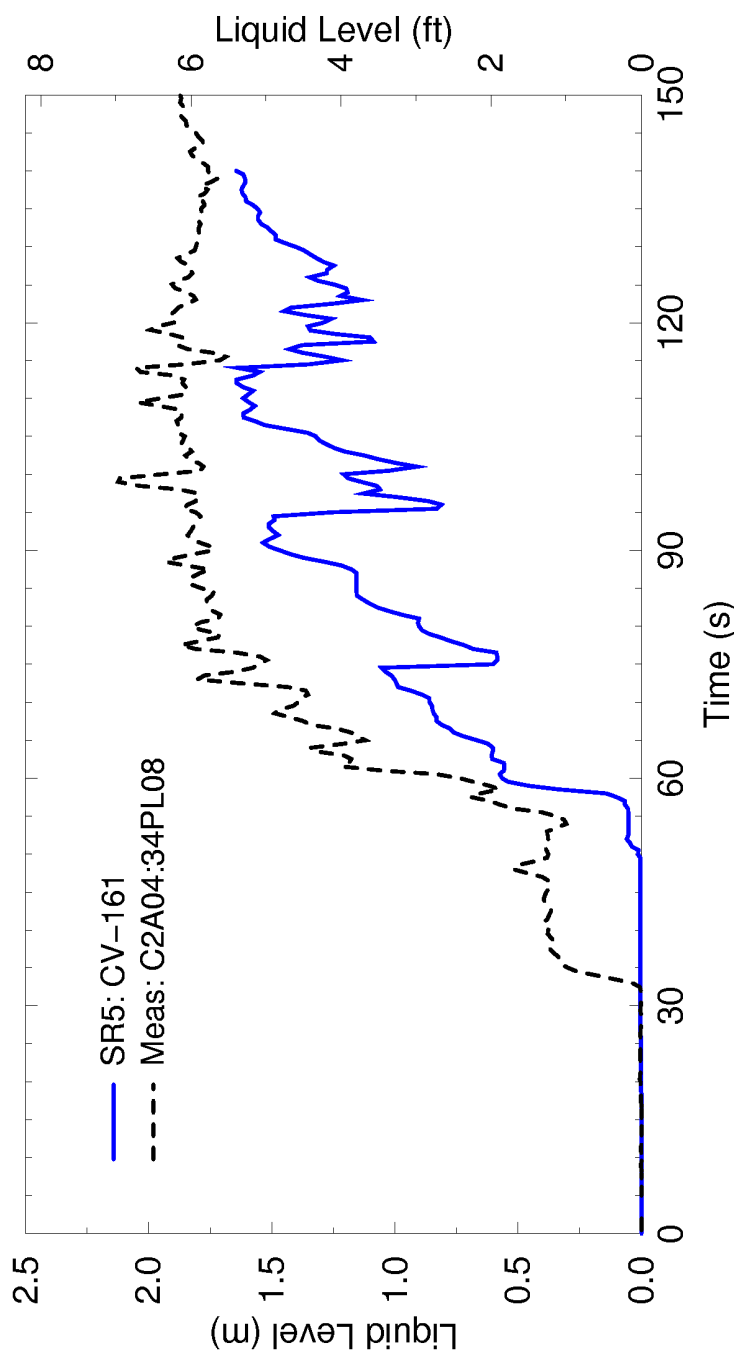


**Figure 4.63: Lower Plenum Liquid Level Comparison  
UPTF Test 6 Run 131**

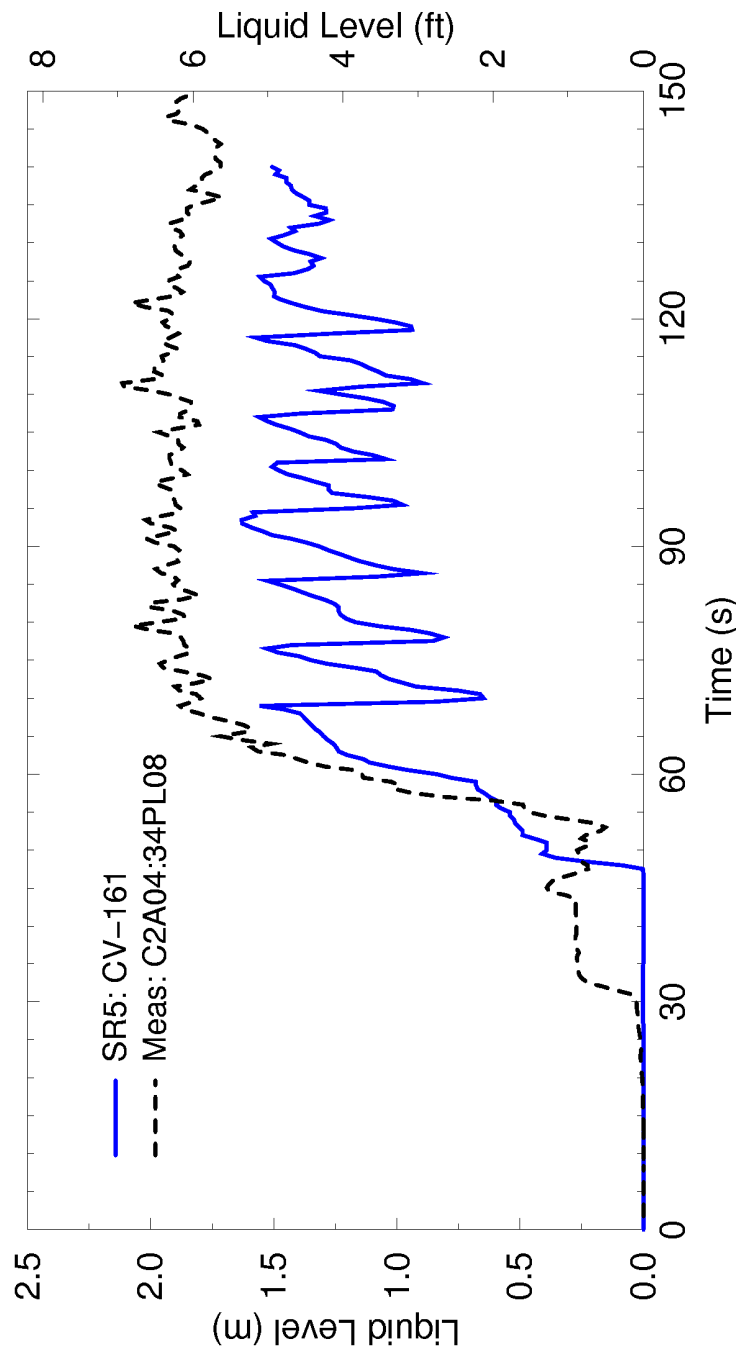


**Figure 4.64: Lower Plenum Liquid Level Comparison  
UPTF Test 6 Run 132**

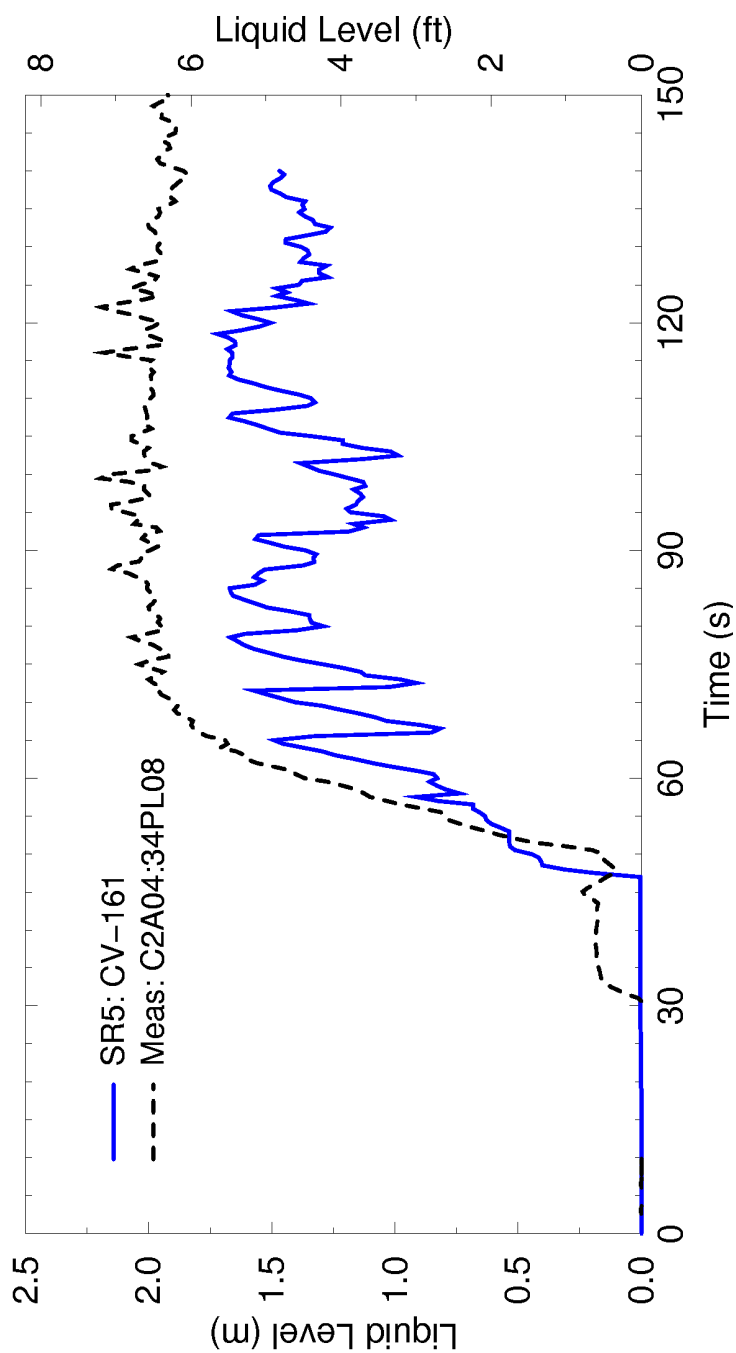


**Figure 4.65: Lower Plenum Liquid Level Comparison  
UPTF Test 6 Run 133**

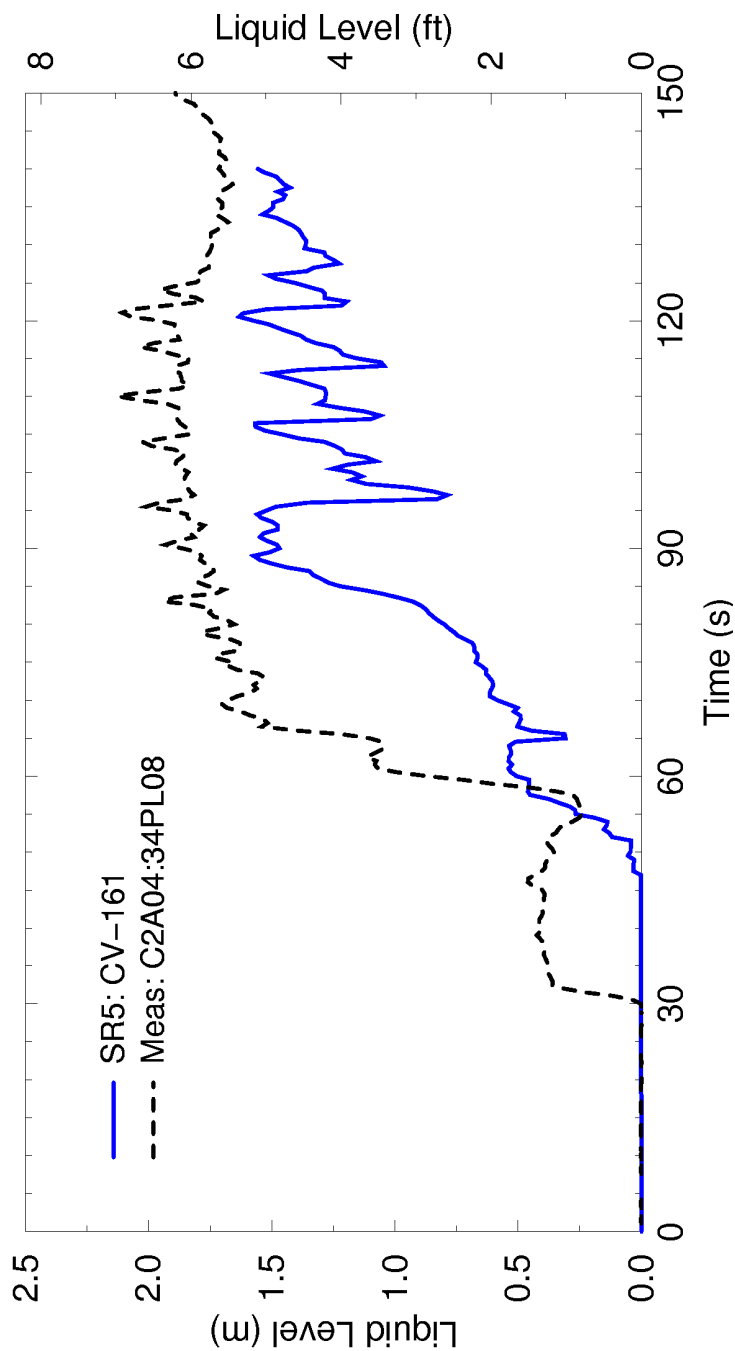


**Figure 4.66: Lower Plenum Liquid Level Comparison  
UPTF Test 6 Run 135**

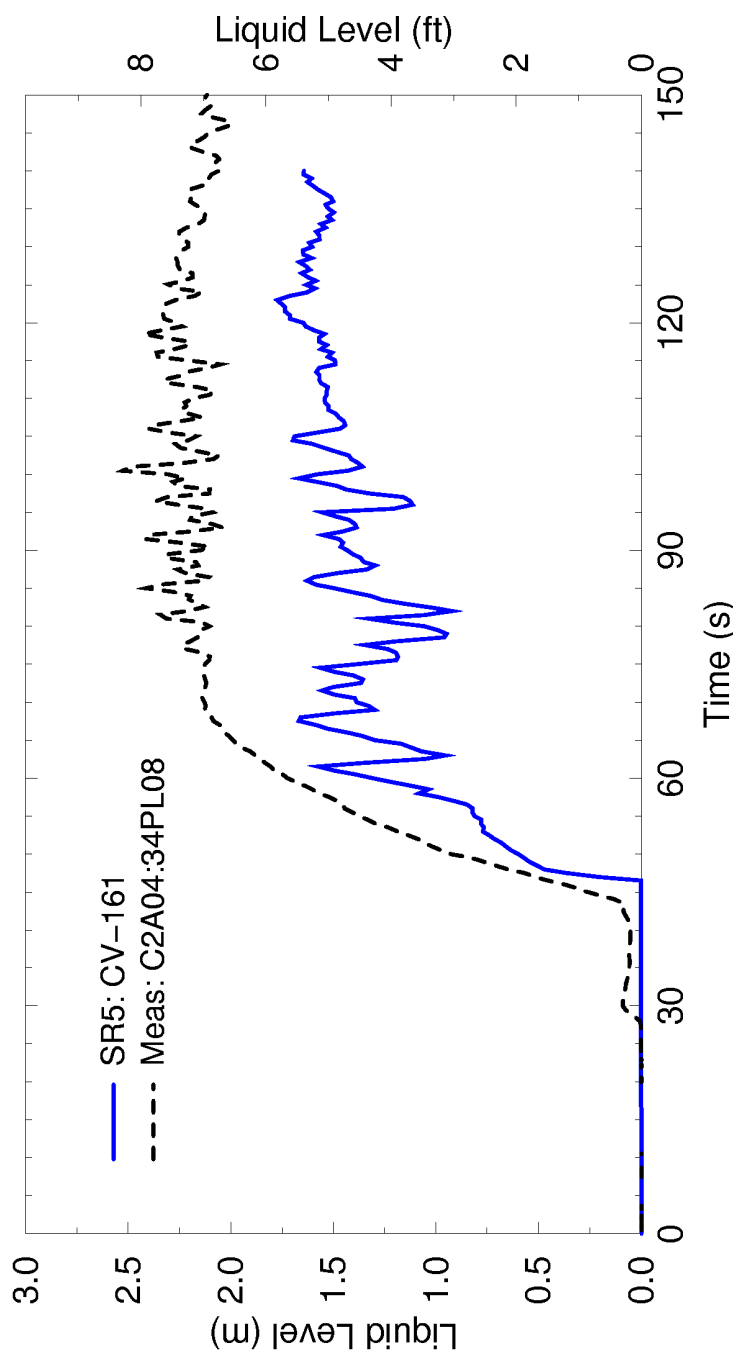


**Figure 4.67: Lower Plenum Liquid Level Comparison  
UPTF Test 6 Run 136**

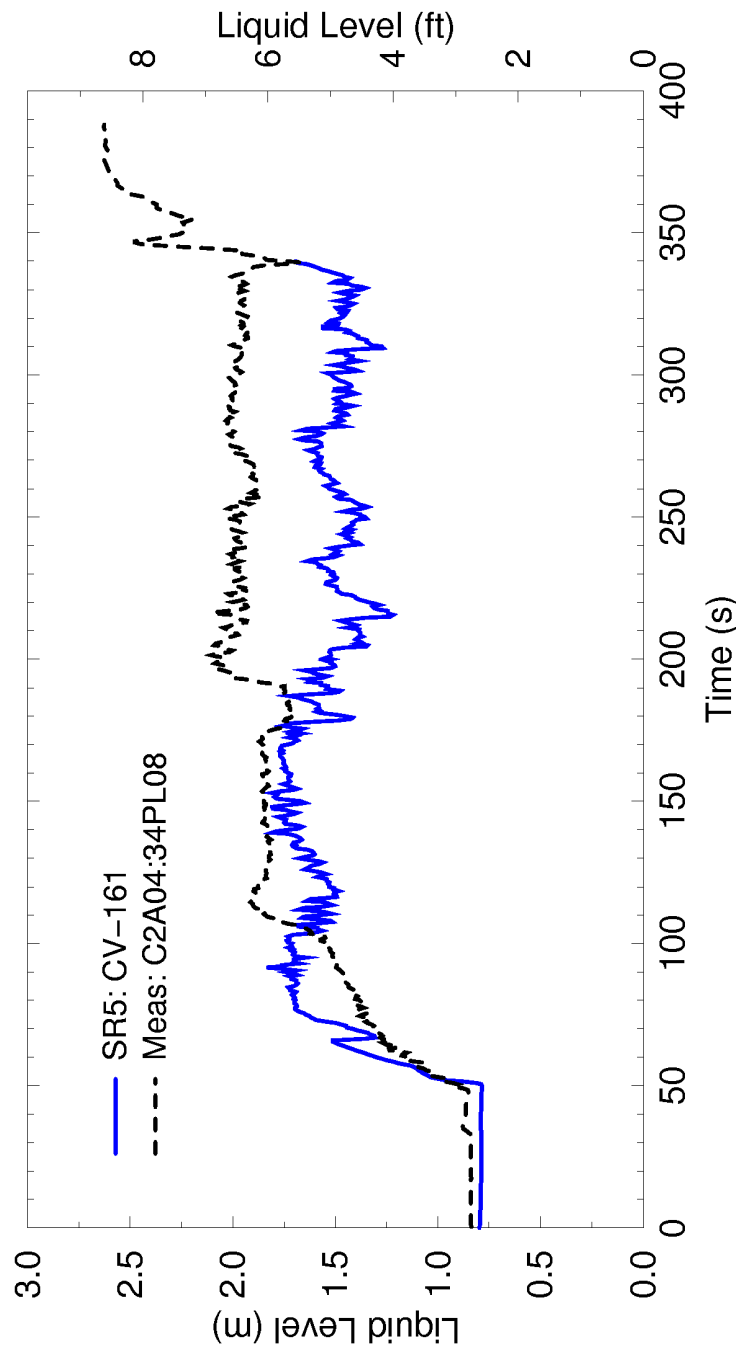


**Figure 4.68: Lower Plenum Liquid Level Comparison  
UPTF Test 7 Run 203**

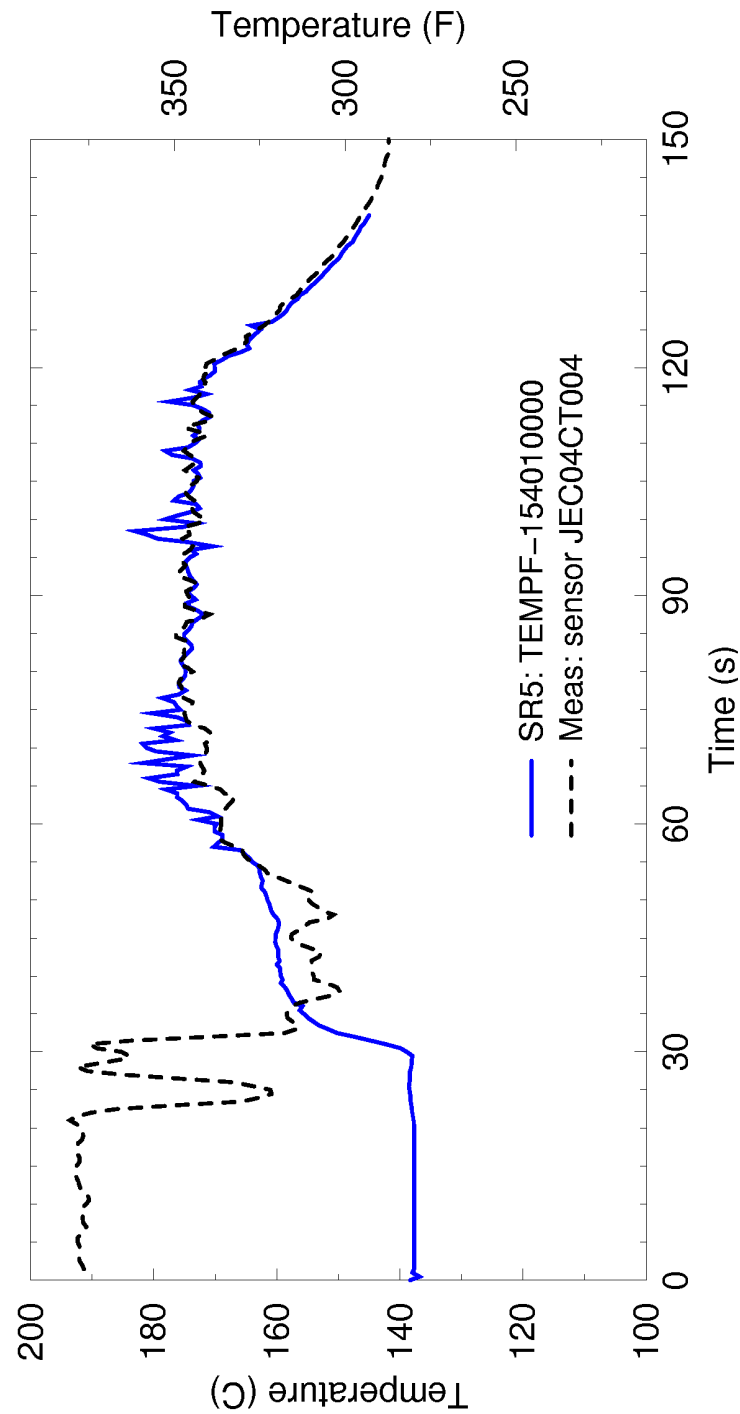


**Figure 4.69: Broken Cold Leg Liquid Temperature  
UPTF Test 6 Run 135**



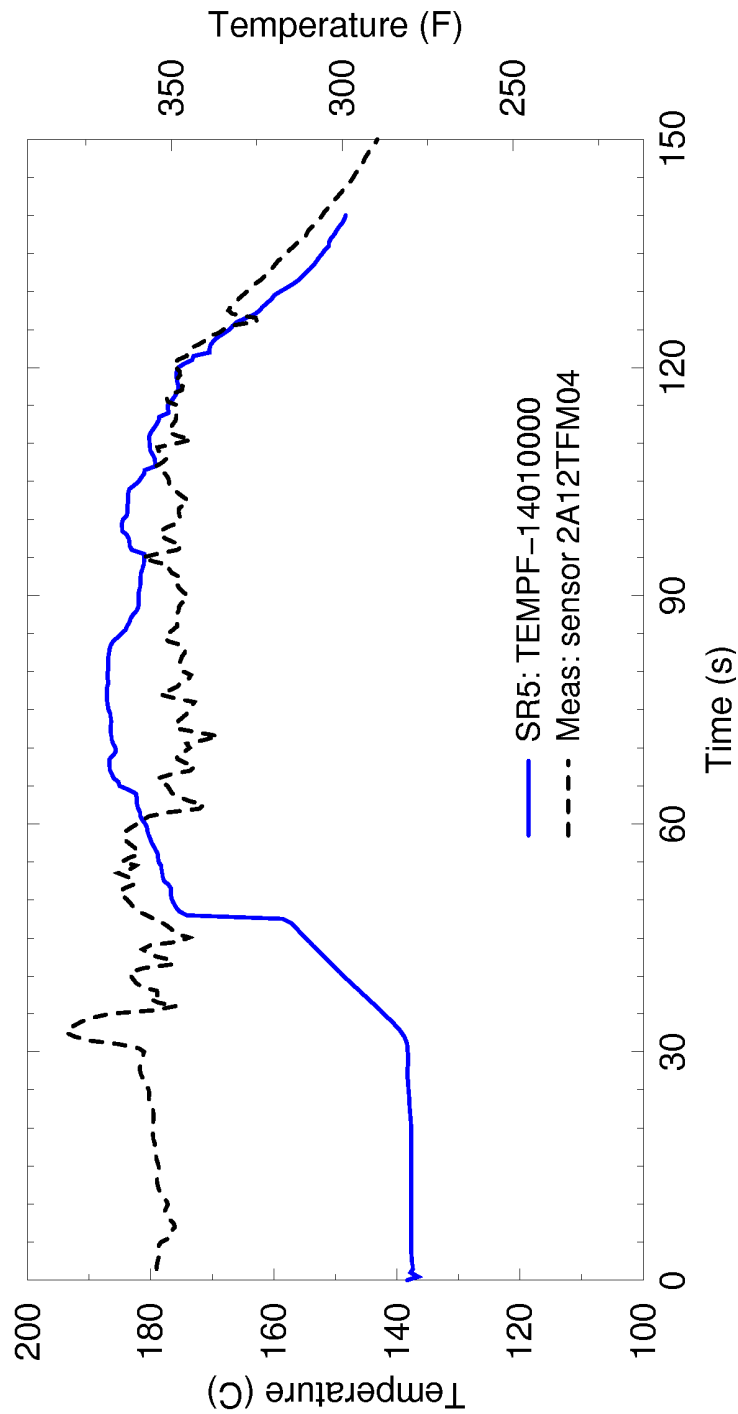


**Figure 4.70: Lower Head Liquid Temperature  
UPTF Test 6 Run 135**

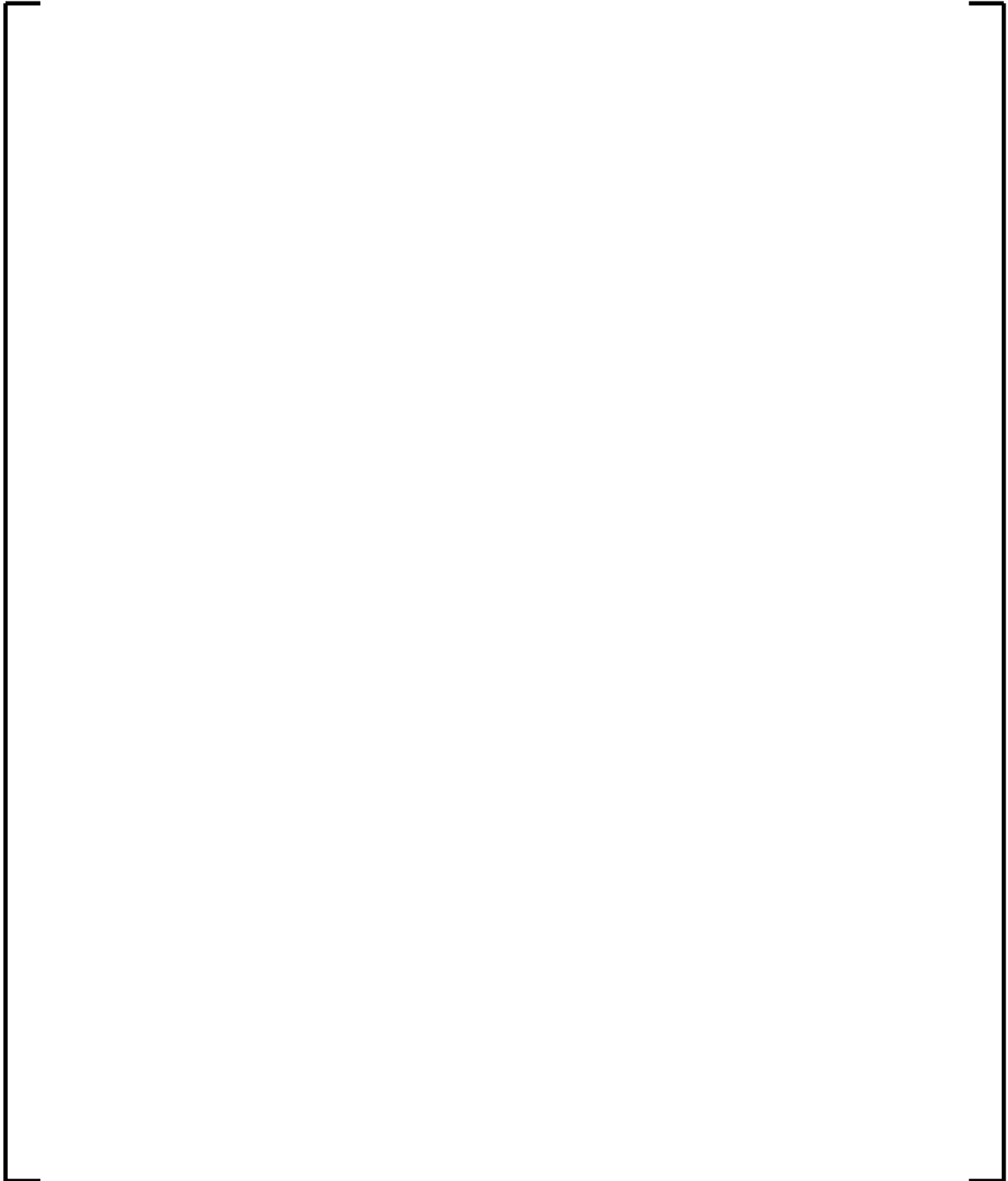


**Figure 4.71: Total Cold Leg Break Flow  
UPTF Test 6 Run 135**

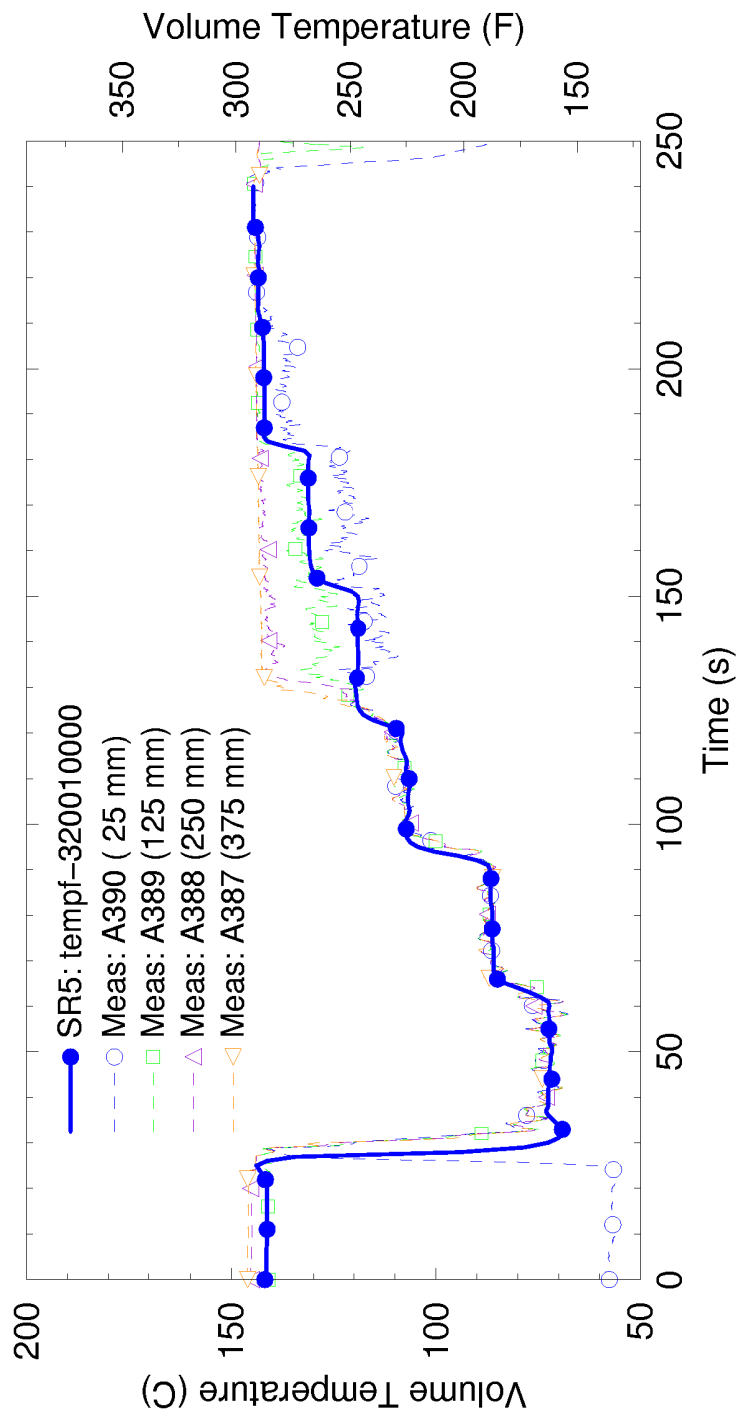


**Figure 4.72: Cold Leg Temperature Comparison  
UPTF Test 8 Run 111**

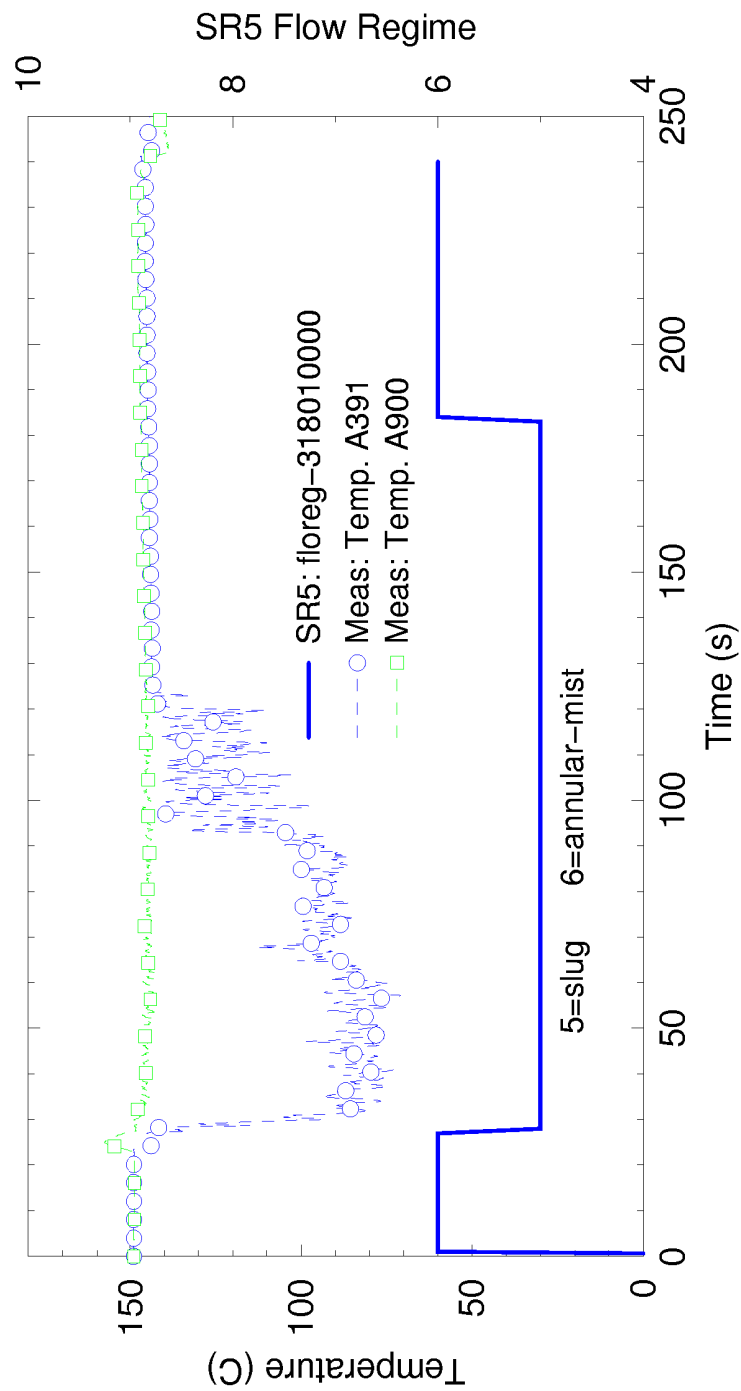


**Figure 4.73: Flow Regime Comparison  
UPTF Test 8 Run 111**

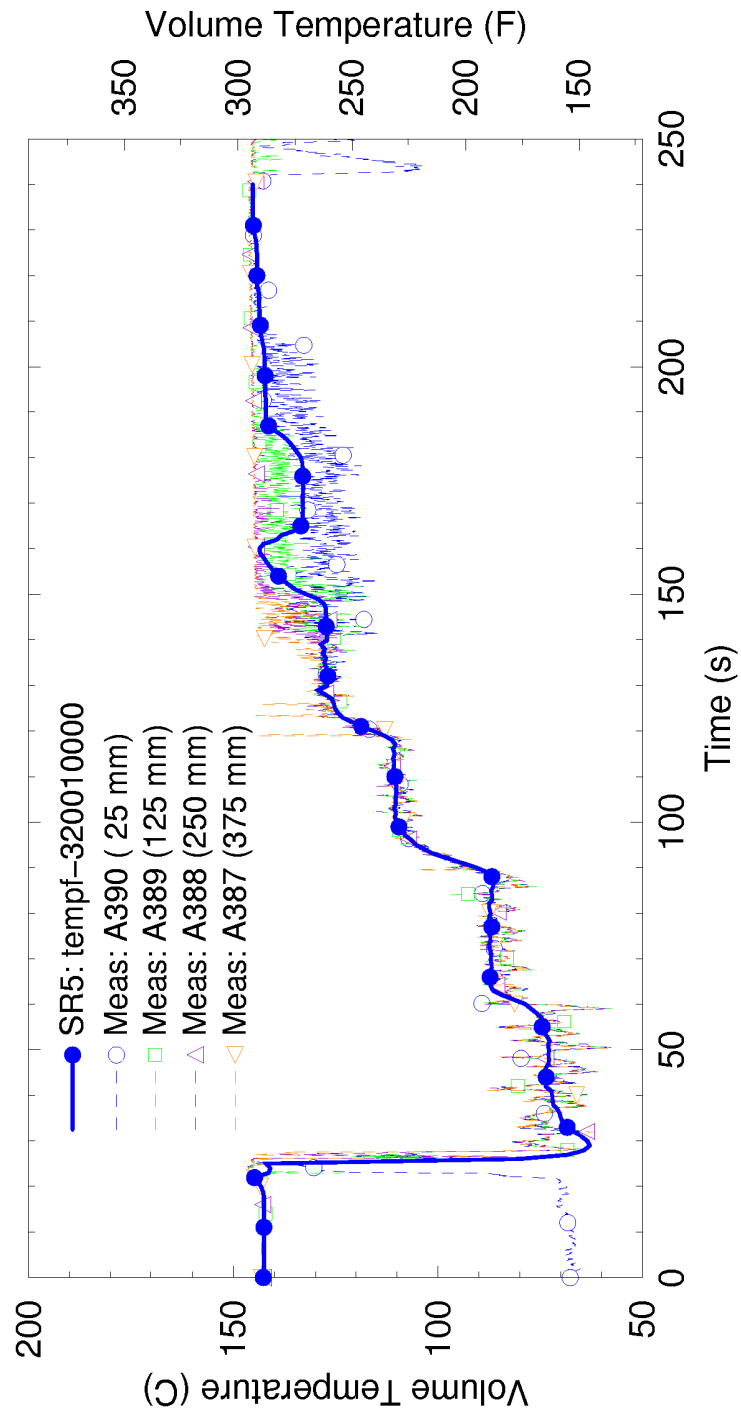


**Figure 4.74: Cold Leg Temperature Comparison  
UPTF Test 8 Run 112**

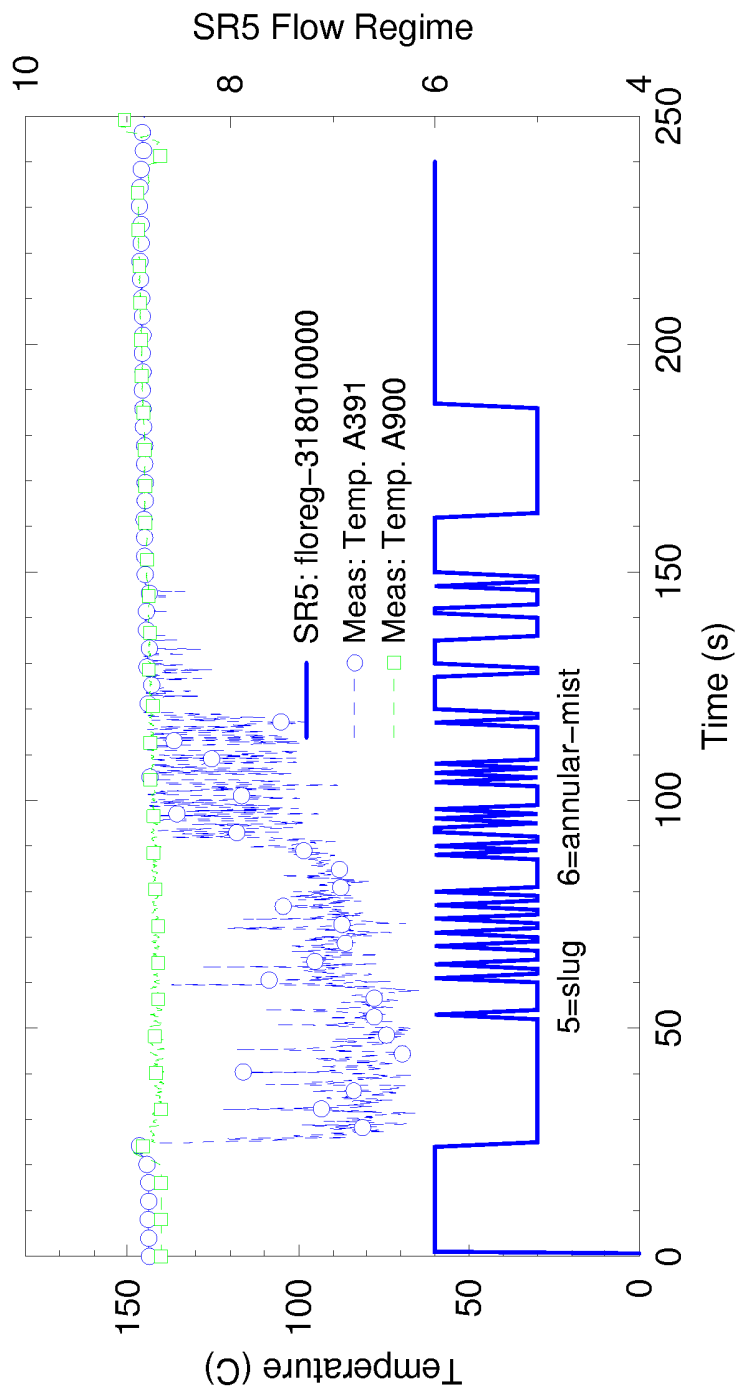


**Figure 4.75: Flow Regime Comparison  
UPTF Test 8 Run 112**

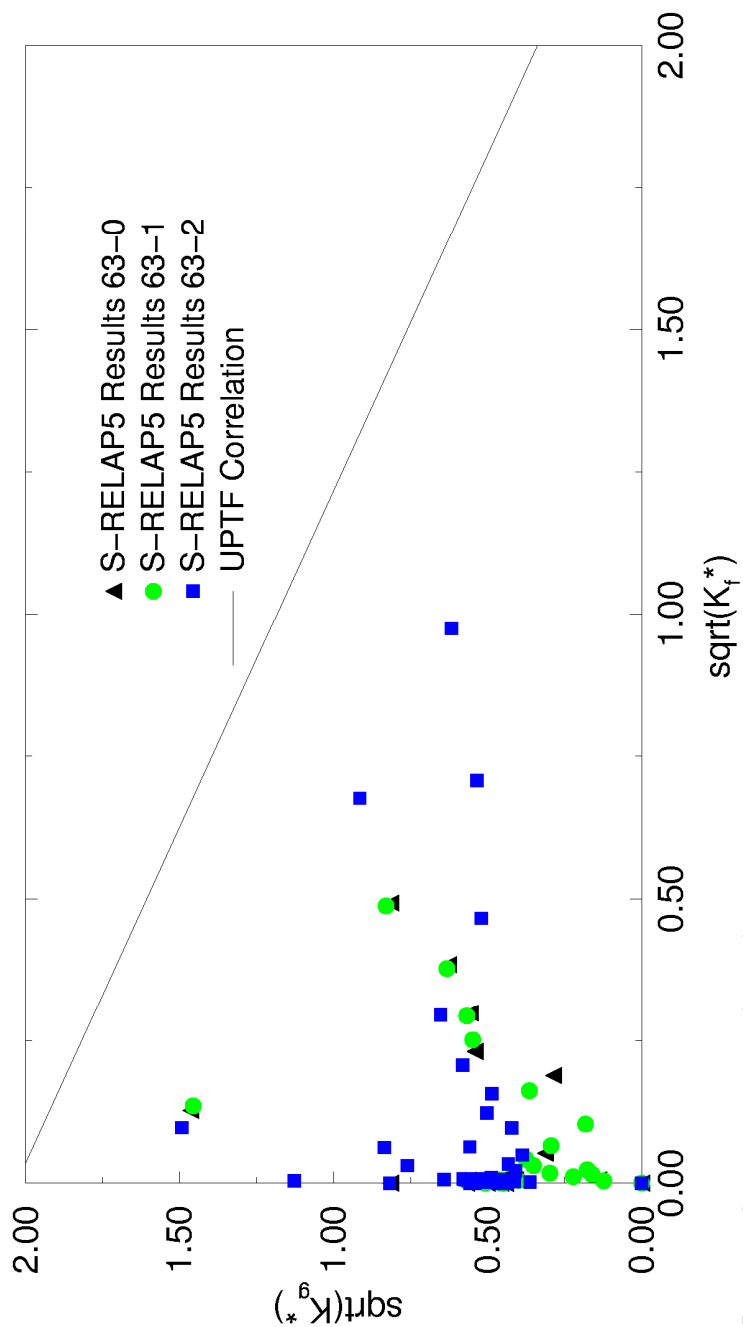


**Figure 4.76: Countercurrent Flow of Steam and Water  
UPTF Test 10 Run 081**

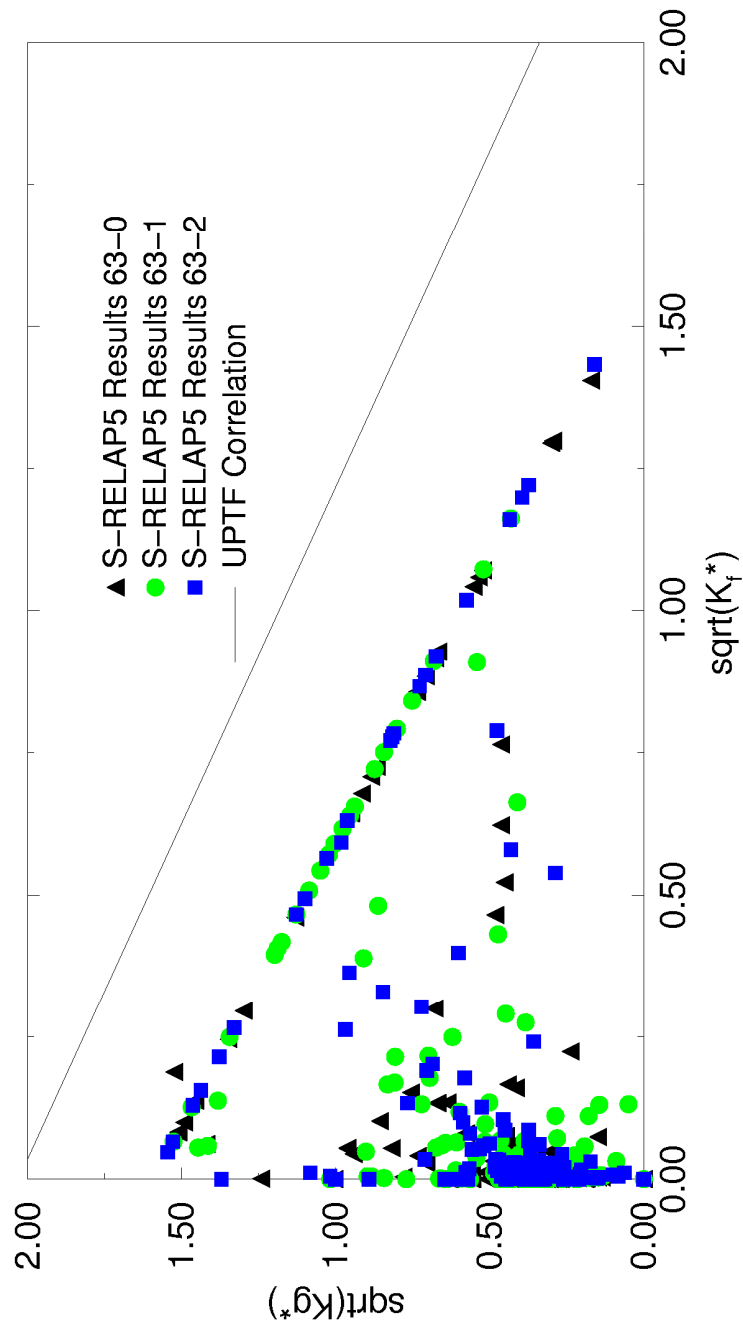


**Figure 4.77: Countercurrent Flow of Steam and Water  
UPTF Test 29 Run 212/211**



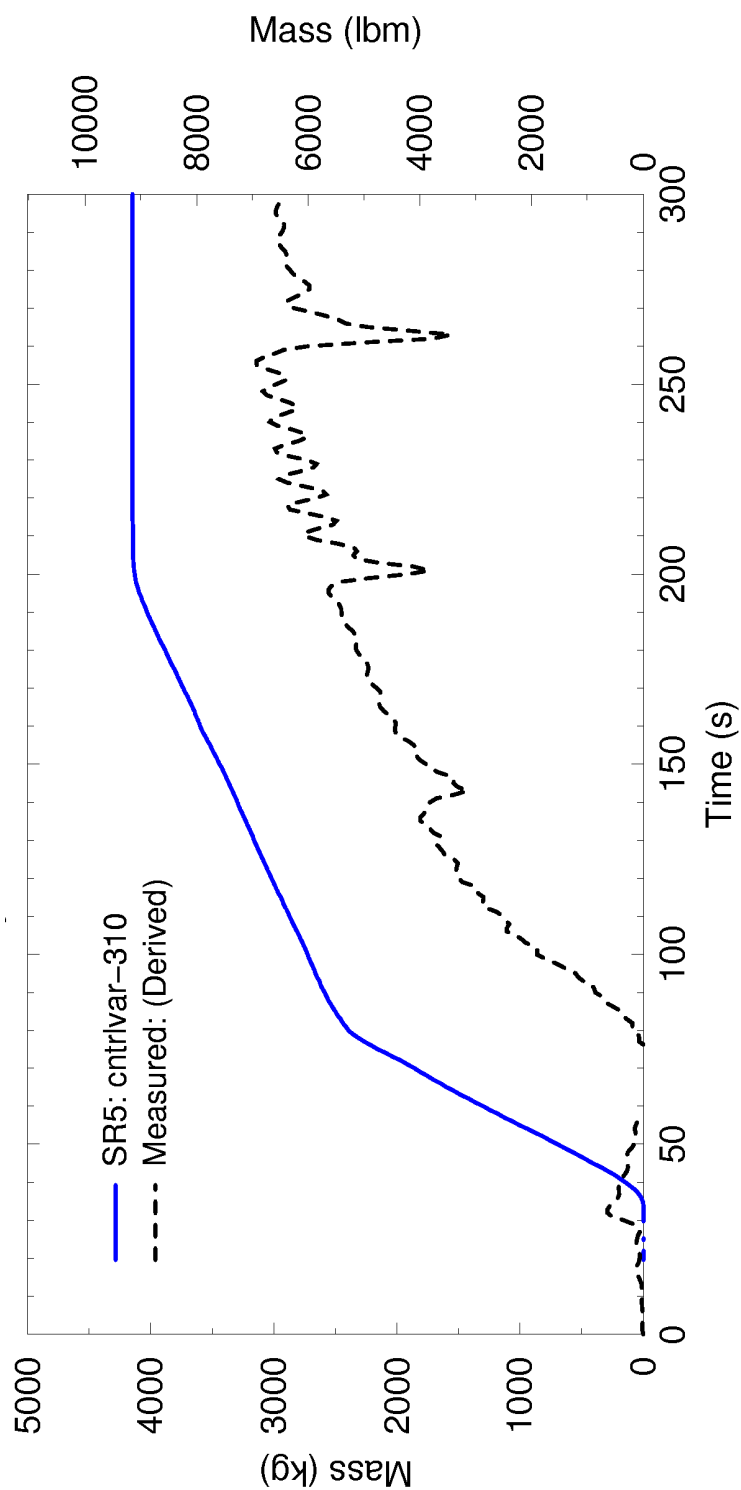


**Figure 4.78: Carryover to Steam Generators**  
**UPTF Test 10 Run 081**

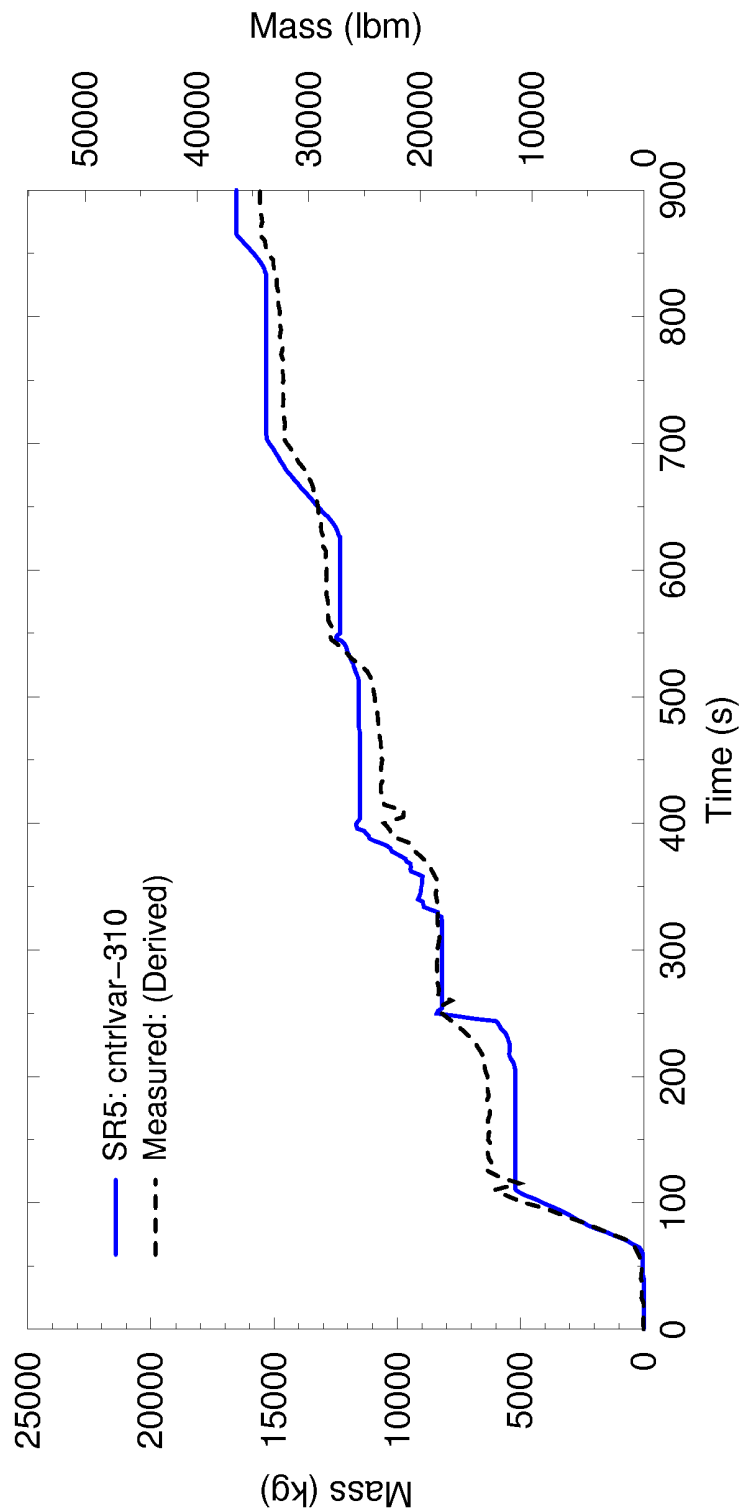


**Figure 4.79: Cumulative Water Carryover to Steam Generators  
UPTF Test 29 Run 211/212**

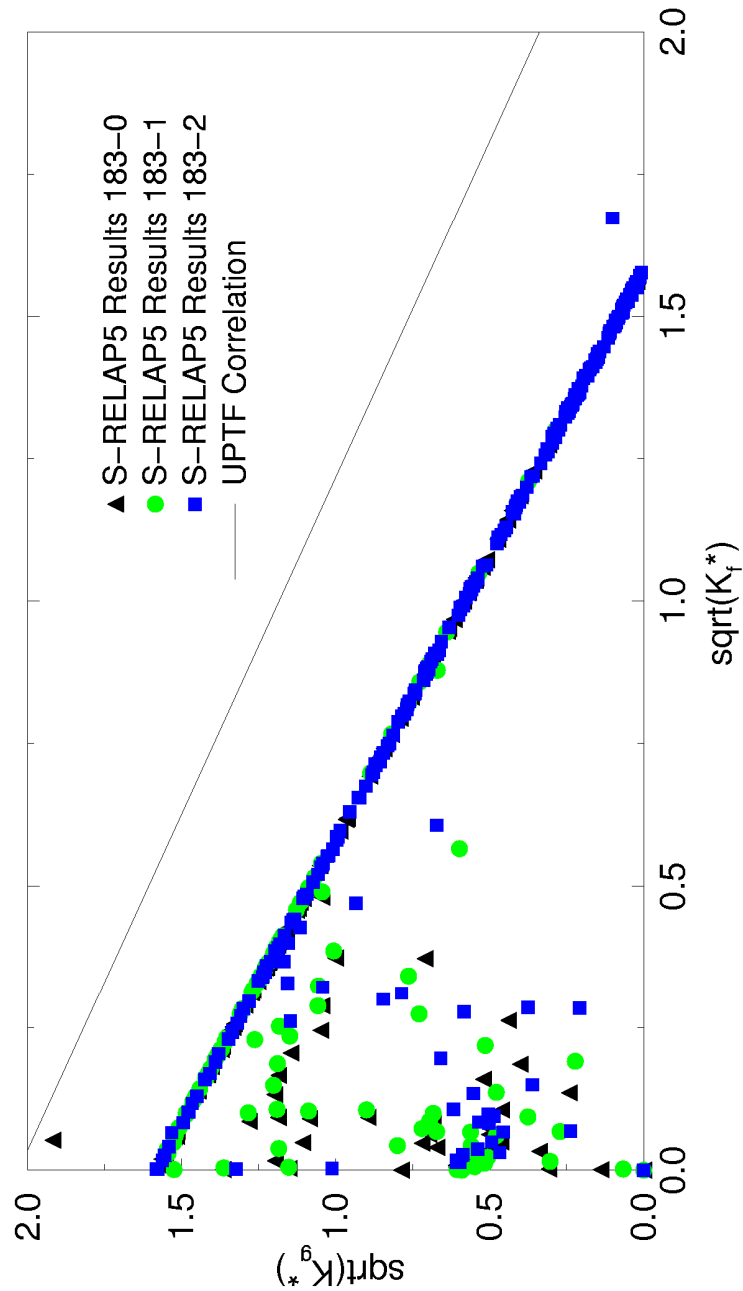


**Figure 4.80: Countercurrent Flow of Steam and Water  
UPTF Test 10 Run 080**

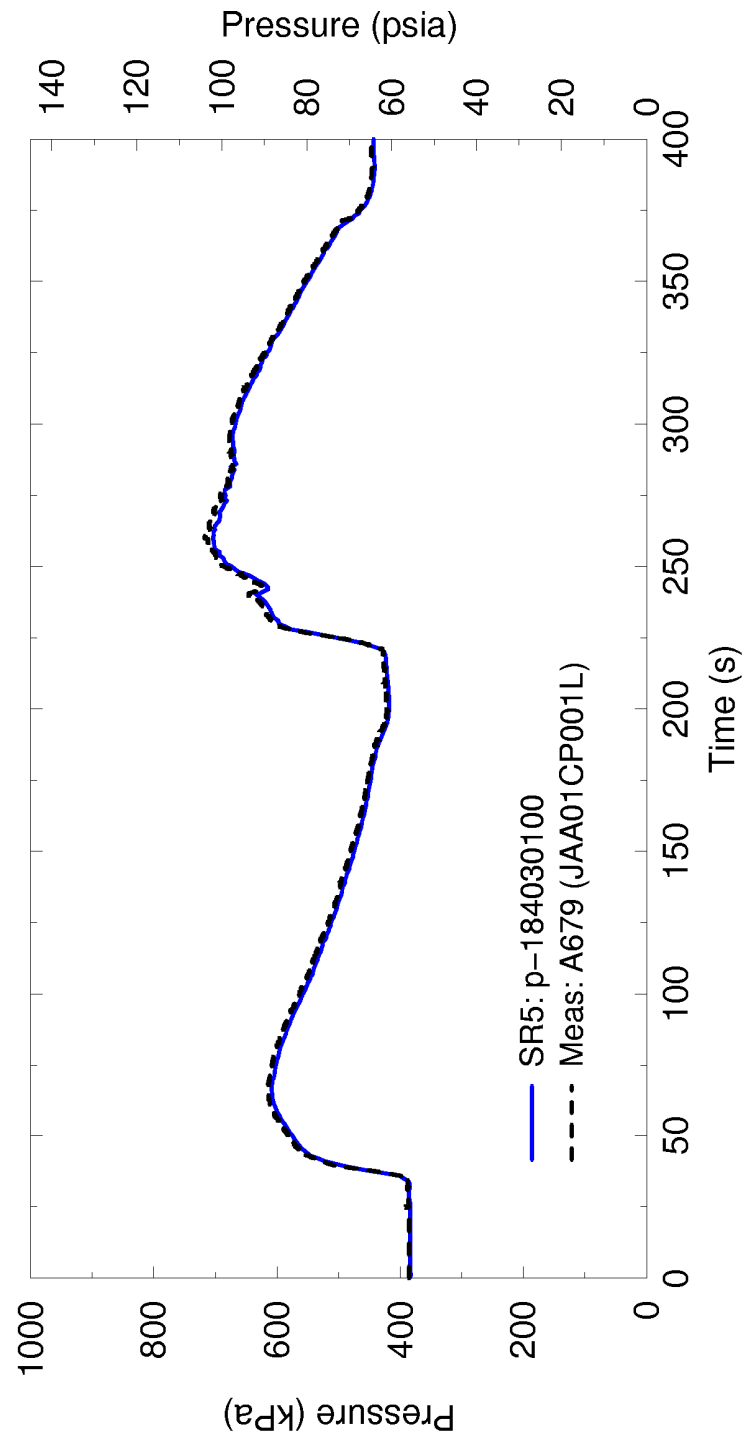


**Figure 4.81: Upper Plenum Pressure Comparison  
UPTF Test 10 Run 080**

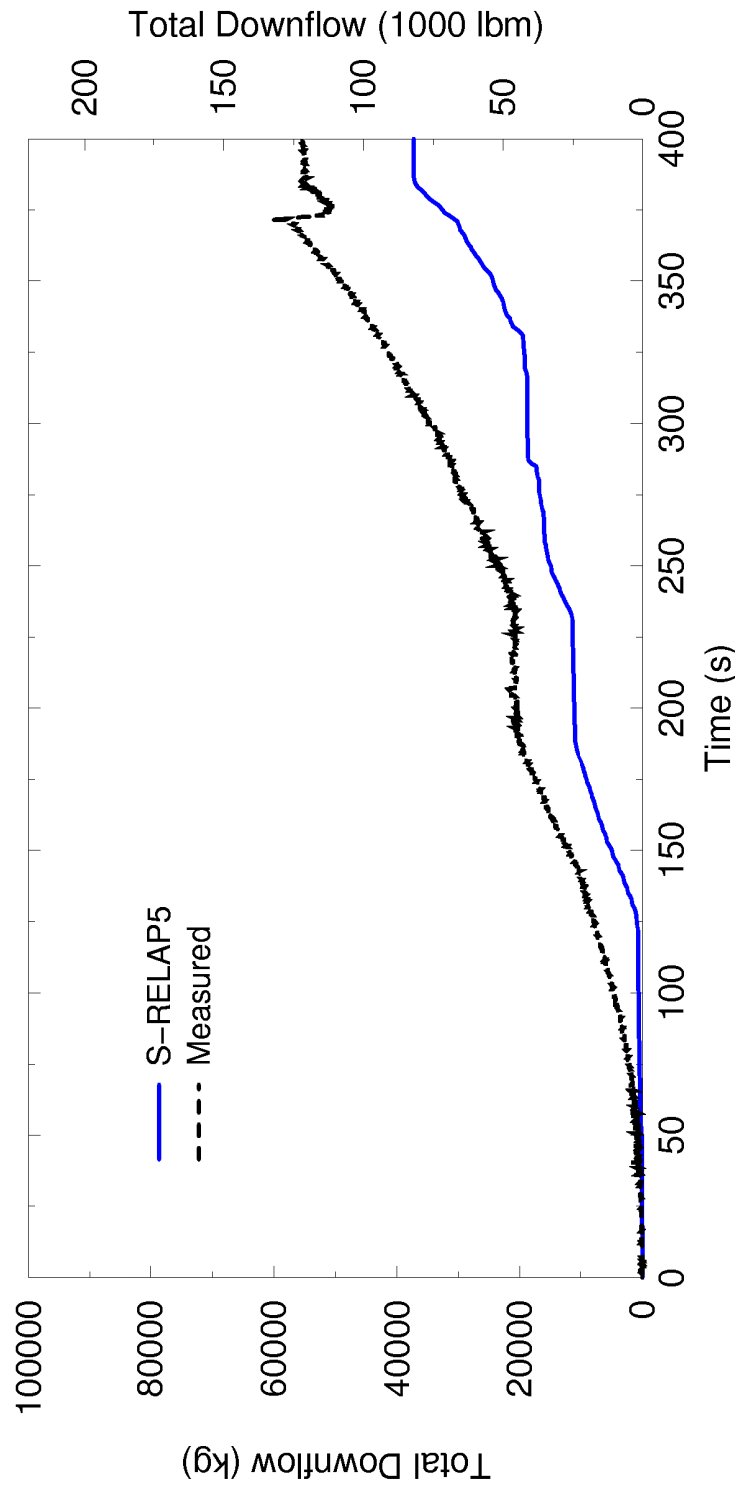


**Figure 4.82: Calculated Downflow Comparison  
UPTF Test 10 Run 080**

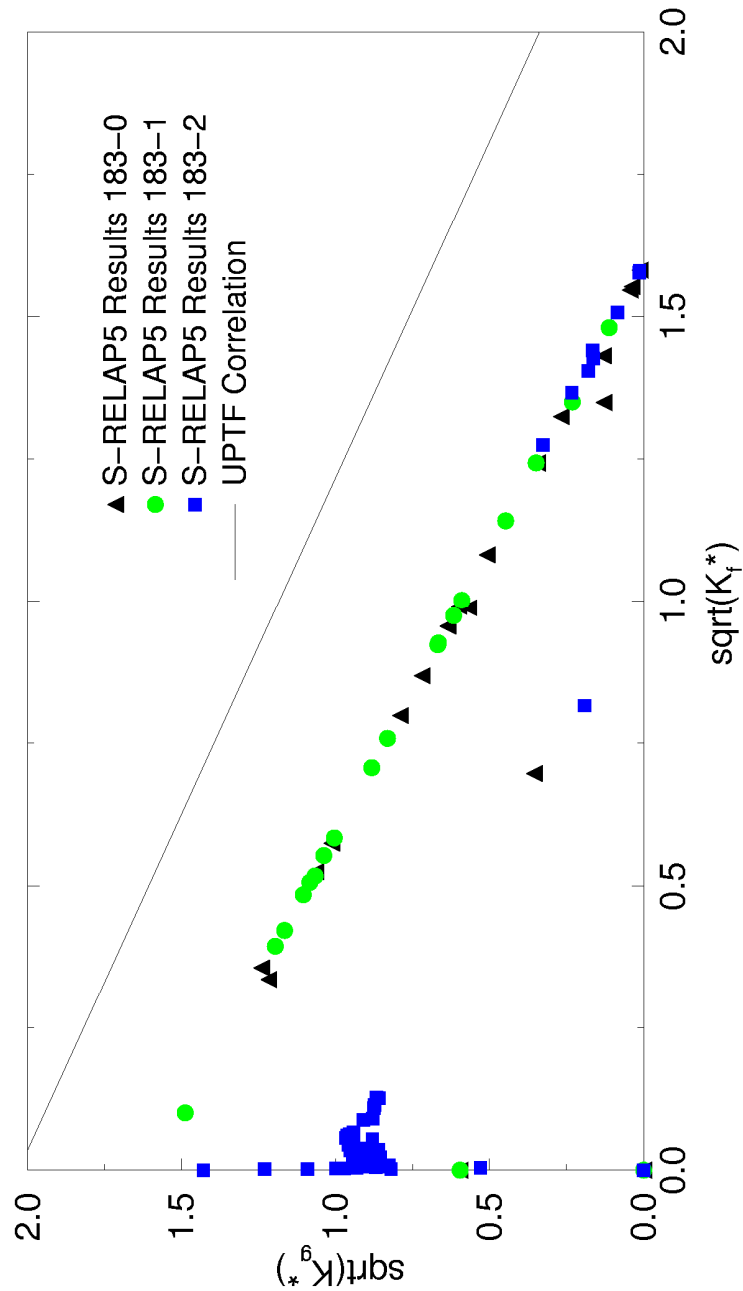


**Figure 4.83: Countercurrent Flow of Steam and Water  
UPTF Test 12 Run 014**

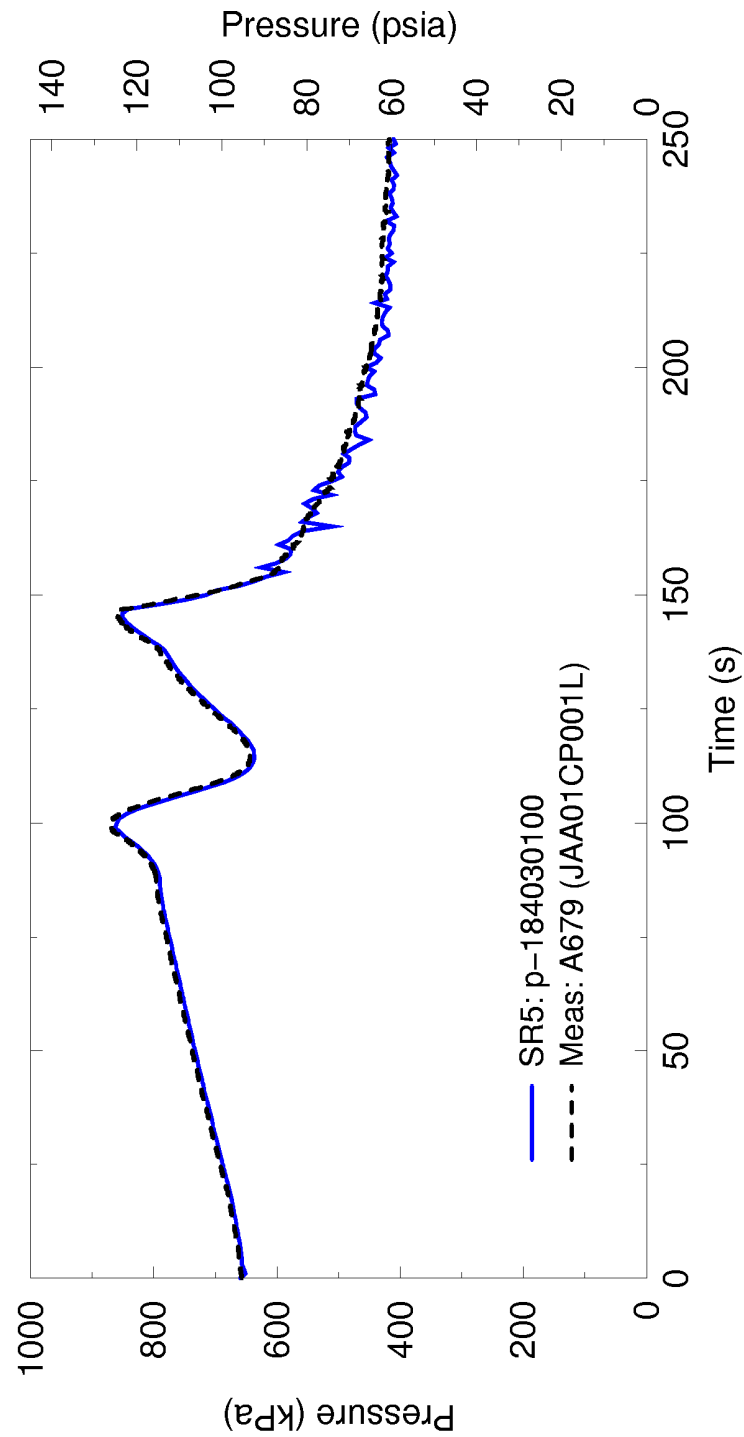


**Figure 4.84: Upper Plenum Pressure Comparison**  
**UPTF Test 12 Run 014**

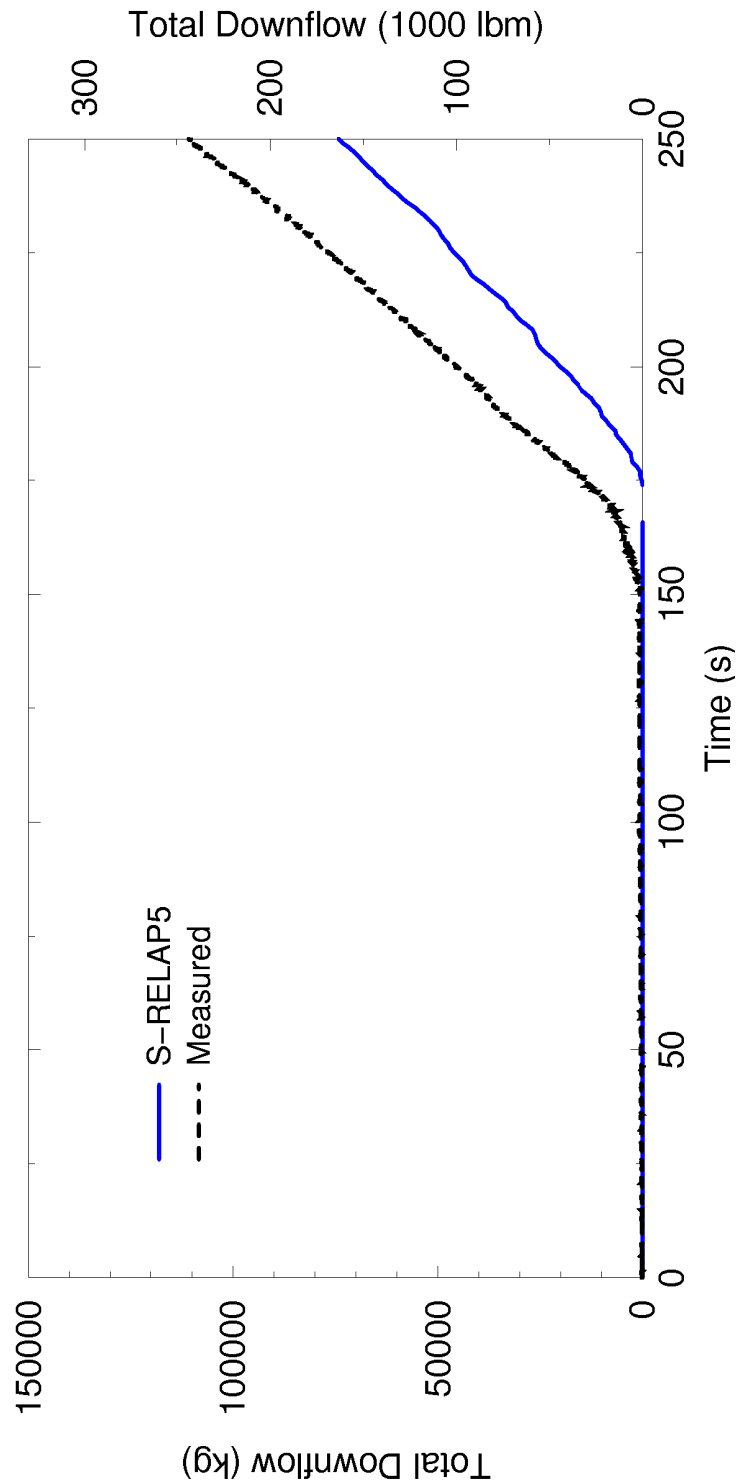


**Figure 4.85: Calculated Downflow Comparison  
UPTF Test 12 Run 014**



#### 4.3.1.12 CCTF Tests

Four, from a series of 29, Cylindrical Core Test Facility (CCTF) CORE-II tests were chosen as a diverse sample of behaviors to evaluate the capability of S-RELAP5 to predict core and primary system thermal-hydraulic phenomena occurring during the reflood phase of LBLOCA in a PWR. CCTF Core-II tests were conducted under the 2D/3D program to provide a major and useful database of LBLOCA reflood behavior in PWRs. Of particular interest are the simulations of reflood behavior in Westinghouse 4-loop PWRs in which ECC is injected into the cold leg. CCTF is a full-height, 1/21 scale model of the RCS of a 4-loop PWR plant. The facility was designed to reasonably simulate the flow conditions, including ECC flow behavior in the downcomer, and reactor core responses in the primary system of a PWR during the refill and reflood phases of a LBLOCA.

Tests 54, 62, 67, and 68 were chosen to evaluate the performance of S-RELAP5 during vessel reflood. The tests are representative of a series of CCTF system gravity reflood tests with certain aspects of refill included. Simulation of these tests provides an understanding of key reflood phenomena and comparisons of predicted and measured results for assessment of various S-RELAP5 thermal-hydraulic models and their dynamic interactions. Table 4.10 summarizes the key test parameters.

Since CCTF is a full-height, 1/21 scale model of the primary coolant system of a 4-loop plant, the RLBLOCA guidelines were used, wherever possible, to model the test facility. The downcomer is represented by a 9x8 2-dimensional ( $z, \theta$ ) component. The lower plenum is divided into two axial nodes. The upper plenum is modeled using two two-dimensional ( $z, r$ ) components each having three axial levels. One component represents the region in the guide assembly simulators; it is divided into two radial rings. The second component represents the remainder of the upper plenum; it is divided into three radial rings.

The bundle region is modeled using an 18x4 two-dimensional ( $z, r$ ) component. The lower 17 axial nodes represent the 3.66 meter (144 inch) active core region and Node 18 represents the distance between the top of the active core and the upper core tie plate. The four radial flow channels correspond to the three power zones. The first radial ring represents the hot assembly and the second ring represents the remainder of the high-power region, Region-A. The third and fourth rings represent the medium power region, Region-B, and the low power region, Region-C. The bundles in each ring are represented by one rod. In the hot channel (central

ring) there is an additional rod that represents a hot rod. Bundle heat transfer multipliers, FILMBL and DFFBHTC are set to [ ]. Since all the heated rods in a bundle have the same power, and the PCTs in all the tests simulated are below 1800°F, the rod-to-rod radiation model was not used.

The steam generator tube region is modeled using eight nodes and the cold leg piping from the pump discharge to the downcomer inlet is modeled using four nodes. The cold leg condensation model (summarized in Section 4.3.3.1.14 and described in detail in Section 5.2 of Reference 5) is used in the intact cold legs.

To get acceptable liquid entrainment out of the steam generator inlet plenum, the following input modeling recommended from the UPTF Tests 10 and 29 benchmarks (Section 4.3.1.11.3) was used.

The CCTF tests, input model, and assessment results are discussed in detail in Section 3.11 of Reference 5. During the reflood phase of a LBLOCA, some of the important reflood phenomena are core heat transfer, void generation/distribution and entrainment/ deentrainment in the core, entrainment/deentrainment in the upper plenum and in the hot legs, and steam binding in the steam generator. All of these reflood phenomena were calculated reasonably well by S-RELAP5. Selected key parameters are discussed below.

- The calculated pressures in the primary system for all four tests agree reasonably well with the data as shown in Figure 4.86 through Figure 4.89.
- The calculated axial differential pressures in the downcomer for all four cases agree reasonably well with the data as shown in Figure 4.90 through Figure 4.93. The small difference between the data and the calculation in some cases during the steady-state can be due to the uncertainty in the  $\Delta P$  measurements. S-RELAP5 calculated higher amplitude oscillations than in the tests, especially during the early phase of the transient, which represents the accumulator injection period. This is primarily due to the atypical ECC injection modes in the tests. During the early phase of the transient, ECC, that simulates accumulator injection, is injected into the lower plenum. The ECC injection is switched to the cold legs a few seconds after reflood initiation, when the downcomer level is nearly full and the system is reasonably stable. This approach was selected in both SCTF and CCTF tests in order to minimize unstable conditions at the start of cold water injection into the stagnant primary system. In a PWR, the ECC injection into the cold legs starts while the system is blowing down and the transition from the refill to the reflood phase is a continuous process. The oscillations in the later phase of the transients in the calculation are primarily due to cold leg condensation.
- The calculated axial differential pressures in the core region for all four cases agree reasonably well with the data as shown in Figure 4.94 through Figure 4.97. These results indicate that, in all four cases, the code calculates the proper liquid inventory in the bundle region.
- The core and downcomer  $\Delta P$  results also reflect the primary system response. Therefore, these  $\Delta P$  results indicate S-RELAP5 calculates acceptable loop and downcomer oscillations when compared to the CCTF tests. From these results, it can be concluded the code will calculate acceptable downcomer and loop oscillations during the reflood phase of a LBLOCA.
- CCTF has active scaled steam generators. Therefore, the tests realistically simulate the entrainment process and droplet evaporation in the tube region. However, little information is available to make a direct comparison between the measured and calculated liquid entrained to the tube region. The pump side break is connected to a containment tank (Containment Tank II), which has a liquid separator at the top. This separator traps all liquid exiting from the broken loop steam generator side of the break. S-RELAP5-calculated and the measured Containment Tank II levels for the four tests are shown in Figure 4.98 through

Figure 4.101. Considering the differences in the droplet evaporation in the steam generator tube region between the test and calculation, and the uncertainty in the dimensions of Containment Tank II, the S-RELAP5 calculated entrainment rate to the tube region is considered acceptable.

- Table 4.11 gives the measured and calculated PCT and the time of PCT for the four test cases. The calculated PCTs range from an overprediction of 95 K to an underprediction of 49 K. The calculated time of PCT occurs later than the test data for all four cases. S-RELAP5 also calculates later quench times for all the cases as can be seen from the cladding thermal response at 2.035 meters as shown in Figure 4.102 through Figure 4.105. These and other cladding thermal response results given in Section 3.11 of Reference 5 indicate that the higher amplitude oscillations in the core and downcomer  $\Delta P$  calculations have a negligible effect on the cladding thermal response. Figure 4.106 through Figure 4.109 show that S-RELAP5 generally calculates higher PCTs above the mid-plane for all four cases.

In summary, the assessment results show S-RELAP5 calculates the important reflood phenomena occurring in all four CCTF tests with reasonable-to-conservative agreement to the data. The assessments demonstrate S-RELAP5 will calculate acceptable thermal-hydraulic phenomena during the reflood phase of a LBLOCA in a PWR including PCT, quench front propagation, and loop and downcomer oscillations.

**Table 4.10: CCTF Test Conditions**

Run	Core Power	LPCI Flow $\left(\frac{\text{m}^3}{\text{s}}\right)$	System Pressure (MPa)
54	ANSx1.0 + Actinide * 1.1	0.011	0.20
62	ANSx1.2 + Actinide * 1.1	0.011	0.20
67	ANSx1.2 + Actinide * 1.1	0.011	0.15
68	ANSx1.0 + Actinide * 1.1	0.025	0.20

**Table 4.11: Summary Comparison of Measured and Calculated PCT,  
CCTF Tests 54, 62, 67, and 68**

Run	Measured PCT (K)	Time of Measured PCT (s)	Calculated PCT (K)	Time of Calculated PCT (s)
54	1113	130	1064	226
62	1132	154	1116	235
67	1143	164	1238	385
68	1122	144	1123	246

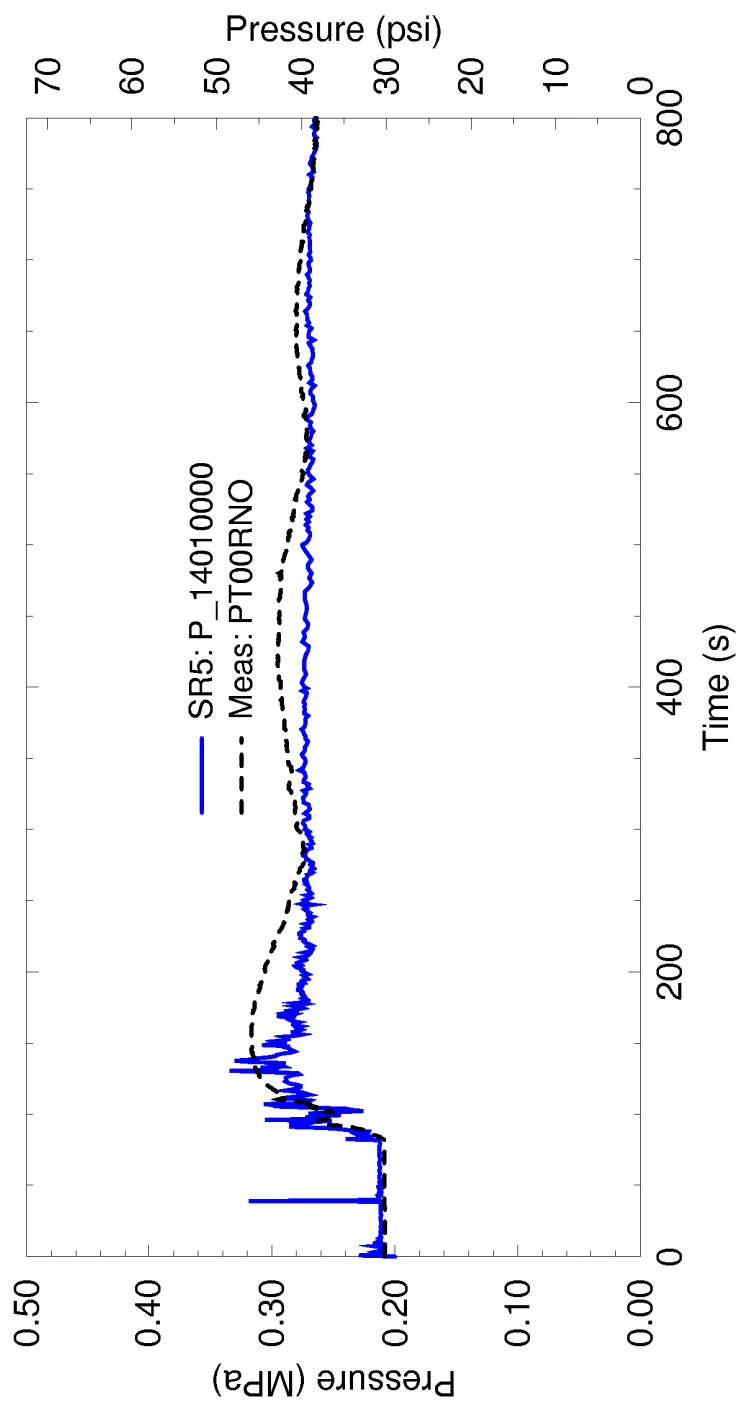


**Figure 4.86: Calculated and Measured Vessel Bottom Pressures  
CCTF Test Run 54**

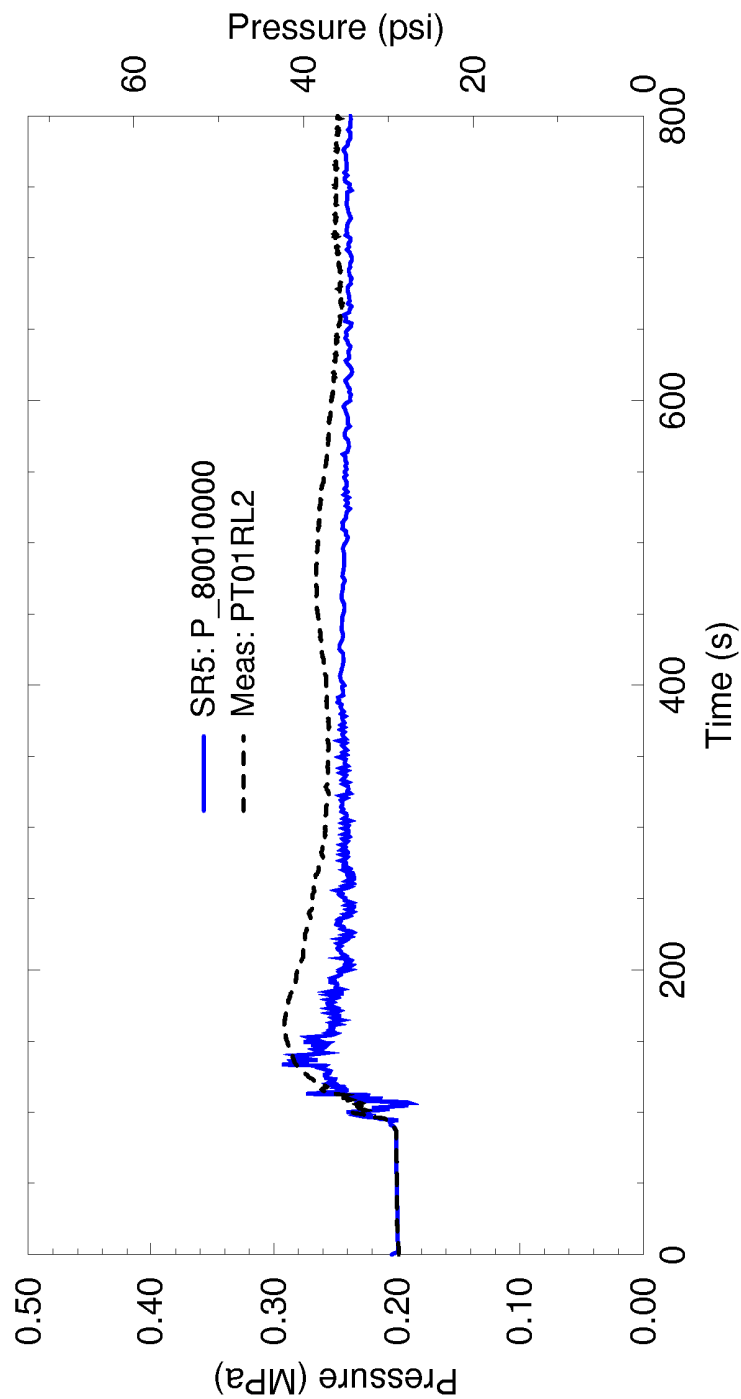


**Figure 4.87: Calculated and Measured Upper Plenum Pressures  
CCTF Test Run 62**

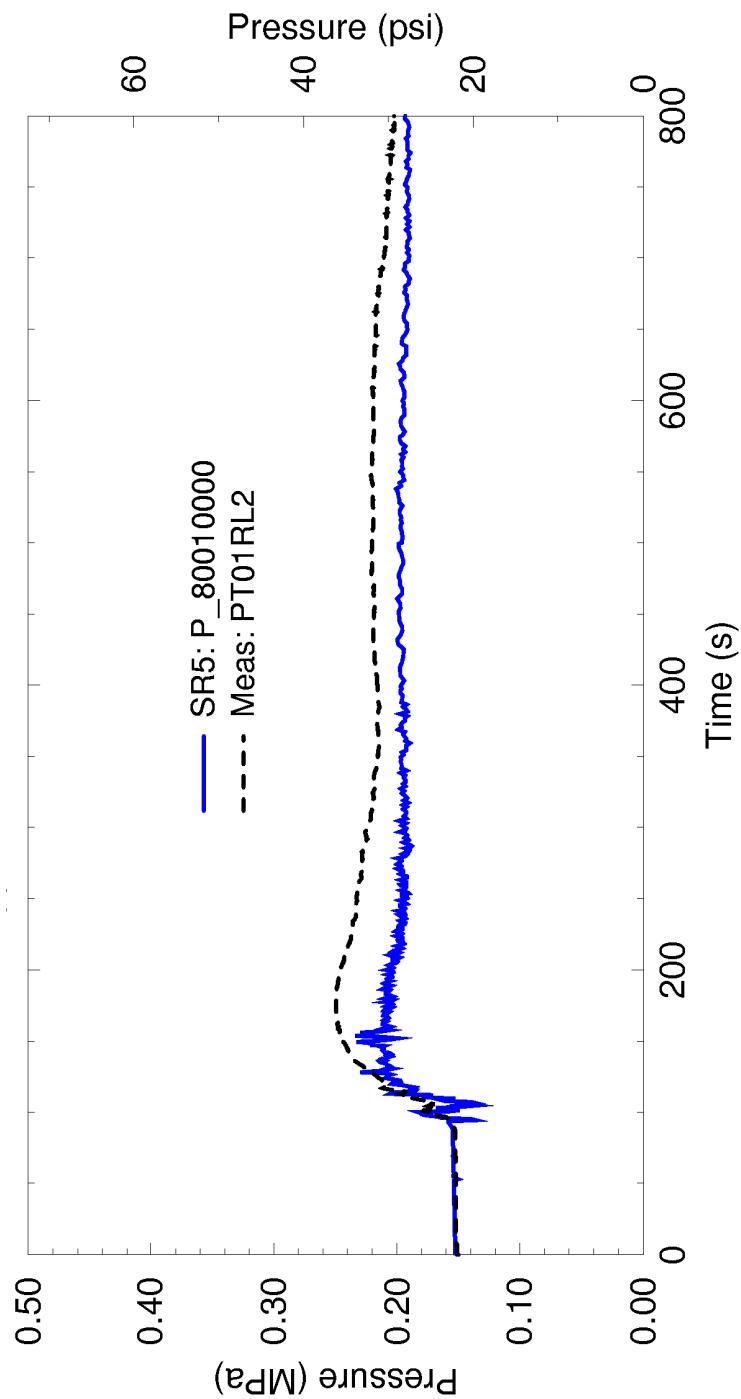


**Figure 4.88: Calculated and Measured Upper Plenum Pressures  
CCTF Test Run 67**



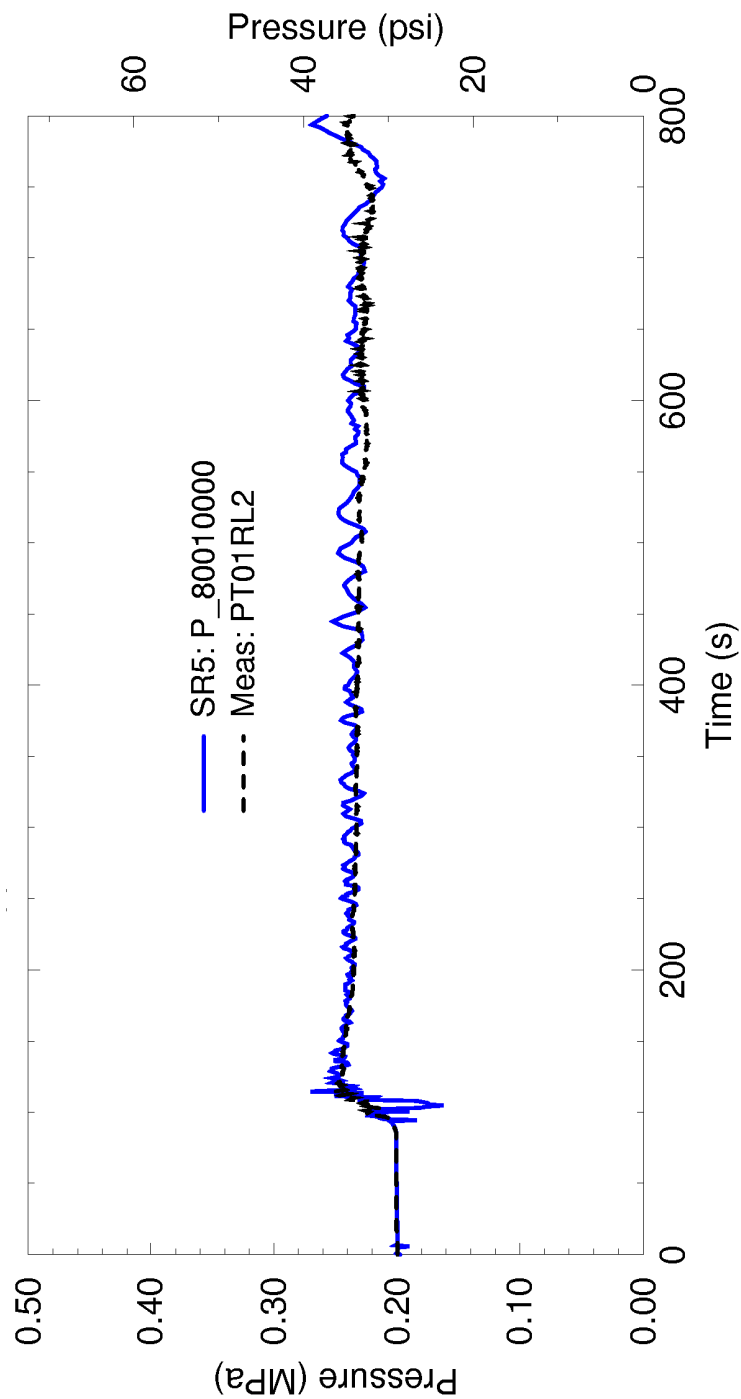


**Figure 4.89: Calculated and Measured Upper Plenum Pressures  
CCTF Test Run 68**

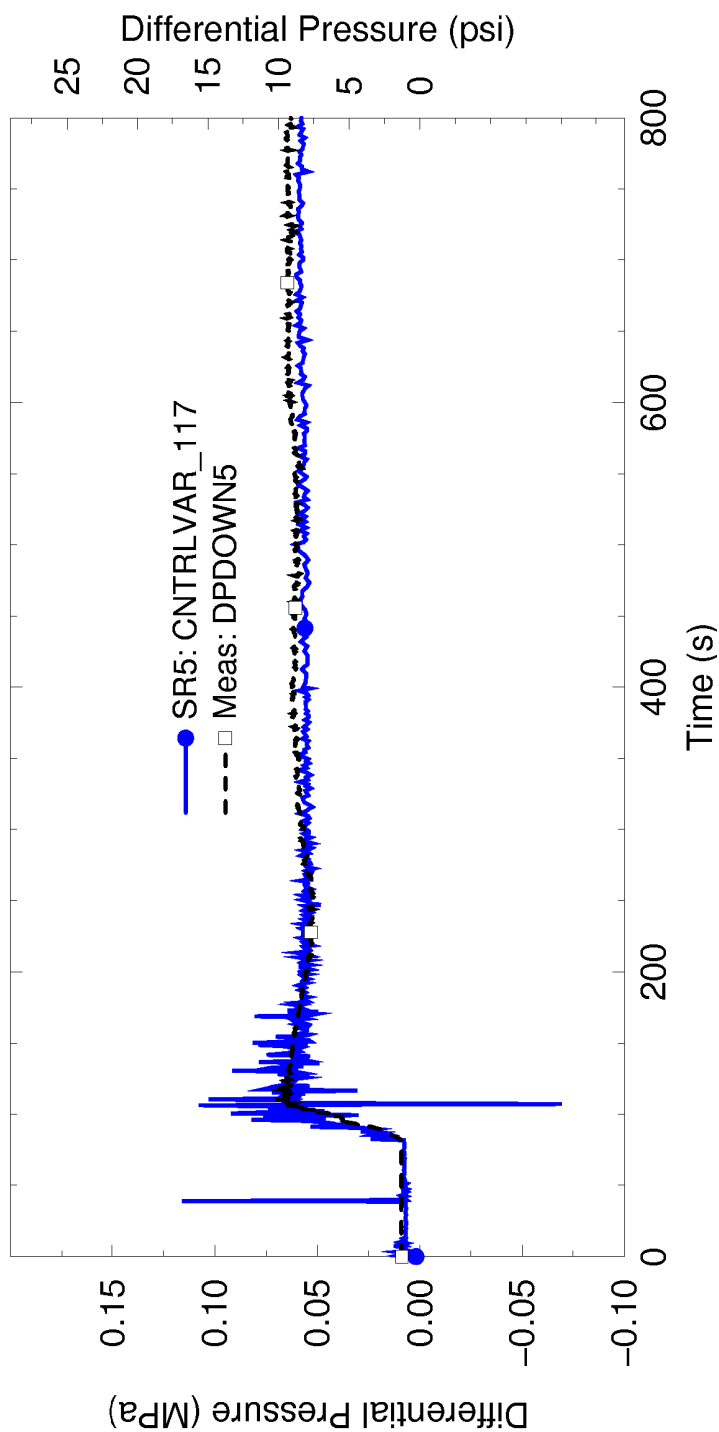


**Figure 4.90: Calculated and Measured Downcomer Differential Pressure CCTF Test Run 54**

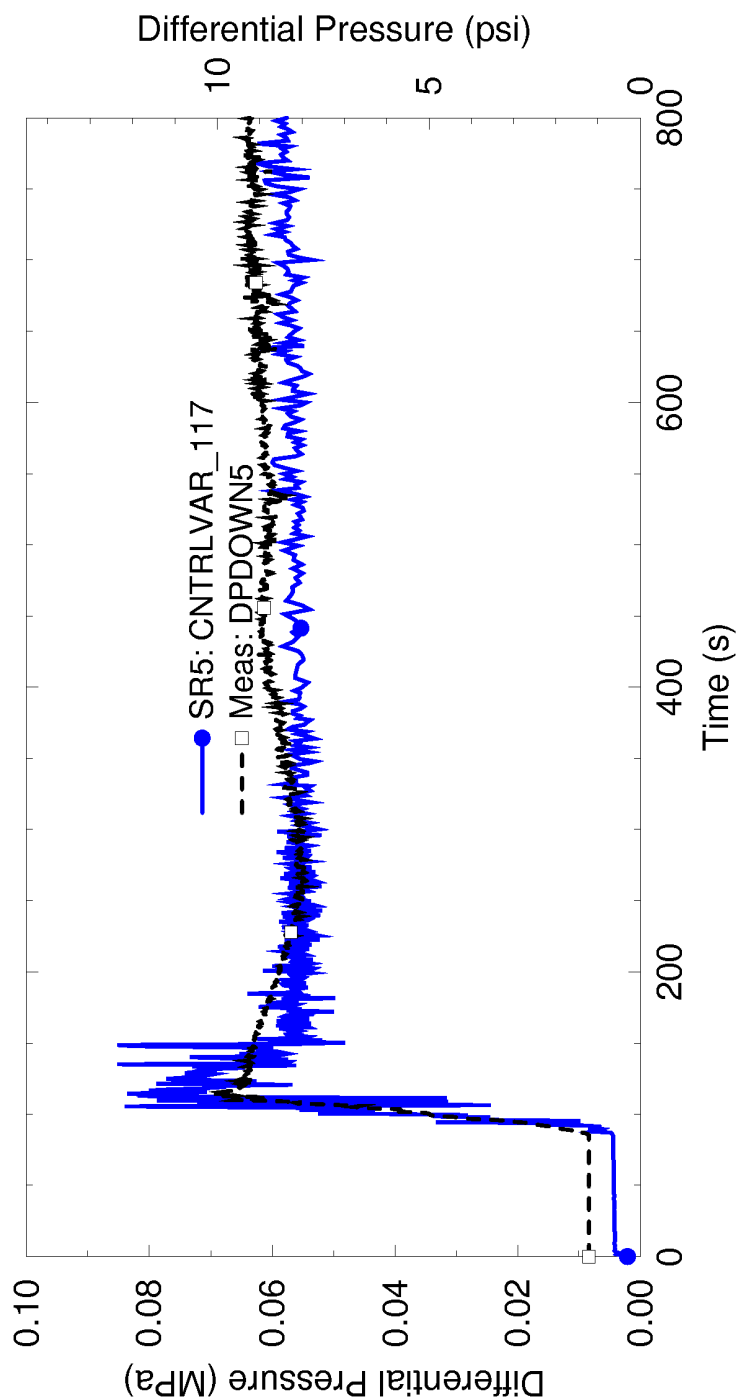


**Figure 4.91: Calculated and Measured Downcomer Differential Pressure CCTF Test Run 62**

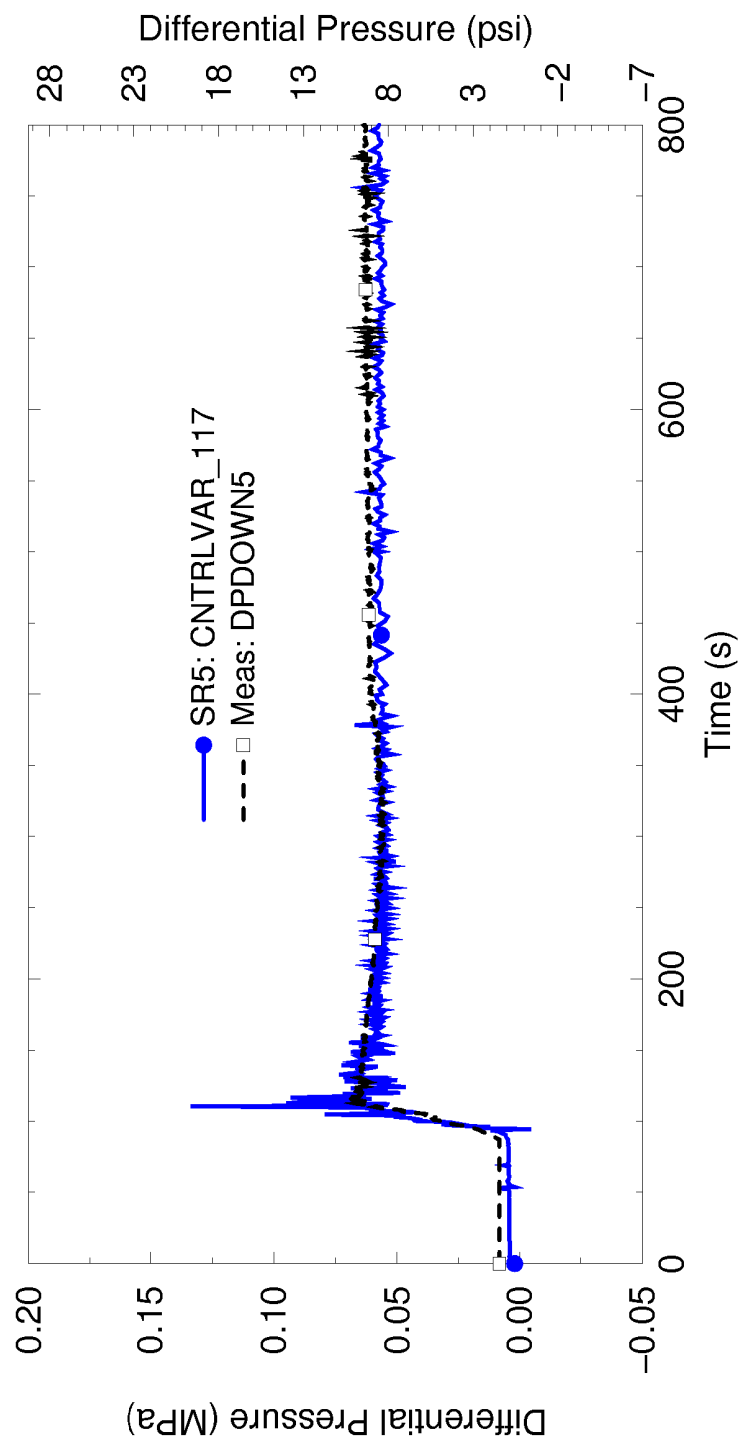


**Figure 4.92: Calculated and Measured Downcomer Differential Pressure CCTF Test Run 67**

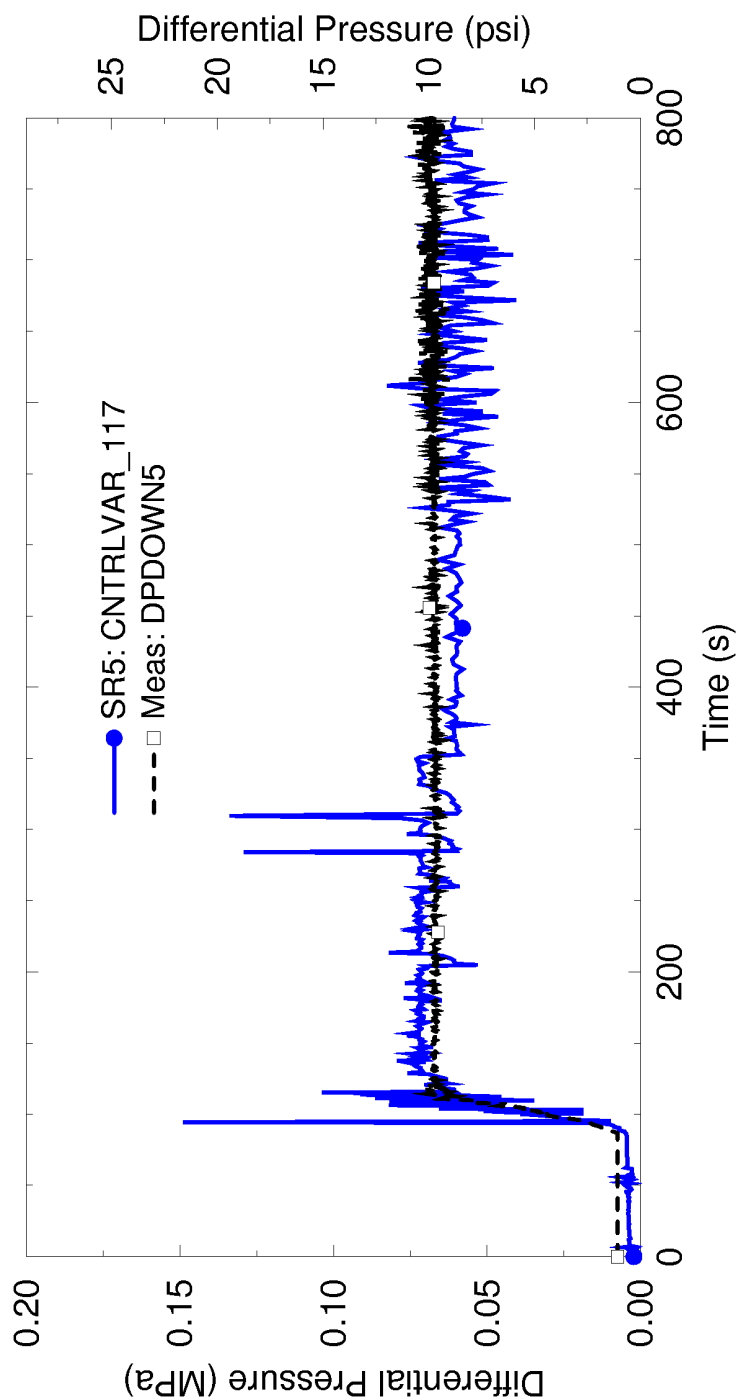


**Figure 4.93: Calculated and Measured Downcomer Differential Pressure CCTF Test Run 68**

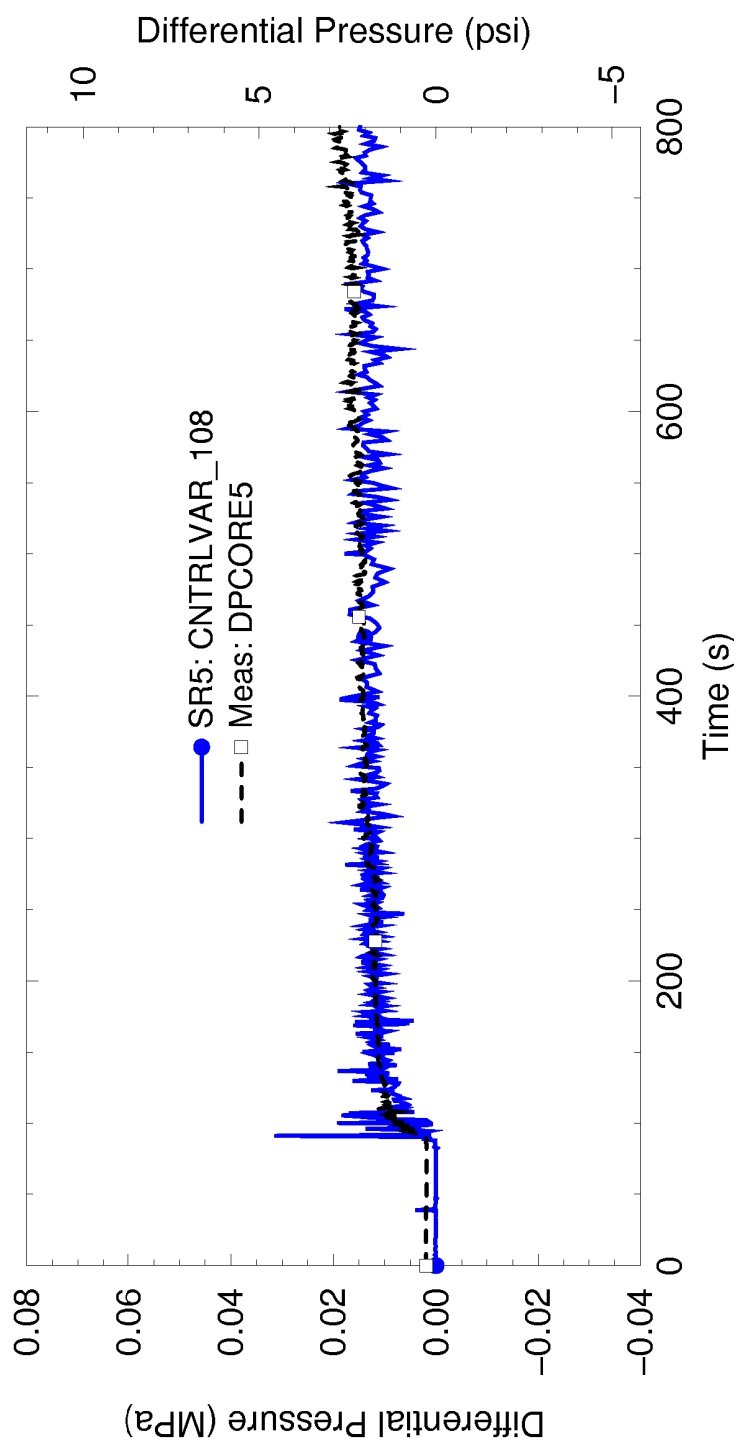


**Figure 4.94: Comparison of Core Differential Pressures  
CCTF Test Run 54**

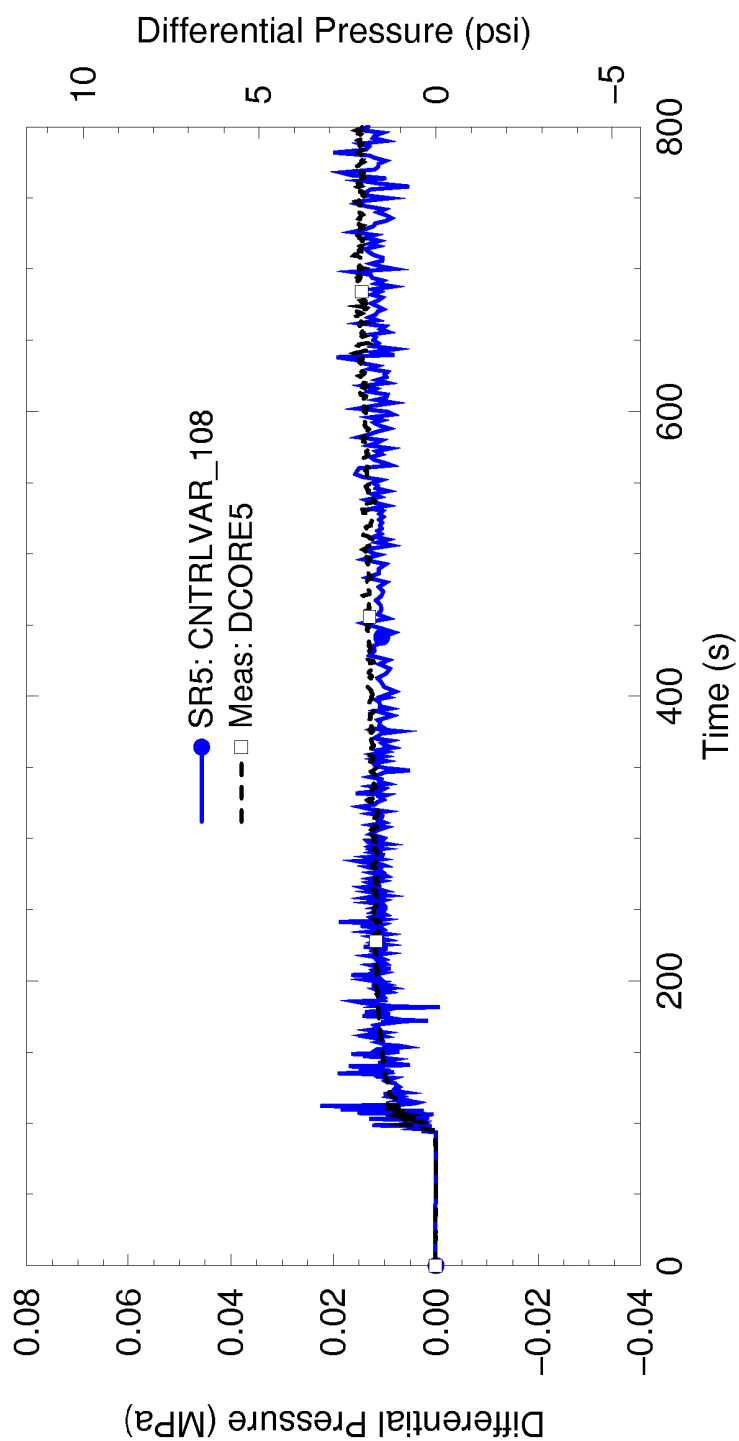


**Figure 4.95: Comparison of Core Differential Pressures  
CCTF Test Run 62**

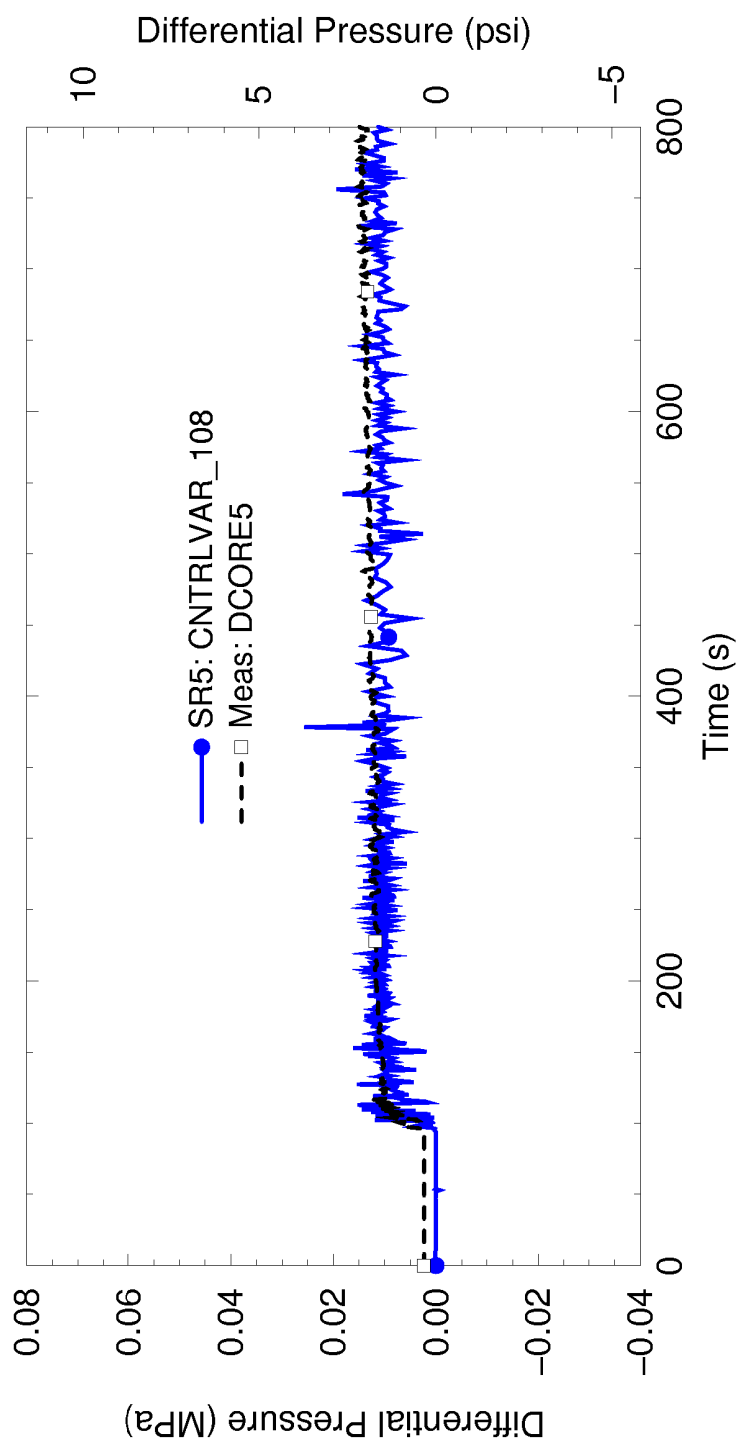


**Figure 4.96: Comparison of Core Differential Pressures  
CCTF Test Run 67**



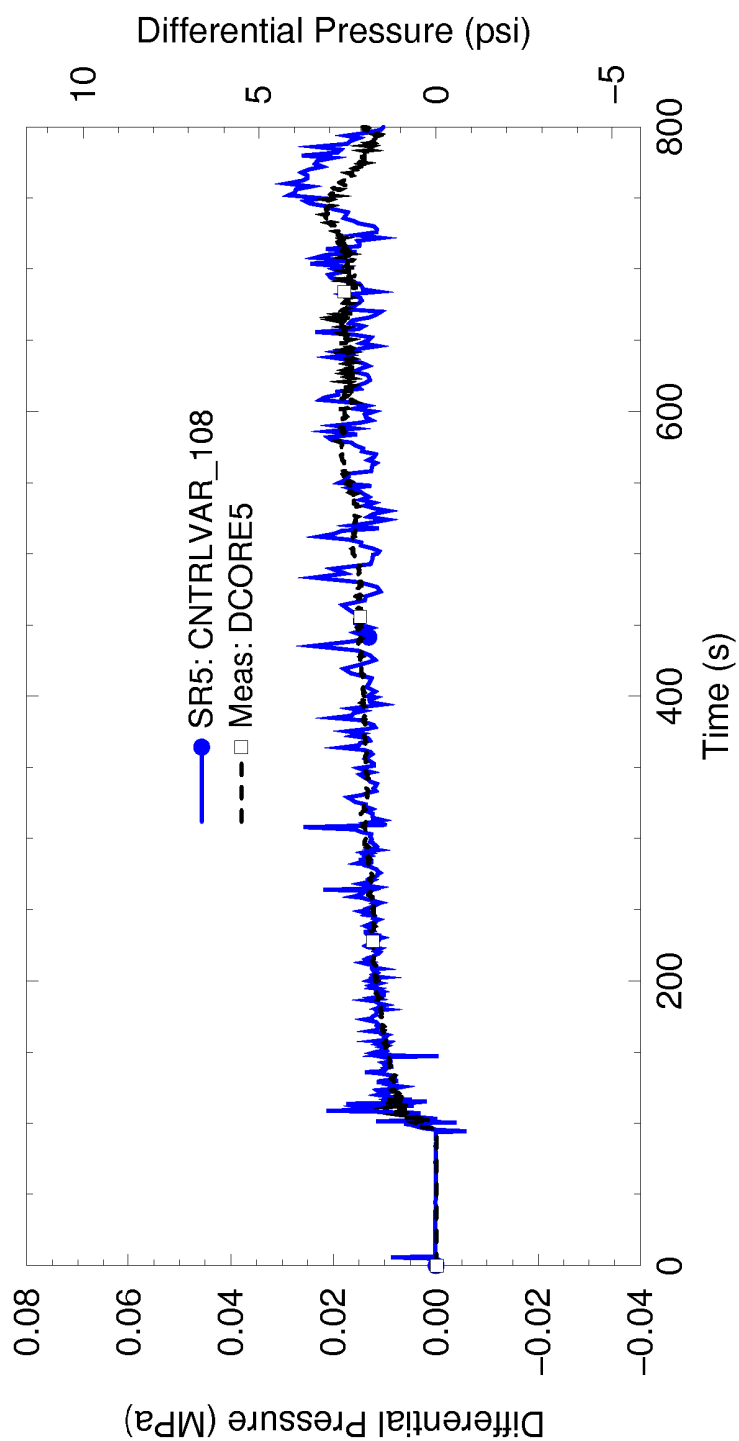


**Figure 4.97: Comparison of Core Differential Pressures  
CCTF Test Run 68**

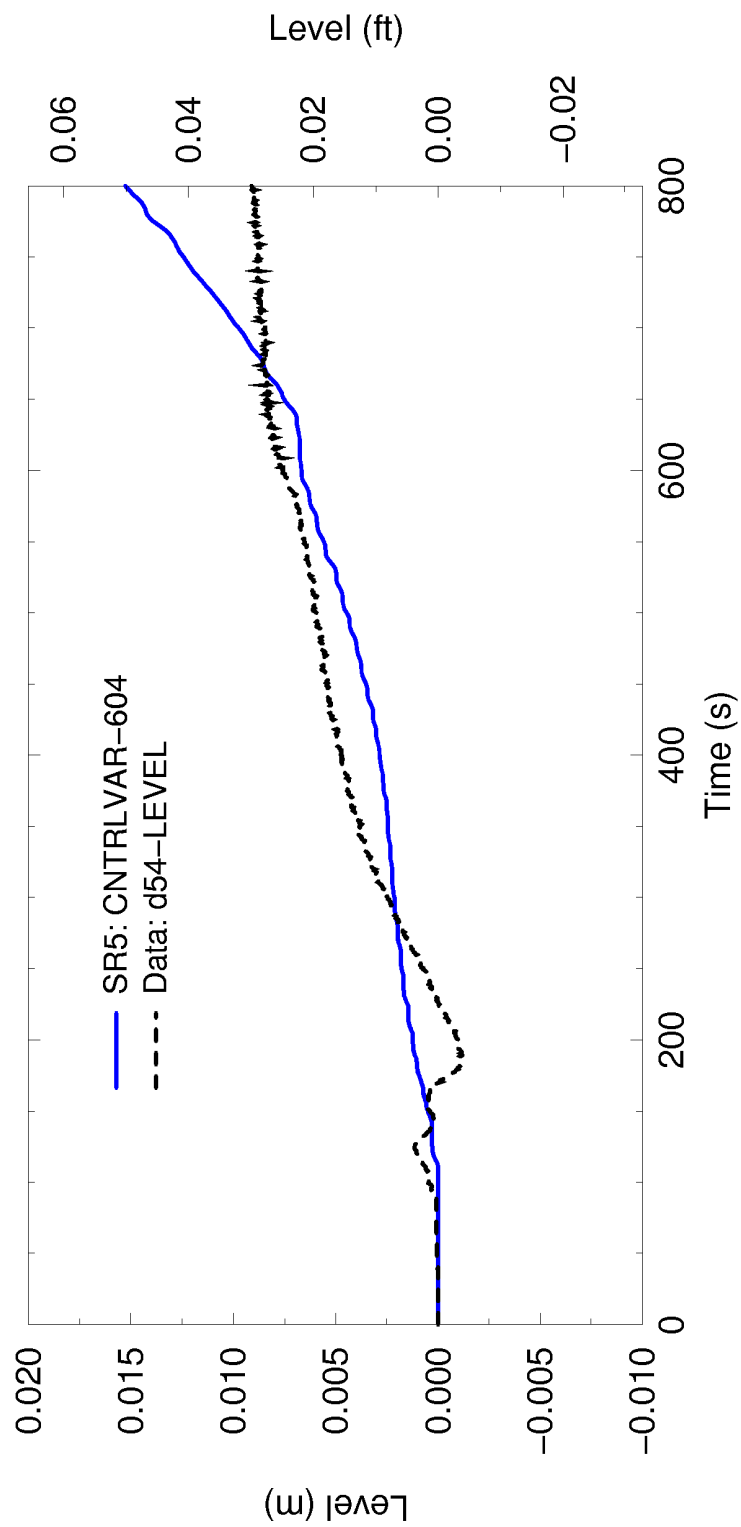


**Figure 4.98: Comparison of Liquid Level in Containment Tank II  
CCTF Test Run 54**

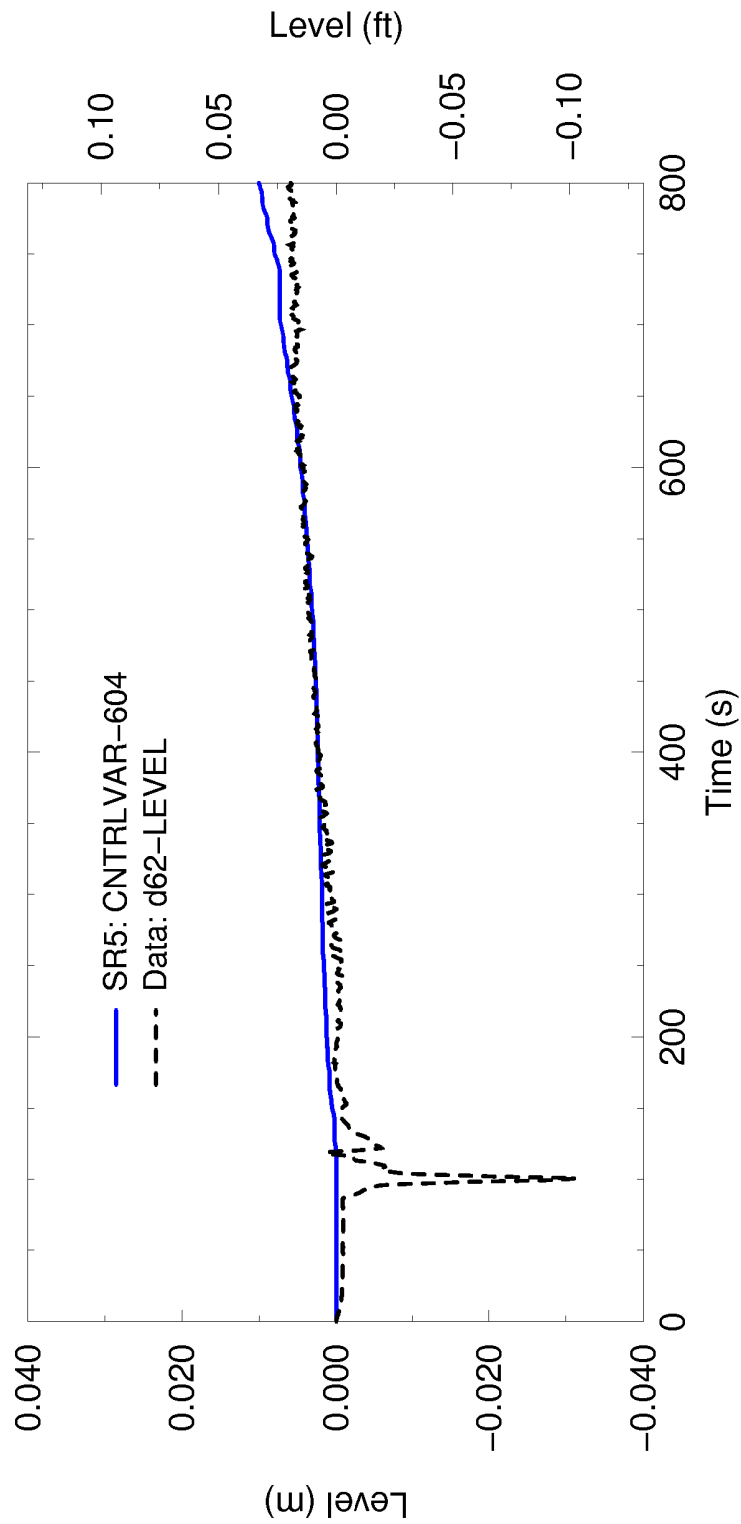


**Figure 4.99: Comparison of Liquid Level in Containment Tank II  
CCTF Test Run 62**

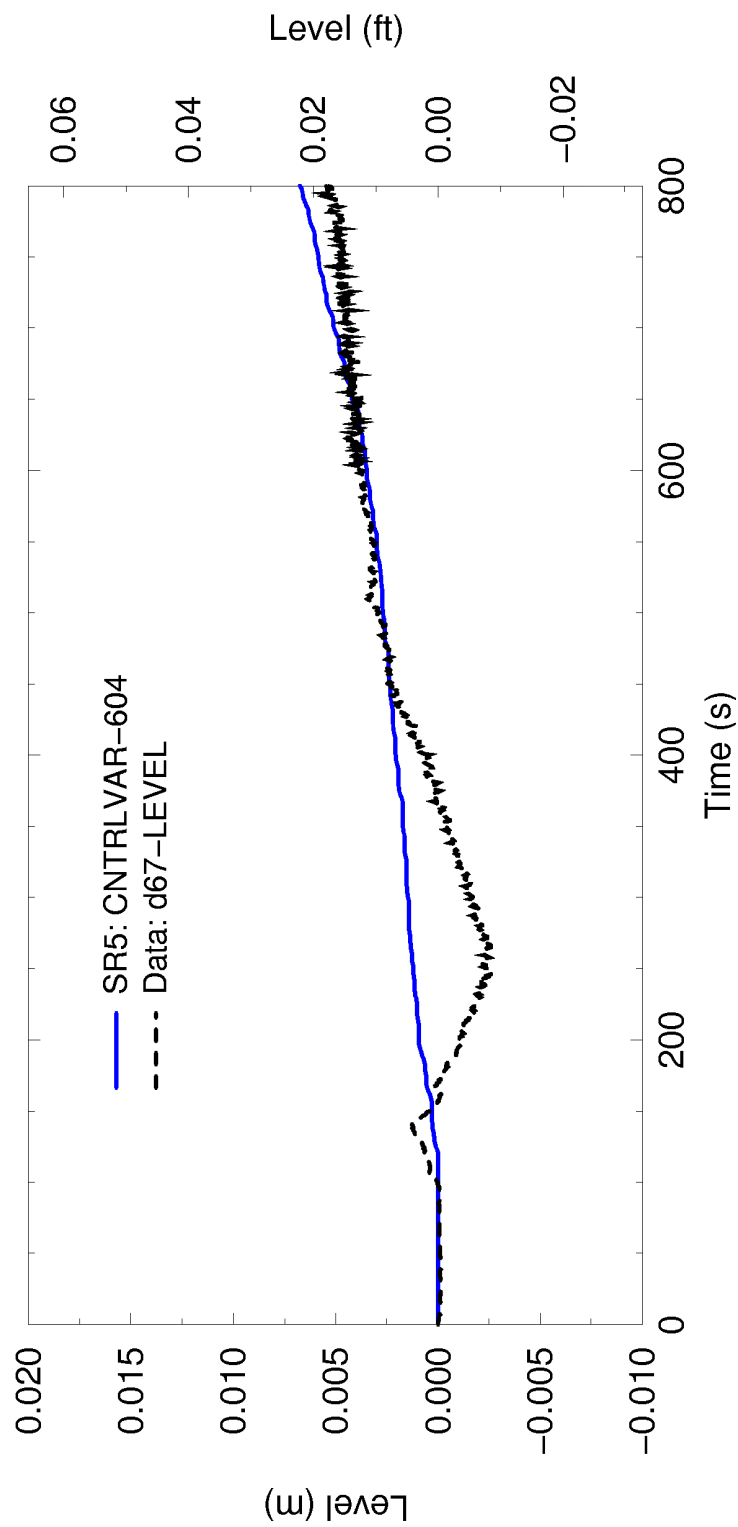


**Figure 4.100: Comparison of Liquid Level in Containment Tank II  
CCTF Test Run 67**

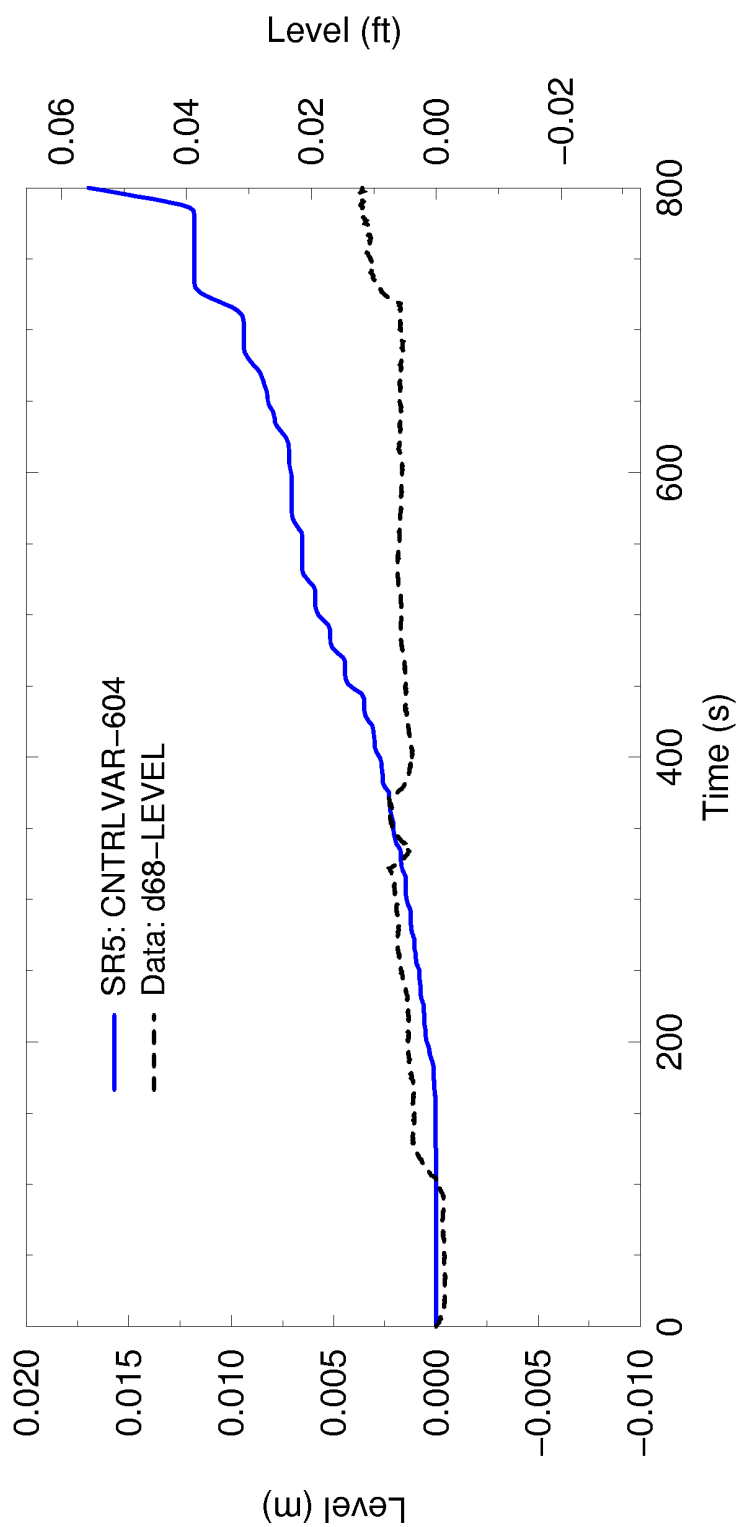


**Figure 4.101: Comparison of Liquid Level in Containment Tank II  
CCTF Test Run 68**

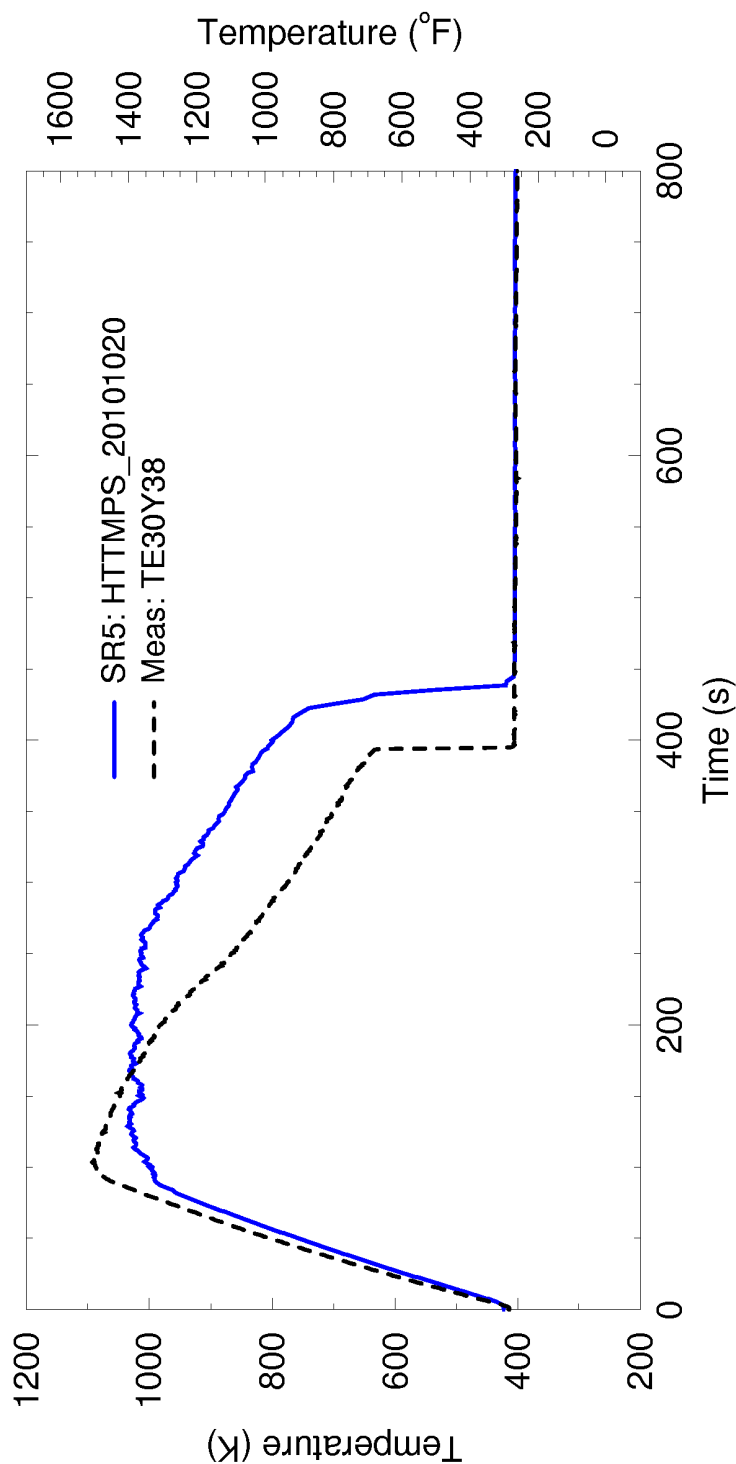


**Figure 4.102: Comparison of Rod Surface Temperatures for High Power Bundles at 2.035 meters Elevation CCTF Test Run 54**

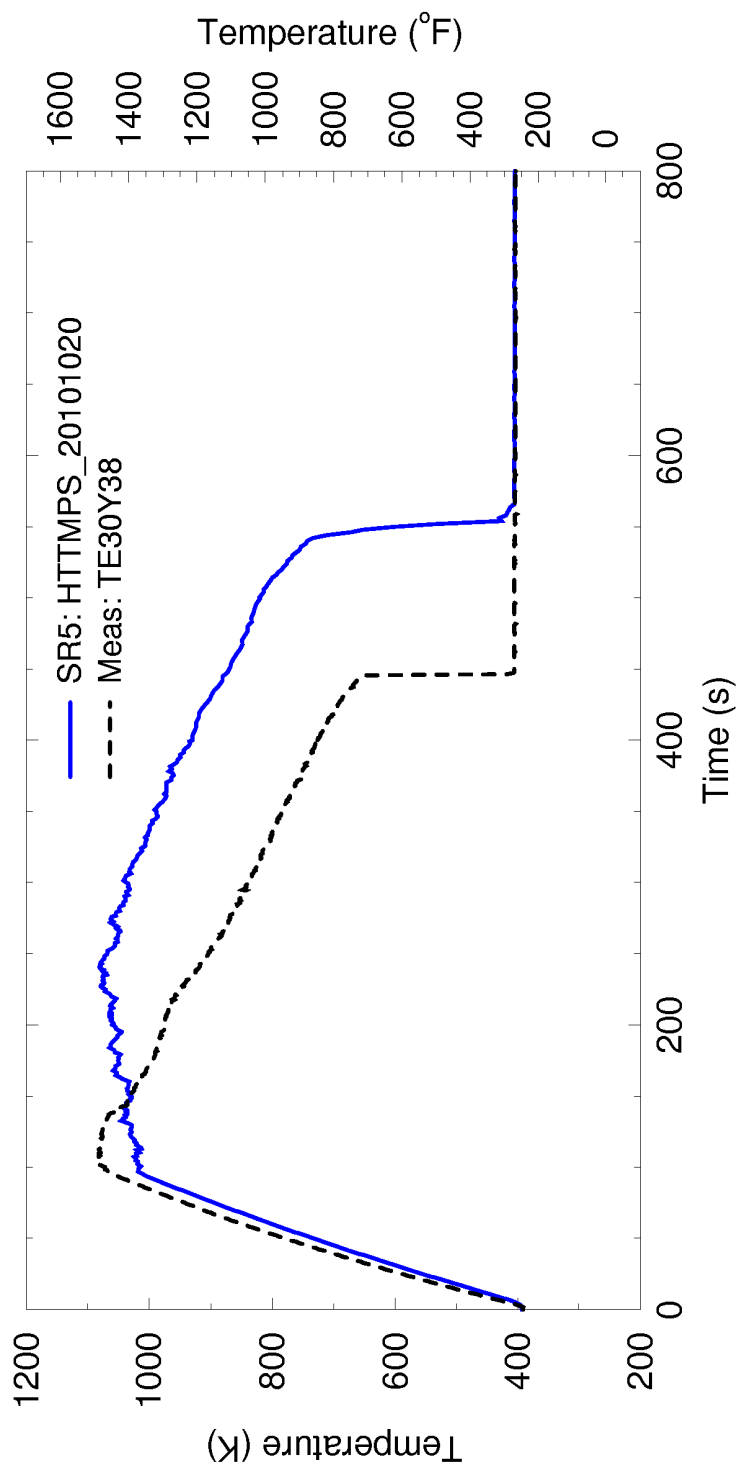


**Figure 4.103: Comparison of Rod Surface Temperatures for High Power Bundles at 2.035 meters Elevation CCTF Test Run 62**

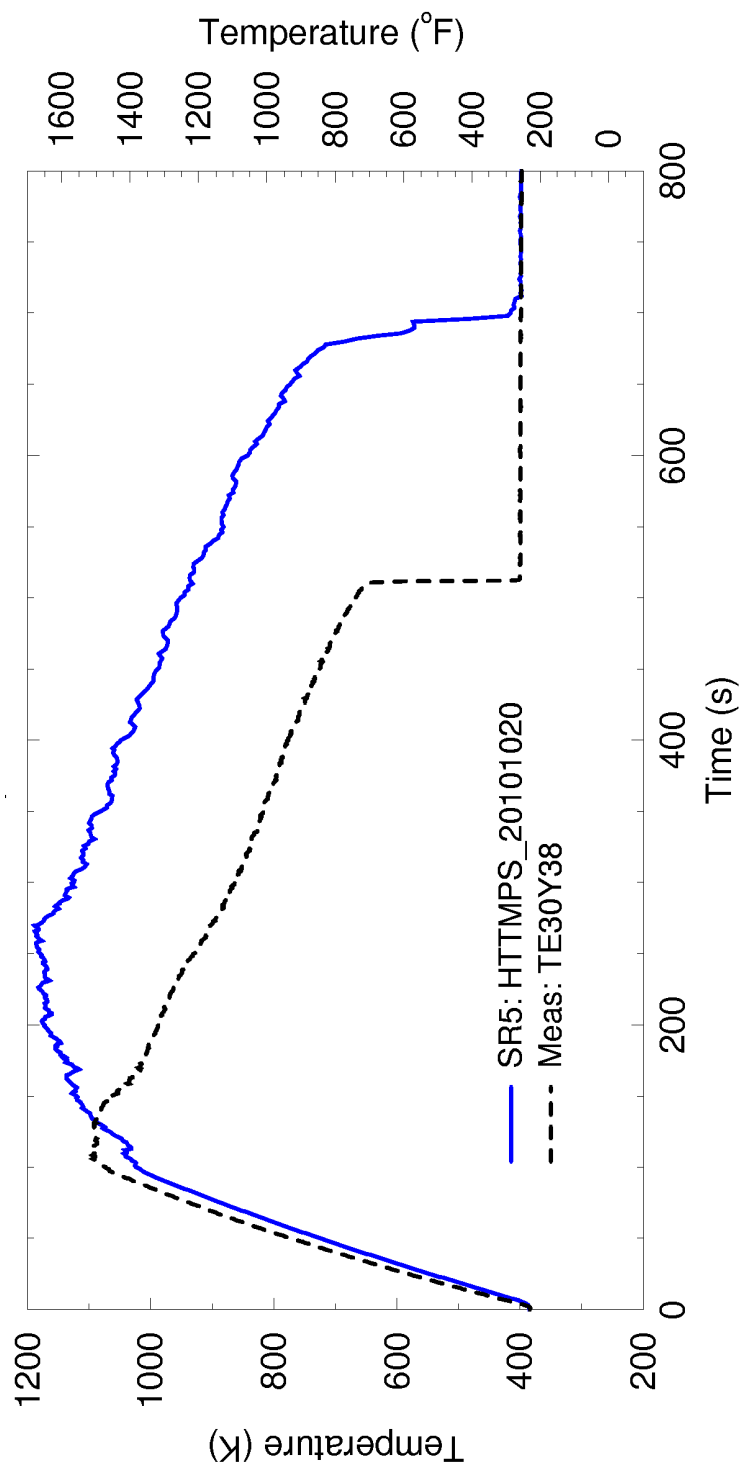


**Figure 4.104: Comparison of Rod Surface Temperatures for High Power Bundles at 2.035 meters Elevation CCTF Test Run 67**



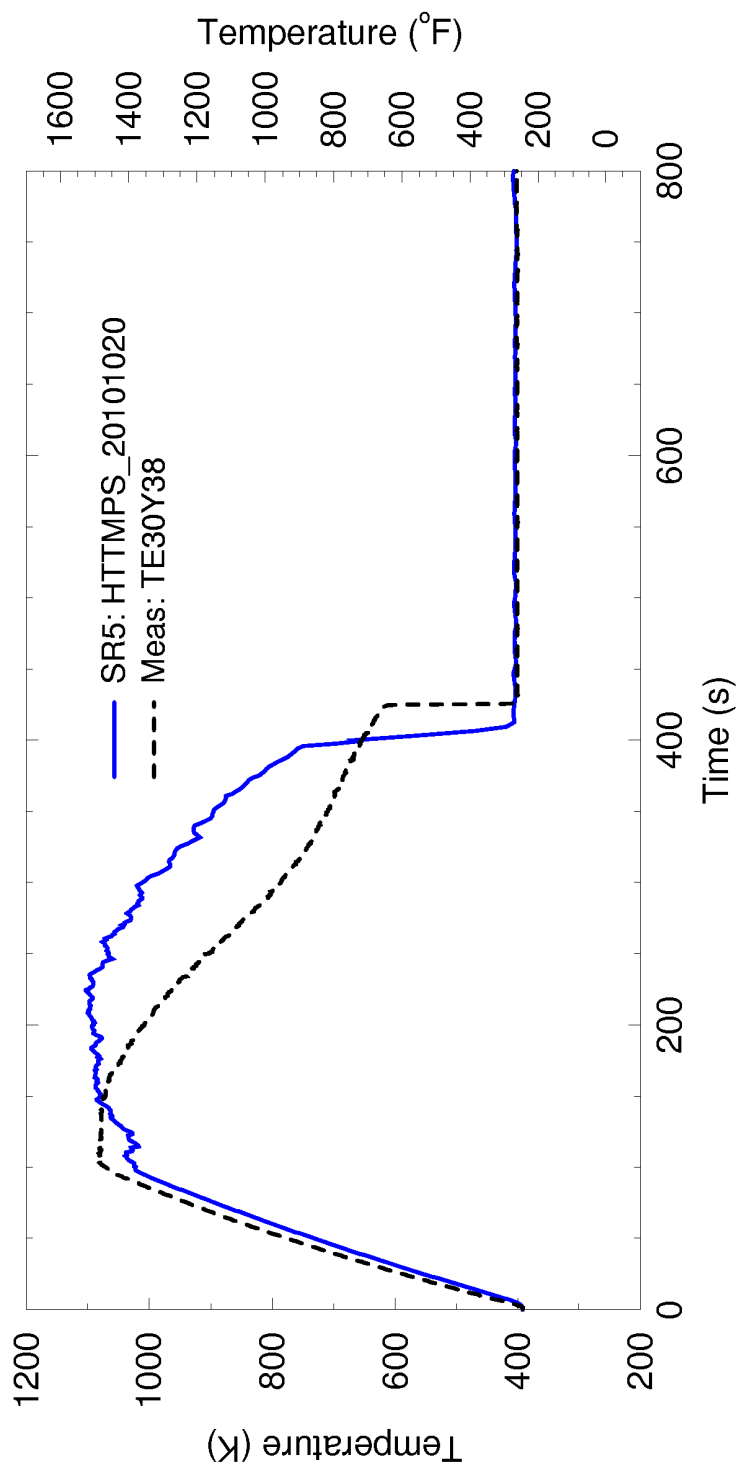


**Figure 4.105: Comparison of Rod Surface Temperatures for High Power Bundles at 2.035 meters Elevation CCTF Test Run 68**

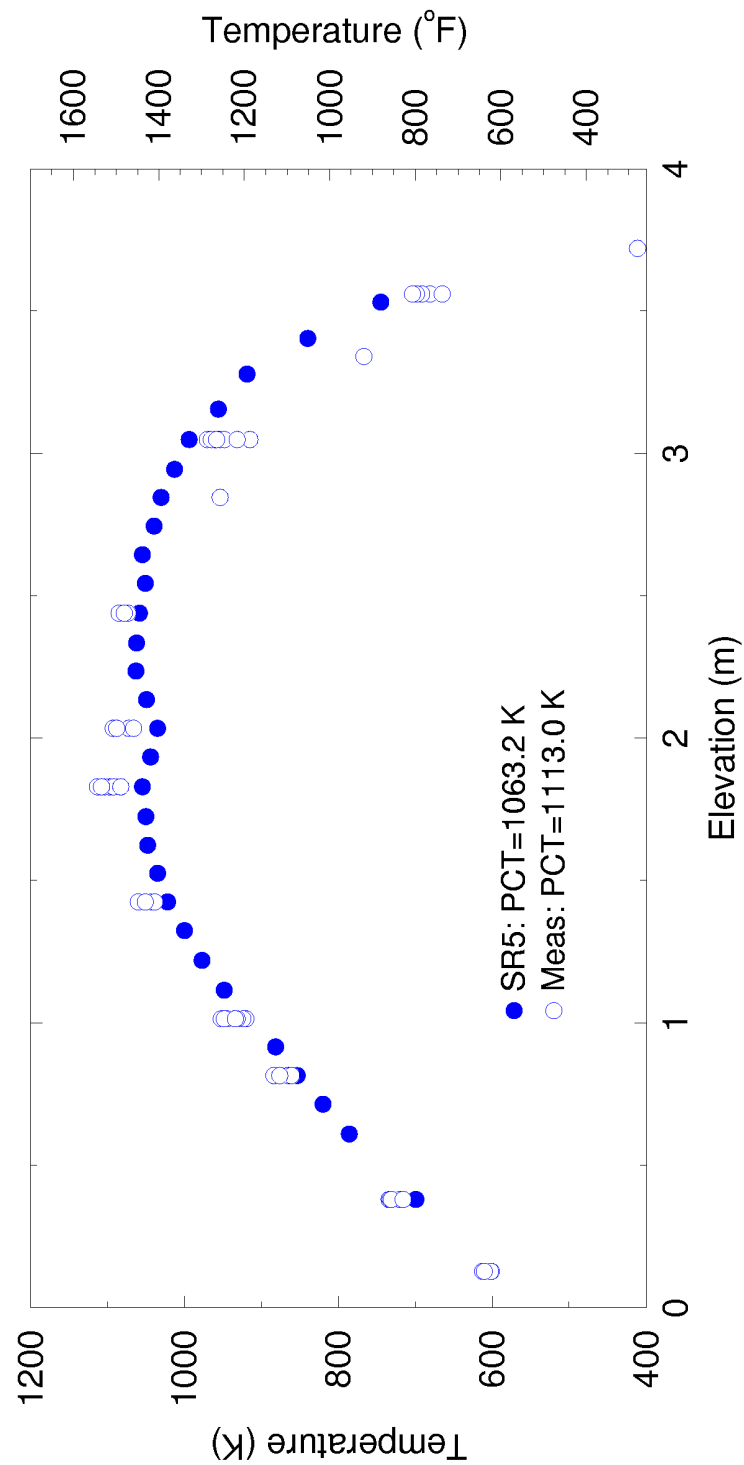


**Figure 4.106: Comparison of Peak Surface Temperatures versus Elevation for High Power Bundles CCTF Test Run 54**

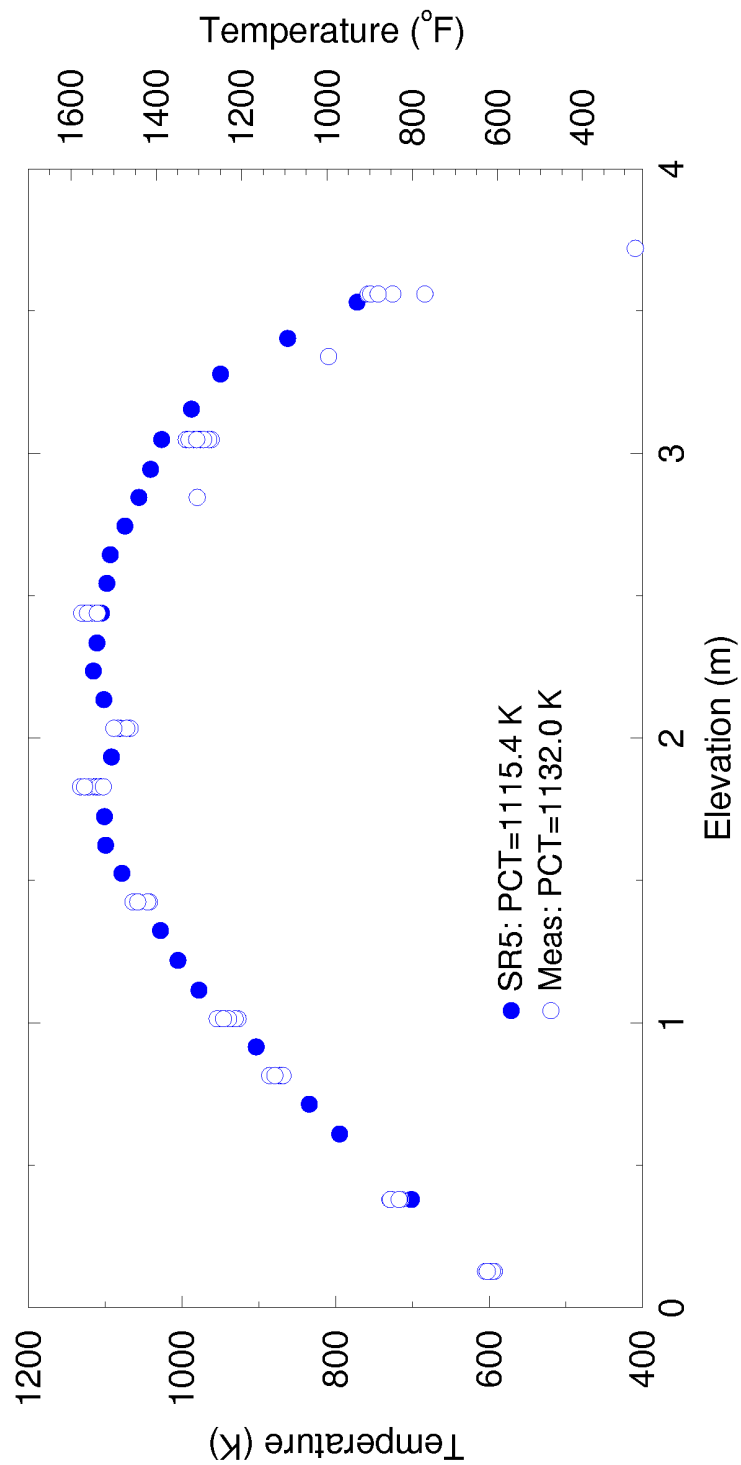


**Figure 4.107: Comparison of Peak Surface Temperatures versus Elevation for High Power Bundles CCTF Test Run 62**

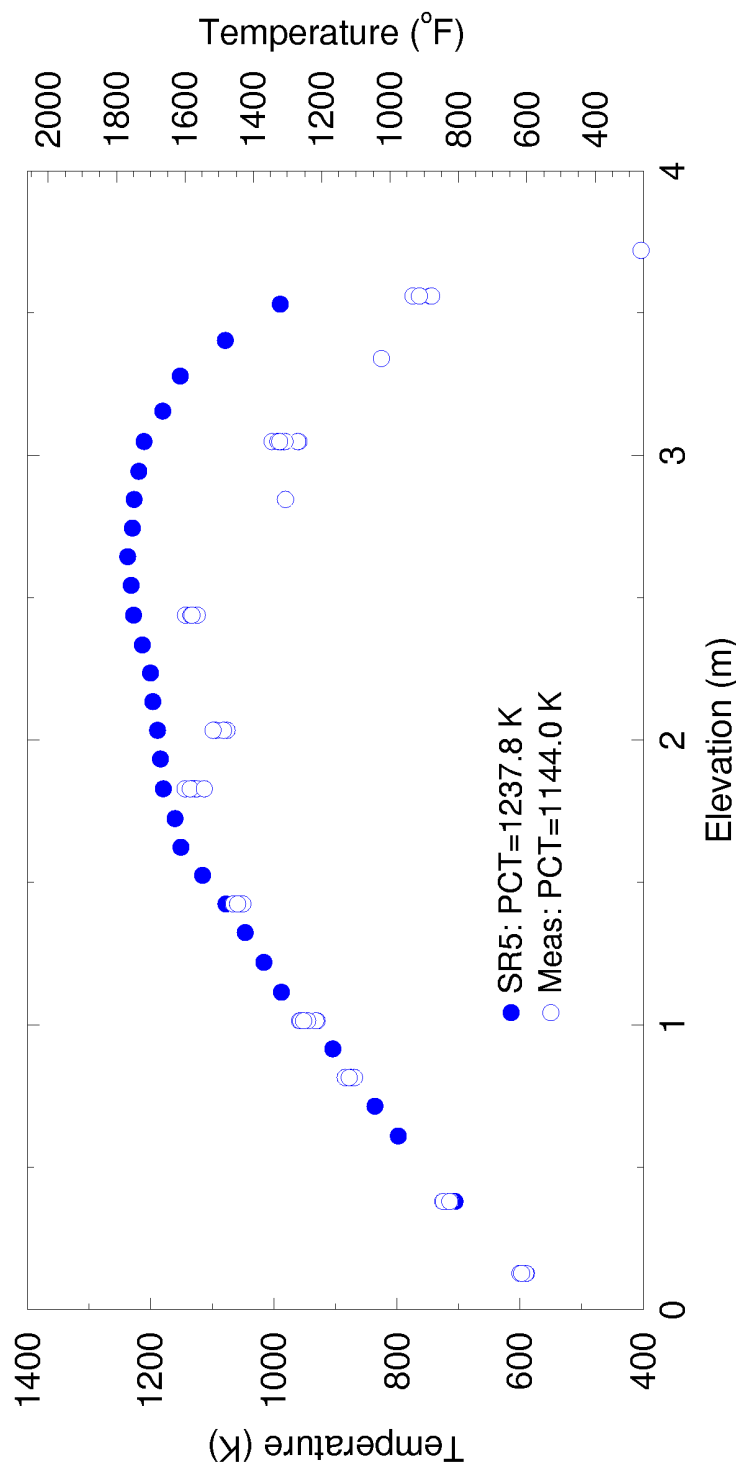


**Figure 4.108: Comparison of Peak Surface Temperatures versus Elevation for High Power Bundles CCTF Test Run 67**

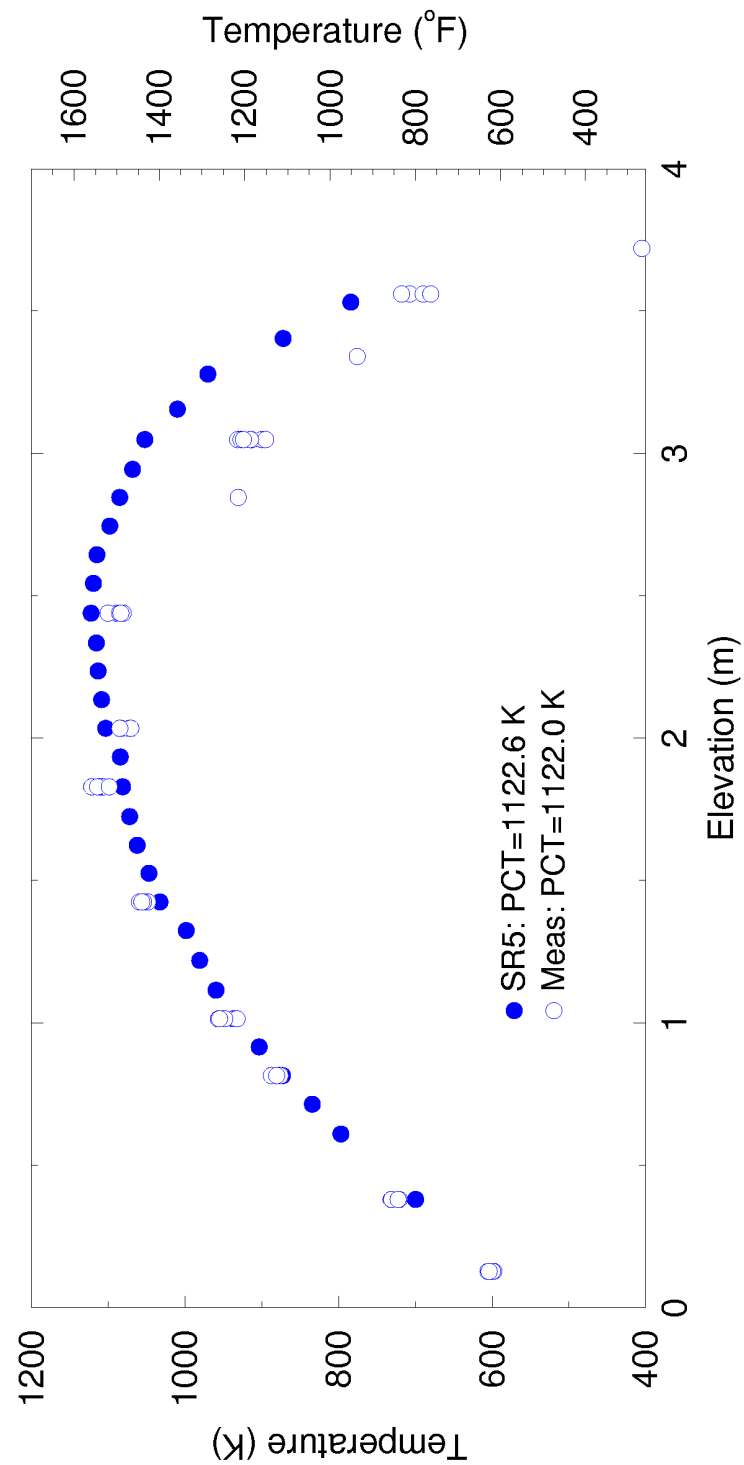


**Figure 4.109: Comparison of Peak Surface Temperatures versus Elevation for High Power Bundles CCTF Test Run 68**

#### 4.3.1.13 SCTF Tests

Two gravity feed and four forced feed SCTF CORE-II tests (from a series of 27 tests) were chosen as a diverse sample of behaviors to evaluate the ability of S-RELAP5 to predict the core and the pressure vessel thermal-hydraulic phenomena occurring during the reflooding phase of a LBLOCA in a PWR. The study has two objectives: (1) to assess the capability of the code to simulate both forced and gravity reflood transients and (2) to study the effect of radial nodalization on reflood behavior.

The SCTF Core-II test series was undertaken under the 2D/3D program in part to obtain information useful in assessing thermal-hydraulic models in best-estimate evaluation models. The SCTF test facility was designed to investigate two-dimensional thermal-hydraulic behavior in the pressure vessel during the reflood phase of a PWR LBLOCA. To meet this objective, SCTF simulated a full-radius slab section of a PWR core with eight bundles arranged in a row. The heating power for each bundle can be controlled independently.

In the SCTF test series, two test modes were adopted: gravity- and forced feed. In the gravity feed tests, the valve between the lower downcomer and lower plenum was open so that there was communication between the downcomer and the bundle region. In these tests, ECC was initially injected into the lower plenum. After several seconds, ECC injection was switched to the cold leg. In the force-feed tests, the valve between the lower downcomer and lower plenum was closed and ECC was injected into the lower plenum only. Although the first mode is considered to be a better simulation of integral reactor behavior, the boundary conditions at the core inlet (mass flow rate and subcooling) are affected by changes in various parameters (change of system pressure and core heating, etc.). Therefore, to investigate the effect of parameter changes on the 2-D thermal-hydraulic behavior in the pressure vessel, the forced feed test mode was adopted to obtain accurate boundary conditions at the core inlet.

Two "gravity reflood" tests (Tests S2-SH1 and S2-AC1) and four "forced reflood" tests (Tests S2-10, S2-11, S2-17, and S2-18) were selected for the S-RELAP5 code assessment. Test S2-SH1 is a gravity-reflood based test. During Test S2-SH1, the downcomer was not blocked from the lower plenum (i.e., hydraulic communication existed between the lower plenum and the downcomer). In the test, ECC was first injected into the lower plenum. After core reflood started and the downcomer was almost full, ECC injection was switched to the intact cold leg. Test S2-AC1 differs from Test S2-SH1 in the accumulator injection rate and duration.

Test S2-10 is a forced-reflood based test. In Test S2-10, ECC was injected into the lower plenum only, with no hydraulic communication between the lower plenum and the downcomer. The ECC injection rate was specified to match the core inlet flow rate achieved in gravity feed Test S2-SH1. Test S2-11 differs from S2-10 in that a high accumulator flow rate was used to match the core inlet flow rate achieved in gravity feed Test S2-AC1.

Tests S2-17 and S2-18 are also forced reflood tests with the primary difference between them being in the radial power distribution. Test S2-17 has a flat power profile and Test S2-18 has a steep power profile. The assessment of these two tests with their widely different radial power distributions provides a good test for S-RELAP5.

Table 4.12 shows the test conditions for each of the tests examined. The six SCTF Core-II reflood experiment tests were selected to assess forced reflood, gravity reflood, and the effect of core radial nodalization. The assessment matrix is summarized as follows:

- Forced versus Gravity Reflood (Phase I): In this assessment phase, two sets of counterpart tests were chosen to study the differences between forced and gravity reflood. The first set consists of Tests S2-11 and S2-AC1 and the second set consists of Tests S2-10 and S2-SH1. A nominal nodalization of two bundles per core channel was modeled for this study.
- Effect of Radial Nodalization (Phase II): In this assessment phase, two tests were chosen to study the effect of radial nodalization on reflood behavior. These tests are S2-18 and S2-17. Both tests were simulated using the nominal axial nodalization. In addition, Test S2-18 was simulated using a fine-nodalization—one bundle per channel.

Since the primary purpose of the tests was to study the core and vessel thermal-hydraulic phenomena, the RLBLOCA guidelines are used, wherever possible, to model the test vessel, hot leg, the steam-water separator inlet plenum, and the cold leg piping from the ECC injection to the downcomer. A simple modeling approach is used to model the remaining portion of the test facility. The downcomer is represented by nine axial nodes, and the lower plenum is divided into two nodes. The core region is modeled using a 25x4 TWODEE component. Axial Nodes 1 through 24 model the active core, and Node 25 represents the distance between the top of the active core and the upper core tie plate. As previously explained, for the base model each radial segment consists of two fuel bundles. The axial nodes are divided such that each grid spacer is at a node boundary. Bundle heat transfer multipliers, FILMBL and DFFBHTC are

set to [ ] Since all the heated rods are represented by an average rod and the PCTs in all the tests simulated are below 1800 °F, the rod-to-rod radiation model was not used. The cold leg condensation model (summarized in Section 4.3.3.1.14 and described in detail in Section 5.2 of Reference 5) is used in the intact cold leg. To achieve proper liquid entrainment out of the steam-water separator inlet plenum, the following input modeling recommended from the UPTF Tests 10 and 29 benchmarks (Section 4.3.1.11.3) was used.

To study the radial power distribution effect, Test S2-18 was also simulated using a fine nodalization in the fuel bundle and upper plenum regions. In this model, an 8x25 TWODEE component, with one test bundle per radial segment, is used to model the bundle region and an 8x3 TWODEE component is used to model the upper plenum.

The SCTF tests, S-RELAP5 input model, and simulation results are discussed in detail in Section 3.10 of Reference 5. During the reflood phase of a LBLOCA, some of the important reflood phenomena are: core heat transfer, multi-dimensional flow phenomena in the core region, void generation/distribution, cold leg condensation, entrainment/ deentrainment in the core, entrainment/deentrainment in the upper plenum and in the hot legs, and steam binding in the steam generator. Except for steam binding effects in the steam generator, all other



important reflooding phenomena were observed in the SCTF tests and were calculated reasonably well by S-RELAP5. Selected important parameters are discussed below.


- The calculated pressures in the primary system for all six tests agree reasonably well with the data as shown in Figure 4.110 through Figure 4.115.
- The calculated axial differential pressures in the core region for all six cases agree reasonably well with the data as shown in Figure 4.116 through Figure 4.121. These results indicate that, in all six cases, the code calculates proper liquid inventory in the bundle region.
- The calculated differential pressure between the upper plenum and downcomer for all six cases agree reasonably well with the data as shown in Figure 4.122 through Figure 4.127.
- The core and the upper plenum to downcomer  $\Delta P$  results indicate S-RELAP5 calculates acceptable loop and downcomer oscillations in the SCTF tests. The oscillations in the later phase of the transients are primarily due to cold leg condensation. In some cases, S-RELAP5 calculated higher amplitude oscillations than in the tests during the early phase of the transient, which represents the accumulator injection period. This is primarily due to the atypical ECC injection modes in the tests. During the early phase of the transient, ECC, that simulates accumulator injection, is injected into the lower plenum in all the tests. In the gravity feed tests, the ECC injection is switched to the cold legs a few seconds after reflood initiation, when the downcomer level is nearly full and the system is reasonably stable. This approach was selected in SCTF and CCTF tests in order to minimize unstable conditions at the start of cold water injection into the stagnant primary system. In a PWR, the ECC injection into the cold legs starts while the system is blowing down and the transition from the refill to the reflood phase is a continuous process. Considering these differences, it can be concluded the code will calculate acceptable downcomer and loop oscillations during the reflood phase of a LBLOCA in the plant.
- SCTF hot leg geometry is atypical. The inside geometry is elliptical with height (major axis) close to the inside diameter of a typical 4-loop PWR. The width (minor axis) is narrow to preserve the volume flow area scaling. In the S-RELAP5 model, the oval geometry is approximated as a circular pipe while maintaining the same volume flow area. In SCTF, there is no active steam generator. A steam-water separator is used to simulate the primary side of the steam generator. The inlet chamber represents the inlet plenum of four scaled steam generators. The outlet chamber collects the liquid that is entrained from the inlet chamber. In the tests, the liquid level in the outlet chamber is measured. This collected

liquid represents the liquid that would be entrained in the tube region during a LBLOCA in a scaled PWR. The measured and S-RELAP5 calculated liquid levels for the six tests are shown in Figure 4.128 through Figure 4.133. Considering the atypical SCTF hot leg and the approximation used in modeling the hot leg, the S-RELAP5 calculated liquid entrainment to the steam-water separator is acceptable. These results are consistent with the core  $\Delta P$  results.

- Table 4.13 and Table 4.14, and the cladding thermal responses at 1.905 meters shown in Figure 4.134 through Figure 4.139 indicate that the S-RELAP5 results, including the PCT and quench time for all the six cases, agree reasonably well with the data.
- The results for Test S2-18 shows the core thermal-hydraulic behavior is not sensitive to the radial nodalization.

In summary, the assessment results show that S-RELAP5 calculates the important reflood phenomena occurring in all six SCTF tests with reasonable agreement to data. The assessments demonstrate that S-RELAP5 will calculate acceptable thermal-hydraulic phenomena during the reflood phase of a LBLOCA in a PWR including PCT, quench front propagation, and loop and downcomer oscillations.





**Table 4.13: Phase I Assessment Results, SCTF Tests**

		<b>S2-10</b>	<b>S2-11</b>	<b>S2-AC1</b>	<b>S2-SH1</b>
PCT (°F)	S-RELAP5	1126.0	1069.0	1067.0	1112.0
	Data (MIN/MAX)	1114/1168	1042/1085	1052/1085	1081/1166
Time of PCT (s)	Data	193.5	125.5	127.0	251.5
	S-RELAP5	180.0	125.0	125.0	175.0
Quench Time (s)	Data (elev 2.76 m)	520.0	425.0	465.0	570.0
	S-RELAP5	572.0	445.0	480.0	625.0

**Table 4.14: Phase II Assessment Results, SCTF Tests**

		<b>S2-17</b> (nominal nodalization)	<b>S2-18</b> (nominal nodalization)	<b>S2-18</b> (fine nodalization)
PCT (°F)	S-RELAP5	1050.0	1048.0	1076.0
	Data (MIN/MAX)	1080	1036/1116	1036/1116
Time of PCT (s)	Data	180.0	125.0	125.0
	S-RELAP5	173.0	128.0	123.0
Quench Time (s)	Data (elev 2.76 m)	498.0	455.0	455.0
	S-RELAP5	570.0	570.0	570.0

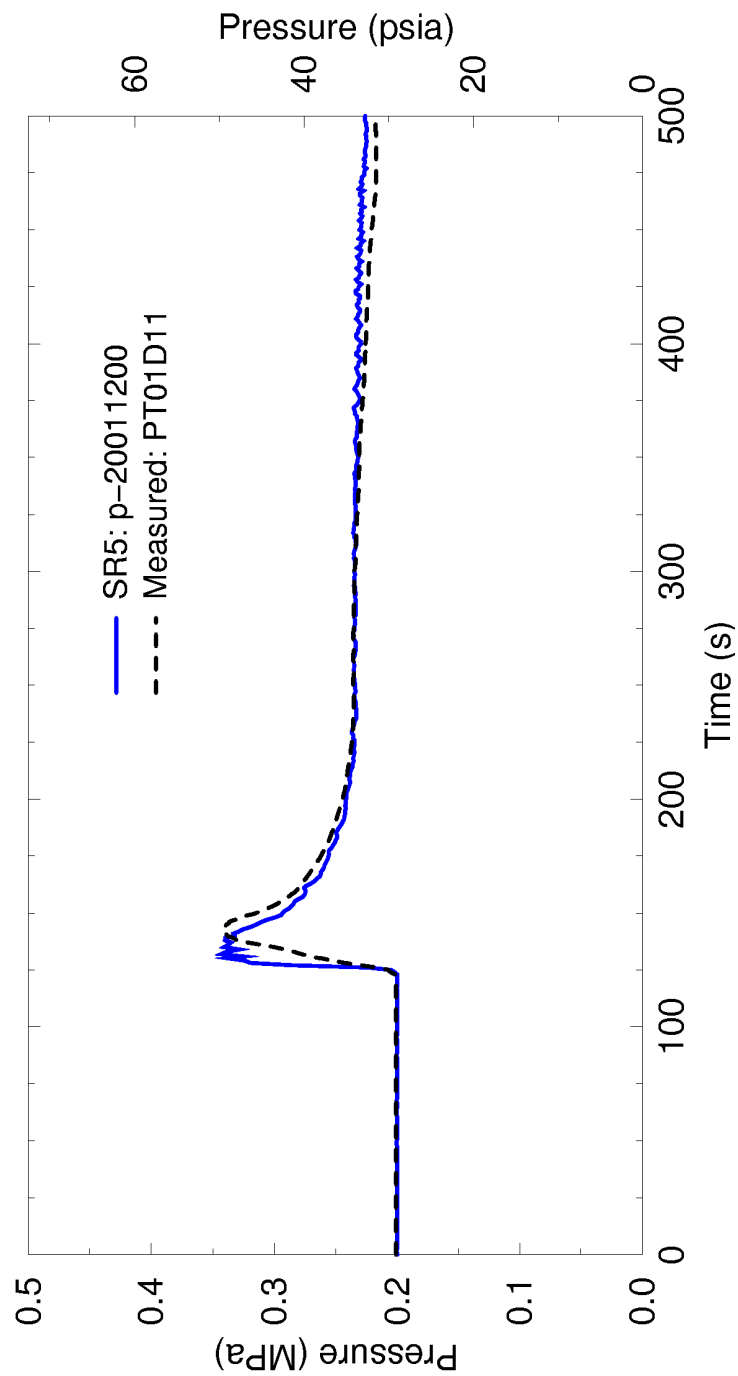


**Figure 4.110: Fuel Assembly Pressure Comparison  
SCTF-II S2-11**

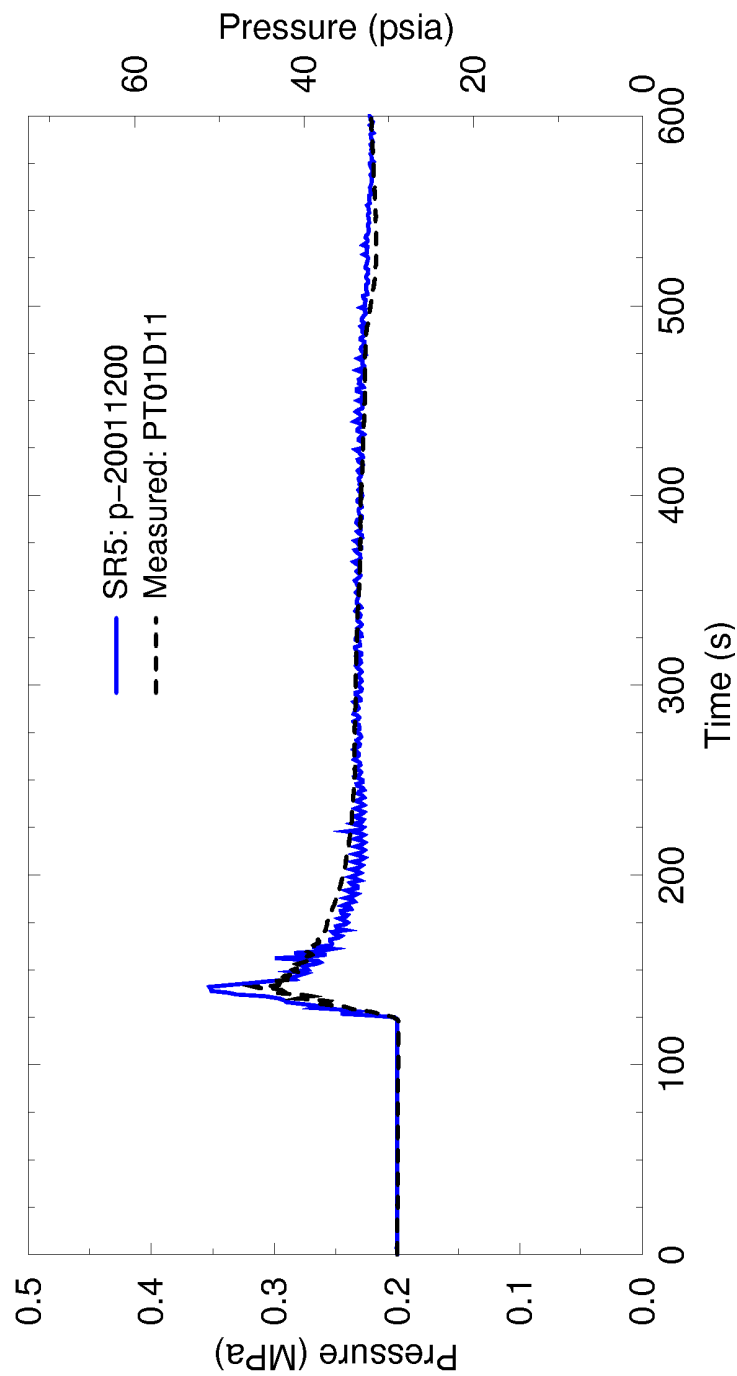


**Figure 4.111: Fuel Assembly Pressure Comparison  
SCTF-II S2-AC1**

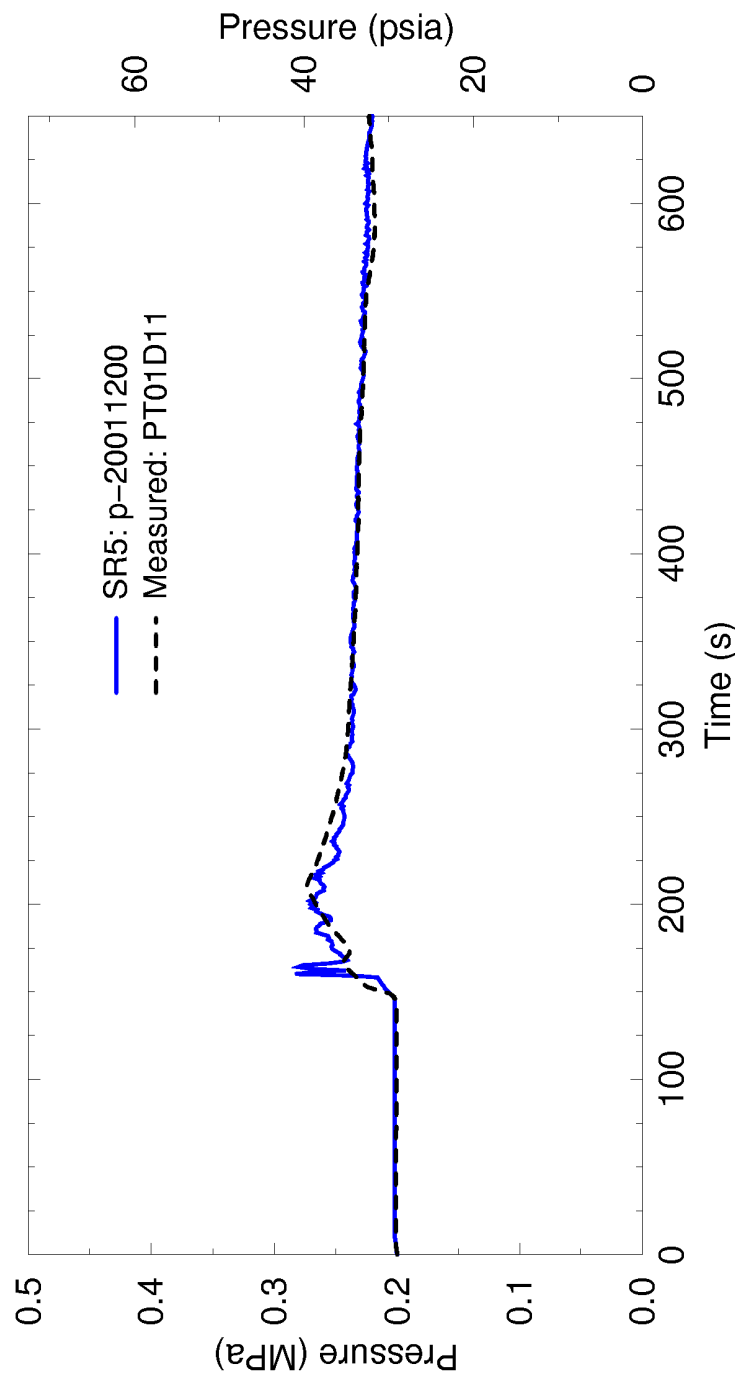


Figure 4.112: Fuel Assembly Pressure Comparison SCTF-II S2-10



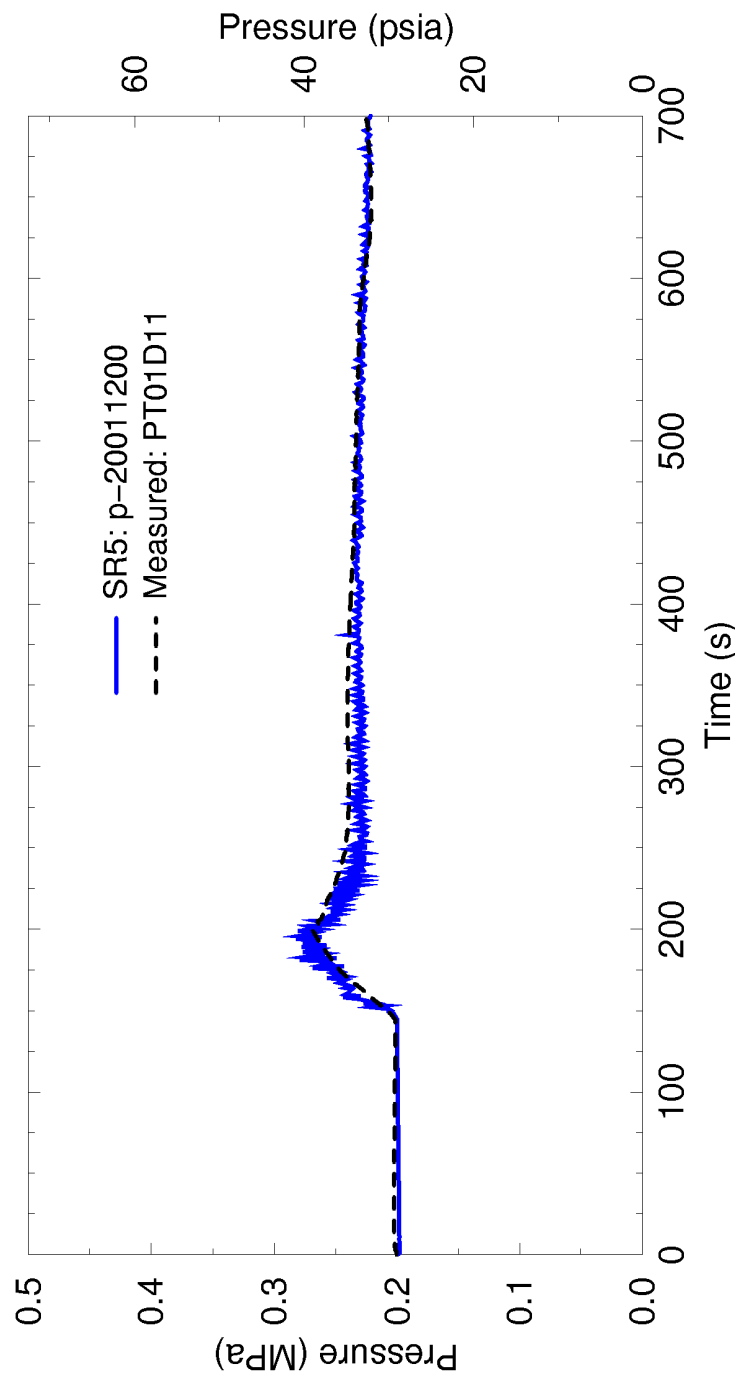


Figure 4.113: Fuel Assembly Pressure Comparison SCTF-II S2-SH1

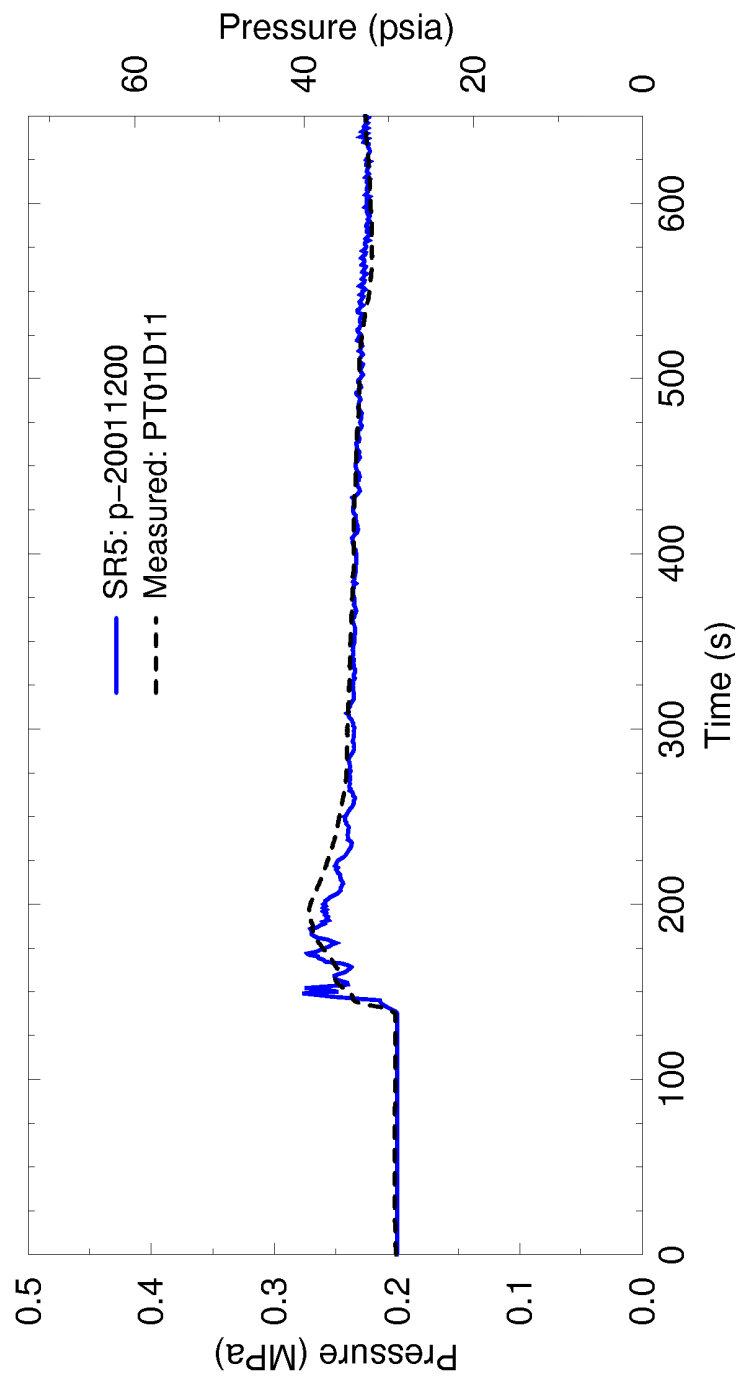
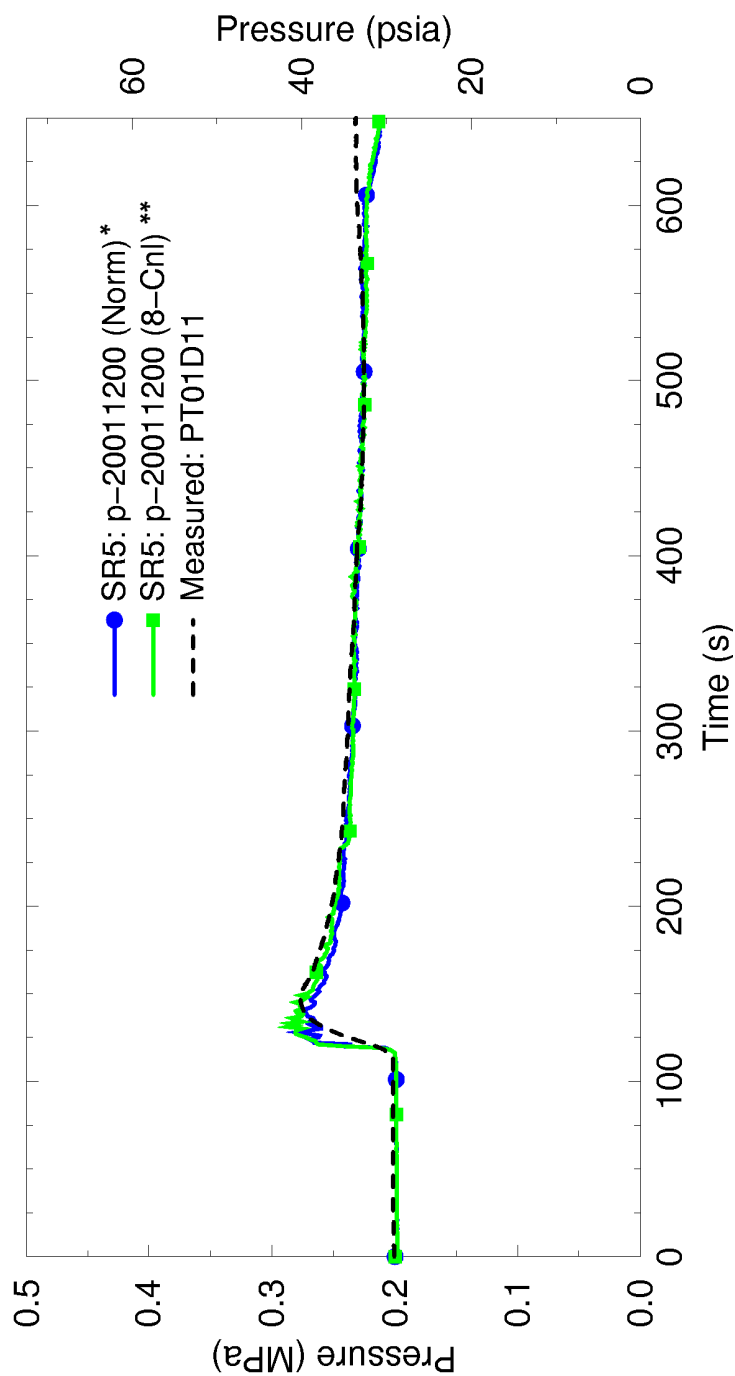


Figure 4.114: Fuel Assembly Pressure Comparison SCTF-II S2-17



\* Coarse noding, 2 bundles per segment  
\*\* Fine noding, 1 bundle per segment

Figure 4.115: Fuel Assembly Pressure Comparison  
SCTF-II S2-18

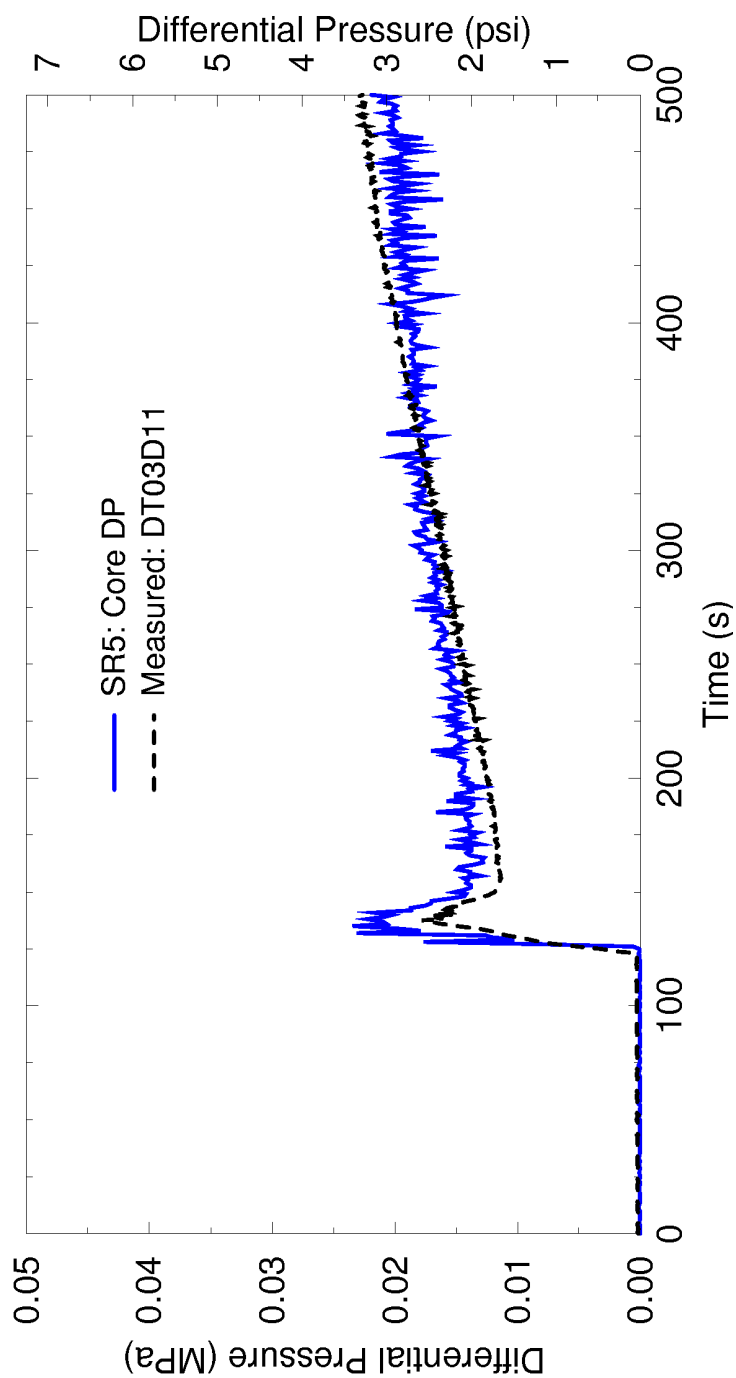
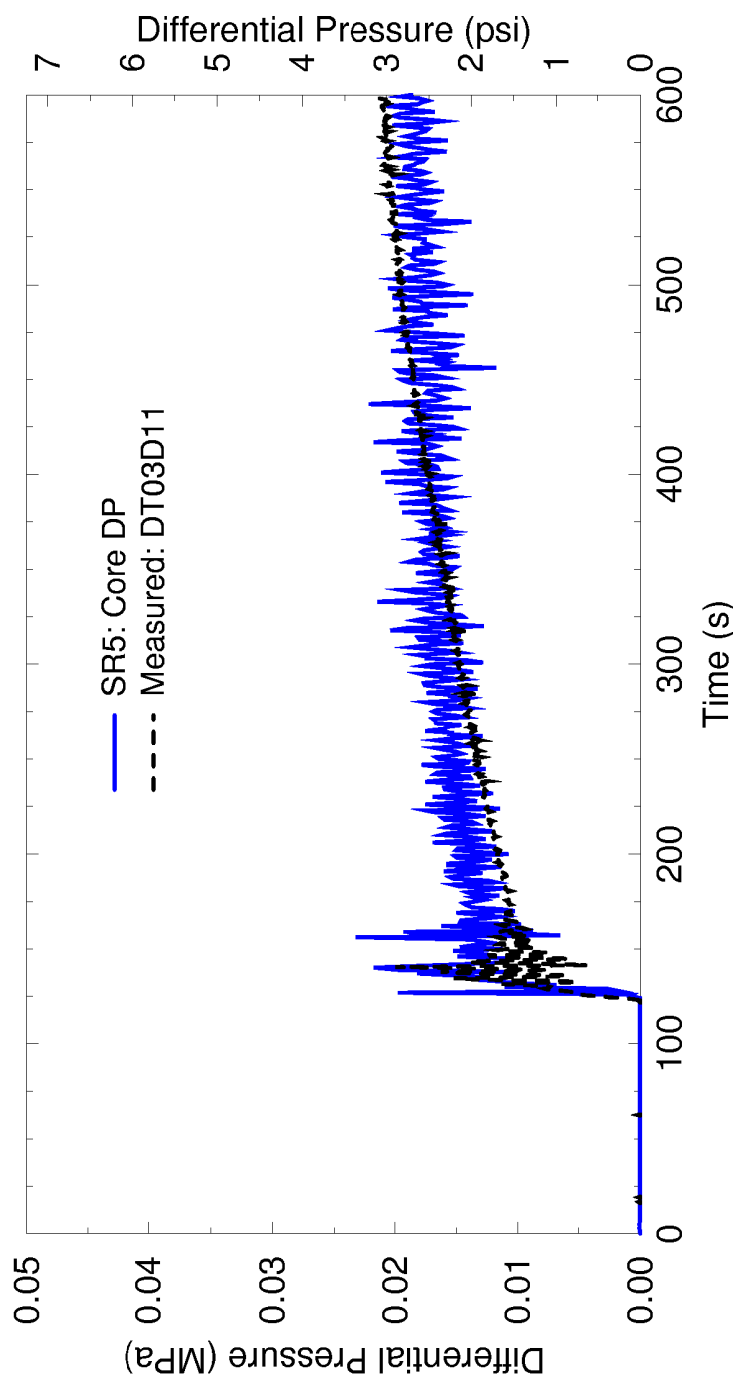
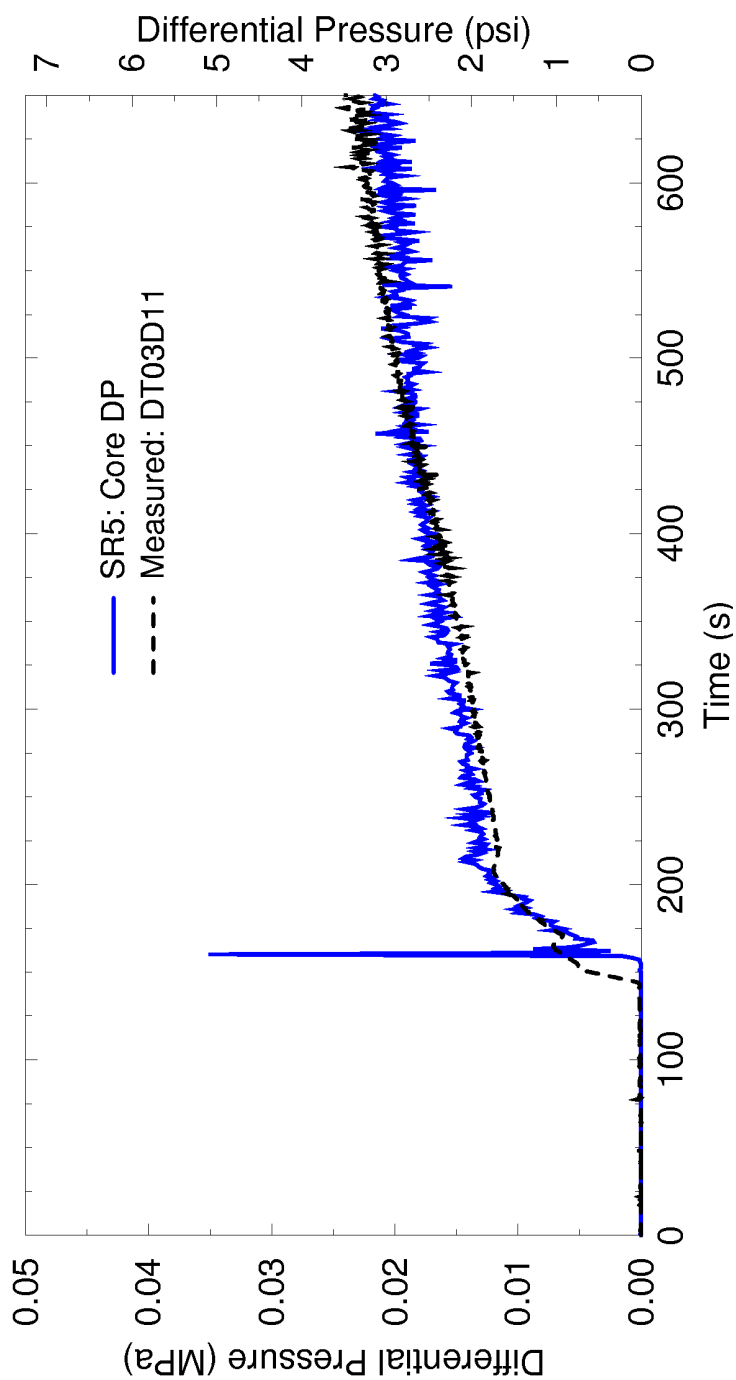


Figure 4.116: Core Differential Pressure Comparison SCTF-II S2-11



**Figure 4.117: Core Differential Pressure Comparison  
SCTF-II S2-AC1**



**Figure 4.118: Core Differential Pressure Comparison SCTF-II S2-10**

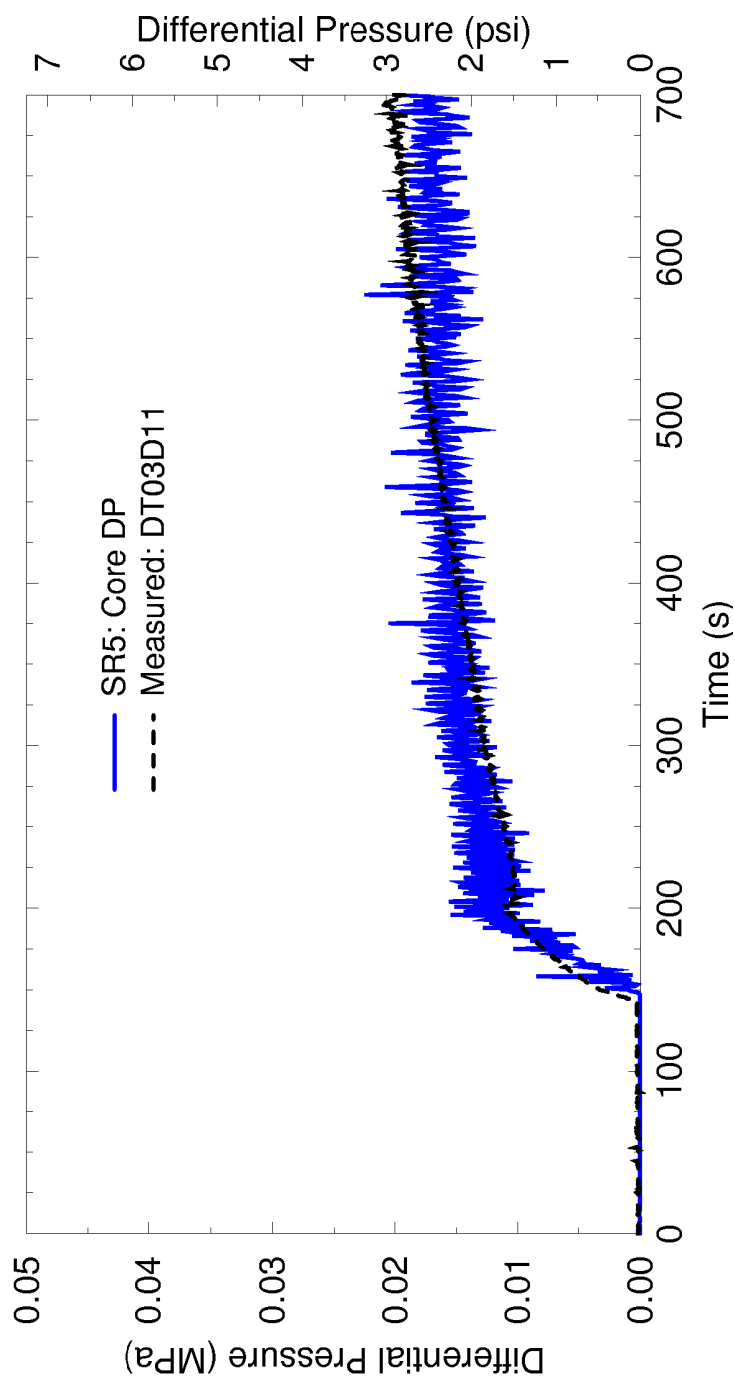


**Figure 4.119: Core Differential Pressure Comparison  
SCTF-II S2-SH1**

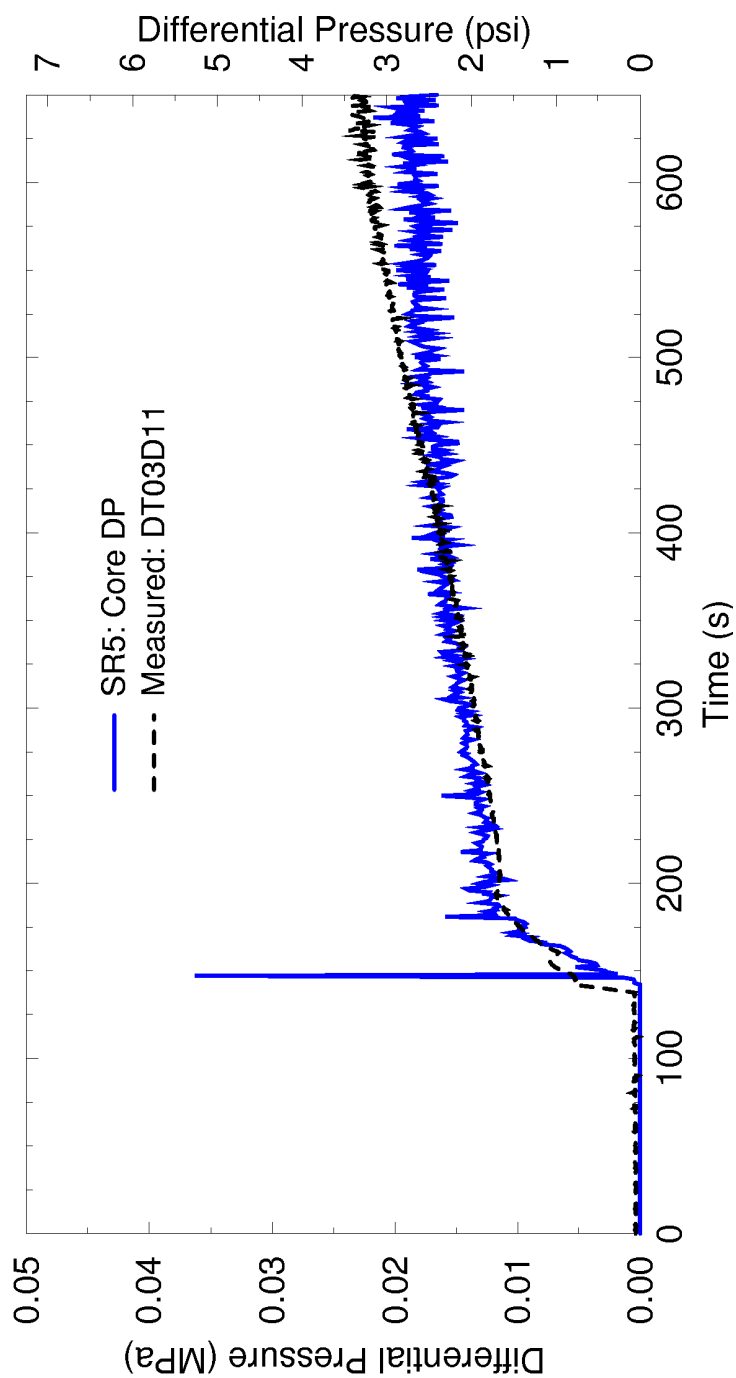


Figure 4.120: Core Differential Pressure Comparison SCTF-II S2-17



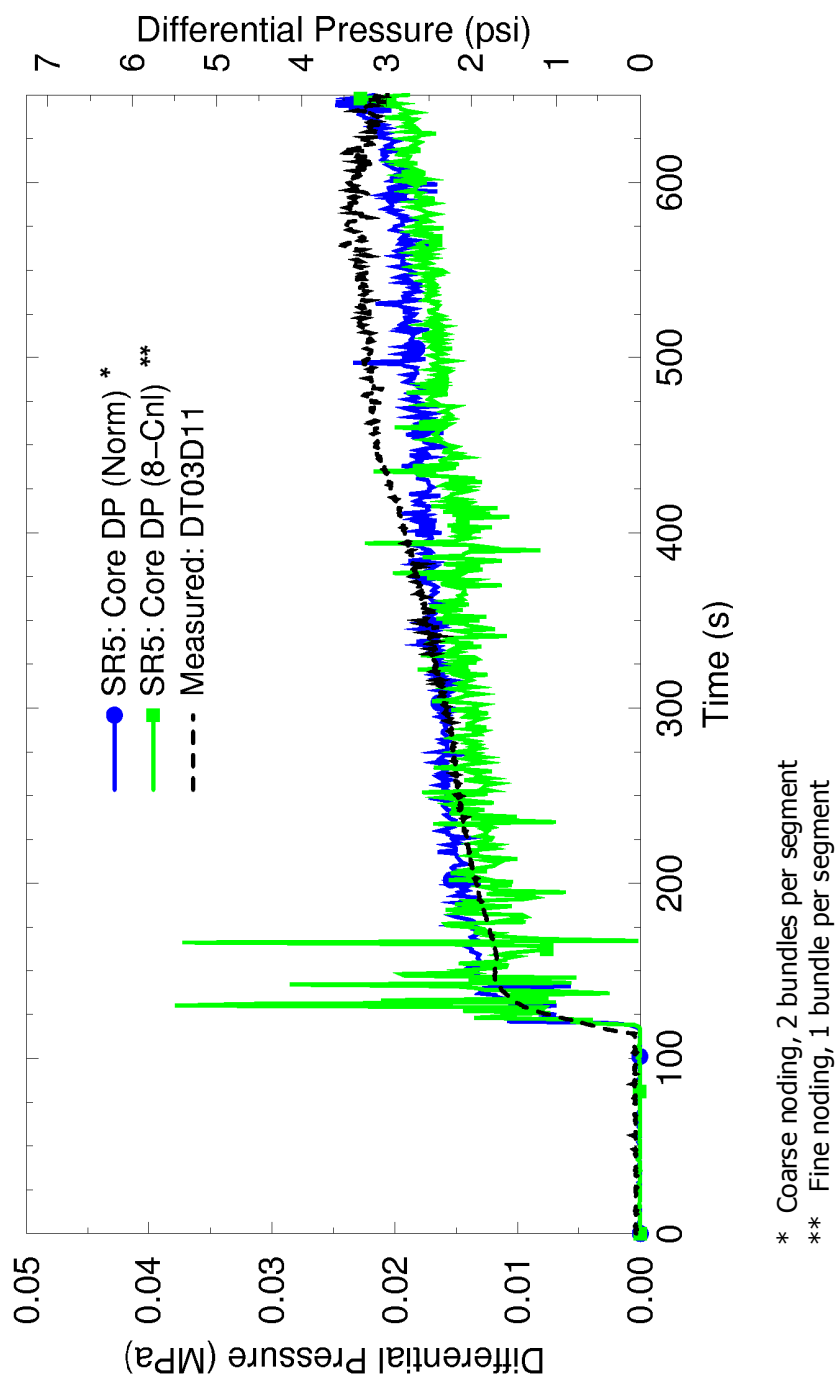
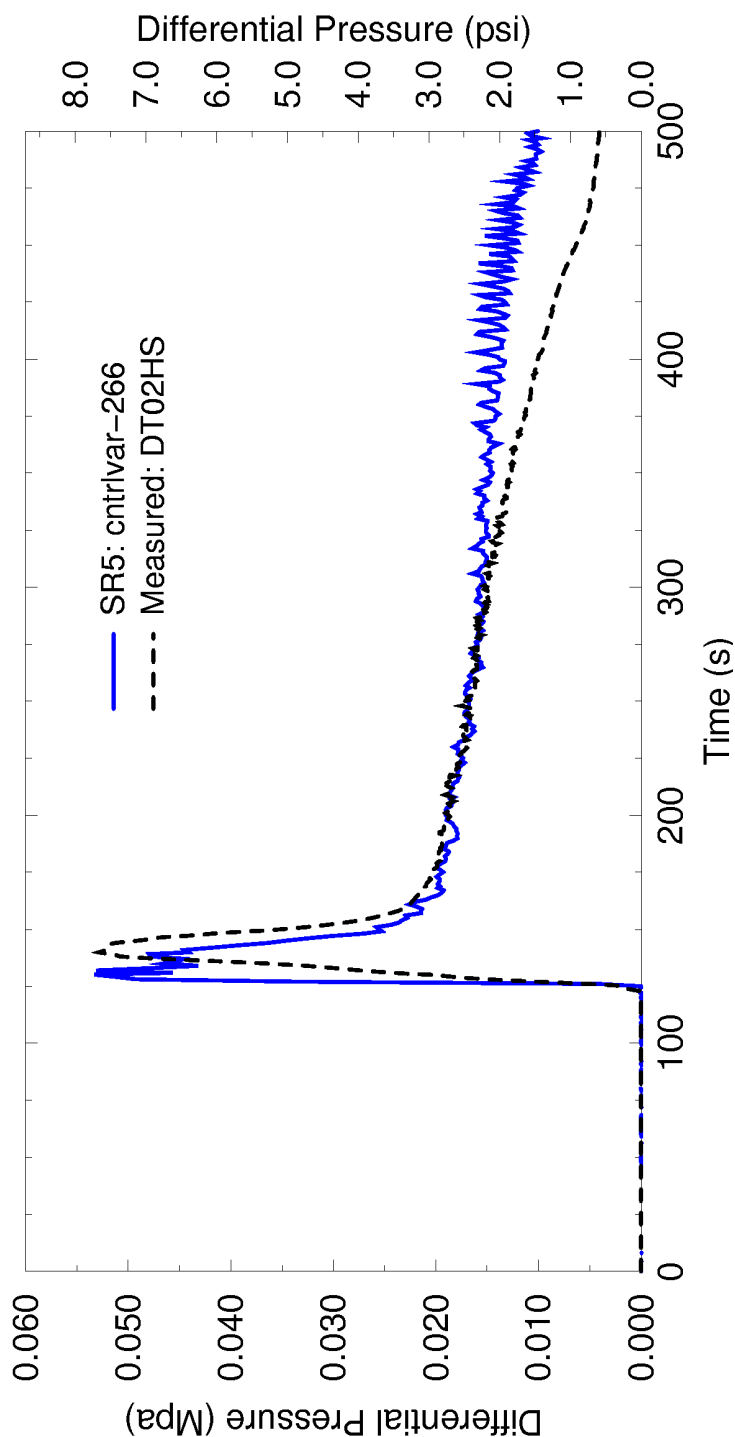
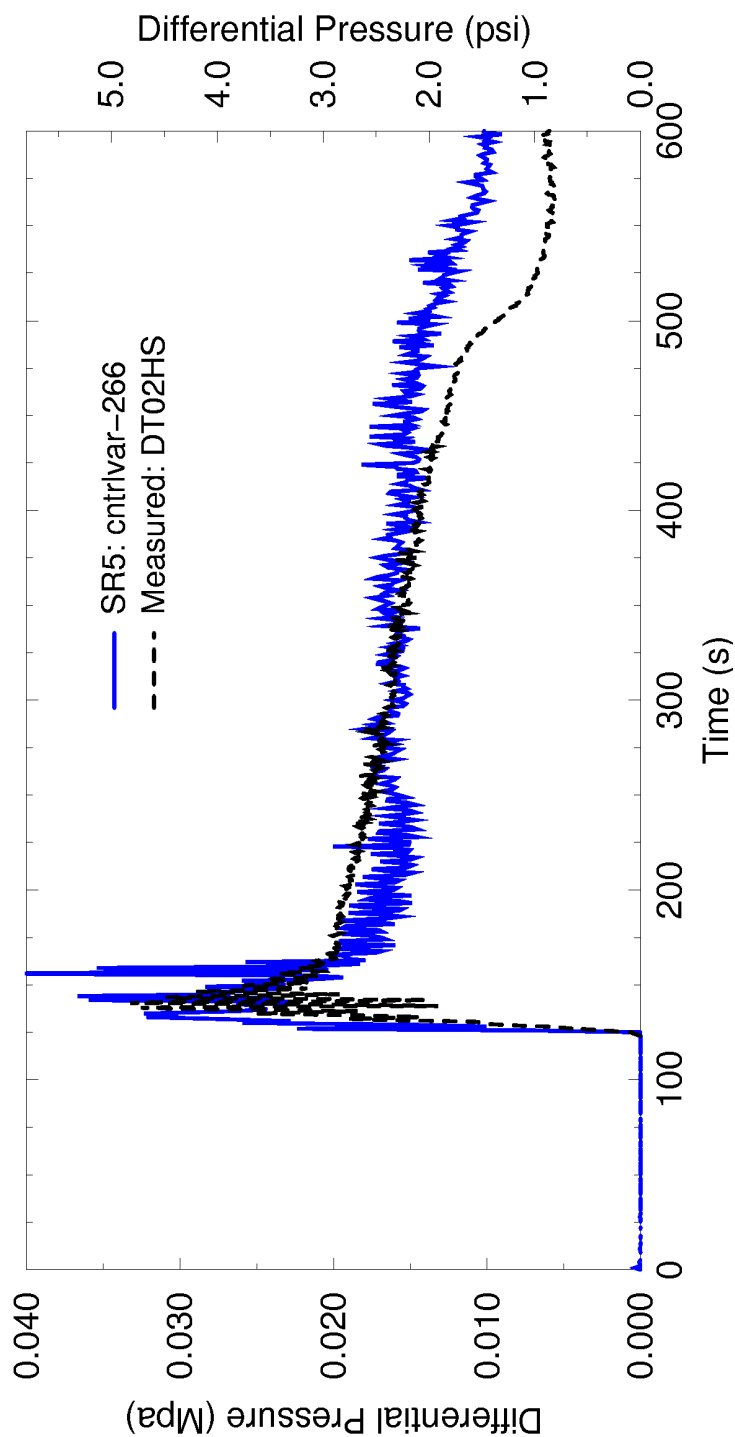


Figure 4.121: Core Differential Pressure Comparison SCTF-II S2-18



**Figure 4.122: Differential Pressure: Upper Plenum – Downcomer  
SCTF-II S2-11**



**Figure 4.123: Differential Pressure: Upper Plenum – Downcomer  
SCTF-II S2-AC1**

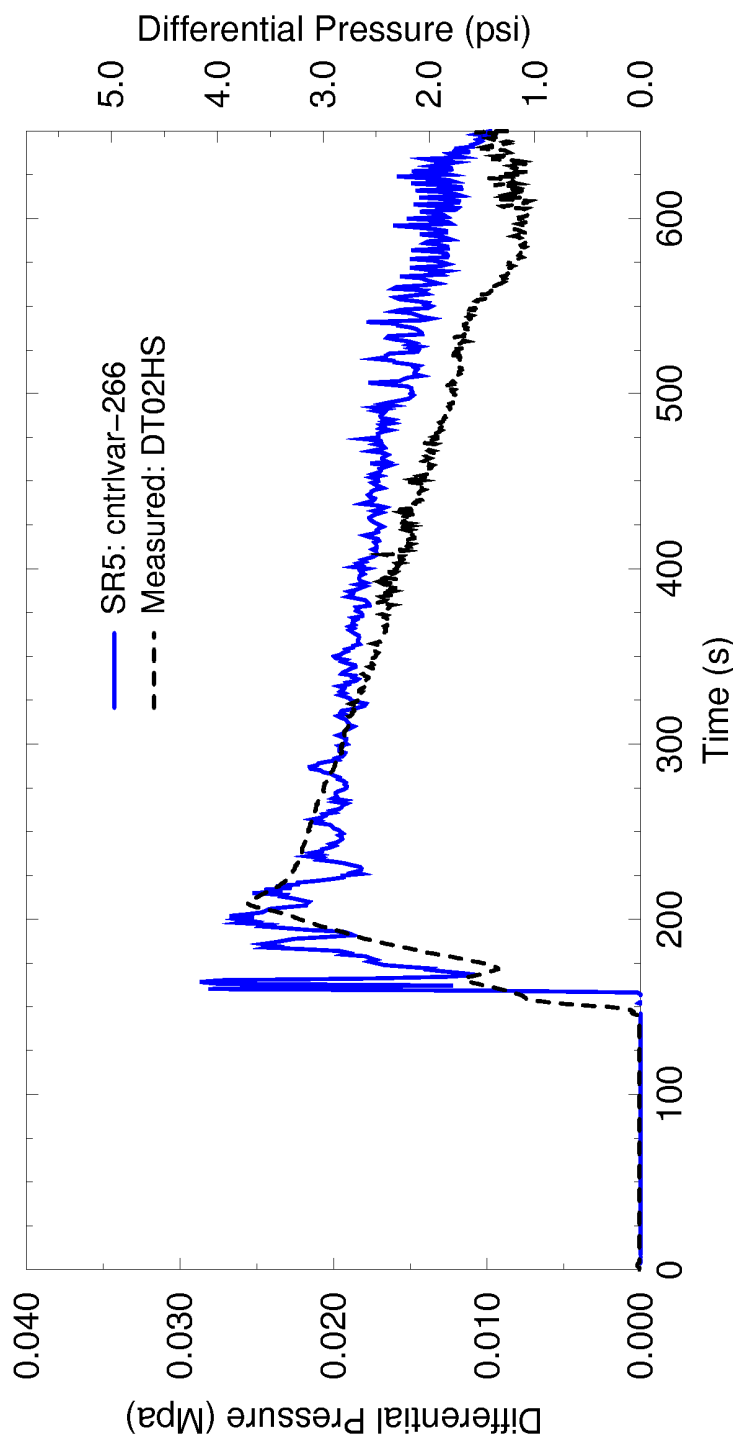


**Figure 4.124: Differential Pressure: Upper Plenum – Downcomer  
SCTF-II S2-10**

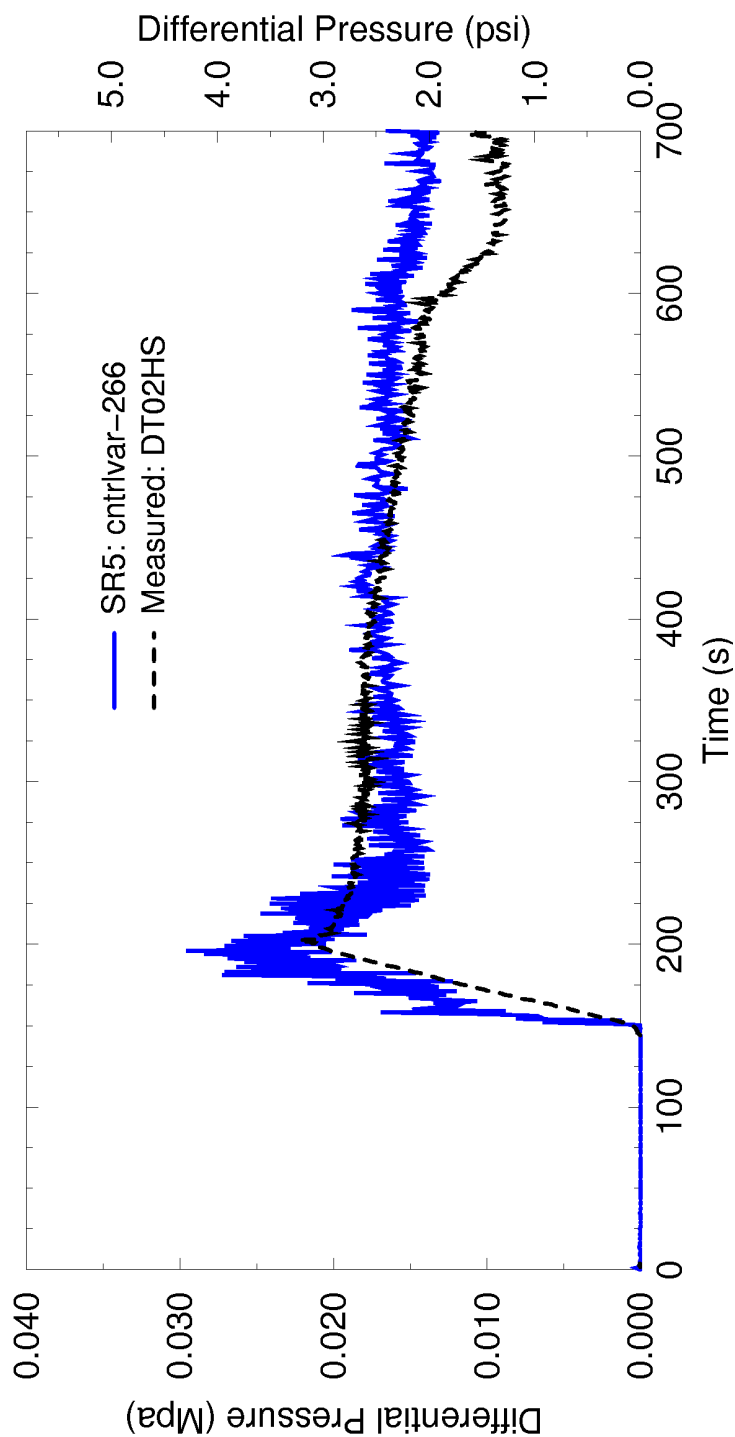


**Figure 4.125: Differential Pressure: Upper Plenum – Downcomer  
SCTF-II S2-SH1**

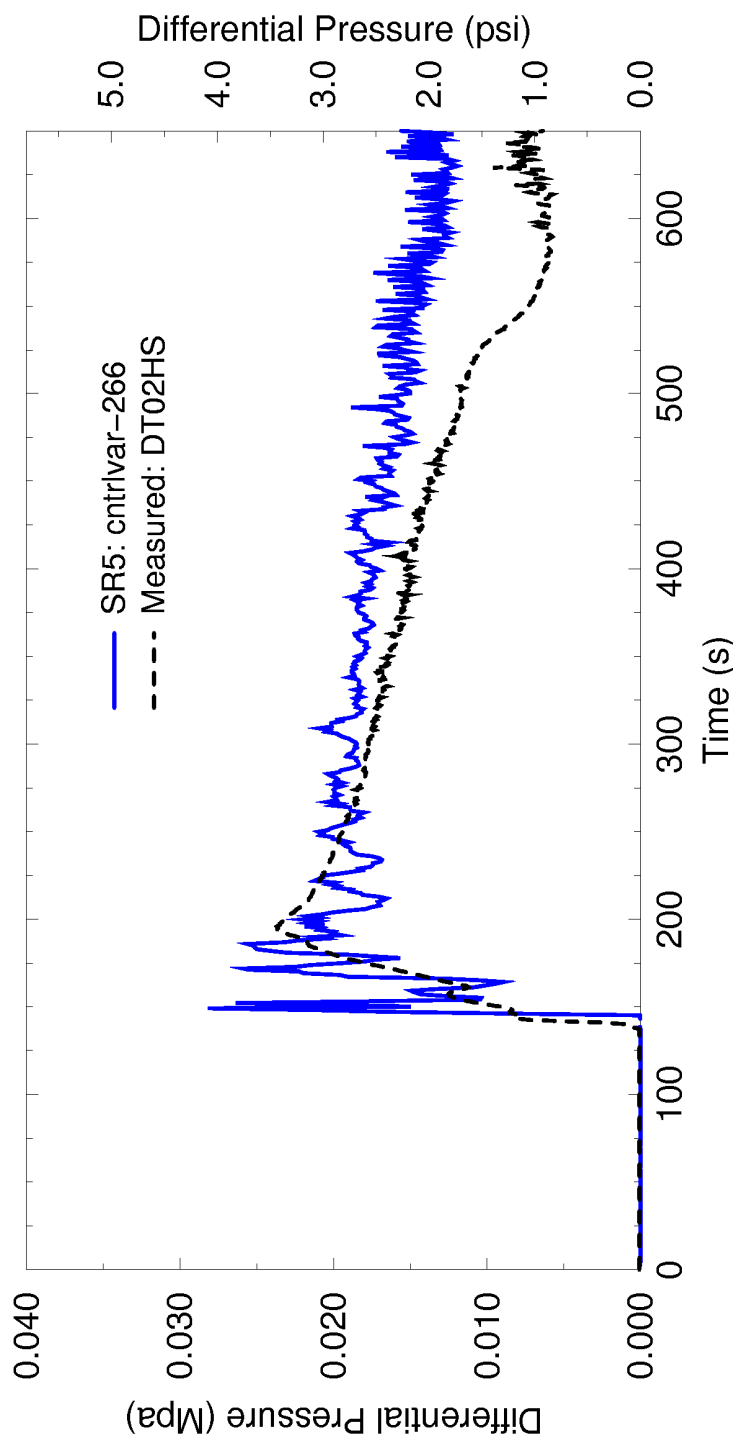


**Figure 4.126: Differential Pressure: Upper Plenum – Downcomer  
SCTF-II S2-17**

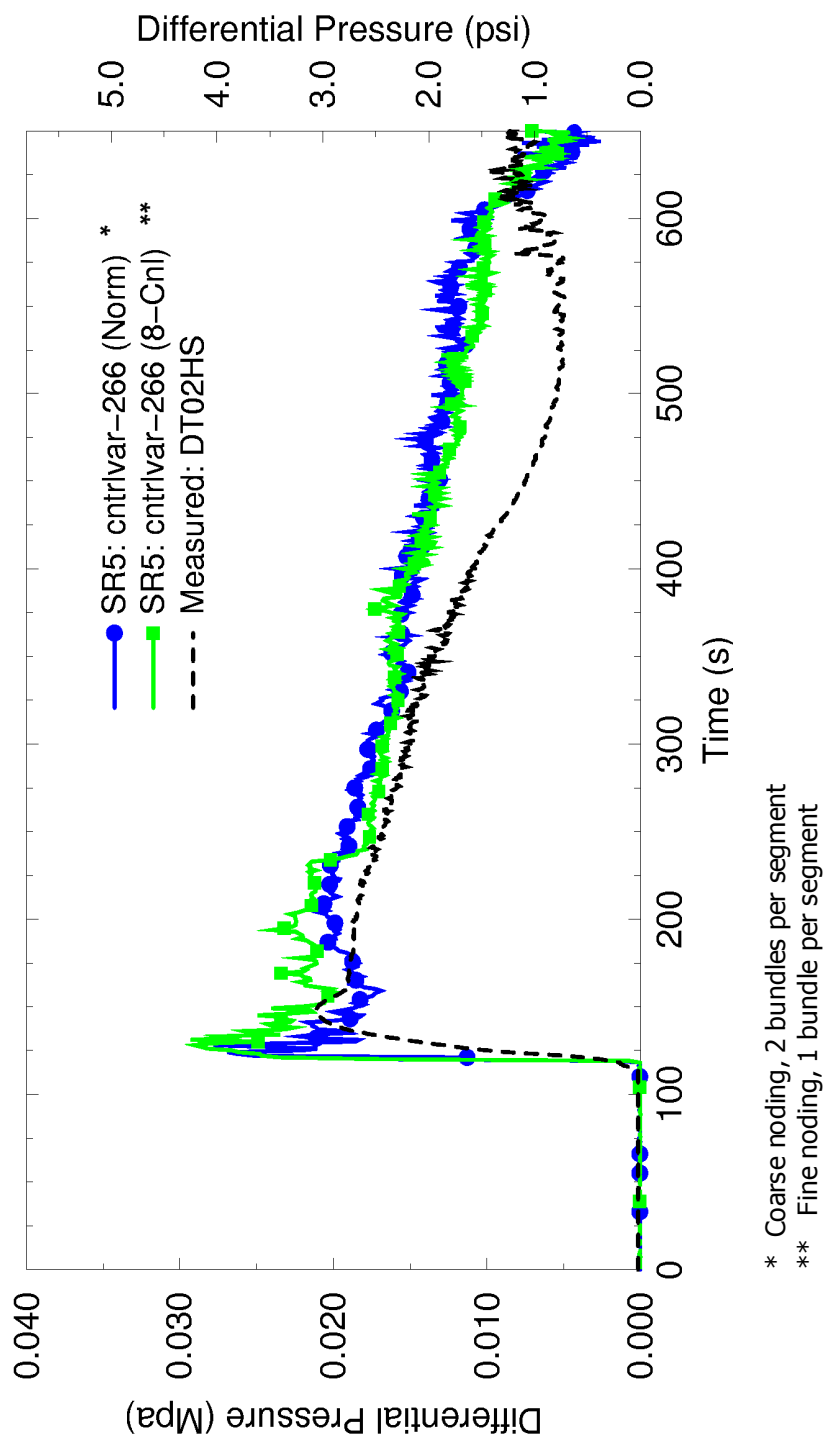


Figure 4.127: Differential Pressure: Upper Plenum – Downcomer  
SCTF-II S2-18

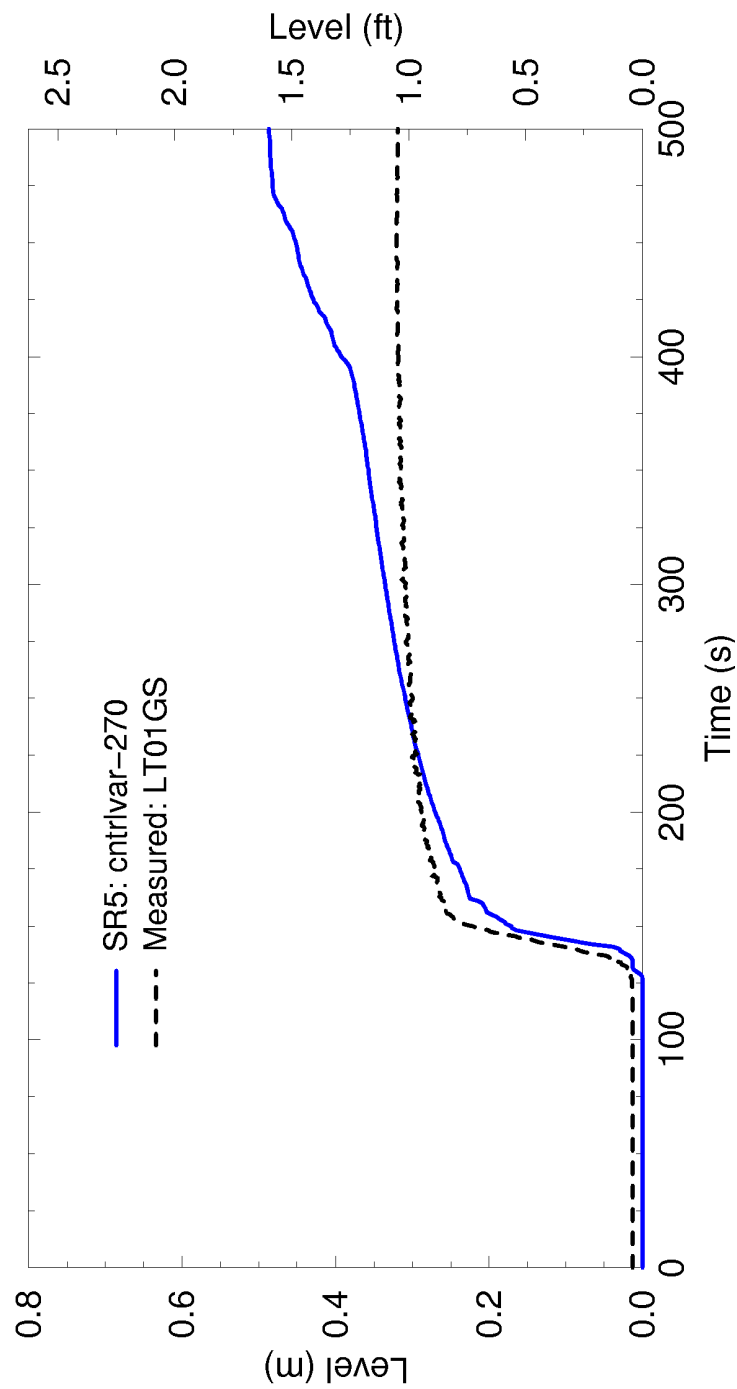


Figure 4.128: Liquid Level in S/W Separator SCTF-II S2-11



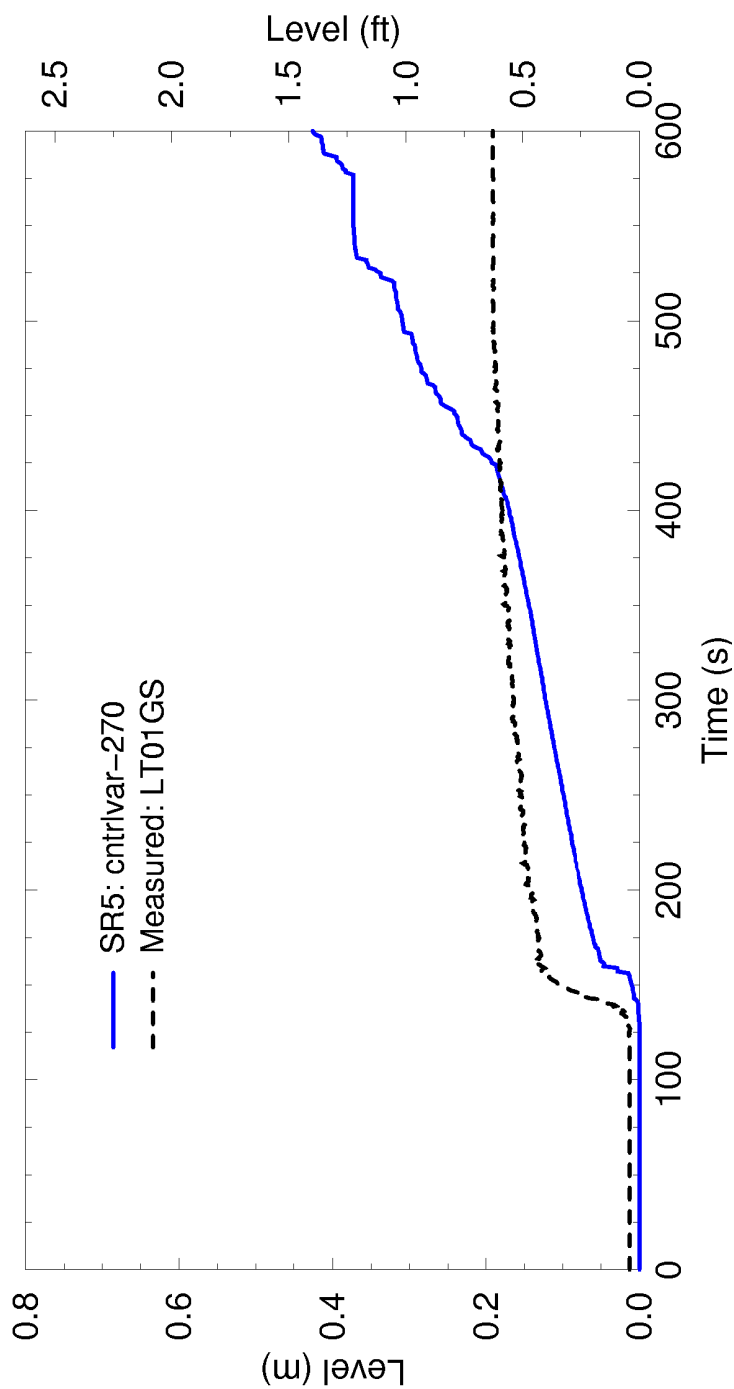


Figure 4.129: Liquid Level in S/W Separator SCTF-II S2-AC1

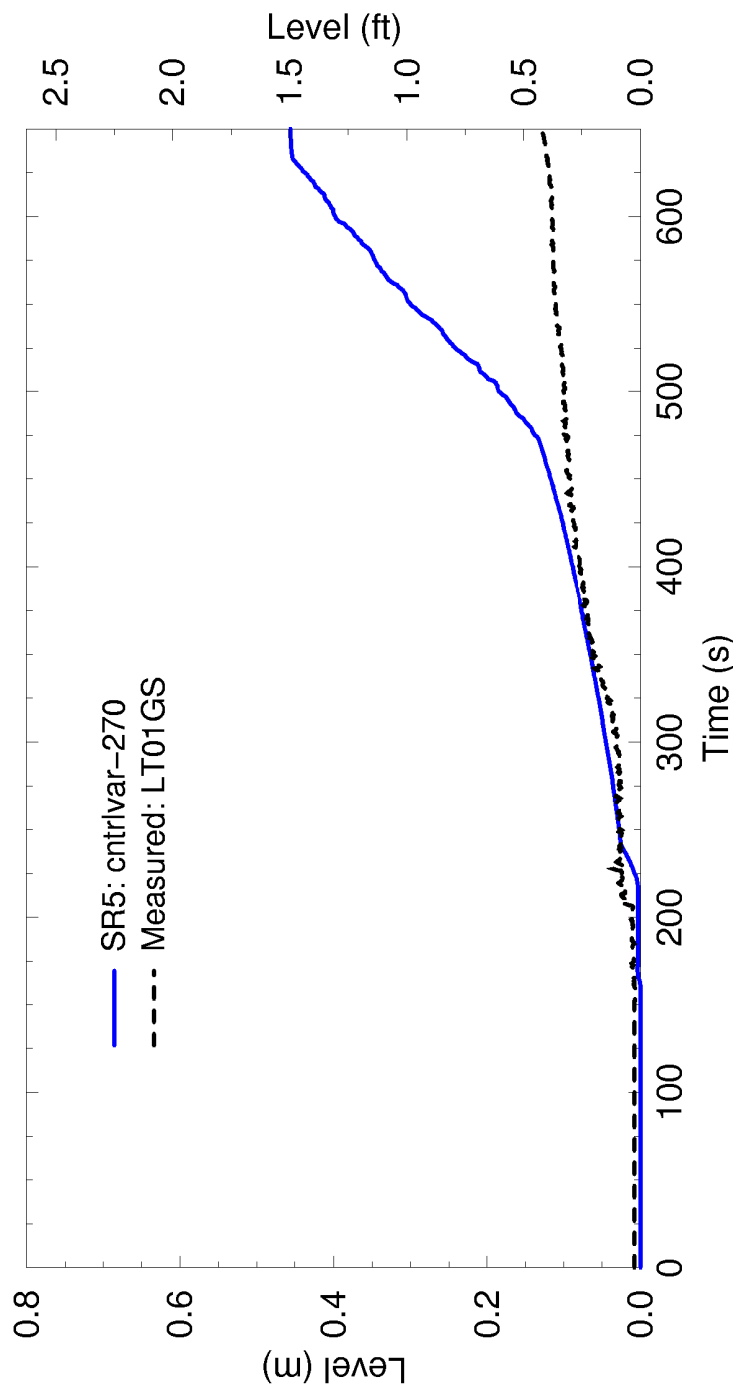


Figure 4.130: Liquid Level in S/W Separator SCTF-II S2-10

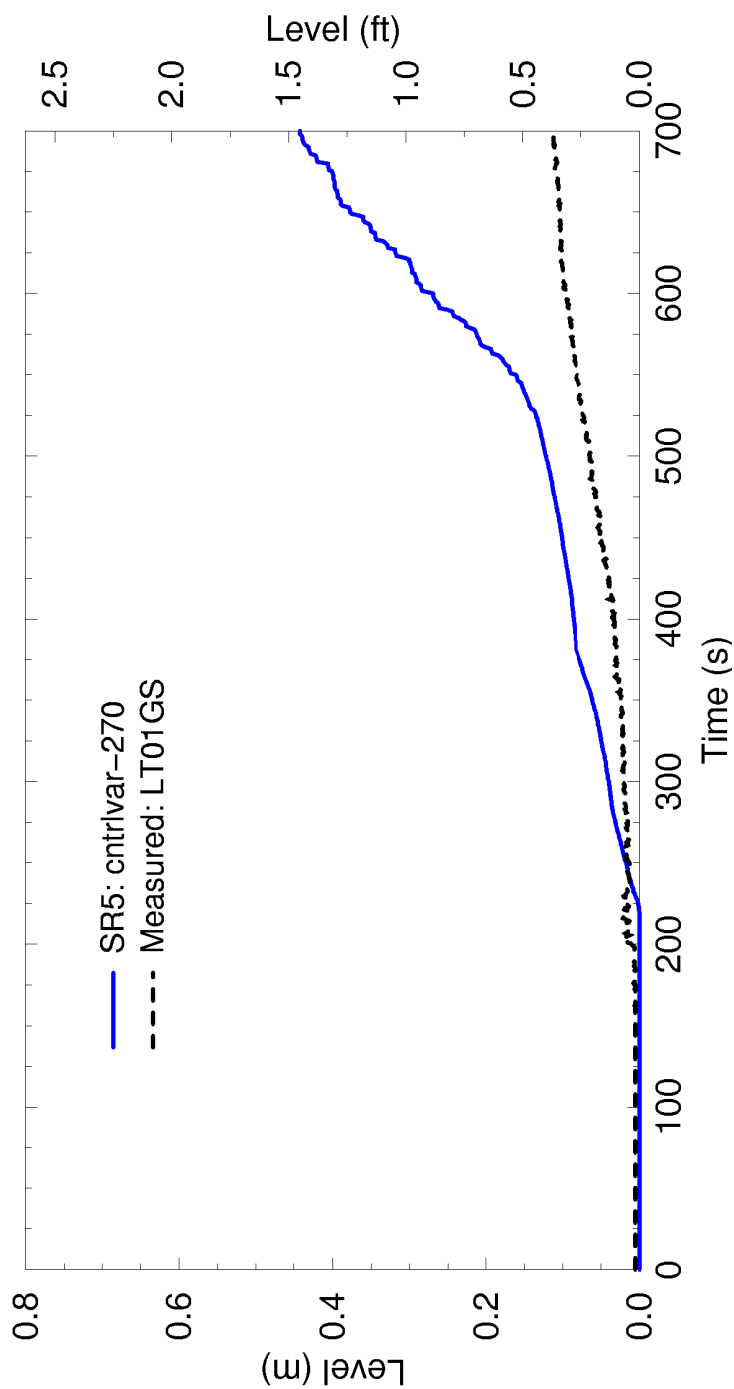


Figure 4.131: Liquid Level in S/W Separator SCTF-II S2-SH1

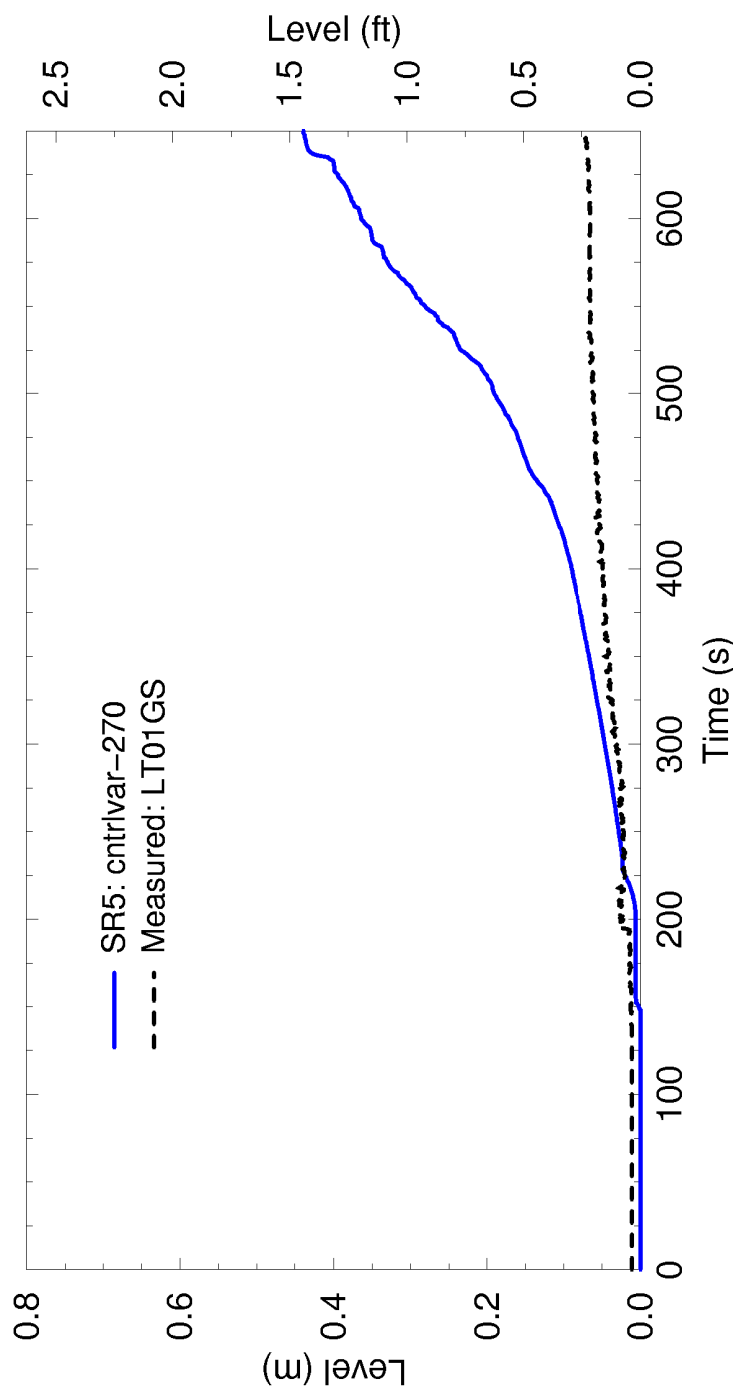
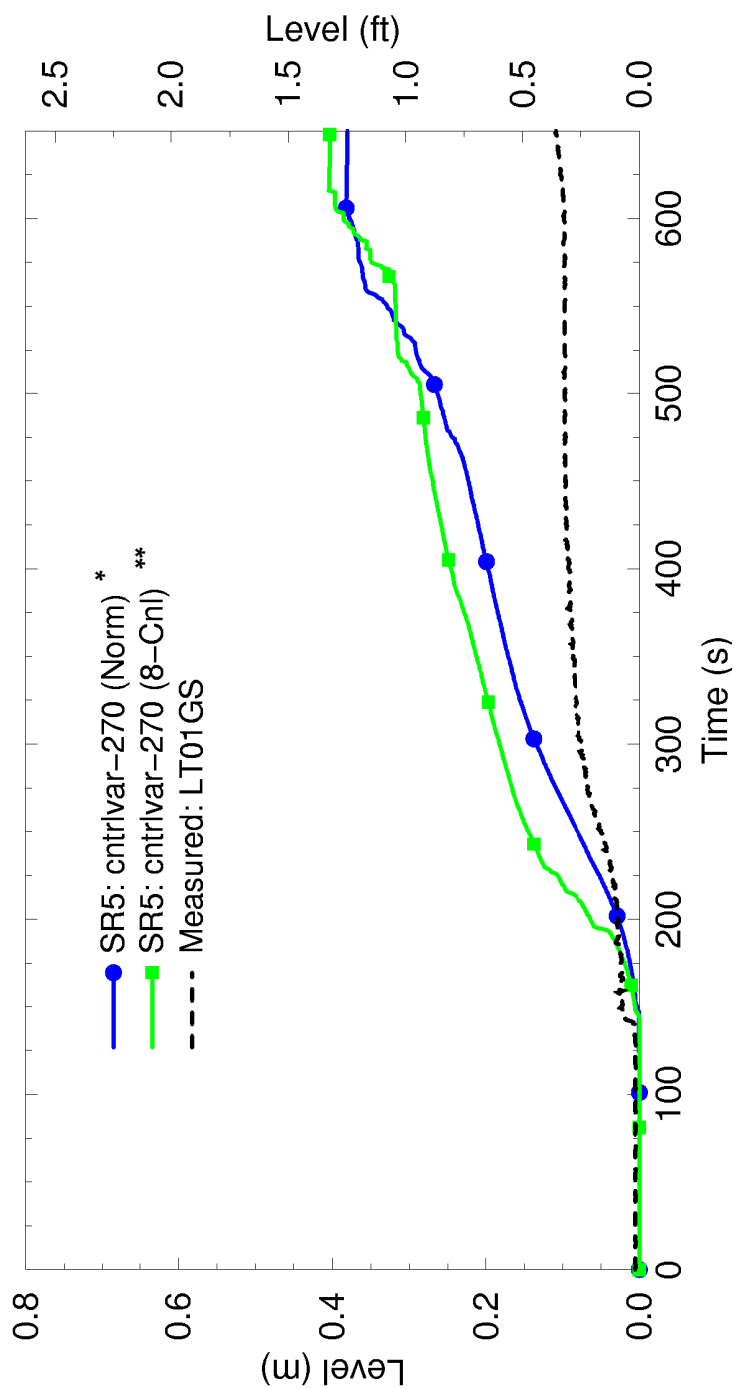
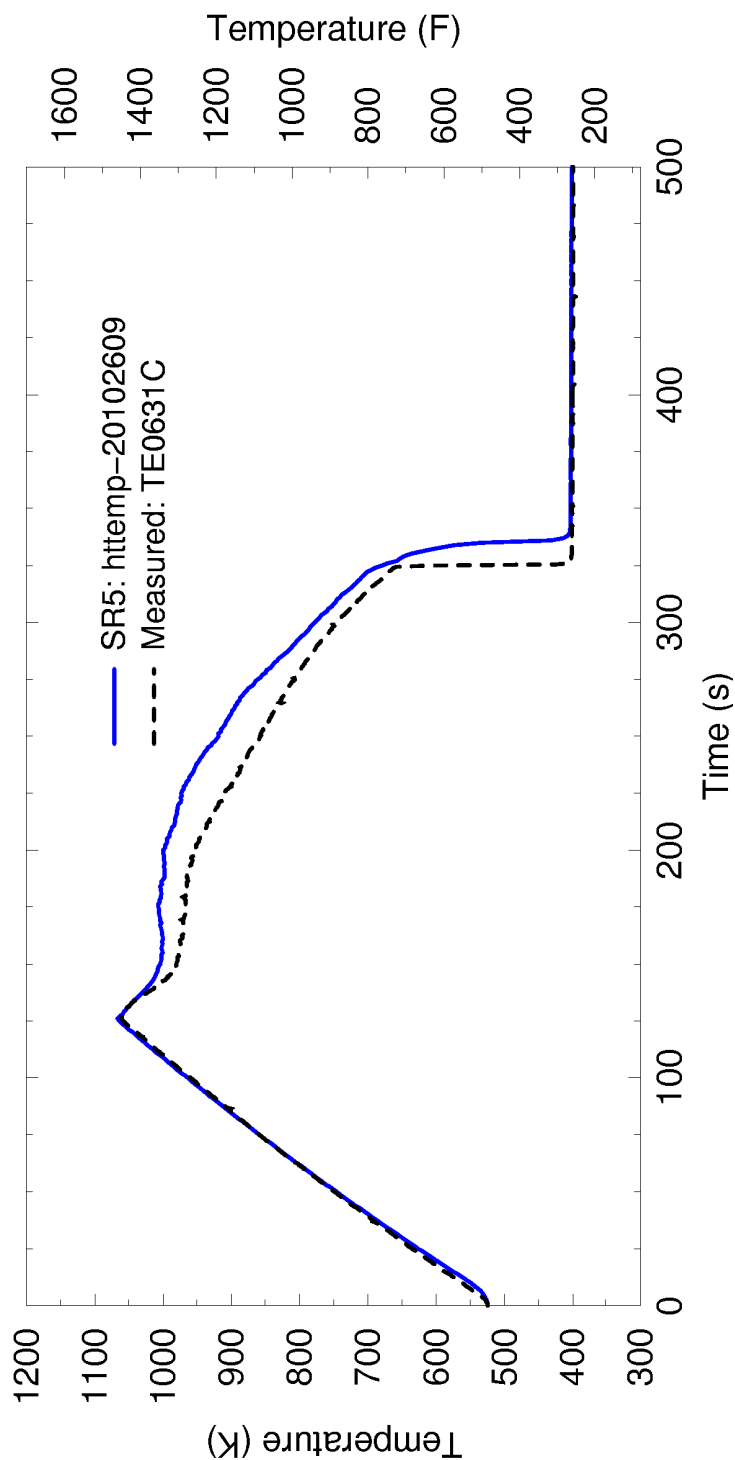


Figure 4.132: Liquid Level in S/W Separator SCTF-II S2-17



\* Coarse noding, 2 bundles per segment  
\*\* Fine noding, 1 bundle per segment

Figure 4.133: Liquid Level in S/W Separator SCTF-II S2-18



**Figure 4.134: Temperature Comparison at 1.905 meters  
SCTF-II S2-11**

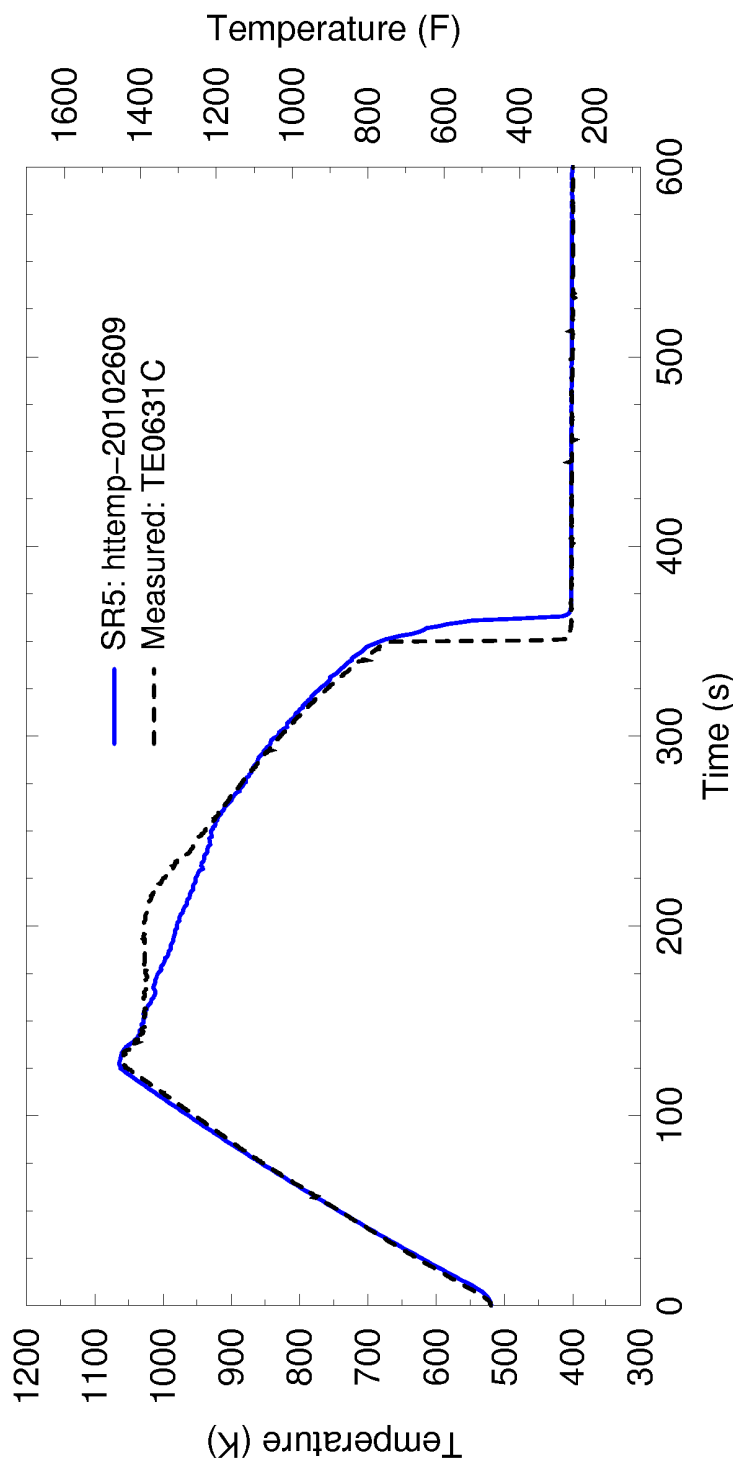


**Figure 4.135: Temperature Comparison at 1.905 meters  
SCTF-II S2-AC1**

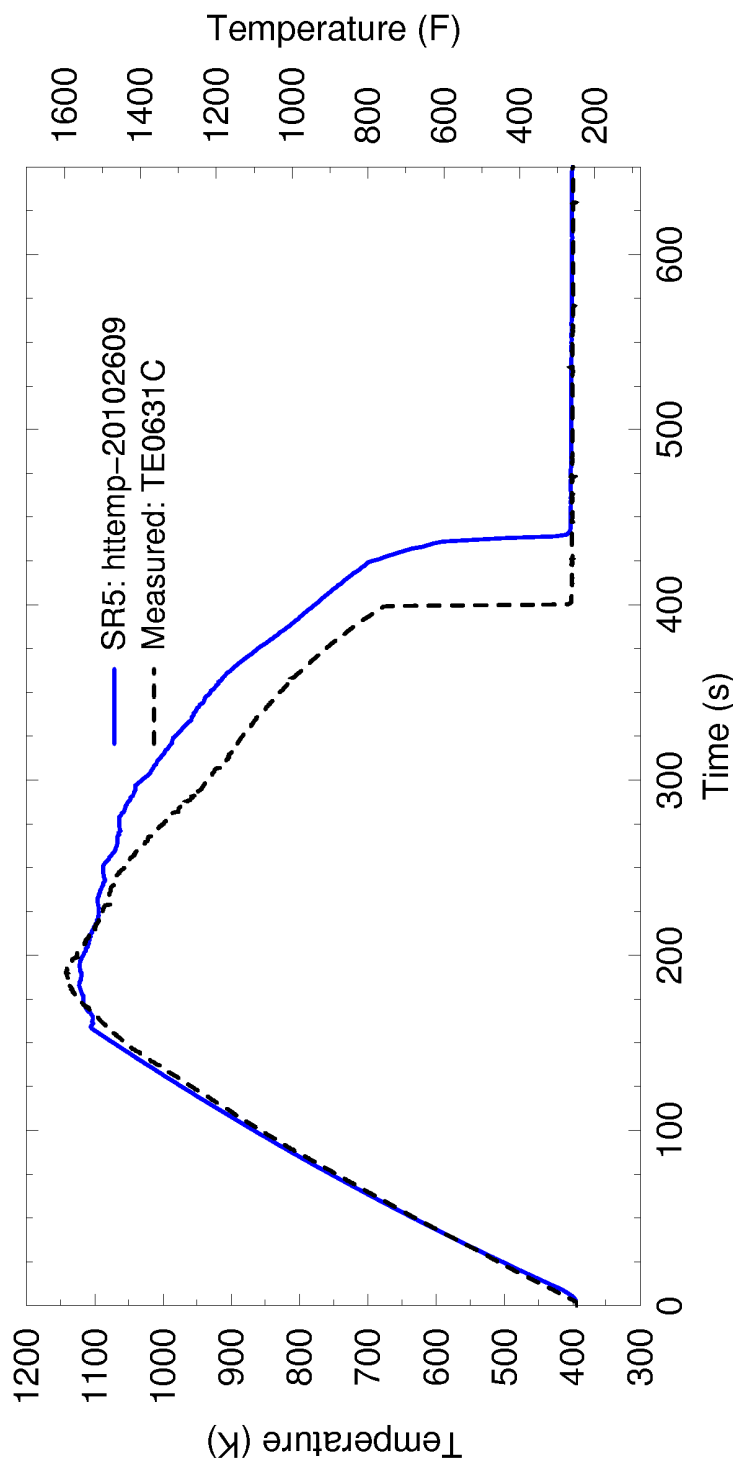


**Figure 4.136: Temperature Comparison at 1.905 meters  
SCTF-II S2-10**



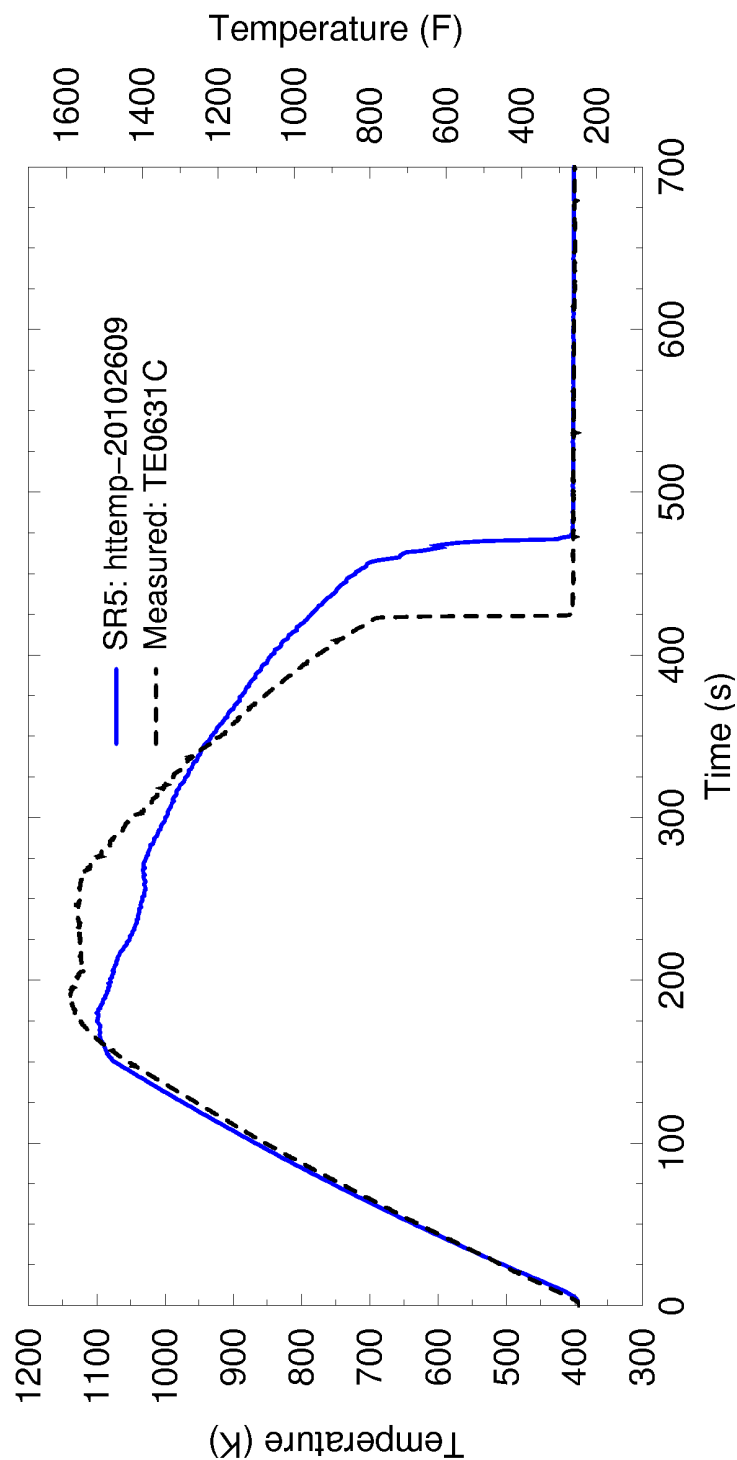


**Figure 4.137: Temperature Comparison at 1.905 meters  
SCTF-II S2-SH1**

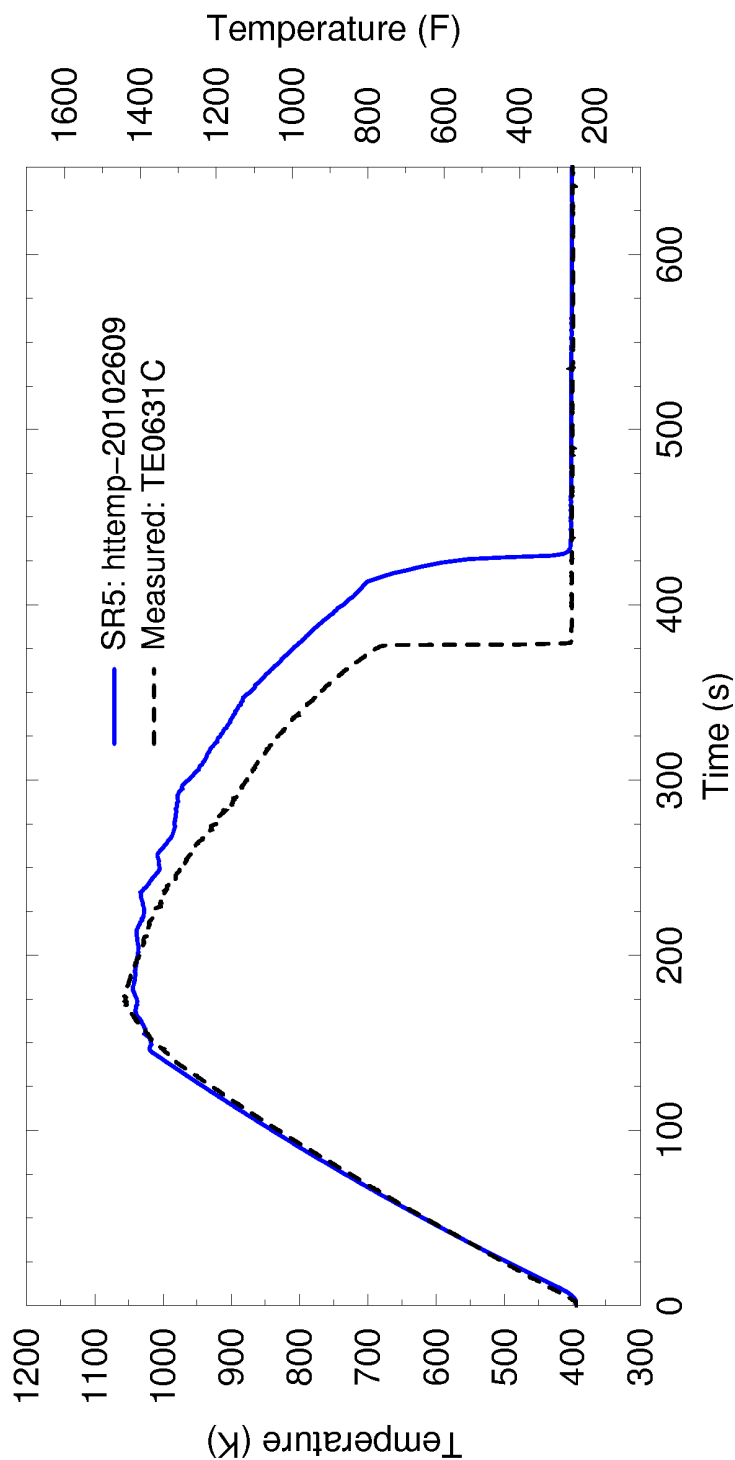


**Figure 4.138: Temperature Comparison at 1.905 meters  
SCTF-II S2-17**

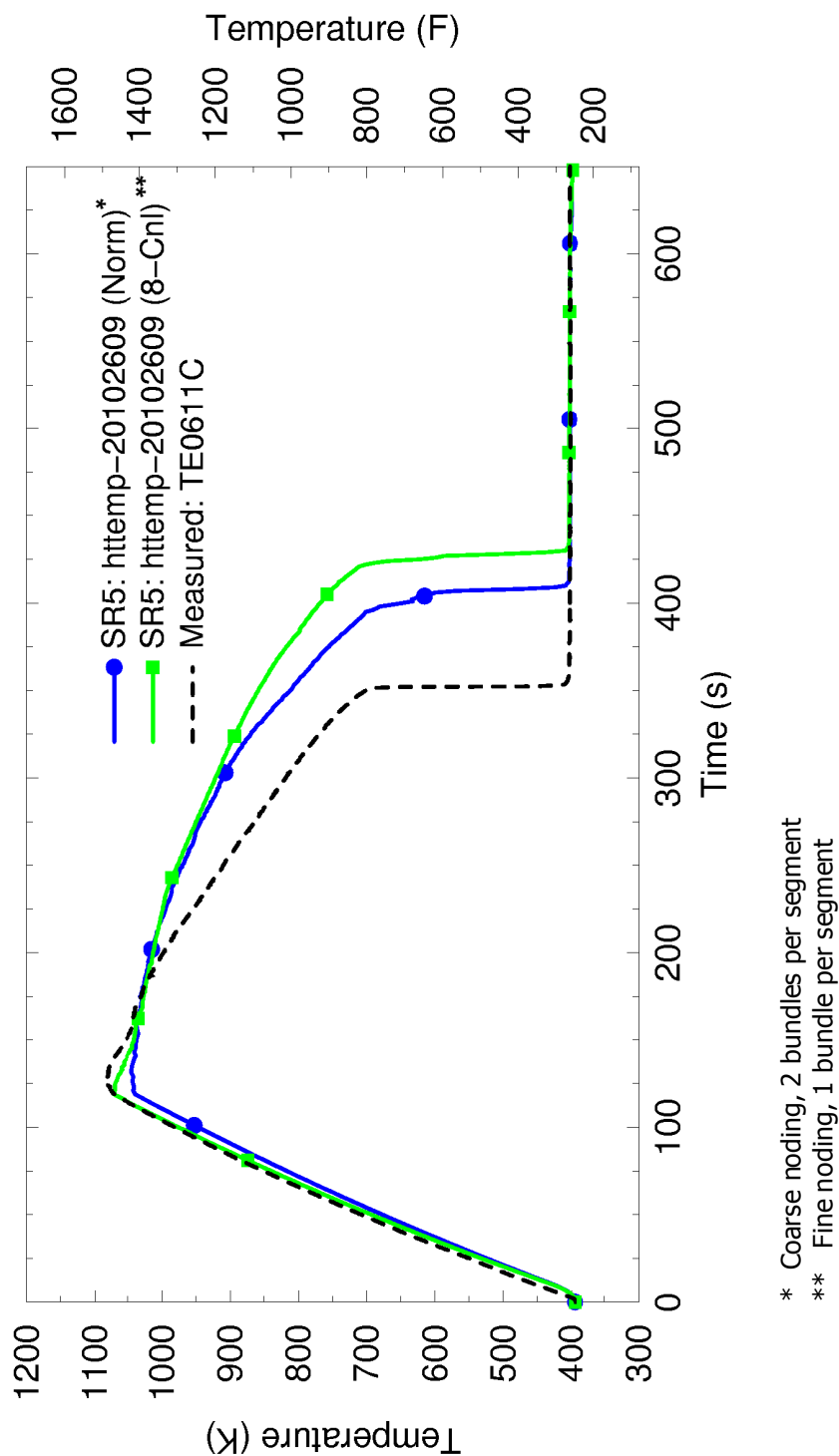


Figure 4.139: Temperature Comparison at 1.905 meters  
SCTF-II S2-18

#### 4.3.1.14 ACHILLES Tests

An ACHILLES test, identified as International Standard Problem Number 25 (ISP 25), was simulated using S-RELAP5 to evaluate the ability of the code to predict pressure vessel thermal-hydraulic behavior due to the accumulator cover gas nitrogen release during a LBLOCA in a PWR. The ACHILLES test simulated the latter phase of accumulator injection during a LBLOCA.

The accumulator release of nitrogen into the primary system during a LBLOCA in a PWR creates a complicated pressure vessel thermal-hydraulic behavior for several seconds after the nitrogen release. When the accumulators empty of liquid, the nitrogen cover gas enters the RCS where it flows to the upper part of the downcomer, causing the pressure to increase. The pressure increases due to two primary reasons: (1) the loss of condensation in the cold legs and (2) the vessel side break will not be able to remove the cover gas released and the un-condensed steam flowing through the intact loops. The increased pressure depresses the liquid level in the downcomer, resulting in a surge of water into the core. The surge of water in the core momentarily increases core heat transfer resulting in an increase steam binding, which causes an outsurge of water from the core back to the downcomer. The insurge back into the downcomer has the potential to increase the liquid flow out of the vessel side break, which can adversely affect the core heat-up later in the transient. Thus, the impact of nitrogen release from the accumulators on core thermal response is difficult to evaluate.

The ACHILLES test facility is designed to simulate the latter stages of accumulator injection in a LBLOCA. The test bundle had 69 electrically heated rods with geometry similar to that of a Westinghouse 17x17 fuel assembly design. The rods were held together using eight spacer grids and housed within a pipe. The exit region has a centrifugal separator to collect carryover water. The steam then joins the nitrogen bypass flow and exits. The downcomer is a simple pipe connected to the bottom of the core. A valve, located between the downcomer and the bundle region, is closed before nitrogen injection begins, holding the water in the downcomer until injection occurs. Another valve (bypass valve) is open before injection begins. It provides a flow path for the pumped water so that it does not enter the core. This valve closes on initiation of nitrogen injection.

The nitrogen tank is connected to the top of the simulated downcomer and a valve, which is initially closed, opens to initiate the nitrogen flow. Nitrogen forces flow through the core by

increasing the pressure on the downcomer. Nitrogen also flows through a bypass path to join the steam that is produced in the bundle region, and then exits through the break valve. A flow meter measures the nitrogen flow from the tank and another flow meter measures the bypass flow.

Each simulated fuel rod has multiple thermocouples on the surface of the rod. The PCT level (2.13 meters) is heavily instrumented with 66 thermocouples.

As the appropriate valves are operated to initiate the event, an immediate pressure transient occurs at the top of the downcomer. The initial pressurization of the downcomer causes a rapid surge of liquid into the simulated core. As the nitrogen leaves the system via the bypass, the pressure drops at the top of the downcomer, the levels in the core and downcomer recover, and the core reflooding now depends on the pumped water flow, which is entering both the downcomer and the core.

ACHILLES ISP 25 was analyzed using S-RELAP5 modeling consistent in the bundle region with the modeling guidelines. Since the remaining test facility piping is atypical to the RLBLOCA evaluation model, a simplified, but logical, modeling approach is selected in developing the input model.

Figure 4.140 presents the range of variation in the thermocouples at the PCT elevation (2.13 meters). The wide variation shown is not a consequence of power variations because the rods are all at the same power. Three rods set the lower bound and all three of these rods are located next to the shroud in the test assembly. The early quench indicates that the flow field near the shroud is far different from that in the interior.

The remaining fuel rods can be divided into a group that tracks the maximum fairly well and a group that falls well below the maximum, but not as dramatically as the three rods setting the lower limit. Thus, the test data shows that a multi-dimensional analysis is required to get a reasonable prediction of core temperatures.

The radial and azimuthal inhomogeneity is greater than would be experienced in the interior region of a typical PWR. Thus, predicting the thermal-hydraulic behavior for this test assembly is significantly more challenging than for a typical PWR core. One of the main reasons for this is that there is a relatively large flow area between the rod bundle and the test vessel, which

resulted in a large degree of radial and azimuthal inhomogeneity in the fuel rod flow areas. The ISP-25 summary report (Reference 28) concluded that “none of the codes produced a completely satisfactory prediction,” which further indicates the atypicality of the ACHILLES test.

The bundle region is modeled as a two radial region TWODEE component because of the inhomogeneity in the bundle region. The central 21 rods in the test assembly were modeled as one channel and the remaining 48 rods and the shroud were modeled as the other channel using a TWODEE component. [

] Since a hot pin is not modeled separately, the rod-to-rod-radiation heat transfer option is not used in the bundle region. The CCFL model is not applied at the bundle exit since in the test facility there is a steam/water separator in the upper plenum, which is modeled in the S-RELAP5 input model. The test facility, S-RELAP5 input model, and simulation results are discussed in detail in Section 3.13 of Reference 5.

The calculated nitrogen flow rate agreed well with the data until frost was formed in the throat of the venturi at about 7 seconds. Thereafter, the gas release data and the S-RELAP5 comparison are of questionable value. The calculated liquid carryover and the steaming rate at the core exit show reasonable agreement with the data.

The downcomer  $\Delta P$  measurements indicate an insurg of water in the core as soon as the nitrogen injection starts. The core  $\Delta P$  measurements indicate an increase in the core level. The data indicate that most of the insurg of water was pushed out of the core within 5 seconds. This is not completely reflected in the downcomer  $\Delta P$  measurements. Insufficient information is available to understand this difference. The calculated results show less insurg into the core and as a result the downcomer level increased during this early phase of the transient. Once the cover gas effect subsides, the calculated downcomer and core levels agreed reasonably well with the data. The results indicate that S-RELAP5 will underpredict the liquid insurg into the core, resulting in less core cooling after the accumulator tanks empty and the cover gas from the tanks enters the primary system.

Calculated temperatures for the central region were compared to measured temperatures for the 21 rods in the middle of the assembly. The maximum, minimum, and average temperatures were compared with the calculated temperature for elevations from 1.08 to 3.18 meters. The calculated values are mostly in good agreement with the measured values. The PCT elevation

is at 2.13 meters and, at this elevation, the calculated PCT is about 50 K lower than the data. At all other elevations, the calculated peak temperature exceeds the measured values, except for the 2.65 meter elevation where the prediction is about 50 K lower than the data. As discussed earlier, there is a considerable amount of inhomogeneity in the bundle, which may not be completely captured by the S-RELAP5 two-region simulation. Considering the observed atypicality in the bundle flow behavior, the differences in results are considered acceptable.

The impact of the nitrogen injection, which is the focus of this assessment, can be seen in the first 25 seconds of the transient. Figure 4.141 through Figure 4.146 show the effect of nitrogen on temperature. The rod thermocouples all show a transient temperature reduction at the beginning of the event, which is consistent with the downcomer and core  $\Delta P$  measurements. This initial cool-down is caused by the initial nitrogen surge. S-RELAP5 calculates a conservatively small cool-down compared to the data. In all cases, the calculated downward temperature transient accompanying the nitrogen injection is smaller than the measured temperature decrease. This indicates that S-RELAP5 underpredicts the cool-down due to the nitrogen injection. The smaller decrease in the calculated cladding temperature results in lower core steam production, resulting in a lower system pressure increase compared to the data as shown in Figure 4.147. These results support the conclusions drawn earlier from the core and downcomer  $\Delta P$  results.

In summary, S-RELAP5 predicted a lower pressure increase and less surge of water into the core region compared to the ACHILLES data, resulting in less clad cooling following nitrogen injection. From these results, it can be concluded that S-RELAP5 will calculate a conservative cladding thermal response resulting from cover gas release into the primary system when the accumulator empties following a LBLOCA in a PWR.

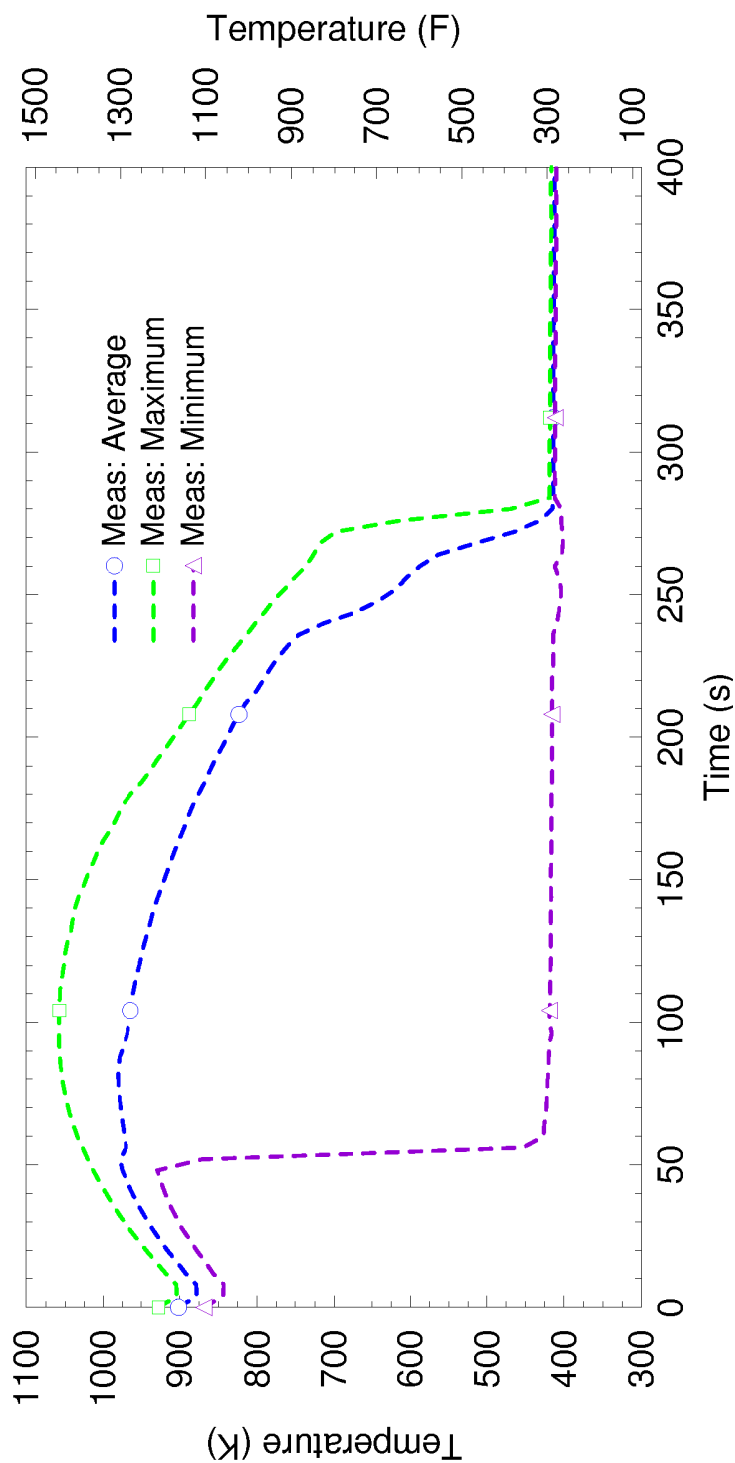


**Figure 4.140: Thermocouple Variation Range at the PCT Elevation  
ACHILLES ISP 25**



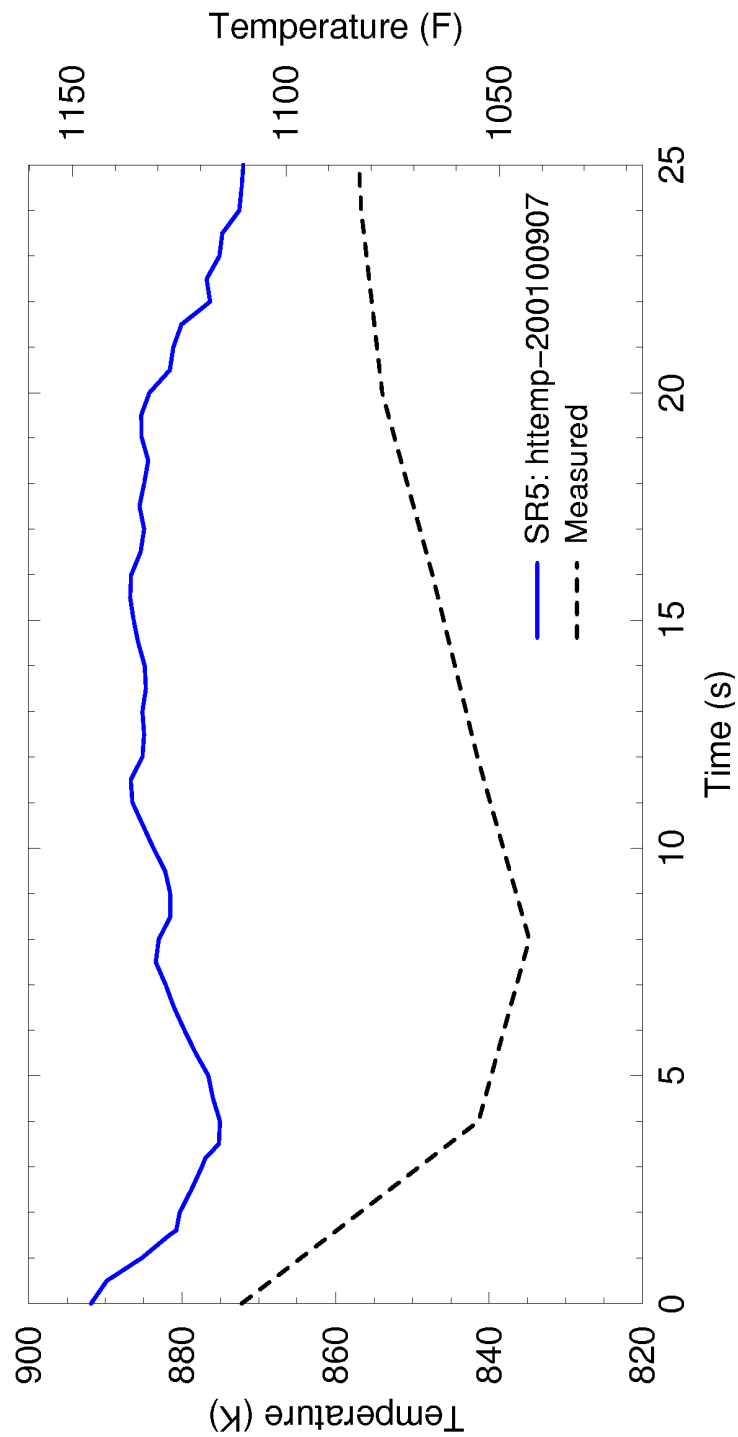


**Figure 4.141: Nitrogen Insurge Impact at 1.08 meters  
ACHILLES ISP 25**

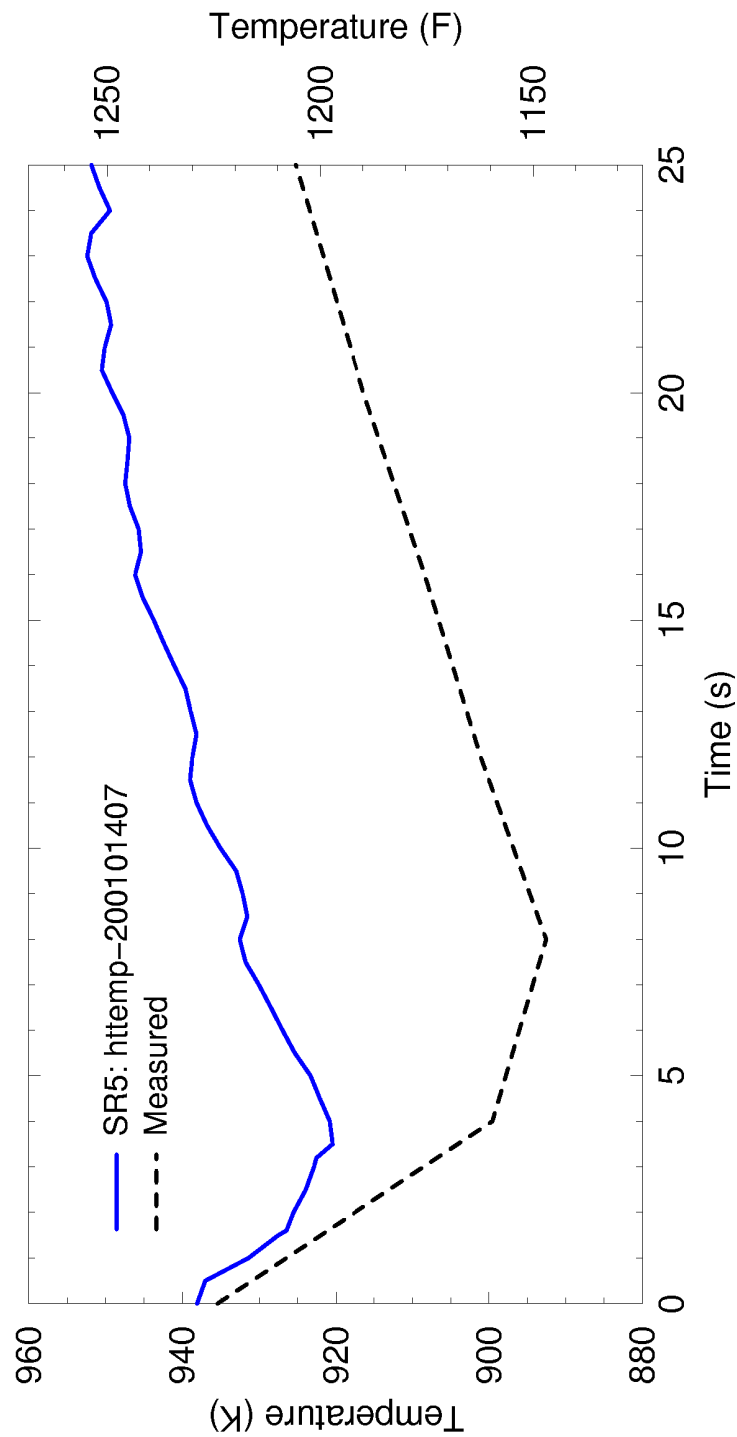


**Figure 4.142: Nitrogen Insurge Impact at 1.81 meters  
ACHILLES ISP 25**

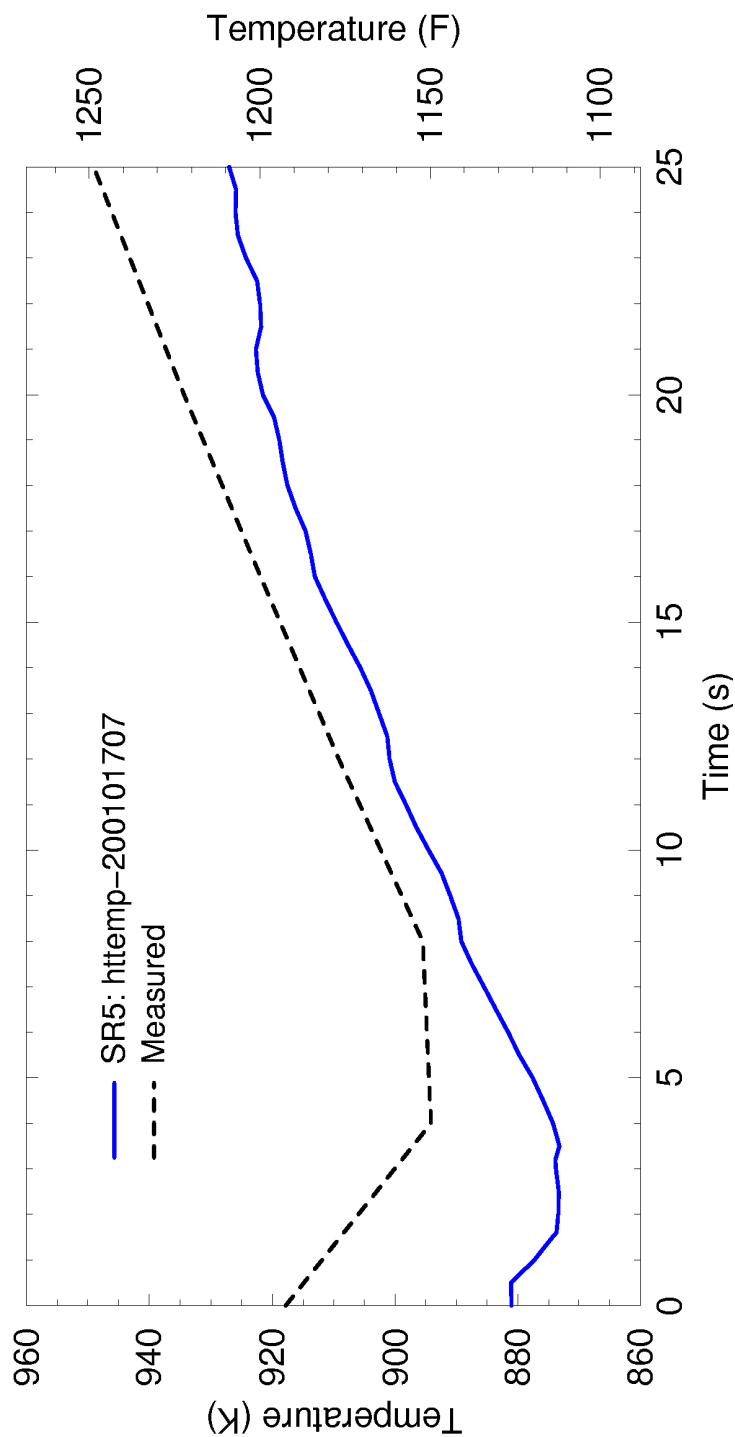


**Figure 4.143: Nitrogen Insurge Impact at 2.13 meters  
ACHILLES ISP 25**

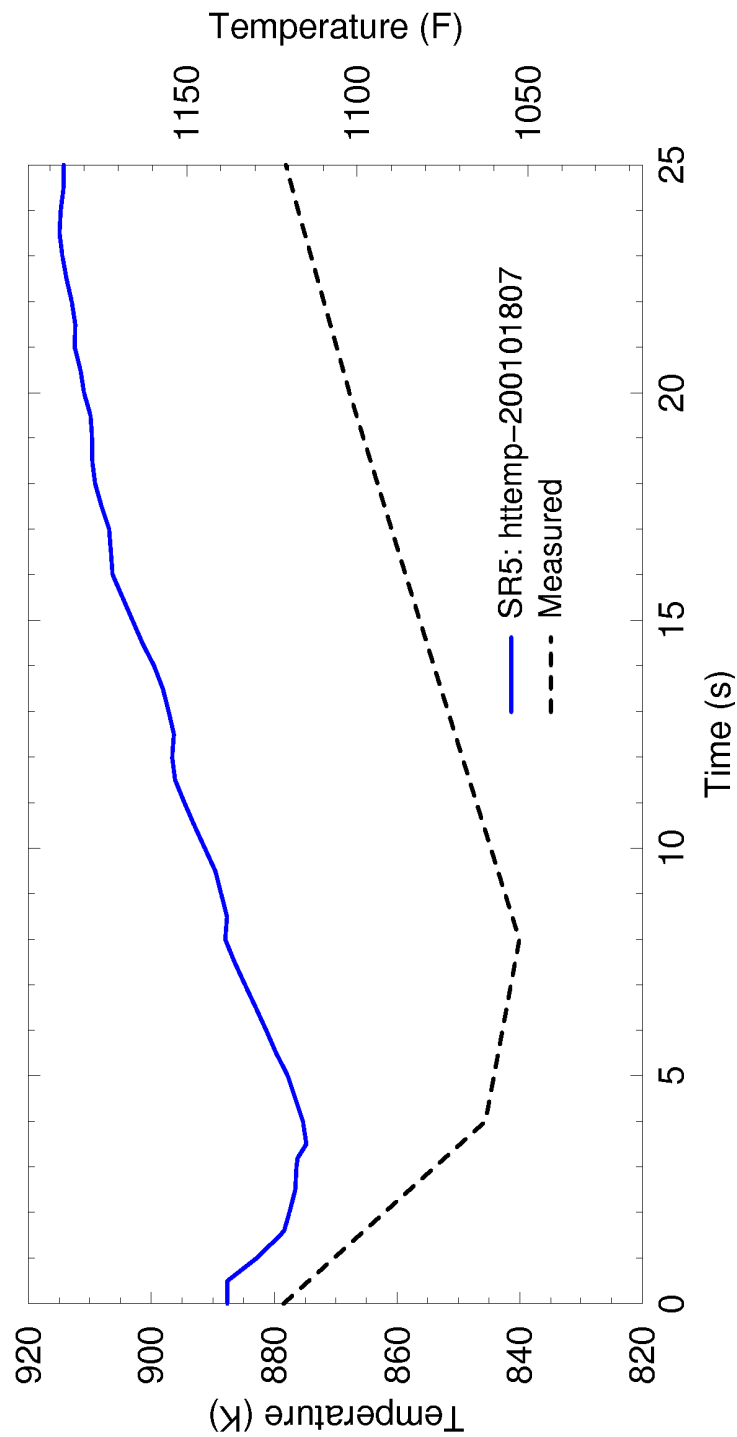


**Figure 4.144: Nitrogen Insurge Impact at 2.33 meters  
ACHILLES ISP 25**

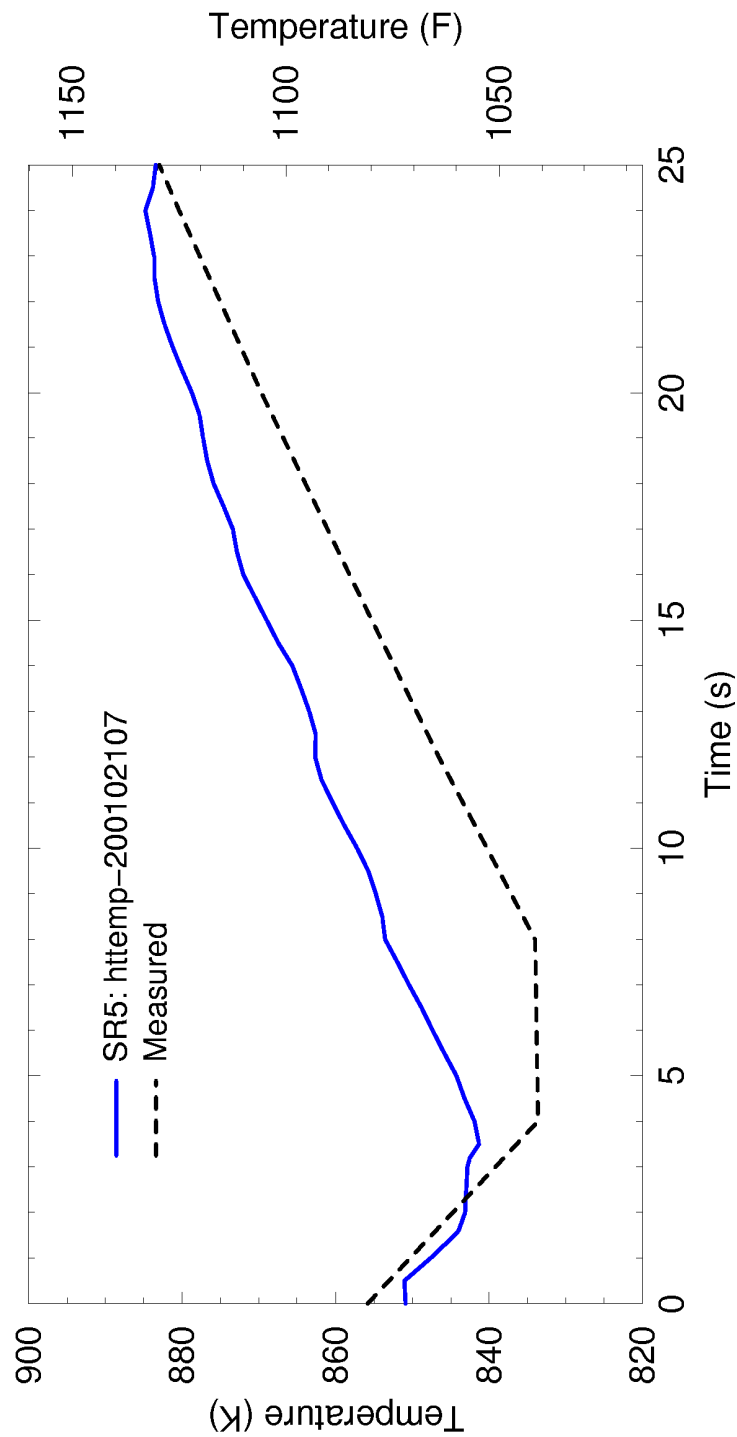


**Figure 4.145: Nitrogen Insurge Impact at 2.65 meters  
ACHILLES ISP 25**

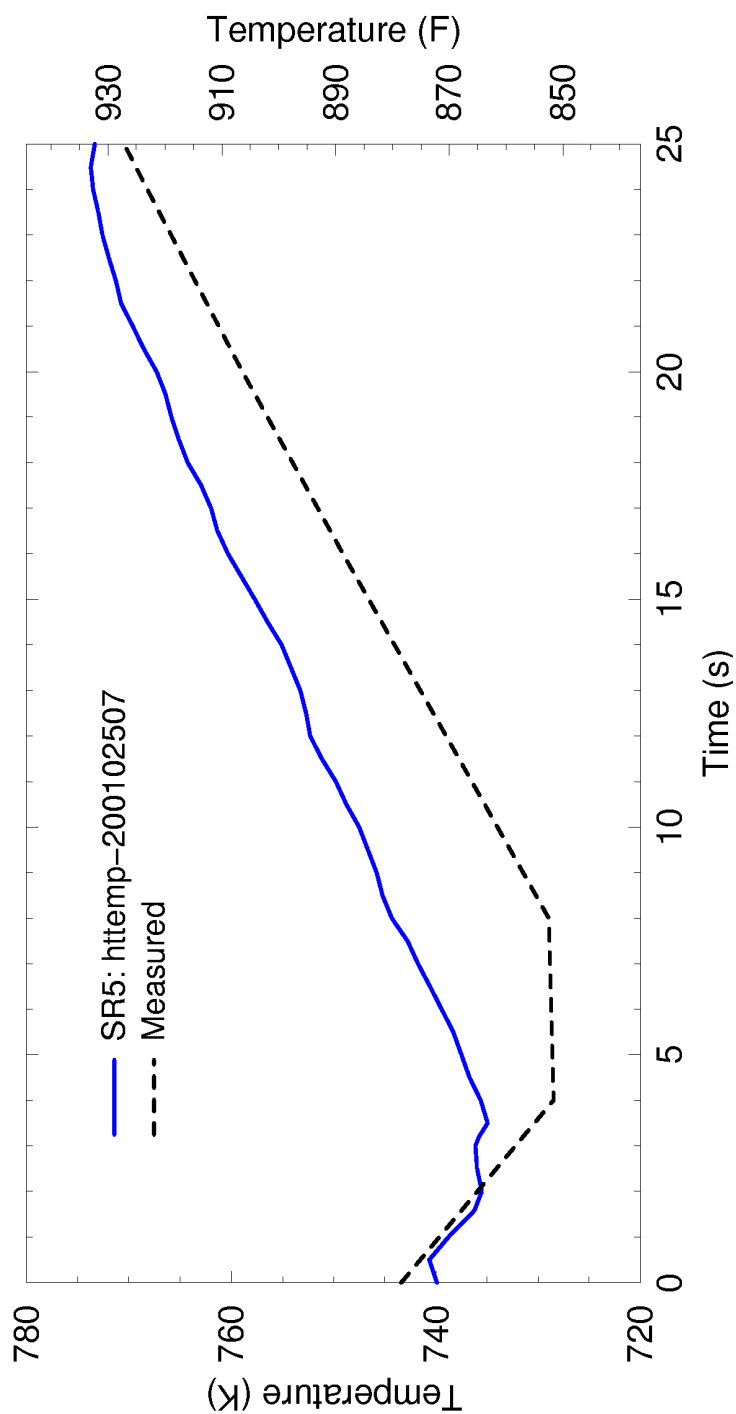


**Figure 4.146: Nitrogen Insurge Impact at 3.18 meters  
ACHILLES ISP 25**

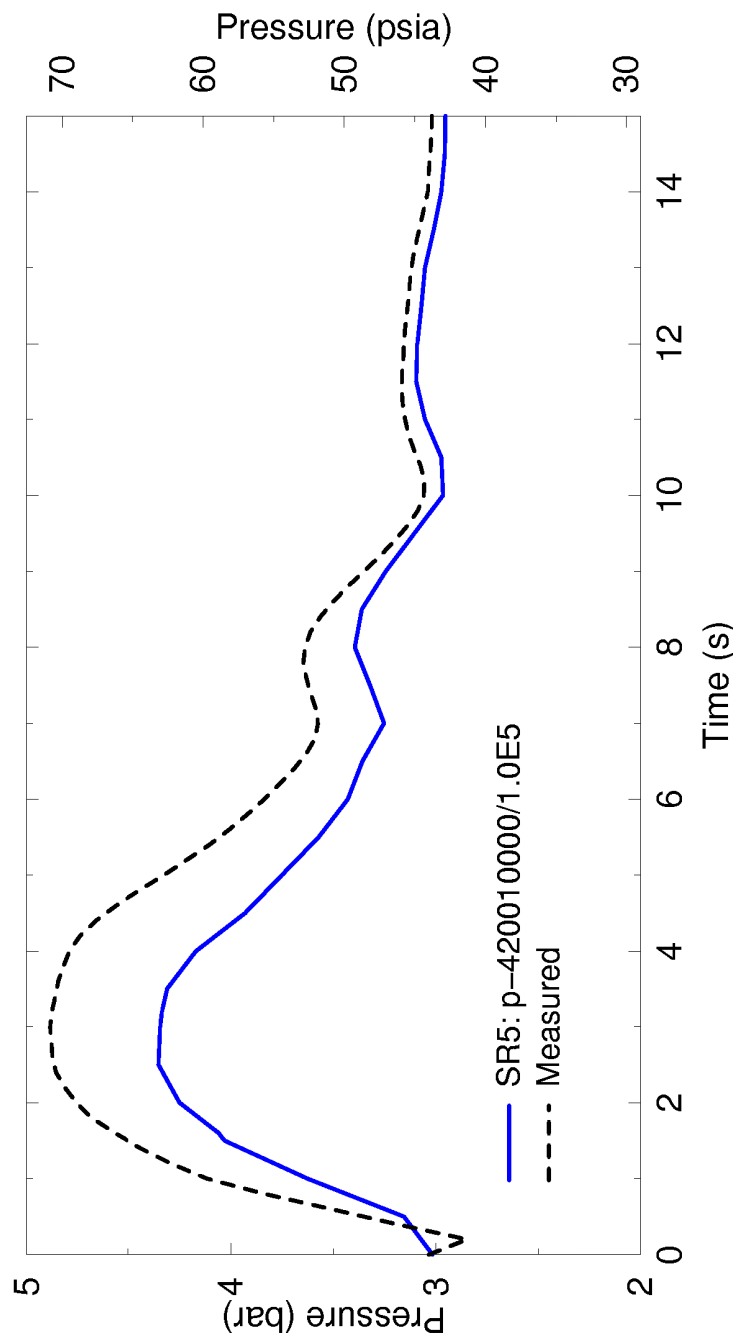


Figure 4.147: Downcomer Pressure Comparison ACHILLES ISP 25

#### 4.3.1.15 Multi-Dimensional Flow Testing

The Westinghouse Flow Blockage tests were performed using simulated PWR fuel assemblies. These tests provided data on single-phase flow redistribution for non-uniform core inlet and outlet conditions that can be used to assess multi-dimensional models in system codes such as S-RELAP5. The S-RELAP5 assessment of these tests is presented in detail in Section 3.12 of Reference 5. No bias or uncertainty is derived from or used in this assessment.

The test section consisted of two 14x14 array rod bundles, a 0.426 inch rod diameter, and a pitch to diameter ratio of 1.28. The simulated fuel assemblies are about 38 inches long and are enclosed in a rectangular canister. For the bulk of the testing, the gap between the two simulated fuel assemblies was left open, but for some tests a perforated plate was inserted between the two assemblies. Because of the detail of the measurements and the nearly prototypic geometry (in the radial, or x-y, direction), these tests have become a standard for benchmarking flow redistribution codes.

The tests consisted of introducing asymmetric flows in the inlet region with blocked or unblocked exit regions and measuring flow recovery in the bundle with an array of Pitot tubes. The first array is 2.5 inches above the inlet while the remaining arrays are located at 5 inch intervals, with the last one at the 32.5 inch level.

The test section was modeled in S-RELAP5 as a TWODEE component with 10 vertical (x) volumes and 14 horizontal (y) volumes. This, in effect, collapses the test assembly in the direction perpendicular to the asymmetric flows. Selection of 14 horizontal volumes resulted in volumes that corresponded to the Pitot tube measurement locations. The vertical volumes had lengths that made the first volume match the bottom of the rodded region (4.5 inches) and each of the others match the elevation of a velocity measurement point (Pitot tube location).

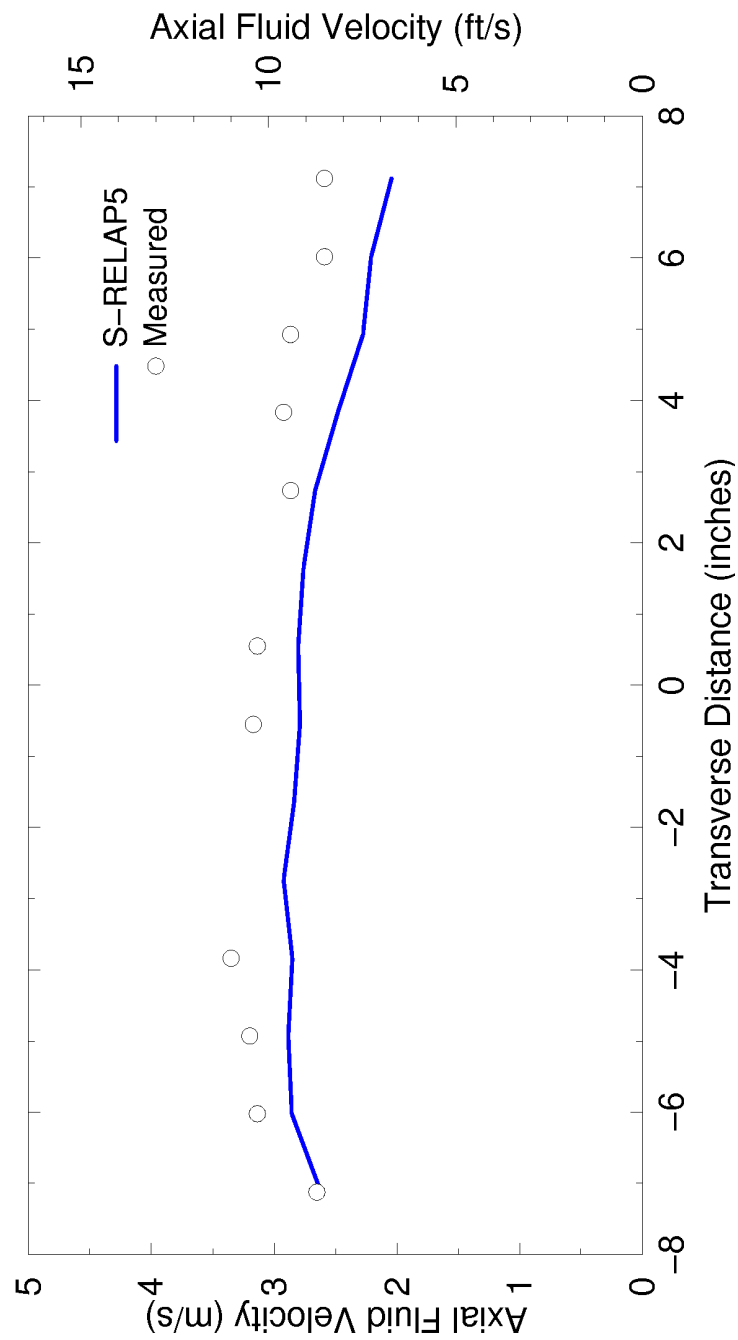
Figure 4.148 provides a comparison of the Test 1 measured and S-RELAP5 calculated flow distributions at the uppermost set of Pitot tubes. The reported axial fluid velocities were calculated by S-RELAP5 with test data-based inlet flows of 1138 and 512 gpm (as opposed to the reported nominal values of 1100 and 550 gpm, respectively). The measured velocities are almost all higher than the S-RELAP5 velocities at this elevation. Figure 4.149 compares the reported mass flow fraction in the high flow bundle with that calculated by S-RELAP5.



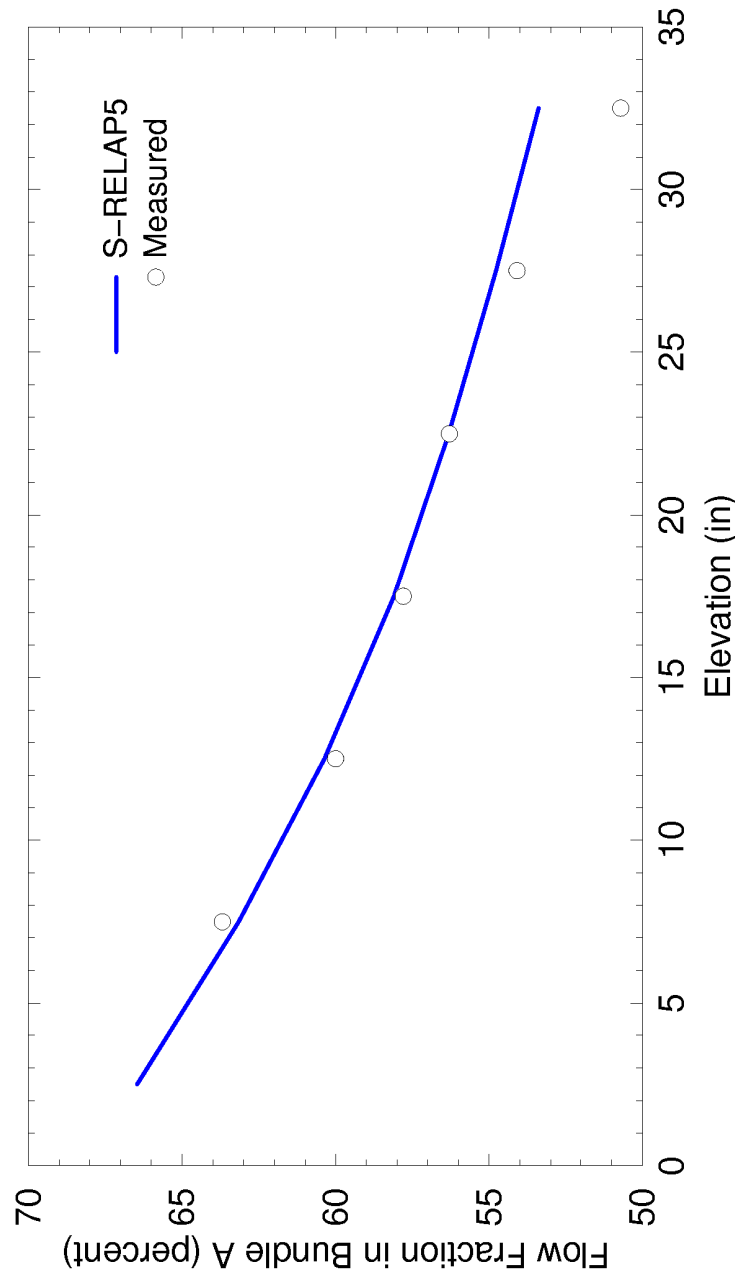
Figure 4.150 provides a comparison of the Test 2 measured and S-RELAP5 calculated flow distributions at the uppermost set of Pitot tubes. The reported axial fluid velocities were calculated by S-RELAP5 with a test data-based inlet flow of 1281 gpm (as opposed to a reported nominal value of 1500 gpm). For this test, the inlet to one bundle was blocked. In general, the agreement is excellent. The largest discrepancy occurs on the side of the inlet-blocked bundle next to the wall. Here, S-RELAP5 calculates a tendency to back flow. The measurement velocities, which are based on Pitot tube readings, show that the flow stops near the wall. Figure 4.151 compares the fractional flow in the unblocked bundle. The agreement is good over most of the axial height of the bundle. Near the exit, the measured flow was nearly equal for the two bundles. The calculated flow distribution is still about a 60:40 split for S-RELAP5. The overall agreement is good.

Figure 4.152 compares the reported axial fluid velocities for Test 3 to those calculated by S-RELAP5 at the uppermost set of Pitot tubes. This test has the inlet and exit of one assembly blocked and a perforated plate inserted between the two simulated fuel assemblies. The inlet flow to the unblocked assembly is 1300 gpm. The agreement for these data is good for the reported elevation and, in fact, for all measurement levels. The most notable difference is the tendency of S-RELAP5 to predict reverse flow near the wall in the blocked assembly—similar to the result in Test 2.

In summary, a series of flow blockage tests were analyzed using the S-RELAP5 two-dimensional component. The code was able to calculate the axial flow redistribution within the two test assemblies in a reasonable manner and was in acceptable agreement with the measured data. Therefore, the S-RELAP5 two-dimensional yields acceptable single-phase flow performance. The comparison of S-RELAP with the flow blockage data indicates that the two-dimension model in S-RELAP is sufficient to describe flow redistribution in multi-dimensional problems.



**Figure 4.148: Axial Velocities at 32.5 inches, Asymmetric Flow - Test 1**



**Figure 4.149: Axial Flow Fractions for Asymmetric Flow - Test 1**

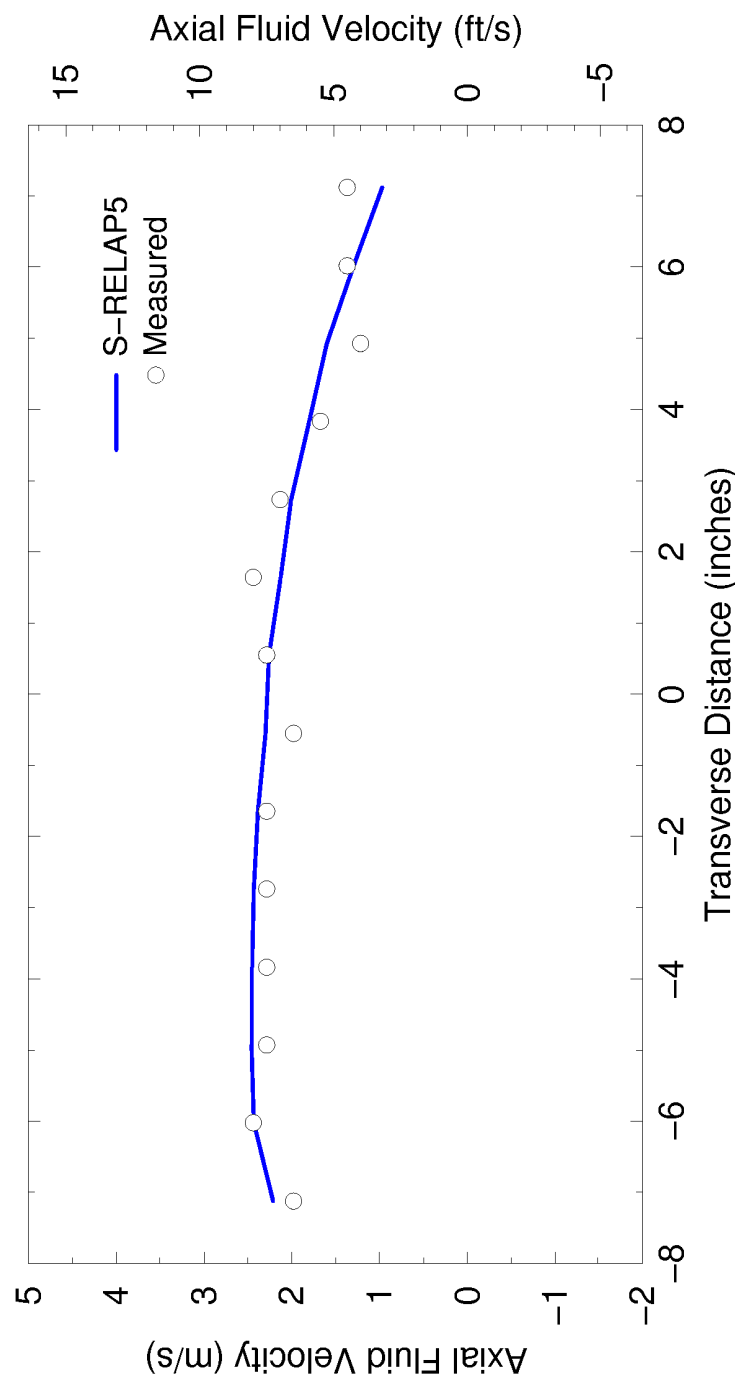


**Figure 4.150: Axial Velocities at 32.5 inches, for Asymmetric Flow - Test 2**

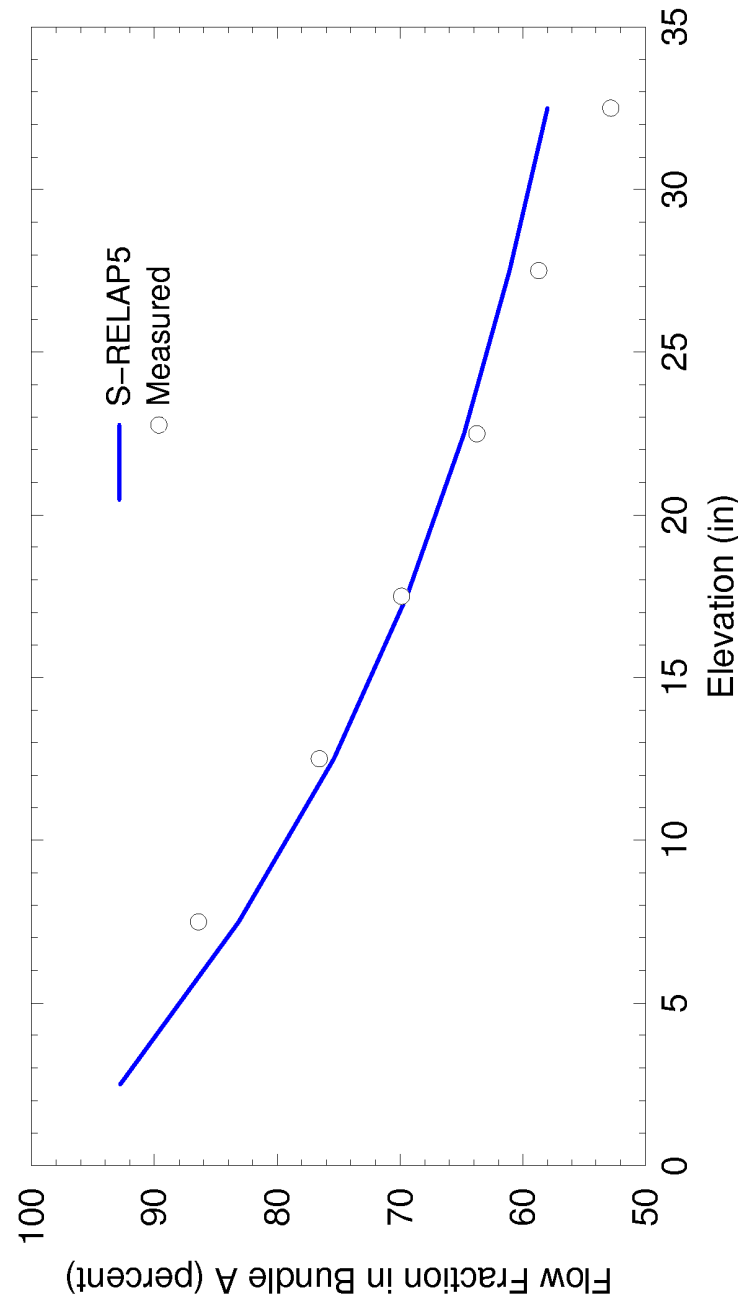


**Figure 4.151: Axial Flow Fractions for Asymmetric Flow – Test 2**

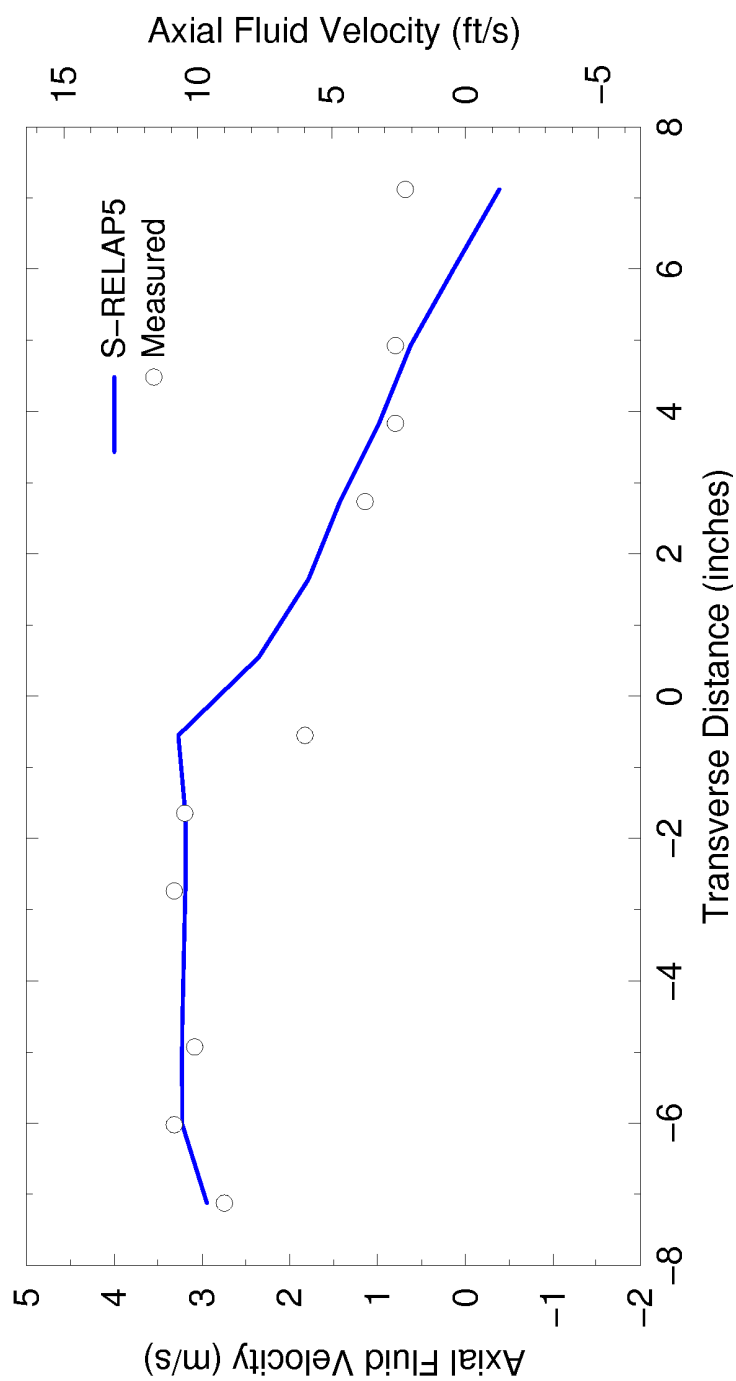


**Figure 4.152: Axial Velocities at 32.5 inches, for Asymmetric Flow - Test 3**

#### 4.3.1.16 Moby Dick Test 3141

The calculation of critical flow is an important consideration in the area of nuclear reactor safety. The fluid velocity at the location of the break, or other restrictions, can exceed the local sound speed, which causes the fluid flow rate to become insensitive to downstream pressure changes. Of particular importance are choking conditions at pipe break locations where fluid conditions are low pressure, subcooled liquid and the vapor space is saturated with nitrogen. These are the conditions that exist in the cold leg after the accumulator empties and the nitrogen cover gas escapes from the ECC injection point immediately upstream of the break plane.

For this S-RELAP5 assessment, Moby-Dick Test 3141 is used since this test establishes choked flow for a two-component (nitrogen/water) flow in a divergent nozzle, similar to the flow exiting the break during a postulated LBLOCA event. The S-RELAP5 assessment of these tests is presented in detail in Section 3.15 of Reference 5.

The facility consists of a vertical pipe with the dimensions given in Table 4.15 with piping for the water and nitrogen sources and a catch tank surrounding the diffuser outlet. The inlet pressure was  $5.619 \times 10^5$  Pa (81.48 psia) and the outlet pressure was  $1.03178 \times 10^5$  Pa (14.96 psia). This pressure drop, along with a nitrogen injection of  $6.101 \times 10^{-3}$  kg/s ( $1.345 \times 10^{-2}$  lb/s), gave a choked mass flow rate of 1.222 kg/s (2.694 lb/s).

The S-RELAP5 nodalization mimicked the facility dimensions with the insignificant exception of having a 0.993 meter (3.26 feet) distance between the nitrogen injection point and diffuser entrance due to node spacing. The same pressures and nitrogen injection flow were used. The S-RELAP5 choked flow rate was 1.2769 kg/s (2.813 lb/s). The calculated axial pressures are shown in Figure 4.153 along with the test data.

The results show S-RELAP5 predicted the pressure gradient in the straight pipe well, before and after the divergent nozzle. Flashing occurred at the diverging nozzle entrance and choked flow was calculated by S-RELAP5 using the HEM critical flow model. The calculated choked flow rate compares well (within 5 percent) to the test steady-state flow rate.

The critical flow model with non-condensables present in S-RELAP5 was examined and was determined to be performing as intended and the model was behaving in an acceptable manner. When the injected nitrogen gas causes a pressure increase, choking at the break becomes

possible, depending both on the magnitude of the pressure rise and the flow area at the break. A benchmark of the S-RELAP5 critical flow calculation, with nitrogen surging into the system and passing out the break, compares well with test data obtained from the Moby Dick Critical Flow Experiments. Therefore, the critical flow model with non-condensables present is expected to capture the appropriate phenomena when the nitrogen cover gas surges into the RLBLOCA plant model as the accumulator empties.



**Table 4.15: Moby Dick Facility Dimensions**

Parameter	Dimension
Straight Inlet Section Length	2.668 m (8.75 ft)
Internal Diameter	0.014 m (0.046 ft)
Nitrogen Injection Upstream of Nozzle	0.985 m (3.23 ft)
Conical Convergent Nozzle Length	0.2534 m (0.83 ft)
Straight Outlet Section Length	0.420 m (1.38 ft)
Internal Diameter	0.045 m (0.148 ft)
Nozzle Divergent Angle	7 degrees

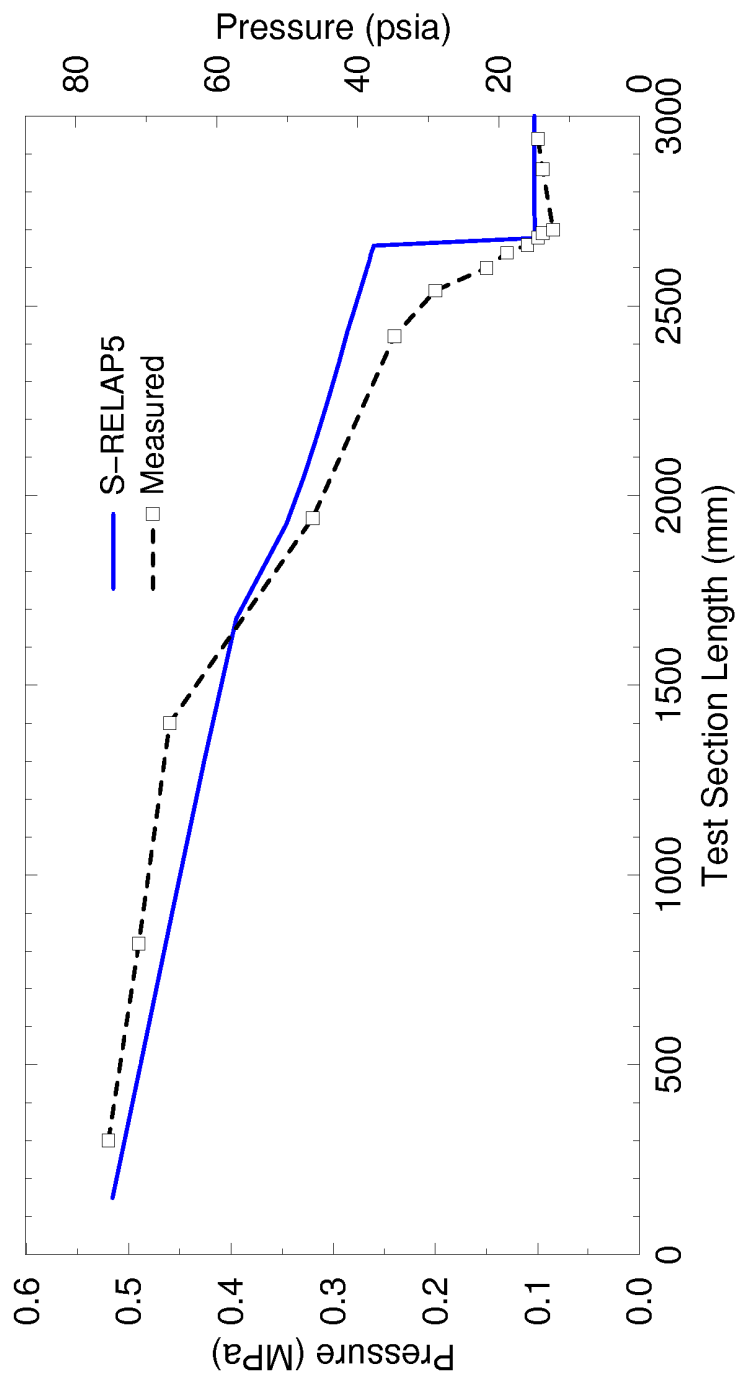


**Figure 4.153: Comparison of Moby Dick Data and S-RELAP5 Calculated Pressures**

#### 4.3.1.17 Assessment of Total Heat Transfer in FLECHT-SEASET Test 31504

The post-CHF heat transfer model now includes provisions for thermal radiation between structures (rod-to-rod). This adds to the current model which already includes thermal radiation from structures to the fluid (rod-to-droplets and rod-to-steam). The heat transfer uncertainties developed previously (discussed in Section 5.1.2 of Reference 5), assumed that rod-to-rod radiation was implicitly included in that development. Consequently, [

]. As a result, the heat transfer uncertainty with rod-to-rod radiation was determined using the same (Revision 0) FLECHT-SEASET tests as before, but with modified input to explicitly account for the rod-to-rod radiation contribution. Discussion of those results is provided in Section 5.1.3 of Reference 5.

The application of the heat transfer uncertainties to the hot rod requires a different strategy than previously used (i.e., Revision 0). First, a model conducive to including rod-to-rod radiation heat transfer needs to be developed. Referring to the thermal radiation analysis in Reference 29, the 161-rod FLECHT-SEASET bundle was collapsed into a 5x5 array, including a guide tube, plus a boundary that surrounds the hot rod. The researchers used test measurements for the boundary and array elements, steam temperature, and droplet size and distribution to establish the total radiation contribution to the heat transfer over a span of 100 seconds. Applying this arrangement to the plant model requires some simplifications since it is not practical to extract either individual rod temperatures or groups of rod temperatures from a reflood analysis.

By assuming the rods, including guide tubes, in the 5x5 and boundary have the same temperature, the 5x5 boundary can be collapsed into one structure surrounding the hot rod. This simplified arrangement can be treated as concentric cylinders. However, assuming a constant temperature distribution is acceptable only if a bounding temperature is used.

Additional heat structures were added to the otherwise unchanged (except for numbering) S-RELAP5 input model discussed in Section 3.3.5 of Reference 5. A new 'hot rod' structure was created. It differs from the original (Revision 0) bundle structure by the heat transfer surface area factors (one rod versus 159 rods) and its power level (adjusted to be suitable for one rod). A new 'aux rod' structure was created which differs from the original bundle structure by the heat transfer surface area factor (approximately 49 rods versus 159 rods) and the power level (reduced to be suitable for a 49 rod structure). Additionally, the power level was further

reduced until sufficient radiation heat transfer between this structure and the hot rod was calculated. This amount was determined by comparison with results presented in Reference 29. A 10 percent reduction in power was required to obtain a total radiation contribution that was approximately 35 percent of the total heat transfer.

The RLBLOCA heat transfer multipliers [ ] were applied to the base structure that represented the 161-rod bundle. This arrangement is meant to achieve a best-estimate response and is also similar in application to the plant model. The hot rod and auxiliary rod used [ ]. These values represent the median values from the post-CHF probability distributions given in Section 5.1.3 of Reference 5.

The radiation modeling in S-RELAP5 of the FLECHT-SEASET tests does not include the test vessel components (guide tubes) other than the test bundle, nor is it possible to supply an effective rod temperature distribution as found in Test 31504. Consequently, the ratio of convective heat transfer to total heat transfer at 100 seconds (time of PCT) was determined to be the figure of merit for comparison. The results from Test 31504 are shown in Figure 4.154. The data was estimated from Figure 6-12 in Reference 29.

The total heat transfer coefficient is presented in Figure 4.155 and the total convection heat transfer coefficient is presented in Figure 4.156. Also in Figure 4.155 are the measured heat transfers coefficients estimated from Figure H-6 on page H-5 from Reference 29. The measurements are from three separate rods, while the estimates are from the estimated maximum and minimum heat transfer coefficients from 50 to 200 seconds. A quadratic was fitted to the calculation over the span of 30 to 300 seconds to give an estimate of the average magnitude to the computed heat transfer coefficient due to the oscillations present. S-RELAP5 tends to briefly reduce droplet generation immediately after a node quenches and before the quench front moves up to the next node. This process causes the apparent increased heat transfer immediately following a severe decrease in heat transfer when the droplet production ceases momentarily. The regression shows a truer estimate of the average heat transfer coefficient. The average total heat transfer coefficient at 100 seconds is  $9.7 \text{ BTU/h-ft}^2\text{-}^\circ\text{F}$ .

A cubic was fitted to the calculated heat transfer coefficient in Figure 4.156. Without the radiation heat transfer present, the character of the heat transfer coefficient changed slightly so

that a cubic provided a better fit to the calculation. The magnitude of the average convective heat transfer coefficient at 100 seconds is  $6.4 \text{ BTU/h-ft}^2\text{-}^\circ\text{F}$ .

Summarizing, the FLECHT-SEASET input decks were modified to include rod-to-rod radiation by adding a radiation enclosure model to the existing 161-rod bundle. The cases were executed and a post-CHF heat transfer probability distribution was generated. Additional results from Test 31504 were generated by using the Test 31504 input deck from the distribution analysis. In this instance, [

]

for the heat transfer multipliers from the new heat transfer uncertainty distribution that includes rod-to-rod radiation. From this analysis, at 100 seconds, the total heat transfer coefficient has an average value of  $9.7 \text{ BTU/h-ft}^2\text{-}^\circ\text{F}$  and the convection heat transfer coefficient has an average value of  $6.4 \text{ BTU/h-ft}^2\text{-}^\circ\text{F}$ . Based on this comparison, the appropriate amount of thermal radiation is being computed in the S-RELAP5 post-CHF heat transfer model at the time of PCT. This indicates that when the S-RELAP5 post-CHF heat transfer model is applied to a LBLOCA plant analysis, the total amount of heat transfer at the time of PCT is appropriate.

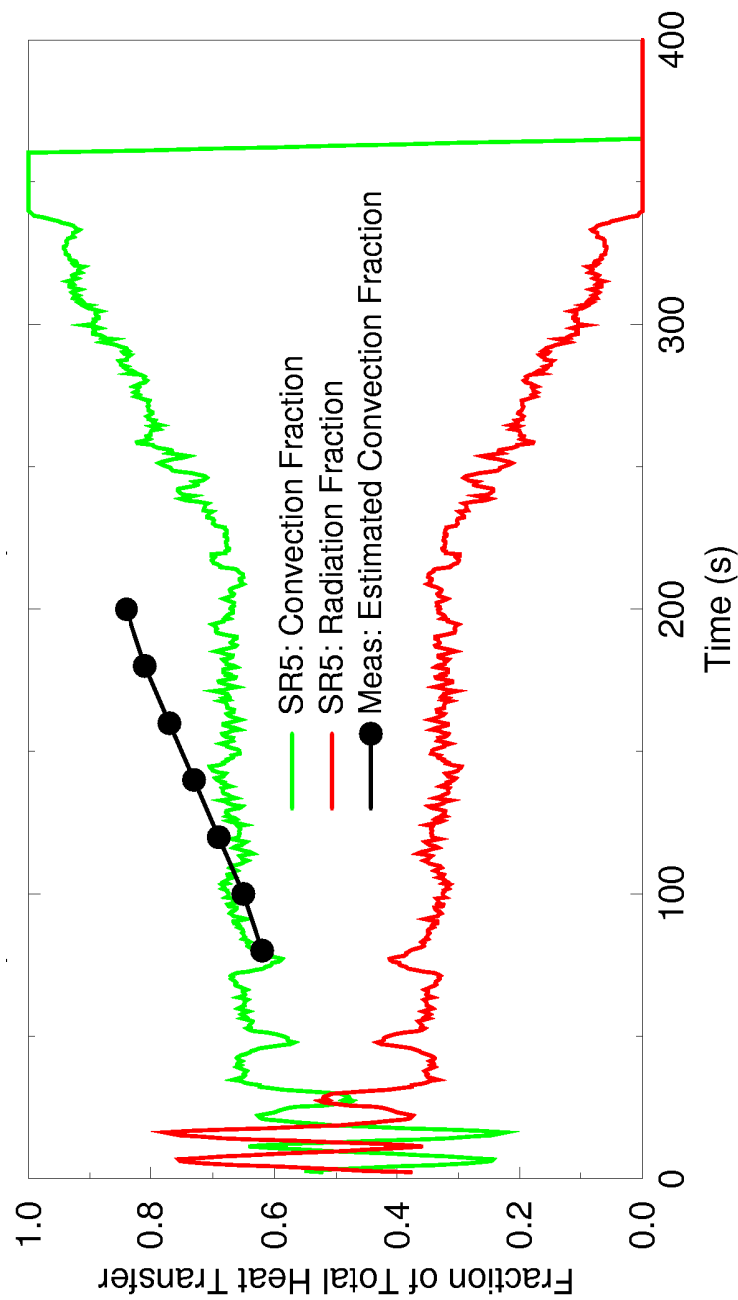


**Figure 4.154: Ratio of Convective to Total Heat Transfer, Calculated and Measured**

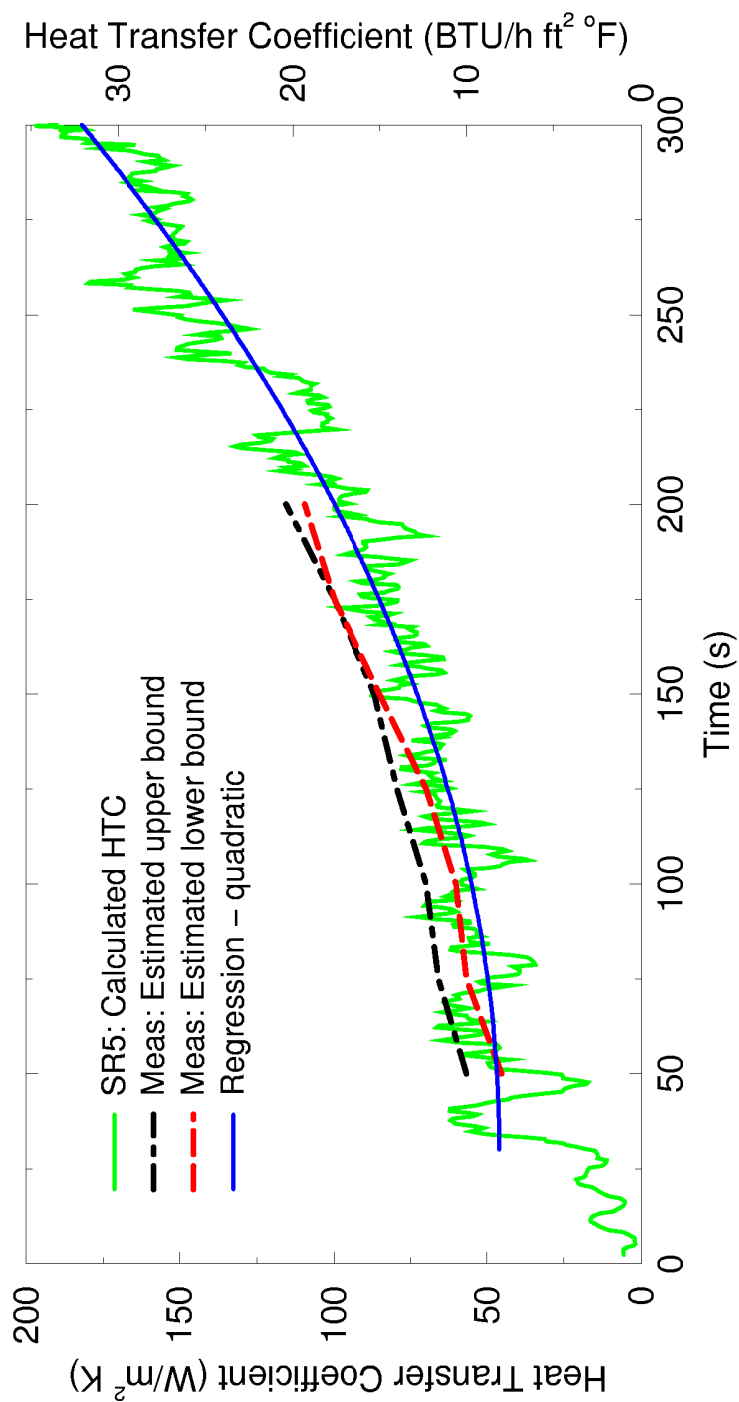


**Figure 4.155: Total Heat Transfer Coefficient, Calculated and Measured**

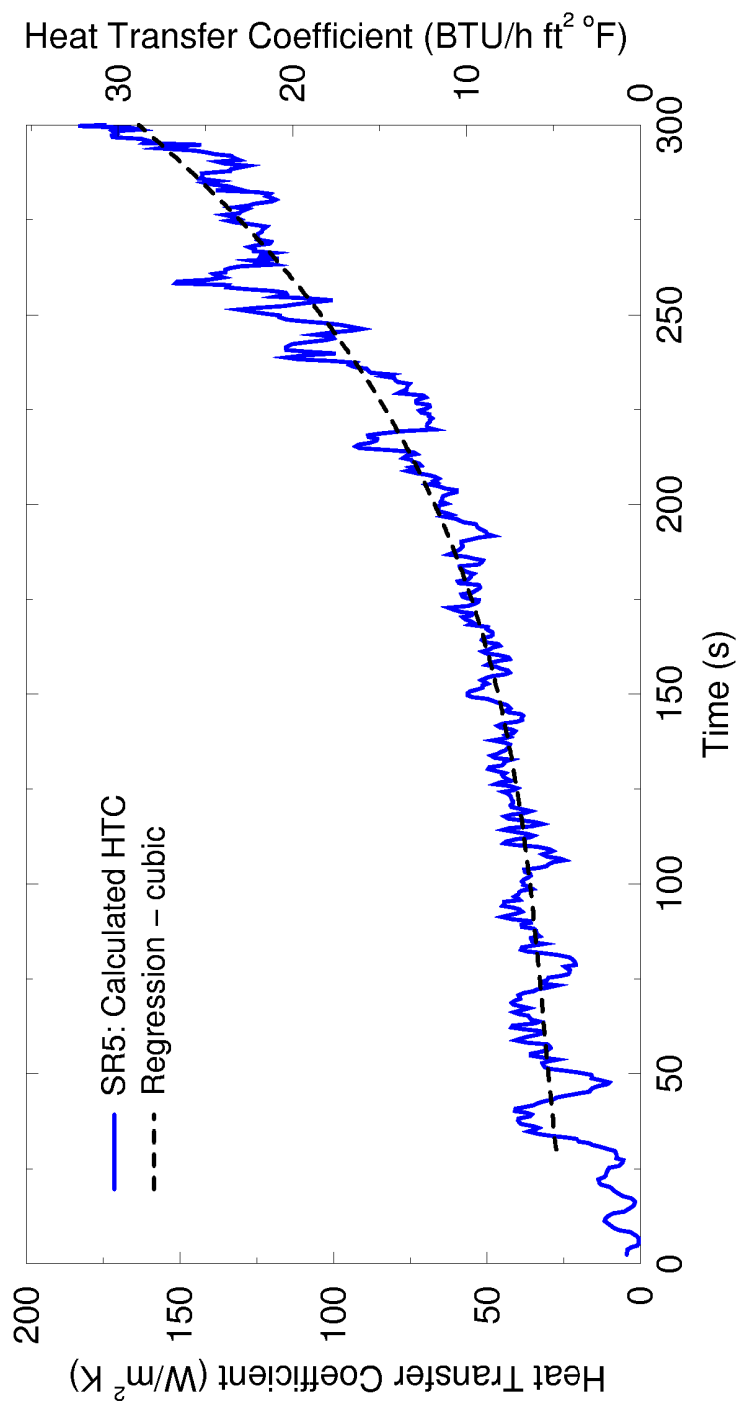


**Figure 4.156: Convective Heat Transfer Coefficient**



#### 4.3.2 Integral Effects Tests

The SETs presented in Section 4.3.1 assess the code capability and provide information to quantify the uncertainty to predict specific phenomena identified by the PIRT. In addition to the SETs, assessments are performed for IETs to evaluate the overall code capability to predict the integrated LBLOCA scenario and the interacting phenomena in facilities of differing scale. Some of the tests conducted using the facilities discussed with the SETs, such as SCTF, CCTF, and UPTF are large scale and include integral interacting-phenomena effects. However, these tests are still limited in that only a portion of the RLBLOCA scenario is addressed. For this reason, AREVA regarded these tests as SETs.

IETs covering the entire RLBLOCA scenario were performed in the LOFT facility and the smaller scale Semiscale test facility. AREVA assessed tests from both of these facilities [

] These assessments are reported in detail in Reference 5 and are summarized in the following sections.

##### 4.3.2.1 LOFT Assessments

Assessments of LOFT Tests L2-3, L2-5, LP-02-6, and LP-LB-1 were performed to justify the use of AREVA's RLBLOCA methodology and the S-RELAP5 code developed by AREVA for realistic analysis of LBLOCA. The assessment results demonstrate the accuracy of the COPENIC2, RODEX3A, and S-RELAP5 codes, and their capability of simulating LBLOCA phenomena observed during the LOFT tests. The RODEX3A and S-RELAP5 codes were assessed with the LOFT tests in the previous RLBLOCA methodology, Reference 6. Steady-state exposure results were compared between the COPENIC2 and RODEX3A models with differences being consistent with the different physical models used in the two fuel codes. In this assessment, COPENIC2 is used. Although COPENIC2 is not specifically approved for use with Zircaloy clad fuel, the physical models in COPENIC2 do not exclude the use of Zircaloy cladding. Consequently, the LOFT assessment demonstrates the adequacy of the combined S-RELAP5 and COPENIC2 codes in the LBLOCA scenario.

#### 4.3.2.1.1 LOFT Facility

The LOFT facility was an NRC-sponsored 50 MWt PWR nuclear experimental test facility designed to simulate the nuclear and thermal-hydraulic phenomena that take place in a Westinghouse 4-loop PWR during a hypothetical LBLOCA. The LOFT results are widely used to validate thermal-hydraulic codes that analyze PWR accident and transient phenomena. Key LOFT LBLOCA tests are included in the CSAU assessment matrix (Reference 4) and RELAP5/MOD3 developmental assessment matrix. LOFT assessments were performed to verify RELAP5/MOD2 and MOD3 by various members of the NRC-sponsored International Code Assessment Program (Reference 30).

The facility included five major subsystems, an intact loop, a broken loop, a reactor vessel, an emergency core cooling system, and a blowdown suppression system. The LOFT facility was fully instrumented so that system parameters could be measured during the tests.

The LOFT reactor had a single active intact loop that simulated the combined three intact loops of a Westinghouse 4-loop PWR. The intact loops included an active steam generator, two reactor coolant pumps (RCP) in parallel, a pressurizer, a loop seal, and connecting piping.

The broken loop in the LOFT facility was an inactive flow loop during normal operation. The loop consisted of a hot leg, a steam generator simulator, a pump simulator, and a cold leg. It became an active flow loop and simulated the broken loop of a 4-loop PWR during LOCA tests. The broken loop cold leg (BLCL) was divided into two parts: a pump side that connected the pump simulator to the blowdown suppression system, and a vessel side that connected the vessel downcomer to the blowdown suppression system. The steam generator and pump simulators provided flow resistances representative of a PWR during a LOCA. Both sides of the broken cold legs contained quick-opening blowdown valves that opened to initiate the transient.

The LOFT reactor vessel had an annular downcomer, a lower plenum, below core hardware, a nuclear core, above core hardware, and an upper plenum. The downcomer was connected to the intact and broken cold legs and the upper plenum was connected to the hot legs. The core contained 1300 fuel rods arranged in five square (15x15) and four triangular (corner) assemblies with an average linear heat generation rate (LHGR) of about 7.0 kW/ft at full power. The LOFT fuel rods and pitch were typical of a PWR 15x15 fuel rod array, except that the active length was only 1.68 meters (5.5 feet) compared to a typical value of 3.66 meters (12 feet). For

Tests L2-5, LP-02-6, and LP-LB-1, all the fuel rods in the central assembly (except the outside row) were pressurized with helium to 2.51 MPa (350 psig) and all the fuel rods in the peripheral assemblies were unpressurized. For Test L2-3, all of the fuel rods were unpressurized.

The LOFT intact loop had two separate ECCSs connected to the cold leg. Each system contained an accumulator, a HHSI, and a LHSI. Only one set of the pumped injection systems were used during a LOCA test; the other set was used as backup for plant protection in case of unplanned emergency situations that might occur during the test. The ECCS was not connected to the broken loop. For the LBLOCA tests, ECC was injected into the intact loop cold leg (ILCL). The HHSI and LHSI were connected to the accumulator injection piping. The LOFT blowdown suppression system consisted of a header and a suppression tank that simulated the PWR containment pressure and temperature environment expected to occur during a LBLOCA.

The LOFT facility was designed with a primary system volume-to-core power ratio similar to that of a PWR. The design objective for the LOFT facility was to produce, on a reduced scale, the significant thermal-hydraulic phenomena with representative conditions and a representative sequence of events that could occur in a PWR during postulated LOCAs. Volumetric scaling generally was used for the design of LOFT components. Primary system components (e.g., lower plenum, core region, upper plenum, outlet piping, steam generator, and inlet piping) also were designed with relative volumes equivalent to those in a PWR. LOFT is a reduced-scale facility that is not uniformly scaled. Therefore, scaling distortions exist that must be considered when applying the results of the LOFT tests.

The accumulator gas volume is scaled so that the ratio of accumulator gas volume to accumulator liquid volume injected is made equal to that of a typical 4-loop PWR by adjusting the standpipe height. The LOFT accumulator liquid volume is scaled to represent three of the four accumulators of a typical 4-loop PWR, assuming that the liquid in the fourth accumulator is lost out of the break. The LOFT HHSI flow rate for the LBLOCA tests is volume-ratio scaled using the ratio of the LOFT to PWR total primary system fluid volume plus the single failure criterion and the assumption that flow from one of four lines of injection is lost out of the break. The LHSI flow rate is scaled based on the combined downcomer and core flow areas. The single failure criterion and the assumption that flow from one of four injection lines is lost out of the break are also used for LHSI scaling.

The major differences between the LOFT and a Westinghouse 4-loop PWR are:

- The LOFT facility has one active operating (intact) loop and a passive blowdown (broken) loop with only a steam generator simulator and a pump simulator, while the PWR has four operating loops.
- The LOFT facility has two pumps connected in parallel in the operating loop, while the PWR has only a single pump in each loop.
- The LOFT core has a 1.68 meter (5.5 feet) active fuel length, while PWR core lengths are typically 3.66 meter (12 feet). The axial power distribution of the LOFT core is similar to a beginning-of-life, bottom-skewed power distribution in a PWR core.
- The LOFT facility has a short steam generator relative to a PWR.
- The LOFT cold leg ECC injection location is close to the vessel inlet, while the PWR ECC injection lines are located near the pump outlet.
- Axial lengths and elevations of hydraulic components are not preserved relative to a PWR.

The LOFT scaling philosophy was to reduce the component coolant volume and flow areas by the core power ratio. The volume and power scaling was not achieved completely, and vertical scaling was not preserved. Despite these component differences and scaling distortions, the LOFT components were functionally similar to those of a PWR and provide sufficient similarity to permit the LOCA data to be used to validate the ability of the S-RELAP5 code to properly evaluate PWR LOCA/ECCS performance.

#### 4.3.2.1.2 LOFT Test Descriptions

AREVA selected four LOFT LBLOCA tests (L2-3, L2-5, LP-02-6, and LP-LB-1) for assessment with S-RELAP5. Key test parameters are provided in Table 4.16. All of the selected tests simulate cold leg guillotine breaks. The major differences between these tests are: L2-3 and L2-5 were initiated from about 75 percent power while LP-02-6 and LP-LB-1 were initiated from nearly full power. The RCP flywheels were not attached during the coastdown of Tests L2-5 and LP-LB-1, but were attached when the pump speed was above 750 rpm (78.54 rad/s) in Test LP-02-6 and were left running for Test L2-3. These tests were used to validate the S-RELAP5 code for the blowdown, refill, and reflood phases of a LBLOCA. The tests were selected for S-RELAP5 assessment for the following reasons:

- The boundary conditions and the initial test conditions most closely simulate the "design basis accident" LOCA conditions for typical Westinghouse 4-loop PWR.
- Test L2-3 provides scaling data when compared to Semiscale Test S-06-3.
- The LOCA phenomenology for Tests L2-5 and LP-LB-1 is similar to that expected for a Westinghouse 3-Loop PWR, and the LOCA phenomenology for Test LP-02-6 is similar to that expected for a Westinghouse 4-Loop PWR.
- Test L2-3 was designated as United States Standard Problem 10 for code assessment by the NRC.
- Test L2-5 was designated as ISP 13 for code assessment by the Organization for Economic Cooperation and Development.
- Other code assessment calculations of L2-5, LP-02-6, and LP-LB-1 are available for comparison.

#### 4.3.2.1.3 LOFT Assessment Summary

The LOFT assessment calculations were performed with an input model developed to be consistent with the nodalization to be applied for PWR plant calculations. For the LOFT benchmarks a nodalization scheme (in terms of number and distribution of volumes, junctions, heat structures, and input specifications) corresponding to the RLBLOCA evaluation model was used to represent corresponding components in the LOFT and plant models. Exceptions are made only where significant LOFT geometry differences justify a different, but consistent scheme.

Reference 5 contains detailed comparisons of the results of the LOFT L2-3, L2-5, LP-02-6, and LP-LB-1 tests with calculated results using the RLBLOCA evaluation model. The LOFT benchmark results demonstrate the ability of S-RELAP5 to realistically simulate the key system phenomena relevant to a LBLOCA that were observed in the LOFT LBLOCA tests. These include: (1) system depressurization, (2) core flow reversal and core dry-out, or CHF, (3) the fuel cladding temperature excursion and PCT, (4) two-phase pump flow and critical flows at the breaks, (5) prevention of core bottom-up quench during the early blowdown period, (6) ECC downcomer penetration and bypass, and (7) core refill, reflood, and final quench.

As shown by the results presented in Reference 5, the RLBLOCA evaluation model produced results in good agreement with the observations for LOFT tests L2-3, L2-5, LP-02-6, and LP-LB-1. The results are summarized as follows:

- The COPENIC2-calculated fuel initial centerline fuel temperatures were within 10 percent of the measured data.
- The S-RELAP5 code results agree with the hydraulic responses of the LOFT tests. That is, the calculated results were: (1) within measured uncertainties or followed the major trends of the data, if not within measured uncertainties, or (2) conservative with respect to the data, if the phenomena were not simulated. The intact loop mass flow rates, broken loop break flow, and loop volume densities were all well calculated. Coolant temperatures also were well calculated. Pressurizer draining was overpredicted, but because the pressurizer liquid tended to flow to the broken loop and was removed from the system, that trend produced conservative results. Calculated pump speeds were accurately predicted up to the time where a two-phase mixture appeared, after which the pump speeds were lower than the measured data and, thus, acceptable.
- The code accurately calculated the thermal response (fuel centerline temperature and cladding temperature). The centerline temperatures closely match the data. The cladding temperature results generally were in reasonable agreement with the measured data. The hot rod PCT is well calculated, considering test measurement uncertainty. The cladding quench times are significantly delayed with respect to the measured data. The early bottom-up core quenching found in Tests L2-3 and LP-02-6 was not simulated in the code calculations. The upper regions of the core showed delayed dry-out with respect to the test data. However, once the upper regions went through dry-out, the calculated rewet was much later than measured. In general, the code predicted higher than measured temperatures in the middle core region, lower than measured temperatures in the upper core region, and approximately measured temperatures in the lower core region. In all cases, the calculated PCT was either within or greater than the measured PCT with analytical uncertainties included. The measured PCT is reported with the fin cooling bias applied (Reference 70), and shown separately on the PCT versus core elevation plots.
- The calculated ECC injection rates for the low pressure safety injection (LPSI) system and accumulator tended to underpredict the measured data and, hence, are acceptable.

#### 4.3.2.1.4 LOFT Test L2-3 Assessment

Test L2-3 was the second LBLOCA test conducted in the LOFT facility. The test represented a hypothetical cold leg guillotine break that simulated a double-ended, offset, shear break in a 4-loop PWR. The test was initiated at 75 percent thermal power (36 MWt) and a 12.22 kW/ft LHGR.

Table 4.17 shows the measured and calculated event times for LOFT Test L2-3, while Figure 4.157 compares the calculated and measured PCT versus core elevation. This figure refers to the PCT as a maximum cladding surface temperature, either calculated or measured at the various locations, during the LOCA transient history. The highest PCT of 942 K (1236 °F) was measured at the 15 inch elevation while the calculated PCT was 993 K (1328 °F).

#### 4.3.2.1.5 LOFT Test L2-5 Assessment

Test L2-5 was the third LBLOCA test conducted in the LOFT facility. The test represented a hypothetical cold leg guillotine break that simulated a double-ended, offset, shear break in a typical 4-loop PWR. The test was initiated at 75 percent thermal power (36 MWt) and a 12.22 kW/ft maximum LHGR.

Table 4.18 shows the measured and calculated event times for LOFT Test L2-5 while Figure 4.158 depicts the final comparison of the calculated and measured PCT versus core elevation. The highest LOFT test reportable PCT of 1106 K (1531 °F) was measured at the 24 inch elevation and the calculated PCT of 1088 K (1499 °F) only slightly underpredicts the measured PCT in the high-power core region and, thereby, the results are considered to be in reasonable agreement with the data.

#### 4.3.2.1.6 LOFT Test LP-02-6 Assessment

LOFT Test LP-02-6 was the fourth LOFT nuclear powered core LBLOCA test conducted with pressurized nuclear fuel rods and with a specification of minimum U.S. ECC injection rates. The maximum LHGR of 14.87 kW/ft was the typical technical specification currently used for licensing analyses of PWR fuel rods with the same approximate pellet diameter used in a 15x15 fuel pin array. Test LP-02-6 represented an NRC "design basis accident" test and was supposed to run at 100 percent power, 50 MWt, but because of questions concerning the integrity of the pressurized fuel rods in the central hot assembly, the power level was reduced to

mitigate possible safety problems. Test LP-02-6 is an important LBLOCA test for code assessment because it addresses the issues relating to safety margins associated with the response of a PWR to the NRC "design basis accident" scenario, including delayed minimum ECC safeguards.

Test LP-02-6 simulated a cold leg guillotine break coincident with a loss-of-offsite power. It was conducted with a delayed and degraded high and low pressure ECC injection. During the test, the RCPs were tripped and coasted down with their flywheels attached. The result was an early partial core rewet from the bottom up. When RCP speed dropped below 750 rpm (78.54 rad/s), the flywheels were uncoupled from the pumps to increase the pump speed deceleration. The attached flywheels produced pump coast down characteristics typical of a commercial Westinghouse 4-loop PWR.

Before the initiation of blowdown, the power level in the reactor core was steadily increased and then held at 46 MWt  $\pm$  1.2 MWt to ensure an appropriate decay heat power level would be obtained once the control rods were inserted into the reactor core. Table 4.19 shows the measured and calculated event times for LOFT Test LP-02-6 while Figure 4.159 compares the calculated and measured PCT versus core elevation. The highest PCT of 1105.0 K (1530 °F) was measured at the 26 inch elevation while the calculated PCT was 1135 K (1584 °F).

#### 4.3.2.1.7 LOFT Test LP-LB-1 Assessment

The fifth LOFT LOCA test, LP-LB-1, simulated a hypothetical double-ended cold leg guillotine break initiated from conditions representative of a PWR operating near its licensing limits. The initial core power was near the facility design limit of 50 MWt with maximum LHGR of 15.8 kW/ft. Included in the boundary conditions of the test were loss-of-offsite power coincident with the LOCA, a rapid RCP coastdown, and a minimum safeguard ECCS injection assumption from a European PWR. To minimize possible fuel pin damage, all of the fuel rods in the core were initially unpressurized.

Table 4.20 shows the measured and calculated event times for LOFT Test LP-LB-1 while Figure 4.160 compares the calculated and measured PCT versus core elevation. The measured PCT is 1284.0 K (1852 °F) at the 24 inch elevation with a calculated maximum PCT of 1297 K (1875 °F).



**Table 4.16: LOFT Nuclear Large Break Test Parameters**

Test	Power (MWt)	MLHGR (kW/ft)	Pump Operation	Fuel Pressurized	ECCS			PCT (K)
					HPI	LPI	Accum.	
L2-3 - Double end-cold leg break, with break area scaled to simulate PWR double-end cold leg break, US Appendix K ECC	36	11.9	On	No	2/3	1/2	3/4	914
L2-5 - Similar to L2-3, with pumps turned off and decoupled from their external flywheels within 1 s, US Appendix K ECC with 58% L2-3 HPIS	36	12.2	Off(A)	Yes	1/3	1/2	3/4	1078
LP-02-6 - Similar to L2-5, with pumps turned off but initial coast down with external flywheels, US Appendix K ECC, increased core power and MLHGR	46	14.9	Off(N)	Yes	1/3	1/2	3/4	1077
LP-LB-1 - Similar to LP-02-6, with pump turned off and decoupled from their external flywheels within 1 s, UK minimum safeguards ECC, and slightly increased core power and MLHGR	49.3	15.8	Off(A)	No	0/3	1/2	2/4	1256

A – Atypical rapid pump coastdown

N – Normal pump coastdown

**Table 4.17: Event Sequence for LOFT Test L2-3**

<b>Event</b>	<b>Measured Data Time (s)</b>	<b>S-RELAP5 Time (s)</b>
Test Initiation	0.00	0.0
Reactor Scram	0.103	0.016
PCT Reached	5.0	5.2
Pressurizer Empty	≈10.0	≈20.0
HPIS Initiation	14.0	14.0
Accumulator Injection Initiation	16.0	16.6
Lower Plenum Refill Started	Not Reported	≈24
Lower Plenum Refill Completed	Not Reported	≈30
Core Reflood Initiated	Not Reported	≈30
LPIS Initiation	29.0	29.0
Accumulator Empty	45.0	39.4
Core Reflood Completed	Not Reported	≈70
Core Cladding Quench	>50.0	≈70

**Table 4.18: Event Sequence for LOFT Test L2-5**

<b>Event</b>	<b>Measured Data Time (s)</b>	<b>S-RELAP5 Time (s)</b>
Test Initiation	0.00	0.0
Reactor Scram	$0.24 \pm 0.01$	0.014
Primary Coolant Pump Trip	$0.94 \pm 0.01$	1.75
Pressurizer Empty	$15.40 \pm 1.0$	$\approx 16$
Accumulator Injection Initiation	$16.80 \pm 0.1$	16.0
Lower Plenum Refill Started	22.0	$\approx 22$
HPIS Initiation	$23.90 \pm 0.02$	23.90
PCT Reached	$28.47 \pm 0.02$	26.5
Lower Plenum Refill Completed	31.0	$\approx 32$
Core Reflood Initiated	37.0	$\approx 32$
LPIS Initiation	$37.32 \pm 0.02$	37.32
Accumulator Empty	$49.60 \pm 0.1$	$\approx 55.0$
Core Reflood Completed	$55.30 \pm 1.5$	$\approx 130$
Core Cladding Quench	$65.00 \pm 2.0$	$\approx 130$

**Table 4.19: Event Sequence for LOFT Test LP-02-6**

<b>Event</b>	<b>Measured Data Time (s)</b>	<b>S-RELAP5 Time (s)</b>
Test Initiation	0.00	0.0
Reactor Scram	$0.06 \pm 0.01$	0.01
Primary Coolant Pump Trip	$1.28 \pm 0.01$	1.28
PCT Reached	$4.9 \pm 0.2$	5.2
Pressurizer Empty	$15.5 \pm 0.5$	$\approx 15$
Accumulator Injection Initiation	$17.5 \pm 0.5$	16.0
Lower Plenum Refill Started	Not Reported	$\approx 22$
HPIS Initiation	$24.77 \pm 0.01$	24.77
Lower Plenum Refill Completed	30.7	$\approx 30$
Core Reflood Initiated	Not Reported	$\approx 30$
LPIS Initiation	$37.32 \pm 0.02$	37.32
Accumulator Empty	45.0	39.2
Core Quench Completed	$56.0 \pm 0.2$	$\approx 120$
Core Reflood Completed	$59.0 \pm 1.0$	$\approx 120$

**Table 4.20: Event Sequence for LOFT Test LP-LB-1**

<b>Event</b>	<b>Measured Data Time (s)</b>	<b>S-RELAP5 Time (s)</b>
Test Initiation	0.00	0.0
Reactor Scram	$0.13 \pm 0.01$	0.012
Primary Coolant Pump Trip	$0.24 \pm 0.01$	1.2
Blowdown PCT Reached	$12.9 \pm 0.5$	9.8
Pressurizer Empty	$15 \pm 1.0$	$\approx 15$
Accumulator Injection Initiation	$17.5 \pm 0.05$	15.8
Refill/Reflood PCT Reached	$26.8 \pm 0.5$	21.4
LPIS Initiation	$32.0 \pm 1.0$	31.0
Lower Plenum Refill Completed	$34.5 \pm 0.5$	$\approx 32$
Accumulator Empty	$40.0 \pm 1.0$	30.4
Accumulator Injection Completed	$46.0 \pm 2.0$	50.0
Core Quench Completed	$72.0 \pm 1.0$	$\approx 200$

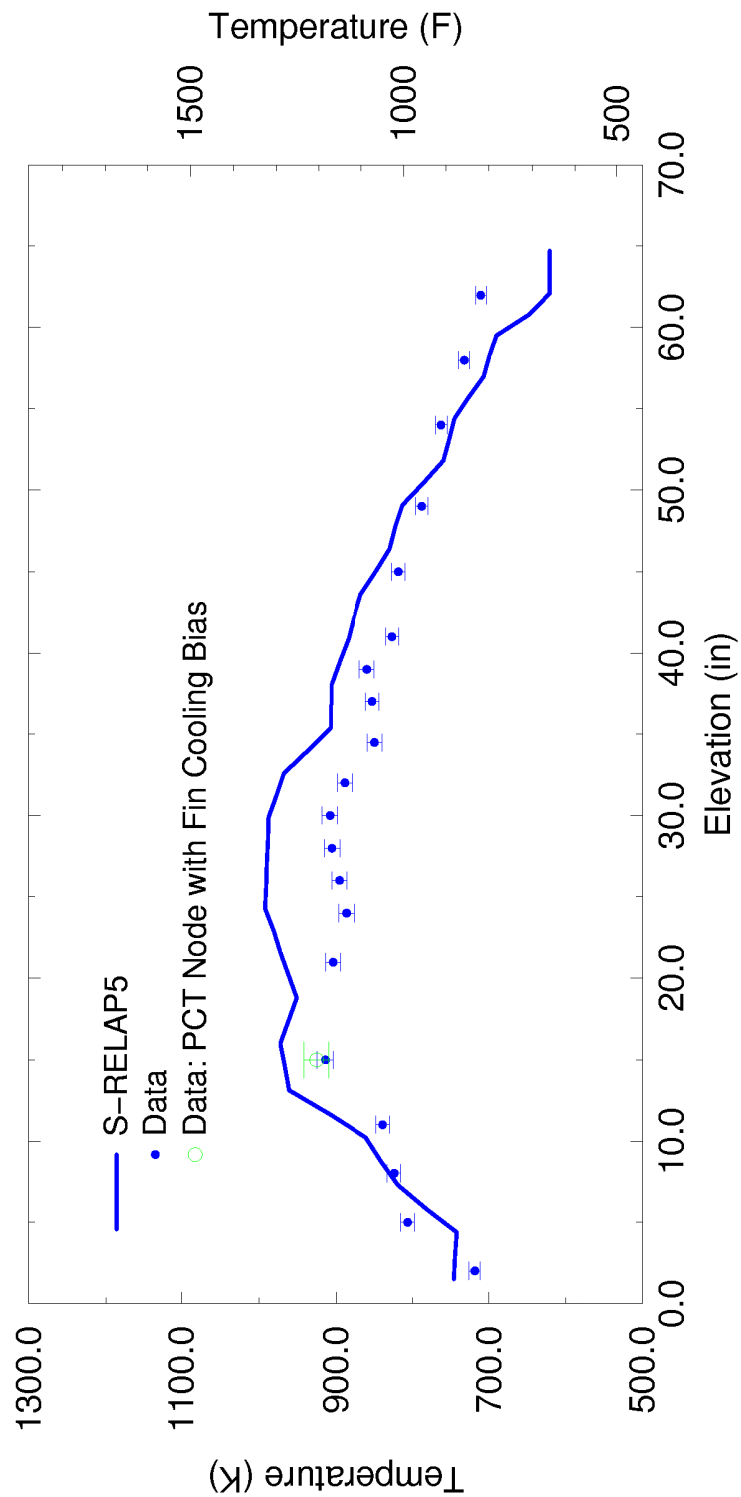


**Figure 4.157: Comparison of PCTs versus Core Elevations LOFT  
Test L2-3 with S-RELAP5**

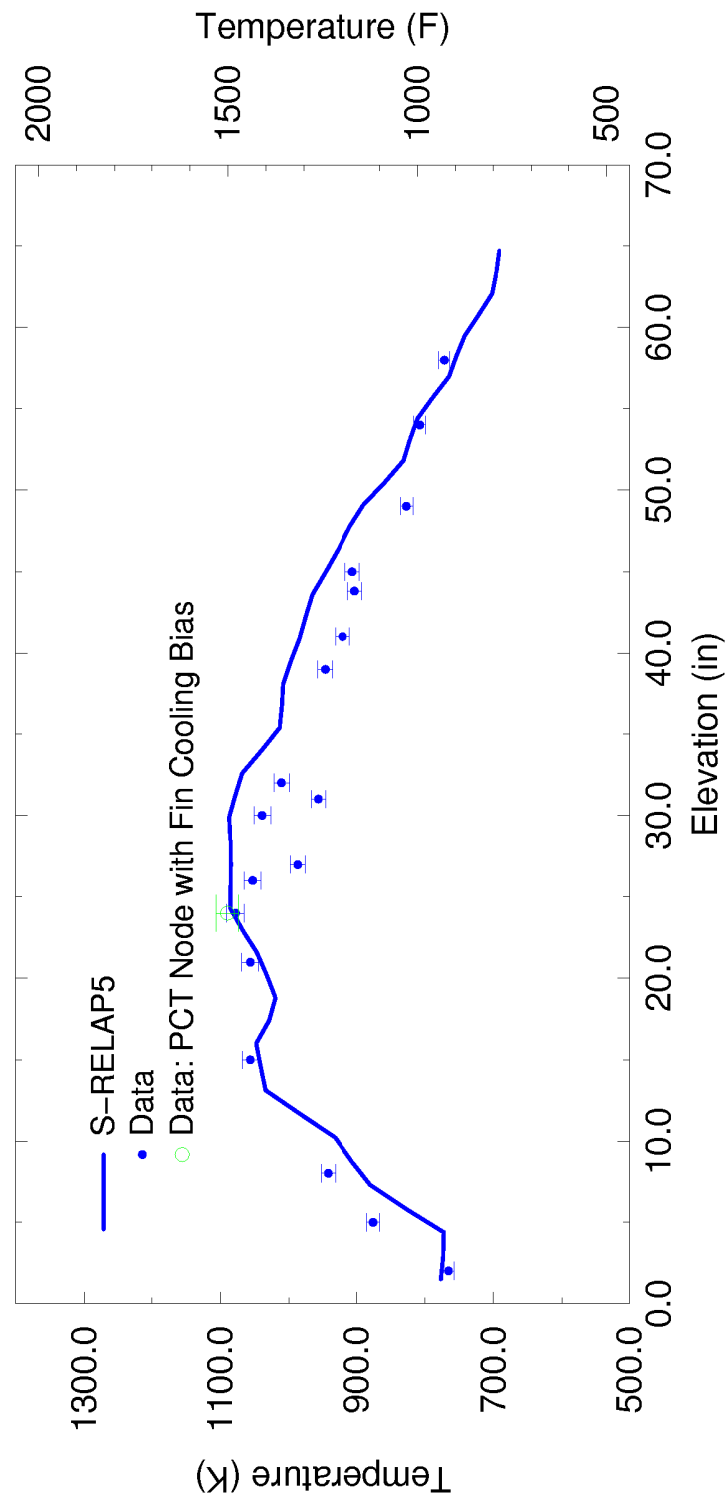


**Figure 4.158: Comparison of PCTs versus Core Elevation, LOFT Test L2-5**

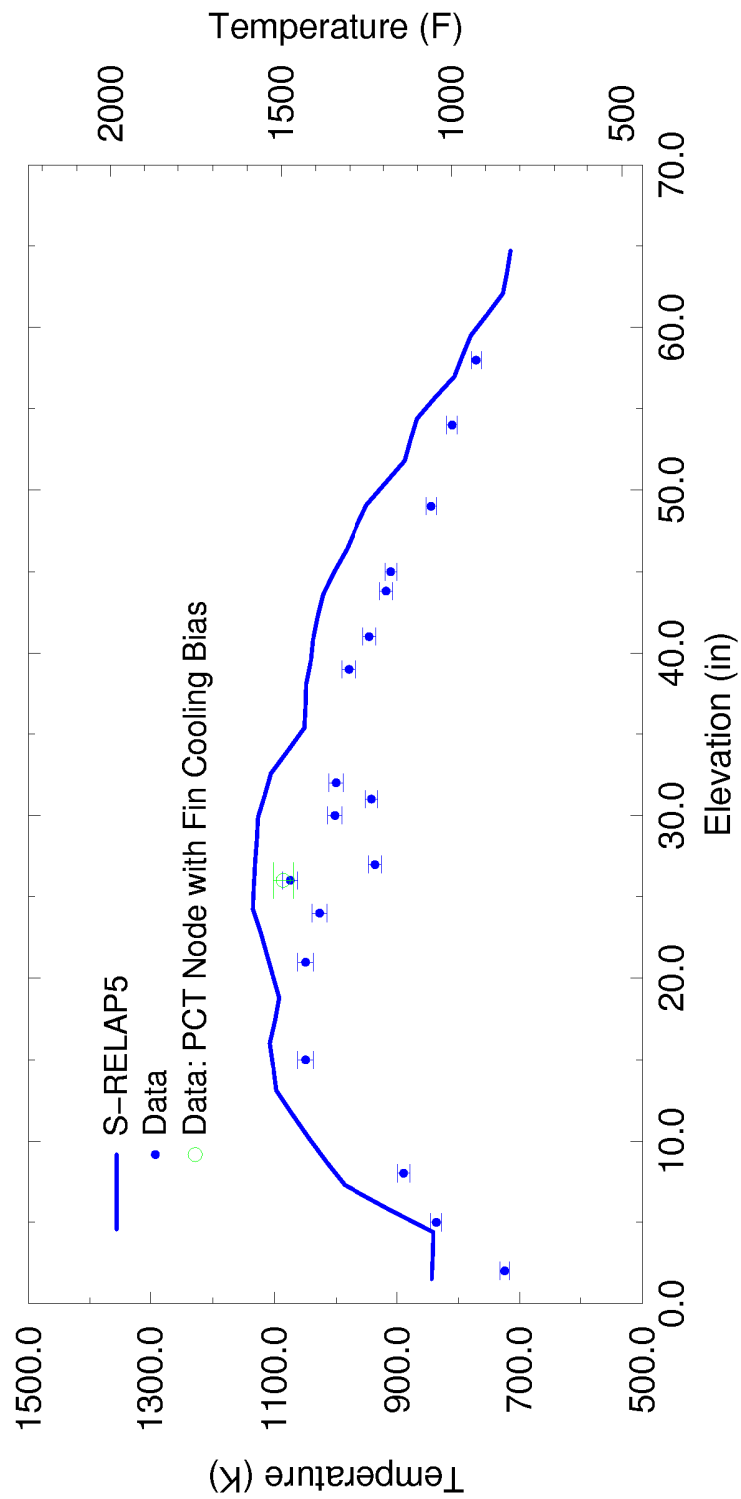


**Figure 4.159: Comparison of PCTs versus Core Elevations,  
LOFT Test LP-02-6**



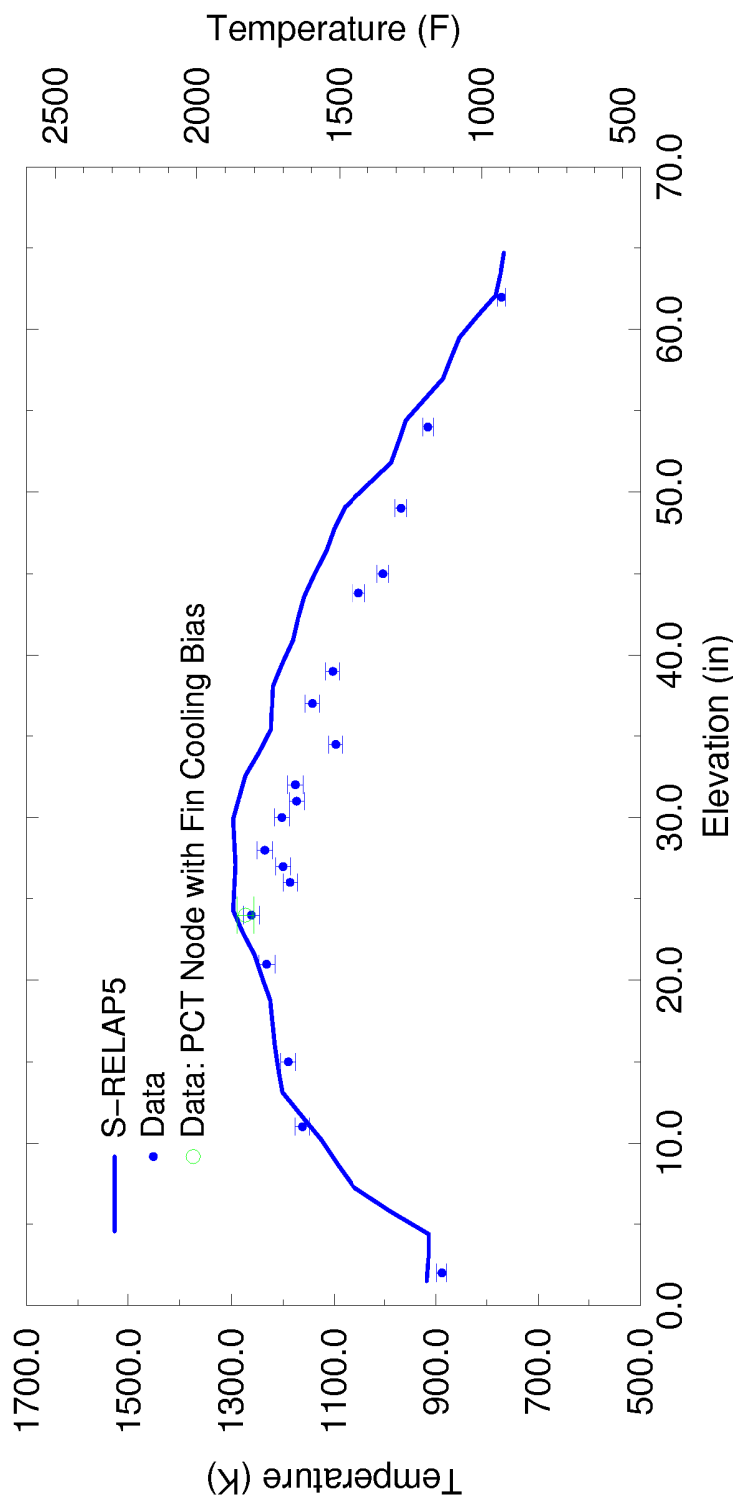


**Figure 4.160: Comparison of PCTs versus Core Elevation, LOFT Test LP-LB-1**

#### 4.3.2.2 Semiscale Tests

S-RELAP5 was assessed against Semiscale LBLOCA tests S-06-3 and S-07-1. Test S-06-3 was performed in the Semiscale MOD-1 facility. The MOD-1 facility was scaled from the LOFT facility. Test S-06-3 was performed as a counterpart to LOFT Test L2-3 and provides assessment for the blowdown, refill, and reflood phases of a LBLOCA. The results presented for this assessment are used to verify the capability of the S-RELAP5 code to calculate integral LOCA phenomena in facilities of different scale.

Semiscale Test S-07-1 is a blowdown test performed in the Semiscale MOD-3 facility with cold leg ECC injection. The results presented for this assessment are used to verify the capability of the code to calculate blowdown film boiling heat transfer in the core.

Both assessments are presented in detail in Section 4.2 of Reference 5.

##### 4.3.2.2.1 Semiscale Facilities

###### MOD-1 Facility

The Semiscale MOD-1, 1½-loop facility was scaled to the LOFT facility, which in turn was scaled to a 4-loop PWR. It is designated as a 1½-loop system because it is configured with one active loop and one passive blowdown loop. Subsequent Semiscale facilities have included components that have made the facility more typical of a PWR. All the other Semiscale facilities were designed with 1/1600 to 1/2000 volume scaling, with full height, in reference to a 4-loop, 3400 MWt PWR.

The MOD-1 system contains a reactor vessel with internals, including a 40-rod electrically heated core, an active intact loop scaled to represent three loops of a PWR, and a broken loop scaled to a single loop of a PWR. The intact loop contains an active steam generator, an active RCP, and a pressurizer. The broken loop contains hydraulic steam generator and pump simulators, and break simulators or rupture assemblies connected to a blowdown suppression system. The blowdown suppression system simulates containment pressure.

The 40-rod electrically heated core has a PWR fuel pin pitch of 0.563 inches, a heated length of 5.5 feet, and an outside diameter of 0.42 inches. They are identical to the nuclear fuel rods of the LOFT core.

Semiscale Test Series 6 was performed to assist the LOFT program in planning the first nuclear test series. Test S-06-3 was performed as a counterpart to LOFT Test L2-3. For this test, the four central heater rods were operated at approximately 39.4 kW/m, 32 rods were operated at approximately 24.9 kW/m, and four rods were unpowered to simulate passive rod locations. This configuration yielded a peaked power profile that simulates that of the LOFT facility and provides a total core power of 1.004 MWt.

The safety injection includes the HHSI, LHSI, and accumulators. For Test S-06-3, two HHSI pumps and two LHSI pumps delivered flow into the intact loop cold leg along with the intact loop accumulator. The RCP was powered for the entire transient.

### MOD-3 Facility

The Semiscale MOD-3 facility is constructed with two fully active coolant loops. The intact loop, retained from the Semiscale MOD-1 system, was scaled to the LOFT facility, which in turn was scaled to a 4-loop PWR. The broken loop, on the other hand, was scaled directly to a 4-loop commercial PWR. The Semiscale MOD-3 facility was designed with 1/1600 to 1/2000 volume scaling and full height, in reference to a 4-loop, 3400 MWt PWR.

The vessel in the MOD-3 system consists of an upper plenum with internals required to represent guide and support tubes, an upper head, a 25-rod electrically heated core, and an external single pipe downcomer. The active intact loop is scaled to represent three loops of a PWR and the active broken loop is scaled to represent a single loop of a PWR. The intact loop contains a pump and a short Type I steam generator, and is connected to a pressurizer. The broken loop contains the taller Type II steam generator, a pump simulator, and break simulators or rupture assemblies connected to a blowdown suppression system. The blowdown suppression system simulates containment pressure.

The 25-rod electrically heated core is characterized by fuel pin pitch of 0.563 inches and an outside diameter of 0.422 inches typical of a PWR. The heated length of the MOD-3 core is 12 feet, identical to a 4-loop PWR core.

Test S-07-1 was performed to establish the baseline performance of the MOD-3 system during a blowdown with cold leg ECC injection. It was conducted to obtain core heat transfer and departure from nucleate boiling (DNB) characteristics of the heater rods. The MOD-3 system

was initialized in the experiment to a primary pressure of 15.95 MPa, total-loop flow of 9.4 kg/s, and cold-leg temperatures of 559 K for the intact loop and 557 K for the broken loop at a core power level of 2.01 MWt nominal. The system was subjected to a double-ended cold-leg break through a rupture assembly and two non-communicative nozzles.

#### 4.3.2.2.2 Semiscale Test Descriptions

##### Test S-06-3

In Test S-06-3, the MOD-1 system was initialized to a primary pressure of 15.769 MPa, cold leg temperature of 563 K, and inlet flow of 6.68 l/s (liters per second) at an initial core power level of 1.004 MWt. The system was subjected to a double-ended cold leg break through two rupture assemblies and two LOFT facility counterpart nozzles, each having a break area of 0.000243 m<sup>2</sup> (0.00262 ft<sup>2</sup>). The effluent from the primary system was ejected into the pressure suppression system.

After initiating blowdown, power to the heated core was reduced to simulate the predicted heat flux response of the nuclear fuel rods during a LOCA. Blowdown was accompanied by ECC injection into the cold leg piping of the intact loop. Coolant injection from the HHSI began at blowdown and continued until test termination (300 seconds). Coolant injection from the accumulator started at approximately 18.5 seconds after rupture and terminated at approximately 90 seconds. LHSI began at 25.5 seconds after rupture, at a pressure of 1900 kPa, and continued until test termination.

##### Test S-07-1

The specific test conditions simulated in the S-RELAP5 calculation are:

- The 23 rods in the square matrix of the 25-rod electrically heated core were operated at approximately 36.9 kW/m with a flat radial power profile, resulting in a total core power level of 2.01 MWt nominal. One corner rod was unpowered and another corner rod was replaced by a liquid level probe. The normalized axial power profile is a chopped cosine.
- During the blowdown transient, power to the electrically heated core was automatically controlled to simulate the thermal response of nuclear heated fuel rods. The power history is modeled based on the measured core power decay.

- The accumulators for the ILCL and BLCL were pressurized with nitrogen to 4137 kPa (600 psia). Intact loop accumulator injection began at 19 seconds and nitrogen discharge began at 72 seconds. BLCL accumulator injection began at 12.5 seconds and nitrogen discharge began at 35 seconds. The ILCL and BLCL accumulator injected flows are modeled based on the measured data. The accumulators are actuated in the calculation on time, not pressure, to match the injection timing of the experiment.
- The simulation extended from the time of pipe rupture until the time before nitrogen injection. The earliest nitrogen was injected at 35 seconds, originating from the BLCL accumulator. Therefore, the simulated transient is 35 seconds long.
- The initial containment pressure is 246 kPa nominal. The transient containment pressure is modeled based on the measured data.
- The maximum break area which is modeled, corresponding to a double-ended break is  $0.849 \text{ in}^2$  ( $5.48 \text{ cm}^2$ ). This implies that each of the two blowdown nozzles had a break area of  $0.424 \text{ in}^2$  ( $0.849/2$ ) ( $2.74 \text{ cm}^2$ ). This maximum break area was determined from the ratio of the maximum break area to the primary liquid volume of a PWR system applied to the primary liquid volume of the Semiscale MOD-3 system.
- The intact and broken loop RCPs coast down during the test. The ILCL and BLCL pumps are modeled based on the measured data.
- HHSI flow into the intact and broken loops started at 3.5 seconds at a pressure of 12,410 kPa (1800 psia) and continued until test termination. The ILCL and BLCL HHSI injected flows are modeled based on the measured data. The HHSI pumps are actuated in the calculation on time, not pressure, to match the injection timing of the experiment.
- The LHSI started into the ILCL and BLCL at 27 seconds at a pressure of 2000 kPa (290 psia) and continued until test termination. The ILCL and BLCL LPIS injected flows are modeled based on the measured data. The LPIS pumps are actuated in the calculation on time, not pressure, to match the injection timing of the experiment.
- The measured fluid temperature in the intact loop and broken loop ECCS injection lines indicate that the ECCS (HHSI, LHSI, and accumulator) water temperature is approximately 300 K (80.6 °F). Therefore, the ILCL and BLCL ECCS water are both modeled at a temperature of 300 K.
- The broken loop pump speed was increased by a factor of about 2.5 to match the steady-state flow in the broken loop.

- Based on scoping analyses performed for Revision 0 of the RLBLOCA methodology, the discharge coefficients were determined to be (0.80, 1.5) at the pump side and (0.85, 0.7) at the vessel side, where the first value refers to the subcooled discharge coefficient and the second value refers to the two-phase discharge coefficient.

#### 4.3.2.2.3 Test S-06-3 Assessment

The discharge coefficients were set to 1.0 for both the vessel side and pump side break junctions for both the subcooled and two-phase flows to obtain initial break flow agreement with the data. Otherwise, the nodalization of the input model was developed to be as consistent as possible with the RLBLOCA analysis guidelines.

The S-RELAP5 initial condition results match reasonably well with the Semiscale Test S-06-3 data. The detailed comparisons of predicted versus measured results for the important transient phenomena are shown in Reference 5, and are not repeated here. The calculation results were compared to test data for the three test phases (blowdown, refill, and reflood). While reasonable agreement is obtained between code results and data for the major thermal-hydraulic variables, the MOD-1 Test S-06-3 experienced apparent ECC bypass that could not be well predicted by the RLBLOCA methodology. This was caused by the small scale and the proximity of the ECC injection to the break, resulting in earlier refill being calculated and consequently earlier reflood and quenching of the heater rods. The PCT of 1152 K in the test occurs at an elevation of 21 inches above the bottom of the heated length at 20.7 seconds after pipe rupture. The calculated PCT of 1236 K occurs during blowdown at an elevation of 32.3 inches above the bottom of the heated length at 26.8 seconds after pipe rupture. Figure 4.161 shows the calculated versus measured maximum temperatures as a function of elevation in the simulated core for Semiscale Test S-06-3.

#### 4.3.2.2.4 Test S-07-1 Assessment

S-RELAP5 was assessed against Semiscale Test S-07-1. The calculation results were compared to test data. Reasonable to good agreement is obtained between code results and data for the major thermal-hydraulic variables including upper plenum pressure, break flow rates, coolant temperatures, and rod temperatures. The comparison demonstrates that S-RELAP5 is capable of simulating the blowdown film boiling heat transfer phenomena expected of a PWR LBLOCA transient. In particular, the code conservatively predicted the

average of the measured PCTs at all elevations. For instance, the calculated maximum temperature at an elevation of 72.4 inches is 1118 K compared to the average measured PCT of 1056 K at this elevation (based on eight thermocouple readings). In addition, the highest calculated PCT is 1120 K, compared to the highest measured (not average) PCT of 1101 K. Figure 4.162 shows the calculated versus measured maximum temperatures as a function of elevation in the simulated core for Semiscale Test S-07-1.

Overall, these assessments show the S-RELAP5 models and correlations are valid for the prediction of core blowdown and reflooding conditions, and can be used in RLBLOCA applications.

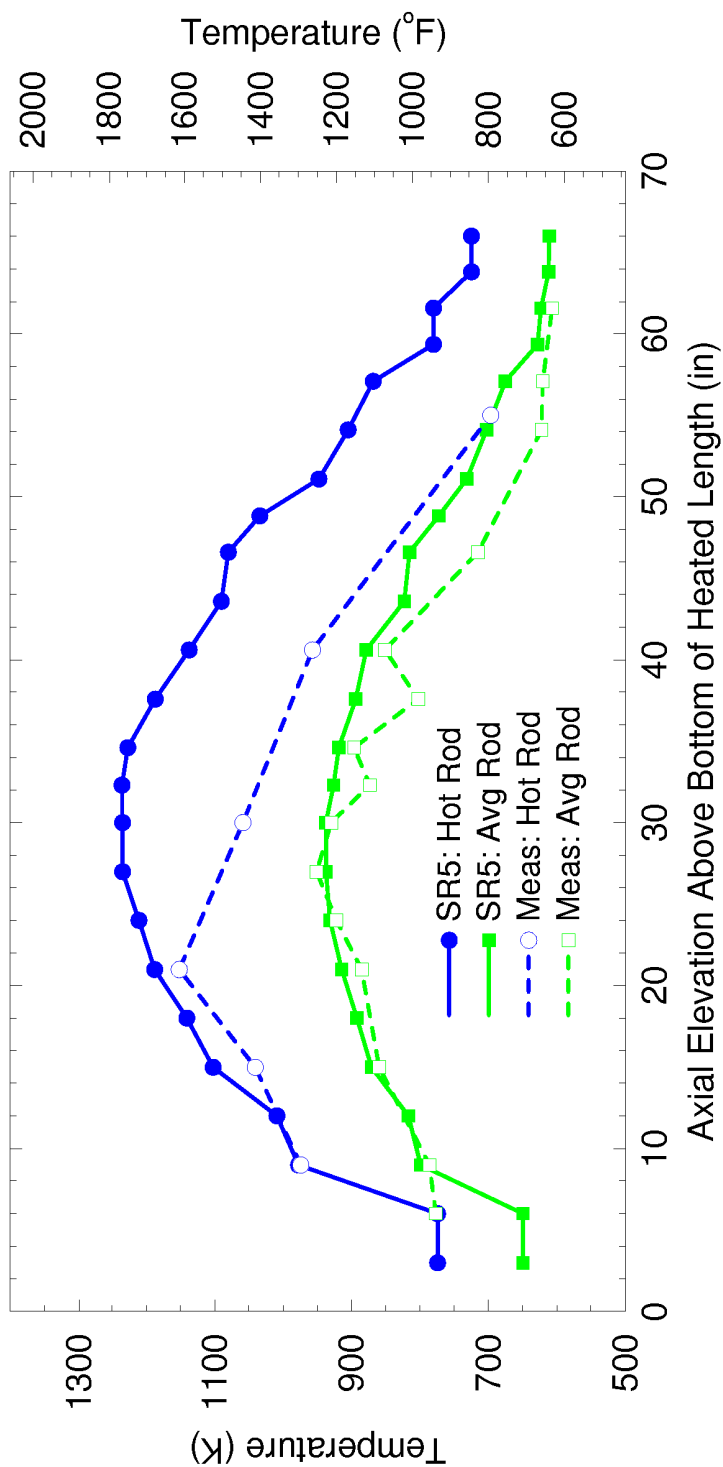
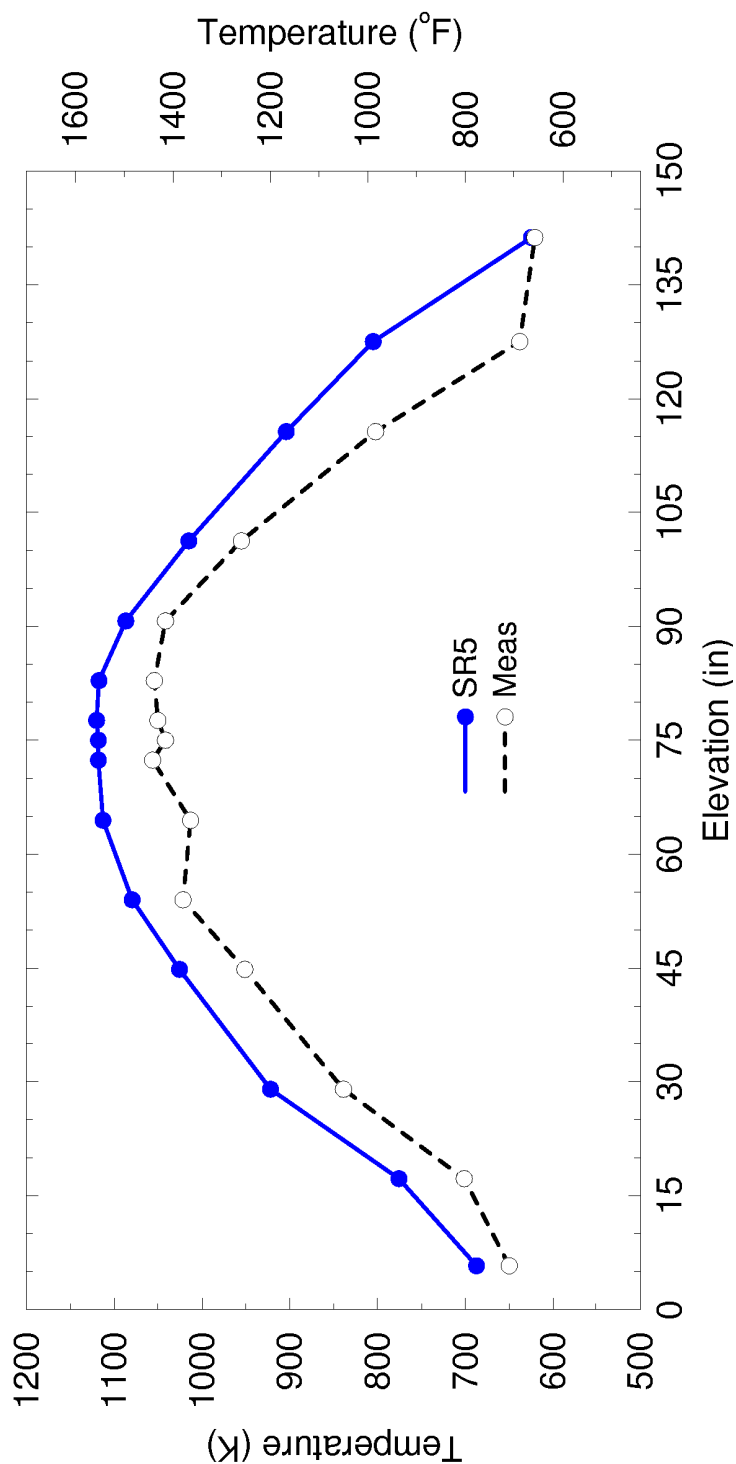


Figure 4.161: Assessment of Semiscale LBLOCA Test S-06-3, PCTs





**Figure 4.162: Assessment of Semiscale LBLOCA Test S-07-1,  
PCTs versus Elevation**

#### 4.3.3 Methodology Treatment of PIRT Phenomena

Sections 4.3.1 and 4.3.2 reviewed the extensive assessment of the S-RELAP5 code with regard to its capability to predict the important phenomena identified in the LBLOCA PIRT. In some cases statistical information was determined with regard to the mean values and uncertainties for predicting a specific phenomenon. Much of this information is also contained in Section 5 of Reference 5. In other cases, S-RELAP5 was shown to calculate the phenomenon conservatively and no evaluation of a bias or uncertainty was performed. In these situations, the conservatism associated with these phenomena was simply accepted as unquantified conservatism in the methodology. Table 4.21 summarizes the important PIRT phenomena and how those phenomena are being addressed in the methodology.

##### 4.3.3.1 Important PIRT Phenomena Not Treated Statistically

From the comparison of the S-RELAP5 predictions and data for both the SET and IET assessments, a number of important PIRT phenomena were found to be predicted conservatively by the code. The conservative predictions were either because of a conservative model in S-RELAP5 or the use of conservative input. These phenomena are indicated in Table 4.21 as being treated in the methodology as an "inherent conservatism" or an "input conservatism." By "inherent conservatism," it is meant that a code model or combination of models was demonstrated to conservatively predict these phenomena. By "input conservatism," it is meant that the input being provided to the code was demonstrated to be conservative and will be used in NPP analyses. These conservatisms are accepted in the methodology as an unquantified conservatism above that indicated by the statistical analysis. These phenomena are discussed individually in the following sections.

##### 4.3.3.1.1 Core Multi-Dimensional Flow and Void Distributions

The core flow distribution and void distribution are determined by the initial power distributions and [

] In

effect this will result in a wide variation of calculated flow and void distributions in the core.

The ability of S-RELAP5 to calculate void distributions has been demonstrated in the SET assessments performed for the THTF Level Swell, the GE Level Swell, the FRIGG-2, the FLECHT-SEASET and the FLECHT Skewed tests. For all these assessments, the agreement between code prediction and measured void fractions was good to excellent (Section 4.3.1 and Reference 5). The THTF and FRIGG-2 tests are high pressure tests and the GE Level Swell test is a transient depressurization test from high pressure. The FLECHT-SEASET and FLECHT Skewed test facilities are instrumented to measure  $\Delta P$ s in the bundle at 12 inch intervals. At low flow conditions, which typically occur during the reflood phase of a LOCA, the  $\Delta P$ s directly give the void distribution in the bundle. The assessments of several FLECHT-SEASET and FLECHT Skewed tests, discussed in Section 4.3.1 and in Reference 5, show the code calculated  $\Delta P$ s agree with the data reasonably well. These assessments indicate S-RELAP5 is capable of calculating acceptable void distributions in the core at high and low pressure conditions.

The FLECHT-SEASET tests were also used to calculate the heat transfer biases and uncertainties. The prediction of flow and void distributions is an integral part of determining the code heat transfer biases and uncertainties. [

]

The ability of S-RELAP5 to calculate flow distributions in the core was demonstrated in the SET assessments (Section 4.3.1 and Reference 5) performed for the multi-dimensional flow tests, CCTF, and SCTF. The multi-dimensional flow tests demonstrated S-RELAP5 was capable of modeling and predicting the measured flows in these tests. The SCTF tests were conducted specifically to study the two-dimensional flow behavior in the core region during the reflood phase of the LOCA. The overall bundle  $\Delta P$ s and PCTs are good indications of the core flow distribution. The assessments of several of the SCTF tests show that S-RELAP5 calculated hot bundle  $\Delta P$ s and PCTs agree with the data reasonably well. In addition, the calculated void fraction in the upper region of the hot bundle is somewhat higher than the data. These assessments demonstrated that the combined code and core nodalization was capable of predicting the effects of changes in radial power distribution and associated flows during the reflood period of a LBLOCA.

The CCTF assessments further demonstrated that the combined code and core nodalization were able to predict the core flows, hot bundle  $\Delta P$ s, and resulting PCTs in a cylindrical facility. The cylindrical bundle region modeling used is consistent with the input modeling used in the methodology NPP nodalization.

Based on the information in the previous paragraph, the combination of these assessments clearly demonstrates S-RELAP5 is capable of realistically predicting the core flows and void distributions as the statistical parameters are being varied in the statistical analysis of a LBLOCA.

#### 4.3.3.1.2 Liquid Entrainment in the Core

The liquid entrainment in the core has been demonstrated to be conservatively calculated by S-RELAP5 and the methodology nodalization. This is shown in the assessments performed for CCTF, UPTF, and FLECHT-SEASET, and reported in Section 5.6 of Reference 5. In the CCTF tests examined (Tests 54, 62, 67, and 68), the conclusion was that the liquid entrained from the core into the upper plenum was overpredicted by S-RELAP5 during the early part of the test. This overprediction occurred until about 400 to 500 seconds into the test. After that, the code underpredicted the amount of liquid in the upper plenum. Only after quenching occurred in the test did the data indicate higher levels. Both the measured and calculated time of PCT occurred before the calculation began to underpredict the liquid in the upper plenum.

For the FLECHT-SEASET tests, as shown in Figures 3.3.89 through 3.3.97 in Reference 5, the mass of water in the test section is underpredicted by S-RELAP5 and the methodology nodalization. This is consistent with the results provided in Figures 3.3.98 through 3.3.103 in Reference 5, which show that S-RELAP5 is overpredicting the water carryover from the test assembly.

In conclusion, S-RELAP5 predicted liquid carryout from the core to the upper plenum was examined in three different test facilities. In all three test facilities, the amount of liquid carryout of the core into the upper plenum was overpredicted. Given these results from three different test facilities, it is concluded that the code and methodology prediction of core entrainment is conservative and no bias or uncertainty was developed to take credit for this conservatism.

#### 4.3.3.1.3 Core Flow Reversal/Stagnation

The reversal and stagnation of flow in the core is the result of the size of the break and the rate of coolant loss versus the rate of coolant injection from the ECC systems. Generally, a combination of other phenomena occur to determine the limiting set of conditions that result in the worse situation where the flow in the core is essentially stagnant or has a low reflood rate for the longest period of time. This condition is addressed by the random variation of the other dominant phenomena. [

]

#### 4.3.3.1.4 Upper Plenum Liquid Entrainment/Deentrainment

When liquid droplets are entrained in the core and carried up into the upper plenum, they can remain there, fall back into the core (deentrainment), or be carried out into the hot leg (entrainment). The major modeling concern for a LBLOCA is that allowing too much liquid to fall back into the core would result in a top-down quench and a significant underprediction of the PCT. It would also reduce steam binding. Several SCTF, CCTF, and UPTF tests were used to demonstrate S-RELAP5 will carry over an acceptable amount of liquid to the steam generator tube region, thus limiting the liquid accumulation in the upper plenum to an acceptable amount.

Several input options were developed to make sure S-RELAP5 will entrain an acceptable amount of liquid to the steam generator tube region during the reflood phase of a LOCA in a PWR plant. The simulation of UPTF Test 10, Run 080 and Test 12, Run 014, demonstrate that by using a Kutateladze-type CCFL correlation, S-RELAP5 will conservatively calculate liquid down flow from the upper plenum. A Wallis-type CCFL correlation developed by MPR using UPTF Test 11 is applied at the hot leg-to-steam generator inlet plenum junction to limit the liquid drain back to the upper plenum. UPTF Test 10, Run 081 and Test 29, Runs 211 and 212, were simulated to develop upper plenum, hot leg, and steam generator inlet plenum input options to ensure acceptable liquid entrainment to the tube region. These benchmarks are discussed in Section 4.3.1.11.

In the simulation of several CCTF and SCTF tests, all the above discussed input options were used. The SCTF hot leg geometry is atypical due to the inside geometry being elliptical. The height (major axis) of the hot leg is close to the inside diameter of a typical 4-loop PWR. In order to preserve the volume flow area scaling of a 4-loop PWR, the width (minor axis) of the hot leg is very narrow. In the S-RELAP5 model, the oval geometry is approximated by a circular pipe while preserving the total volume flow area. In SCTF there is no active steam generator; a steam-water separator is used to simulate the primary side of the steam generator. The inlet chamber represents the inlet plenum of four scaled steam generators. The outlet chamber collects the liquid entrained from the inlet chamber. In the tests, the liquid level in the outlet chamber is measured. This collected liquid represents the liquid entrained in the tube region during a LOCA in a scaled PWR. Six SCTF Core-II tests were simulated using S-RELAP5. The results are summarized in Section 4.3.1.13 and discussed in detail in Section 3.10 of Reference 5. The measured and S-RELAP5 calculated liquid levels for the two gravity feed (Tests S2-AC1 and S2-SH1) and four forced feed tests (S2-10, S2-11, S2-17, and S2-18) are shown in Figure 4.128 through Figure 4.133. Considering the atypicality of the SCTF hot leg and the approximation used in modeling the hot leg in the S-RELAP5 input model, the calculated liquid entrainment to the steam-water separator is considered acceptable.

Four CCTF tests (Tests 54, 62, 67, and 68) were simulated using S-RELAP5. CCTF has active scaled steam generators. Therefore, the tests realistically simulate the entrainment process and droplet evaporation in the tube region. However, there is little information available to make a direct comparison between measured and calculated liquid entrained to the tube region. In CCTF, the pump side break is connected to a containment tank (Containment Tank II), which has a liquid separator at the top. This separator traps all liquid exiting the broken loop steam generator side of the break. With the assumption that the calculated droplet evaporation in the tube region is comparable to the data, a comparison between the measured and calculated liquid collected in Containment Tank II provides a reasonable comparison to the measured and calculated liquid entrainment to the tube region of the broken loop steam generator. The results are summarized in Section 4.3.1.12 and discussed in detail in Section 3.11 of Reference 5.

S-RELAP5 calculated and measured Containment Tank II levels for the four tests are shown in Figure 4.98 through Figure 4.101. Considering the differences in the broken loop steam generator tube region heat transfer between the test and the S-RELAP5 prediction, the uncertainty in the extent to which the piping is adiabatic (as it is modeled in S-RELAP5), and the

uncertainty in the dimensions of Containment Tank II (dimensioned drawings were not available at the time of the analysis), the S-RELAP5 calculated entrainment rate to the tube region is considered acceptable.

In summary, several input options are developed to make sure an acceptable amount of liquid is entrained into the upper plenum and carried over to the steam generator tube region during the reflood phase of a LOCA in a PWR. This approach will also limit the liquid accumulation in the upper plenum to an acceptable level during the reflood phase of a LOCA.

#### 4.3.3.1.5 Countercurrent Flow Limit

The CCFL correlations with specific CCFL parameters are applied [

]

These models are applied in all the appropriate benchmarks and are used in the plant models.

Therefore, the conservative set of parameters used in the assessments is also used in the NPP analysis so that the CSAU requirement that the assessments use the same model as the NPP analysis is satisfied.

#### 4.3.3.1.6 Hot Leg Entrainment/Deentrainment

As discussed in Section 4.3.3.1.4, several input options are developed to make sure an acceptable amount of liquid is entrained into the upper plenum and carried over to the steam generator tube region during the reflood phase of a LOCA in a PWR. This approach also limits liquid accumulation in the hot leg to an acceptable level during the reflood phase.

#### 4.3.3.1.7 Two-Phase Pump Degradation

Two-phase pump degradation is addressed in the methodology as a best-estimate input. Based on the sensitivity study described in Reference 6 for a limiting break on both a 3-loop and a 4-loop plant, it is shown that two-phase pump degradation is not an important phenomenon for the limiting LBLOCA case. The use of the Semiscale two-phase degradation model, instead of the CE/EPRI two-phase degradation model, produced essentially no impact on the 3-loop

results and only an 18 °F (10 K) change in PCT for the 4-loop plant. Therefore, the best-estimate CE/EPRI model is used in the RLBLOCA methodology.

#### 4.3.3.1.8 Pump Differential Pressure Loss

The pump differential pressure loss is addressed in the methodology strictly as a best-estimate model. The S-RELAP5 code has the ability to input the pump-specific homologous curves for the NPP being analyzed and this option is used. The homologous curves for the specific NPP pumps are obtained from the utility and, if plant data are available, a pump coast down benchmark is performed to ensure the behavior is consistent with plant data.

#### 4.3.3.1.9 Noncondensable Transport

The treatment of noncondensibles in the S-RELAP5 code was demonstrated to be conservative through the assessment of the ACHILLES ISP 25. The rod thermocouples in the test all clearly showed a reduction in temperature following the introduction of nitrogen into the system. The S-RELAP5 code conservatively underpredicted this cooldown, as shown in Figure 4.141 through Figure 4.146. Figure 4.147 shows the calculated increase in system pressure is lower than the data, which also potentially reduces the core cooling because of the effect of system pressure on steam binding. Thus, the impact of the nitrogen injection following the accumulator emptying of water will be conservatively predicted in the NPP analysis.

#### 4.3.3.1.10 Downcomer Entrainment

The S-RELAP5 code prediction of the ECC bypass during the refill phase of a LOCA was demonstrated to be conservative through the assessment of UPTF Tests 6 and 7 (Section 4.3.1.11.1 and Reference 5). In addition, a CCFL correlation developed by MPR Associates is used in the sample plant cases given in Appendix B to demonstrate S-RELAP5 conservatively calculates the bottom of core recovery (or beginning of core reflood) time. The MPR correlation is described in Section 4.4.2.2.7. Acceptable downcomer entrainment during the reflood phase was demonstrated for the CCTF benchmarks discussed in Section 4.3.1.12 and also in Reference 5.

Based on these results, it is concluded that S-RELAP5 will appropriately calculate the ECC bypass, the core recovery time, and will calculate realistic downcomer entrainment during the



reflood phase of a LBLOCA in PWRs where the ECCS delivery to the reactor vessel is not limited to locations adjacent to the broken cold leg.

#### 4.3.3.1.11 Downcomer Liquid Level Oscillations

Downcomer liquid level oscillation is another phenomenon that is controlled primarily by other important phenomena such as steam-ECC water mixing in the cold legs. A special cold leg condensation model (summarized in Section 4.3.3.1.14 and discussed in detail in Section 5.2 of Reference 5) was developed using UPTF Test 8, UPTF Test 25, and the EPRI 1/3-scaled tests. The cold leg condensation model is used in all the benchmarks discussed in Sections 4.3.1 and 4.3.2 where there is ECC injection into the cold legs. The simulation results for UPTF Test 8, discussed in Section 4.3.1.11.2, shows S-RELAP5 predicted the observed flow regimes reasonably well which indicates the code is capable of calculating the appropriate phenomena associated with steam-ECC mixing in the cold leg in the plant. However, since the complete UPTF primary system was not modeled using S-RELAP5, the system oscillations were not calculated by the code. The CCTF, SCTF and LOFT benchmarks (Sections 4.3.1.12, 4.3.1.13, 4.3.2.1, respectively) compared the calculated and measured differential pressures. These results show the code calculated acceptable oscillations during the refill and reflood phases of the transients.

In summary, from the simulation of the above tests, it can be concluded S-RELAP5 will calculate the acceptable primary system and downcomer oscillations during a LBLOCA in a PWR.

#### 4.3.3.1.12 Lower Plenum Sweepout

The conservatism of the S-RELAP5 lower plenum sweepout is demonstrated in the essentially full-scale UPTF Test 6 and 7 assessments. Again, these tests were performed with a constant ECC injection rate and with various steam flow rates up the downcomer. The measured versus code prediction of the lower plenum level is provided in Figure 4.63 through Figure 4.67 for Test 6 and Figure 4.68 for Test 7.

The large sweepout events predicted in the UPTF Test 6 and 7 assessments, but not seen in the measured data, are a direct result of the 1-D nodalization used in the lower plenum to simulate a highly multi-dimensional flow phenomenon during the refill phase.

#### 4.3.3.1.13 Steam Binding

Steam generator liquid entrainment was examined in the code assessments for CCTF and UPTF. As discussed in Section 4.3.3.1.4 and Section 4.3.3.1.6, several input options are developed using UPTF 10B and 29B (Section 4.3.1.11.3) to assure an acceptable amount of liquid is entrained into the upper plenum and carried over into the steam generator tube region during the reflood phase of a LBLOCA. One of the input options is the interphase drag bias which is applied at the tube inlet junctions. These input options are used in the SCTF and CCTF tests assessments. From the tests assessments, it can be concluded that S-RELAP5 entrains an acceptable amount of liquid into the steam generator tube region during the reflood phase of a LBLOCA.

#### 4.3.3.1.14 Cold Leg Condensation

A cold leg condensation model was developed using several Westinghouse/EPRI 1/3-scaled Tests, UPTF Test 8 (Phase A, Run 111 and Phase B, Run 112) and Test 25, to calculate a proper cold leg condensation rate during the accumulator and pumped injection period. The tests selected for this development generally cover both periods and the input models used are similar to those used in the benchmarks discussed in Section 4.3.1. The condensation model consists of biases (multipliers) on the liquid and vapor side heat transfer coefficients that determine the condensation due to steam–water mixing. The condensation model is described in detail in Section 5.2 of Reference 5. A summary of the model is described below.

During cold leg condensation, due to ECC mixing with steam in the cold leg, the vapor side heat transfer primarily affects desuperheating of the steam. It was determined that [

]. The condensation is primarily determined by the liquid side heat transfer and a void dependent multiplier, CONMAS, as shown in Figure 4.163. CONMAS is used to calculate the liquid temperature as it enters the downcomer. The ECC injection node void fraction is used to determine the value of CONMAS. It is applied to the intact cold leg piping, from the pump discharge location to the downcomer, and to the pump discharge side of the broken cold leg. In addition, since the flow regime in the ECC injection location is highly complex, the non-stratified flow regime option is selected in the ECC injection node. During the accumulator injection period, the flow regime in the cold leg piping downstream from the injection location is generally slug (plug) flow and the void fraction is generally below 50 percent. During the pumped injection

period, especially with the consideration of a single failure, the steam energy available will generally exceed the ECC condensation potential, the flow regime in the cold leg will generally be stratified and the void fraction is high (80 to 95 percent). During this period, the liquid side heat transfer [

] With these input options, S-RELAP5 is found to calculate acceptable cold leg condensation for the selected UPTF and EPRI tests. These results are discussed in detail in Section 5.2 of Reference 5.

Additional EPRI tests were simulated using S-RELAP5 and the results are discussed in Section 4.3.1.9. These input modeling options are used in all the benchmarks discussed in Section 4.3 where there is cold leg ECC injection and are summarized in Table 4.25. This option will be used to model cold leg condensation in plant application cases.

In summary, S-RELAP5 calculates acceptable cold leg condensation during both the accumulator and pumped injection periods of a LBLOCA in a PWR.

#### 4.3.3.1.15 Fuel Rod, Stored Energy, Gap Conductivity

The gap conductivity from the fuel performance code (COPERNIC2 or RODEX3A) under the fuel and system conditions calculated by S-RELAP5 is used throughout the transient evaluation. The fuel codes are considered best-estimate solutions to the thermal performance of the fuel rods. They were benchmarked against experimental data, Reference 5, to determine any appropriate bias and uncertainty. Uncertainty in the prediction of gap conductivity is accounted for by the adjustment of the thermal conductivity of the fuel pellet. This adjustment is comprised of a burnup dependent bias and a sampled uncertainty, implemented at the beginning of the steady-state initialization for each case calculation and maintained throughout the transient. The adjustment controls the primary factor of the initial energy within the fuel pellet and also responds to the ability to transport energy to the coolant during the transient. As such, the approach is considered acceptable for a best-estimate methodology and no further assessment is required.

#### 4.3.3.1.16 Fuel Rod, Stored Energy, Axial and Radial Peaking

The axial and radial peaking is set conservatively for each case of the sample set. Radial peaking for the hot assembly and hot rod is set in accordance with plant technical specification maximums. Axial peaking is sampled, with a flat distribution, between that expected at normal operation for the hot rod and that which would provide a peak local heating rate equal to the  $F_q$  limit for the plant at the case burnup. The local power peak is a dominant factor in determining cladding temperature and oxidation responses. Off normal values for the local power result from plant maneuvering; they are time wise random occurrences and are rare. Thus, a realistic probability distribution would be exponential in nature and the assumed flat distribution used in the RLBLOCA methodology is conservative. No further assessment is required.

#### 4.3.3.1.17 Fuel Rod, Decay Heat, Ballooning, Rupture and Post-Rupture Fuel Relocation

Decay heat, post-shutdown specific energy generation, is treated statistically in the RLBLOCA evaluation model and discussed in Section 4.3.3.2.3. This section documents the treatment of the potential for an increase in cladding heat load due to possible clad ballooning and rupture followed by fuel relocation. The phenomenon is referred to as fuel relocation and the scenario proceeds as: during a LOCA, fuel pins are placed under a condition of stress tending to strain the cladding outward away from the fuel pellet; at relatively moderate LOCA cladding temperatures, 1500 to 1700 °F, the clad will balloon outward and rupture; cracked pellet material from the region just above the ballooned region may separate from the pellet and fall into the cup of the ballooned region; the heat load on the cladding at this location is now increased because more heat producing material is located there.

The importance, or effect, of fuel relocation is dependant on when it occurs during the accident. Provided there is a reasonably constant supply of coolant at qualities somewhat below 1.0, cooling mechanisms are induced by ballooning and rupture that act to decrease the cladding temperature below that experienced at unruptured locations on the fuel rod. However, if the flow should degrade to steam only for a period of more than several seconds, some of these cooling mechanisms will become ineffective and a rapid clad temperature excursion may occur. During reflood, core flow is upward, relatively constant, and forced by significant driving heads. This results in continuous coolant conditions conducive to providing effective cooling for the ballooned and ruptured locations. Prior to the reflood phase, during blowdown and refill, the core flow is erratic—changing from upward to downward and possibly stagnating—and periods

of steam only coolant can not be prevented with any assurance. The occurrence of ballooning and rupture during the blowdown and refill phases may lead to uncontrollable cladding temperature excursions. Thus, if that condition is to be allowed, an explicit modeling of clad ballooning, rupture and fuel relocation must be provided to assure that the condition can be controlled.

#### Pre-Reflood Clad Ballooning and Rupture

[

]

#### Reflood Clad Ballooning and Rupture

[

]

Support for this position is provided by consideration of the phenomena involved, analysis of the effects, and experimental results. The impact of rupture and ballooning on clad cooling occurs through several rupture or ballooning-induced cooling mechanisms and three detrimental heating effects:

Cooling effects:

1. Increased heat transfer surface area at the ballooned elevation
2. Increased velocities within the ballooned and ruptured regions

3. Increased turbulence within the ballooned and ruptured regions
4. Droplet shattering resulting in increased interphase heat transfer and steam desuperheating
5. Decrease in gap heat transfer if the fuel does not strongly relocate
6. Decrease in pellet thermal conductivity if the fuel relocates
7. Potential formation of local quench-fronts in ballooned and ruptured regions

Heating effects:

8. Diversion of flow around ballooned and ruptured regions
9. Cladding heat load increased due to fuel relocation
10. Cladding heat load increased due to interior oxidation

Experience with Appendix K methodologies has shown that the aggregate of these effects acts to decrease the cladding temperatures when no fuel relocation occurs. This was demonstrated in Appendix B, Section B.2 of Revision 0 (Reference 6) and the response to RAI 28 on Revision 0 (page 79 of Amendment 1 to Reference 6) with sensitivity studies on both 3- and 4-loop PWRs with 15x15 and 17x17 fuel designs. The studies included increased heat transfer surface area, increased local coolant velocities, a decrease in gap heat transfer, flow diversion, and interior cladding oxidation. The effects of increased turbulence, droplet shattering, and potential local quenching were not included within the modeling. Decrease in pellet thermal conductivity and a clad heat load increase were not included because these studies did not address fuel relocation. Even without half of the cooling mechanisms, the cladding temperatures and local oxidations were reduced when reasonable accounting for the cooling mechanisms was made. This effect has also been observed in the Flooding Experiments with Blocked Arrays (FEBA) and FLECHT test series.

Under a condition of fuel relocation, wherein the fuel above the ballooned region drops into the ballooned region, it has been postulated that increased decay heat generation will lead to an increase in cladding heat flux resulting in higher cladding temperatures. Various presentations (Reference 69 Articles 1 and 12, for example) purport to show the effect. However, these studies have uniformly incorporated extreme assumptions on the conditions of relocation and the resultant heat transfer processes. Few include provisions for rupture-induced cooling mechanisms. Most assume that the cladding expands circularly without being encumbered by the remainder of the fuel assembly. In fact, a free expansion of the fuel rod is only possible up to pin strains in the mid-30 percents, for higher strains the local gap volume no longer increases

faster than the clad surface area. Finally, the packing factor of the rubble filling the ballooned region is overpredicted. If reasonable, yet conservative, assumptions had been made, the results would lead to the expectation that fuel relocation, which is real, does not pose a condition by which the ruptured or ballooned regions will exceed the consequence of the non-ballooned regions of the hot pin.

This was observed experimentally in the KfK experiments as reported in RAI 131 on Revision 0 (page 120 of Amendment 1 to Reference 6). In the KfK in Pile Tests, fuel relocation into the ballooned area of the fuel rod occurred, but did not adversely affect the subsequent clad temperature behavior. To determine when the fuel relocates, two tests were performed with thermocouples located at the top of the pellet stack. One test comprised low burnup fuel which maintained its pellet geometry after rupture. The other test was of higher burnup fuel which relocated. The traces from the upper thermocouples, for the test that relocated, showed the temperature at the top of the pellet stack displayed a significant drop at the time of fuel rod rupture. For this test, following the rupture, the heatup rate at the rupture elevation was reduced relative to the heatup rate prior to the rupture. This reduction in heatup rate would indicate that the PCT at the time of turnover would be less than would be reached if rupture had not occurred, even with the increase in localized decay heat from the pellet rubble residing at the ruptured region. Thus, the KfK experiments demonstrate that analyses which ignore the beneficial effects of swelling and rupture provide unduly high clad temperature estimates for the ruptured region during reflood, even when fuel relocation occurs.

## Conclusions

The RLBLOCA evaluation model does not incorporate a clad ballooning, rupture and fuel relocation model. To support this modeling, the cladding temperature and pin stress evolution for individual cases in the case set will be assessed against rupture criteria appropriate for the cladding being evaluated. [

] when comparing it to the 10 CFR 50.46 criterion.

#### 4.3.3.1.18 Downcomer, Flow Pattern, CCFL, Slug Flow, and Non-Equilibrium

The downcomer LBLOCA phenomena of multidimensional flow patterns, CCFL and non-equilibrium flow primarily affect the refill period by influencing the duration of ECCS bypass.

UPTF Test 6 (Runs 131, 132, 133, 135, and 136) and Test 7 (Run 203) were designed specifically to examine downcomer countercurrent flow behavior during blowdown, ECC bypass, and lower plenum refill with cold leg ECC injection. The ECC injection is activated in a PWR during the end-of-blowdown and refill phases of a cold leg break LBLOCA transient. These interactions play a key role in determining the rate at which ECC water is able to refill the lower plenum.

The tests were analyzed to demonstrate the ability of S-RELAP5 to self-limit countercurrent flow in the downcomer and predict reasonable refill behavior including ECC bypass compared to experimental data. For these runs, the UPTF system was configured to simulate the late blowdown and refill phases of a cold leg break PWR LBLOCA. These tests all were initiated with no water inventory in the lower plenum. Steam injected in the core region traveled downward to the lower plenum, and then exited the vessel via the downcomer and broken cold leg. An identical pattern of ECC injection was used for all the runs analyzed, with a constant injection rate into each of the three intact cold legs. A wide range of steam flow rates was used for the various runs and, depending on the downcomer steam flow rate, the ECC water entering the downcomer either bypassed to the broken cold leg or penetrated downward to fill the lower plenum.

The following general observations regarding UPTF Tests 6 and 7 were found to be true of both the experiments and their corresponding S-RELAP5 simulations.

- Little water was delivered to the downcomer and lower plenum during the period that the intact cold legs were filling with ECC water. Only after the cold legs were filled did a significant amount of ECC penetration to the downcomer and lower plenum begin.
- When ECC penetration to the lower plenum did occur, the rate of that penetration tended to vary inversely with the rate of steam flow in the downcomer.
- During the period of ECC penetration, ECC water from the two cold legs opposite the broken cold leg tended to penetrate directly downward to the lower plenum. ECC water



from the cold leg immediately adjacent to the broken cold leg tended to be bypassed to the broken cold leg.

- Highly unstable flow conditions were observed in the downcomer during the entire period of ECC injection.

The specific LBLOCA refill phenomena addressed by the analyses of Tests 6 and 7 include the following:

- Downcomer multi-dimensional effects - Both calculated steam flow and calculated ECC water flow are shown to distribute themselves azimuthally in multidimensional patterns that were consistent with test results.
- Downcomer countercurrent and slug flow - The various runs were performed with a wide range of downcomer steam flow rates and with two-phase flow conditions including countercurrent and slug flow. In all cases, the code was demonstrated to conservatively (adequate to reasonable agreement with data) predict downcomer penetration of ECC water with the RLBLOCA lower plenum plant nodalization.
- Downcomer condensation and non-equilibrium flow - The various runs were performed with a wide range of ECC subcoolings (and downcomer condensation rates) and in all cases, the code was demonstrated to conservatively predict downcomer penetration of ECC water with the RLBLOCA plant lower plenum nodalization.

In summary, from the simulation results of UPTF Tests 6 and 7, it can be concluded that S-RELAP5 will conservatively calculate lower plenum sweep-out, lower plenum refill, and ECC bypass rates. This results in a conservative beginning of core recovery time during LBLOCA in a PWR. S-RELAP5 also calculates acceptable downcomer condensation rates due to steam-ECC water interaction.

#### 4.3.3.1.19 Downcomer, Multi-D Phenomena

As discussed in the previous section, simulations of UPTF Tests 6 and 7 were used in part to verify the refill and ECC bypass flow behavior compared to experimental data. The comparisons showed that the multidimensional flow patterns of both steam and ECC liquid were consistent with test results. This indicates that the multidimensional phenomena in the downcomer are being properly included in the methodology.

#### 4.3.3.1.20 Downcomer, Downcomer Boiling, Noding

Although boiling in the downcomer occurs during blowdown, the biggest potential for impact on clad temperatures is during late reflood following the end of accumulator injection. The impact of downcomer boiling is primarily dependent on the wall heat release rate and on the ability to slip steam up the downcomer and out of the break. The higher the downcomer wall heat release, the more steam is generated within the downcomer and the larger the impact on core reflooding. Similarly, the quicker the passage of steam up the downcomer, the less resident volume within the downcomer is occupied by steam and the lower the impact on the downcomer average density. Therefore, the ability to properly simulate downcomer boiling depends on both the heat release (boiling) model and on the ability to track steam rising through the downcomer.

The S-RELAP5 heat release modeling was validated by a sensitivity study on wall mesh point spacing and a benchmark against a closed form solution (see Figure 4.166). Steam tracking was validated through both an axial and an azimuthal fluid control volume sensitivity study done at low pressures. The axial noding study was based on an ice condenser plant that is near atmospheric pressure during reflood. These studies demonstrated that S-RELAP5 delivers energy to the downcomer liquid volumes at an appropriate rate and that the downcomer noding detail is sufficient to track the distribution of any steam formed. The results indicated that the modeling accuracy within the RLBLOCA methodology is sufficient to resolve the effects of downcomer boiling and that, to the extent that boiling occurs, the methodology properly resolves the impact on the cladding temperature and cladding oxidation rates. Thus, the required methodology for the prediction of downcomer boiling at system pressures approximating those achieved in plants with pressures as low as ice condenser containments was demonstrated.

#### 4.3.3.1.21 Loop, Flow Oscillation

Loop flow oscillations arise when steam in the cold leg (post-blowdown) is condensed by cold ECC water and forms a liquid plug. The flow rate decreases and the cold leg flow transitions to the stratified flow regime, allowing the steam flow to increase again. This sweeps the liquid out again.

UPTF Test 8 was used to verify the S-RELAP5 cold leg condensation model. The model is applied to the ECC injection node and all downstream nodes in the intact loop cold legs. This

includes the selection of the non-stratified option in the ECC injection nodes. The cold leg condensation model is summarized in Section 4.3.3.1.14.

The primary results from the comparisons of S-RELAP5 to the UPTF data for Test 8 Run 111 and Run 112 are:

- The primary objective of the test simulation was to validate the adequacy of the prediction of the water temperature entering the downcomer, due to its effect on downcomer boiling during the post-accumulator injection period of a postulated LBLOCA. S-RELAP5 correctly predicted the cold leg liquid temperature for both runs.
- The S-RELAP5 calculated flow regimes are in general agreement with the thermocouple data from the tests.

In summary, it can be concluded that the S-RELAP5 cold leg condensation model correctly calculates the temperature of the water entering the downcomer during the reflood phase of a postulated LBLOCA. This will result in realistic calculation of loop flow oscillations.

**Table 4.21: Methodology Treatment of Important PIRT Phenomena**

--	--

A large, empty rectangular frame with a thin black border, intended for a drawing or image. The frame is centered on the page and occupies most of the available space. It is a simple black rectangle with no internal markings or text.

[illegible]



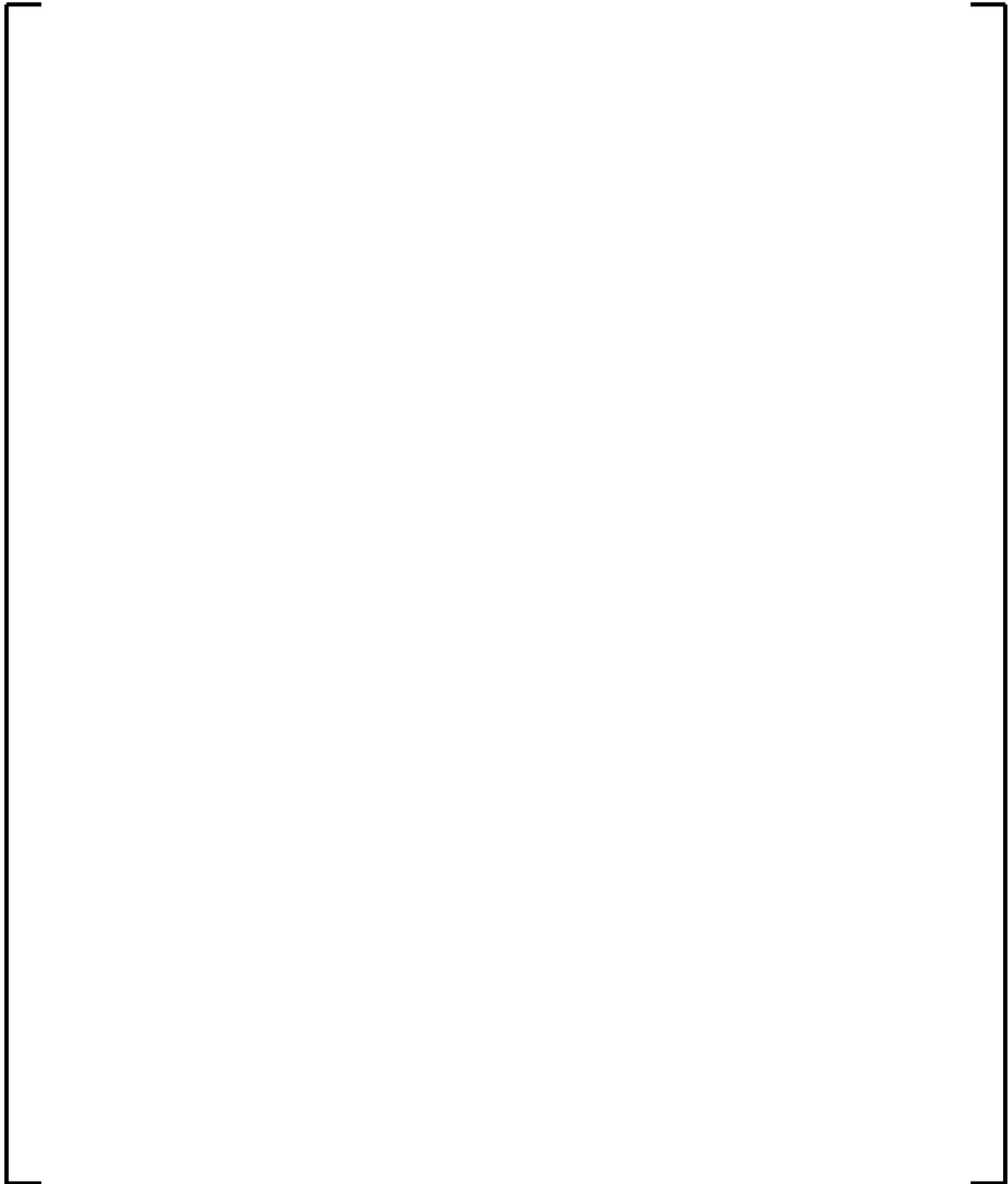


**Figure 4.163: CONMAS Multiplier as a Function of Cold Leg Void Fraction**



#### 4.3.3.2 Important PIRT Phenomena Treated Statistically

A summary, giving the parameter bias and uncertainty, and how they are to be applied in the methodology, is provided in this section. The determination of code or physical phenomena uncertainties is presented in Section 5 of Reference 5. Other parameters treated statistically are discussed in detail, including background information, justification of the statistical approach and explanation of the objective of the statistical treatment.

Table 4.22 presents a summary of the key parameters treated statistically in the AREVA RLBLOCA methodology. The table lists the biases and provides a description of the statistical treatment of uncertainty for each key parameter.

##### 4.3.3.2.1 Stored Energy

Revision 2 of the RLBLOCA methodology incorporates both RODEX3A and COPENIC2 (References 9 and 10, respectively) as fuel performance codes from which the initial fuel conditions and the fuel thermal mechanical correlations are determined. These codes are used for Uranium oxide fuel pellets with and without Gadolinia. COPENIC2 will be used for fuel with M5® cladding, which comprises the vast majority of the applications of this methodology. In cases requiring an evaluation of Zircaloy cladding, the RODEX3A code will be applied.

The analysis of stored energy uncertainty was performed in Section 5.8 and 5.9 of Reference 5 by assessing COPENIC2 and RODEX3A predictions for centerline fuel temperature relative to data (see data discussions in References 7, 8, 9, and 10). The assessment for each code was established as a bias and an uncertainty in the form of the difference of measured and predicted temperatures ratioed to the predicted temperatures. For the development in Reference 5, the form was:

$$\frac{(T_{\text{Predicted}} - T_{\text{Measured}})}{T_{\text{Predicted}}}.$$

This gives an adjustment proportional to the magnitude of the predicted centerline fuel temperature and is easy to apply within a code structure. The  $(T_{\text{Predicted}} - T_{\text{Measured}})$  means the negative of the adjustment is provided.

## COPERNIC2

COPERNIC2 is an NRC-approved current generation fuel performance code. The assessment database used to develop the bias and uncertainty for the RLBLOCA methodology was that incorporated in the code approval. The approval resulted in the assignment of a zero bias and, for deterministic evaluations, a 71 C increase in the centerline fuel temperature to achieve a 95/95 prediction. This adjustment is an absolute and not dependent on the magnitude of the prediction. For RLBLOCA, it is replaced with a proportional adjustment of the form

$$(T_{\text{Predicted}} - T_{\text{Measured}}) / T_{\text{Predicted}} \cdot [$$

]

In line with the realistic treatment of uncertainty, the adjustment is sampled separately for each member analysis of the case set and is sampled as both a positive and a negative adjustment. Figure 4.164 gives the uncertainty used in the methodology as a cumulative distribution in comparison to the actual cumulative distribution of the benchmarked database. Within the range of negative adjustments to temperature, the adjustment is somewhat less than the data would justify making the methodology slightly conservative.

The restriction on the use of COPERNIC2 to M5<sup>®</sup> cladding only is not due to limitations in the physical models in the code, but is rather based on SER restrictions associated with the current NRC approval of COPERNIC2. The physical models in COPERNIC2 allow for the use of Zircaloy cladding, and much of the validation of the code was based on test results using Zircaloy cladding. Based on the evidence presented in Reference 10, COPERNIC2 is capable of accurately analyzing fuel with Zircaloy cladding.

## RODEX3A

RODEX3A was approved for use in the RLBLOCA methodology with the approval of EMF-2103(P)(A)Revision 0 (Reference 6). However, the benchmark database was limited to fuel rod burnups of 30 GWd/mtU. For Revision 2, the database was expanded to include fuel rod burnup data over 100 GWd/mtU.

An examination of the data, Section 5.8 of Reference 5, shows the uncertainty in low burnup data is higher than in the high burnup data. Revision 2 of the RLBLOCA methodology applies the same uncertainty—a Gaussian distribution with a 130 °F standard deviation—distribution that was previously applied in Revision 0. This approach is quite conservative, but sufficient.

The total fuel centerline temperature bias for Revision 2 of the RLBLOCA methodology is a combination of 1) the bias developed in Section 5.8 of Reference 5 for the expanded benchmark database and 2) an adjustment to properly compute burnup dependent pellet thermal conductivity degradation. This adjustment was resolved through consultation with industry experts and informal comparisons to current generation thermal performance codes that explicitly model the effects of thermal conductivity degradation.

The result is the burnup dependent bias function shown in Figure 4.165. Here, the final bias is contrasted to the original RODEX3A bias applied in Revision 0 of the methodology.

#### 4.3.3.2.2 Oxidation

Energy released through the oxidation of cladding is calculated using the Cathcart-Pawel correlation (Reference 33) for oxide layer growth:

$$\frac{\delta_{\phi}^2}{2} = 0.01126 \exp(-35890 / RT),$$

where  $R$  is the universal gas constant (1.987 cal/mole-K) and  $T$  is clad temperature. This is given in the S-RELAP5 Models and Correlations document (Reference 11 Section 7.3.4) as:

$$\frac{\partial \Delta r_{\phi}}{\partial t} = \frac{0.000002252}{2\Delta r_{\phi}} \exp(-18062 / T).$$

In Reference 33, uncertainties are provided for both the constant term and the exponential term. It is reported that the 90 percent confidence limits on the constant term is –23 percent to +30 percent and on the exponential term, it is ±2.2 percent. A standard deviation is calculated from the upper one-sided 95 percent probability point (+30 percent, 2.2 percent).

Assuming a normal distribution, this corresponds to 1.645 standard deviations (Reference 34, page 791); hence, the standard deviation is  $30 \text{ percent} / 1.645 = 18.237 \text{ percent}$  on the constant

term and  $2.2 \text{ percent} / 1.645 = 1.337 \text{ percent}$  on the exponential term. Both terms are sampled within the methodology employing Gaussian distributions with the above standard deviations and no bias (Reference 33).

When calculating the total oxidation of the cladding, a best-estimate steady-state corrosion value is added to the predicted maximum transient oxidation. The sum of the steady-state and transient oxidation is then compared to the total cladding maximum oxidation limit.

#### 4.3.3.2.3 Decay Heat

Decay heat calculations are based on the 1979 ANSI/ANS standard (ANSI/ANS-5.1-1979, Reference 35). This standard is applicable to light water reactors containing low enriched uranium as the initial fissile material. The treatment of fission product decay and actinide decay are separated in the methodology with differing approaches used to assure representative yet conservative treatment.

##### Fission Product Decay

The RLBLOCA methodology utilizes the decay curve of the standard for fully saturated decay chains and infinite operation, with the total fission energy coming from U-235 and the energy per fission being 200 Mev (Reference 35).

No bias is assigned to this phenomenon, but an uncertainty derived from the U-235 fission product decay of the standard is incorporated and sampled. The uncertainty for the decay of U-235 fission products has an initial standard deviation of about 3 percent, which drops to around 2 percent by 2 seconds and is below 2 percent by 8 seconds. The uncertainty remains near, but below, 2 percent for over 400 seconds. Because peak cladding temperatures occur prior to 400 seconds, and in general sooner than 200 seconds, the uncertainty is characterized by a standard deviation of approximately 2 percent. The RLBLOCA methodology utilizes a random sampling of a Gaussian distribution based on a 2 percent standard deviation for the fission product decay energy uncertainty. The sampling is two-sided and done at the beginning of each transient.

There are five principle applications of the fission product decay model within a RLBLOCA simulation:

- Fresh fuel – hot pin,
- Once-burned fuel – hot pin,
- Fresh fuel assemblies,
- Once-burned fuel assemblies, and
- Twice-burned fuel assemblies.

For once- and twice-burned fuel, substantial plutonium accumulates such that the ratio of plutonium-to-uranium fission-energy production rate is substantial and increasing. Because the decay energy resulting from plutonium fissions is less than that from uranium, the decay energy, for infinite operation, is reduced as the fuel is burned. Thus, as burnup increases, the RLBLOCA decay heat modeling, U-235 only, accrues conservatism. The conservatism applies to all regions of the core according to the mix of burnup represented within each region.

The fresh fuel hot pin and assembly begin operation with no plutonium. Therefore, the reduction in decay heat due to plutonium build-up is not applicable to these regions for the initial period of the cycle. However, there will not be any long decay term fission products to build in. The lack of long decay term sources comprises a reduction in decay heat rate of several percent over the first several months of operation, making the infinite operation assumption conservative for the period that plutonium is accumulating.

In conclusion, the choice of infinite operation with pure U-235 decay heat provides a base model that is conservative. Sampling this model based on the uncertainty of the U-235 decay chain provides something of the realistic treatment subject to the conservatism imbedded in the approach.

#### Actinide Decay

In addition to fission product decay heat, actinide capture product decay power is computed using the ANS standard equations and added to the fission product decay heat. In this calculation, a conservative conversion ratio, appropriate for the time in cycle analyzed, is obtained from core neutronic calculations. The ANS standard also provides equations to calculate the addition of decay heat from neutron capture in fission products. These equations are included in S-RELAP5 and the contribution to the total decay heat from this source is included in the methodology.

#### 4.3.3.2.4 Departure from Nucleate Boiling

Results from the THTF Heat Transfer SETs contributed to identifying a bias in the Biasi CHF correlation (Reference 5). [

] The CHF scaling is applied for RLBLOCA calculations, and the statistical information on heat transfer is used along with other test data (Section 4.3.3.2.5) to derive the uncertainty parameters on film boiling and dispersed flow film boiling heat transfer (Section 4.3.3.2.5).

#### 4.3.3.2.5 Core Post-CHF Heat Transfer

The post-CHF heat transfer model now includes provisions for thermal radiation between structures (rod-to-rod). This adds to the current model which already includes thermal radiation from structures to the fluid (rod-to-droplets and rod-to-steam). The rod-to-rod radiation model is only applied to the hot rod since its power level is elevated compared to its surroundings. Applying rod-to-rod radiation exclusively to the hot rod logically leads to the development of separate heat transfer uncertainties for the hot rod and the rest of the core.

The core wide heat transfer uncertainty was developed from code comparisons using the FLECHT-SEASET reflood test data as discussed in Section 5.1 of Reference 5. These comparisons were used to derive the heat transfer multipliers that are applied to film boiling (FILMBL) heat transfer and dispersed flow film boiling heat transfer (DFFBHTC). [

]

[

]

The  
distribution was integrated to form the cumulative probability, which compared favorably with a

[ ] . However, the uncertainties from the low pressure reflood multipliers FILMBL and DFFBHTC conservatively bound the  $2\sigma$  interval from the high pressure multiplier. Therefore, the low pressure reflood multipliers and biases will be applied to the post-CHF heat transfer for the entire LBLOCA event.

The single-phase vapor heat transfer was assessed in Reference 5 (Section 3.16) and [

] in the FLECHT-SEASET, FLECHT Skewed and THTF assessments. The results from those assessments did not show adverse or unrealistic behavior or temperatures. Based on this analysis, the single-phase vapor heat transfer is unbiased.

The assessments that were used in the bias and uncertainty determinations previous discussed used [

]

#### 4.3.3.2.6 $T_{min}$

A set of seven FLECHT-SEASET tests was used to evaluate the trends in  $T_{min}$  at low pressure. Quench temperatures improve at higher pressures; hence, a  $T_{min}$  uncertainty based on low pressure data was expected to bound high pressure data. This was validated in the Reference 6 methodology with data from ROSA/TPTF, the ORNL/THTF and the Westinghouse G1/G2 tests. Examination of FLECHT-SEASET data showed that, based on observable conservatisms, only the 3 in/s reflood rate test (Test Number 31302) was necessary to evaluate a bounding  $T_{min}$  uncertainty (Reference 5).

From the FLECHT-SEASET data and from an evaluation of code uncertainty with regard to how the LBLOCA multiplier relates to  $T_{min}$ , [

] . The uncertainty evaluation was demonstrated to be a conservative bounding distribution relative to other datasets.



#### 4.3.3.2.7 Break Flow

Break flow is a function of break area and critical flow uncertainty. [

] The S-RELAP5 HEM critical flow model applied in this methodology was assessed by comparison to full-scale critical flow tests at the Marviken facility, Section 4.3.1.8. From these assessments, [

]

#### 4.3.3.2.8 Accumulator Discharge

Accumulator discharge can be influenced by piping flow resistances and pressure. Most plants provide best-estimate data that maybe used to accurately model flow resistance; hence, the largest uncertainty to accumulator discharge is accumulator pressure. To support the technical specification of a plant for accumulator pressure and liquid inventory ranges, these parameters are sampled over the technical specification ranges, using a uniform probability distribution.

#### 4.3.3.2.9 Reactor Vessel Hot Walls

The heat release from the reactor vessel walls affects the ECC bypass during the early refill phase of a LBLOCA when the primary system is depressurizing. During the reflood phase, the heat release from the downcomer walls affects downcomer boiling. The results from UPTF

Tests 6 and 7 demonstrated that S-RELAP5 will overpredict ECC bypass; however, the downcomer wall temperature was much lower than would be expected in an actual operating plant. Therefore, the hot wall effects can only be partially evaluated using these tests. The hot wall effect can be separated out since it is expected that there is a direct relationship with the degree of nucleate boiling in the downcomer and ECC bypass. To maximize the hot wall effect, heat transfer in the downcomer can be locked into nucleate boiling during the refill phase by raising the CHF point to a high value. In the AREVA methodology, the hot wall effect during the refill phase [

].

During the reflood phase, the downcomer vessel wall heat release is conduction limited and depends on the mesh spacing used in the S-RELAP5 input model. The mesh spacing used to model the downcomer vessel was verified by using a simple benchmark having a closed form solution. The results, shown in Figure 4.166, show that S-RELAP5 will adequately calculate the heat release from the downcomer vessel wall during the reflood phase of a LBLOCA in a PWR.

#### 4.3.3.2.10 Containment Pressure

Containment pressure is ranged [

]. A conservative

containment pressure for the post-blowdown portion of a LOCA implies a low containment pressure. A low containment pressure is conservative since it results in an increase in steam binding, and thus reduces reflood rates to the core. Reduced reflood rates means a longer transient, and thus, higher cladding temperatures. [

]

#### 4.3.3.2.11 Upper Head Temperature, Initial Coolant Temperature

This is the initial temperature in the upper head of the reactor vessel. Plant data are examined to determine an average operating temperature and uncertainty range. During the case runs, the temperature is adjusted over the uncertainty range by adjusting the flows into and out of the upper head region of the reactor vessel. As such the value for the upper head temperature

corresponds to the expected operating conditions of the plant and requires no further assessment.

[illegible][illegible]



**Figure 4.164: COPENIC2 Cumulative Centerline Fuel Temperature  
Error Distribution**



**Figure 4.165: RODEX3A Bias as a Function of Fuel Pin Burnup**

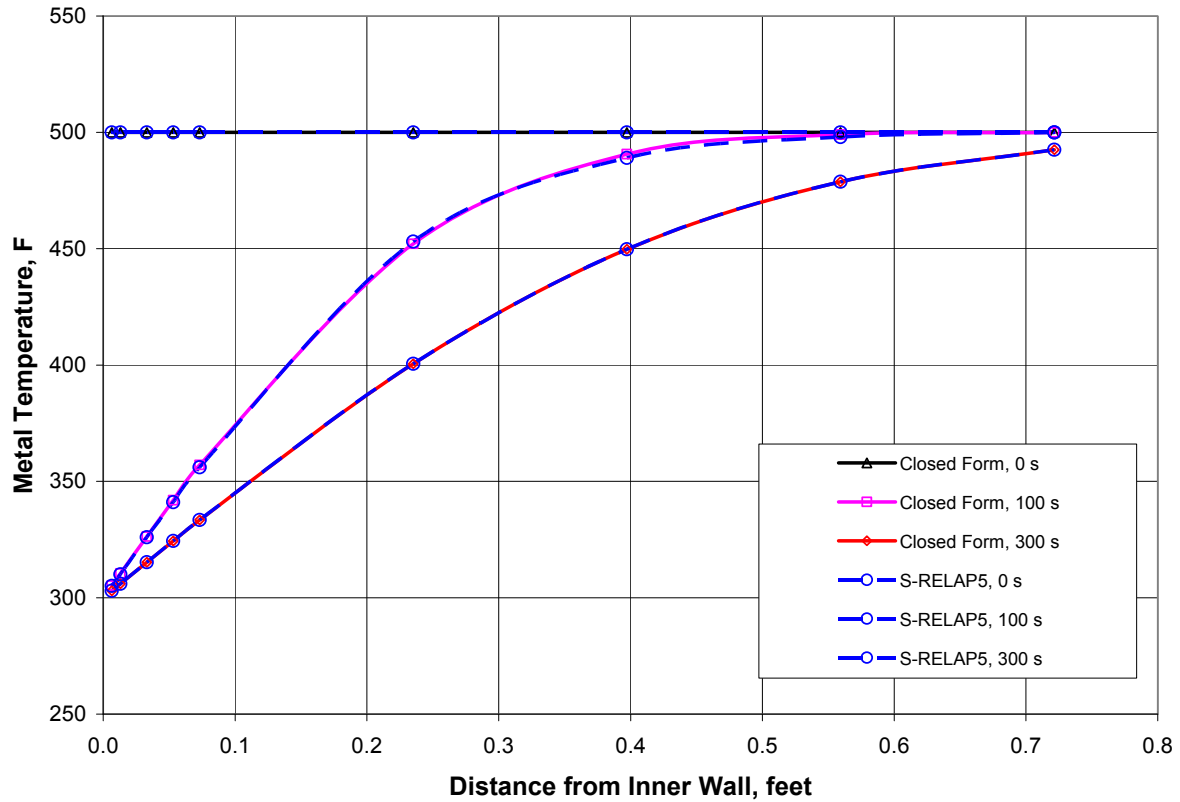


**Figure 4.166: Temperature Distribution in the Vessel Wall –  
S-RELAP5 versus Exact Solution**

#### 4.3.4 Application of Code Biases


This section summarizes the biases applied to the assessments presented in the previous sections. The biases were developed from uncertainty analyses performed on the SETs. In most instances, each bias developed has an uncertainty associated with it, but the uncertainties were not included in the assessments.

The biases listed below were taken from Table 4.22:

--	--

Listed in Table 4.25 are the assessments and the biases used in those assessments. [





#### 4.4 ***Determine Effect of Scale (CSAU Step 10)***

The basis for the analysis of a LBLOCA is the entire methodology being used, not just the base code, S-RELAP5. When S-RELAP5 is referenced in this section, it means the combination of the code and the associated methodology. As noted in Appendix C of Reference 4, there are two premises upon which the scalability of the methodology is based. The first premise is that the tests are scalable to a LBLOCA and the second is that the models in S-RELAP5 and the implementation result in scalability of the code predictions. For the first premise to be true, the selection of tests needs to be such that all of the important phenomena in a PWR LBLOCA are captured by one or more appropriately scaled tests. For the second premise to be true, the phenomenological models in S-RELAP5 should apply to both the PWR LBLOCA and the scaled test.

Throughout the assessment program (Reference 5), S-RELAP5 was used to simulate a variety of tests. These tests are a significant portion of the basis for the RLBLOCA methodology, having been used to demonstrate the ability of S-RELAP5 to predict the test outcomes. Because of the cataclysmic nature of a design-basis LBLOCA, no tests exist that fully replicate a LOCA at full-scale. All of the IETs and some of the SETs are scaled. One exception is the UPTF, which is full-scale, but has no core and no steam generators. The ability of the scaled tests to capture the phenomena of a LBLOCA is then pivotal to the applicability of the assessments for S-RELAP5.

##### 4.4.1 Test Scaling

Tests are scaled to preserve certain features of the full-scale phenomena. For this reason, tests with different scaling are used to address different phases or aspects of a LBLOCA. If a test is considered appropriately scaled for the phenomena of interest, then assessment conclusions to that data is considered applicable to the full-scale NPP. A common scaling approach, power-to-volume ratio, was shown (Reference 36) to preserve system response results as substantially the same under most circumstances. Its application and other approaches are discussed in reference to specific portions of the methodology in the following subsections.

#### 4.4.1.1 Blowdown

Power-to-volume scaling for the blowdown period was demonstrated in Reference 4. Five system tests with powers from  $1/48^{\text{th}}$  of a typical PWR to  $1/30,000^{\text{th}}$  were used as a basis for the comparison. Each of these facilities was scaled such that the ratio of power to volume was preserved. The peak temperature during blowdown was plotted as a function of linear power for each of these test facilities. The measured peak temperatures all fell within 350 °F of a linear regression line (temperature versus LHGR). The data scatter for a single facility was as great as, or greater than, any differences between facilities. As a result, it is concluded that tests which preserve the power-to-volume ratio of a PWR will scale properly for the blowdown phase of the LBLOCA.

#### 4.4.1.2 Refill

During refill and early reflood, scale dependent multi-dimensional flow behavior has been observed in the downcomer for facilities using power-to-volume scaling. The Semiscale and LOFT facilities were compared for analogous tests in Reference 36. Under ideal scaling, the two tests should have shown the same behavior. However, during the refill portion of the simulation, the downcomer flow was observed to be generally upward for the Semiscale test before the pressure increase accompanying the emptying of the accumulator. For the analogous test in the LOFT facility, the flow was asymmetric; downward for the regions near the intact loop and upward for the region near the broken loop. This was attributed to differences in the downcomer gap and the distance between the cold leg penetrations. This allows multi-dimensional flow effects to dominate the flow in the LOFT facility, whereas they do not occur to the same extent in the Semiscale facility. The downcomer gap, volume and surface area-to-fluid volume ratios do not scale between these two facilities in such a manner as to preserve the transit time and the heat transfer to the fluid from the walls.

The UPTF facility (Reference 37) was designed to simulate a four-loop 3900 MWt PWR primary system and to provide a full-scale simulation of thermal-hydraulic behavior in the primary system during the end of blowdown and refill phases of a PWR LBLOCA. The reactor vessel, the core barrel, and the greater part of the vessel internals are full-sized representations of the reference PWR, as are the four hot and cold legs that simulate three intact loops and one broken loop. The dimensions of the test vessel are those of the reactor pressure vessel of the reference PWR, with the exception that the vessel wall is thinner. The downcomer annulus,

which is formed by the vessel wall and the core barrel, has a gap width that varies from 0.25 meters (0.82 feet) in the lower part to 0.21 meters (0.69 feet) in the upper part. The loop geometry and flow areas correspond to the 4-loop PWR.

With the exception of the wall thickness, the UPTF is full-scale. The hot-wall effect should be slightly under-estimated, because of the slight reduction in vessel mass and stored energy. However, there is an ample amount of metal in the vessel so that the UPTF tests are applicable to the refill portion of a LBLOCA.

#### 4.4.1.3 Reflood

Scaling issues associated with reflood were addressed in Reference 4, where the effects of refill scaling were removed from the data by comparing the temperature rise to reflood rates. The temperature rise considered is the change from the beginning of reflood to the PCT.

Temperature rise data were collected for eight facilities with volumes scaled from 1/21<sup>st</sup> to 1/1700<sup>th</sup>, all of which were power-to-volume scaled. Figure 34 of Reference 4 compares the temperature rise for all eight facilities to the reflood rate. The data were fit with a regression relation and the tolerance bands added. As with the blowdown data, the spread in the data for a single facility was as great as or greater than the difference between the facilities. Tests which scale by maintaining the power-to-volume are applicable to the reflood phase of a LBLOCA.

#### 4.4.2 Code Scaling

The issue of code scaling is primarily determined by the ability of the correlations and closure relations used to describe complicated thermal-hydraulic phenomena that are not treated from a mechanistic, theoretical approach. Generally, phase transitions, heat transfer, phasic interactions and CHF fall in this category. The models, correlations, and closure relations used in S-RELAP5 are described in Reference 11. To a lesser extent, the numerical implementation may be subject to scaling issues. Generally, issues of numerics are treated by addressing the converged nature of the nodalization and time step criteria. This demonstrates that the computer code can solve the mathematical model correctly over the applicable range for the tests and a LBLOCA. This leaves the issue of scaling of the correlations and the closure relations employed in LBLOCA analysis.

Code scaling evaluation will focus on those items identified by the sensitivity studies of PIRT phenomena as having the greatest impact on LBLOCA. Table 4.1 shows the results of sensitivity studies on the PIRT phenomena in a PWR LBLOCA. The models, related to these phenomena and the scalability of each of these models, are discussed in the following paragraphs.

Items related to fuel rod performance are not affected by scaling, because the basis for the fuel-stored energy and dynamic response are based on COPENIC2 (Reference 10) and RODEX3A (Reference 8), each of which was benchmarked to data from actual fuel rods.

#### 4.4.2.1 Post-CHF and Reflood Heat Transfer

When heat flux from the fuel rods and any other metal masses exceeds the CHF, the heat transfer is calculated using correlations specific to the heat transfer regimes. The single-phase vapor, transition boiling and film boiling regimes constitute the post-CHF heat transfer regimes. For each of these regimes, the effects of radiation heat transfer also are considered. Single-phase vapor heat transfer is the maximum of the Wong-Hochreiter correlation (Reference 38) for forced flow regimes (turbulent and laminar) and the turbulent natural convection heat transfer recommended by Holman (Reference 39). In general, the Wong-Hochreiter correlation determines the heat transfer.

The natural convection heat transfer model is based on data from the flow between vertical plates. If the boundary layer is small compared to the diameter of the rod, then heat transfer through this layer would be very similar to that through the boundary layer on a plate. With the Prandtl number near unity and the rod diameter large compared to the boundary layer, the Holman formulation for natural convection heat transfer used in S-RELAP5 applies (Reference 40) as long as

$$D/L \geq 35 \cdot (Gr)^{-0.25},$$

where  $D$  is the rod diameter,  $L$  is the length used in calculating the Grashof number and  $Gr$  is the Grashof number. When these conditions are met, the flat plate solution does not differ by more than 5 percent from the solution for the cylinder. In the turbulent flow regime, this implies  $0.02 \leq D/L \leq 0.2$ . For a 17x17 fuel design, with a pin diameter of 0.376 inches, the length can be as low as 1.9 inches and as large as 19 inches. Within the RLBLOCA methodology, normal

heat transfer lengths in the core [

]. These fall well within the range of applicability of the natural convection heat transfer correlation.

The Wong-Hochreiter correlation was developed from steam cooling tests performed on the FLECHT-SEASET test facility; consequently it is scaled to the desired geometry. The steam temperature data was taken at low pressure and temperature for Reynolds numbers ranging from 3,000 to 20,000 with provisions for lower Reynolds numbers. The Reynolds and Prandtl numbers are functions of thermodynamic and transport properties and scale appropriately with pressure and temperature. Figure 4.167 shows the data from Figure 4-10 of Reference 38 along with the Wong-Hochreiter fit. In this figure, the Dittus-Boelter correlation (Reference 41) is shown for comparison to demonstrate its inadequacy when applied to tube bundle geometries.

In conclusion, the model for single-phase vapor heat transfer used in S-RELAP5 can be applied to a full-scale PWR LBLOCA.

Transition boiling is not really a heat transfer regime in the sense that it can be characterized by a homogeneous, steady, heat transfer mechanism. It is a combination of dynamically varying heat transfer mechanisms, including nucleate boiling, film boiling and vapor heat transfer. The amount of time a region spends in one of these heat transfer modes determines the effective heat transfer rate. Few measurements are available for transition boiling heat transfer and they do not cover a wide range. In addition, the unsteady nature of the process makes modeling the process physically challenging.

Despite the complexity of this regime, exact modeling of the transition boiling heat transfer is not particularly important for a LBLOCA because most volumes in the core move through this heat transfer regime rather quickly and are not sensitive to the details of the modeling. The main requirement for simulating a LBLOCA is that the point at which the code predicts the beginning and end of the transition region be reliable. In addition, the heat transfer in the transition region should be significantly better than the vapor heat transfer and it should remain below the CHF. The value of CHF in this region is computed using the modified Zuber CHF correlation (Reference 11).

The major assumption in modeling this regime is that it can be modeled by a combination of steady-state boiling heat transfer to liquid and convective heat transfer to vapor. In this model,

the heat flux is bounded by the CHF at the lowest wall temperatures and it approaches the flux based on single-phase vapor heat transfer as the wall temperature rises. The heat transfer is based on a modified Chen correlation for transition heat transfer (Reference 17 and 42). This model makes a smooth transition from the CHF to the single-phase vapor heat transfer, with the calculated fraction of liquid heat transfer based on the wall temperature. The Chen correlation was tested against data and behaves adequately, which is sufficient for LBLOCA transition boiling.

Film boiling occurs when the wall temperature exceeds the minimum temperature for stable film boiling and the void fraction lies in the appropriate range. The coolant consists of vapor and water droplets in this mode. The heat transfer mechanisms consist of boiling heat transfer to liquid droplets, convective heat transfer to vapor, and radiative heat transfer to droplets and vapor.

[

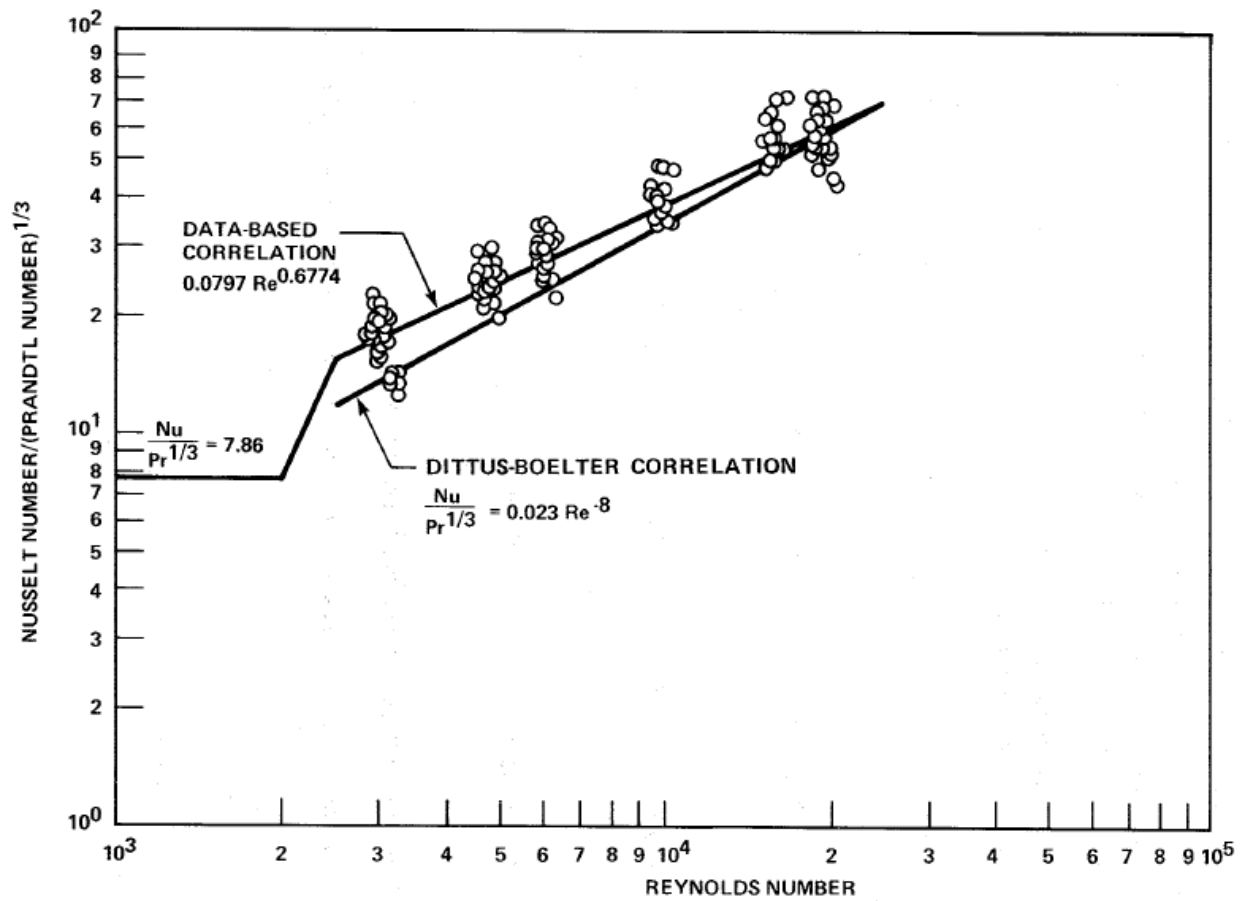


Figure 4.167: Data Based Nusselt Number versus Reynolds Number  
for FLECHT-SEASET Steam Cooling Tests Compared with  
Dittus-Boelter Correlation



#### 4.4.2.2 Scaling from Tests

While analytical arguments (see prior section) can provide a basis for code scaling for selected cases, often the issue of scaling needs to be addressed by a comparison to test data. Code scaling and the tests making up the basis are discussed in the following paragraphs.

##### 4.4.2.2.1 Film Boiling Heat Transfer

A series of tests was performed in the THTF at Oak Ridge National Laboratory to measure heat transfer at higher pressures and flows. These included 22 steady-state dry-out tests (Reference 50), three transient boil-off tests (Reference 51) and two sets of transient reflood tests (References 52 and 53). The reactor core was simulated by an 8x8 array of heated rods with dimensions corresponding to those of a Westinghouse 17x17 fuel assembly. The axial power shape was uniform. The FLECHT-SEASET used 161 full-length simulated fuel rods and axially-dependent power shapes (Reference 23). Based on rod count, these two test facilities differ by a scaling factor of 2.5.

These tests were used to evaluate the film boiling heat transfer. Table 4.26 compares the ranges for LBLOCA calculations for parameters that affect heat transfer with the ranges covered by the THTF tests and FLECHT-SEASET. Given the near prototypic nature of the fuel rod simulators and the extent to which the tests span the applicable ranges for LBLOCA, it is concluded that the heat transfer models, including correlations and closure relations, in S-RELAP5 are sufficient to allow direct application to a PWR LBLOCA and that the uncertainties obtained from these tests are applicable.

##### 4.4.2.2.2 Core Entrainment

Entrainment of water droplets by the steam flow in the core can affect the predicted core cooling flow. The primary determinant of entrainment is the drag exerted on the liquid droplets by the steam flowing up out of the core. This drag, in turn, depends on the vertical flow regime in the core model. The determinants of the model applicability to a PWR LBLOCA are primarily local and, in the core, principally related to the conditions within the flow channel between the fuel rods. The axial effects predominate in this phenomenon. Radial redistribution is a second-order effect, in that it makes fluid available in a channel or removes it. The RLBLOCA

methodology makes use of the TWODEE component in S-RELAP5 to model the radial behavior in the core.

The tests used in the assessments, CCTF (Reference 31), FLECHT-SEASET (Reference 23), and THTF (References 50, 51, 52, and 53), use bundles of full-length fuel rods. ACHILLES (Reference 28) also used full-length rods, but the gaps between the rods and the piping containing the rods caused some radial flow redistributions which made it less suitable for confirming scaling of core entrainment. The LOFT and Semiscale Test S-06-03 cores were too short for entrainment scaling. Based on the comparisons to CCTF, FLECHT-SEASET and THTF, the core entrainment model in S-RELAP5 is conservative and will scale suitably to a full-scale PWR LBLOCA.

#### 4.4.2.2.3 Critical Flow at Break

The choked flow model used for AREVA RLBLOCA analyses is the homogeneous equilibrium model (HEM). Choking for break flow occurs when the flow velocity reaches the speed of sound at the break. The critical flow model is not scale dependent; however, the Marviken Full-Scale Critical Flow Test data were used to determine the S-RELAP5 critical flow multipliers and uncertainties as discussed in Section 4.3. The Marviken test facility and S-RELAP5 results are discussed in detail in Section 3.5 of Reference 5.

The test facility consists of four major components: a full-scale BWR vessel, a discharge pipe attached to the bottom of the vessel, a test nozzle connecting to the downstream end of the discharge pipe, and a rupture disk assembly attached to the downstream end of the nozzle. Nozzles of various length-to-diameter ratios are used in the tests. The Marviken test data are widely used in assessing critical flow models of various system codes over a range of flows to confirm the scalability. The Marviken tests provide a suitable basis for code scaling verification and the determination of uncertainties.

#### 4.4.2.2.4 Carry-over to Steam Generator

Steam binding during the reflood phase of a LBLOCA in a PWR occurs as a result of steam production in the steam generator. This steam production occurs when water carried over from the core enters the hot steam generator. The resulting vaporization expansion increases the

pressure drop through the steam generator and produces steam binding that reduces the core reflood rate.

Several UPTF, SCTF and CCTF tests were used to benchmark and verify the RLBLOCA methodology and S-RELAP5. The UPTF is a full-scale simulation of a German PWR. However, the geometry of UPTF is also close to a Westinghouse 4-loop PWR. In UPTF, the steam generators are replaced with steam separators and the pumps are simulated with mechanical resistance. The CCTF and SCTF are scaled such that they are prototypic of a Westinghouse PWR in the dimension parallel to flow and scaled down ( $\sim 0.2$ ) in the orthogonal directions.

The UPTF has no core per se, and reflood is simulated with steam and water injection in the core simulator region. The CCTF and SCTF have electrically heated rods in the core. The upper plenum region was tested at full-scale in the UPTF, as were the hot legs and the steam generator inlet plenum. The steam generator tubing geometry is prototypical in the CCTF (although the number of tubes is smaller). In SCTF, a steam-water separator is used instead of an active steam generator. As discussed in Section 4.3.3.1.4 and 4.3.3.1.6, several input options are developed to make sure that an acceptable amount of liquid that is entrained to the upper plenum during the reflood phase of a large break LOCA is carried over to the steam generator tube region. One of the input options is the [

]. These input options are used in the UPTF, SCTF, and CCTF tests assessments. In all the assessments, S-RELAP5 entrained an acceptable amount of liquid into the steam generator tube (or tube simulator) region. While each test by itself has some deficiencies in terms of simulating a PWR and in terms of scale, the combination of the simulation of tests from these three different test facilities provides a substantial basis to justify the ability of the code to calculate an acceptable amount of liquid entrainment into the steam generator tube region during the reflood phase of a large break LOCA in a PWR.

#### 4.4.2.2.5 Pump Scaling

The S-RELAP5 code uses normalized single-phase homologous curves for a full-scale reactor coolant pump as code input. The use of full-scale data for the pump makes code scaling moot for the pump. These homologous curves are set to applicable values by entering plant-specific values for rated head, torque, moment of inertia, etc. The coastdown of the pump is driven by the torque and moment of inertia of the rotating mass. The torque includes the effects of friction

and back EMF (pump torque) and of the loop pressure losses (hydraulic torque). Although the two-phase degradation of RCP performance is not considered a phenomenon of significance (Table 3.1), the single-phase pump head and torque curves are adjusted for two-phase effects based on the EPRI two-phase degradation data (Reference 54). The pumps in the EPRI test program are similar to PWR coolant pumps and the data represents a best estimate approximation of both the single phase and two phase performance.

#### 4.4.2.2.6 Cold Leg Condensation

As discussed in Section 4.3.3.2, several EPRI 1/3 scale tests, in combination with UPTF Test 8 Phase A (Run 111) and Phase B (Run 112) and Test 25, were simulated using S-RELAP5. The simulation results were used to develop the biases (multipliers) on the liquid-side (CONMAS) and vapor-side (CONMSG) interphase heat transfer coefficients. The tests selected generally cover both the accumulator and pumped injection period of the LOCA transient. In addition, additional EPRI tests were simulated using S-RELAP5 and the results are discussed in Section 4.3.1.9. The UPTF is close to a full-scale facility and the EPRI test facility is a 1/3<sup>rd</sup> scaled facility.

Correlations based on the Stanton numbers are used to calculate the interphase condensation. These correlations are generally insensitive to geometry as demonstrated by the EPRI and UPTF benchmark results. The interphase heat transfer correlations used in S-RELAP5 are discussed in detail in Section 3.4 of Reference 11.

In summary, with the biases determined from the tests conducted in these facilities, S-RELAP5 will calculate acceptable condensation in the cold legs during a large break LOCA in a PWR.

#### 4.4.2.2.7 ECC Water Bypass of Downcomer during Refill and Lower Plenum Sweep-Out

The S-RELAP5 code prediction of the ECC bypass during the refill phase of a LOCA was demonstrated to be conservative through the assessment of UPTF Tests 6 and 7 (Section 4.3.1.11.1 and Reference 5). In addition, a CCFL correlation developed by MPR Associates is used in the sample plant cases given in Appendix B to demonstrate S-RELAP5 conservatively calculates the bottom of core recovery (or beginning of core reflood) time.

As discussed in Section 4.3.1.11.1, UPTF Tests 6 and 7 were steady-state downcomer counter current flow tests. UPTF Tests 6 and 7 were specifically designed under the 2D/3D program to

examine downcomer countercurrent flow behavior, ECC bypass, and lower plenum refill during the refill phase in plants with cold leg ECC injection. In these tests the lower plenum fill rate was measured as a function of time. The comparison of the lower plenum liquid level for UPTF Test 6 is provided in Figure 4.63 through Figure 4.67 and for UPTF Test 7 in Figure 4.68. The liquid level comparisons show S-RELAP5 underpredicts the lower plenum level which indicates the code is overpredicting ECC bypass. Since UPTF is a full scale test facility, results from the Tests 6 and 7 simulations demonstrate S-RELAP5 will conservatively calculate ECC bypass, lower plenum fill, and the core recovery time during the LOCA in a PWR.

Under the 2D/3D program, MPR Associates developed a Wallis-type CCFL correlation using UPTF data from the steady-state countercurrent flow tests (which included UPTF Test 5, Phase B, and UPTF Tests 6 and 7) to calculate the liquid downflow into the lower plenum during the refill phase:



The details of this CCFL correlation are given in Reference 26. In this correlation,  $J_{g,eff}^*$  is the net steam flow rate available to entrain the ECC liquid to the break and its value determines the potential for ECC bypass. If  $J_{g,eff}^*$  is zero, or negative, the steam flow is insufficient to entrain liquid, and bypass will not occur (complete end-of-bypass). If  $J_{g,eff}^*$  is positive, then partial or full bypass occurs.

Since the correlation is normalized using the downcomer flow area and circumference, it is directly applicable to calculate the ECC bypass in the plant during the refill phase. This correlation has already been approved by the NRC to calculate the complete end-of-bypass time ( $J_{g,eff}^* < 0.0$ ) as part of AREVA's Appendix K-based Recirculating Steam Generator Evaluation Model (Reference 55).

The correlation is used in the sample plant cases discussed in Appendix B to estimate the beginning of core reflood time in order to demonstrate S-RELAP5 will calculate the beginning of core reflood time appropriately. To estimate the beginning of core reflood time, the correlation is used to calculate the complete end-of-bypass time. At this time the liquid volume in the lower

head, lower plenum, and downcomer below the active core region is determined. Knowing this time, the ECC injection rates in the intact cold legs and the remaining fluid volume below the active core region that need to be filled with water, the beginning of core reflood time can be estimated. The results for the sample cases (Figure B.18, Figure B.36, Figure B.53, and Figure B.71) demonstrate S-RELAP5 calculates the beginning of core reflood time appropriately.

The highly separated flow behavior observed in the full-scale UPTF tests (see Figure 4.1-3 in Reference 56) were not observed in scaled facilities like LOFT and Semiscale. Therefore, the tests conducted in these scaled facilities cannot be used to determine code scalability of ECC bypass, and the multi-dimensional flow phenomena that will occur in the downcomer and lower plenum during the refill phase.

In summary, it is demonstrated that S-RELAP5 will appropriately calculate the ECC bypass during refill and the beginning of core reflood time during the large break LOCA in a PWR.

#### 4.4.2.2.8 Loop Oscillations

UPTF Test 8 (References 57 and 58) investigated the behavior during the end-of-blowdown, refill, and reflood phases of a postulated LOCA with cold leg ECC injection. The focus of the test was the pressure and fluid oscillations in the cold legs. These oscillations arise when the steam is condensed by the ECC water and forms a liquid plug in the cold leg. The ECC flow rate was varied from typical accumulator flows down to pumped injection flows. The test results show the flow regimes switching from the slug (plug) flow during the accumulator injection period to stratified flow during the pumped injection period. Test 8, Runs 111 and 112, were performed by isolating one intact loop at the pump simulator, opening a second intact loop to stabilize the pressure drop between the upper plenum and the downcomer, opening the break valves on the broken loop, injecting steam into the test vessel, and varying ECC water injection into the third intact loop cold leg downstream from the pump simulator. The S-RELAP5 simulation of the Test 8 modeled the cold leg piping for the third loop from the steam generator simulator to the pump simulator (including loop seal), the pump simulator, and the cold leg piping from the pump simulator to the vessel downcomer; all of which are full-scale.

The simulation is discussed in Section 4.3.1.11.2. S-RELAP5 predicted the observed flow regimes reasonably well which indicate the code is capable of calculating the appropriate

phenomena associated with steam-ECC mixing in the cold leg in the plant. However, since the complete UPTF primary system was not modeled using S-RELAP5, the system oscillations were not calculated by the code.

The CCTF, SCTF and LOFT benchmarks (Sections 4.3.1.12, 4.3.1.13, and 4.3.2.1, respectively) compared the calculated and measured differential pressures. The results show the code calculated acceptable oscillations during the refill and reflood phases.

In summary, from the simulation of the above tests, it can be concluded that S-RELAP5 will calculate the acceptable loop oscillations during a large break LOCA in a PWR.

**Table 4.26: Test Ranges for Film Boiling Heat Transfer Test Comparison**

Parameter	Maximum		Minimum	
	Tests	LBLOCA	Tests	LBLOCA
Pressure (MPa)	8.2	10.8	0.13	0.22
Mass Flux Vapor (kg/s-m <sup>2</sup> )	907	367	0	0
Mass Flux Liquid (kg/s-m <sup>2</sup> )	4254	945	0	0
Void Fraction	1	1	0.13	0.13
Saturation Temperature (K)	570	589	381	390
Vapor Temperature (K)	1294	1160	384	391
Wall Temperature (K)	1525	1400	390	396
Quality	1	1	-0.11	0



## 5.0 Sensitivity and Uncertainty Analysis

The objective of this section is to describe how plant compliance to the criteria of 10 CFR 50.46 with high probability is demonstrated. For the AREVA RLBLOCA evaluation model, high probability was defined as having 95 percent confidence that 95 percent of LBLOCAs will meet the acceptance criteria of 10 CFR 50.46. This is accomplished by applying non-parametric statistical techniques to the calculation results of the evaluation. The key premise is that the RLBLOCA evaluation tool, S-RELAP5 and the attendant codes, is accurate in representing the possible LBLOCAs and the frequency with which specific LBLOCA results will occur. Thus, S-RELAP5 contains the domain of all possible LBLOCA results within the scenario defined in Section 3.1. Extracting information about this domain is done by random sampling (running individual LOCA calculations referred to as cases or events) with random values for the initial conditions and the parameter values, including those that alter the simulation of important phenomena and deducing from those samples the content of the domain. To accomplish this entails two requirements: 1) the calculation evaluation tool, S-RELAP5 and COPENIC2 or RODEX3A, must be established as sufficiently accurate or conservatively biased such that any calculation provides a result that is accurate or conservative for the sampled choices and 2) a method of evaluating the results sampled from the domain be established to provide accurate probability and confidence. Section 5.1 presents the establishment and evaluation of the first requirement, and Sections 5.2 and 5.3 present the second. Sample RLBLOCA evaluations illustrating the analysis steps described below are provided for representative Westinghouse 3- and 4-loop and CE 2x4 plants in Appendix B.

### 5.1 *Determination of the Effect of Reactor Input Parameters and State (CSAU Step 11)*

The uncertainties associated with the prediction of LOCA results can be categorized into three groups:

1. Fixed design factors (e.g., system geometry, etc.) that do not change, but that can still only be rendered in approximation,
2. Operational processes (e.g., core power peaking, etc.), which do not change during the transient, but vary across the spectrum of conditions at which a LOCA may occur, and

3. Phenomena, which evolve during the transient (e.g., core heat transfer coefficients, etc.), and may take on differing normalized performance across the spectrum of LOCAs within the domain.

The treatment of fixed design factors and operational processes are discussed in Section 5.1.1 and Section 5.1.2, respectively. The treatment and development of uncertainty distributions for phenomena is presented in Section 4.3 and Section 4.4.

#### 5.1.1 Fixed Design Factors

Uncertainties associated with fixed design parameters are addressed by maintaining adherence to nodalization guidelines and identifying phenomenological uncertainties from code assessment studies applying those guidelines. Within the development of the methodology the guidelines for fixed structure or condition are applied, contingent on experimental restrictions, to a wide variety of experiments and benchmark evaluations, Section 4.0. The benchmarks serve to develop the uncertainties of correlations or phenomena modeling and to establish the ability of the modeling guidelines to produce fixed design models capable of allowing replication of the LOCA physical phenomena. This is the subject of the entire Section 4.0 and discussed specifically in Sections 4.2 and 4.3, which describe CSAU Steps 8 and 9.

#### 5.1.2 Operational Process

In contrast to phenomenological or fixed design factors, process parameters characterize the state of operation of the plant and are, to various degrees, controllable by plant operators such that realistic variations can be expected. The importance of these parameters must be established and, for those of significance, the ability of the model to predict appropriate results must be validated and an appropriate uncertainty distribution established.

##### 5.1.2.1 Determining Important Process Parameters

From an operational standpoint, the NPP operating state is a function of the time in cycle (burnup and power distribution) and the actual conditions present in the various NPP components. Treating these process parameters statistically accounts for higher order behavior by including all possible combinations in the domain of possible LOCAs.

As part of the AREVA RLBLOCA methodology development, a review was performed to identify the NPP parameters that are to be addressed in the performance of a LBLOCA analysis. The identified parameters are provided in Table 5.1. The basis for inclusion in this list comes from three sources: PIRT, plant-specific technical specifications, and utility requests.

Determination of which process parameters to treat statistically begins with identifying the relationship a particular parameter has to any PIRT phenomenon. Table 5.2 lists process parameters determined to be important based on their potential influence to the moderate-to-high ranked phenomena given in the PIRT, Table 3.1.

A refinement of the conclusions presented in Table 5.1 and Table 5.2 based on sensitivity studies is within the precepts of the methodology. Such studies can be employed to adopt a bias over an uncertainty distribution for process parameters or to assist in the quantification of an uncertainty range or distribution.

Other process parameters are considered of lower importance and are generally treated on a nominal basis. As with any parameter, there is no prohibition to treating these parameters on a statistical basis.

#### 5.1.2.2 Quantifying Uncertainty for Process Parameters

To treat a parameter statistically, the parameter uncertainty must be quantified in terms of biases and distributions. Quantifying this uncertainty with plant data is the best approach. At most plants, histories of parameters values such as RCS flow rate, core inlet temperature, pressurizer condition, accumulator parameters, and containment temperature are maintained and useable for quantifying RLBLOCA analysis uncertainties. Operational uncertainty is defined as the true fluctuation of a parameter during normal operation. Setting the uncertainty distribution for a process parameter requires addressing the impact of measurement uncertainty for the parameter.

The choice of distribution may be influenced by how a utility manages a given process parameter. For example, using a uniform distribution may properly reflect the control provided for a parameter, if that control is random within a range. A uniform distribution is also considered a conservative approach in that equal likelihood is given for values at the limits of the distribution where the strongest influence is expected. However, if there is an

expectation that the true distribution is substantially non-uniform, the actual distribution can be used.

As shown in Table 5.1, some parameters lack explicit definition (technical specifications or data). For parameters for which no plant data are available, ranges may be established based on physical constraints or by analytical methods. An example of a physical limit is ranging the reactor vessel upper head temperature to a maximum value of the hot leg temperature. It may also be demonstrated that a particular parameter has a limited range of influence based on a set of sensitivity studies.

#### 5.1.2.3 Treatment of Time in Cycle

The time in cycle establishes the fuel rod properties and the lower bound for the global power peaking factor,  $F_q$ . Power history calculations are performed using an NRC-approved methodology (References 59 and 60). Typically, fuel rod data for 20 to 40 burnup steps are explicitly written from a cycle power history calculation. The methodology examines potential limiting fuel conditions during both the first and second cycle of fuel rod operation. Fuel rod data are, therefore, provided for the first and second cycle of fuel rod operation. Third cycle fuel is sufficiently depleted that it can not rise to the possibility of being the limiting fuel within the core and is not evaluated by the methodology.

In contrast to a traditional safety analysis, which assumes conservative fuel rod models consistent with Appendix K requirements, [

4. [

]

The data produced by this method are used primarily to develop input for the RODEX3A or COPERNIC2 fuel rod sub-codes within S-RELAP5. [

]

#### 5.1.2.4 Treatment of Axial and Radial Power Shapes

Once the fuel rod histories for the fuel rod sub-code are found as described above, the axial and radial power shapes for the S-RELAP5 core model are selected as follows. To support plant Technical Specification for the core peaking factor,  $F_q$ , the axial power shape must be adjusted from the nominal axial power shape extracted for the limiting fuel rod. During normal operation,  $F_q$  will likely occur relatively near the nominal  $F_q$  represented in the power history files. [

] The resultant normalized axial power distribution is used for fresh fuel in all core radial regions and the supplemental hot rods representing fresh fuel. Similar calculations are performed to select an axial profile for once-burned fuel using a different table of shapes generated at applicable burnups.

#### 5.1.2.5 Treatment of GDC-35 Criteria

GDC-35 states that the plant shall be able to mitigate design basis accidents with or without off site power available. The methodology does this by determining the most severe condition between these two configurations and then performing the RLBLOCA statistical analysis for the plant with off site power availability set to the most severe condition. Further details are provided in Appendix B, Section B.1.3.

### 5.2 ***Performance of NPP Sensitivity Calculations and Determination of Combined Bias and Uncertainty (CSAU Steps 12 and 13)***

As previously discussed, the evaluation applies non-parametric statistical techniques. To do this, the calculation of several individual LOCA possibilities must be conducted. Each of these possibilities must have the performance of key parameters or conditions determined randomly. This is accomplished by assigning an individual PDF to each of the parameters to be varied or sampled by the methodology. The PDFs are then seeded, using standard techniques, with independent random numbers to specify the performance of each parameter for a given case. After the accumulation of the results for several possible LOCAs, the group of results is evaluated to determine the probability of compliance to LOCA criteria.

#### 5.2.1 Statistical Approach



- First step : Defining the partition function



- **Second step : sorting the samples**

- **Third step : constructing the blocks**

- **Fourth step: Constructing the tolerance region**







#### 5.2.2 Application of Methodology

The AREVA RLBLOCA methodology is a statistics-based methodology; therefore, the application does not involve the evaluation of different deterministic calculations. Instead, a minimum set of LOCA calculations, consistent with the previous table, are performed with the

values of key parameters randomly varied over identified uncertainty ranges. As previously explained, the methodology has the advantage of being able to treat a large number of parameters by randomly varying each parameter in each single calculation. This random selection process is repeated to define a large number of RLBLOCA calculations, all of which are then run. [

]

### **5.3 *Determination of Combined Bias and Uncertainty and Determination of Total Uncertainty (CSAU Steps 13 and 14)***

CSAU Step 13 provides for the determination of the combined bias and uncertainty for the NPP. This is basically the application of the process described in Section 5.2. The procedure is executed for each of three sample problems in Appendix B.

The total uncertainty for the evaluation is determined by comparing the bounding parameter value for the limiting parameter to the 50/50 probability value for that parameter within the domain defining the high probability of compliance. Examples of this value are also reported for each of the sample problem in Appendix B.

**Table 5.1: NPP Parameters for Consideration in the Performance of  
a RLBLOCA Analysis**

--	--

**Table 5.2: Relationship of PIRT to Operational Parameters**

--	--



## 6.0 References

1. *Emergency Core Cooling Systems; Revisions to Acceptance Criteria*, Federal Register, Vol. 53, No. 180, September 16, 1988, 10 CFR Part 50.
2. NUREG/1230, *Compendium of ECCS Research for Realistic LOCA Analysis*, December 1988.
3. *Best-Estimate Calculations of Emergency Core Cooling System Performance*, Regulatory Guide 1.157, May 1989.
4. NUREG/CR-5249, *Quantifying Reactor Safety Margins, Application of Code Scaling, Applicability, and Uncertainty Evaluation Methodology to a Large Break, Loss-of-Coolant Accident*, December 1989.
5. EMF-2102(P) Revision 2, *S-RELAP5 Code Verification and Validation*, November 2010.
6. EMF-2103(P)(A) Revision 0, *Realistic Large Break LOCA Methodology*, Framatome ANP Richland, Inc., April 2003.
7. ANF-90-145(P)(A), *RODEX3 Fuel Rod Thermal-Mechanical Response Evaluation Model*, Volume 1, "Theoretical Manual," and Volume 2, *Thermal and Gas Release Assessments*, April 1996.
8. EMF-1557(P) Revision 8, *RODEX3A: Theory and User's Manual*, May 2007.
9. EMF-2417(P) Revision 0, *RODEX3A Code Verification and Programmers Guide for Version USEP98*, July 2000.
10. BAW-10231P-A Revision 1, *COPERNIC Fuel Rod Design Computer Code*, AREVA NP Inc., January 2004.
11. EMF-2100(P) Revision 14, *S-RELAP5 Models and Correlations Code Manual*, December 2009.
12. EMF-2101(P) Revision 3, *S-RELAP5 Programmers Guide*, May 2004.
13. EMF-CC-097(P) Revision 23, *S-RELAP5 Input Data Requirements*, October 2009.
14. EMF-CC-039(P) Revision 4, *ICECON Code User's Manual: A Computer Program Used to Calculate Containment Back Pressure for LOCA Analysis (Including Ice Condenser Plants)*, December 2007.
15. EMF-CC-039(P) Supplement 1 Revision 5, *ICECON Code User's Manual: A Computer Program Used to Calculate Containment Back Pressure for LOCA Analysis (Including Ice Condenser Plants)*, July 2007.
16. NUREG-0800, *U.S. Nuclear Regulatory Commission Standard Review Plan*.

17. NUREG/CR-4312, EGG-2396, Revision 1, *RELAP5/MOD2 code Manual, Volume 1: Code Structure, Systems Models, and Solution Methods*, March 1987.
18. NUREG/CR-5535, INEL-95/0174, *RELAP5/MOD3 Code Manual*, August 1995.
19. TID-4500, ANCR-1219, *CONTEMPT-LT – A computer Program for Predicting Containment Pressure-Temperature Response to a Loss-Of-Coolant Accident*, June 1975.
20. NUREG/CR-5535, S. Shieh, V. H. Ransom, R. Krishnamurthy, *RELAP5/MOD3 Code Manual, Validation of Numerical Techniques in RELAP5/MOD3*, Volume 6, August 1994.
21. R. R. Schultz, *RELAP5-3D Code Manual, User's Guidelines*, INEEL-EXT-98-00834, February 2001.
22. O. Nylund, et al., *Hydrodynamic and Heat Transfer Measurements on a Full-Scale Simulated 36-Rod Marviken Fuel Element with Uniform Heat Flux Distribution*, R4-447/RTL-1007, ASEA and AB Atomenergi, 1968.
23. Loftus, M. J. et al, *PWR FLECHT-SEASET Unblocked Bundle, Forced and Gravity Reflood Task Data Report*, NUREG/CR-1532, Volumes 1 and 2, June 1980.
24. NUREG/CR-2671 MXC-301, *The Marviken Full Scale Critical Flow Tests*, May 1982.
25. EMF-2102(P) Revision 0, *S-RELAP5 Code Verification and Validation Document*, Framatome ANP Richland, Inc., April 2003.
26. MPR Report, *Summary of Results from the UPTF Downcomer Separate Effects Tests, Comparisons to Previous Scaled Tests, and Application to U.S. Pressurized Water Reactors*, MPR-1163, July 1190.
27. MPR Report, *Summary of Results from the UPTF Cold Leg Flow Regime Separate Effects Tests, Comparison to Previous Scaled Tests, and Application to U.S. Pressurized Water Reactors*, MPR-1208, October 1992.
28. Holmes, B. J, *I25 Comparison Report*, NEA/CSNI/R(91)1, AEA-TRS-1043, February 1991.
29. NUREG/CR-2256, EPRI NP-2013, WCAP-8891, *FLECHT-SEASET Program, PWR FLECHT SEASET Unblocked Bundle, Forced and Gravity Reflood Task Data Evaluation and Analysis Report*, November 1981.
30. NUREG/IA-0128, *International Code Assessment and Application Program: Summary of Code Assessment Studies Concerning RELAP5/MOD2, RELAP5/MOD3, and TRAC-B*, December 1993.
31. *Data Report on Large Scale Reflood Test-43 – CCTF CORE-II Shakedown Test C2-SH2 (Run 054)*, JAERI-memo 58-155, Japan Atomic Energy Research Institute, May 1983.

32. E. H. Karb et al., *KfK In Pile Tests on LWR Fuel Rod Behavior During the Heatup Phase of a LOCA*, KfK 3028, Kemforschungszentrum Karlsruhe GmbH, Karlsruhe.
33. J. V. Cathcart and R.E. Pawel, *Zirconium Metal-Water Oxidation Kinetics: IV. Reaction Rate Studies*, ORNL/NUREG-17, August 1977.
34. Kreyszig, E., *Advanced Engineering Mathematics*, Second Edition, John Wiley & Sons, Inc., 1967.
35. ANSI/ANS-5.1-1979, *American National Standard for Decay Heat Power in Light Water Reactors*, approved August 29, 1979.
36. NURGE/CR-0410, *Comparisons of Thermal-Hydraulic Phenomena During Isothermal Loss-Of-Coolant Experiments and Effect of Scale in LOFT and SEMISCALE MOD-1*, December 1978.
37. *UPTF: Program and System Description*, U9 414/88/023, Siemens AG, KWU Group (Erlangen), November 1988.
38. Wong, S., Hochreiter, L. E., *Analysis of the FLECHT SEASET Unblocked Bundle Steam Cooling and Boiloff Tests*, NUREG/CR 1533, EPRI NP 1460, WCAP-9729, January 1981.
39. Holman, J. P., *Heat Transfer*, 5<sup>th</sup> Edition, McGraw-Hill, New York, 1981.
40. Gebhart, B., *Heat Transfer*, 2<sup>nd</sup> Edition, McGraw-Hill, New York, 1971.
41. Dittus, F. W. and L. M. K. Boelter, *Heat Transfer in Automobile Radiators of the Tubular Type*, Publications in Engineering, Volume 2, pp. 443-461. University of California, Berkeley, 1930.
42. Chen, J. C., R. K. Sundaram, F. T. Ozkaynak, *A Phenomenological Correlation for Post-CHF Heat Transfer*, NUREG-0237, June 1977.
43. Bromley, L.A., *Heat Transfer in Stable Film Boiling*, Chemical Engineering Progress, Volume 46, pp. 221-227, 1950.
44. Berenson, P. J., *Film Boiling Heat Transfer from a Horizontal Surface*, Journal of Heat Transfer, pp. 351-358, 1961.
45. Drucker, M., Dhir, V. K., *Studies of Single and Two Phase Heat Transfer in a Blocked Four Rod Bundle*, EPRI-NP 3485, Electric Power Research Institute (1984).
46. M. J. Meholic, L. E. Hochreiter, J. H. Mahaffy, J. Spring, *Increased Convective Heat Transfer Caused by Spacer Grids in Laminar High Void Fraction Flows*, 2008 ANS Winter Meeting, Reno.
47. S. C. Yao, L. E. Hochreiter and W. J. Leech, *Heat Transfer Augmentation in Rod Bundles Near Grid Spacers*, Trans. ASME, 104, pp. 76-81, February 1982.

48. Sun, K.H., J.M. Gonzales-Santalo and C.L. Tien, *Calculations of Combined Radiation and Convection Heat Transfer in Rod Bundles Under Emergency Cooling Conditions*, Journal of Heat Transfer, pp. 414-420, 1976.
49. Taylor, D. D. et al., *TRAC-BD1/MOD1: An Advanced Best Estimate Computer Program for Boiling Water Reactor Transient Analysis, Volume 1: Model Description*, NUREG/CR-3633, EGG-2294, April 1984.
50. NUREG/CR-2435, ORNL-5822, *Dispersed Flow Film Boiling in Rod Bundle Geometry – Steady State Heat Transfer Data and Correlation Comparisons*, Oak Ridge National Laboratory, March 1982.
51. NUREG/CR-2469, ORNL/NUREG-85, *An Analysis of Transient Film Boiling of High-Pressure Water in a Rod Bundle*, Oak Ridge National Laboratory, March 1982.
52. NUREG/CR-2455, ORNL-5846, *Experimental Investigations of Bundle Boiloff and Reflood Under High-Pressure Low Heat Flux Conditions*, Oak Ridge National Laboratory, April 1982.
53. NUREG/CR-2114, ORNL/NUREG/TM-446, *ORNL Small-Break LOCA Heat Transfer Test Series I: High-Pressure Reflood Analysis*, Oak Ridge National Laboratory, August 1981.
54. *Pump Two-Phase Performance Program*, EPRI NP-1556, Volumes 1 through 8, September 1980.
55. BAW-10168-A, Revision 3, *RSG LOCA – BWNT Loss-of-Coolant Accident Evaluation Model for Recirculating Steam Generator Plants*, Volume I – Large Break, December 1996.
56. Damerell, P. S., Simsons, J. W., *Reactor Safety Issues Resolved by the 2D/3D Program*, NUREG/IA-0127, July 1993.
57. *Upper Plenum Test Facility, Test No. 8 Cold/Hot Leg Flow Pattern Test Experimental Data Report*, U9 316/88/12, Siemens AG, Erlangen Germany, September 1988.
58. *Upper Plenum Test Facility, Test No. 8 Cold/Hot Leg Flow Pattern Test Quick Look Report*, U9 316/88/11, Siemens AG, Erlangen Germany, September 1988.
59. XN-75-27(A), *Exxon Nuclear Neutronic Design Methods for Pressurized Water Reactors*, Exxon Nuclear Company, April 1977.
60. EMF-96-029(P)(A), *Reactor Analysis System for PWRs*, January 1997.
61. Wilks, S. S., *Determination of Sample Sizes for Setting Tolerance Limits*, Ann. Math. Stat., Vol. 12, pp. 91-96, 1941.
62. Somerville, P. N., *Tables for Obtaining Non-Parametric Tolerance Limits*, Ann. Math. Stat., Vol. 29, No. 2, pp 599-601, June 1958.

63. *An Acceptable Model and Related Statistical Methods for the Analysis of Fuel Densification*, Regulatory Guide 1.126, Revision 1, U.S. Nuclear Regulatory Commission, March 1978.
64. A. Wald, *An Extension of Wilk's Method for Setting Tolerance Limits*, Annals of Mathematical Statistics, Volume 14 (1943), 45-55.
65. J. W. Tukey, *Non-Parametric Estimation. II. Statistically Equivalent Blocks and Tolerance Regions – The Continuous Case*, Annals of Mathematical Statistics, Volume 18 (1947), 529-539.
66. A. Guba, M. Makai and L. Pal, *Statistical Aspects of Best Estimate Method—I*, Reliability Engineering and System Safety 80 (2003), 217–232.
67. Abramowitz, M. and I. Stegun, *Handbook of Mathematical Functions with Formulas, Graphs, and Mathematical Tables*, National Bureau of Standards, Applied Mathematics Series 55, 1966.
68. NAI 8907-09, Revision 10, Version 7.2b(QA), *GOTHIC Containment Analysis Package Qualification Report*, EPRI, Palo Alto, California, March 2009.
69. NEA/CSNI/R(2004)19, *SEGFSM Topical Meeting on LOCA Fuel Issues*, Argonne National Laboratory, May 25-26 2004, Published by Organization for Economic Cooperation and Development Nuclear Energy Agency, Isy-les-Moulineaux, France, November 2004.
70. V. T. Breta, et al., *Determination of the Bias in LOFT Fuel Peak Cladding Temperature Data from the Blowdown Phase of Large-Break LOCA Experiments*, NUREG/CR-6061, May 1993.

## **Appendix A Time Step Sensitivity**

For the AREVA RLBLOCA methodology, solution convergence is demonstrated by performing sensitivity studies in which the calculation time step was varied for three appropriate plant designs. This is an accepted approach to demonstrate solution convergence while recognizing that a certain degree of variability is to be expected.

This sensitivity study was performed by first regenerating steady-state plant analysis decks for three types of plants appropriate for this methodology, i.e., 3- and 4-loop Westinghouse designs, and a CE design. These decks were then brought to typical steady-state conditions, and a transient initiated with a DEG break with nominal parameters, other than decay heat. Each transient used 120 percent of nominal decay heat to drive the temperatures sufficiently high that code models would be challenged.

The recommended time step selection strategy is to set a single maximum time step during the portions of the transient of most significance to safety, that is, the blowdown, refill, and early reflood phases. The requested time step should then be increased during late reflood when the flooding phenomena are reasonably stable. This approach was found to provide a reasonable compromise between optimal numerical stability and run time. It should be noted that the time step requested by the user is actually the maximum time step allowed by the code for that time period, and that in fact the code will reduce the requested time step should instability be detected. The nominal or base case used a requested time step of 0.002 seconds from 0 to 400 seconds, and then 0.004 seconds from 400 to 600 seconds, 0.008 seconds from 600 to 800 seconds and 0.010 seconds beyond 800 seconds. Code convergence and stability at the nominal time step of 0.002 seconds were demonstrated by incrementally varying the time step from 0 to 400 seconds over a range from the nominal time step to an order of magnitude smaller.

[

]

The nominal case for each of the designs noted in the time step sensitivity study was repeated with this new time step and it was determined that the code continued to proceed through the analysis with the requested time steps, indicating code stability, with a minor deviation at the time of quench at the core hot spot.

Figure A.1, Figure A.3, and Figure A.5 show the calculated PCTs from the 3-loop, 4-loop, and CE studies, respectively. S-RELAP5 shows stability and convergence for all design types during the blowdown period. During refill and early reflood, there is some noticeable divergence in the results; however this has little impact on the PCT. Figure A.2, Figure A.4, and Figure A.6 show the variability about the mean PCT from the 3-loop, 4-loop, and CE studies, respectively. The data for these figures were generated by averaging the calculated PCTs for each design, and then calculating the maximum deviation, whether it is above or below the mean. As shown in these figures, the nominal variability for the 3-loop design is approximately 15 K (27 °F), the 4-loop design is approximately 12 K (21 °F), and the CE design is approximately 15 K (27 °F).

[

]

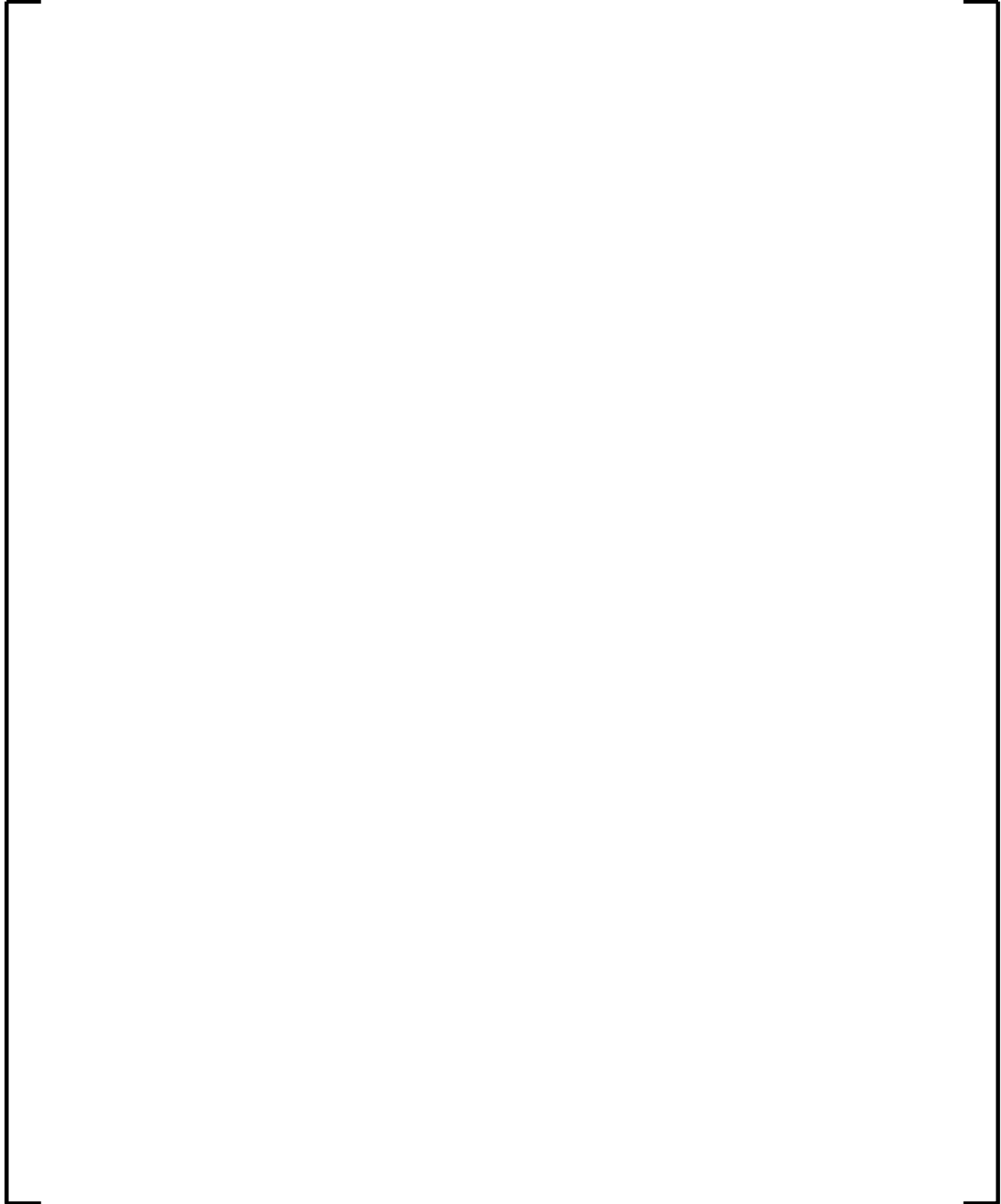


**Figure A.1: Time Step Sensitivity of Westinghouse 3-Loop Analysis**



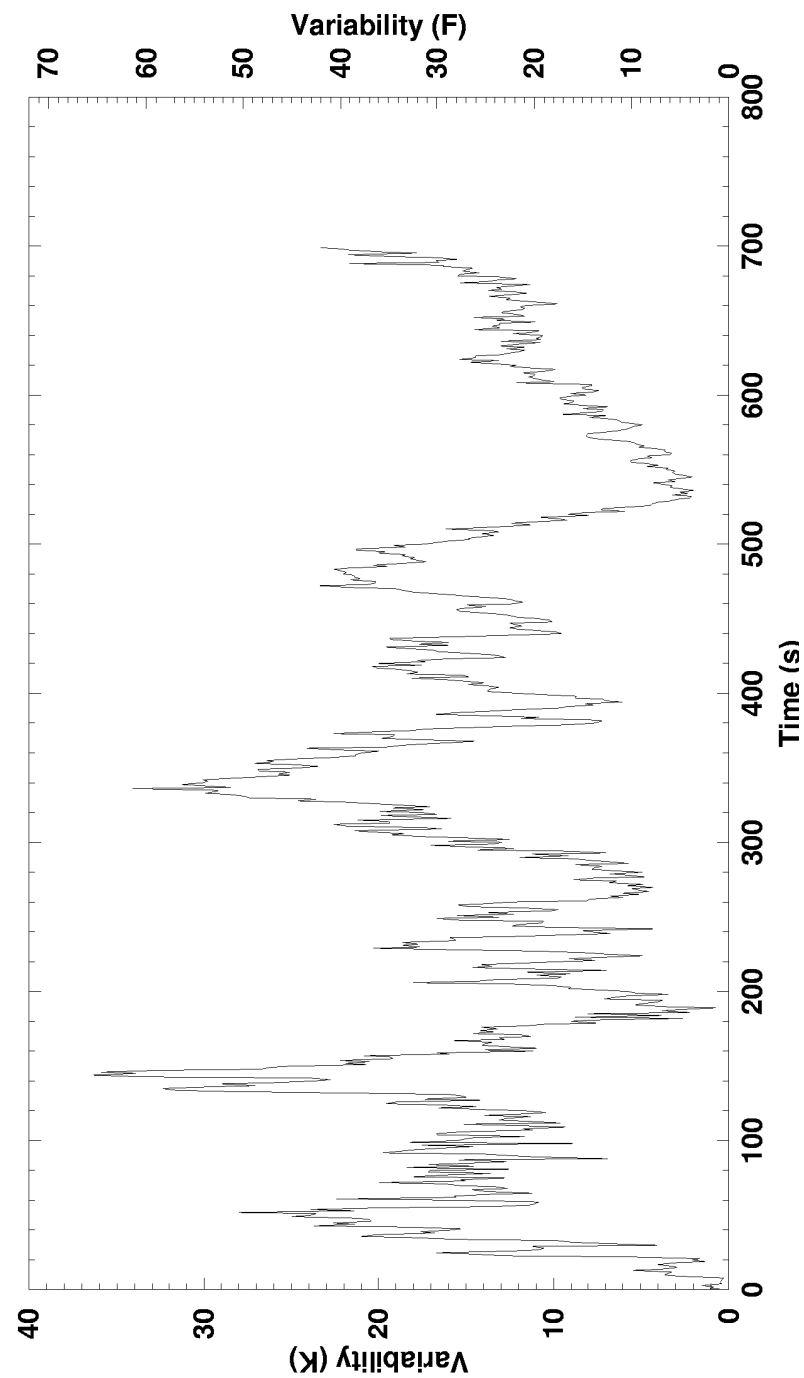
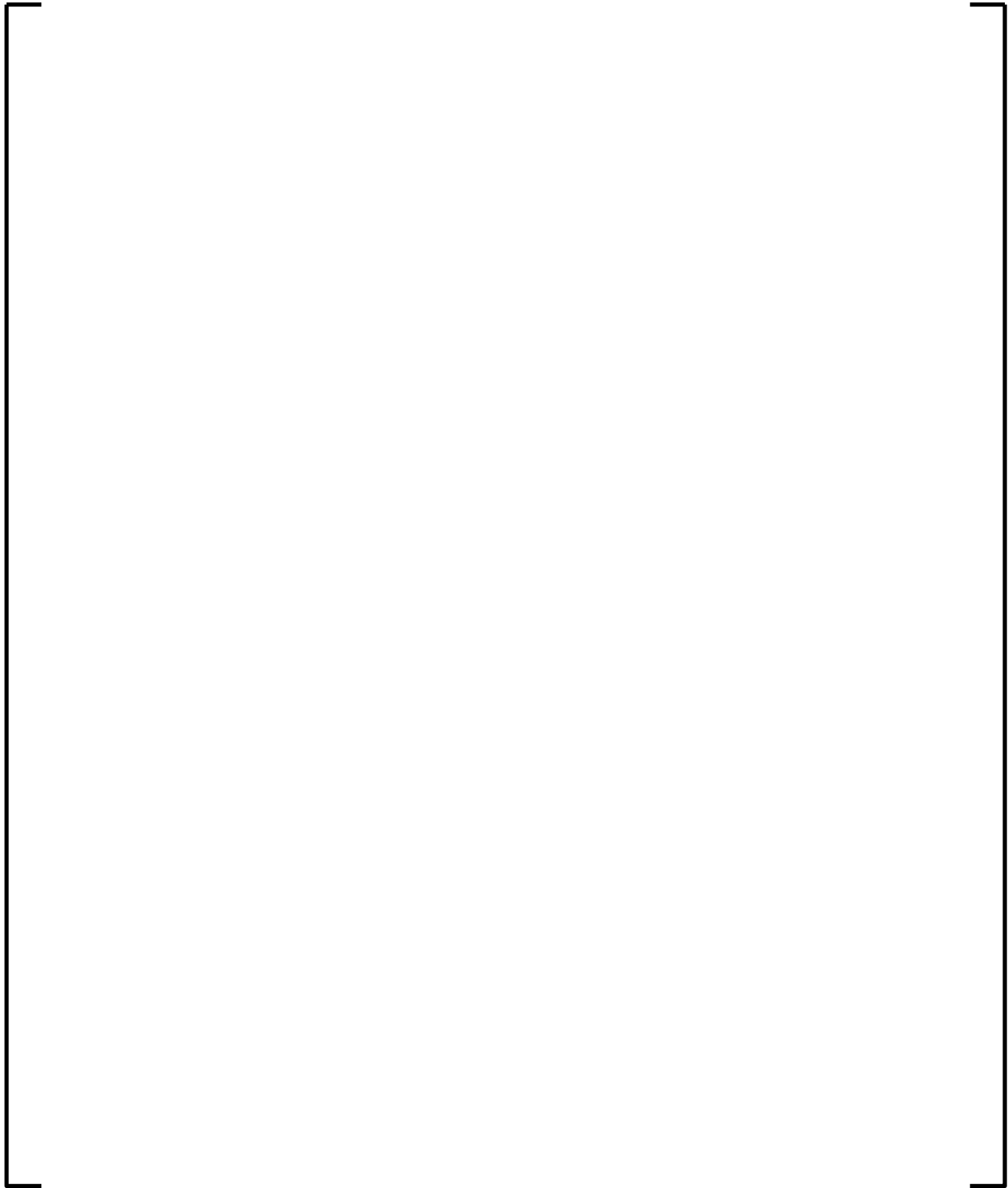


Figure A.2: Variability of Westinghouse 3-Loop Analysis



**Figure A.3: Time Step Sensitivity of Westinghouse 4-Loop Analysis**

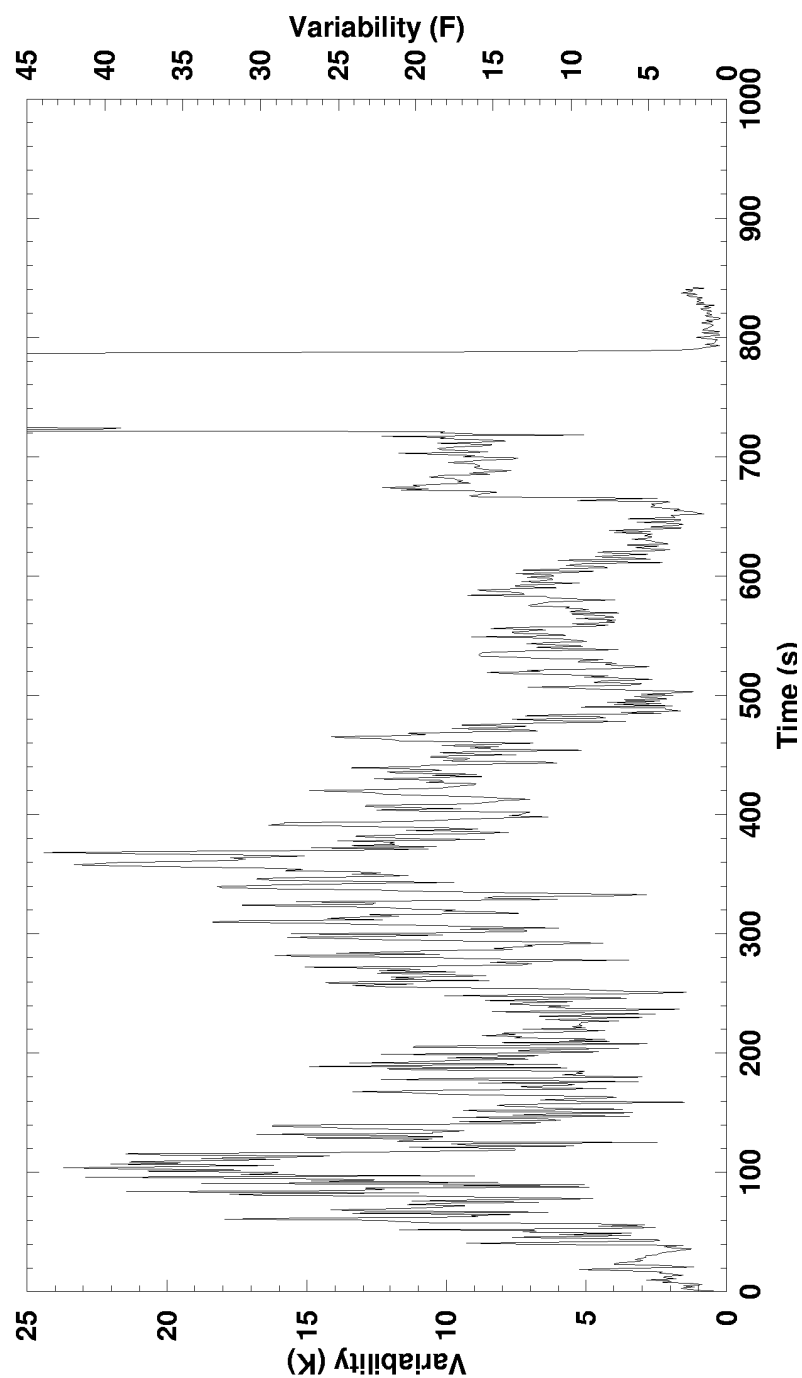
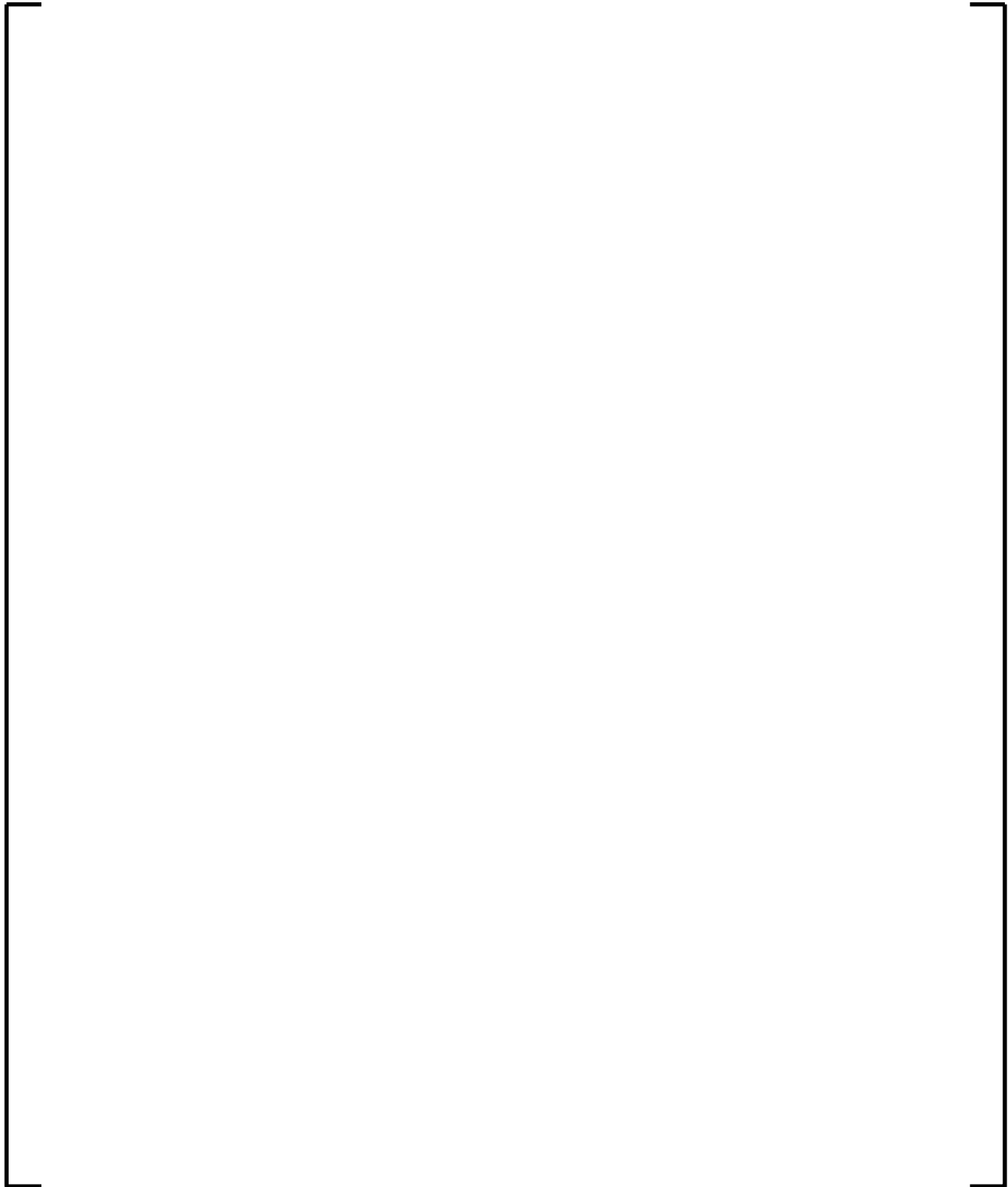


Figure A.4: Variability of Westinghouse 4-Loop Analysis



**Figure A.5: Time Step Sensitivity of CE Analysis**

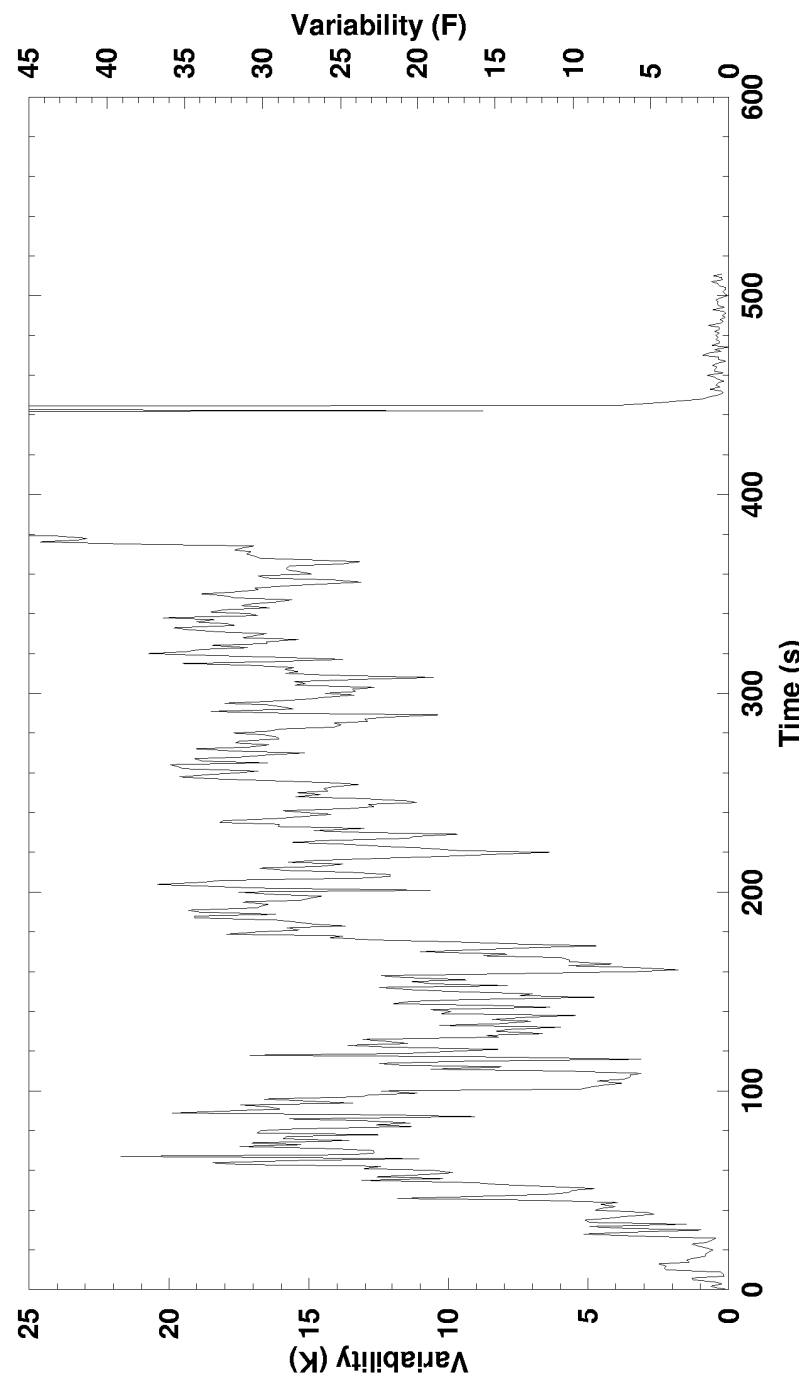


Figure A.6: Variability of CE Analysis

## **Appendix B    Sample PWR Licensing Analyses**

### **B.1    Introduction**

This appendix provides sample RLBLOCA analyses for a Westinghouse 3- and 4-loop PWR and a Combustion Engineering 2x4 PWR. These sample analyses are presented to provide representative solutions to the RLBLOCA evaluation and the reporting or recording of such analyses. None of the sample problems are fully representative of any specific plant. The analyses contain inconsistencies relative to nominal core designs but each has been reviewed to assure that it offers an accurate representation of the RLBLOCA evaluation model findings and conclusions. The first three sample analyses have AREVA fuel with M5<sup>®</sup> cladding and utilize the COPENIC2 code for fuel calculations within S-RELAP5. The fourth sample analysis has AREVA fuel with Zirc-4 cladding and utilizes the RODEX3A code for fuel calculations within S-RELAP5.

RLBLOCA analyses, as illustrated by the sample analyses, are designed to support operation for a typical reload cycle. It also applies to subsequent cycles, unless changes in the Technical Specifications, Core Operating Limits Report, fuel design, plant hardware, or plant operation cause model input revisions.

The non-parametric statistical methods inherent in the AREVA RLBLOCA methodology considers a full spectrum of break sizes, break configurations (guillotine or split break), axial shapes, and plant operational parameters. A conservative single failure assumption is applied in which the negative effects of both the loss of a low pressure safety injection pump and the loss of a diesel generator are simulated. The effects of Gadolinia bearing fuel rods and peak fuel rod exposures are also considered.

Section B.1.1 describes the criteria that the RLBLOCA analyses will analyze. Section B.1.2 of this report describes the models used in the analysis. Section B.1.3 describes the GDC-35 limiting condition. Section B.1.4 describes the statistical compliance to the acceptance criteria. Section B.1.5 discusses the application of heat transfer correlations. Section B.2 describes the 3-loop PWR plant analysis, Section B.3 describes the 4-loop PWR plant analysis, and Section B.4 describes the CE 2x4 PWR plant analyses.

### B.1.1 Analysis

The purpose of the analysis is to verify typical technical specification peaking factor limits and the adequacy of the ECCS by demonstrating that the following 10 CFR 50.46(b) criteria are met:

- The calculated maximum fuel element cladding temperature shall not exceed 2200 °F.
- The calculated total oxidation of the cladding shall nowhere exceed 0.17 times the total cladding thickness before oxidation.
- The calculated total amount of hydrogen generated from the chemical reaction of the cladding with water or steam shall not exceed 0.01 times the hypothetical amount that would be generated if all of the metal in the cladding cylinders surrounding the fuel excluding the cladding surrounding the plenum volume were to react.

As discussed in Section 2.1, the two remaining 10 CFR 50.46(b) criteria require evaluations beyond the capability of this methodology and are treated separately during plant evaluations.

### B.1.2 Description of Analytical Models

The modeling of plant components is performed by following guidelines developed to ensure accurate accounting for physical dimensions and that the dominant phenomenon expected during a LBLOCA event are captured. The basic building block for modeling is the hydraulic volume for fluid paths and the heat structure for a heat transfer surface. In addition, special purpose components exist to represent specific components such as the pumps or the steam generator separators. All geometries are modeled at the resolution necessary to best resolve the flow field and the phenomena being modeled within practical computational limitations.

A typical calculation using S-RELAP5 begins with the establishment of a steady-state, initial condition with all loops intact. The input parameters and initial conditions for this steady-state calculation are chosen to reflect plant technical specifications or to match measured data. Specific parameters are discussed in Sections B.2.2, B.3.2, and B.4.2.

Following the establishment of an acceptable steady-state condition, the transient calculation is initiated by introducing a break into one of the loops. The evolution of the transient through blowdown, refill, and reflood is computed continuously using S-RELAP5. Containment pressure is calculated by the ICECON module within S-RELAP5.

A detailed assessment of the S-RELAP5 computer code was made through comparisons to experimental data. These assessments were used to develop quantitative estimates of the ability of the code to predict key physical phenomena in a PWR LBLOCA. The final step of the best-estimate methodology is to combine all the uncertainties related to the code and plant parameters and estimate the PCT at 95 percent probability and 95 percent confidence. The steps taken to derive the PCT uncertainty estimate are summarized below:

### *1. Base Plant Input File Development*

First, base COPENIC2 (or RODEX3A) and S-RELAP5 input files for the plant (including the containment input file) are developed. Code input development guidelines are applied to ensure that the model nodalization is consistent with the model nodalization used in the code validation.

### *2. Sampled Case Development*

The non-parametric statistical approach requires that many “sampled” cases be created and processed. For every set of input created, each “key LOCA parameter” is randomly sampled over a range established through code uncertainty assessment or expected operating limits (provided by plant technical specifications or data). Those parameters considered “key LOCA parameters” are listed in Table B.1. This list includes both parameters related to LOCA phenomena (based on the PIRT provided in Section 3.3) and to plant operating parameters.

### *3. Determination of Adequacy of ECCS*

The RLBLOCA methodology uses a non-parametric statistical approach to determine that the first three criteria of 10 CFR 50.46 (PCT < 2200 °F, local oxidation < 17 %, and core-wide oxidation < 1 %) are met with a probability higher than 95 percent with 95 percent confidence.

#### **B.1.3      GDC-35 Limiting Condition Determination**

GDC-35 states that the plant shall be able to mitigate design basis accidents with or without off site power available. The methodology does this by determining the most severe condition between these two configurations and then performing the RLBLOCA statistical analysis for the plant with off site power availability set to the most severe condition.



To determine the limiting assumption, a sensitivity study of two LBLOCA cases is performed with and without offsite power available. The plant conditions incorporated in this study are set to those expected to challenge the ECCS capability, such that the validity of the result is established for conditions expected to be representative of those that will eventually determine the LBLOCA results which will be compared to the 10 CFR 50.46 criteria.

An examination of the PIRT (Table 3.1) for high ranking items resulted in the selection of the following parameters (where appropriate, representative values used in the sensitivity studies are also provided):

- Core Power (set to nominal power plus uncertainty)
- Decay Heat (1.02 multiplier)
- Initial Stored Energy (set to upper value of the standard deviation)
- $F_q$  (Set to Technical Specification maximum)
- Time in Cycle – Fresh Fuel (time of peak assembly power)
- Time in Cycle – Burned Fuel (time of peak assembly power)
- Axial Skew (Only requirement is to have positive ASI)
- Break (double-ended guillotine, 2 x cold leg pipe area)
- Break Discharge Loss Coefficients (set to 0.9917)
- BIASI Critical Heat Flux (set to 0.86)
- Film Boiling (randomly selected value of FILMBL reduced by 75 percent)
- Dispersed Flow Film Boiling HTC (set to 0.75)
- $T_{min}$  (set to the median value, 636.0 K)
- Condensation Interphase HTC (set to 75.0 for vapor side, void dependent multiplier for liquid side)
- Accumulator Cover Gas Pressure (set to the lower bound)
- Accumulator Volume (set to average of lower and upper bound)

The study is performed with and without off site power available. As mentioned previously, the conditions assumed will be based on those considered to be representative of the LBLOCA results that be compared to the 10 CFR 50.46 criteria. The statistical case set, set of LBLOCA sample events, is then run under the assumption that off site power is always either available or unavailable according to the study result.

#### B.1.4 Overall Statistical Compliance to Criteria

For the RLBLOCA analyses the determination of compliance to the criteria is treated as a [ ] with all three of the first three criteria of 10 CFR 50.46 using non-parametric statistics. The approach is outlined in detail in Section 5.2 of this report. [ ]

[ ] Generally, the minimum margins for each of the three parameters of interest will be established by different cases. For the sample evaluations presented in this appendix, a case set size of 208 was selected. At this size, the 95/95 metric value is provided by the [ ] for the criterion of interest.

#### B.1.5 Application of Heat Transfer Correlations

During a transient simulation, different heat transfer correlations may be applied at any given time. The best way to demonstrate how the S-RELAP5 simulation of a LBLOCA is supported by correlation development and validation studies is to first identify (or map) the “simulation-space” and compare it to the “assessment-space.” The assessment-space represents the combination of the applicability range from separate-effects investigation (i.e., correlation development or derivation), the expanded applicability range from uncertainty analysis, and validation from integral-effects benchmark calculations. The simulation-space is evaluated through the examination of the limiting calculations (in terms of PCT) for the 3- and 4-loop and CE sample problems for key correlation dependent parameters. The key parameters are defined as those engineered parameters that can be designed into a thermal-hydraulic test matrix. The most common engineered parameters used in thermal-hydraulic testing and correlation development are pressure, power (in terms of LHGR, or heat flux), and mass flux (may also be given as Reynolds number or mass flow).

The comparison of the simulation-space and the assessment-space provides quantitative support to CSAU Step 6, Determination of Code Applicability (Reference B.1). As stated in Reference B.1, “if inadequacies are noted, they should be fully documented and, if possible, quantified.” Ideally, the assessment-space will span the simulation-space; however,

realistically, there will likely be holes in the assessment-space. To prioritize the effort in demonstrating adequate coverage, AREVA presented a PIRT for the LBLOCA in Section 3.3. This PIRT identified and ranked the relevant phenomena of importance for a LBLOCA. The important heat transfer regimes are nucleate boiling, CHF (DNB), transition boiling, and film boiling. It was the conclusion of the AREVA PIRT team that the other heat transfer regimes were either not present or had negligible impact on peak clad temperatures. In fact, it was concluded that nucleate boiling has a relatively low ranking during a LBLOCA event.

The best resource for information about the heat transfer regimes and their application can be found in Section 4 of Reference B.2. The selection logic for each heat transfer regime is presented in Figure 4.1 of that document. As a summary, Table B.2 highlights the heat transfer correlations used in S-RELAP5. Table B.15, Table B.24, Table B.34, and Table B.35 summarize the different heat transfer regimes, the heat transfer correlations used, and the approximate parameter ranges for the 3- and 4-loop and CE sample problems.

### **Time Period: Early Blowdown**

Immediately following the postulated LBLOCA, portions of the core will, for a brief time, be in the nucleate boiling heat transfer regime until CHF is achieved. The duration of this period depends on the size of the break; however, for the typical limiting PCT break, this period will last only several seconds, at most. This period is more influenced by the CHF correlation, rather than the nucleate boiling heat transfer correlation, because CHF triggers the time of transition to the low heat transfer regimes (post-CHF). Table B.3 provides a comparison of the simulation-space (taken from Table B.15, Table B.24, Table B.34, and Table B.35) and the range of applicability evaluated for the assessment-space for the CHF correlation.

### **S-RELAP5 Implementation of CHF**

Early in the transient, heat transfer in the core rapidly advances to post-CHF conditions. Nonetheless, the Biasi correlation was assessed against the tests performed on the THTF at Oak Ridge National Laboratory and a bounding bias was determined for application in the RLBLOCA methodology. This study is presented in Section 4.3.1.1. Further discussion is provided in Section 4.13 of EMF-2100 (Reference B.2).

Table B.3 provides a comparison of the simulation-space (taken from Table B.15, Table B.24, Table B.34, and Table B.35) and the range of applicability evaluated for the assessment-space for the Biasi CHF correlation. Note that the assessment-space includes three components as previously described: (1) the test conditions used in correlation development, (2) relevant uncertainty analysis, and (3) integral-effects validation.

### **Time Period: Blowdown**

As the RCS depressurizes and CHF is reached in the core, vapor generation is rapid and the steam quality increases. This post-CHF period is characterized by film boiling, single-phase steam convection, and radiation (although radiation is not expected to be significant; hence, it does not appear in the PIRT). As long as the steam maintains some wetness, the total heat transfer includes all three heat transfer mechanisms; however, single-phase steam convection dominates heat transfer when void fractions are above about 0.90. Post-CHF heat transfer includes uncertainty not only from the application of the correlations, but also from contributions of interfacial drag and heat transfer phenomena. For this reason, total post-CHF heat transfer, rather than the individual correlations, is a statistically treated parameter. Table B.4 provides a comparison of the simulation-space (taken from Table B.15, Table B.24, Table B.34, and Table B.35) and the range of applicability evaluated for the assessment-space for the film boiling correlation.

### **S-RELAP5 Implementation of Film Boiling Heat Transfer**

Within S-RELAP5 both the modified Bromley and the Wong-Hochreiter correlation are used outside their derived range of applicability; however, applied statistical uncertainty on the total heat transfer provides the means for expanding the range of applicability. The primary deviations from the original range of applicability are:

- The modified Bromley correlation is limited to the condition where vapor void fraction is less than 0.9, rather than 0.4.
- Both correlations are used for the full range of pressure from 2250 psia to atmospheric.
- Wong-Hochreiter is used at Reynolds numbers lower than 2500.

A discussion of the statistical treatment of total heat transfer is presented in S-RELAP5 Verification and Validation document, EMF-2102 (Reference B.3). The uncertainty analysis applies data from the FLECHT-SEASET tests. The applicability of these tests was evaluated by

analysis of the breadth of the data in terms of key correlation parameters and the density of the data in terms of the parameters for which the correlation is most sensitive, pressure and void fraction. [

] The IETs were initiated from full pressure conditions.

#### S-RELAP5 Implementation of Single-Phase Vapor Convection

Single-phase vapor heat transfer was assessed using the 161-rod bundle FLECHT-SEASET steam cooling tests (Reference B.3). The LOFT and Semiscale integral tests during the refill period and the separate effect assessments, including FLECHT-SEASET, CCTF and SCTF, during the early period of adiabatic heat-up were used to validate single-phase heat transfer at low flows.

Low flows that directionally oscillate are characteristic during refill in both the tests and the calculations. In LBLOCA calculations during vessel refill, vapor flow rates decelerate and directionally oscillate as a result of the transition to refill. This will last until the beginning of core reflood, which is a period typically less than 15 seconds. During this unsettled period, core flow will likely remain turbulent; however, vapor Reynolds numbers will be low.

In general, the S-RELAP5 results conservatively bound the measured results (higher clad temperatures). While the results of the assessments demonstrated that the Wong-Hochreiter correlation is adequate for post-blowdown periods during a LOCA (and lower Reynolds numbers), single-phase vapor heat transfer is treated implicitly in the evaluation of uncertainty in the total post-CHF heat transfer (see previous section).

#### S-RELAP5 Implementation of Radiation

Thermal radiation [ ] provides a significant contribution to the total heat transfer. The wall-to-fluid radiation is intrinsic to the heat transfer model and is implicitly validated in all post-CHF assessments. The wall-to-structure component is activated through input and required a separate assessment of the performance of the model and a separate assessment of the rod-to-rod radiation model's implementation into the plant model.

[

]

#### **Time Period: Refill**

During the refill period, the RCS has nearly depressurized and the core region is devoid of coolant. Heat transfer in the core is almost all from single-phase vapor. As previously stated, single-phase vapor heat transfer is predicted using the Wong-Hochreiter correlation. The core conditions during this time are consistent with both the derived range of applicability and the FLECHT-SEASET steam cooling tests. While post-CHF total heat transfer is a statistically treated parameter, there is no bias or uncertainty applied when void fraction equals 1.0. As assessed from the FLECHT-SEASET steam cooling tests, the Wong-Hochreiter correlation is slightly conservative relative to the data. Analysis of the integral tests assessment cases support this finding.

Since the single-phase vapor heat transfer is a component of film boiling, refer to Table B.4 for a comparison of the simulation-space (taken from Table B.15, Table B.24, Table B.34, and Table B.35) and the range of applicability evaluated for the assessment-space for the single-phase vapor heat transfer correlation.

### **Time Period: Reflood**

By this time, the RCS pressure has established some equilibrium with the relative low pressure containment. ECCS coolant from the accumulator begins to reach the lower portions of the core and a definite two-phase mixture is present throughout the core region. With the constant supply of coolant, a quench front is established at the bottom of the core that slowly moves upward. At some point the coolant supply from the accumulator ends and core heat removal relies solely on that provided by the pumped injection safety systems. This may result in a late reflood heat up. Nonetheless, in time, this supply of coolant will be able to completely quench all the fuel rods in the core.

For the duration of this period, the heat structure nodes with the highest temperatures are removing heat by film boiling. Table B.4 provides a comparison of the simulation-space (taken from Table B.15, Table B.24, Table B.34, and Table B.35) and the range of applicability evaluated for the film boiling assessment-space. This period ends with the fuel rod quenched, which will occur shortly after meeting the conditions for transition boiling.

#### **S-RELAP5 Implementation of Reflood Heat Transfer**

When core reflood is enabled in S-RELAP5 (provided in the input model), a heat transfer regime profile covering the entire boiling curve is established along the modeled heat structure. Proceeding from the bottom of the core, this will be single-phase liquid and/or nucleate boiling, transition boiling, and single-phase vapor and/or film boiling. The same heat transfer correlations apply that would apply otherwise; the only major difference is the forced mapping of the heat transfer profile that keys on the calculation of CHF wall temperature from the Modified Zuber CHF correlation.

The uncertainty and bias for the total post-CHF heat transfer includes data from FLECHT-SEASET simulations that modeled reflood heat transfer. The range of applicability was presented previously in the discussion of film boiling.

#### **S-RELAP5 Implementation of Transition Boiling**

In general, the application of the modified Chen correlation is within its range of applicability; however, system pressures will likely be lower than the 61 psia used in the derived range of applicability. In limiting RLBLOCA simulations (high clad temperatures), the PCT sensitivity to

transition boiling is minimal. This is because the location of PCT in these limiting cases is well above the quench plane. Once heat transfer moves into the transition boiling regime, the feedback from the cooler cladding temperature enhances heat transfer rapidly and within seconds the heat transfer moves into the nucleate boiling regime. Considering the distance between the quench location and the PCT location, heat transfer below the quench front has little direct influence on PCT when there is no bulk boiling.

The results of several test validation problems including LOFT, CCTF and Semiscale, presented in Section 4.3 (also Sections 3 and 4 in Reference B.3), show that the quenching of the cladding occurs soon after the heat transfer regime is switched from film boiling to transition boiling. Therefore, the determination of the transition point is more important than the transition boiling heat transfer. For this reason, a  $T_{\min}$  model defining the transition from film boiling to transition boiling is used in S-RELAP5.

Table B.5 provides a comparison of the simulation-space (taken from Table B.15, Table B.24, Table B.34, and Table B.35) and the range of applicability evaluated for the assessment-space for the Modified Chen transition boiling correlation. [

]

### **Time Period: Long-Term Cooling**

This period is characterized by single-phase liquid or nucleate boiling heat transfer. Peak clad temperatures are not influenced by this condition. Calculations are terminated after whole-core quench.

#### **S-RELAP5 Implementation of Nucleate Boiling Heat Transfer**

Since nucleate boiling is not considered to have a significant influence on clad temperatures, no formal assessment was performed. S-RELAP5 was assessed for the few high pressure boil-off tests presented in Reference B.3; however, the focus of these tests is the more dominant film boiling phenomena.

Table B.6 provides a comparison of the simulation-space (taken from Table B.15, Table B.24, Table B.34, and Table B.35) and the range of applicability evaluated for the assessment-space for the Chen nucleate boiling correlation. Note: the assessment-space includes three



components as previously described—the test conditions used in correlation development, relevant uncertainty analysis, and integral-effects validation.

## Summary

As has been presented, individual correlations have been programmed into S-RELAP5; however, during a LBLOCA calculation multiple correlations will be employed simultaneously to calculate a total heat transfer during post-CHF conditions. In addition, correlations for interfacial phenomena will also influence this calculation. For this reason, it is the superposition of these individual correlations that becomes the post-CHF heat transfer correlation in S-RELAP5. The pedigree of this “correlation” relies on the range of applicability of the individual correlations, the range of applicability provided by the uncertainty analysis using FLECHT-SEASET datasets and the RLBLOCA analysis methodology, and the various benchmarks.

Table B.7 presents a collective summary of the coverage of the assessment-space provided in the discussion of the heat transfer regimes (including data provided in Table B.3 through Table B.6). This includes the derived range of applicability, the expanded range of applicability based on statistical treatment (the uncertainty analysis), and code-to-data comparisons. In general, the FLECHT-SEASET test-spaces, used to expand the range of applicability, encompass the original derived range of applicability. In addition, a number of integral test simulations were performed and are presented in Section 4.3.2 and in Reference B.3. The integral tests, including LOFT, CCTF, SCTF, and Semiscale, provide the largest coverage of the assessment-space; that is, they were performed at typical LBLOCA conditions. The demonstration of acceptable agreement among these validation cases sufficiently completes the assessment-space and the assessment-space provides sufficient coverage over the simulation-space.

**Table B.1: Sampled LBLOCA Parameters**

Phenomenological	
	Time in cycle (peaking factors, axial shape, rod properties, burnup)
	Break type (guillotine versus split)
	Break size
	Critical flow discharge coefficients (break)
	Decay heat
	Critical flow discharge coefficients (surge line)
	Initial upper head temperature
	Pump 2-phase degradation
	Film boiling heat transfer
	Dispersed film boiling heat transfer
	Critical heat flux
	$T_{\min}$ (intersection of film and transition boiling)
	Initial stored energy
	Downcomer hot wall effects
	Steam generator interfacial drag
	Condensation interphase heat transfer
	Metal-water reaction
Plant <sup>1</sup>	
	Pressurizer pressure
	Pressurizer level
	Accumulator pressure
	Accumulator level
	Accumulator temperature
	Containment temperature
	Containment volume
	Initial flow rate
	Initial operating temperature
	RWST temperature

<sup>1</sup> Uncertainties for plant parameters are based on typical plant-specific data with the exception of "Offsite power availability," which is specified in the RLBLOCA Analysis Guideline.

**Table B.2: Identification of Heat Transfer Parameters during a Limiting  
LBLOCA Simulation**

Heat Transfer Regime	Correlations	Reference
Single-phase liquid convection	Dittus-Boelter	B.4
Nucleate boiling	Chen	B.5
Critical Heat Flux, $G < 100 \text{ kg/m}^2\text{-s}$	Modified Zuber	B.6
Critical Heat Flux, $G > 200 \text{ kg/m}^2\text{-s}$	Biasi	B.7
Transition boiling	Modified Chen	B.8
Film boiling, $\alpha < 0.9$	Modified Bromley	B.9
Single-phase vapor convection	Wong-Hochreiter	B.3
Condensation	Carpenter and Colburn	B.10
Convection to noncondensable-water mixture	RELAP5/MOD2	B.11
Radiation to fluid	Sun (Stefan-Boltzman)	B.12
Radiation to walls	Theoretical	N/A

**Table B.3: Simulation and Application Space for CHF during Blowdown**

Parameter	Simulation-Space	Application-Space		
		Derivation	Uncertainty Analysis	Validation
Pressure (psia)	< 2320	40 < P < 2050 (Biasi)	630 < P < 1900 (THTF)	< 2250 (LOFT, blowdown)
LHGR <sub>max,avg</sub> (kW/ft)	q <sub>chf</sub>	q <sub>chf</sub>	q <sub>chf</sub>	q <sub>chf</sub>
Core Inlet Mass Flux (kg/s-m <sup>2</sup> )	< 3700	< 6000 (Biasi)	< 4250 (THTF)	< 4250 (THTF)

**Table B.4: Simulation and Application Space for Film Boiling Heat Transfer Including Thermal Radiation**

Parameter	Simulation-Space	Application-Space		
		Derivation	Uncertainty Analysis	Validation
Pressure (psia)	< 1575	14.7 – 103 (Modified Bromley) 40 (Wong-Hochreiter)	20 – 60 (FLECHT-SEASET)	< 2250 (LOFT, SemiScale) 20-60 (FLECHT-SEASET, FLECHT Skewed) 350-600 (THTF)
LHGR <sub>max,avg</sub> (kW/ft)	< 1.68	< 0.9 (Modified Bromley)	< 0.7 (FLECHT-SEASET)	< 0.1 to 5.5 (THTF) < 1.03 (LOFT, SemiScale) < 0.82 (CCTF)
Core Inlet Mass Flux (kg/s-m <sup>2</sup> )	< 1400	< 300 (Modified Bromley)	< 150 (FLECHT-SEASET)	< 1100 (LOFT, SemiScale, CCTF) < 4250 (THTF)
Vapor Reynolds Number	< 1.46x10 <sup>5</sup>	2.5x10 <sup>3</sup> < Re < 2.0x10 <sup>4</sup> (Wong-Hochreiter)	0 < Re < 20000 (FLECHT-SEASET)	2500-2.0x10 <sup>4</sup> (FLECHT-SEASET Steam Cooling) 0 < Re < 5x10 <sup>4</sup> (LOFT, SemiScale, others)
Void	< 1.0	< 0.4 (Modified Bromley) 1.0 (Wong-Hochreiter)	< 1.0	< 1.0 (LOFT, SemiScale)

**Table B.5: Simulation and Application Space for Transition Boiling Heat Transfer**

Parameter	Simulation-Space	Application-Space		
		Derivation (Modified Chen)	Uncertainty Analysis	Validation
Pressure (psia)	< 28	61 – 2830	20 – 60 (FLECHT-SEASET)	30 - 40 (LOFT, SemiScale)
LHGR <sub>max,avg</sub> (kW/ft)	< 0.40	< 13.5	< 0.7 (FLECHT-SEASET)	< 0.82 (CCTF)
Core Inlet Mass Flux (kg/s-m <sup>2</sup> )	< 300	< 26	< 150 (FLECHT-SEASET)	< 200 (CCTF) < 50 (LOFT, SemiScale)
Void	< 0.95	N/A	< 1.0	< 1.0 (LOFT, SemiScale)

**Table B.6: Simulation and Application Space for Nucleate Boiling Heat Transfer (late reflood)**

Parameter	Simulation-Space	Application-Space	
		Derivation (Chen)	Validation
Pressure (psia)	< 28	< 510	< 40 (LOFT, SemiScale)
LHGR <sub>max,avg</sub> (kW/ft)	< 0.40	< q <sub>chf</sub>	< 0.82 (CCTF)
Core Inlet Mass Flux (kg/s-m <sup>2</sup> )	< 1000	N/A	< 200 (CCTF) < 50 (LOFT, SemiScale)

**Table B.7: Summary of Full Range of Applicability**

Heat Transfer Mode	Heat Transfer Correlations	Pressure (psia)	LHGR <sub>max,avg</sub> (kW/ft)	Core Inlet Mass Flux (kg/s-m <sup>2</sup> )	Vapor Reynolds Number
CHF*	Zuber (< 100 kg/s-m <sup>2</sup> ) Biasi (> 200 kg/s-m <sup>2</sup> )	< 2250	< q <sub>chf</sub>	< 6000	N/A
Film Boiling	Modified Bromley ( $\alpha < 0.9$ ) Wong-Hochreiter	< 2250	< 5.5	< 4250	< 10 <sup>6</sup>
Single-Phase Vapor ( $\alpha = 1.0$ )	Wong-Hochreiter	< 2250	< 0.7	< 4250	< 2.5x10 <sup>4</sup>
Transition Boiling	Modified Chen Transition boiling	< 2830	< 13.5	< 200	N/A
Nucleate Boiling	Chen Nucleate Boiling	< 510	< q <sub>chf</sub>	< 200	N/A

\* Interpolation between correlations is performed between 100 kg/s-m<sup>2</sup> < mass flux < 200 kg/s-m<sup>2</sup>.

## **B.2 Westinghouse 3-Loop PWR**

### **B.2.1 Summary**

The parameter specification for this analysis is provided in Table B.9. The analysis assumes full-power operation at 3200 MWt, a tube plugging level of up to 3 percent per steam generator, a total peaking factor ( $F_q$ ) of 2.44 including uncertainties, and a nuclear enthalpy rise factor ( $F_{\Delta H}$ ) of 1.73 (including a 4 percent uncertainty). The analysis supports operation with AREVA 17x17 HTP design fuel using standard  $UO_2$  fuel with 2, 4, 6, and 8 weight percent  $Gd_2O_3$  for fresh and standard  $UO_2$  fuel with 4, 6, and 8 weight percent  $Gd_2O_3$  for once-burned assemblies. The analysis addresses typical operational ranges or technical specification limits (whichever is applicable) with regard to pressurizer pressure and level; accumulator pressure, temperature (containment temperature), and level; core inlet temperature; core flow; containment pressure and temperature; and refueling water storage tank temperature. The analysis explicitly analyzes fresh and once-burned fuel assemblies. The two GDC 35 cases were run<sup>1</sup> and Loss of Offsite Power produced the limiting PCT; therefore, the 208 case set was run in this configuration.

The evaluation resulted in meeting the 10 CFR 50.46 criteria with a minimum margin of 11.8 percent with 95 percent coverage and 95 percent confidence. The parameter which set this margin was the PCT of 1940 °F and occurred in a fresh fuel rod with 17.4 GWd/mtU burnup.

### **B.2.2 Plant Description and Summary of Analysis Parameters**

The plant analysis presented in this section is a Westinghouse designed PWR, having three loops, each with a hot leg, a U-tube steam generator, and a cold leg with a RCP. The RCS also includes a pressurizer. The ECCS comprises three accumulators, one per loop, and one full train of LHSI and HHSI injection (after applying the single failure assumption). The HHSI and LHSI feed into common headers (cross connected) that are connected to the accumulator lines.

The S-RELAP5 model explicitly describes the RCS, reactor vessel, pressurizer, and ECCS back to the common LHSI header and accumulators. This model also describes the secondary-side

---

<sup>1</sup> This sample problem exceeded the recommendations provided in Section B.1.3 and was analyzed with a decay heat multiplier of 1.04.



steam generator that is instantaneously isolated (closed MSIV and feedwater trip) at the time of the break.

As described in Section 4.0, many parameters associated with RLBLOCA phenomenological uncertainties and plant operation ranges are sampled. A summary of those parameters sampled is given in Table B.1. Values for process or operational parameters, including ranges of sampled process parameters, and fuel design parameters used in the analysis are given in Table B.9. Plant data are analyzed to develop uncertainties for the process parameters sampled in the analyses. Table B.9 summarizes the uncertainties used in the analyses. Two parameters (RWST temperature and diesel start time) are set at conservative bounding values for all calculations.

Where applicable, the sampled parameter ranges are based on technical specification limits. Plant data are used to define range boundaries for loop flow (high end) and containment temperature (low end).

### B.2.3 Realistic Large Break LOCA Results

A case set of 208 cases was performed sampling the parameters listed in Table B.1. The minimum retained margin to criteria was 11.8 percent at 95 percent coverage with 95 percent confidence and was associated with case number 104, which resulted in a PCT of 1940 °F. For the set of cases (LOCA events) that lie within the 95/95 range, the maximum local oxidation was 9.5833 percent (Case 27) and the maximum core-wide oxidation 0.1498 percent (Case 123). Table B.8 is a summary of the major parameters for the minimum margin case. Table B.9 is the plant input parameters and operating range supported by the analysis. Table B.10 provides the containment initial and boundary conditions. Table B.11 describes the passive heat sinks for the containment input. Table B.12 provides the statistical distribution for the process parameters. The minimum margin case is characterized in Table B.13 and Table B.14. The heat transfer parameter range for the limiting margin case is provided in Table B.15. Table B.16 provides the twenty minimum margin cases used to establish the probability evaluation.

The analysis plots for the minimum margin case are shown in Figure B.1 through Figure B.17. Figure B.1 shows linear scatter plots of the key parameters sampled for the case set. Parameter labels appear to the left of each individual plot. These figures illustrate the parameter ranges used in the analysis.

Figure B.2 and Figure B.3 show PCT scatter plots versus the time of PCT and versus break size from the set of cases (LOCA events) that lie within the 95/95 range. The scatter plots for the maximum oxidation and total oxidation are shown in Figure B.4 and B.5, respectively.

Figure B.6 through Figure B.17 show key parameters from the S-RELAP5 calculations for the minimum margin case. Figure B.6 is the plot of PCT, independent of elevation. Figure B.18 compares the bottom of core recovery times for the set of cases that lie within the 95/95 range to the BOCR time predicted using the MPR CCFL correlation.

#### B.2.4 Conclusions

The results of this RLBLOCA analysis show 11.8 percent minimum margin to any of the first three 10 CFR 50.46 criterion at 95 percent coverage with 95 percent confidence.

**Table B.8: 3-Loop Westinghouse Summary of Major Parameters for  
Minimum Margin Case**

Parameter	Value
Time in Cycle (hrs)	7708.98
Burnup (GWd/mtU)	17.4
Core Power (MWt)	3200
Core Peaking ( $F_q$ )	2.354
Radial Peak ( $F_{\Delta H}$ )	1.73
Axial Offset	+0.1520
Local Peaking ( $F_l$ )	1.051
Break Type	DESB
Break Size (ft <sup>2</sup> /side)	2.2802
Offsite Power Availability	not available
Decay Heat Multiplier	1.02402

**Table B.9: 3-Loop Westinghouse Plant Operating Range Supported by the  
RLBLOCA Analysis**

Event		Operating Range
<b>1.0</b>	<b>Plant Physical Description</b>	
	1.1 Fuel	
	a) Cladding outside diameter	0.376 in.
	b) Cladding inside diameter	0.328 in.
	c) Cladding thickness	0.024 in.
	d) Pellet outside diameter	0.3215 in.
	e) Initial Pellet density	[ ]
	f) Active fuel length	144 in.
	g) Gd <sub>2</sub> O <sub>3</sub> concentrations	2, 4, 6, 8 w/o
	1.2 RCS	
	a) Flow resistance	Analysis
	b) Pressurizer location	Analysis assumes location giving most limiting PCT (broken loop)
	c) Hot assembly location	Anywhere in core
	d) Hot assembly type	17x17
	e) SG tube plugging	≤ 3 percent
<b>2.0</b>	<b>Plant Initial Operating Conditions</b>	
	2.1 Reactor Power	
	a) Analyzed reactor power	3200 MWt
	b) $F_q$	≤ 2.44
	c) $F_{\Delta H}$	≤ 1.73 <sup>1</sup>
	d) MTC	≤ 0 at HFP
	2.2 Fluid Conditions	
	a) Loop flow	109.2 Mlbm/hr ≤ M ≤ 117.8 Mlbm/hr
	b) RCS average temperature	582.0 °F ≤ T ≤ 594.8 °F
	c) Upper head temperature	~Tcold Temperature <sup>2</sup>
	d) Pressurizer pressure	2200 psia ≤ P ≤ 2288 psia
	e) Pressurizer level	53.25 percent ≤ L ≤ 66.75 percent
	f) Accumulator pressure	599.7 psia ≤ P ≤ 679.7 psia
	g) Accumulator liquid volume	994.6 ft <sup>3</sup> ≤ V ≤ 1029.4 ft <sup>3</sup>
	h) Accumulator temperature	80 °F ≤ T ≤ 130 °F (coupled with containment temperature)
	i) Accumulator resistance fL/D	As-built piping configuration
	j) Minimum ECCS boron	≥ 2400 ppm

<sup>1</sup> Includes 4 percent measurement uncertainty.

<sup>2</sup> Upper head temperature will change based on sampling of RCS temperature.

**Table B.9: 3-Loop Westinghouse Plant Operating Range Supported by the RLBLOCA Analysis (continued)**

Event		Operating Range																																																																																																						
3.0	Accident Boundary Conditions																																																																																																							
	a) Break location	Cold Leg Pump Discharge																																																																																																						
	b) Break type	Double-ended guillotine or split																																																																																																						
	c) Break size (each side, relative to cold leg pipe area)	0.05 ≤ A ≤ 1.0 full pipe area (split) 0.05 ≤ A ≤ 1.0 full pipe area (guillotine)																																																																																																						
	d) Worst single-failure	Loss of one train of ECCS																																																																																																						
	e) Offsite power	LOOP																																																																																																						
	f) ECCS pumped injection temperature	125 °F																																																																																																						
	g) HHSI pump delay	17 s (w/ offsite power) 29 s (w/o offsite power)																																																																																																						
	h) LHSI pump delay	27 s (w/ offsite power) 37 s (w/o offsite power)																																																																																																						
	i) Containment pressure	14.7 psia, nominal value																																																																																																						
	j) Containment temperature	80 °F ≤ T ≤ 130 °F																																																																																																						
	k) Containment sprays delay	0 s																																																																																																						
	l) Containment spray water temperature	40 °F																																																																																																						
	m) LHSI Flow																																																																																																							
	<table><tr><th colspan="2">BROKEN_LOOP</th><th colspan="2">INTACT_LOOP1</th><th colspan="2">INTACT_LOOP2</th></tr><tr><td colspan="2">* RCS pressure LHSI flow</td><td colspan="2">* RCS pressure LHSI flow</td><td colspan="2">* RCS pressure LHSI flow</td></tr><tr><td colspan="2">* -----</td><td colspan="2">* -----</td><td colspan="2">* -----</td></tr><tr><td colspan="2">----</td><td colspan="2">----</td><td colspan="2">----</td></tr><tr><td>psia</td><td>gpm</td><td>psia</td><td>gpm</td><td>psia</td><td>gpm</td></tr><tr><td>0.</td><td>1832.0</td><td>0.</td><td>916.0</td><td>0.</td><td>916.0</td></tr><tr><td>15.</td><td>1832.0</td><td>15.</td><td>916.0</td><td>15.</td><td>916.0</td></tr><tr><td>20.</td><td>1791.1</td><td>20.</td><td>895.6</td><td>20.</td><td>895.6</td></tr><tr><td>30.</td><td>1707.6</td><td>30.</td><td>853.8</td><td>30.</td><td>853.8</td></tr><tr><td>35.</td><td>1664.9</td><td>35.</td><td>832.4</td><td>35.</td><td>832.4</td></tr><tr><td>40.</td><td>1621.5</td><td>40.</td><td>810.8</td><td>40.</td><td>810.8</td></tr><tr><td>50.</td><td>1532.5</td><td>50.</td><td>766.3</td><td>50.</td><td>766.3</td></tr><tr><td>70.</td><td>1318.8</td><td>70.</td><td>6208.3</td><td>70.</td><td>6208.3</td></tr><tr><td>120.</td><td>546.2</td><td>120.</td><td>273.1</td><td>120.</td><td>273.1</td></tr><tr><td>125.</td><td>491.9</td><td>125.</td><td>246.0</td><td>125.</td><td>246.0</td></tr><tr><td>125.01</td><td>0.0</td><td>125.01</td><td>0.0</td><td>125.01</td><td>0.0</td></tr><tr><td>3000.</td><td>0.0</td><td>3000.</td><td>0.0</td><td>3000.</td><td>0.0</td></tr></table>	BROKEN_LOOP		INTACT_LOOP1		INTACT_LOOP2		* RCS pressure LHSI flow		* RCS pressure LHSI flow		* RCS pressure LHSI flow		* -----		* -----		* -----		----		----		----		psia	gpm	psia	gpm	psia	gpm	0.	1832.0	0.	916.0	0.	916.0	15.	1832.0	15.	916.0	15.	916.0	20.	1791.1	20.	895.6	20.	895.6	30.	1707.6	30.	853.8	30.	853.8	35.	1664.9	35.	832.4	35.	832.4	40.	1621.5	40.	810.8	40.	810.8	50.	1532.5	50.	766.3	50.	766.3	70.	1318.8	70.	6208.3	70.	6208.3	120.	546.2	120.	273.1	120.	273.1	125.	491.9	125.	246.0	125.	246.0	125.01	0.0	125.01	0.0	125.01	0.0	3000.	0.0	3000.	0.0	3000.	0.0	
BROKEN_LOOP		INTACT_LOOP1		INTACT_LOOP2																																																																																																				
* RCS pressure LHSI flow		* RCS pressure LHSI flow		* RCS pressure LHSI flow																																																																																																				
* -----		* -----		* -----																																																																																																				
----		----		----																																																																																																				
psia	gpm	psia	gpm	psia	gpm																																																																																																			
0.	1832.0	0.	916.0	0.	916.0																																																																																																			
15.	1832.0	15.	916.0	15.	916.0																																																																																																			
20.	1791.1	20.	895.6	20.	895.6																																																																																																			
30.	1707.6	30.	853.8	30.	853.8																																																																																																			
35.	1664.9	35.	832.4	35.	832.4																																																																																																			
40.	1621.5	40.	810.8	40.	810.8																																																																																																			
50.	1532.5	50.	766.3	50.	766.3																																																																																																			
70.	1318.8	70.	6208.3	70.	6208.3																																																																																																			
120.	546.2	120.	273.1	120.	273.1																																																																																																			
125.	491.9	125.	246.0	125.	246.0																																																																																																			
125.01	0.0	125.01	0.0	125.01	0.0																																																																																																			
3000.	0.0	3000.	0.0	3000.	0.0																																																																																																			

**Table B.9: 3-Loop Westinghouse Plant Operating Range Supported by the RLBLOCA Analysis (continued)**

Event				Operating Range			
n) HHSI Flow							
BROKEN_LOOP				INTACT_LOOP1		INTACT_LOOP2	
*				*		*	
* RCS Pressure		HHSI		* RCS Pressure		HHSI	
Flow				Flow			
* -----		-----		* -----		-----	
----				----			
psia		gpm		psia		gpm	
10.		206.3		10.		129.6	
15.		206.3		15.		129.6	
20.		206.1		20.		129.4	
30.		205.7		30.		129.2	
40.		205.3		40.		128.9	
50.		204.9		50.		128.7	
70.		204.1		70.		128.2	
120.		202.1		120.		126.9	
500.		186.3		500.		117.0	
1001.		161.9		1001.		101.7	
1150.		154.0		1150.		96.8	
1609.		124.4		1609.		78.3	
1775.		114.5		1775.		72.4	
2037.		91.2		2037.		58.7	
2141.		72.7		2141.		49.2	
2193.		60.8		2193.		44.6	
2246.		35.1		2246.		28.6	
2296.		0.0		2296.		0.0	

**Table B.10: 3-Loop Westinghouse Containment Initial and Boundary Conditions**

<b>Containment Net Free Volume (ft<sup>3</sup>)</b>	2,266,000 – 2,610,000
<b>Initial Conditions</b>	
Containment Pressure (nominal)	14.7 psia
Containment Temperature	80 °F – 130 °F
RWST Temperature	125 °F
Outside Temperature	40 °F
Humidity	1.0
<b>Containment Spray</b>	
Number of Pumps operating	2
Quench System Total Spray Flow	5000 gpm
Minimum Spray Temperature	40 °F
Fastest Post-LOCA initiation of spray	0 s

**Table B.11: 3-Loop Westinghouse Passive Heat Sinks in  
Containment**

Description	Slab Material	Material Thick. (ft)	Area (ft <sup>2</sup> )
Containment Cylindrical Wall	Paint Carbon Steel Concrete	0.00025 0.021083 3.89608	44290
Containment Dome	Paint Carbon Steel Concrete	0.00025 0.021083 3.02108	6530
Foundation Slab	Paint Carbon Steel Concrete Concrete	0.00025 0.021083 1.02108 12.02108	8720
Miscellaneous Concrete Slab	Paint Concrete	0.0005 1.0005	55790
Miscellaneous Concrete	Paint Concrete	0.0005 0.5005	4650
Miscellaneous Concrete	Paint Concrete	0.0005 3.7505	19880
Miscellaneous Steel	Paint Carbon Steel	0.00025 0.010667	7000
Miscellaneous Steel Slab	Paint Carbon Steel	0.00025 0.041917	11180
Ventilation Ducts	Galvanizing (Zinc)	0.005208	73440
Refueling Cavity Walls	Stainless Steel Concrete	0.005 2.005	14160
Refueling Cavity Floor	Stainless Steel Concrete	0.005 4.005	400
Miscellaneous Concrete	Paint Concrete	0.0005 0.3755	8000
Miscellaneous Concrete	Paint Concrete	0.0005 0.5005	11150
Miscellaneous Concrete	Paint Concrete	0.0005 2.5005	9260
Stainless Steel	Stainless Steel	0.020149	10330

Material Properties	Thermal Conductivity (BTU/hr-ft-°F)	Volumetric Heat Capacity (BTU/ft <sup>3</sup> -°F)
Concrete	1.0	34.2
Carbon Steel	33.6	208.8
Stainless Steel	9.6	60.7
Galvanizing (Zinc)	64	40.6
Paint on Steel	1.5	57.6
Paint on Concrete	0.3	43.2



**Table B.12: 3-Loop Westinghouse Statistical Distribution Used for  
Process Parameters**

<b>Parameter</b>	<b>Operational Uncertainty Distribution</b>	<b>Parameter Range</b>	<b>Measurement Uncertainty Distribution</b>	<b>Standard Deviation</b>
Pressurizer Pressure (psig)	Uniform	2200 - 2288	Normal	0
Pressurizer Level (%)	Uniform	53.25 – 66.75	Normal	0
Accumulator Volume (ft <sup>3</sup> )	Uniform	994.6 – 1029.4	N/A	N/A
Accumulator Pressure (psia)	Uniform	599.7 – 679.7	N/A	N/A
Containment/Accumulator Temperature (°F)	Uniform	80 – 130	N/A	N/A
Containment Volume (x10 <sup>6</sup> ft <sup>3</sup> )	Uniform	2.27 – 2.61	N/A	N/A
Initial Flow Rate (Mlbm/hr)	Uniform	109.2 – 117.8	N/A	N/A
Initial Operating Temperature (°F)	Uniform	582 – 594.8	N/A	N/A

**Table B.13: 3-Loop Westinghouse Compliance with 10 CFR 50.46**

Compliance to Cladding Temperature, Local Oxidation, and Core-Wide Oxidation Criteria			
Minimum Margin to Criteria Limits, %		11.8	
Variable Setting Minimum Margin		PCT	
Characterization of Case Set Determining 95/95 Compliance			
Parameter	Value	Fuel Pin Type	Case Number
Minimum Margin PCT, °F	1940	Fresh UO <sub>2</sub> Rod	104
Minimum Margin Local Maximum Oxidation, %	9.5833	Fresh UO <sub>2</sub> Rod	27
Minimum Margin Total Core-Wide Oxidation, %	0.1498	Fresh UO <sub>2</sub> Rod	123
Characteristics of Case Setting the Minimum Margin			
PCT, °F		1940	
Time of PCT, s		119.1	
Elevation within Core, ft		9.828	
Local Maximum Oxidation, %		8.3607	
Total Core-Wide Oxidation, %		0.1012	

**Table B.14: 3-Loop Westinghouse Calculated Event Times for  
Limiting Margin Case**

Event	Time (sec)
Begin Analysis	0.0
Break Opens	0.0
RCP Trip	N / A
SIAS Issued	0.4
Start of Broken Loop Accumulator Injection	14.1
Start of Intact Loop Accumulator Injection	14.6 & 14.6
Start of HHSI	29.4
Start of Charging	N/A
Beginning of Core Recovery (Beginning of Reflood)	29.5
LHSI Available	37.4
PCT Occurred (1940 °F)	119.1
Broken Loop LHSI Delivery Began	37.4
Intact Loops LHSI Delivery Began	37.4 & 37.4
Broken Loop HHSI Delivery Began	29.4
Intact Loops HHSI Delivery Began	29.4 & 29.4
Broken Loop Accumulator Emptied	38.6
Intact Loop Accumulator Emptied	38.8 & 39.5
Transient Calculation Terminated	1125.4

**Table B.15: Westinghouse 3-Loop Heat Transfer Parameters for  
Limiting Margin Case**

Time (s)	0 – 1.0	1.0 – 28.00	28.00 – 29.53	29.53 – Quench (1030 s)	Quench	Quench – End of Transient (1125.36 s)
LOCA Phase	Early Blowdown	Blowdown <sup>1</sup>	Refill	Reflood	Quench	Long Term Cooling
Heat Transfer Mode	CHF	Film Boiling/ Single-Phase	Film Boiling/ Single-Phase	Film Boiling/ Reflood	Transition Boiling	Transition Boiling
Heat Transfer Correlations	Biasi Zuber	Modified- Bromley Wong- Hochreiter Natural Convection Radiation (Sun) Rod-to-Rod radiation	Modified- Bromley Wong- Hochreiter Natural Convection Radiation (Sun) Rod-to-Rod radiation	Modified- Bromley Wong- Hochreiter Natural Convection Radiation (Sun) Rod-to-Rod radiation	Modified Chen Transition boiling	Chen Nucleate boiling
Maximum LHGR (kW/ft)	15.19 {< q <sub>CHF</sub> }	1.68 {< 5.5}	0.72 {< 5.5}	0.72	0.34	0.34
Pressure (psia)	1629 - 2274 {< 2250 at CHF}	55 - 1629 {< 2250}	35 - 55 {< 2250}	27 - 72 {< 2250 }	27	27 - 28
Core Inlet Mass Flux (kg/s-m <sup>2</sup> )	1100 - 3400 {< 6000}	0 - 1100 {< 4250}	0 - 100	0 - 800 {< 4250}	300	100 -500
Vapor Reynolds Number	6100 - 16000	200 - 37000 {< 10 <sup>6</sup> }	200 - 3000 {< 10 <sup>6</sup> }	1200 - 15000 {< 10 <sup>6</sup> }	5900 - 6000	3400 - 15000
Liquid Reynolds Number	7900 - 462000	100 - 29000	100 - 1000	0 -22000	1400 - 2000	100 - 15000
Vapor Prandtl Number	1.17 – 2.93	0.87 – 1.17	0.88	0.87 – 1.01	1.01	1.01
Liquid Prandtl Number	1.07 – 1.31	0.85 – 1.21	1.21 – 1.36	1.13 – 1.45	1.44	1.44 – 1.45
Superheat (°F)	170	1070	1160	1320	-10	10

<sup>1</sup> End of Blowdown considered as beginning of refill.

**Table B.16: Summary of Limiting Values for Top Minimum Margin Cases within the Set Used to Establish the Probability Evaluation**

Case Number	$\Phi$	PCT	ECR (%)	CWO (%)	S <sub>PCT</sub>	S <sub>ECR</sub>	S <sub>CWO</sub>
104	0.88141	1939.1	8.3607	0.10115	0.88141	0.4918	0.10115
123	0.87541	1925.9	7.0041	0.14978	0.87541	0.412	0.14978
78	0.87291	1920.4	8.7881	0.07743	0.87291	0.51695	0.07743
191	0.87014	1914.3	7.2031	0.12327	0.87014	0.42371	0.12327
195	0.86995	1913.9	7.7159	0.12011	0.86995	0.45388	0.12011
107	0.86505	1903.1	7.4609	0.10226	0.86505	0.43888	0.10226
15	0.86468	1902.3	7.3989	0.09691	0.86468	0.43523	0.09691
178	0.85859	1888.9	8.1883	0.10649	0.85859	0.48166	0.10649
192	0.85673	1884.8	7.6971	0.11437	0.85673	0.45277	0.11437
90	0.85673	1884.8	6.9199	0.13407	0.85673	0.40705	0.13407
30	0.84891	1867.6	7.2293	0.06623	0.84891	0.42525	0.06623
142	0.84877	1867.3	8.0463	0.07128	0.84877	0.47331	0.07128
31	0.84645	1862.2	8.1333	0.10272	0.84645	0.47843	0.10272
46	0.84568	1860.5	7.1879	0.11576	0.84568	0.42282	0.11576
27	0.84359	1855.9	9.5833	0.08127	0.84359	0.56372	0.08127
39	0.84177	1851.9	7.1063	0.11110	0.84177	0.41802	0.1111
201	0.84059	1849.3	5.5743	0.10337	0.84059	0.3279	0.10337
7	0.83873	1845.2	7.1353	0.10869	0.83873	0.41972	0.10869
111	0.83818	1844	5.3797	0.08647	0.83818	0.31645	0.08647
140	0.83632	1839.9	6.5627	0.10637	0.83632	0.38604	0.10637

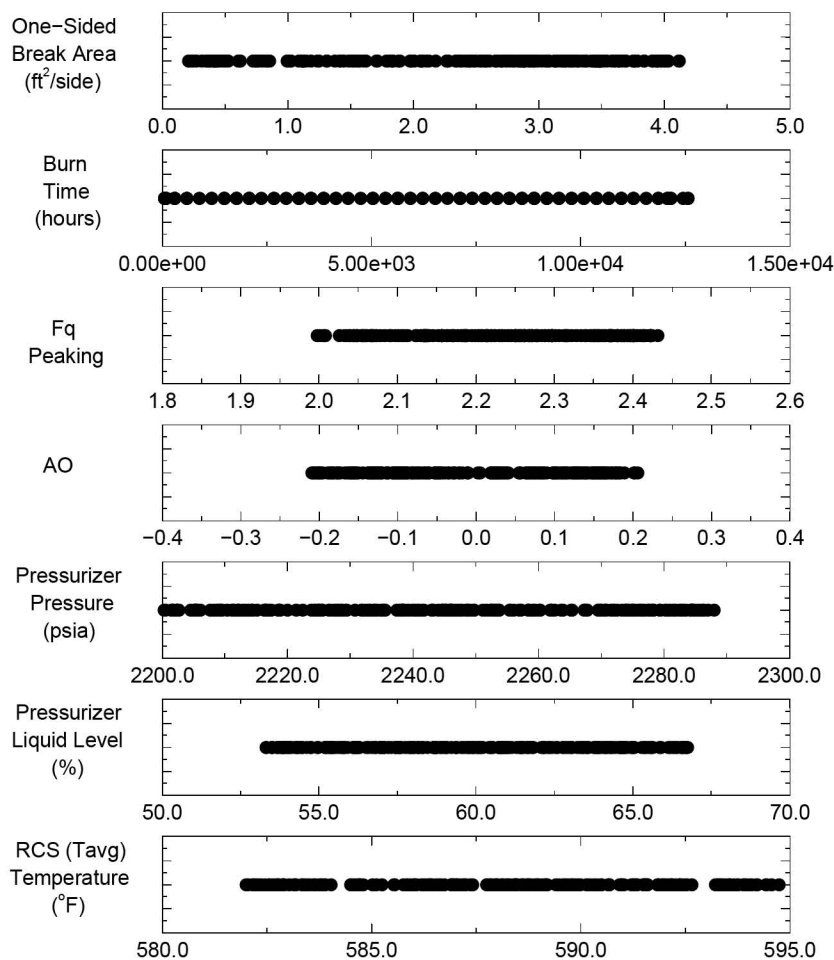


**Figure B.1: 3-Loop Westinghouse Scatter Plot of Operational Parameters**

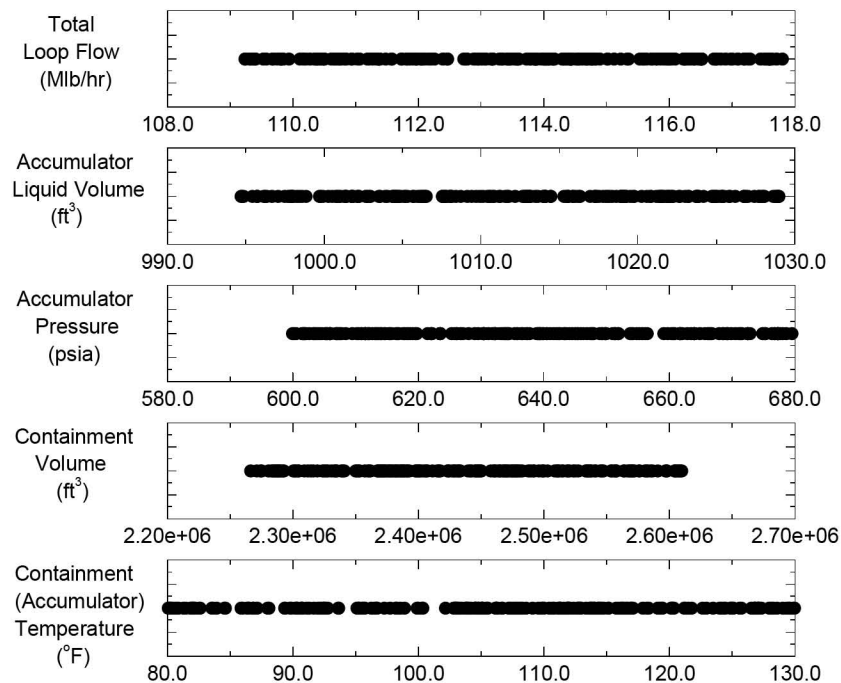


**Figure B.1: 3-Loop Westinghouse Scatter Plot of Operational Parameters (continued)**

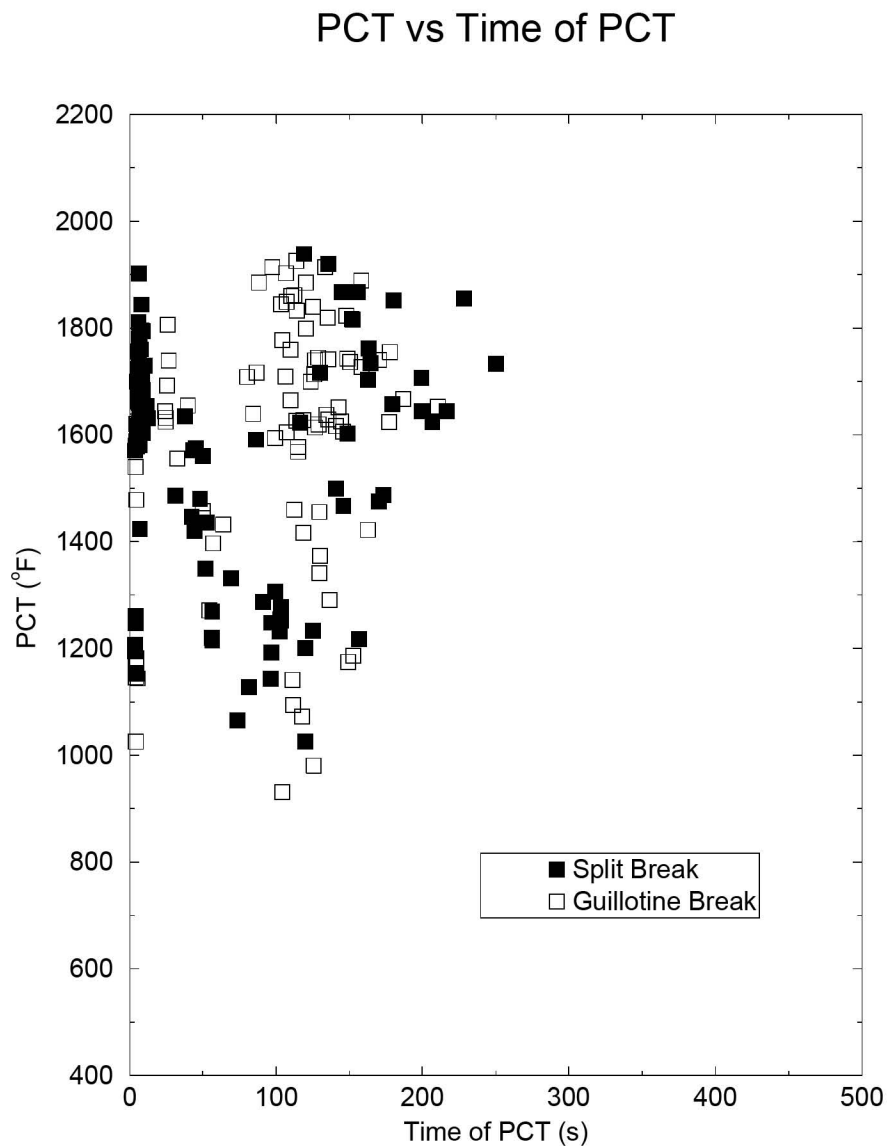


**Figure B.2: 3-Loop Westinghouse PCT versus PCT Time Scatter Plot  
from the Case Set**



### PCT vs One-sided Break Area

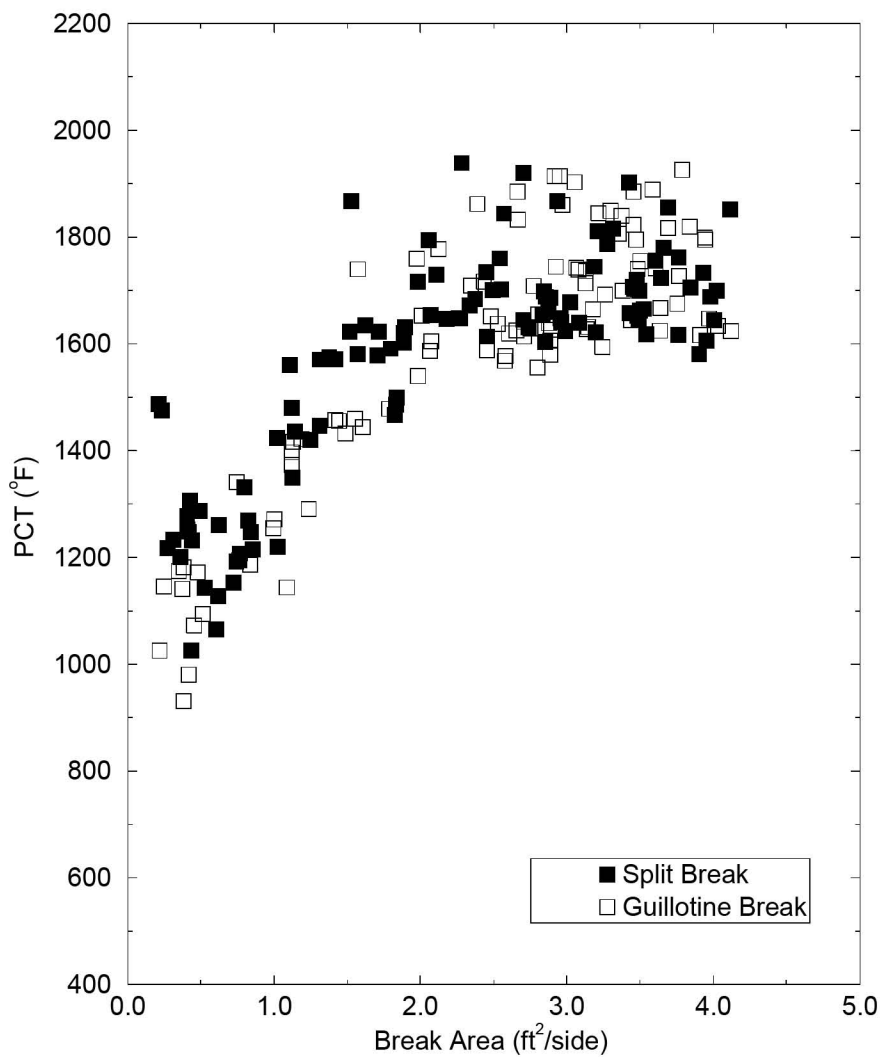


**Figure B.3: 3-Loop Westinghouse PCT versus Break Size Scatter  
Plot from the Case Set**

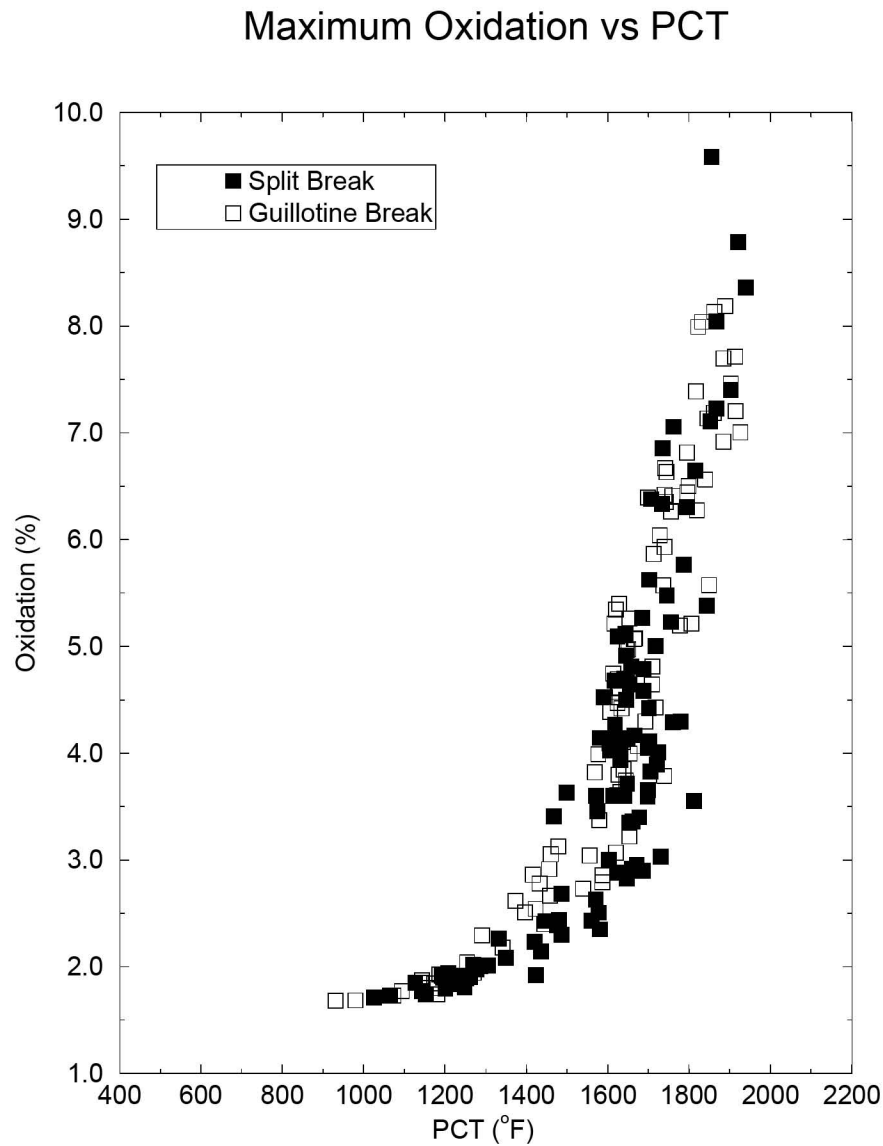


**Figure B.4: 3-Loop Westinghouse Maximum Oxidation versus PCT  
Scatter Plot from the Case Set**

## Total Oxidation vs PCT

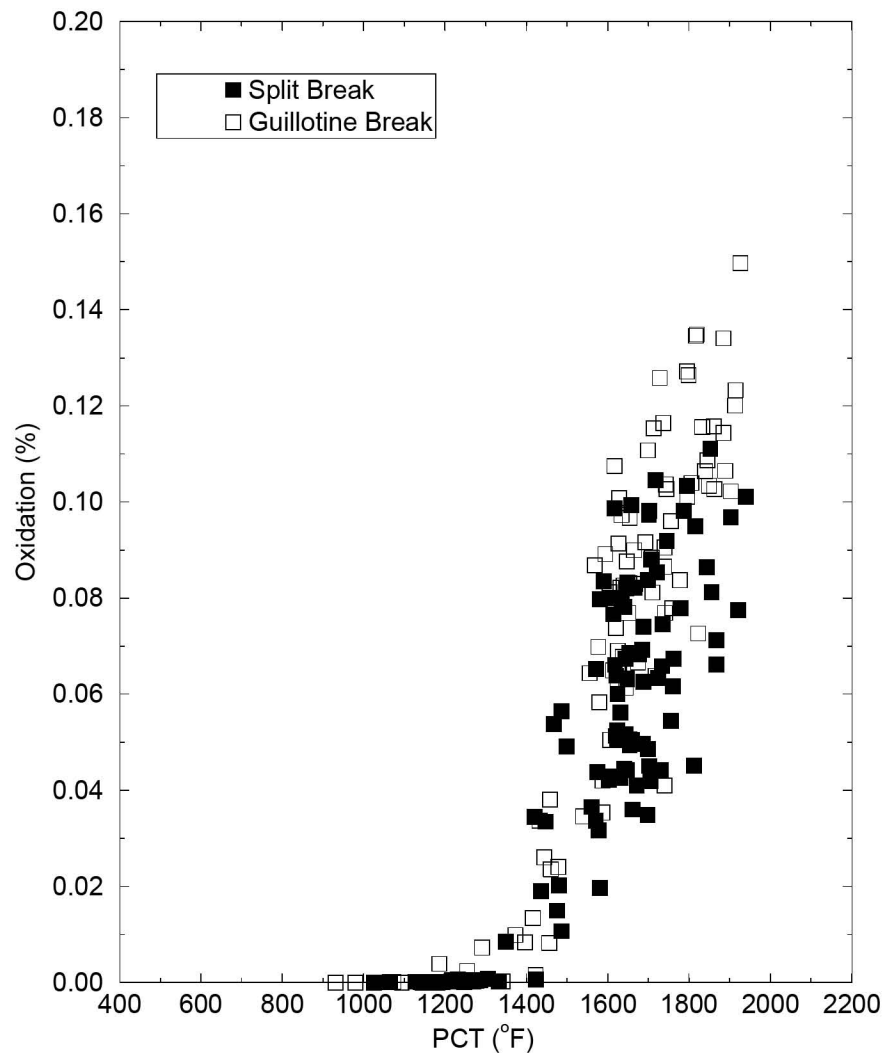


**Figure B.5: 3-Loop Westinghouse Total Oxidation versus PCT  
Scatter Plot from the Case Set**

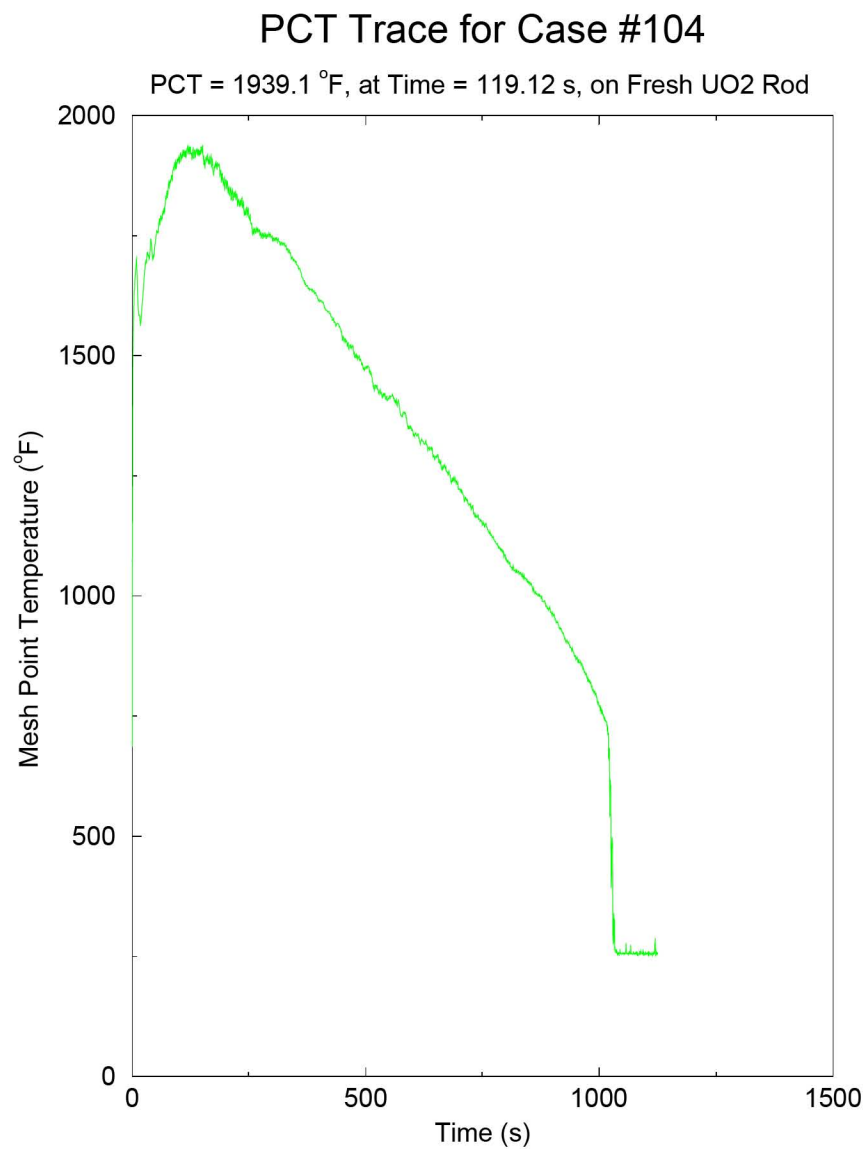


**Figure B.6: 3-Loop Westinghouse Peak Cladding Temperature  
(Independent of Elevation) for the Limiting Margin Case**

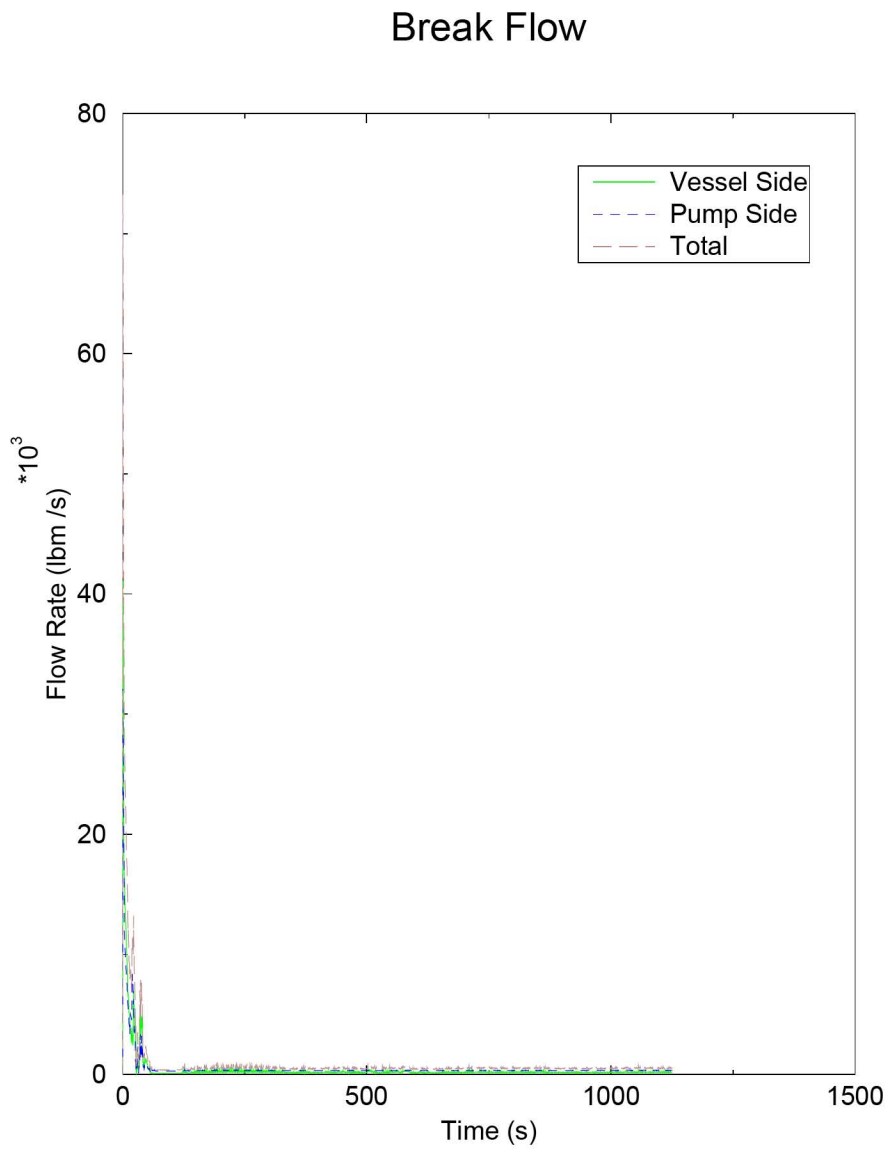


**Figure B.7: 3-Loop Westinghouse Break Flow for the Limiting Margin Case**

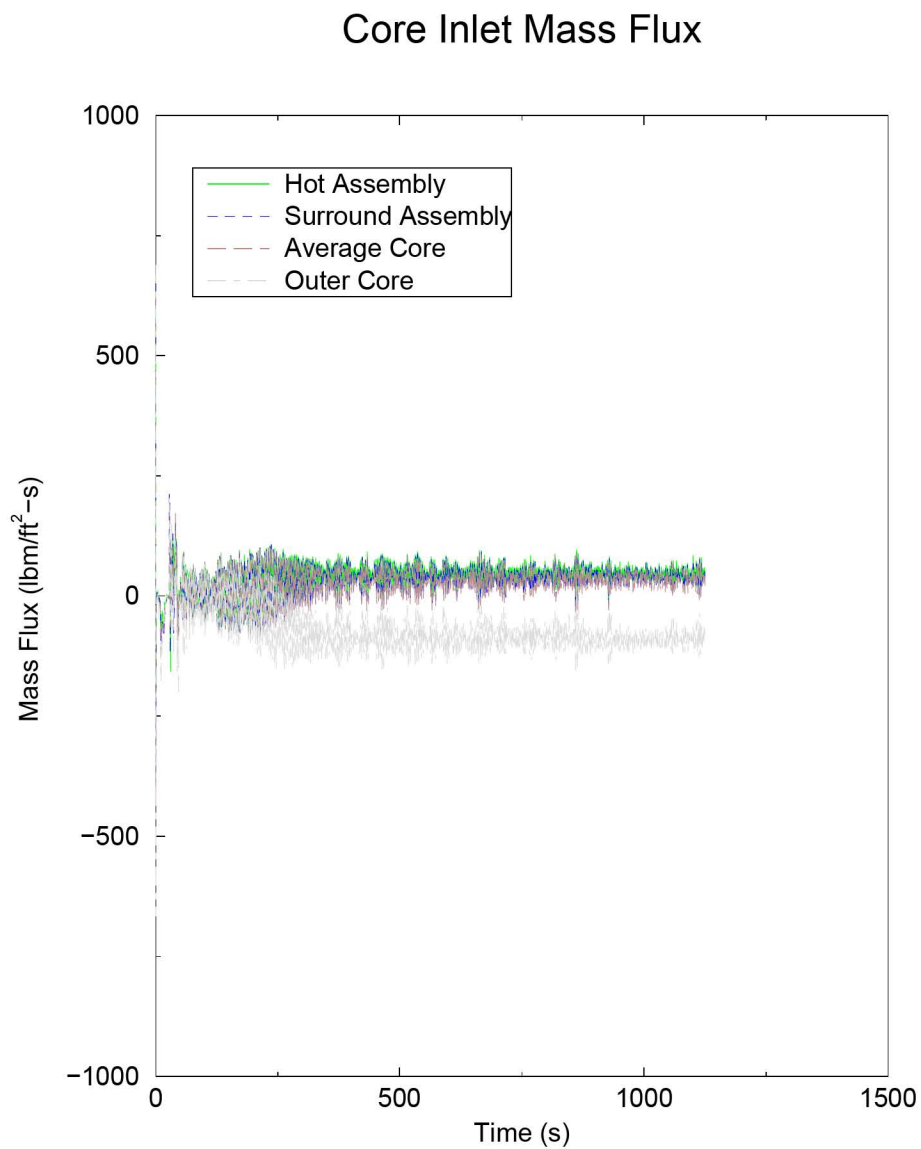


**Figure B.8: 3-Loop Westinghouse Core Inlet Mass Flux for the Limiting Margin Case**

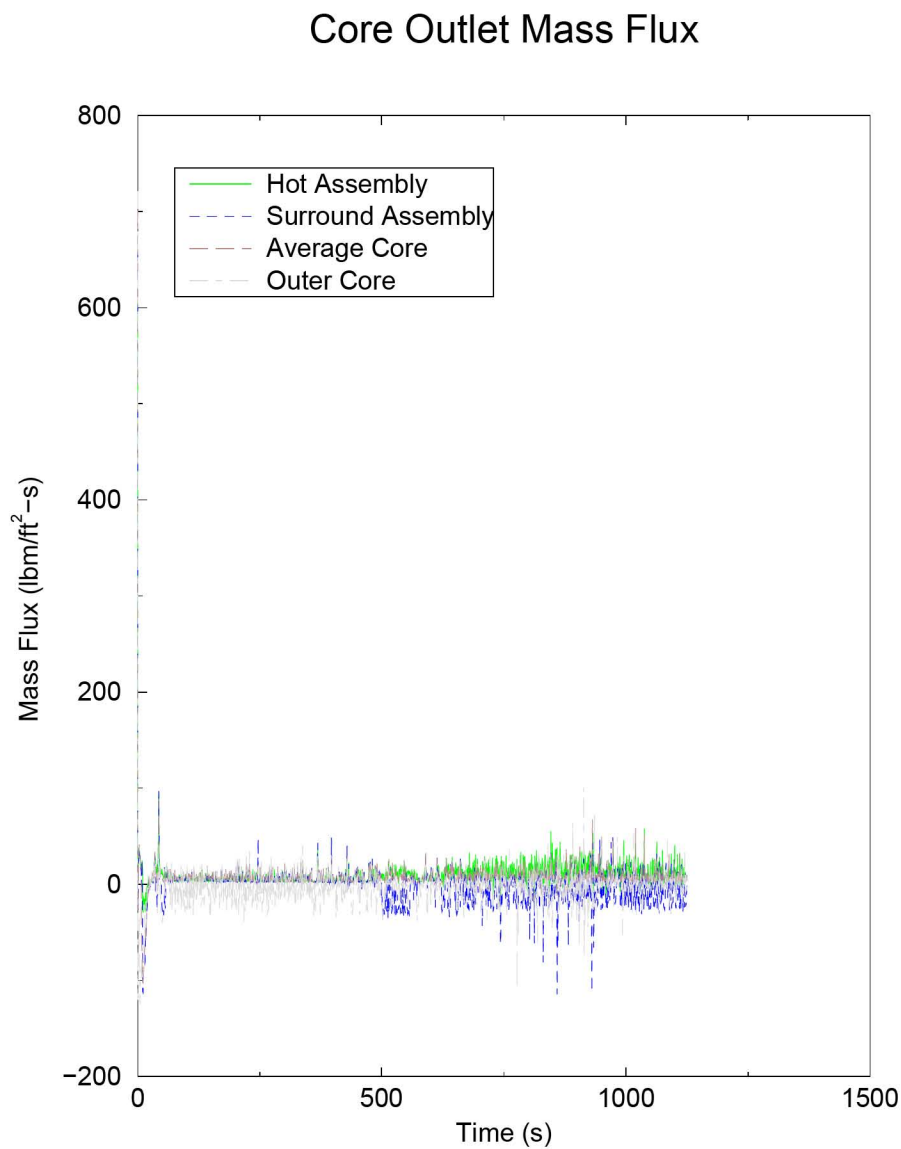


**Figure B.9: 3-Loop Westinghouse Core Outlet Mass Flux for the Limiting Margin Case**

### Pump Void Fraction

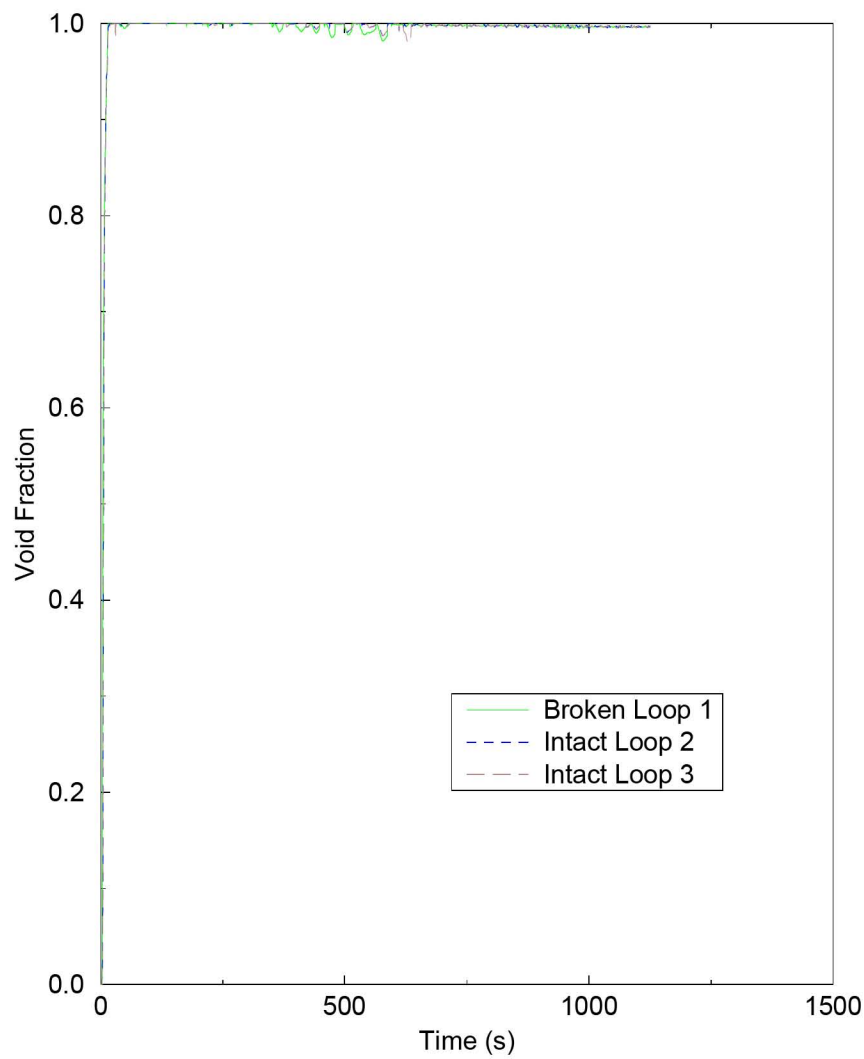


**Figure B.10: 3-Loop Westinghouse Void Fraction at RCS Pumps for the Limiting Margin Case**



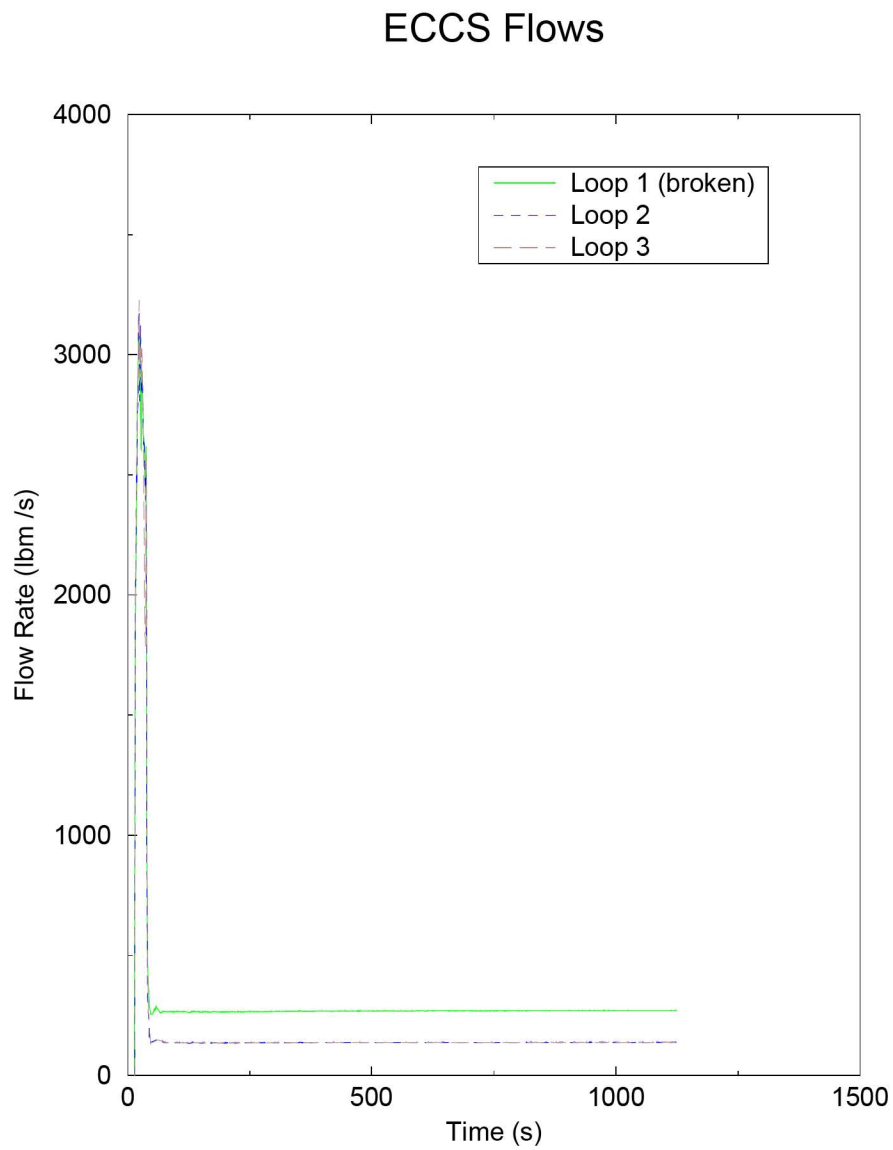


**Figure B.11: 3-Loop Westinghouse ECCS Flows (Includes Accumulator, Charging, SI and RHR) for the Limiting Margin Case**

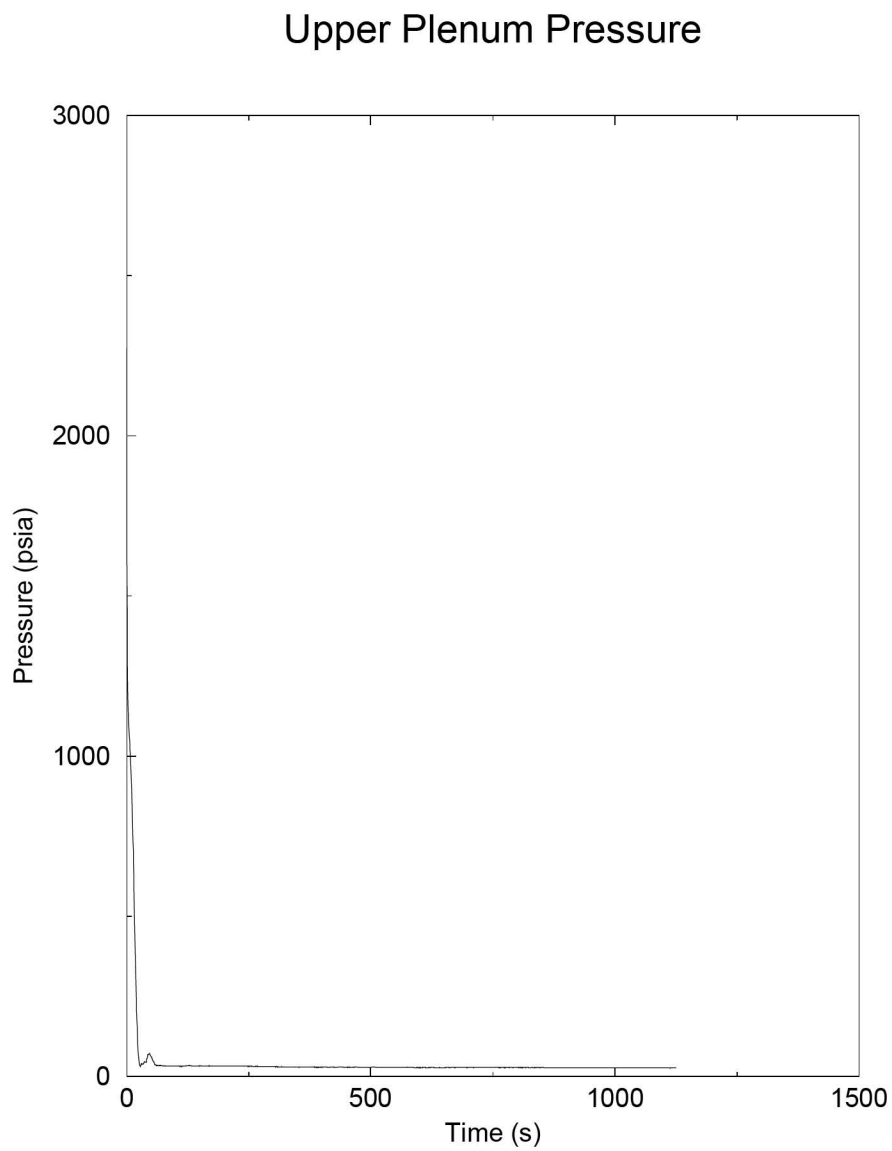


**Figure B.12: 3-Loop Westinghouse Upper Plenum Pressure for the Limiting Margin Case**

### Downcomer Liquid Level

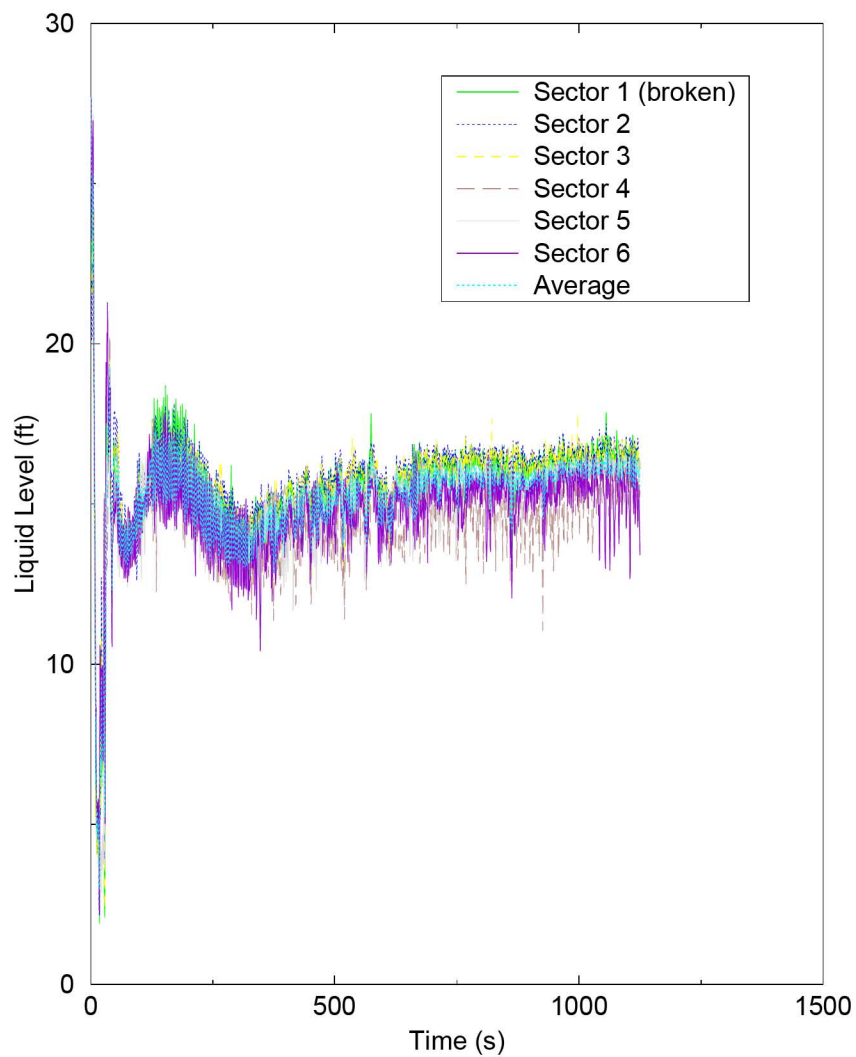


**Figure B.13: 3-Loop Westinghouse Collapsed Liquid Level in the Downcomer for the Limiting Margin Case**

### Lower Vessel Liquid Level

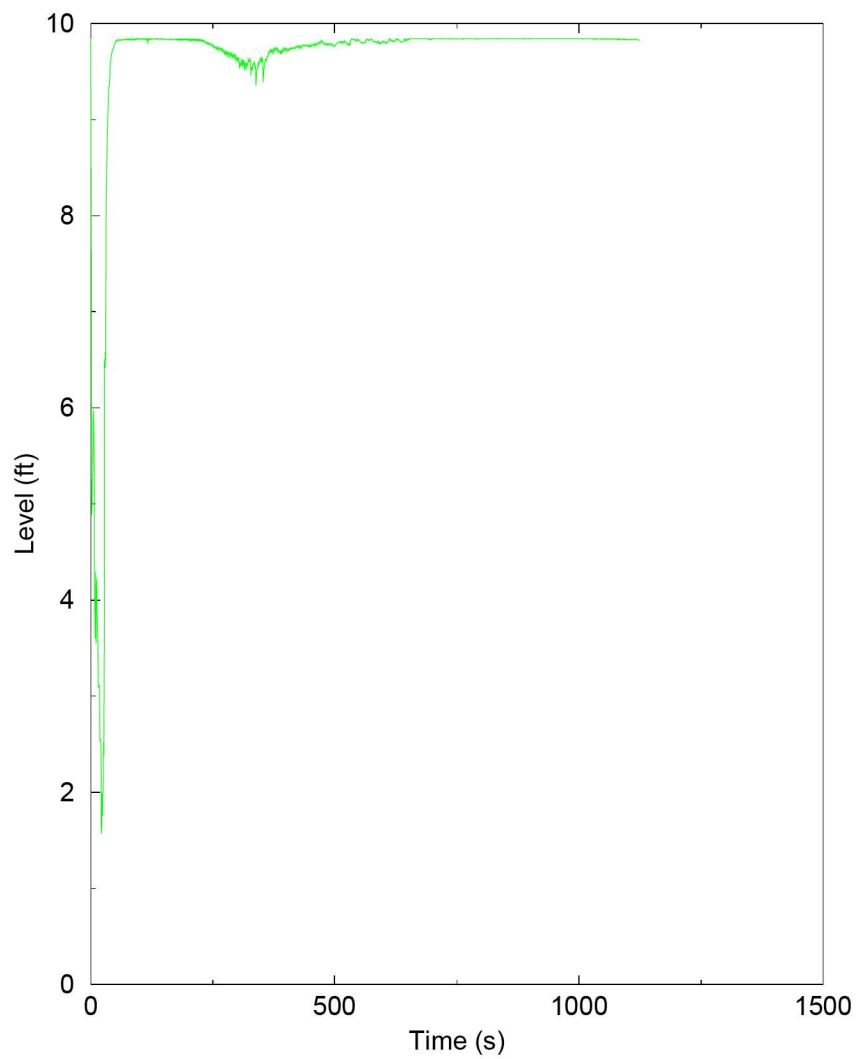


**Figure B.14: 3-Loop Westinghouse Collapsed Liquid Level in the Lower Plenum for the Limiting Margin Case**

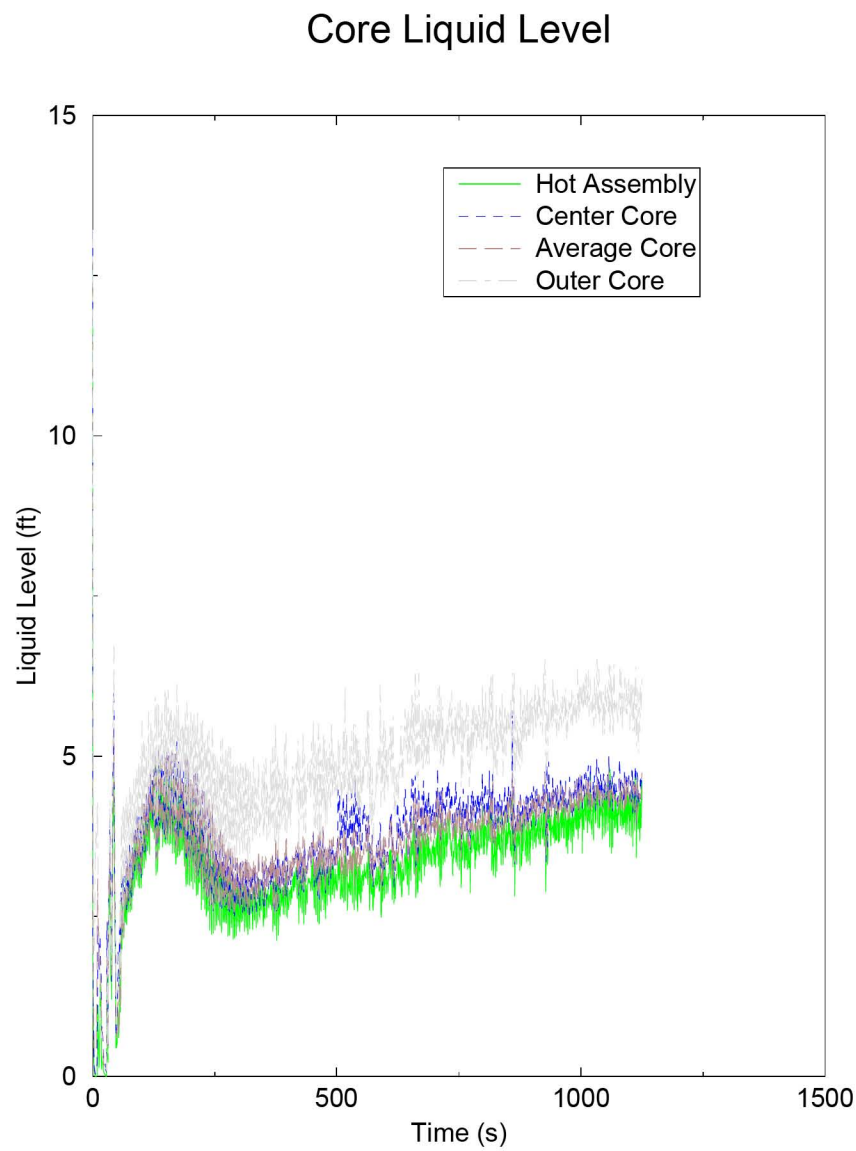


**Figure B.15: 3-Loop Westinghouse Collapsed Liquid Level in the Core for the Limiting Margin Case**

## Containment and Loop Pressures

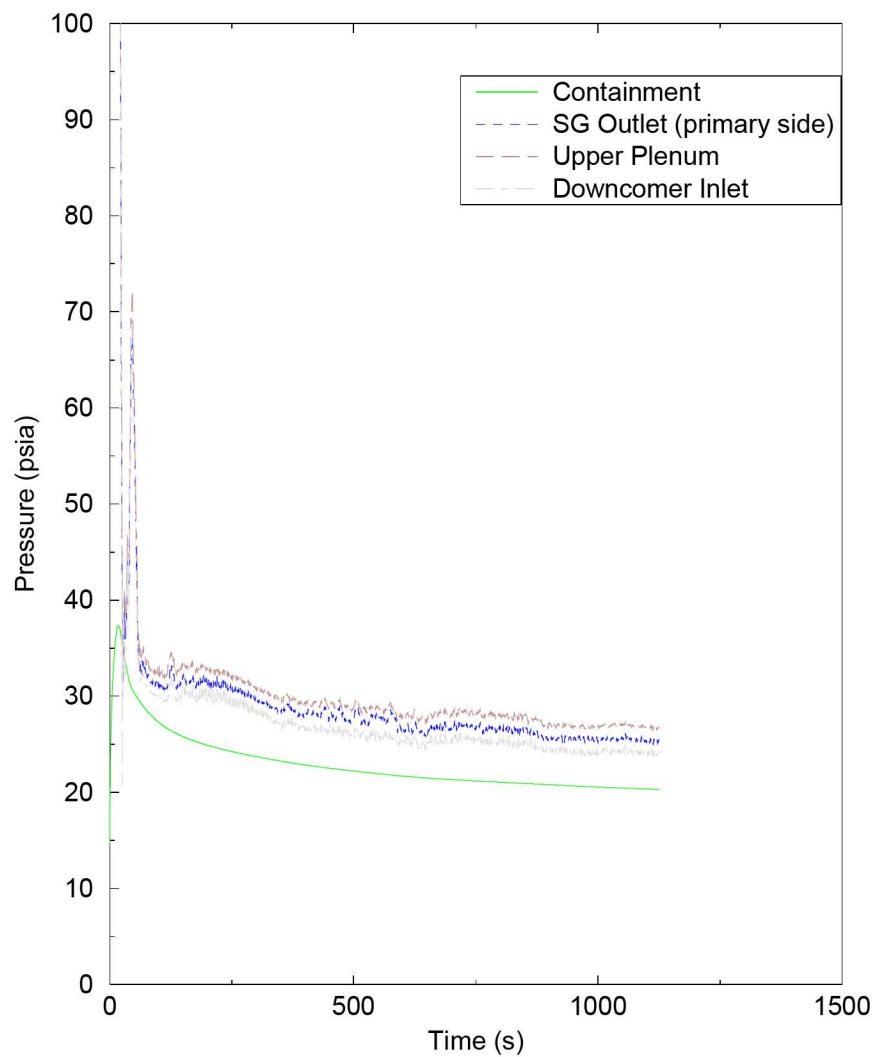


**Figure B.16: 3-Loop Westinghouse Containment and Loop Pressures for the Limiting Margin Case**

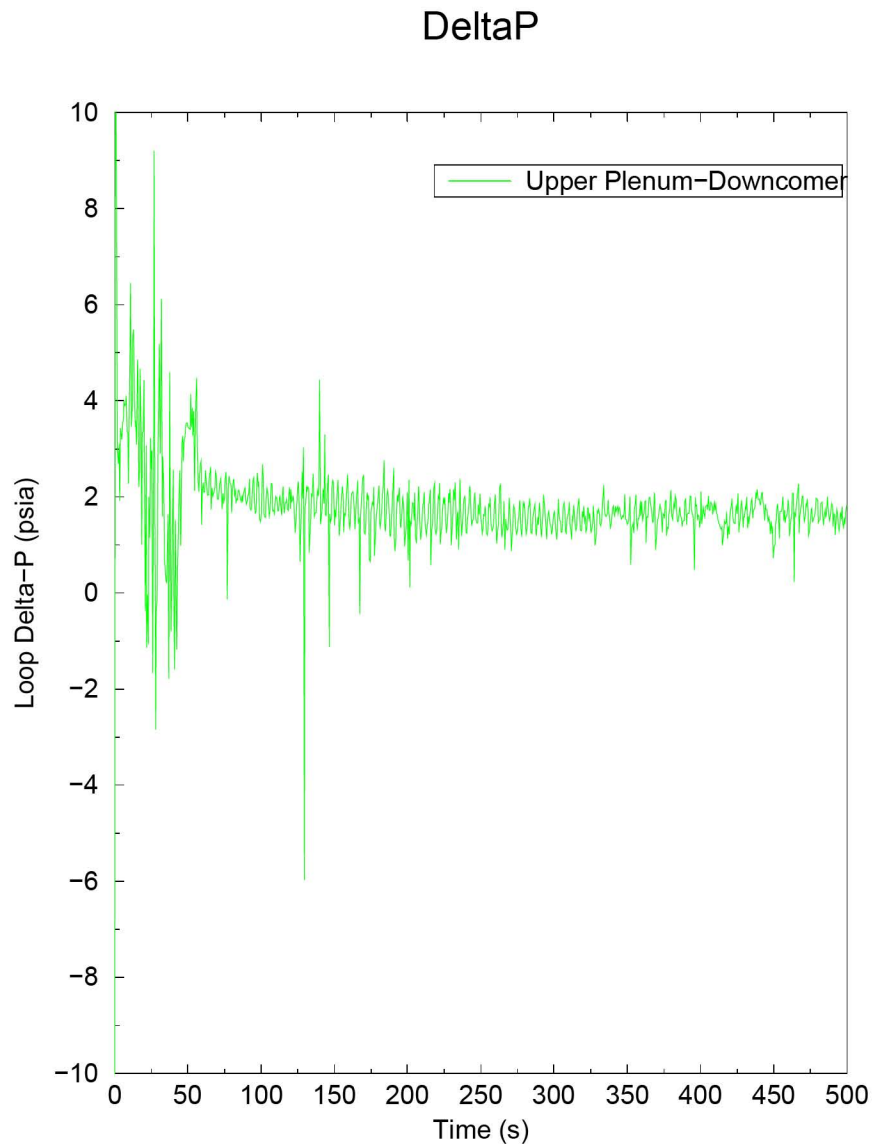


**Figure B.17: 3-Loop Westinghouse Pressure Difference between  
Upper Plenum and Downcomer**

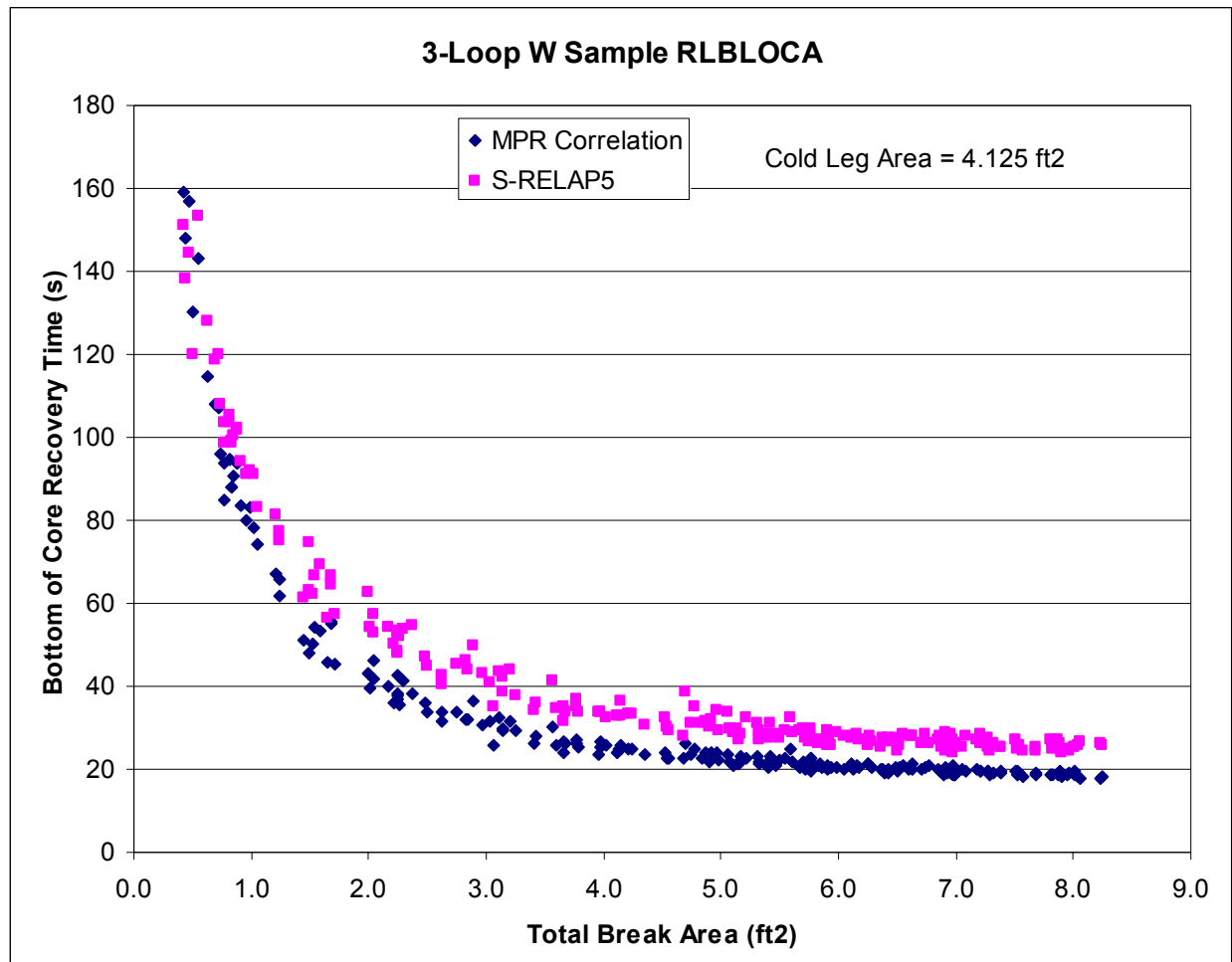


**Figure B.18: 3-Loop Westinghouse Validation of BOCR Time using  
MPR CCFL Correlation**



### **B.3 Westinghouse 4-Loop PWR**

#### **B.3.1 Summary**

The parameter specification for this analysis is provided in Table B.18. The analysis assumes full-power operation at 3800 MWt, a steam generator tube plugging level of up to 15 percent in any generator, a total peaking factor ( $F_q$ ) of 2.335 including uncertainties, and a nuclear enthalpy rise factor ( $F_{\Delta H}$ ) of 1.579 (including 5 percent uncertainty). The analysis supports operation with AREVA 17x17 Mark-BW design fuel using standard  $UO_2$  fuel with 2, 4, 6, and 8 weight percent  $Gd_2O_3$  for fresh and once burned assemblies. This analysis also addresses typical operational ranges or technical specification limits (which ever is applicable) with regard to pressurizer pressure and level; accumulator pressure, temperature (containment temperature), and level; core inlet temperature; core flow; containment pressure and temperature; and refueling water storage tank temperature. The analysis explicitly analyzes fresh and once-burned fuel assemblies. The two GDC 35 cases were run and Loss of Offsite Power produced the limiting PCT; therefore, the 208 case set will be run in this configuration.

The evaluation resulted in meeting the 10 CFR 50.46 criteria with a minimum margin of 13.1 percent with 95 percent coverage and 95 percent confidence. The parameter which set this margin was the PCT of 1912 °F and occurred in a fresh fuel rod with 21.8 GWd/mtU burnup.

#### **B.3.2 Plant Description and Summary of Analysis Parameters**

The plant analysis presented in this appendix is a Westinghouse designed pressurized water reactor (PWR), which has four loops, each with a hot leg, a U-tube steam generator, and a cold leg with a RCP. The RCS also includes one pressurizer. The ECCS includes one charging and one accumulator/SI/RHR injection path per RCS loop (after applying the single failure assumption). The SI and RHR feed into common headers which are connected to the accumulator lines. The charging pumps are also cross-connected.

The S-RELAP5 model explicitly describes the RCS, reactor vessel, pressurizer, and accumulator lines. The charging injection flows are connected to the RCS, and the SI and RHR injection flows are connected to the accumulator lines. This model also describes the secondary-side steam generator that is instantaneously isolated (closed MSIV and feedwater trip) at the time of the break.

As described in the RLBLOCA methodology, many parameters associated with LBLOCA phenomenological uncertainties and plant operation ranges are sampled. A summary of those parameters sampled is given in Table B.1. Values for process or operational parameters, including ranges of sampled process parameters, and fuel design parameters used in the analysis are given in Table B.18. Plant data is analyzed to develop uncertainties for the process parameters sampled in the analyses. Table B.21 presents a summary of the uncertainties used in the analyses. Two parameters (RWST temperature and diesel start time) are set at conservative bounding values for all calculations.

Where applicable, the sampled parameter ranges are based on technical specification limits. Plant data are used to define range boundaries for loop flow (high end) and containment temperature (low end).

### B.3.3 Realistic Large Break LOCA Results

A set of two-hundred eight calculations were performed sampling the parameters listed in Table B.1. The minimum retained margin to criteria was 13.1 percent at 95 percent coverage with 95 percent confidence and was associated with case number 61 which resulted in a PCT of 1912 °F. For the set of cases (LOCA events) that lie within the 95/95 range, the maximum local oxidation was 9.2261 percent (Case 107) and the maximum core wide oxidation was 0.2408 percent (Case 107). Table B.17 is a summary of the major parameters for the minimum margin case. Table B.18 is the plant input parameters and operating range supported by the analysis. Table B.19 provides the containment initial and boundary conditions. Table B.20 describes the passive heat sinks for the containment input. Table B.21 provides the statistical distribution for the process parameters. The minimum margin case is characterized in Table B.22 and Table B.23. The heat transfer parameter range for the limiting margin case is provided in Table B.24. Table B.25 provides the twenty minimum margin cases used to establish the probability evaluation.

The analysis plots for the minimum margin case are shown in Figure B.24 through Figure B.35. Figure B.19 shows linear scatter plots of the key parameters sampled for the 208 calculations. Parameter labels appear to the left of each individual plot. These figures illustrate the parameter ranges used in the analysis. Figure B.20 and Figure B.21 show PCT scatter plots versus the time of PCT and versus break size from the set of cases (LOCA events) that lie within the 95/95 range. The scatter plots for the maximum oxidation and total oxidation are

shown in Figure B.22 and Figure B.23, respectively. Figure B.24 through Figure B.35 show key parameters from the S-RELAP5 calculations for the minimum margin case. Figure B.24 is the plot of PCT, independent of elevation. Figure B.36 compares the bottom of core recovery times for the set of cases that lie within the 95/95 range to the BOCR time predicted using the MPR CCFL correlation.

#### B.3.4 Conclusions

The results of this RLBLOCA analysis show 13.1 percent minimum margin to any of the first three 10 CFR 50.46 criterion at 95 percent coverage with 95 percent confidence.

**Table B.17: Summary of 4-Loop Westinghouse Plant Major  
Parameters for Limiting Transient**

<b>Parameter</b>	<b>Value</b>
Time in Cycle (hrs)	9331.05
Burnup (GWd/mtU)	21.8
Core Power (MWt)	3800
Core Peaking ( $F_q$ )	2.253
Radial Peak ( $F_{\Delta h}$ )	1.579
Axial Offset	+0.2041
Local Peaking (FI)	1.069
Break Type	DEGB
Break Size (ft <sup>2</sup> / side)	2.6935
Offsite Power Availability	not available
Decay Heat Multiplier	0.98943

**Table B.18: 4-Loop Westinghouse Plant Operating Range Supported  
by the LOCA Analysis**

Event		Operating Range
<b>1.0</b>	<b>Plant Physical Description</b>	
	1.1 Fuel	
	a) Cladding outside diameter	0.374 in.
	b) Cladding inside diameter	0.326 in.
	c) Cladding thickness	0.024 in.
	d) Pellet outside diameter	0.3195 in.
	e) Pellet density	[ ]
	f) Active fuel length	144 in.
	g) Gd <sub>2</sub> O <sub>3</sub> concentrations	2, 4, 6, 8 w/o
	1.2 RCS	Analysis
	a) Flow resistance	Analysis assumes
	b) Pressurizer location	most limiting PCT
	c) Hot assembly location	Anywhere in core
	d) Hot assembly type	17x17
	e) SG tube plugging	≤ 15%
<b>2.0</b>	<b>Plant Initial Operating Conditions</b>	
	2.1 Reactor Power	
	a) Nominal Reactor Power	3800 MWt
	b) $F_q$	≤ 2.335
	c) $F_{\Delta H}$	≤ 1.579 <sup>1</sup>
	d) MTC	≤ 0 at HFP
	2.2 Fluid Conditions	
	a) Loop flow	131.6 Mlbm/hr ≤ M ≤ 152.8 Mlbm/hr
	b) Core inlet temperature	578.2 °F ≤ T ≤ 583 °F
	c) Upper head temperature	~Tcold Temperature <sup>2</sup>
	d) Pressurizer pressure	1859.7 psia ≤ P ≤ 2459.7 psia <sup>3</sup>
	e) Pressurizer level	57% ≤ L ≤ 95%

<sup>1</sup> Includes 5 percent measurement uncertainty.

<sup>2</sup> Upper head temperature will change based on sampling of RCS temperature.

<sup>3</sup> Considers both representative plant data and includes ±30 psi measurement uncertainty.

**Table B.18: 4-Loop Westinghouse Plant Operating Range Supported  
by the LOCA Analysis (continued)**

Event		Operating Range
	f) Accumulator pressure	$614.7 \text{ psia} \leq P \leq 697.7 \text{ psia}$
	g) Accumulator liquid volume	$1004.6 \text{ ft}^3 \leq V \leq 1095.4 \text{ ft}^3$
	h) Accumulator temperature	$95 \text{ }^\circ\text{F} \leq T \leq 130 \text{ }^\circ\text{F}$ (coupled to containment lower volume temperature)
	i) Accumulator fL/D	As-Built piping configuration
	j) Minimum ECCS boron	$\geq 2400 \text{ ppm}$
<b>3.0</b>	<b>Accident Boundary Conditions</b>	
	a) Break location	RCS cold leg between RCP and RV
	b) Break type	Double-ended guillotine or split
	c) Break size (each side, relative to cold leg pipe area)	$0.05 \leq A \leq 1.0$ full pipe area (split) $0.05 \leq A \leq 1.0$ full pipe area (guillotine)
	d) Worst single-failure	Loss of one train of ECCS
	e) Offsite power	Not Available <sup>1</sup>
	f) ECCS pumped injection temperature	$110 \text{ }^\circ\text{F}$
	g) Charging pump delay	37 s (w/ offsite power) 27 s (w/o offsite power)
	h) SI pump delay	37 s (w/ offsite power) 27 s (w/o offsite power)
	i) RHR pump delay	37 s (w/ offsite power) 27 s (w/o offsite power)
	j) Containment pressure	14.3 psia, nominal value
	k) Containment upper compartment temperature	$80 \text{ }^\circ\text{F} \leq T \leq 110 \text{ }^\circ\text{F}$
	l) Containment lower compartment temperature	$95 \text{ }^\circ\text{F} \leq T \leq 130 \text{ }^\circ\text{F}$
	m) Containment sprays delay	8 s

<sup>1</sup> This is determined prior to the execution of the set of 208 cases.

**Table B.18: 4-Loop Westinghouse Plant Operating Range Supported  
by the LOCA Analysis (continued)**

Event		Operating Range	
n) Charging pump flow			
Pressure (psia)	Flow total (gpm)	Pressure (psia)	Flow total (gpm)
15.0	108.83	482.0	3497.19
50.0	362.78	675.0	4897.51
75.0	544.17	861.0	6247.05
100.0	725.56	1038.0	7531.29
125.0	906.95	1220.0	8851.80
149.0	1081.08	1392.0	10099.76
179.0	1298.75	1443.0	10469.80
194.0	1407.58	1676.0	12160.35
242.0	1755.85	1902.0	13800.11
291.0	2111.37	2237.0	16230.73
o) SI pump flow			
Pressure (psia)	Flow total (gpm)	Pressure (psia)	Flow total (gpm)
15.0	108.83	242.0	1755.85
50.0	362.78	291.0	2111.37
75.0	544.17	482.0	3497.19
100.0	725.56	675.0	4897.51
125.0	906.95	861.0	6247.05
149.0	1081.08	1038.0	7531.29
179.0	1298.75	1220.0	8851.80
194.0	1407.58	1392.0	10099.76
p) RHR pump flow			
Pressure (psia)	Flow total (gpm)		
15.0	108.83		
50.0	362.78		
75.0	544.17		
100.0	725.56		
125.0	906.95		
149.0	1081.08		
179.0	1298.75		

**Table B.19: 4-Loop Westinghouse Containment Initial and Boundary Conditions**

<b>Containment Net Free Volume</b>	<b>Volume (ft<sup>3</sup>)</b>
Upper Compartment	651,000 – 692,600
Lower Compartment (minimum)	248,500
Ice Condenser	181,400
Dead Ended Compartments	129,900
<b>Initial Conditions</b>	
Initial Mass of Ice	$2.448 \times 10^6$ lbm
Containment Pressure (nominal)	14.3 psia
Upper Containment Temperature	80 °F – 110 °F
Lower Containment Temperature	95 °F – 130 °F
Humidity	100 percent
<b>Containment Spray</b>	
Maximum Total Flow	$2 \times 7700 = 15,400$ gpm
Minimum Spray Temperature	55 °F
Fastest Post-LOCA initiation of spray	10 s (ramped to full flow between 8 and 10 s)
<b>Containment Air Return Fan<sup>1</sup></b>	
Post-LOCA initiation	600 s
Total Flow	120,000 cfm

<sup>1</sup> Due to the relatively late start of the recirculation fan, it is not modeled in this analysis.



**Table B.20: 4-Loop Westinghouse Passive Heat Sinks in Containment**

Heat Sink	Area ft <sup>2</sup>	Thickness ft	Inside Radius ft	Thickness ft	Height ft	Material	Left Side	Right Side
Reactor Cavity Walls	6438	2.02				concrete	Lower Comp.	insulated
Concrete Floor	4444	2.00				concrete	Lower Comp.	insulated
Interior Concrete	8464	1.00				concrete	Lower Comp.	insulated
Reactor Vessel Biological Shield Wall			11	6.0	19.88	concrete	Lower Comp.	Lower Comp.
Steel Lined Refueling Canal in LC			13.	0.02083	21.48	stainless steel	Lower Comp.	
				4.0	21.48	concrete		Lower Comp.
Crane Wall between LC & DE			41.5	3.0	33.72	concrete	Lower Comp.	Dead End
Crane Wall in LC			41.5	3.0	29.37	concrete	Lower Comp.	insulated
Crane Wall in UC			41.5	3.0	32.44	concrete	Upper Comp.	insulated
Refueling Canal in Contact with Upper and Lower Compartment	2551	0.02083				stainless steel	Upper Comp.	
		3.87				concrete		Lower Comp.
Refueling Canal in Contact with Annular Region	1,260	0.02083				stainless steel	Upper Comp.	
		3.0				concrete		annulus
Concrete Structure between Upper and Lower Compartment	13,081	2.34				concrete	Upper Comp.	Lower Comp.
Interior Concrete	2278	3.0				concrete	Upper Comp.	insulated
Containment Shell	24,646	0.05417				carbon steel	Upper Comp.	annulus
LC Steel Heat Sink	24,999	0.03674				carbon steel	Lower Comp.	insulated
UC Steel Heat Sink	11669	0.4229				carbon steel	Upper Comp.	insulated
Dead-End Steel Heat Sink	8610	0.074375				carbon steel	DE Comp.	insulated
<b>Material Properties</b>								
		<b>Thermal Conductivity (BTU/hr-ft-°F)</b>			<b>Volumetric Heat Capacity (BTU/ft<sup>3</sup>-°F)</b>			
Concrete		0.84			30.24			
Carbon Steel		27.3			59.2			
Stainless Steel		9.87			59.22			

**Table B.21: 4-Loop Westinghouse Statistical Distribution Used for  
Process Parameters**

Parameter	Operational Uncertainty Distribution	Parameter Range	Measurement Uncertainty Distribution <sup>1</sup>	Standard Deviation
Pressurizer Pressure (psia)	Uniform	1859.7 – 2459.7	N/A	N/A
Pressurizer Liquid Level (percent)	Uniform	57 – 95	N/A	N/A
Accumulator Liquid Volume (ft <sup>3</sup> )	Uniform	1004.6 – 1095.4	N/A	N/A
Accumulator Pressure (psia)	Uniform	614.7 – 697.7	N/A	N/A
Containment Lower Compartment /Accumulator Temperature (°F)	Uniform	95 – 130	N/A	N/A
Containment Upper Compartment Temperature (°F)	Uniform	80 – 110		
Containment Upper Volume (ft <sup>3</sup> )	Uniform	651,000 – 692,600	N/A	N/A
Initial RCS Flow Rate (Mlbm/hr)	Uniform	131.6 – 152.8	N/A	N/A
Initial RCS Operating Temperature (Tavg) (°F)	Uniform	578.2 – 583	N/A	N/A

<sup>1</sup> All measurement uncertainties were incorporated into the operational ranges.

**Table B.22: 4-Loop Westinghouse Compliance with 10 CFR 50.46**

Compliance to Cladding Temperature, Local Oxidation, and Core-Wide Oxidation Criteria			
Minimum Margin to Criteria Limits, %		13.1	
Variable Setting Minimum Margin		PCT	
Characterization of Case Set Determining 95/95 Compliance			
Parameter	Value	Fuel Pin Type	Case Number
Minimum Margin PCT, °F	1912	Fresh UO <sub>2</sub> Rod	61
Minimum Margin Local Maximum Oxidation, %	9.2261	Fresh UO <sub>2</sub> Rod	107
Minimum Margin Total Core-Wide Oxidation, %	0.2408	Fresh UO <sub>2</sub> Rod	107
Characteristics of Case Setting the Minimum Margin			
PCT, °F		1912	
Time of PCT, s		103.7	
Elevation within Core, ft		10.4	
Local Maximum Oxidation, %		4.8277	
Total Core-Wide Oxidation, %		0.0952	

**Table B.23: 4-Loop Westinghouse Calculated Event Times for  
Limiting Margin Case**

Event	Time (sec)
Begin Analysis	0.0
Break Opens	0.0
RCP Trip	0.0
SIAS Issued	0.1
Start of Broken Loop Accumulator Injection	13.0
Start of Intact Loop Accumulator Injection	20.0, 20.1 & 20.1
Start of SI	27.1
Start of CC	27.1
Beginning of Core Recovery (Beginning of Reflood)	62.1
RHR Available	27.1
PCT Occurred (1912 °F)	103.7
Broken Loop RHR Delivery Began	27.2
Intact Loops RHR Delivery Began	31.5, 31.5, & 31.5
Broken Loop SI Delivery Began	27.1
Intact Loops SI Delivery Began	27.1, 27.1 & 27.1
Broken Loop Accumulator Emptied	98.4
Intact Loop Accumulator Emptied	102.8, 103.0, 102.4
Transient Calculation Terminated	727.3

**Table B.24: Westinghouse 4-Loop Heat Transfer Parameters for  
Limiting Margin Case**

Time (s)	0 – 1.5	1.5 – 20.02	20.02 – 62.12	62.12 – Quench (575 s)	Quench	Quench – End of Transient (727.33 s)
LOCA Phase	Early Blowdown	Blowdown <sup>1</sup>	Refill	Reflood	Quench	Long Term Cooling
Heat Transfer Mode	CHF	Film Boiling/ Single-Phase	Film Boiling/ Single-Phase	Film Boiling/ Reflood	Transition Boiling	Transition Boiling
Heat Transfer Correlations	Biasi Zuber	Modified-Bromley Wong-Hochreiter Natural Convection Radiation (Sun) Rod-to-Rod radiation	Modified-Bromley Wong-Hochreiter Natural Convection Radiation (Sun) Rod-to-Rod radiation	Modified-Bromley Wong-Hochreiter Natural Convection Radiation (Sun) Rod-to-Rod radiation	Modified Chen Transition boiling	Chen Nucleate boiling
Maximum LHGR (kW/ft)	14.05 {< q <sub>CHF</sub> }	1.33 {< 5.5}	0.70 {< 5.5}	0.54	0.35	0.35
Pressure (psia)	1575 - 2038 {< 2250 at CHF}	717 - 1575 {< 2250}	23 - 717 {< 2250}	22 - 63 {< 2250 }	28	24 - 28
Core Inlet Mass Flux (kg/s-m <sup>2</sup> )	300 - 3300 {< 6000}	0 - 1000 {< 4250}	0 - 1000	0 - 900 {< 4250}	200	0 - 800
Vapor Reynolds Number	31700 - 168000	14500 - 146000 {< 10 <sup>6</sup> }	900 - 20000 {< 10 <sup>6</sup> }	1200 - 12000 {< 10 <sup>6</sup> }	7400 - 8000	3100 - 17000
Liquid Reynolds Number	9000 - 418000	400 - 67000	0 - 1000	0 – 23000	15000	100 - 27000
Vapor Prandtl Number	1.47 – 2.36	0.92 – 1.47	0.88 - 0.92	0.88 – 1.00	0.99	0.99 - 1.01
Liquid Prandtl Number	1.05 – 1.24	0.85 – 1.05	0.85 – 1.51	1.16 – 1.53	1.43	1.43 – 1.49
Superheat (°F)	60	480	1270	1420	90	110

<sup>1</sup> End of Blowdown considered as beginning of refill.

**Table B.25: Summary of Limiting Values for Top Minimum Margin Cases within the Set Used to Establish the Probability Evaluation**

Case Number	$\Phi$	PCT	ECR (%)	CWO (%)	S <sub>PCT</sub>	S <sub>ECR</sub>	S <sub>CWO</sub>
61	0.86905	1911.9	4.8277	9.52E-02	0.86905	0.28398	0.0952
193	0.866	1905.2	7.0653	1.94E-01	0.866	0.4156	0.19352
107	0.86155	1895.4	9.2261	2.41E-01	0.86155	0.54271	0.24079
85	0.85977	1891.5	7.0495	1.61E-01	0.85977	0.41468	0.1606
57	0.85909	1890	8.0277	1.32E-01	0.85909	0.47222	0.13177
141	0.85727	1886	7.1683	1.63E-01	0.85727	0.42166	0.16321
47	0.85145	1873.2	5.2807	1.08E-01	0.85145	0.31063	0.10802
39	0.8495	1868.9	5.8207	1.34E-01	0.8495	0.34239	0.13417
161	0.84032	1848.7	7.1497	1.57E-01	0.84032	0.42057	0.15725
65	0.83927	1846.4	7.9441	1.75E-01	0.83927	0.4673	0.17539
145	0.83814	1843.9	8.5891	1.58E-01	0.83814	0.50524	0.15843
35	0.83695	1841.3	7.6507	2.00E-01	0.83695	0.45004	0.20049
69	0.83186	1830.1	5.6567	1.24E-01	0.83186	0.33275	0.12399
67	0.83086	1827.9	5.4053	1.58E-01	0.83086	0.31796	0.15825
46	0.82891	1823.6	7.3055	1.02E-01	0.82891	0.42973	0.10196
29	0.82159	1807.5	7.3257	2.24E-01	0.82159	0.43092	0.22383
22	0.80432	1769.5	4.8187	1.36E-01	0.80432	0.28345	0.13583
45	0.80159	1763.5	6.8639	1.41E-01	0.80159	0.40376	0.14103
73	0.79964	1759.2	5.3569	8.52E-02	0.79964	0.31511	0.0852
43	0.79709	1753.6	4.2769	8.75E-02	0.79709	0.25158	0.0875

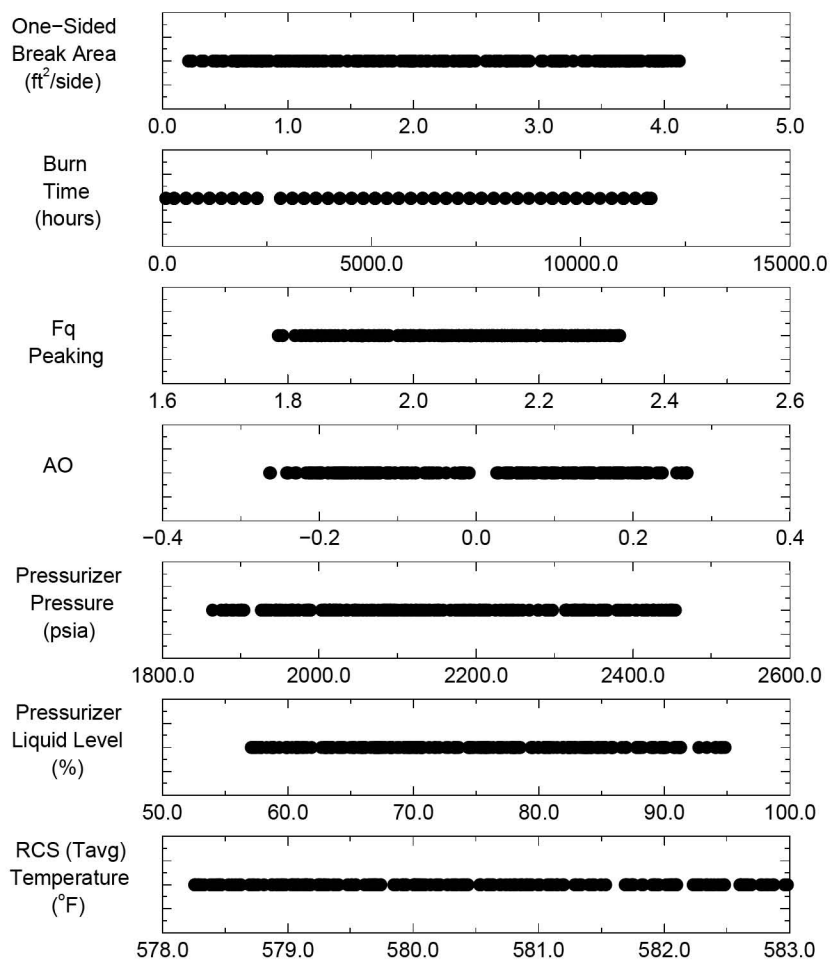


**Figure B.19: 4-Loop Westinghouse Scatter Plot of Operational Parameters**

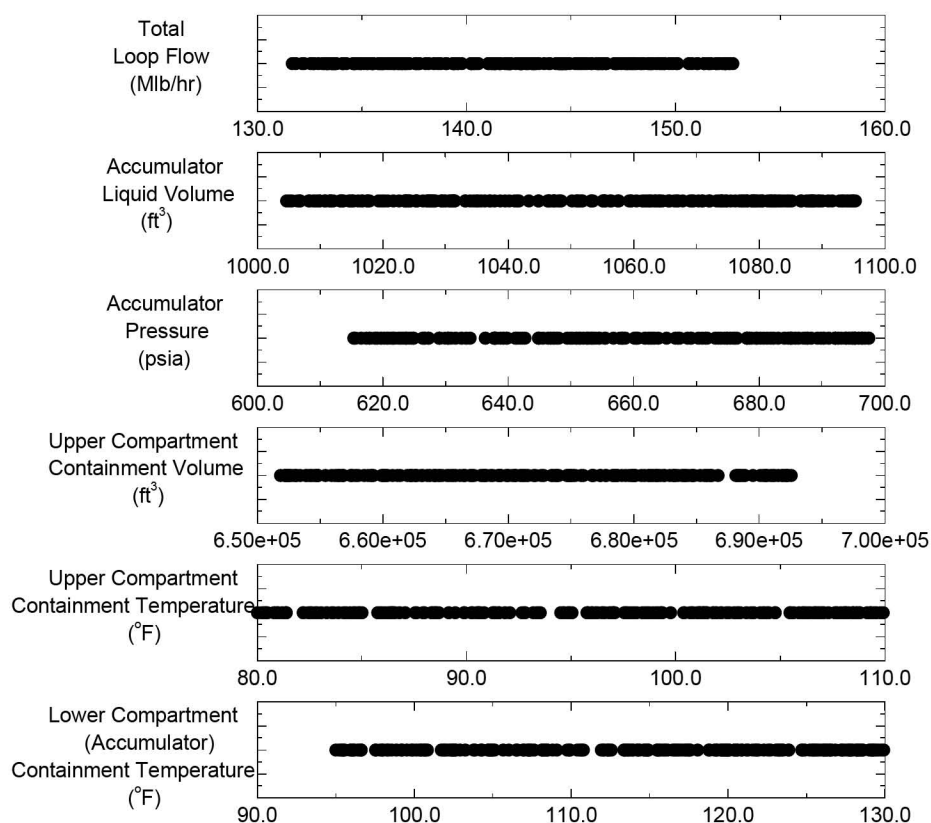


**Figure B.19: 4-Loop Westinghouse Scatter Plot of Operational Parameters (continued)**



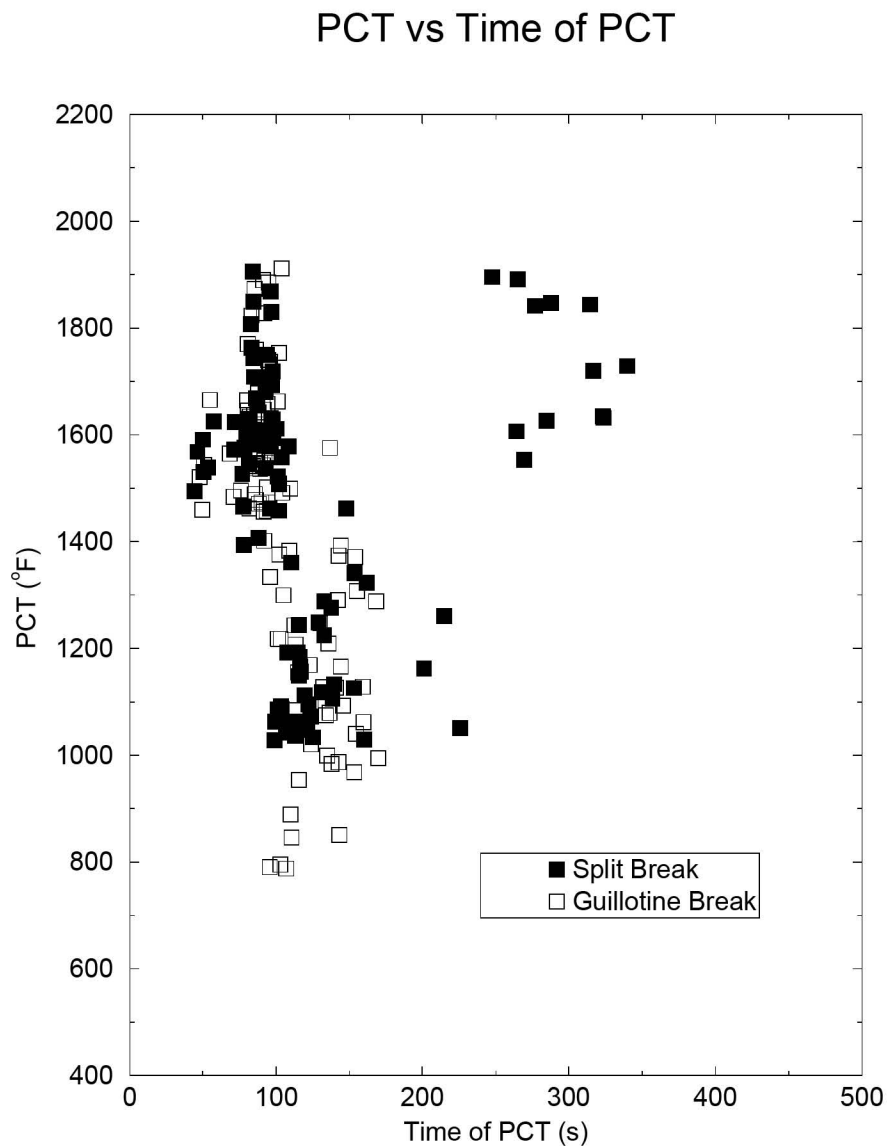


**Figure B.20: 4-Loop Westinghouse PCT versus PCT Time Scatter Plot from the Case Set**

### PCT vs One-sided Break Area

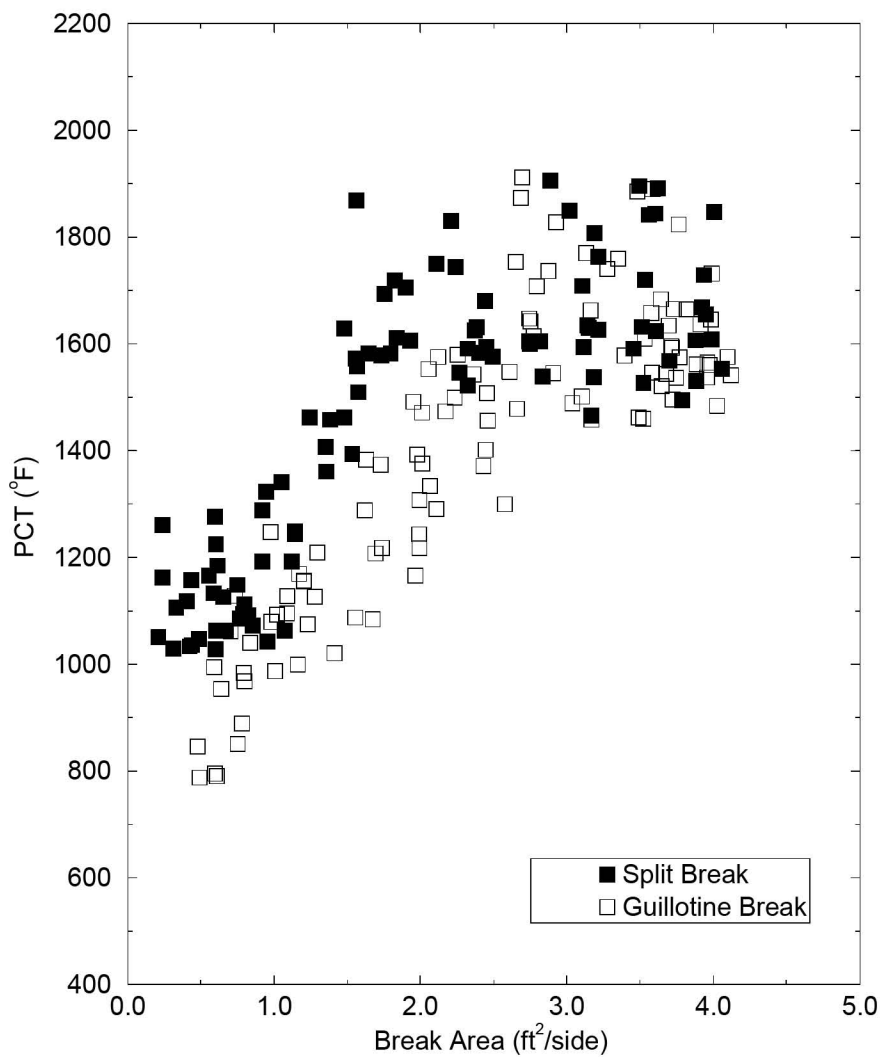


**Figure B.21: 4-Loop Westinghouse PCT versus Break Size Scatter  
Plot from the Case Set**

## Maximum Oxidation vs PCT

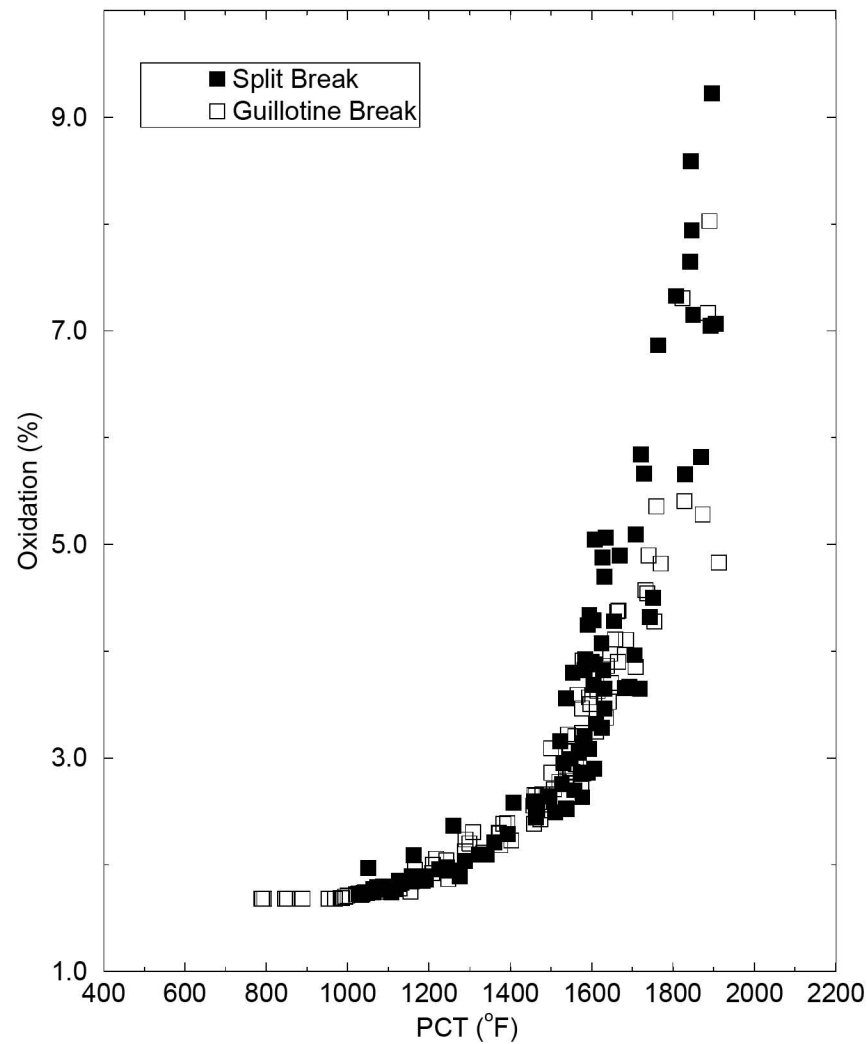


**Figure B.22: 4-Loop Westinghouse Maximum Oxidation versus PCT  
Scatter Plot from the Case Set**

## Total Oxidation vs PCT

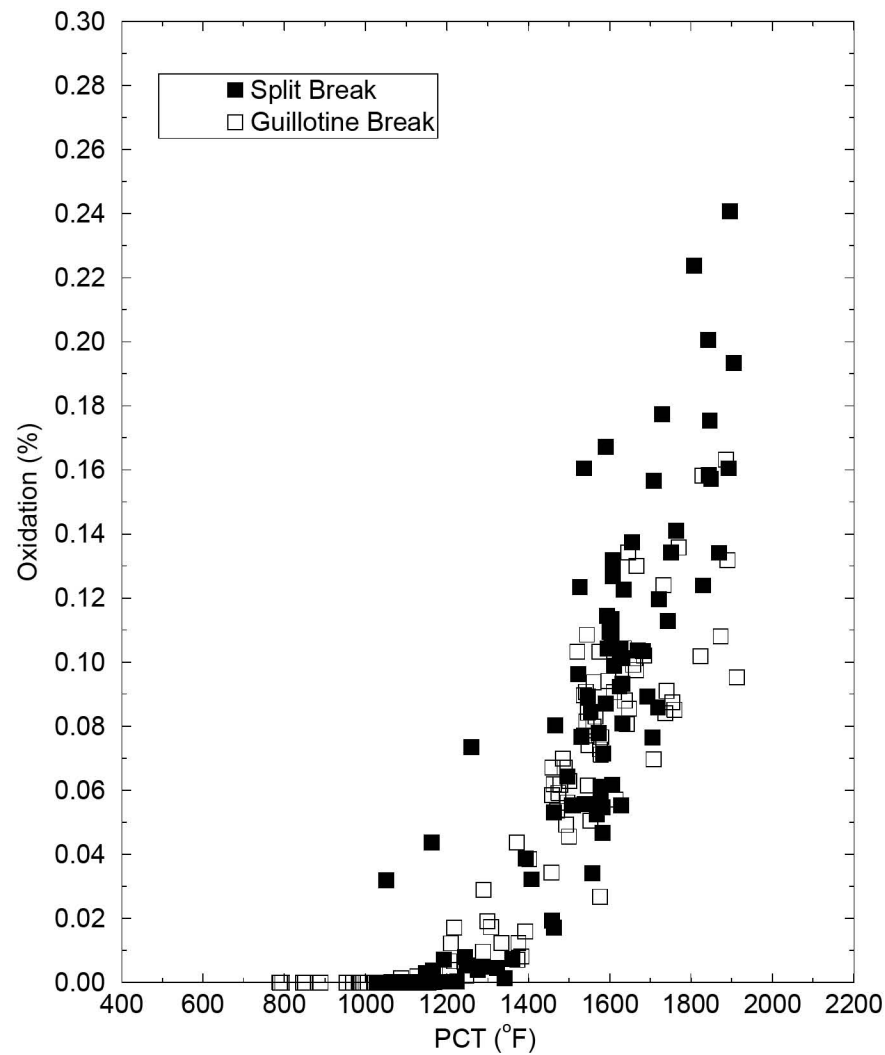


**Figure B.23: 4-Loop Westinghouse Total Oxidation versus PCT  
Scatter Plot from the Case Set**

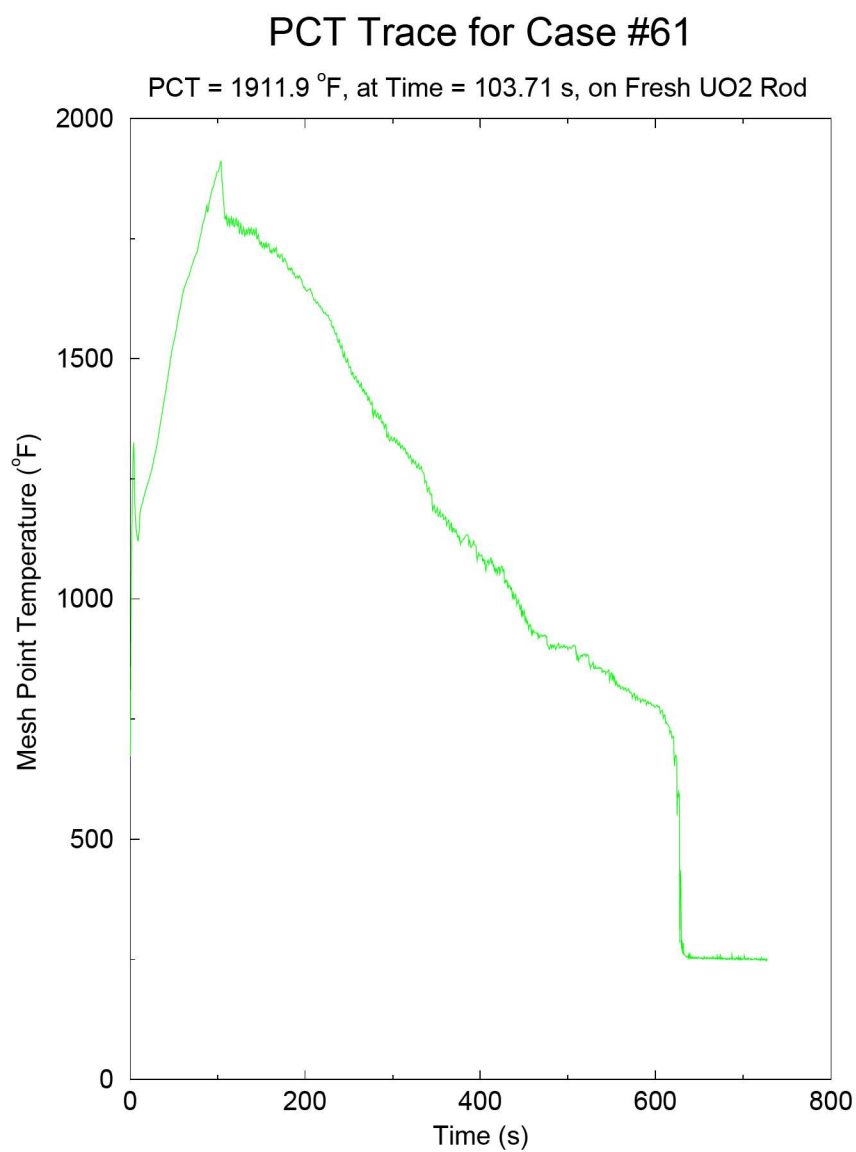


**Figure B.24: 4-Loop Westinghouse Peak Cladding Temperature  
(Independent of Elevation) for the Limiting Margin Case**

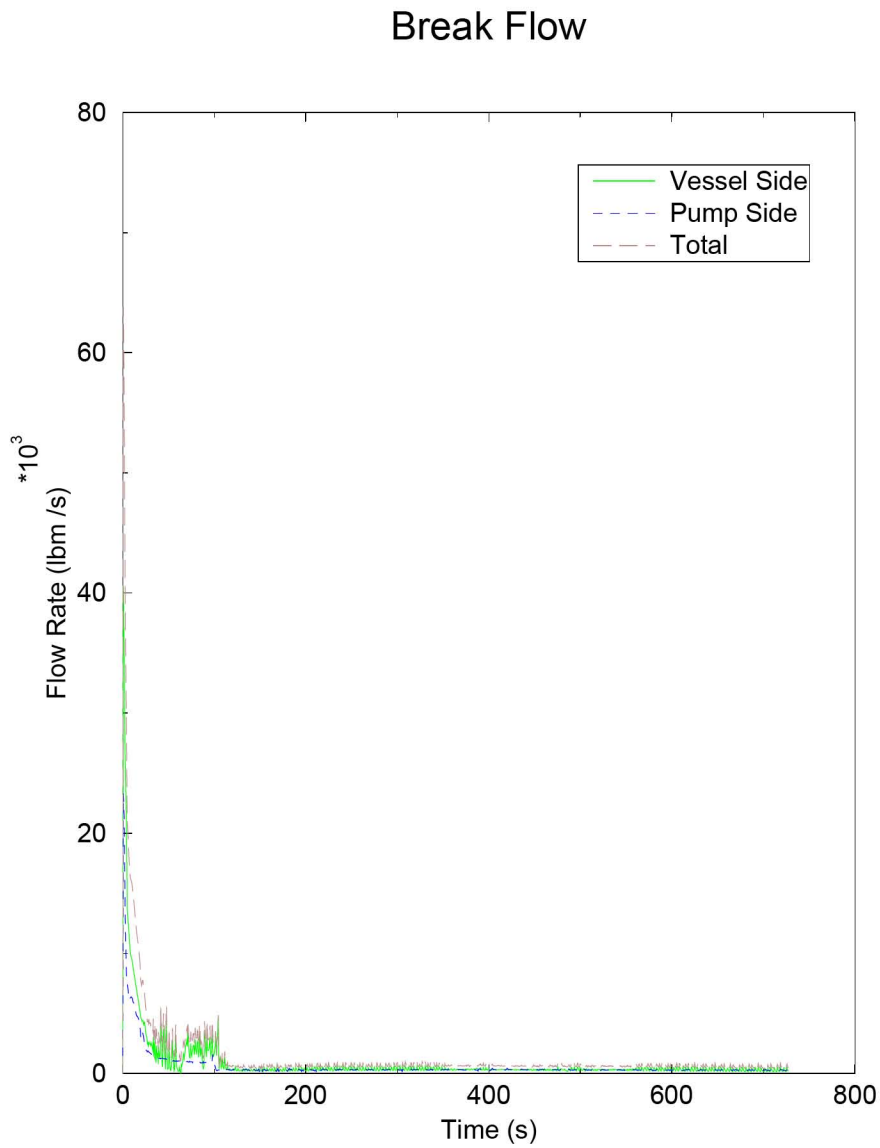


**Figure B.25: 4-Loop Westinghouse Break Flow for the Limiting Margin Case**

## Core Inlet Mass Flux

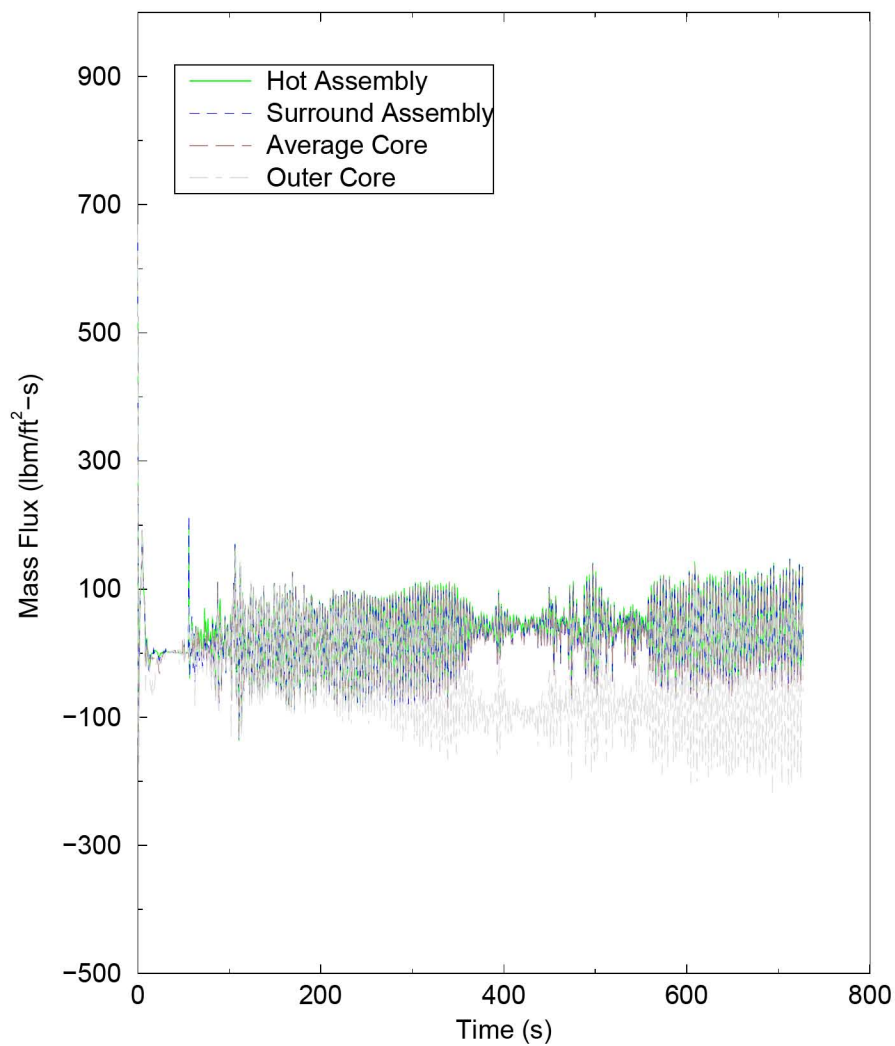


**Figure B.26: 4-Loop Westinghouse Core Inlet Mass Flux for the Limiting Margin Case**

## Core Outlet Mass Flux

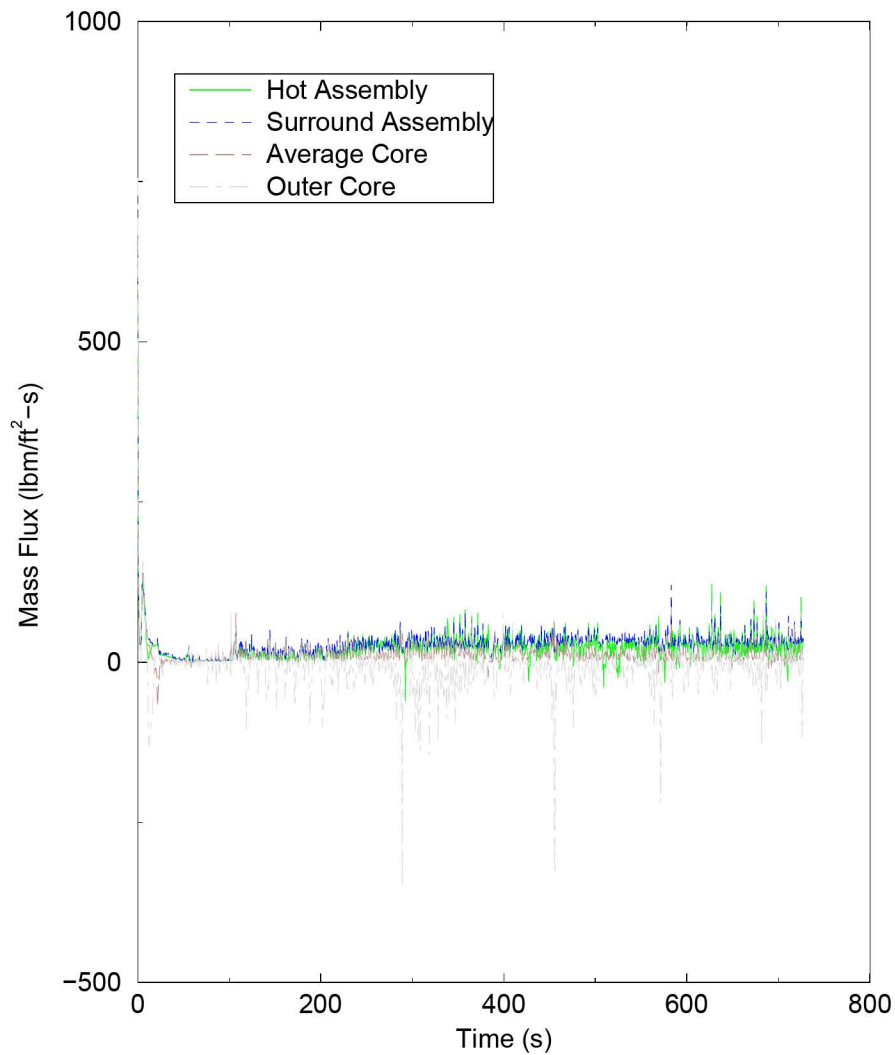


**Figure B.27: 4-Loop Westinghouse Core Outlet Mass Flux for the Limiting Margin Case**



## Pump Void Fraction

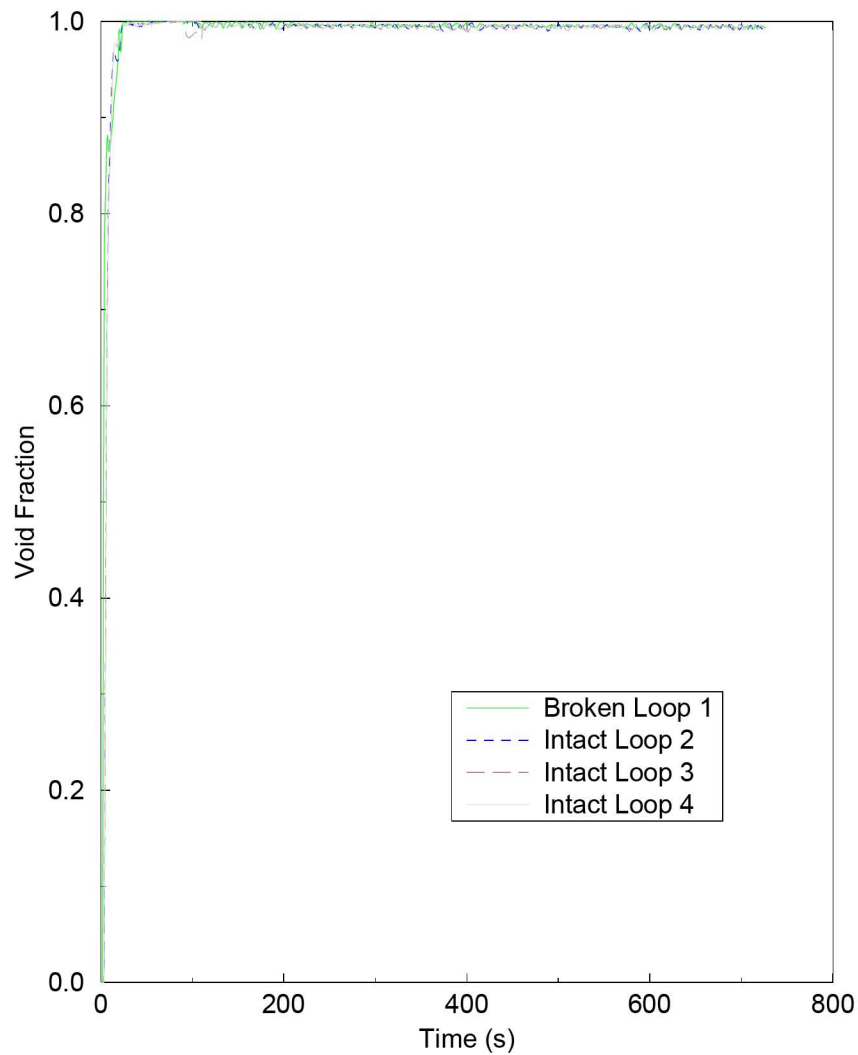


**Figure B.28: 4-Loop Westinghouse Void Fraction at RCS Pumps for the Limiting Margin Case**

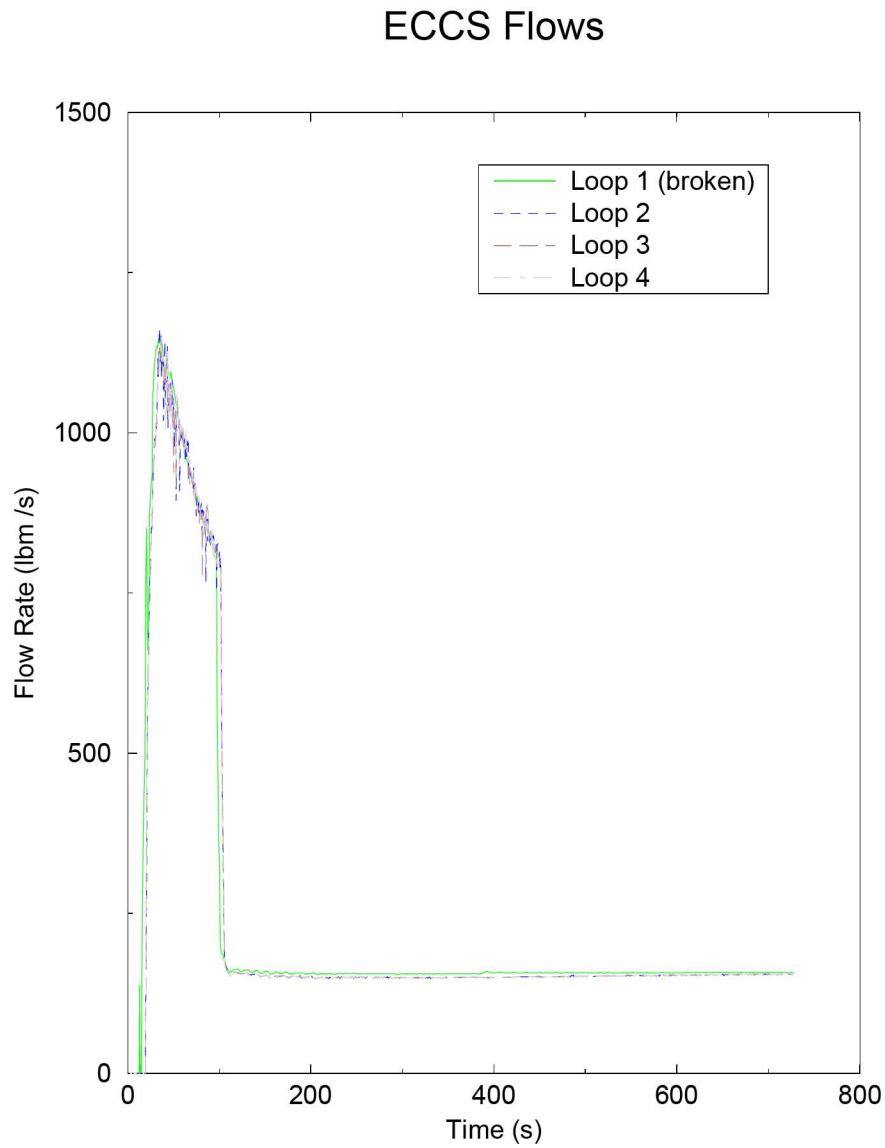


**Figure B.29: 4-Loop Westinghouse ECCS Flows (Includes Accumulator, Charging, SI and RHR) for the Limiting Margin Case**

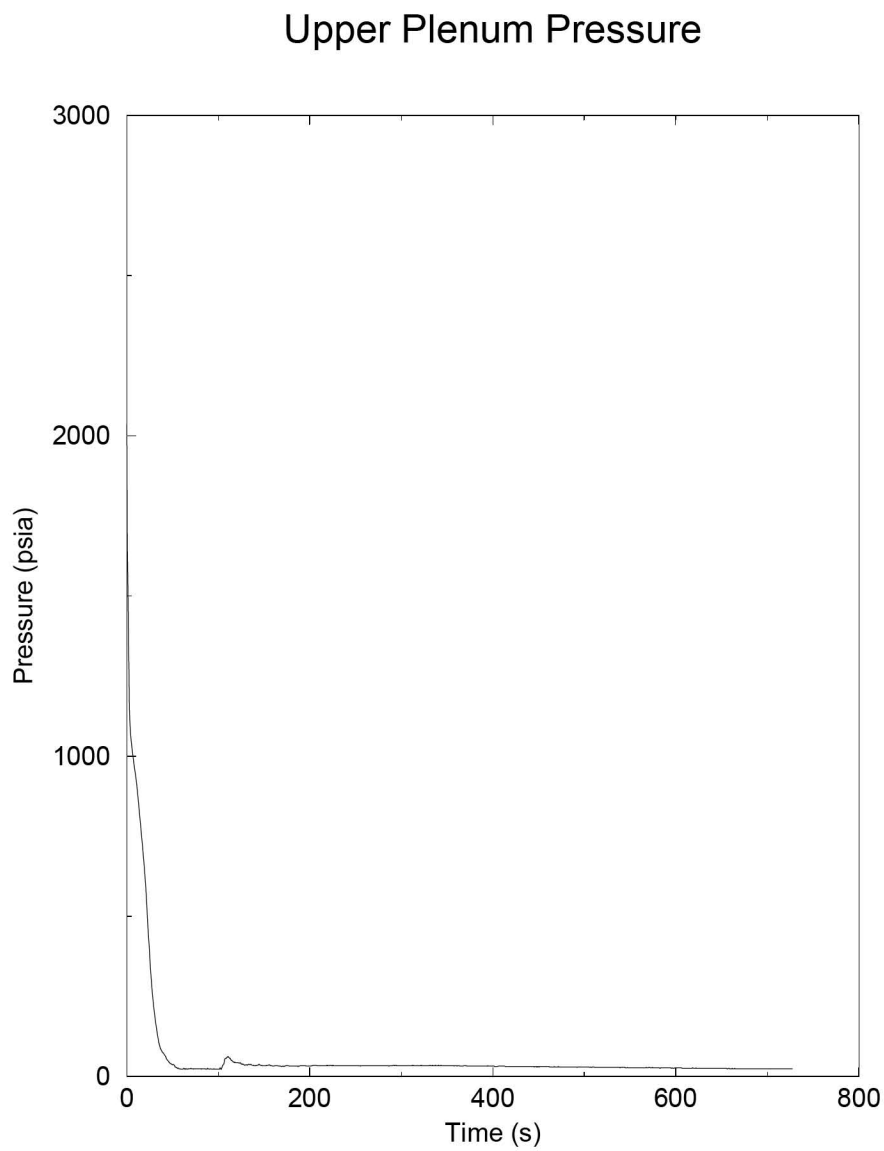


**Figure B.30: 4-Loop Westinghouse Upper Plenum Pressure for the Limiting Margin Case**

## Downcomer Liquid Level

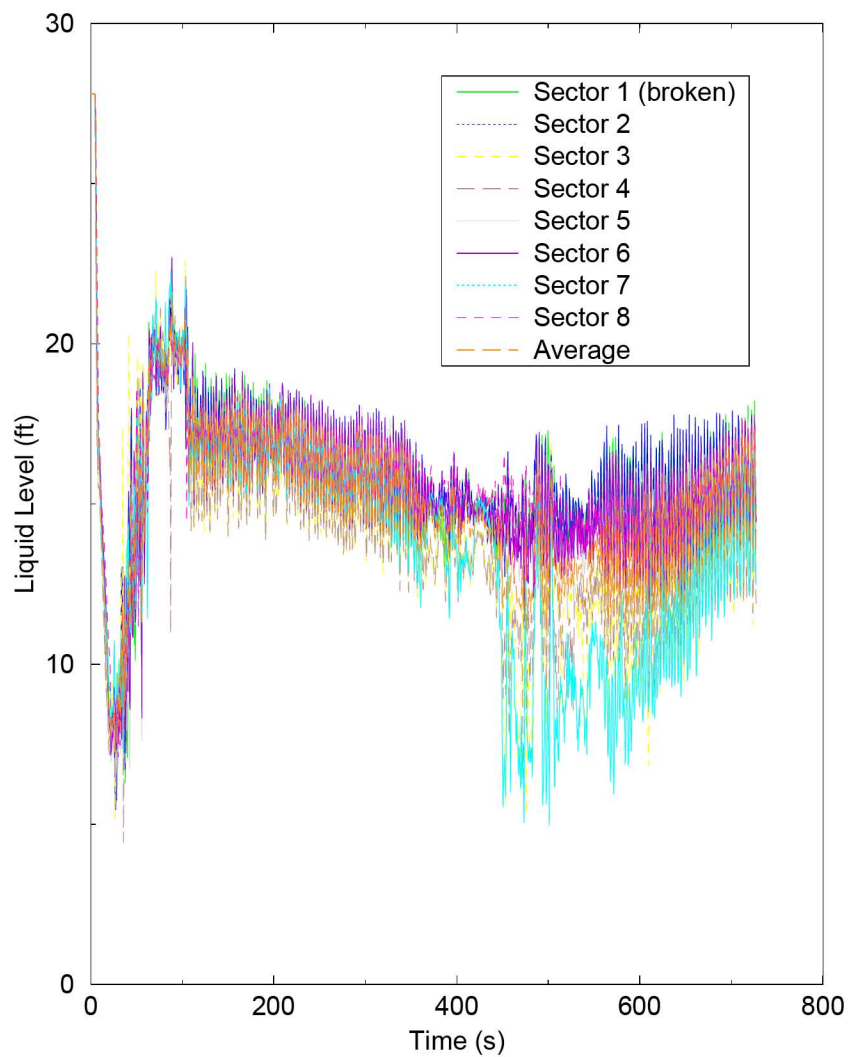


**Figure B.31: 4-Loop Westinghouse Collapsed Liquid Level in the Downcomer for the Limiting Margin Case**

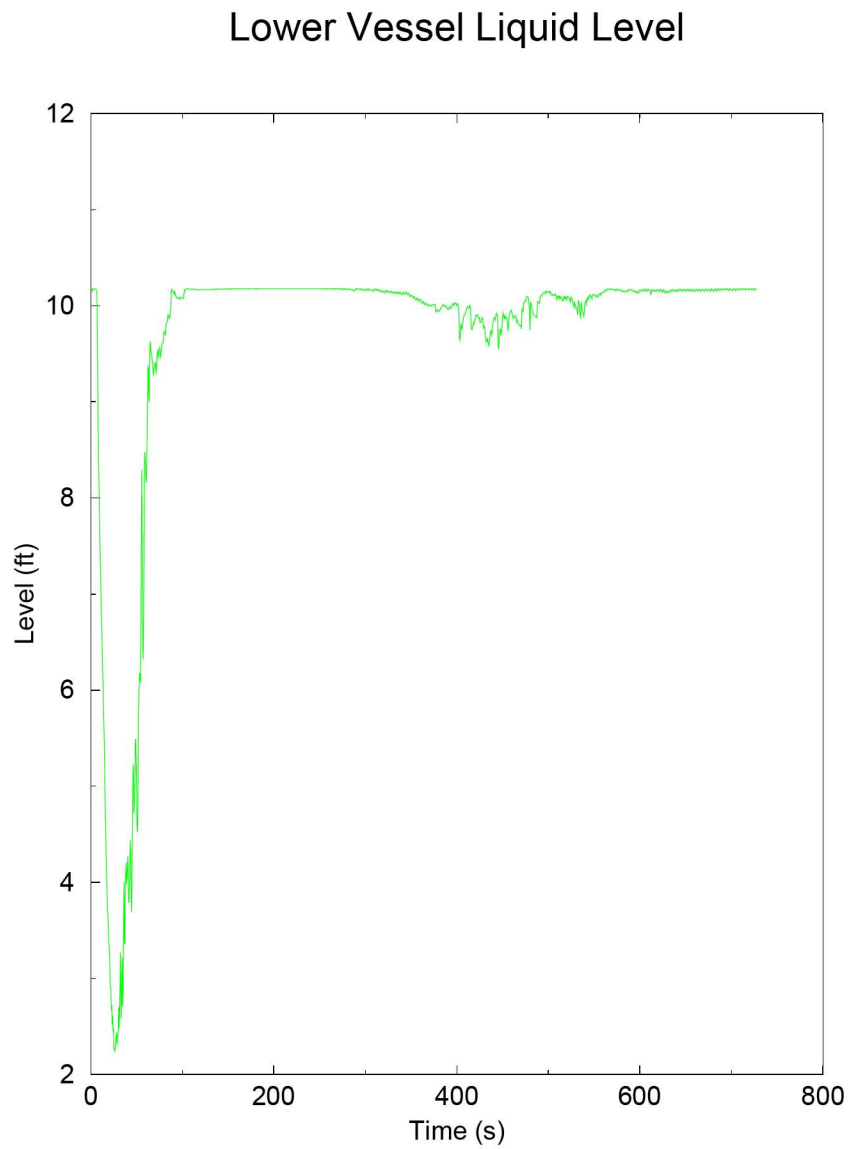


**Figure B.32: 4-Loop Westinghouse Collapsed Liquid Level in the Lower Plenum for the Limiting Margin Case**

## Core Liquid Level

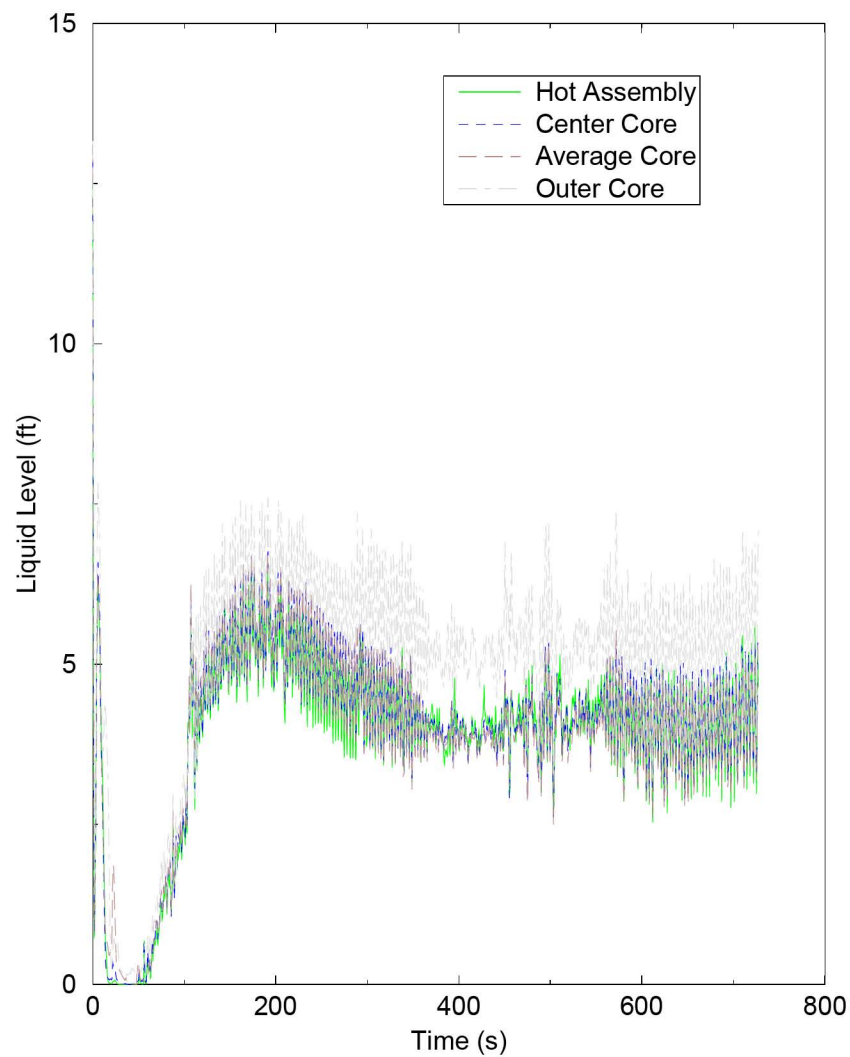


**Figure B.33: 4-Loop Westinghouse Collapsed Liquid Level in the Core for the Limiting Margin Case**

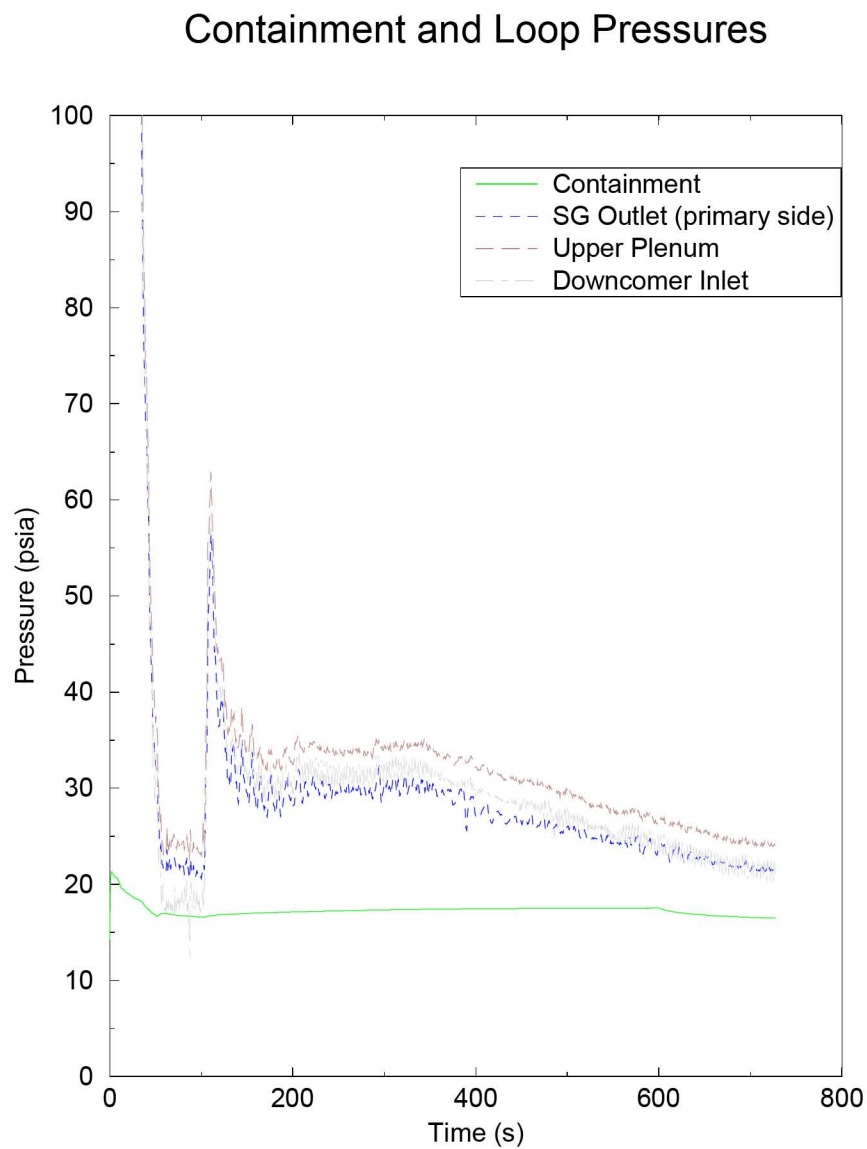


**Figure B.34: 4-Loop Westinghouse Containment and Loop Pressures for the Limiting Margin Case**

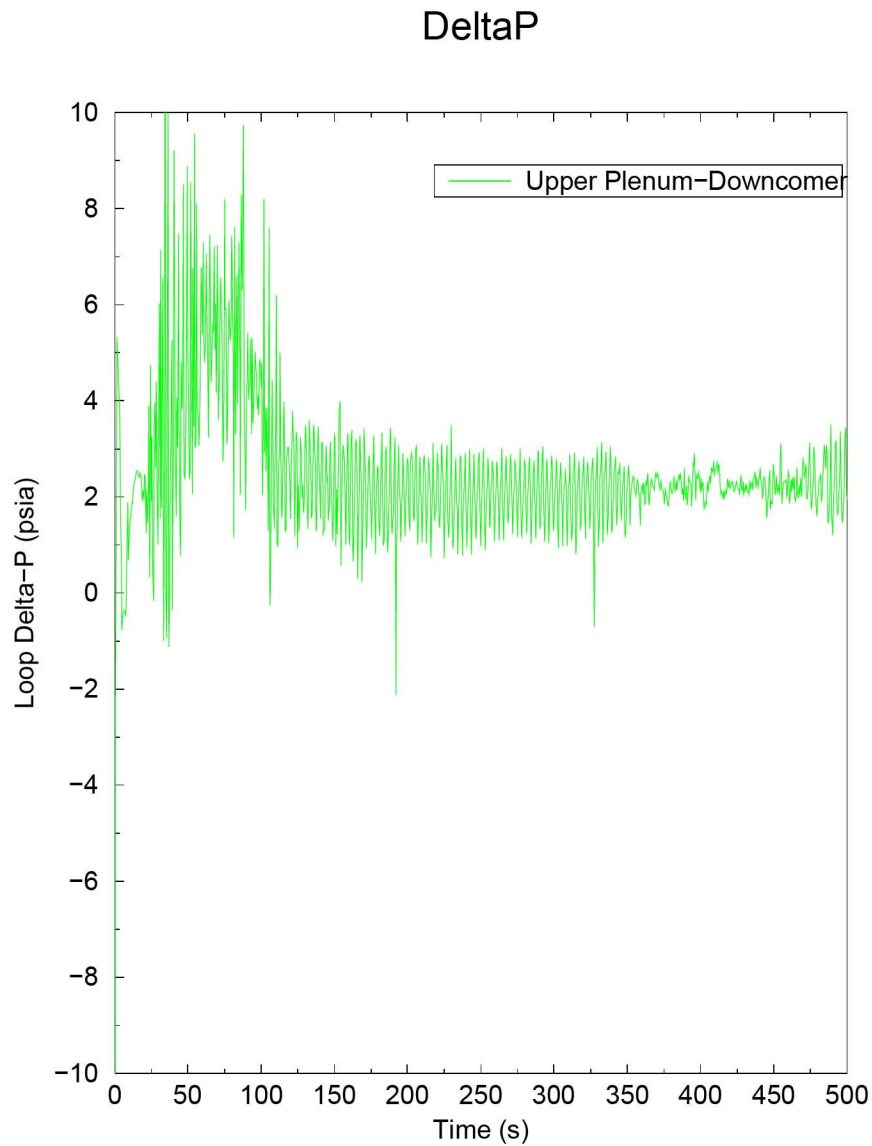


**Figure B.35: 4-Loop Westinghouse Pressure Difference between  
Upper Plenum and Downcomer**



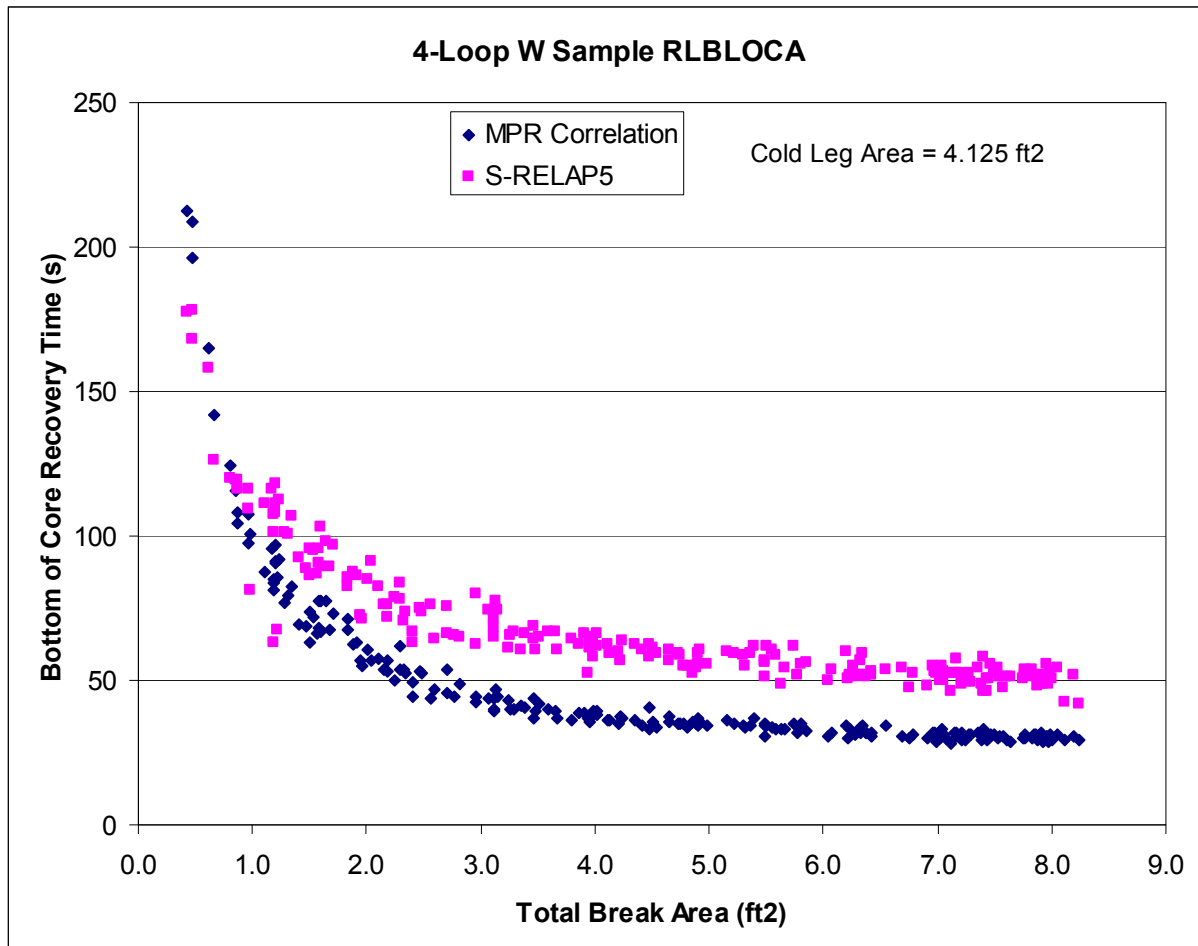


**Figure B.36: 4-Loop Westinghouse Validation of BOCR Time using  
MPR CCFL Correlation**

## **B.4 CE 2x4 PWR**

### **B.4.1 Summary**

The parameter specification for this analysis is provided in Table B.26. The analysis assumes full-power operation at 3300 MWt (plus 0.3 percent uncertainty), a steam generator tube plugging level of up to 10 percent in either generator, a total peaking factor ( $F_q$ ) of 2.175 including uncertainties, and a nuclear enthalpy rise factor ( $F_{\Delta H}$ ) of 1.81 (including 6 percent measurement uncertainty and a 3.5 percent control rod insertion effect). The analysis supports operation with AREVA 14x14 HTP design fuel using standard  $UO_2$  fuel with 2, 4, 6, and 8 weight percent  $Gd_2O_3$  for fresh and 4, 6, and 8 weight percent  $Gd_2O_3$  once burned assemblies. This analysis also addresses typical operational ranges or technical specification limits (which ever is applicable) with regard to pressurizer pressure and level; SIT pressure, temperature (containment temperature), and level; core inlet temperature; core flow; containment pressure and temperature; and refueling water storage tank temperature. The analysis explicitly analyzes fresh and once burned fuel assemblies. The two GDC 35 cases were run<sup>1</sup> and Loss of Offsite Power produced the limiting PCT, therefore the 208 case set will be run in this configuration.

For the sample analysis with M5<sup>®</sup> cladding, the evaluation resulted in meeting the 10 CFR 50.46 criteria with a minimum margin of 21.1 percent with 95 percent coverage and 95 percent confidence. The parameter which set this margin was the PCT of 1735 °F and occurred in a once-burned fuel rod with 27.6 GWd/mtU burnup.

For the sample analysis with Zirc-4 cladding, the evaluation resulted in meeting the 10 CFR 50.46 criteria with a minimum margin of 18.6 percent with 95 percent coverage and 95 percent confidence. The parameter which set this margin was the PCT of 1791 °F and occurred in a fresh fuel rod with 22.6 GWd/mtU burnup.

### **B.4.2 Plant Description and Summary of Analysis Parameters**

The plant analysis presented in this report is for a CE-designed PWR, which has 2X4-loop arrangement. There are two hot legs each with a U-tube steam generator and four cold legs

---

<sup>1</sup> This sample problem exceeded the recommendations provided in Section B.1.3 and was analyzed with a decay heat multiplier of 1.04.

each with a RCP. The RCS includes one Pressurizer connected to a hot leg. The core contains 217 thermal-hydraulic compatible AREVA HTP 14X14 fuel assemblies with 2, 4, 6 and 8 weight percent gadolinia pins. The ECCS includes one high pressure safety injection (HPSI), one LPSI and one SIT injection path per RCS loop. The break is modeled in the same loop as the pressurizer, as directed by the RLBLOCA methodology. The RLBLOCA transients are of sufficiently short duration that the switchover to sump cooling water (i.e., RAS) for ECCS pumped injection need not be considered.

The S-RELAP5 model explicitly describes the RCS, reactor vessel, Pressurizer, and ECCS. The ECCS includes a SIT path and a LPSI/HPSI path per RCS loop. The HPSI and LPSI feed into a common header that connects to each cold leg pipe downstream of the RCP discharge. The ECCS pumped injection is modeled as a table of flow versus backpressure. This model also describes the secondary-side steam generator that is instantaneously isolated (closed MSIV and feedwater trip) at the time of the break.

As described in the RLBLOCA methodology, many parameters associated with LBLOCA phenomenological uncertainties and plant operation ranges are sampled. A summary of those parameters sampled is given in Table B.1. Values for process or operational parameters, including ranges of sampled process parameters, and fuel design parameters used in the analysis are given in Table B.27. Plant data are analyzed to develop uncertainties for the process parameters sampled in the analyses. Table B.30 presents a summary of the uncertainties used in the analyses. Two parameters (RWST temperature and diesel start time) are set at conservative bounding values for all calculations.

Where applicable, the sampled parameter ranges are based on technical specification limits. Plant data are used to define range boundaries for loop flow (high end) and containment temperature (low end).

#### B.4.3 Realistic Large Break LOCA Results

The sample analysis with M5<sup>®</sup> cladding, a set of two-hundred eight calculations, was performed sampling the parameters listed in Table B.1. The minimum retained margin to criteria was 21.1 percent at 95 percent coverage with 95 percent confidence and was associated with case number 200 which resulted in a PCT of 1735 °F. For the set of cases (LOCA events) that lie

within the 95/95 range, the maximum local oxidation was 4.7281 percent (Case 161) and the maximum core-wide oxidation 0.0998 percent (Case 172).

The sample analysis with Zirc-4 cladding, a set of two-hundred eight calculations, was performed sampling the parameters listed in Table B.1. The minimum retained margin to criteria was 18.6 percent at 95 percent coverage with 95 percent confidence and was associated with case number 145 which resulted in a PCT of 1791 °F. For the set of cases (LOCA events) that lie within the 95/95 range, the maximum local oxidation was 6.7168 percent (Case 161) and the maximum core-wide oxidation was 0.1122 percent (Case 162).

Table B.26 is a summary of the major parameters for the minimum margin case. Table B.27 is the plant input parameters and operating range supported by the analysis. Table B.28 provides the containment initial and boundary conditions. Table B.29 describes the passive heat sinks for the containment input. Table B.30 provides the statistical distribution for the process parameters. The minimum margin cases are characterized in Table B.31 through Table B.33, for the COPENIC2 and RODEX3A runs. The heat transfer parameter range for the limiting margin case is provided in Table B.34 (COPENIC2) and Table B.35 (RODEX3A). Table B.36 and Table B.37 provides the twenty minimum margin cases used to establish the probability evaluation.

The analysis plots for the minimum margin case are shown in Figure B.42 through Figure B.53, and Figure B.60 through Figure B.71. Figure B.37 and Figure B.55 shows linear scatter plots of the key parameters sampled for each set of 208 calculations. Parameter labels appear to the left of each individual plot. These figures illustrate the parameter ranges used in the analysis. Figure B.38 and Figure B.39 (COPENIC2) and Figure B.56, and Figure B.57 (RODEX3A) show PCT scatter plots versus the time of PCT and versus break size from the set of cases (LOCA events) that lie within the 95/95 range. The scatter plots for the maximum oxidation and total oxidation are shown in Figure B.40 and Figure B.41 (COPENIC2), and Figure B.58 and Figure B.59 (RODEX3A), respectively. Figure B.42 through Figure B.52 (COPENIC2) and Figure B.60 through Figure B.70 (RODEX3A) show key parameters from the S-RELAP5 calculations for the minimum margin case. Figure B.42 (COPENIC2) and Figure B.60 (RODEX3A) are plots of PCT, independent of elevation. Figure B.54 (COPENIC2) and Figure B.72 (RODEX3A) compare the bottom of core recovery times for the set of cases that lie within the 95/95 range to the BOCR time predicted using the MPR CCFL correlation.

#### B.4.4 Conclusions

For the sample analysis with M5<sup>®</sup> cladding, the results of this RLBLOCA analysis show 21.1 percent minimum margin to any of the first three 10 CFR 50.46 criterion at 95 percent coverage with 95 percent confidence. For the sample analysis with Zirc-4 cladding, there is a 18.6 percent minimum margin to any of the first three 10 CFR 50.46 criterion at 95 percent coverage with 95 percent confidence.

**Table B.26: CE 2x4 Summary of Major Parameters for Limiting  
Transient**

<b>Parameter</b>	<b>COPERNIC2 Run</b>	<b>RODEX3A Run</b>
Time in Cycle (hrs)	8492.65	10694.52
Burnup (GWd/mtU)	34.6	22.6
Core Power (MWt)	3309.9	3309.9
Core Peaking ( $F_q$ )	2.16608	2.1603
Radial Peak ( $F_{\Delta H}$ )	1.81	1.81
Axial Shape Index	+0.0636	+0.0521
Local Peaking (FI)	1.11	1.044
Break Type	DEGB	DEGB
Break Size (ft <sup>2</sup> / side)	2.4638	4.4943
Offsite Power Availability	Not Available	Not Available
Decay Heat Multiplier	1.0070	0.99793

**Table B.27: CE 2x4 Plant Operating Range Supported by the LOCA Analysis**

Event		Operating Range
<b>1.0</b>	<b>Plant Physical Description</b>	
	1.1 Fuel	
	a) Cladding outside diameter	0.440 in.
	b) Cladding inside diameter	0.384 in.
	c) Cladding thickness	0.028 in.
	d) Pellet outside diameter	0.377 in.
	e) Pellet density	[ ]
	f) Active fuel length	136.7 in.
	g) Gd <sub>2</sub> O <sub>3</sub> concentrations	2, 4, 6, 8 w/o
	1.2 RCS	
	a) Flow resistance	Analysis
	b) Pressurizer location	Analysis assumes location giving most limiting PCT (broken loop)
	c) Hot assembly location	Anywhere in core
	d) Hot assembly type	14x14
	e) SG tube plugging	10 percent
<b>2.0</b>	<b>Plant Initial Operating Conditions</b>	
	2.1 Reactor Power	
	a) Nominal reactor power	3309.9 MWt
	b) LHR	16.5 kW/ft
	c) F <sub>q</sub>	2.175
	d) F <sub>r</sub>	1.810 <sup>1</sup>
	2.2 Fluid Conditions	
	a) Loop flow	140.8 Mlbm/hr ≤ M ≤ 164.6 Mlbm/hr
	b) RCS Cold Leg temperature	548.0 °F ≤ T ≤ 554.0 °F
	c) Pressurizer pressure	2210 psia ≤ P ≤ 2290 psia
	d) Pressurizer level	62.6 percent ≤ L ≤ 68.6 percent
	e) SIT pressure	214.7 psia ≤ P ≤ 294.7 psia
	f) SIT liquid volume	1090 ft <sup>3</sup> ≤ V ≤ 1170 ft <sup>3</sup>
	g) SIT temperature	115.5 °F ≤ T ≤ 124.5 °F (coupled with containment temperature)
	h) SIT resistance fL/D	As-built piping configuration
	i) Minimum ECCS boron	≥1900 ppm

<sup>1</sup> The radial power peaking for the hot rod is including 6 percent measurement uncertainty and 3.5 percent allowance for control rod insertion affect.

**Table B.27: CE 2x4 Plant Operating Range Supported by the LOCA  
Analysis (continued)**

Event		Operating Range																																																																																																																																																																																
3.0	Accident Boundary Conditions																																																																																																																																																																																	
	a) Break location	Cold leg pump discharge piping																																																																																																																																																																																
	b) Break type	Double-ended guillotine or split																																																																																																																																																																																
	c) Break size (each side, relative to cold leg pipe area)	0.05 ≤ A ≤ 1.0 full pipe area (split) 0.05 ≤ A ≤ 1.0 full pipe area (guillotine)																																																																																																																																																																																
	d) Worst single-failure	Loss of one emergency diesel generator																																																																																																																																																																																
	e) Offsite power	Available <sup>1</sup>																																																																																																																																																																																
	f) ECCS pumped injection temperature	104 °F																																																																																																																																																																																
	g) HPSI pump delay	19.5 (w/ offsite power) 30.0 (w/o offsite power)																																																																																																																																																																																
	h) LPSI pump delay	19.5 (w/ offsite power) 30.0 (w/o offsite power)																																																																																																																																																																																
	i) Containment pressure	14.7 psia, nominal value <sup>2</sup>																																																																																																																																																																																
	j) Containment temperature	115.5 °F ≤ T ≤ 124.5 °F																																																																																																																																																																																
	k) Containment sprays delay																																																																																																																																																																																	
	<table><tr><th colspan="2">BROKEN_LOOP</th><th colspan="2">INTACT_LOOP1</th><th colspan="2">INTACT_LOOP2</th><th colspan="2">INTACT_LOOP3</th></tr><tr><td colspan="2">* LOOP-1A1</td><td colspan="2">* LOOP-1B1</td><td colspan="2">* LOOP-1A2</td><td colspan="2">* LOOP-1B2</td></tr><tr><td>* RCS pressure</td><td>LPSI</td><td>* RCS pressure</td><td>LPSI</td><td>* RCS pressure</td><td>LPSI</td><td>* RCS pressure</td><td>LPSI</td></tr><tr><td>flow</td><td></td><td>flow</td><td></td><td>flow</td><td></td><td>flow</td><td></td></tr><tr><td>* -----</td><td>-----</td><td>* -----</td><td>-----</td><td>* -----</td><td>-----</td><td>* -----</td><td>-----</td></tr><tr><td>psia</td><td>gpm</td><td>psia</td><td>gpm</td><td>psia</td><td>gpm</td><td>psia</td><td>gpm</td></tr><tr><td>18.32</td><td>1287.</td><td>18.32</td><td>0.0</td><td>18.32</td><td>0.0</td><td>18.32</td><td>926.</td></tr><tr><td>23.48</td><td>1261.</td><td>23.48</td><td>0.0</td><td>23.48</td><td>0.0</td><td>23.48</td><td>902.</td></tr><tr><td>33.47</td><td>1210.</td><td>33.47</td><td>0.0</td><td>33.47</td><td>0.0</td><td>33.47</td><td>853.</td></tr><tr><td>43.02</td><td>1158.</td><td>43.02</td><td>0.0</td><td>43.02</td><td>0.0</td><td>43.02</td><td>804.</td></tr><tr><td>47.64</td><td>1132.</td><td>47.64</td><td>0.0</td><td>47.64</td><td>0.0</td><td>47.64</td><td>780.</td></tr><tr><td>52.14</td><td>1107.</td><td>52.14</td><td>0.0</td><td>52.14</td><td>0.0</td><td>52.14</td><td>755.</td></tr><tr><td>69.04</td><td>1005.</td><td>69.04</td><td>0.0</td><td>69.04</td><td>0.0</td><td>69.04</td><td>657.</td></tr><tr><td>87.73</td><td>877.</td><td>87.73</td><td>0.0</td><td>87.73</td><td>0.0</td><td>87.73</td><td>535.</td></tr><tr><td>103.73</td><td>748.</td><td>103.73</td><td>0.0</td><td>103.73</td><td>0.0</td><td>103.73</td><td>413.</td></tr><tr><td>117.05</td><td>620.</td><td>117.05</td><td>0.0</td><td>117.05</td><td>0.0</td><td>117.05</td><td>291.</td></tr><tr><td>127.72</td><td>492.</td><td>127.72</td><td>0.0</td><td>127.72</td><td>0.0</td><td>127.72</td><td>169.</td></tr><tr><td>135.41</td><td>364.</td><td>135.41</td><td>0.0</td><td>135.41</td><td>0.0</td><td>135.41</td><td>47.</td></tr><tr><td>140.64</td><td>236.</td><td>140.64</td><td>0.0</td><td>140.64</td><td>0.0</td><td>140.64</td><td>0.</td></tr><tr><td>143.98</td><td>82.</td><td>143.98</td><td>0.0</td><td>143.98</td><td>0.0</td><td>143.98</td><td>0.</td></tr><tr><td>144.37</td><td>31.</td><td>144.37</td><td>0.0</td><td>144.37</td><td>0.0</td><td>144.37</td><td>0.</td></tr><tr><td>144.44</td><td>0.</td><td>144.44</td><td>0.0</td><td>144.44</td><td>0.0</td><td>144.44</td><td>0.</td></tr></table>	BROKEN_LOOP		INTACT_LOOP1		INTACT_LOOP2		INTACT_LOOP3		* LOOP-1A1		* LOOP-1B1		* LOOP-1A2		* LOOP-1B2		* RCS pressure	LPSI	* RCS pressure	LPSI	* RCS pressure	LPSI	* RCS pressure	LPSI	flow		flow		flow		flow		* -----	-----	* -----	-----	* -----	-----	* -----	-----	psia	gpm	psia	gpm	psia	gpm	psia	gpm	18.32	1287.	18.32	0.0	18.32	0.0	18.32	926.	23.48	1261.	23.48	0.0	23.48	0.0	23.48	902.	33.47	1210.	33.47	0.0	33.47	0.0	33.47	853.	43.02	1158.	43.02	0.0	43.02	0.0	43.02	804.	47.64	1132.	47.64	0.0	47.64	0.0	47.64	780.	52.14	1107.	52.14	0.0	52.14	0.0	52.14	755.	69.04	1005.	69.04	0.0	69.04	0.0	69.04	657.	87.73	877.	87.73	0.0	87.73	0.0	87.73	535.	103.73	748.	103.73	0.0	103.73	0.0	103.73	413.	117.05	620.	117.05	0.0	117.05	0.0	117.05	291.	127.72	492.	127.72	0.0	127.72	0.0	127.72	169.	135.41	364.	135.41	0.0	135.41	0.0	135.41	47.	140.64	236.	140.64	0.0	140.64	0.0	140.64	0.	143.98	82.	143.98	0.0	143.98	0.0	143.98	0.	144.37	31.	144.37	0.0	144.37	0.0	144.37	0.	144.44	0.	144.44	0.0	144.44	0.0	144.44	0.	
BROKEN_LOOP		INTACT_LOOP1		INTACT_LOOP2		INTACT_LOOP3																																																																																																																																																																												
* LOOP-1A1		* LOOP-1B1		* LOOP-1A2		* LOOP-1B2																																																																																																																																																																												
* RCS pressure	LPSI	* RCS pressure	LPSI	* RCS pressure	LPSI	* RCS pressure	LPSI																																																																																																																																																																											
flow		flow		flow		flow																																																																																																																																																																												
* -----	-----	* -----	-----	* -----	-----	* -----	-----																																																																																																																																																																											
psia	gpm	psia	gpm	psia	gpm	psia	gpm																																																																																																																																																																											
18.32	1287.	18.32	0.0	18.32	0.0	18.32	926.																																																																																																																																																																											
23.48	1261.	23.48	0.0	23.48	0.0	23.48	902.																																																																																																																																																																											
33.47	1210.	33.47	0.0	33.47	0.0	33.47	853.																																																																																																																																																																											
43.02	1158.	43.02	0.0	43.02	0.0	43.02	804.																																																																																																																																																																											
47.64	1132.	47.64	0.0	47.64	0.0	47.64	780.																																																																																																																																																																											
52.14	1107.	52.14	0.0	52.14	0.0	52.14	755.																																																																																																																																																																											
69.04	1005.	69.04	0.0	69.04	0.0	69.04	657.																																																																																																																																																																											
87.73	877.	87.73	0.0	87.73	0.0	87.73	535.																																																																																																																																																																											
103.73	748.	103.73	0.0	103.73	0.0	103.73	413.																																																																																																																																																																											
117.05	620.	117.05	0.0	117.05	0.0	117.05	291.																																																																																																																																																																											
127.72	492.	127.72	0.0	127.72	0.0	127.72	169.																																																																																																																																																																											
135.41	364.	135.41	0.0	135.41	0.0	135.41	47.																																																																																																																																																																											
140.64	236.	140.64	0.0	140.64	0.0	140.64	0.																																																																																																																																																																											
143.98	82.	143.98	0.0	143.98	0.0	143.98	0.																																																																																																																																																																											
144.37	31.	144.37	0.0	144.37	0.0	144.37	0.																																																																																																																																																																											
144.44	0.	144.44	0.0	144.44	0.0	144.44	0.																																																																																																																																																																											

<sup>1</sup> Determined prior to the execution of the set of 208 cases.

<sup>2</sup> Nominal containment pressure range is -0.7 to 0.5 psig. For RLBOCA, a reasonable value between this range is acceptable.



**Table B.27: CE 2x4 Plant Operating Range Supported by the LOCA  
Analysis (continued)**

Event				Operating Range			
m) HPSI flow							
BROKEN_LOOP		INTACT_LOOP1		INTACT_LOOP2		INTACT_LOOP3	
* RCS pressure	HPSI flow	* RCS pressure	HPSI	* RCS pressure	HPSI	* RCS pressure	HPSI flow
* -----	-----	* -----	-----	* -----	-----	* -----	-----
psia	gpm	psia	gpm	psia	gpm	psia	gpm
15.	160.0	15.	151.7	15.	151.7	15.	0.0
315.	137.0	315.	130.0	315.	130.0	315.	0.0
615.	109.0	615.	103.7	615.	103.7	615.	0.0
815.	85.0	815.	81.3	815.	81.3	815.	0.0
1015.	51.0	1015.	48.7	1015.	48.7	1015.	0.0
1115.	16.0	1115.	15.3	1115.	15.3	1115.	0.0
1125.	8.0	1125.	5.7	1125.	5.7	1125.	0.0
1129.	0.0	1129.	0.0	1129.	0.0	1129.	0.0

**Table B.28: CE 2x4 Containment Initial and Boundary Conditions**

<b>Containment Net Free Volume (ft<sup>3</sup>)</b>	2,460,780 – 2,636,550
<b>Initial Conditions</b>	
Containment Pressure (nominal)	14.7 psia
Containment Temperature	115.5 °F – 124.5 °F
Outside Temperature	38 °F
Humidity	1.0
<b>Containment Spray</b>	
Number of Pumps operating	2
Spray Flow Rate (Total, both pumps)	9,000 gpm
Minimum Spray Temperature	36 °F
Fastest Post-LOCA initiation of spray	0 s
<b>Containment Fan Coolers</b>	
Number of Fan Coolers Operating	4
Minimum Post Accident Initiation Time of Fan Coolers (sec)	0
Fan Cooler Capacity (1 Fan Cooler)	
Containment Temperature (°F)	Heat Removal Rate (BTU/sec)
60	0
120	3472
180	8865
220	13,933
264	25,000

**Table B.29: CE 2x4 Passive Heat Sinks in Containment**

Heat Sink	Area (ft <sup>2</sup> )	Thickness (ft)	Material
Containment Shell	86700	0.1171	C Steel
Floor Slab	12682	20.0	Concrete
Misc Concrete	87751	1.5	Concrete
Galvanized Steel	130000	0.0005833	Zinc
	130000	0.01417	C Steel
Carbon Steel	25000	0.03125	C Steel
Stainless Steel	22300	0.0375	S Steel
Misc Steel	40000	0.0625	C Steel
Misc Steel	41700	0.02083	C Steel
Misc Steel	7000	0.17708	C Steel
Imbedded Steel	18000	0.0708	C Steel
	18000	7.07	Concrete
Sump (GSI-191)	7414	0.02895	C Steel
Material Properties	Thermal Conductivity (BTU/hr-ft-°F)	Volumetric Heat Capacity (BTU/ft <sup>3</sup> -°F)	
Concrete	1.0	34.2	
Carbon Steel	25.9	53.57	
Stainless Steel	9.8	54.0	
Galvanizing	64.0	40.6	

**Table B.30: CE 2x4 Statistical Distribution Used for Process Parameters**

Parameter	Operational Uncertainty Distribution	Parameter Range	Measurement Uncertainty Distribution	Standard Deviation
Pressurizer Pressure (psig)	Uniform	2210 - 2290	Normal	N/A
Pressurizer Level (%)	Uniform	62.6 – 68.6	Normal	N/A
SIT Volume (ft <sup>3</sup> )	Uniform	1090 – 1170	N/A	N/A
SIT Pressure (psia)	Uniform	214.7 – 294.7	N/A	N/A
Containment/SIT Temperature (°F)	Uniform	115.5 – 124.5	N/A	N/A
Containment Volume (x10 <sup>6</sup> ft <sup>3</sup> )	Uniform	2.46 - 2.64	N/A	N/A
Initial Flow Rate (Mlbm/hr)	Uniform	140.8 – 164.6	N/A	N/A
Initial Operating Temperature (°F)	Uniform	548 - 554	N/A	N/A

**Table B.31: CE 2x4 COPENIC2 Compliance with 10 CFR 50.46**

<b>Compliance to Cladding Temperature, Local Oxidation, and Core-Wide Oxidation Criteria</b>			
Minimum Margin to Criteria Limits, %		21.1	
Variable Setting Minimum Margin		PCT	
<b>Characterization of Case Set Determining 95/95 Compliance</b>			
<b>Parameter</b>	<b>Value</b>	<b>Fuel Pin Type</b>	<b>Case Number</b>
Minimum Margin PCT, °F	1735	Burned UO <sub>2</sub>	200
Minimum Margin Local Maximum Oxidation, %	4.7281	Fresh UO <sub>2</sub>	161
Minimum Margin Total Core-Wide Oxidation, %	0.0998	Burned UO <sub>2</sub>	172
<b>Characteristics of Case Setting the Minimum Margin</b>			
PCT, °F		1735	
Time of PCT, s		40.2	
Elevation within Core, ft		8.645	
Local Maximum Oxidation, %		3.8531	
Total Core-Wide Oxidation, %		0.0866	

**Table B.32: CE 2x4 RODEX3A Compliance with 10 CFR 50.46**

<b>Compliance to Cladding Temperature, Local Oxidation, and Core-Wide Oxidation Criteria</b>	
Minimum Margin to Criteria Limits, %	18.6
Variable Setting Minimum Margin	PCT

**Characterization of Case Set Determining 95/95 Compliance**

<b>Parameter</b>	<b>Value</b>	<b>Fuel Pin Type</b>	<b>Case Number</b>
Minimum Margin PCT, °F	1791	Fresh UO <sub>2</sub> Rod	145
Minimum Margin Local Maximum Oxidation, %	6.7168	Fresh UO <sub>2</sub> Rod	161
Minimum Margin Total Core-Wide Oxidation, %	0.1122	Fresh UO <sub>2</sub> Rod	162

**Characteristics of Case Setting the Minimum Margin**

PCT, °F	1791
Time of PCT, s	26.1
Elevation within Core, ft	8.906
Local Maximum Oxidation, %	5.8556
Total Core-Wide Oxidation, %	0.0938

**Table B.33: CE 2x4 Calculated Event Times for Limiting Margin  
Case**

Event	Time (sec) (COPERNIC2 w/ M5 <sup>®</sup> Clad)	Time (sec) (RODEX3A w/ Zirc-4 Clad)
Begin Analysis	0.0	0.0
Break Opens	0.0	0.0
RCP Trip	0.0	0.0
SIAS Issued	1.2	1.0
Start of Broken Loop SIT Injection	20.3	14.5
Start of Intact Loop SIT Injection	21.7, 21.8 & 21.8	17.1, 17.2 & 17.2
Start of HPSI	31.2	31.0
Start of Charging	N/A	N/A
Beginning of Core Recovery (Beginning of Reflood)	32.0	26.8
LPSI Available	31.2	31.0
PCT Occurred (1735 °F and 1775 °F, respectively)	40.2	26.1
Broken Loop LPSI Delivery Began	31.2	31.1
Intact Loops LPSI Delivery Began	N/A, N/A & 31.2	N/A, N/A & 31.1
Broken Loop HPSI Delivery Began	31.2	31.1
Intact Loops HPSI Delivery Began	31.2, 31.2 & N/A	31.1, 31.1 & N/A
Broken Loop SIT Emptied	63.9	53.5
Intact Loop SIT Emptied	63.8, 63.1 & 65.8	54.5, 52.7 & 55.4
Transient Calculation Terminated	788.2	743.8

**Table B.34: CE 2x4 Heat Transfer Parameters for Limiting Margin  
Case (COPERNIC2)**

Time (s)	0 – 4.5	4.5 – 30.70	30.70 – 32.01	32.01 – Quench (570 s)	Quench	Quench – End of Transient (788.18 s)
LOCA Phase	Early Blowdown	Blowdown <sup>1</sup>	Refill	Reflood	Quench	Long Term Cooling
Heat Transfer Mode	CHF	Film Boiling/ Single-Phase	Film Boiling/ Single-Phase	Film Boiling/ Reflood	Transition Boiling	Transition Boiling
Heat Transfer Correlations	Biasi Zuber	Modified-Bromley Wong-Hochreiter Natural Convection Radiation (Sun) Rod-to-Rod radiation	Modified-Bromley Wong-Hochreiter Natural Convection Radiation (Sun) Rod-to-Rod radiation	Modified-Bromley Wong-Hochreiter Natural Convection Radiation (Sun) Rod-to-Rod radiation	Modified Chen Transition boiling	Chen Nucleate boiling
Maximum LHGR (kW/ft)	16.20 {< q <sub>CHF</sub> }	1.07 {< 5.5}	0.73 {< 5.5}	0.73	0.40	0.40
Pressure (psia)	1114 - 2268 {< 2250 at CHF}	59 - 1114 {< 2250}	45 - 59 {< 2250}	25 - 70 {< 2250 }	26	23 - 26
Core Inlet Mass Flux (kg/s-m <sup>2</sup> )	0 - 3600 {< 6000}	0 - 600 {< 4250}	0 -100	0 - 900 {< 4250}	200 - 300	0 -600
Vapor Reynolds Number	0 -159000	300 - 31000 {< 10 <sup>6</sup> }	1400 - 3000 {< 10 <sup>6</sup> }	1000 - 15000 {< 10 <sup>6</sup> }	6800 - 7000	1200 - 16000
Liquid Reynolds Number	1900 - 581000	0 - 12000	0	0 - 28000	500 - 1000	100 - 34000
Vapor Prandtl Number	0.92 – 2.94	0.88 – 0.92	0.88	0.87 – 1.01	1.01	1.01
Liquid Prandtl Number	0.93 – 1.09	0.85 – 1.18	1.18 – 1.27	1.13 – 1.47	1.47	1.45 – 1.50
Superheat (°F)	520	1210	1240	1270	-10	10

<sup>1</sup> End of Blowdown considered as beginning of refill.



**Table B.35: CE 2x4 Heat Transfer Parameters for Limiting Margin  
Case (RODEX3A)**

Time (s)	0 – 1.5	1.5 – 24.676	24.68 – 26.77	26.77 – Quench (647 s)	Quench	Quench – End of Transient (743.8 s)
LOCA Phase	Early Blowdown	Blowdown <sup>1</sup>	Refill	Reflood	Quench	Long Term Cooling
Heat Transfer Mode	CHF	Film Boiling/ Single-Phase	Film Boiling/ Single-Phase	Film Boiling/ Reflood	Transition Boiling	Transition Boiling
Heat Transfer Correlations	Biasi Zuber	Modified-Bromley Wong-Hochreiter Natural Convection Radiation (Sun) Rod-to-Rod radiation	Modified-Bromley Wong-Hochreiter Natural Convection Radiation (Sun) Rod-to-Rod radiation	Modified-Bromley Wong-Hochreiter Natural Convection Radiation (Sun) Rod-to-Rod radiation	Modified Chen Transition boiling	Chen Nucleate boiling
Maximum LHGR (kW/ft)	16.48 {< q <sub>CHF</sub> }	1.48 {< 5.5}	0.78 {< 5.5}	0.76	0.40	0.40
Pressure (psia)	1451 - 2320 {< 2250 at CHF}	54 - 1451 {< 2250}	44 - 54 {< 2250}	23- 56 {< 2250 }	23	22 - 24
Core Inlet Mass Flux (kg/s-m <sup>2</sup> )	300 - 3700 {< 6000}	0 - 300 {< 4250}	0 - 100	0 - 1400 {< 4250}	200	0 - 1000
Vapor Reynolds Number	0 – 173000	1100 - 39000 {< 10 <sup>6</sup> }	800 - 3000 {< 10 <sup>6</sup> }	500- 16000 {< 10 <sup>6</sup> }	7600 - 8000	900 - 15000
Liquid Reynolds Number	600 - 599000	0 - 8000	0	0 – 54000	3100 - 4000	100 - 35000
Vapor Prandtl Number	1.38 – 3.09	0.88 – 1.38	0.88	0.86 – 1.01	1.00	1.00 - 1.01
Liquid Prandtl Number	1.01 – 1.10	0.85 – 1.21	1.21 – 1.27	1.20 – 1.51	1.51	1.49 – 1.52
Superheat (°F)	80	1270	1330	1350	10	10

<sup>1</sup> End of Blowdown considered as beginning of refill.

**Table B.36: Summary of Limiting Values for Top Minimum Margin  
Cases within the Set Used to Establish the Probability Evaluation  
(COPERNIC2 with M5<sup>®</sup> Cladding)**

<b>Case Number</b>	<b><math>\Phi</math></b>	<b>PCT</b>	<b>ECR (%)</b>	<b>CWO (%)</b>	<b>S<sub>PCT</sub></b>	<b>S<sub>ECR</sub></b>	<b>S<sub>CWO</sub></b>
200	0.78823	1734.1	3.8531	0.08661	0.78823	0.22665	0.0866
19	0.78291	1722.4	3.5019	0.06637	0.78291	0.206	0.06637
162	0.78095	1718.1	4.3911	0.07933	0.78095	0.2583	0.07933
145	0.77832	1712.3	3.7999	0.06807	0.77832	0.22353	0.06807
62	0.77705	1709.5	3.6167	0.06513	0.77705	0.21275	0.06513
61	0.77505	1705.1	4.7281	0.03429	0.77505	0.27813	0.03429
67	0.77418	1703.2	3.0114	0.06327	0.77418	0.17714	0.06327
92	0.77077	1695.7	3.8483	0.07310	0.77077	0.22637	0.0731
93	0.76977	1693.5	3.9437	0.07698	0.76977	0.23198	0.07698
66	0.76591	1685	3.6373	0.06970	0.76591	0.21396	0.0697
199	0.76186	1676.1	2.8723	0.07096	0.76186	0.16896	0.07096
164	0.75909	1670	3.3862	0.05858	0.75909	0.19919	0.05858
5	0.75882	1669.4	3.8871	0.07612	0.75882	0.22865	0.07612
186	0.758	1667.6	4.4569	0.05989	0.758	0.26217	0.05989
136	0.75718	1665.8	2.4171	0.03470	0.75718	0.14218	0.0347
190	0.75632	1663.9	2.8225	0.07557	0.75632	0.16603	0.07557
74	0.75627	1663.8	3.1048	0.07039	0.75627	0.18263	0.07039
185	0.75382	1658.4	3.9479	0.04760	0.75382	0.23223	0.0476
42	0.75373	1658.2	2.9086	0.06178	0.75373	0.1711	0.06178
54	0.75359	1657.9	2.83	0.04885	0.75359	0.16647	0.04885

**Table B.37: Summary of Limiting Values for Top Minimum Margin  
Cases within the Set Used to Establish the Probability Evaluation  
(RODEX3A with Zirc-4 Cladding)**

<b>Case Number</b>	<b><math>\Phi</math></b>	<b>PCT</b>	<b>ECR (%)</b>	<b>CWO (%)</b>	<b>S<sub>PCT</sub></b>	<b>S<sub>ECR</sub></b>	<b>S<sub>CWO</sub></b>
145	0.81391	1790.6	5.8556	0.09382	0.81391	0.34445	0.09382
2	0.81059	1783.3	5.6286	0.07338	0.81059	0.33109	0.07338
162	0.8075	1776.5	6.3126	0.11221	0.8075	0.37133	0.11221
164	0.80423	1769.3	6.6328	0.08218	0.80423	0.39016	0.08218
93	0.80218	1764.8	5.3622	0.09690	0.80218	0.31542	0.0969
199	0.79827	1756.2	4.9032	0.09545	0.79827	0.28843	0.09545
161	0.79605	1751.3	6.7168	0.04526	0.79605	0.39511	0.04526
186	0.79464	1748.2	6.6318	0.07597	0.79464	0.39011	0.07597
66	0.79327	1745.2	5.1168	0.08717	0.79327	0.30099	0.08717
19	0.79273	1744	5.1782	0.08614	0.79273	0.3046	0.08614
94	0.79091	1740	4.6997	0.06374	0.79091	0.27645	0.06374
62	0.78709	1731.6	5.1218	0.08091	0.78709	0.30128	0.08091
54	0.78668	1730.7	4.8253	0.06072	0.78668	0.28384	0.06071
190	0.78668	1730.7	4.6387	0.09735	0.78668	0.27287	0.09735
92	0.78586	1728.9	5.8296	0.09759	0.78586	0.34292	0.09759
51	0.78573	1728.6	5.0352	0.08765	0.78573	0.29619	0.08765
106	0.78055	1717.2	5.608	0.07232	0.78055	0.32988	0.07232
119	0.78005	1716.1	5.7938	0.09742	0.78005	0.34081	0.09742
110	0.77986	1715.7	4.9146	0.07140	0.77986	0.2891	0.0714
185	0.77927	1714.4	4.9466	0.06535	0.77927	0.29098	0.06535

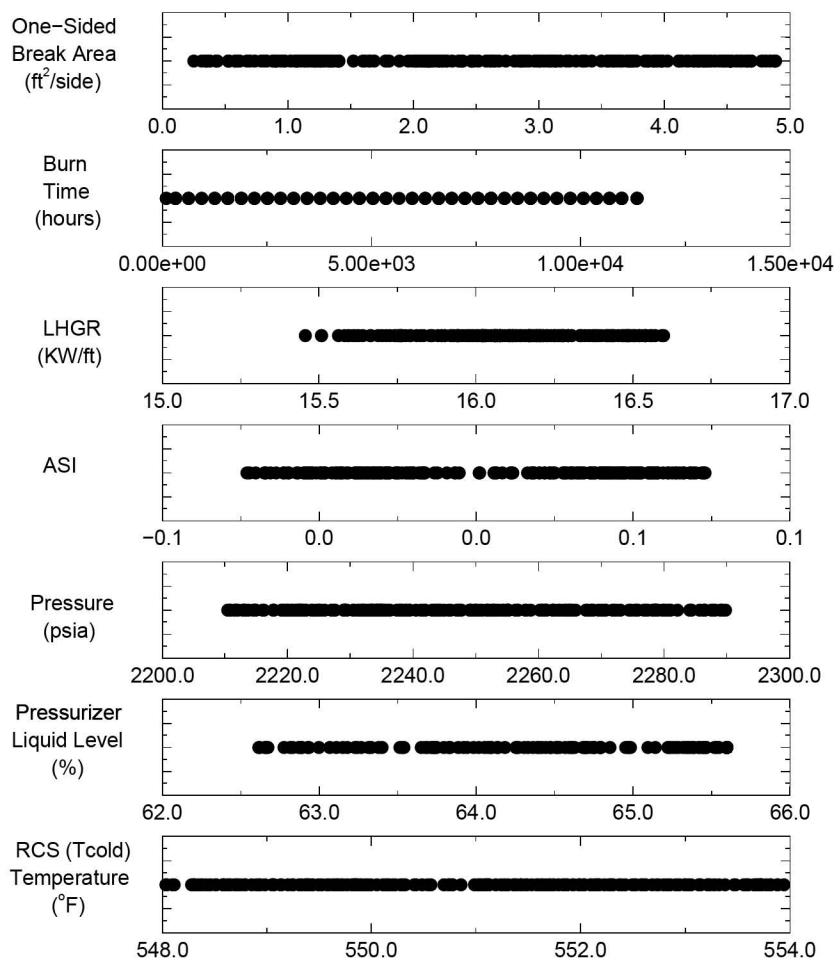


**Figure B.37: CE 2x4 Scatter Plot of Operational Parameters  
(COPERNIC2)**

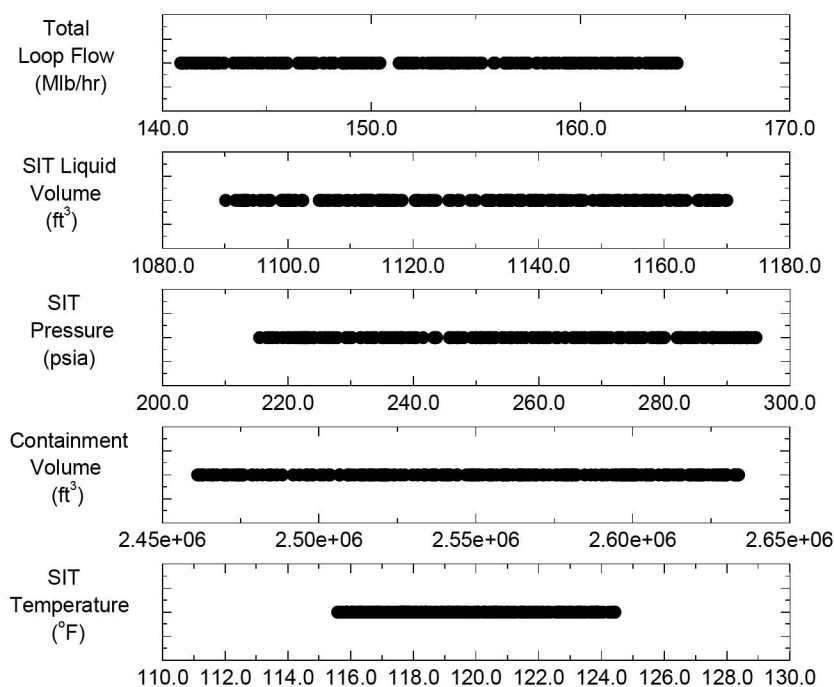


**Figure B.37: CE 2x4 Scatter Plot of Operational Parameters  
(COPERNIC2) (continued)**

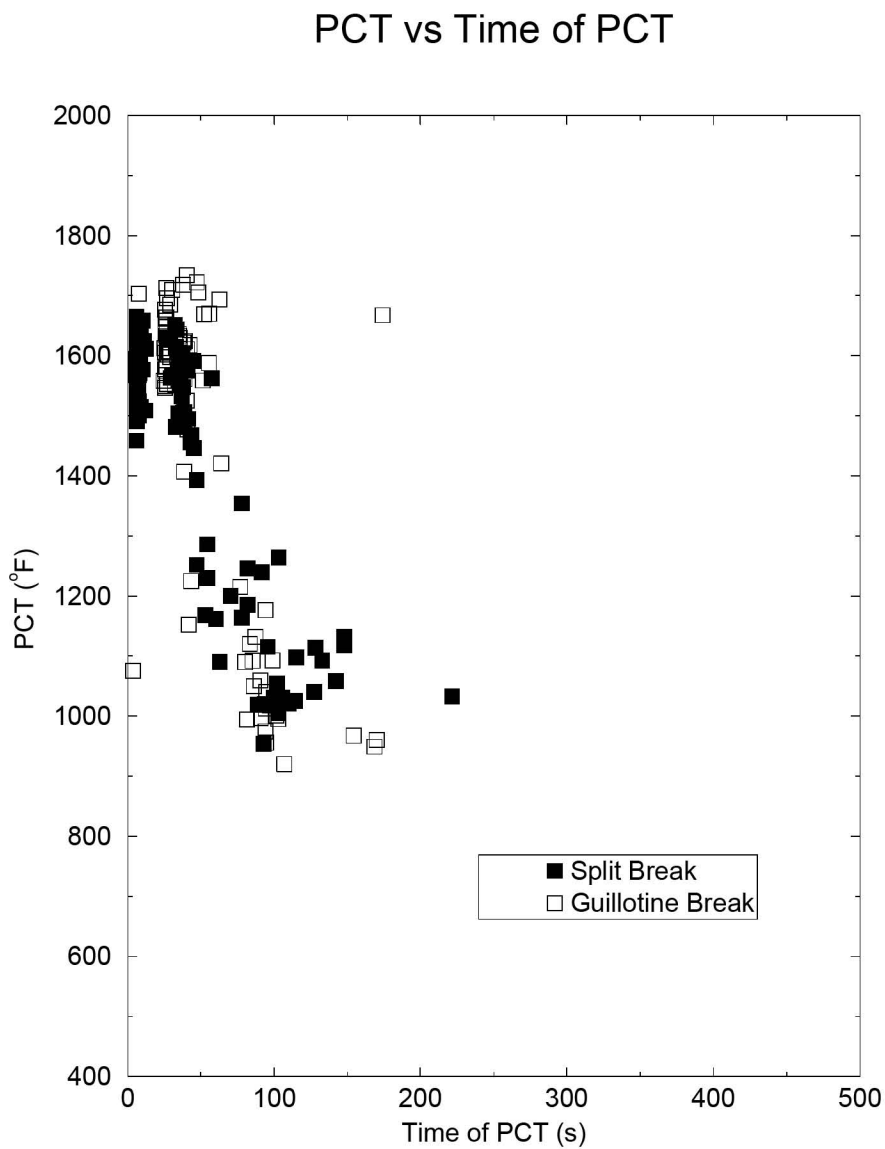


**Figure B.38: CE 2x4 PCT versus PCT Time Scatter Plot from the  
Case Set (COPERNIC2)**

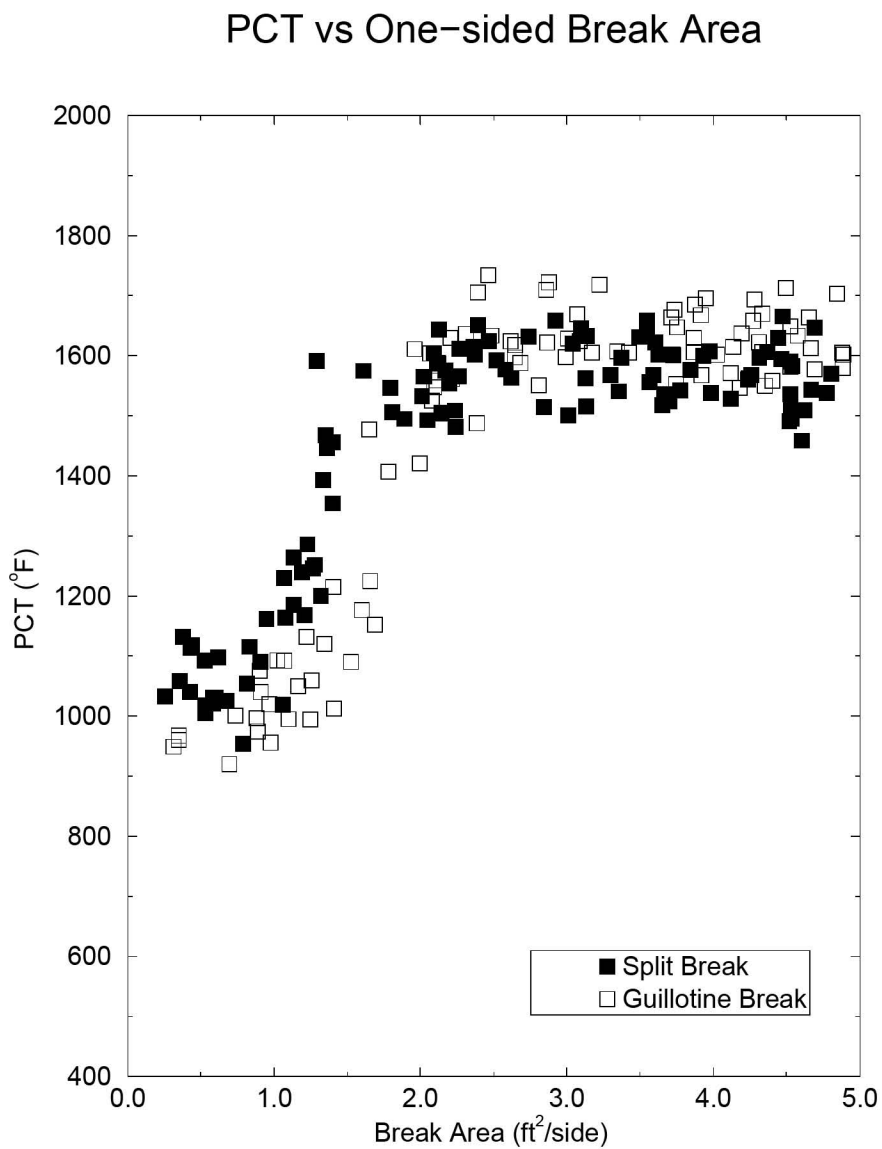


**Figure B.39: CE 2x4 PCT versus Break Size Scatter Plot from the Case Set (COPERNIC2)**

### Maximum Oxidation vs PCT

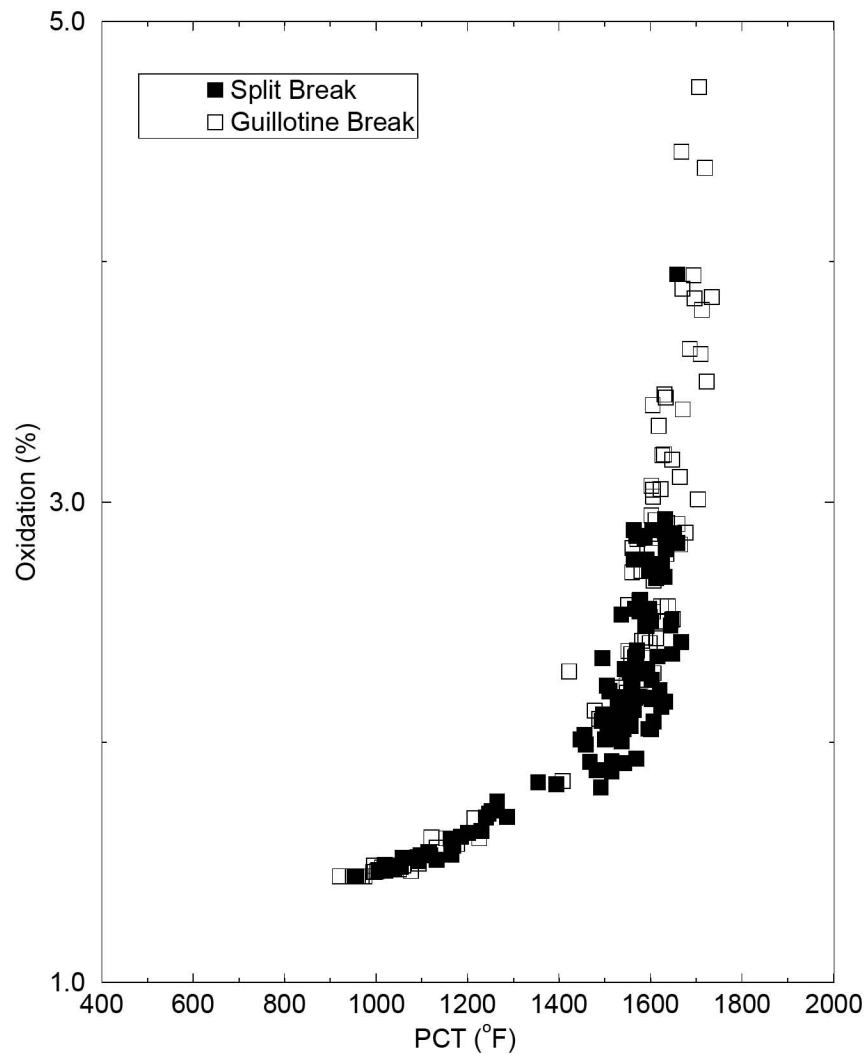


**Figure B.40: CE 2x4 Maximum Oxidation versus PCT Scatter Plot  
from the Case Set (COPERNIC2)**



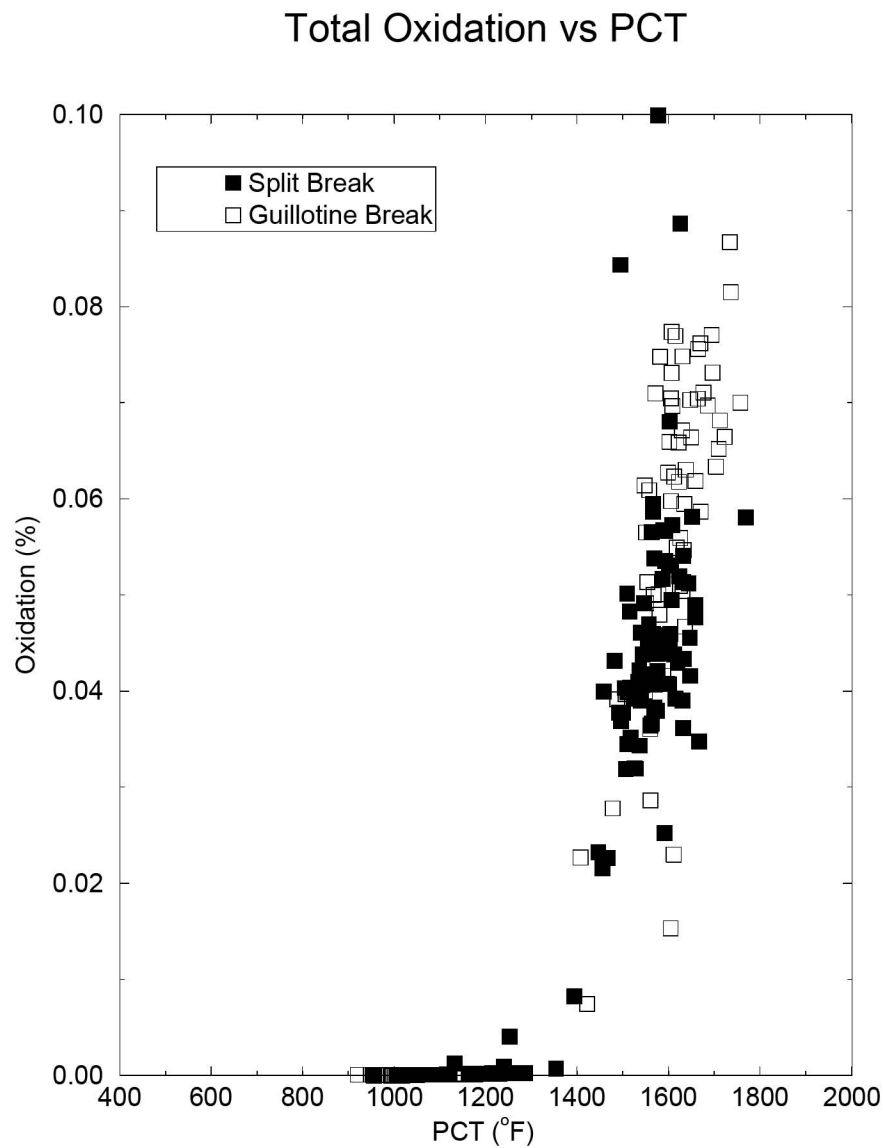


**Figure B.41: CE 2x4 Total Oxidation versus PCT Scatter Plot from the Case Set (COPERNIC2)**

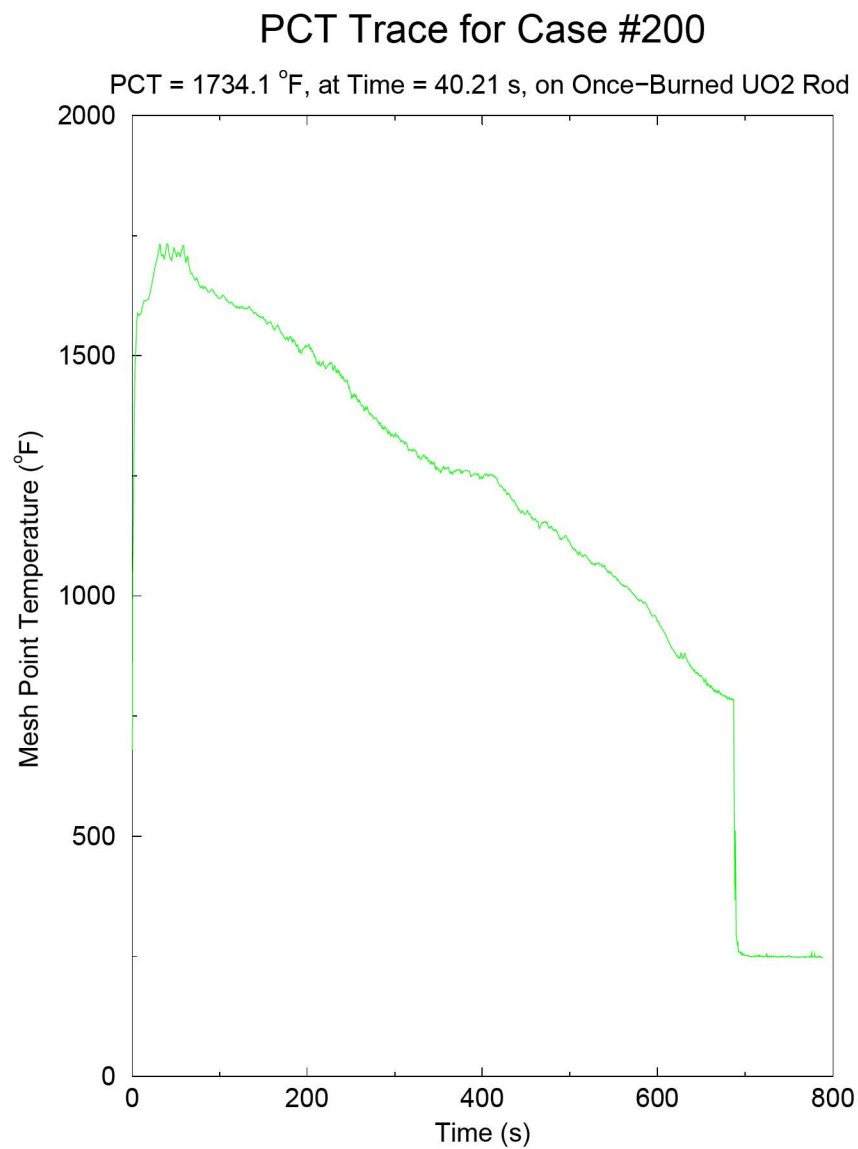


**Figure B.42: CE 2x4 Peak Cladding Temperature (Independent of Elevation) for the Limiting Margin Case (COPERNIC2)**

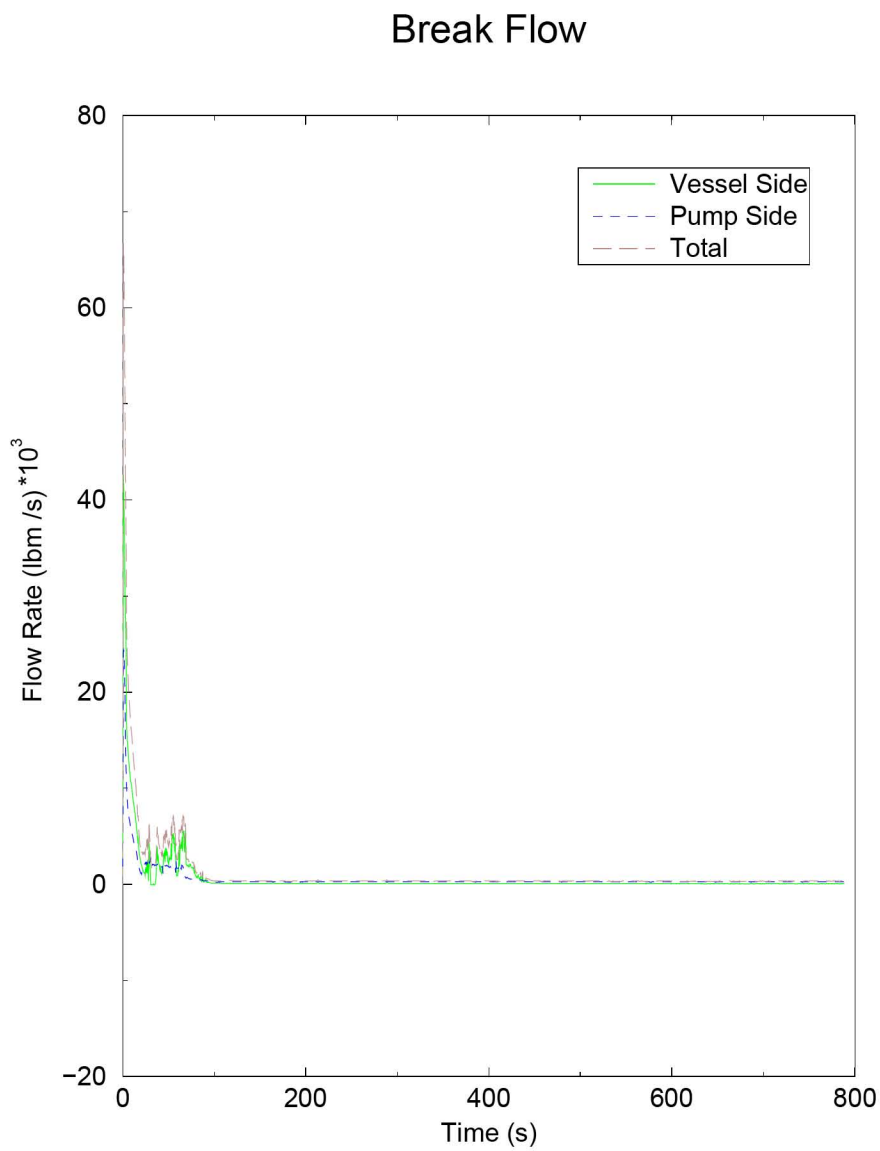


**Figure B.43: CE 2x4 Break Flow for the Limiting Margin Case (COPERNIC2)**

## Core Inlet Mass Flux

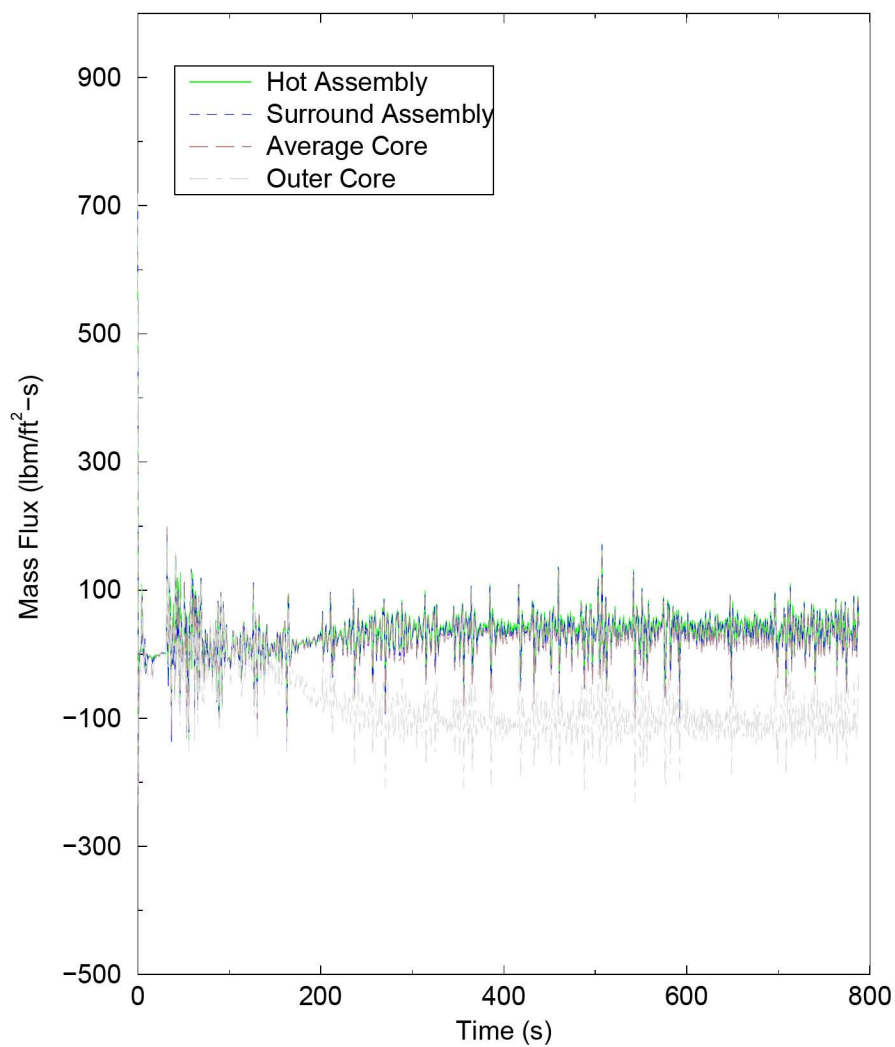


**Figure B.44: CE 2x4 Core Inlet Mass Flux for the Limiting Margin Case (COPERNIC2)**

## Core Outlet Mass Flux

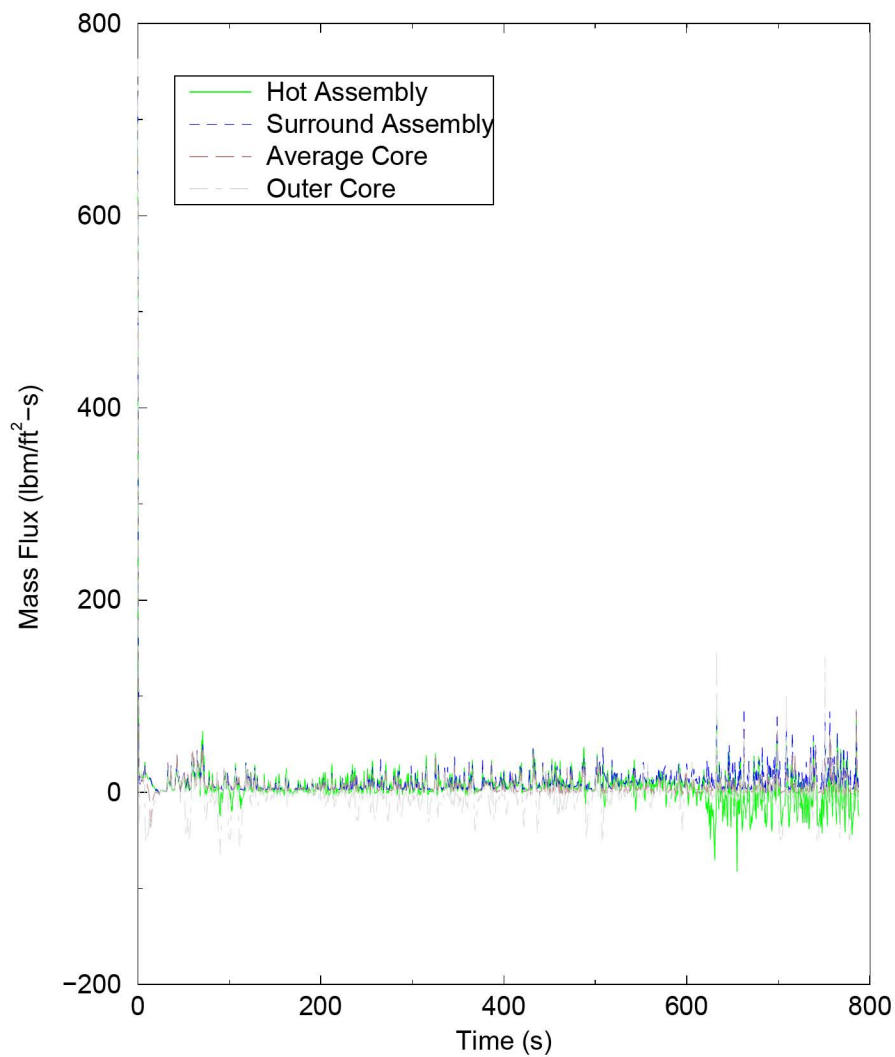


**Figure B.45: CE 2x4 Core Outlet Mass Flux for the Limiting Margin Case (COPERNIC2)**

### Pump Void Fraction

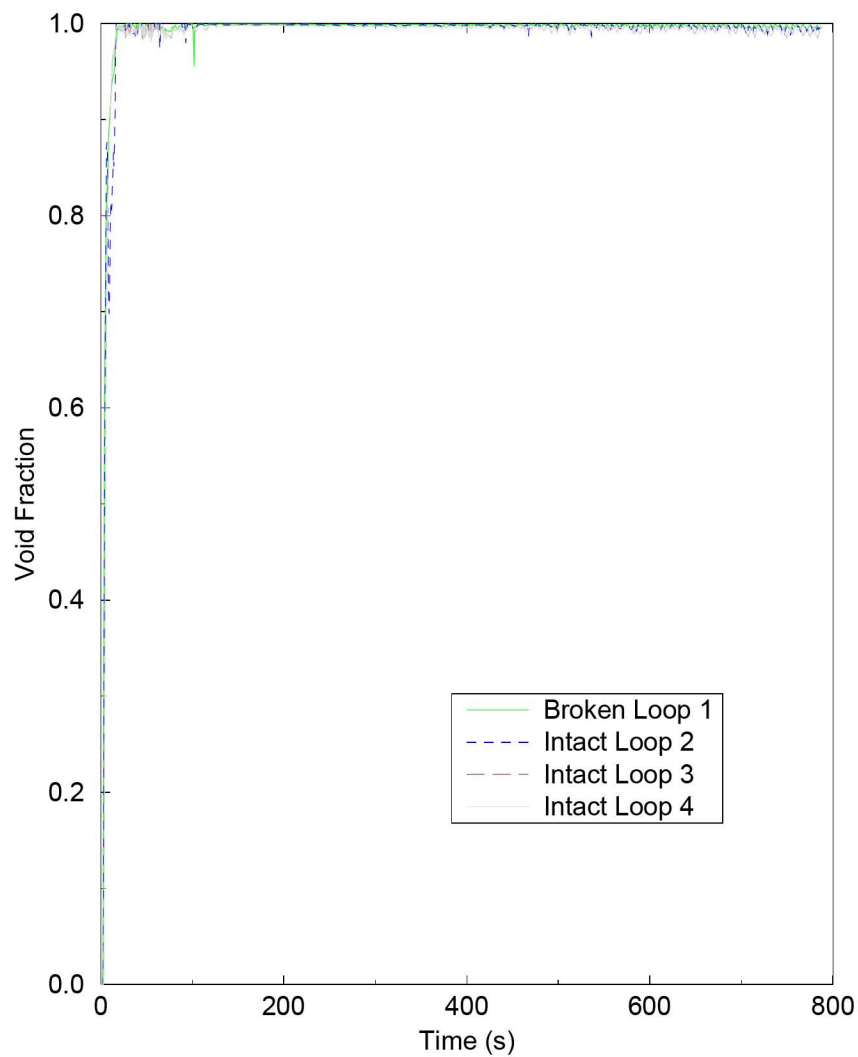


**Figure B.46: CE 2x4 Void Fraction at RCS Pumps for the Limiting Margin Case (COPERNIC2)**

## ECCS Flows

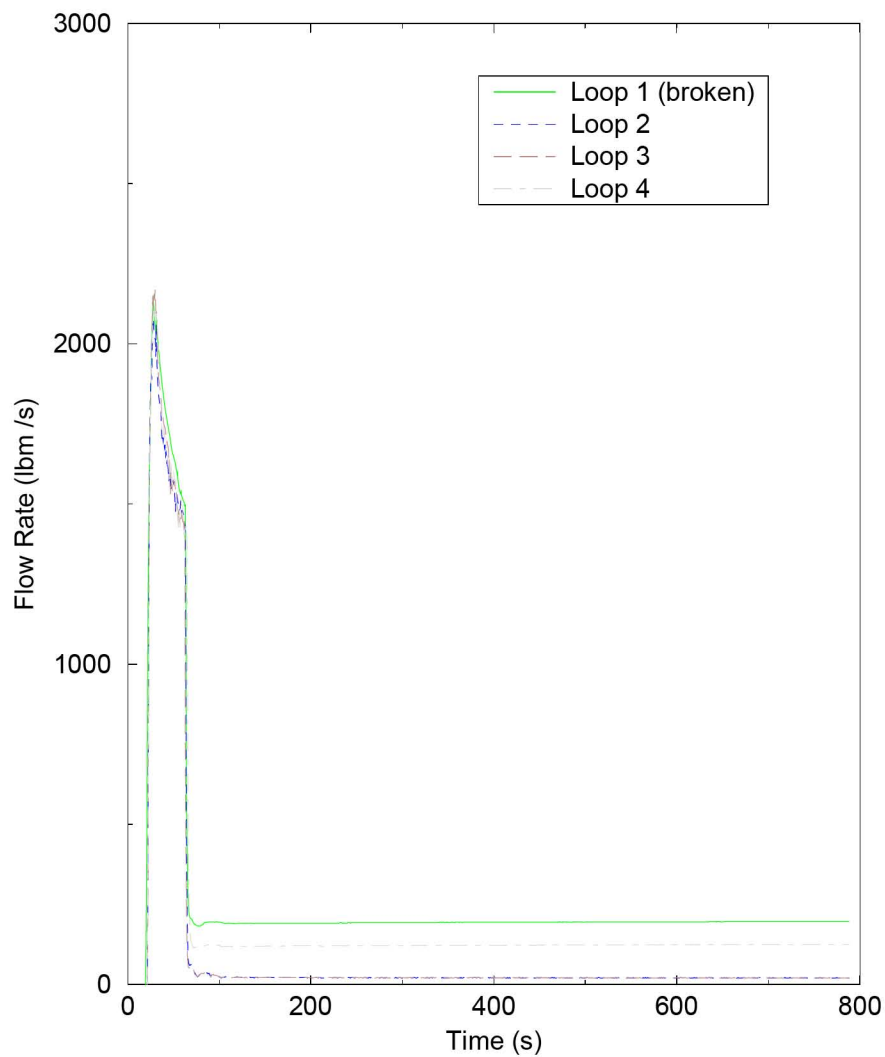


**Figure B.47: CE 2x4 ECCS Flows (Includes SIT, Charging, SI and RHR) for the Limiting Margin Case (COPERNIC2)**

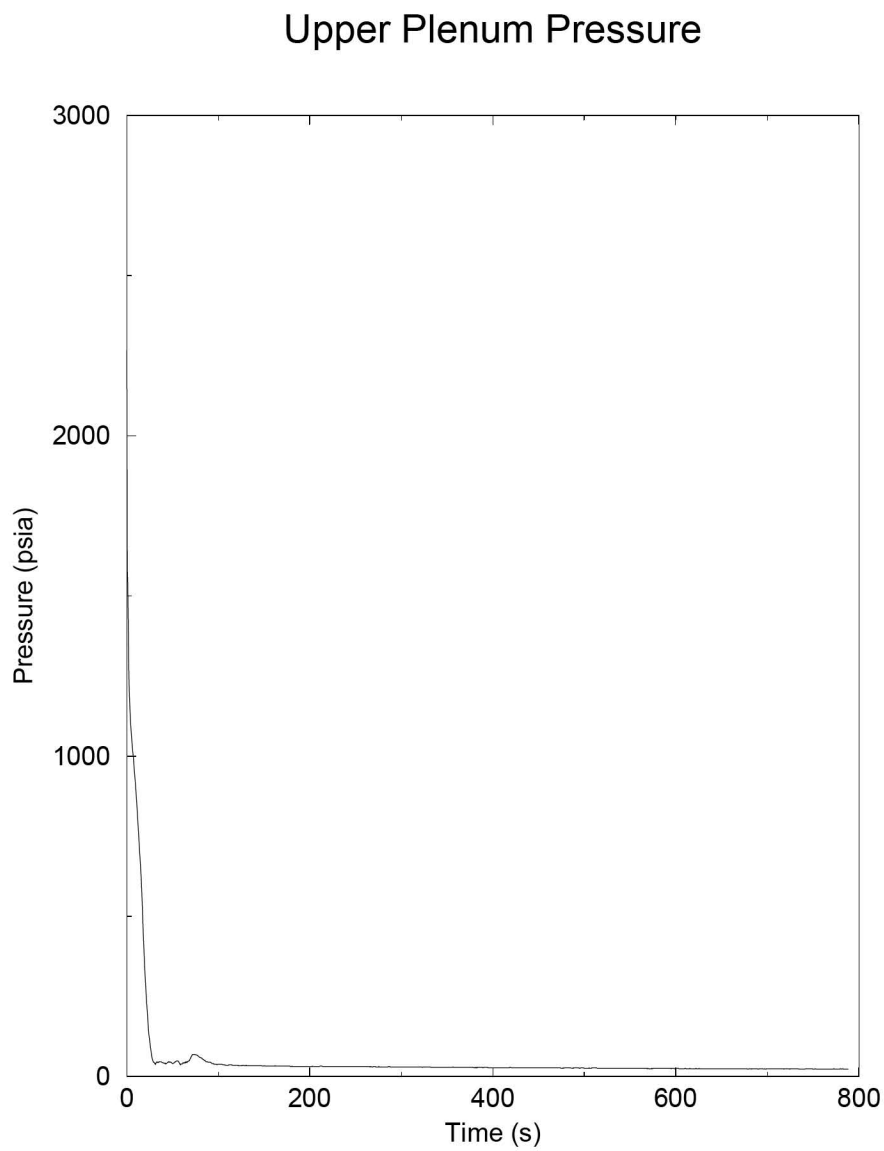


**Figure B.48: CE 2x4 Upper Plenum Pressure for the Limiting Margin Case (COPERNIC2)**



## Downcomer Liquid Level

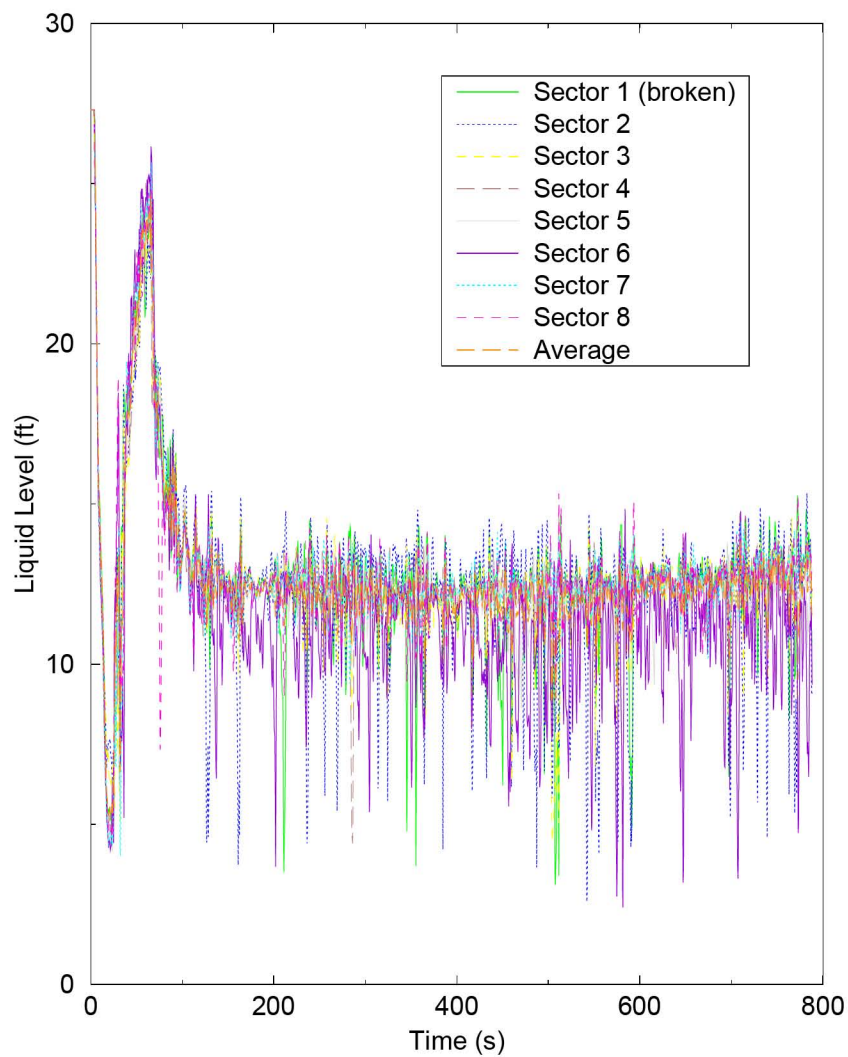


**Figure B.49: CE 2x4 Collapsed Liquid Level in the Downcomer for the Limiting Margin Case (COPERNIC2)**

## Lower Vessel Liquid Level

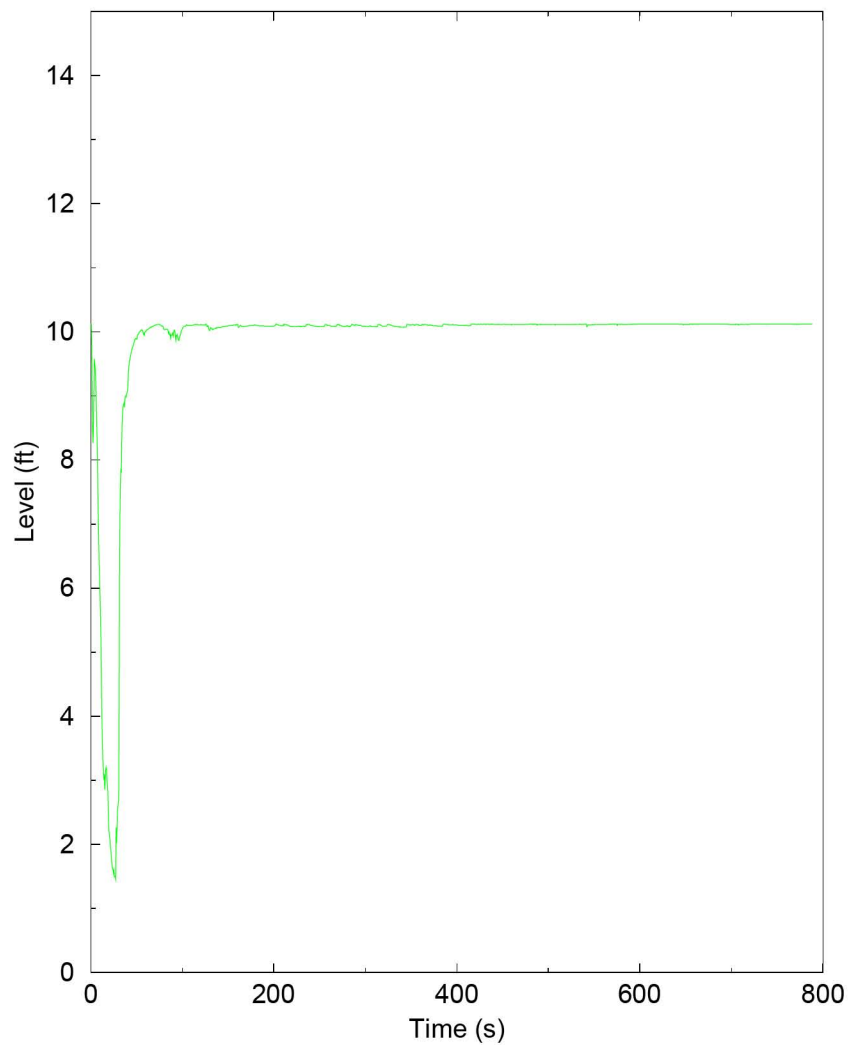


**Figure B.50: CE 2x4 Collapsed Liquid Level in the Lower Plenum for the Limiting Margin Case (COPERNIC2)**

## Core Liquid Level

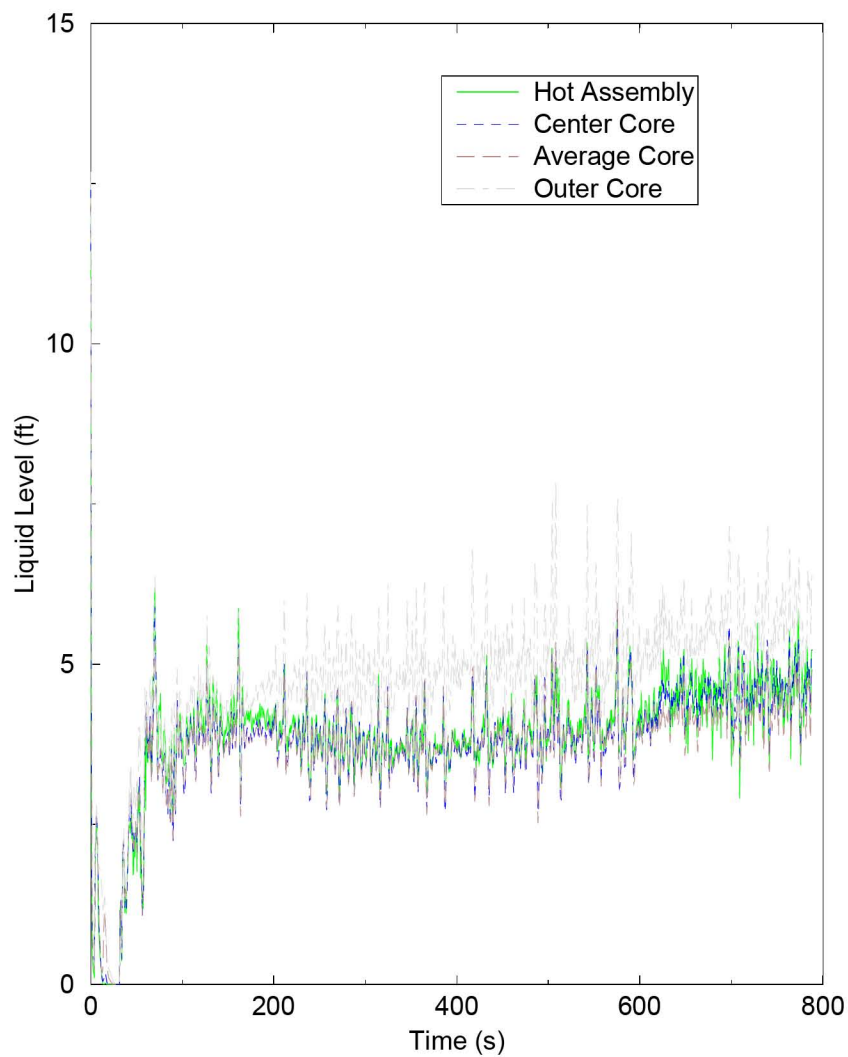


**Figure B.51: CE 2x4 Collapsed Liquid Level in the Core for the Limiting Margin Case (COPERNIC2)**

## Containment and Loop Pressures

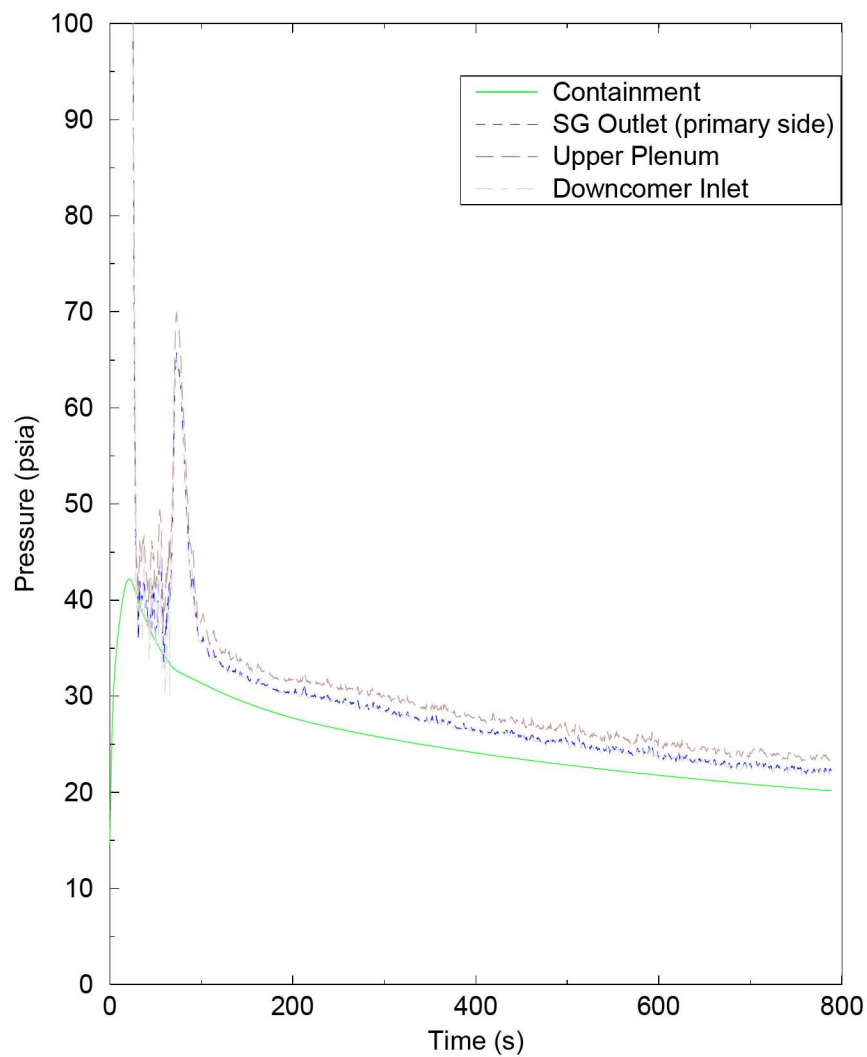


**Figure B.52: CE 2x4 Containment and Loop Pressures for the Limiting Margin Case (COPERNIC2)**

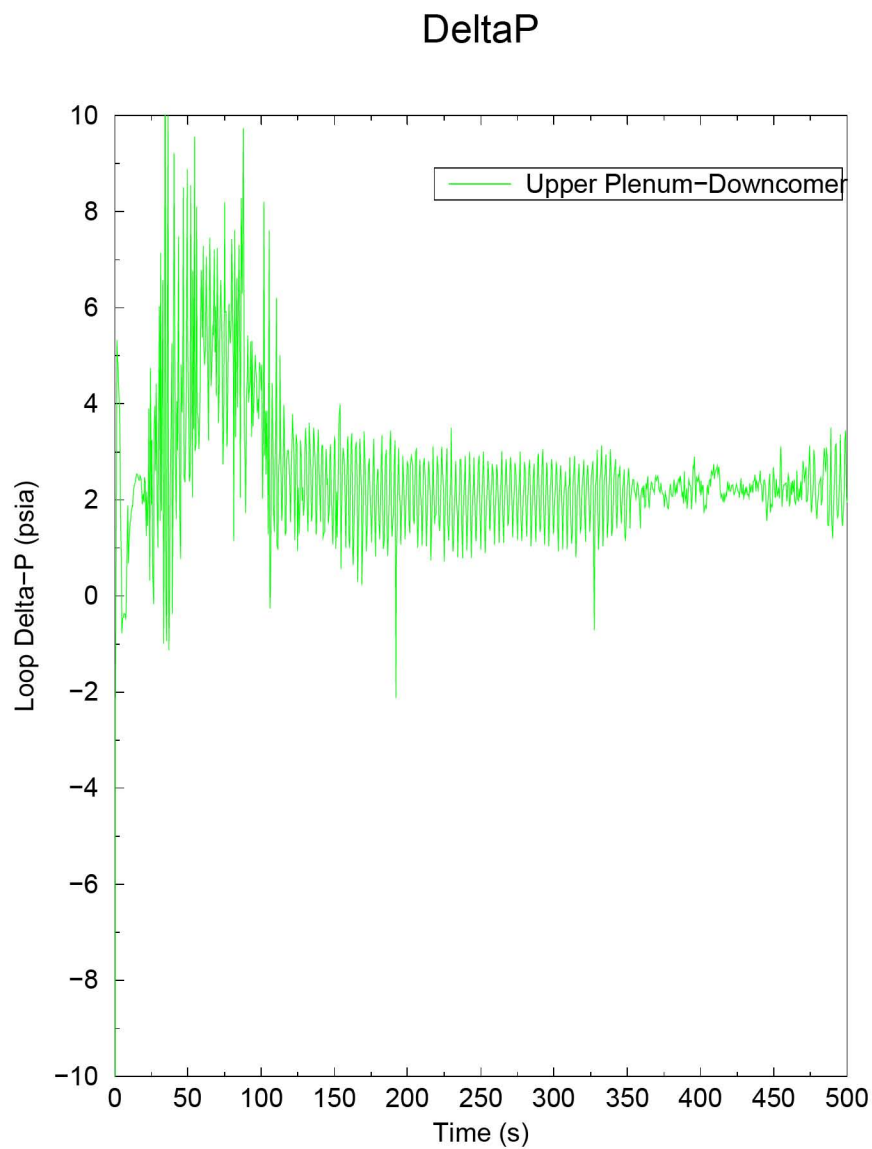


**Figure B.53: CE 2x4 Pressure Difference between Upper Plenum and Downcomer (COPERNIC2)**

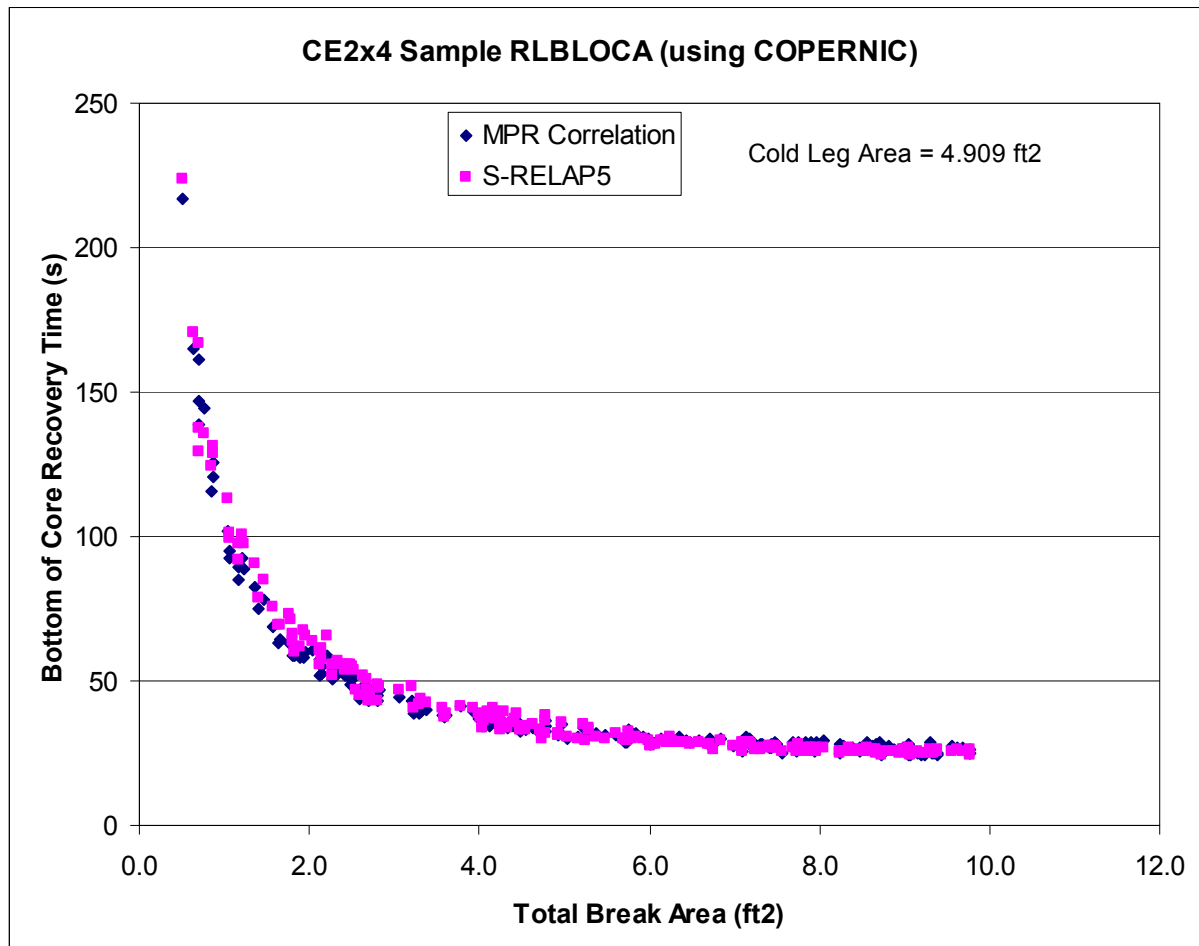


**Figure B.54: CE 2x4 Validation of BOCR Time using MPR CCFL  
Correlation (COPENIC2)**

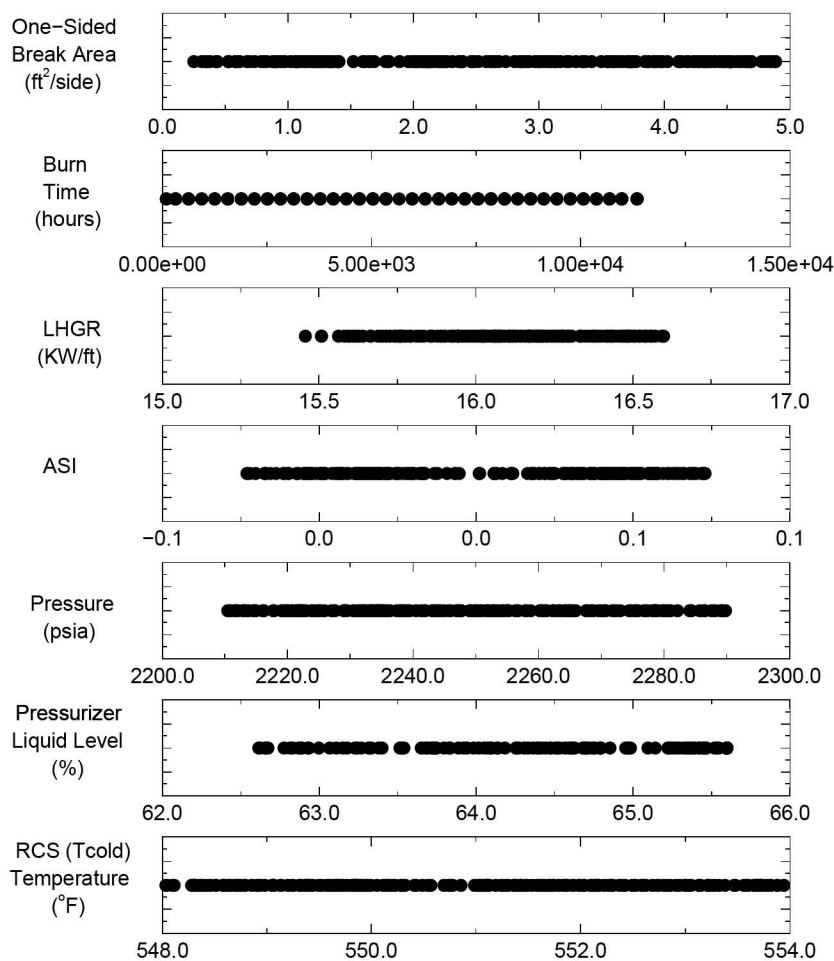


**Figure B.55: CE 2x4 Scatter Plot of Operational Parameters (RODEX3A)**

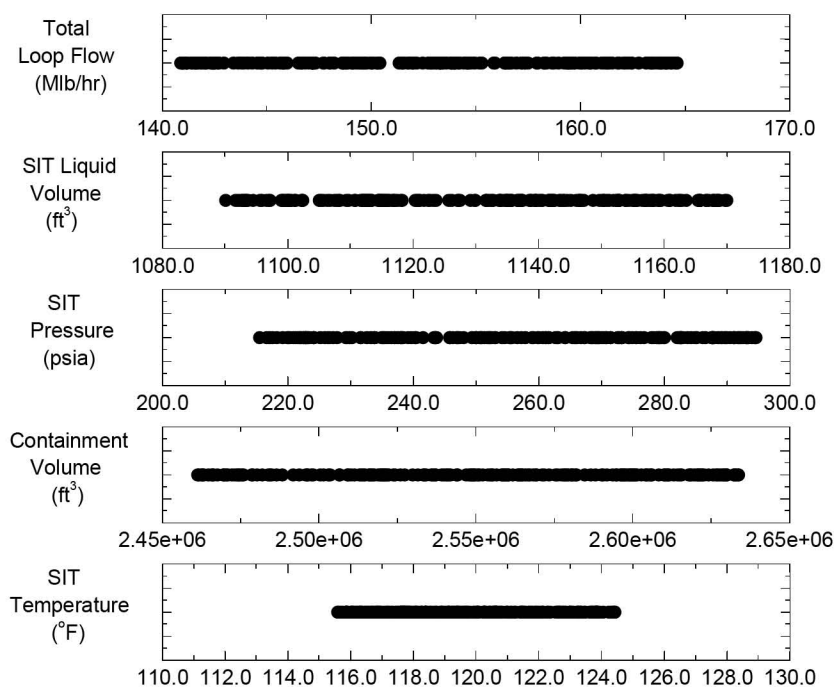


**Figure B.55: CE 2x4 Scatter Plot of Operational Parameters  
(RODEX3A) (continued)**



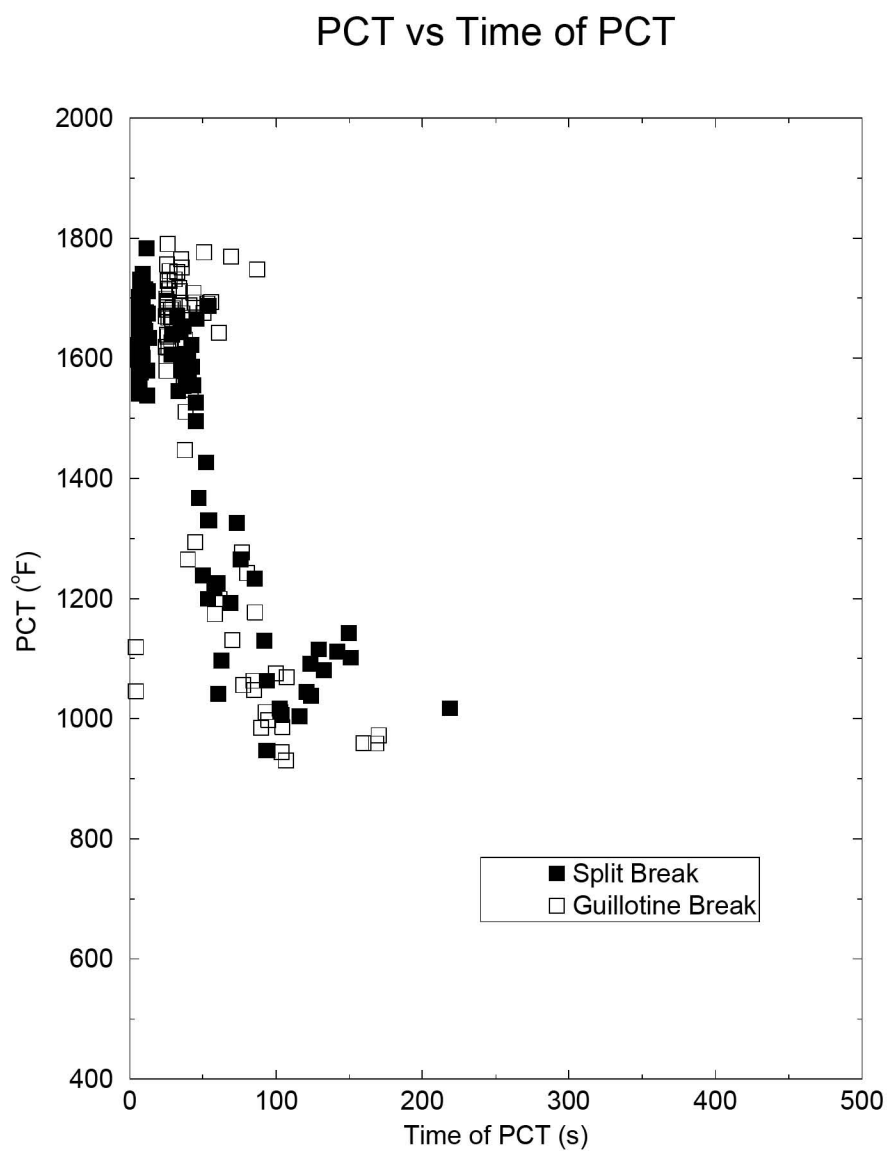


**Figure B.56: CE 2x4 PCT versus PCT Time Scatter Plot from the  
Case Set (RODEX3A)**

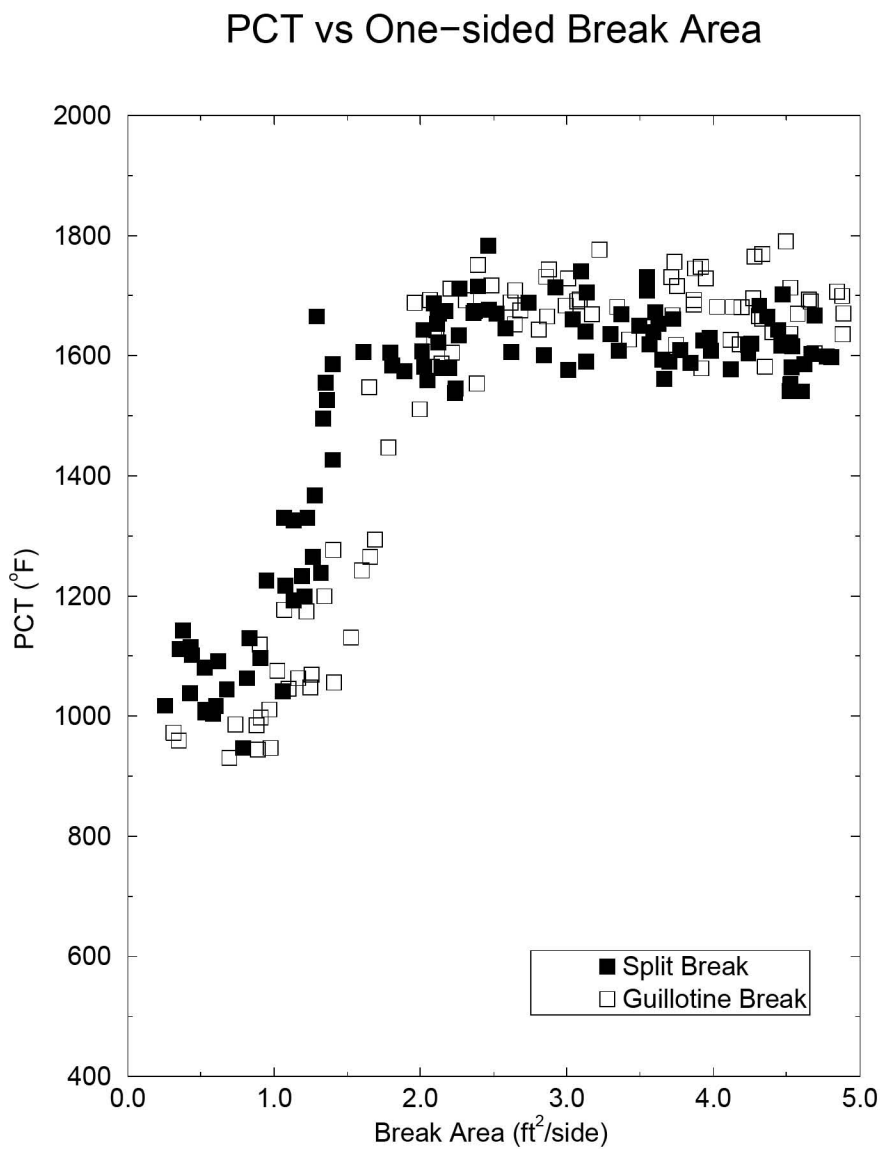


**Figure B.57: CE 2x4 PCT versus Break Size Scatter Plot from the Case Set (RODEX3A)**

### Maximum Oxidation vs PCT

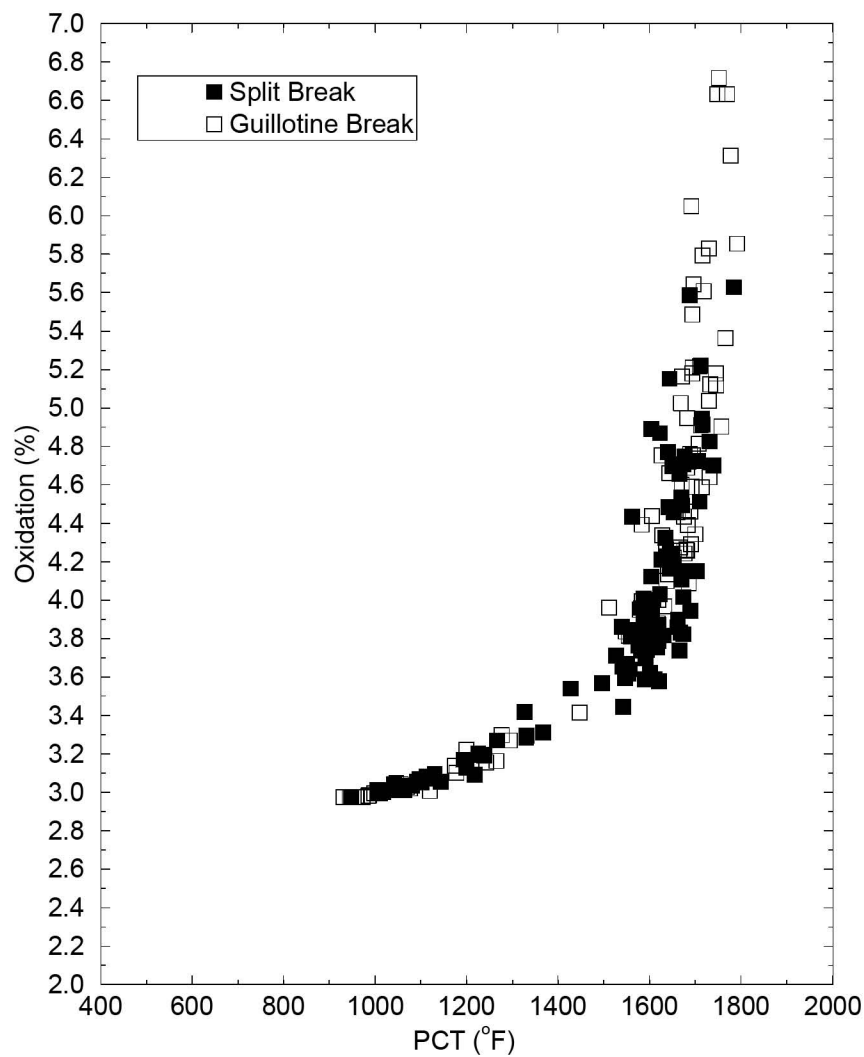


**Figure B.58: CE 2x4 Maximum Oxidation versus PCT Scatter Plot  
from the Case Set (RODEX3A)**

### Total Oxidation vs PCT

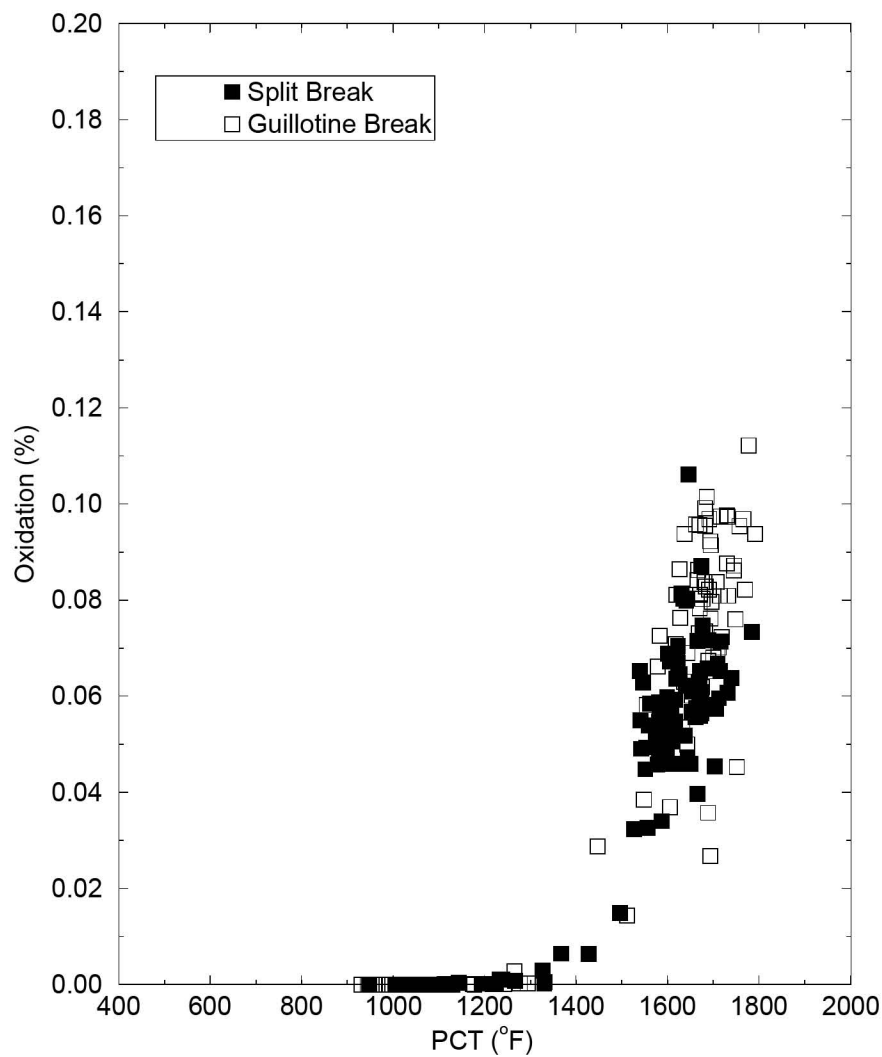


**Figure B.59: CE 2x4 Total Oxidation versus PCT Scatter Plot from the Case Set (RODEX3A)**

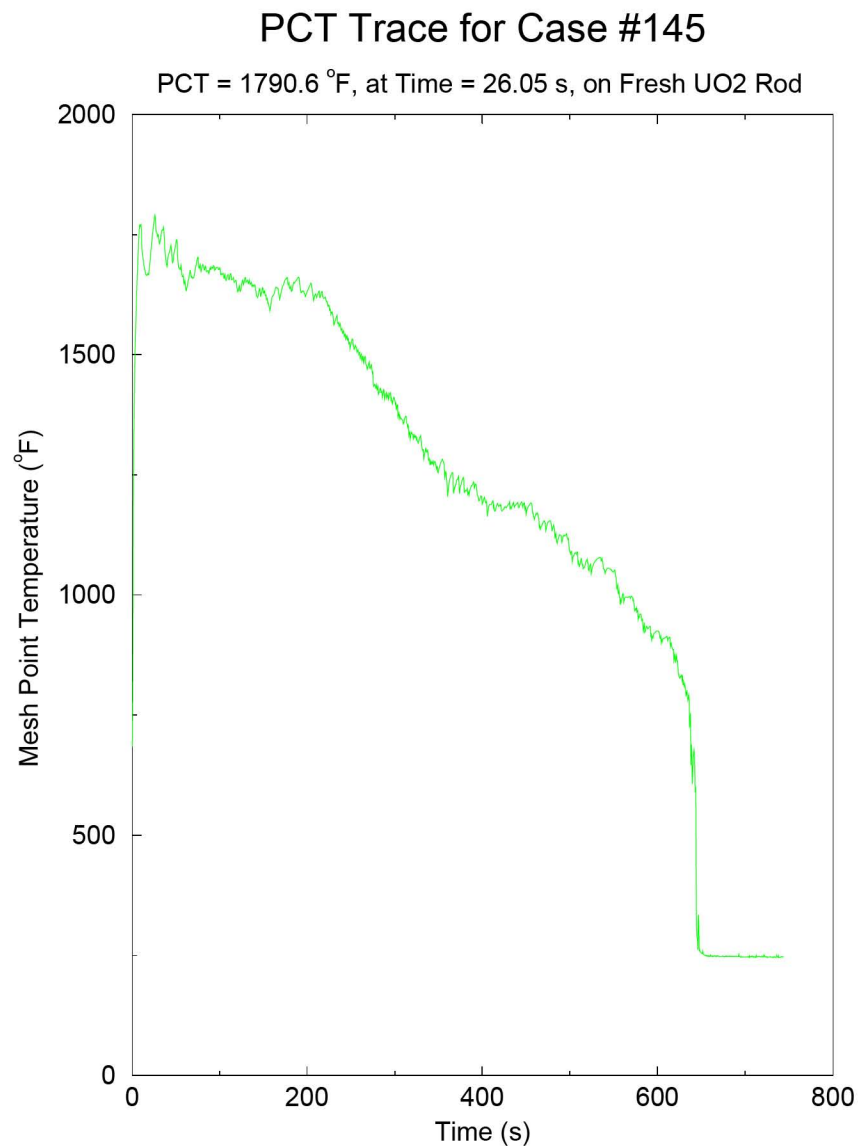


**Figure B.60: CE 2x4 Peak Cladding Temperature (Independent of Elevation) for the Limiting Margin Case (RODEX3A)**

## Break Flow

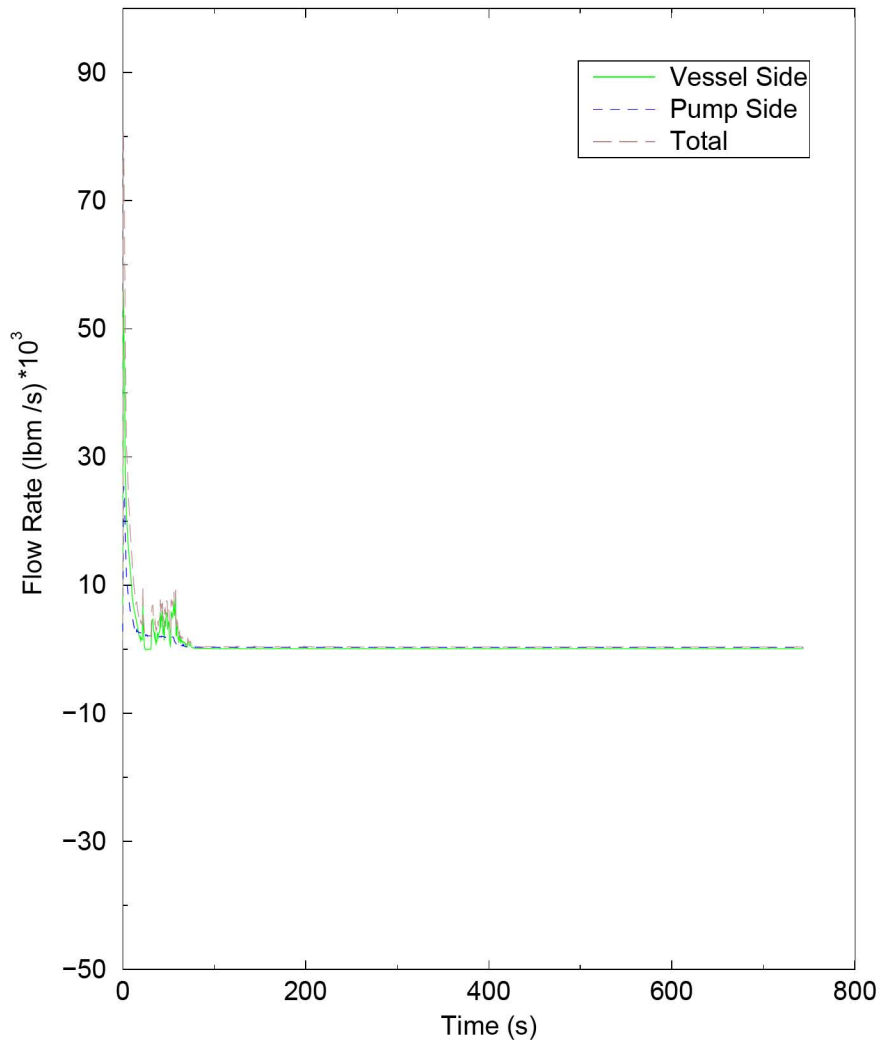


**Figure B.61: CE 2x4 Break Flow for the Limiting Margin Case (RODEX3A)**

## Core Inlet Mass Flux

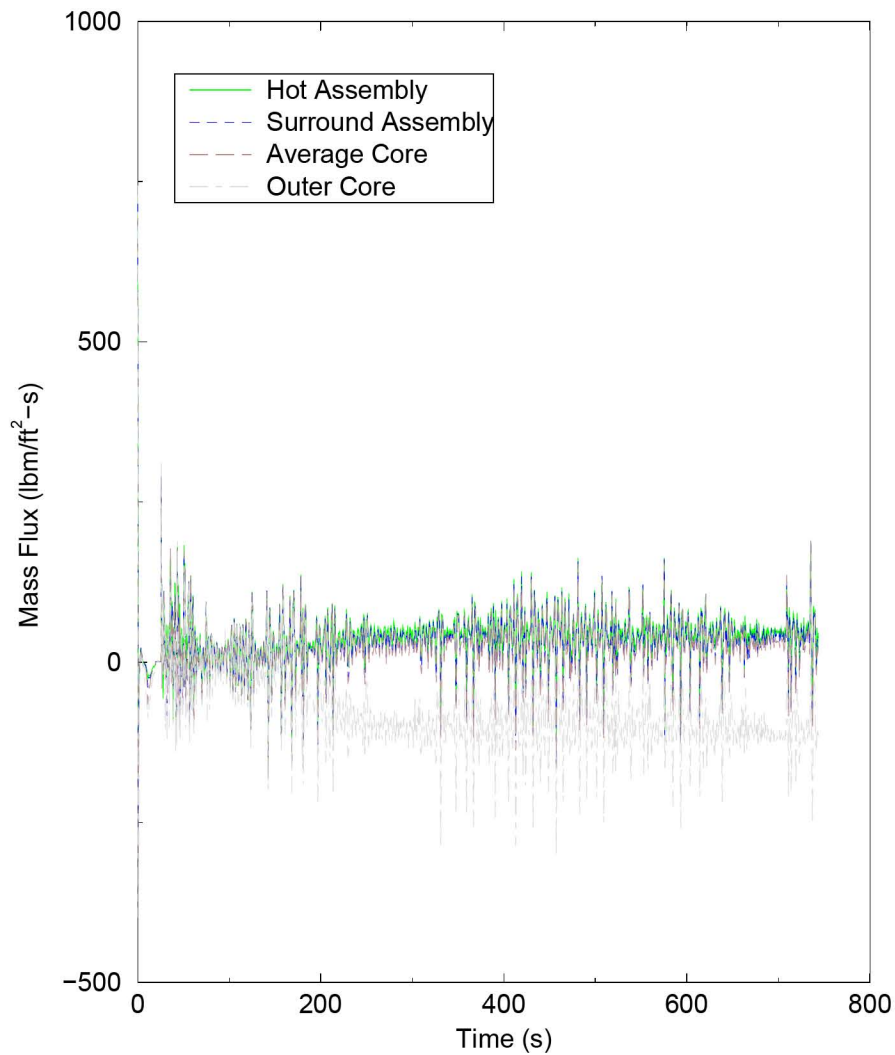


**Figure B.62: CE 2x4 Core Inlet Mass Flux for the Limiting Margin Case (RODEX3A)**

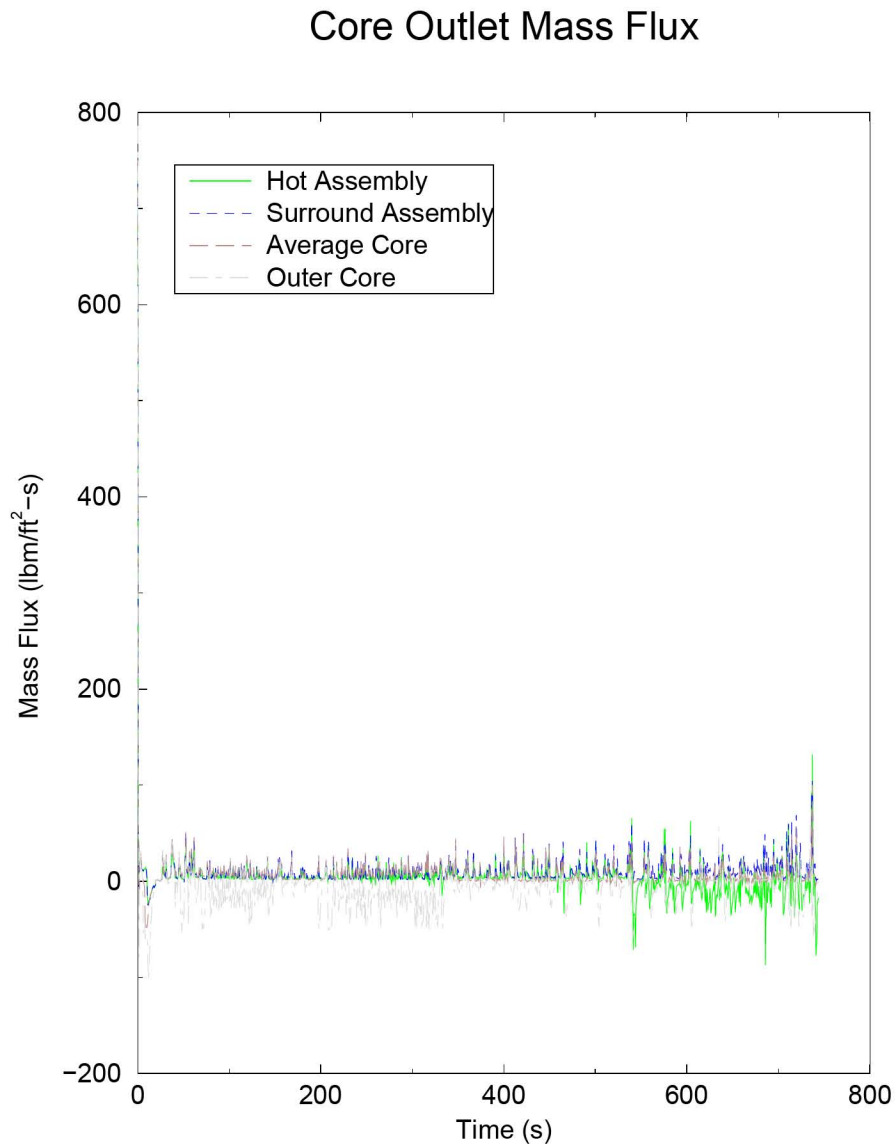


**Figure B.63: CE 2x4 Core Outlet Mass Flux for the Limiting Margin Case (RODEX3A)**



### Pump Void Fraction

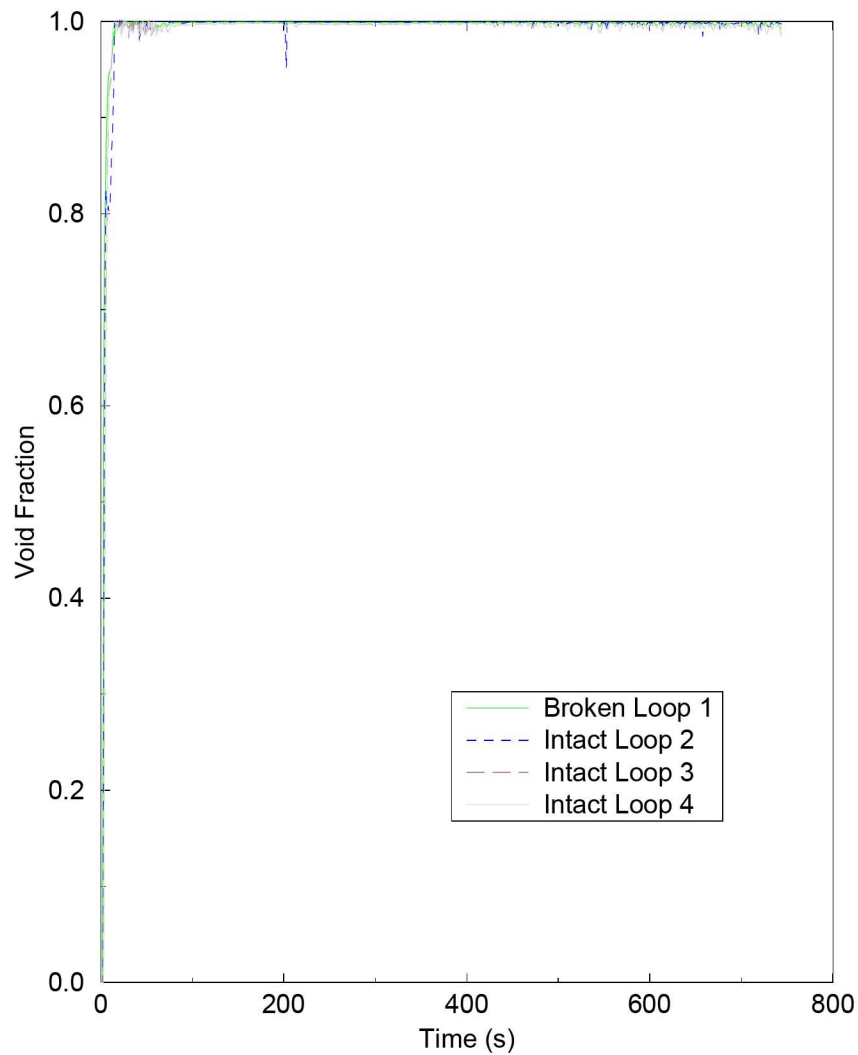


**Figure B.64: CE 2x4 Void Fraction at RCS Pumps for the Limiting Margin Case (RODEX3A)**

## ECCS Flows

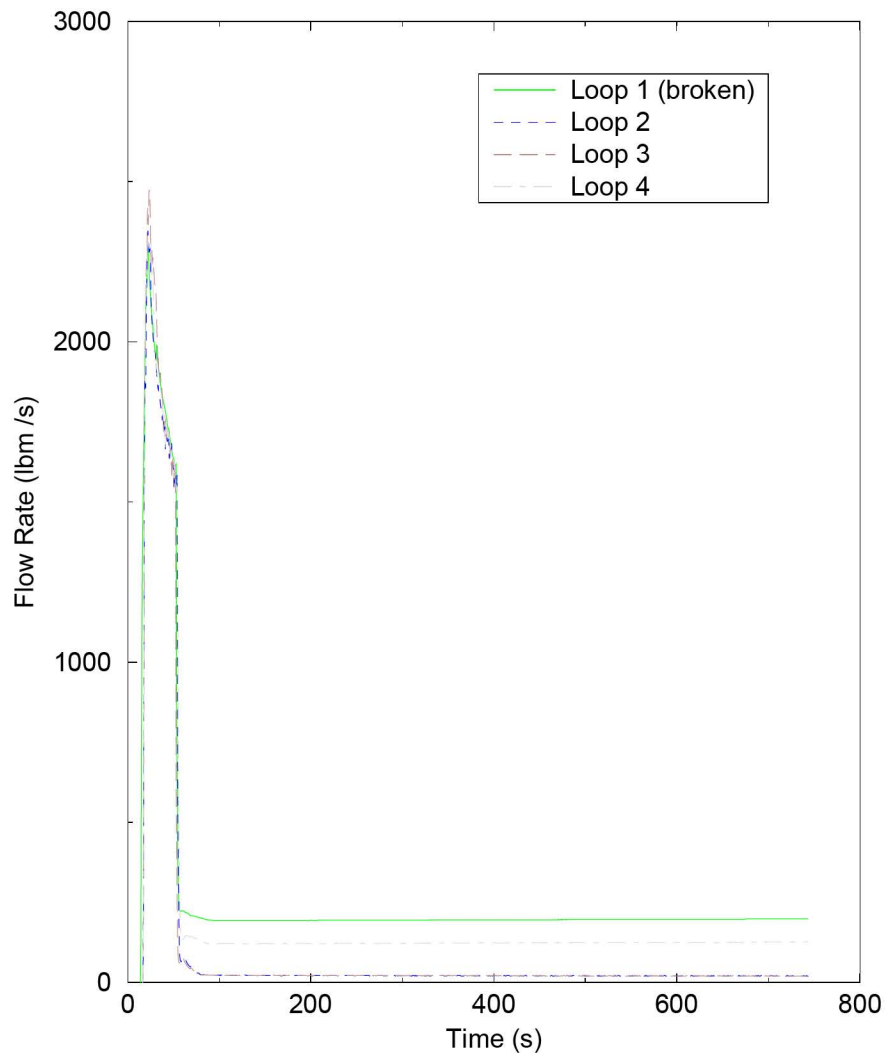


**Figure B.65: CE 2x4 ECCS Flows (Includes SIT, Charging, SI and RHR) for the Limiting Margin Case (RODEX3A)**

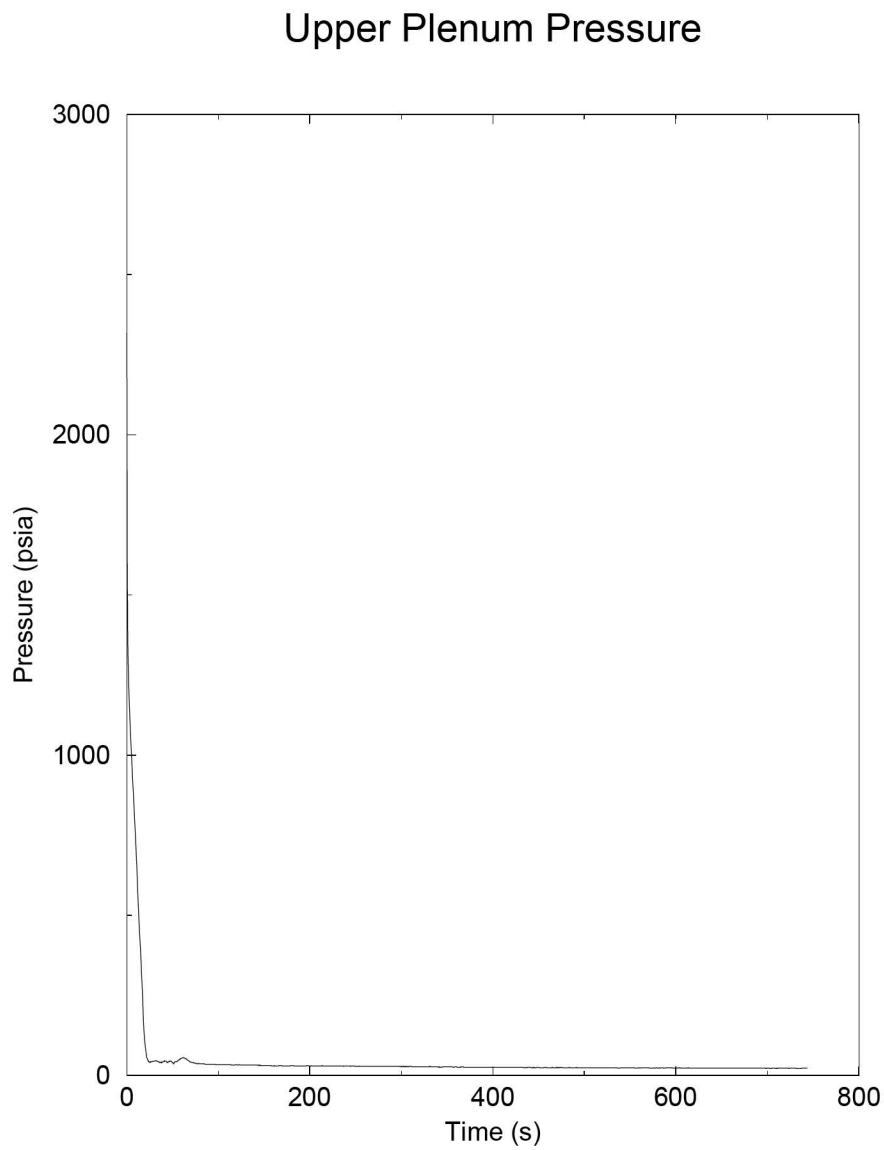


**Figure B.66: CE 2x4 Upper Plenum Pressure for the Limiting Margin Case (RODEX3A)**

## Downcomer Liquid Level

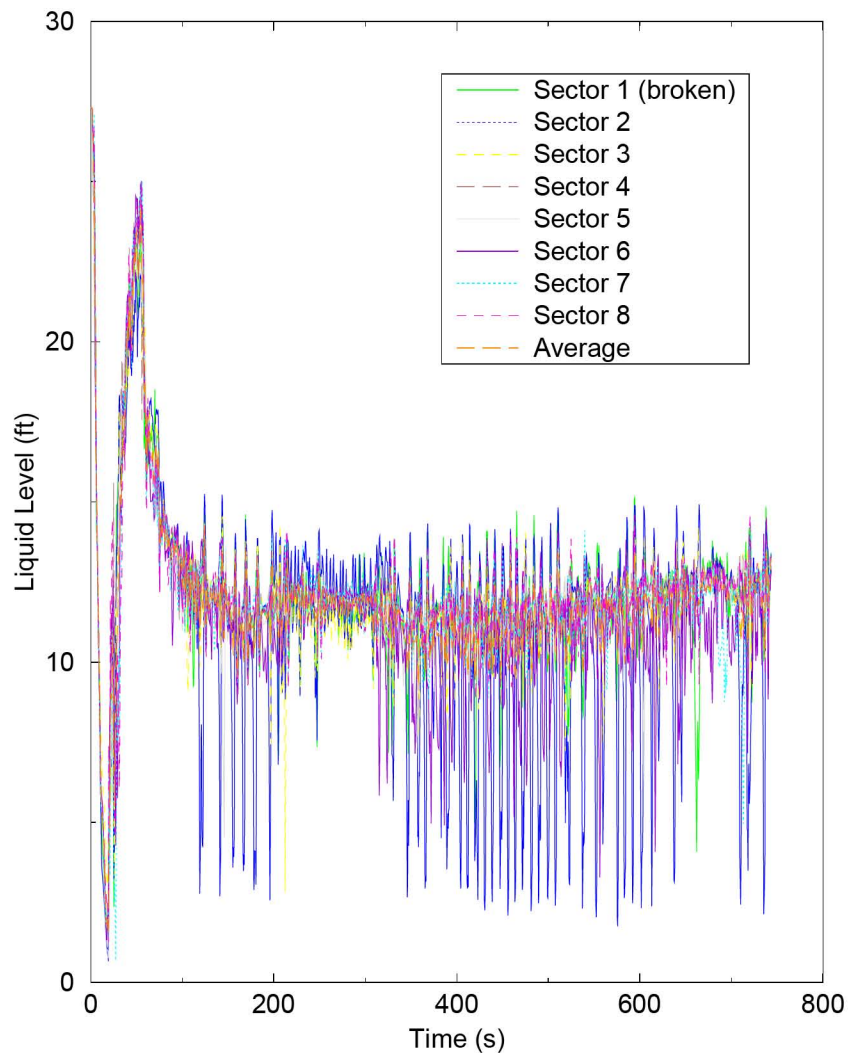


**Figure B.67: CE 2x4 Collapsed Liquid Level in the Downcomer for the Limiting Margin Case (RODEX3A)**

## Lower Vessel Liquid Level

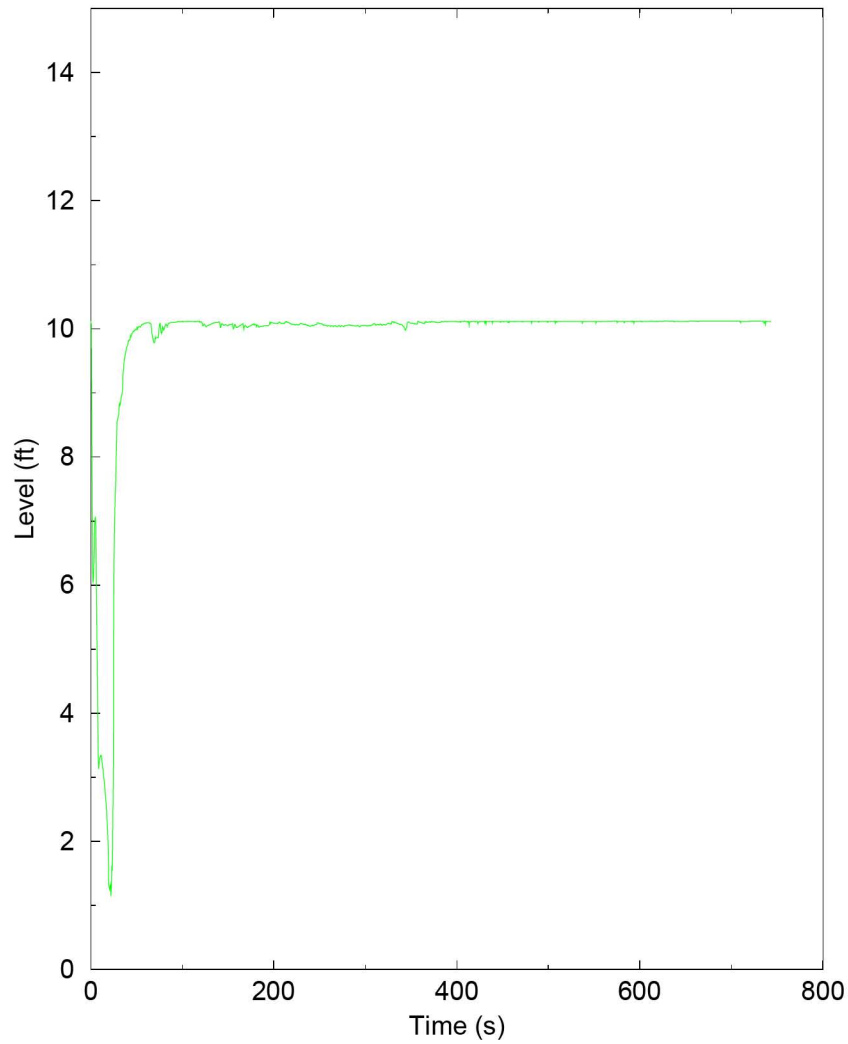


**Figure B.68: CE 2x4 Collapsed Liquid Level in the Lower Plenum for the Limiting Margin Case (RODEX3A)**

## Core Liquid Level

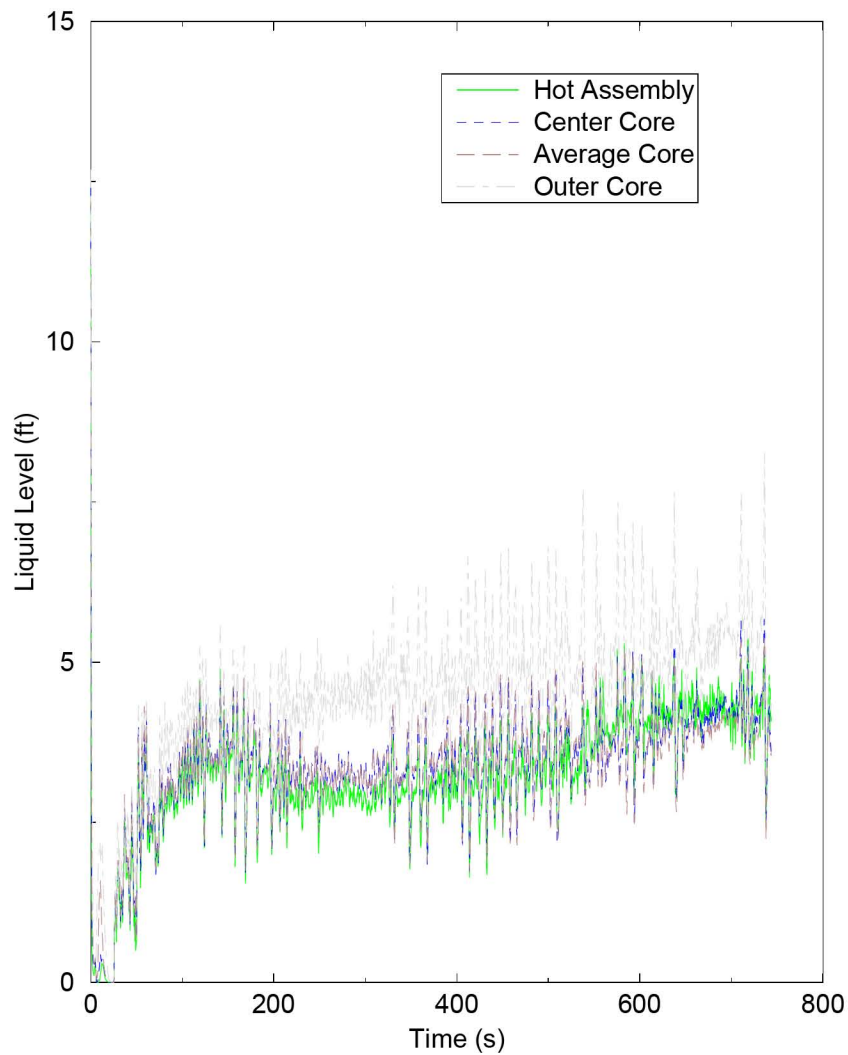


**Figure B.69: CE 2x4 Collapsed Liquid Level in the Core for the Limiting Margin Case (RODEX3A)**

## Containment and Loop Pressures

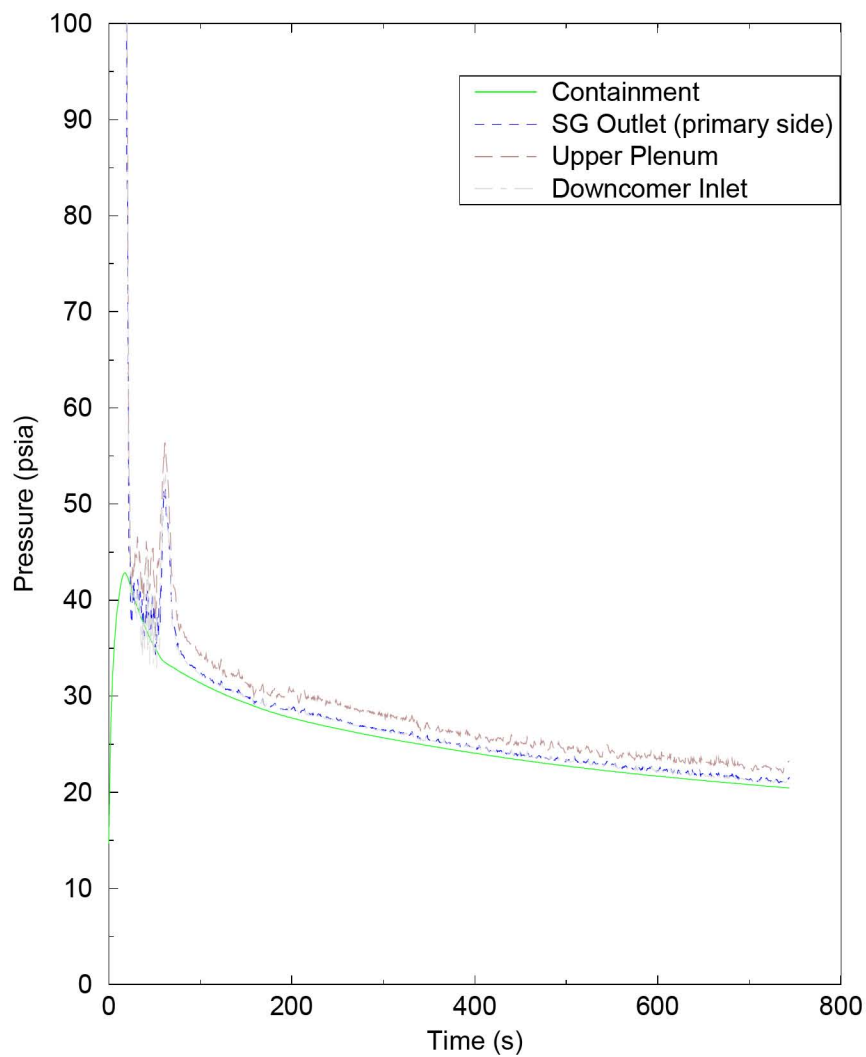


**Figure B.70: CE 2x4 Containment and Loop Pressures for the Limiting Margin Case (RODEX3A)**

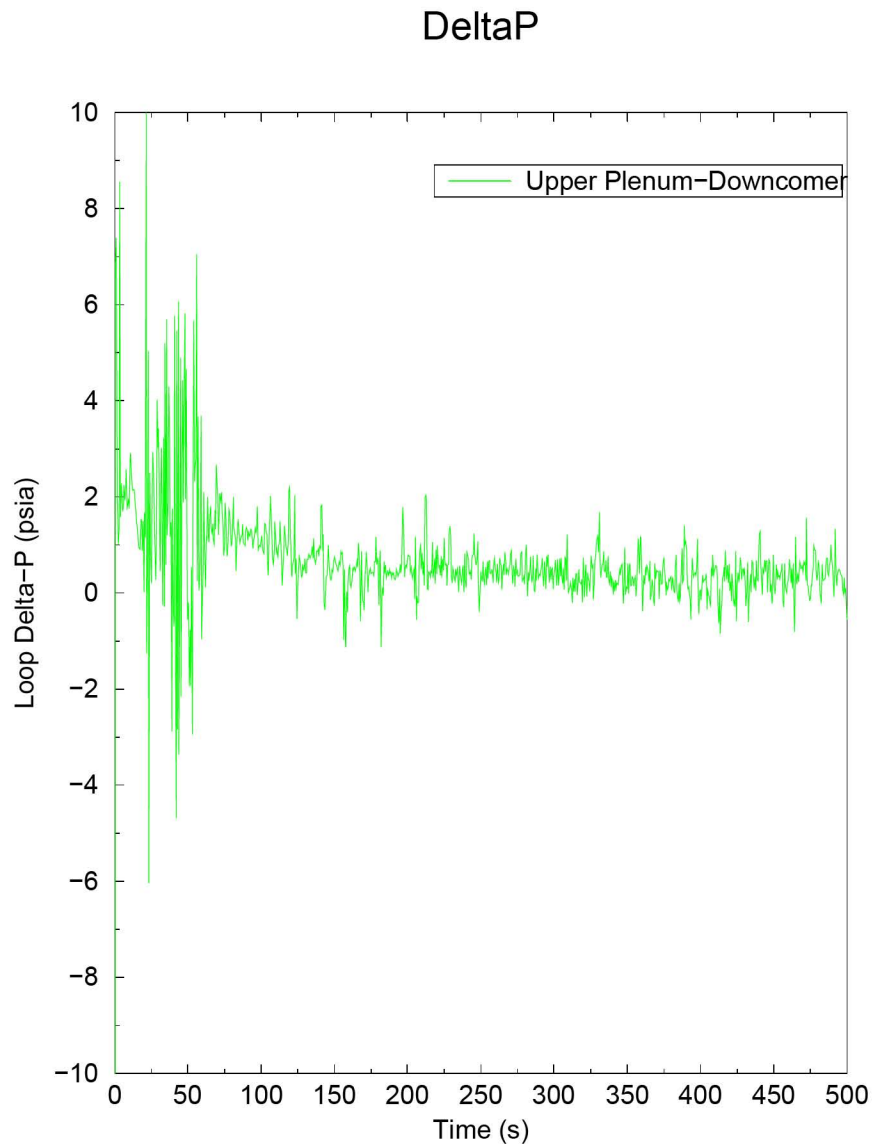


**Figure B.71: CE 2x4 Pressure Difference between Upper Plenum  
and Downcomer (RODEX3A)**



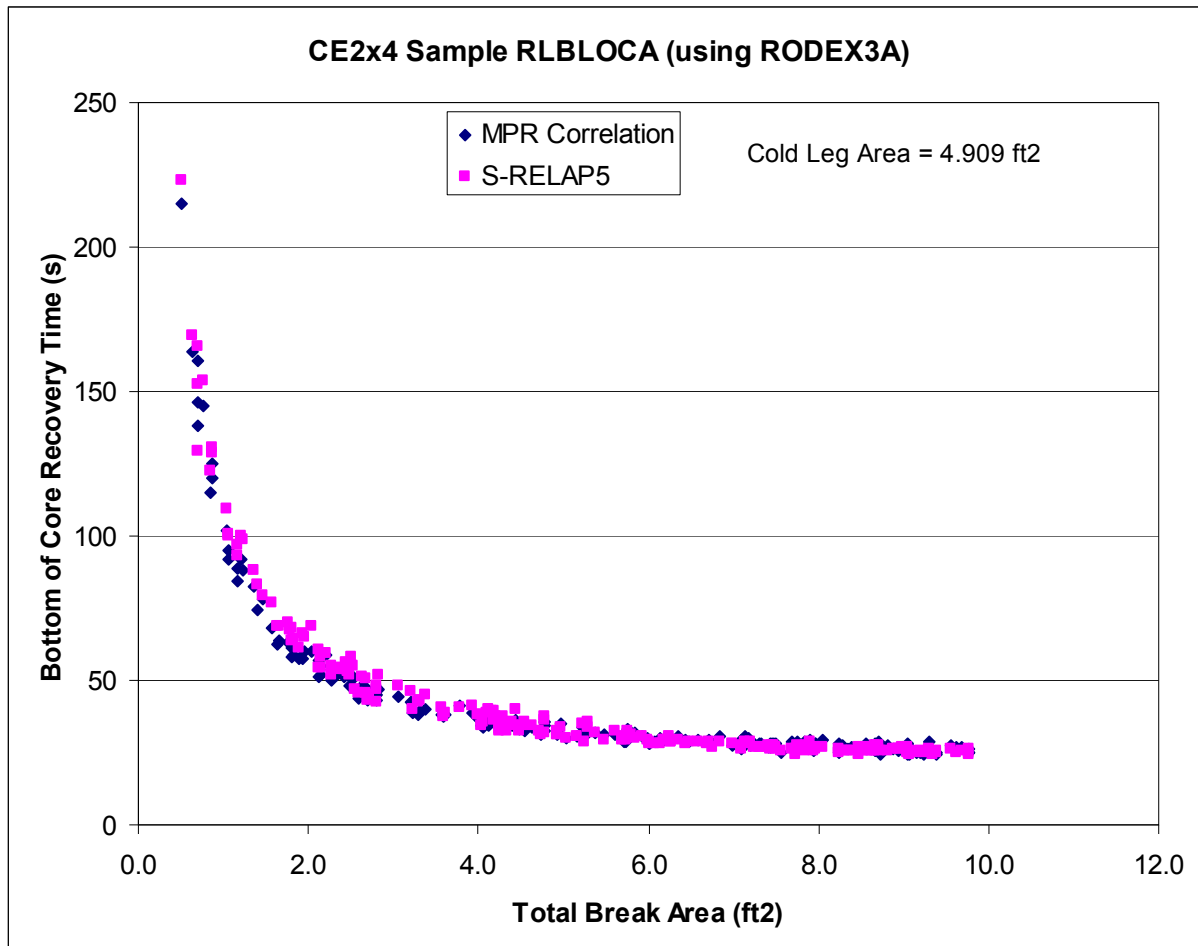


**Figure B.72: CE 2x4 Validation of BOCR Time using MPR CCFL  
Correlation (RODEX3A)**

## B.5 References

- B.1. Technical Program Group, *Quantifying Reactor Safety Margins*, NUREG/CR-5249, EGG-2552, October 1989.
- B.2. EMF-2100(P) Revision 14, *S-RELAP5 Models and Correlations Code Manual*, December 2009.
- B.3. EMF-2102(P) Revision 2, *S-RELAP5 Code Verification and Validation*, November 2010.
- B.4. F. W. Dittus and L. M. K. Boelter, *Heat Transfer in Automobile Radiators of the Tubular Type*, Publications in Engineering, Volume 2, pp. 443-461, University of California, Berkeley, 1930.
- B.5. J. C. Chen, *A Correlation for Boiling Heat Transfer to Saturated Fluids in Convective Flow*, Process Design and Development, Volume 5, pp. 322-327, 1966.
- B.6. N. Zuber, M. Tribus and J. W. Westwater, *Hydrodynamic Crisis in Pool Boiling of Saturated and Subcooled Liquid*, 2<sup>nd</sup> International Heat Transfer Conference, Denver, Colorado, 1961.
- B.7. Biasi, et al., *Studies on Burnout Part 3 - A New Correlation for Round Ducts and Uniform Heating and Its Comparison with World Data*, Energia Nucleare, Volume 14, pp. 530-536, 1967.
- B.8. J. C. Chen, R. K. Sundaram, F. T. Ozkaynak, *A Phenomenological Correlation for Post-CHF Heat Transfer*, NUREG-0237, June 1977.
- B.9. L. A. Bromley, *Heat Transfer in Stable Film Boiling*, Chemical Engineering Progress Volume 46, pp. 221-227, 1950.
- B.10. E. F. Carpenter and A. P. Colburn, *The Effect of Vapor Velocity on Condensation Inside Tubes*, Proceedings of General Discussion on Heat Transfer, Institute Mechanical Engineering/American Society of Mechanical Engineers, pp. 20-26, 1951.
- B.11. V. H. Ransom, et al., *RELAP5/MOD2 Code Manual, Volume 1: Code Structure, Systems Models, and Solution Methods*, NUREG/CR-4312, EGG-2396, Revision 1, March 1987.
- B.12. K. H. Sun, J. M. Gonzales-Santalo, and C. L. Tien, *Calculations of Combined Radiation and Convection Heat Transfer in Rod Bundles Under Emergency Cooling Conditions*, Journal of Heat Transfer, pp. 414-420, 1976.

## Appendix C Incorporation of M5<sup>®</sup> Cladding Properties

This Appendix describes the implementation of the NRC-approved M5<sup>®</sup> cladding material properties into the RLBLOCA methodology. M5<sup>®</sup> is a proprietary variant of Zr1Nb that has desirable high burnup performance. It provides significant improvements in corrosion, hydrogen pick-up, axial growth and diametral creep relative to Zircaloy.

Cladding material properties are required for the fuel performance codes, COPENIC2 and RODEX3A, and the transient analysis code, S-RELAP5. COPENIC2 included M5<sup>®</sup> cladding material properties at the time of its approval by NRC (Reference C.1); thus, the COPENIC2 required properties were previously approved by NRC and require no additional discussion herein. RODEX3A included only Zr-4 properties at the time of its initial approval by the NRC (Reference C.2). Both RODEX3A and S-RELAP5 were updated to include M5<sup>®</sup> cladding properties in Revision 0 of the RLBLOCA methodology (Reference C.3).

M5<sup>®</sup> cladding specific material properties are incorporated into the AREVA RLBLOCA methodology for the purpose of analyzing LBLOCA transients when M5<sup>®</sup> clad fuel rods are present. No modifications to the base methodology are required for the inclusion of the M5<sup>®</sup> properties.

### C.1 References

- C.1. BAW-10231P-A Revision 1, *COPENIC Fuel Rod Design Computer Code*, AREVA NP Inc., January 2004.
- C.2. ANF-90-145(P)(A), RODEX3 Fuel Rod Thermal-Mechanical Response Evaluation Model, Volume 1, *Theoretical Manual*, and Volume 2, *Thermal and Gas Release Assessments*, April 1996.
- C.3. EMF-2103(P)(A) Revision 0, *Realistic Large Break LOCA Methodology*, Framatome ANP Richland, Inc., April 2003.

## **Distribution**

### **E-Mail Notification**

R. L. Baxter  
J. R. Biller  
K. E. Carlson  
B. M. Dunn  
M. E. Garrett  
N. K. Nithianandan  
D. W. Pruitt  
G. S. Uyeda